Atmospheric New Particle Formation and Growth in Diverse Environments in India

A thesis submitted during 2023 to the University of Hyderabad in partial fulfilment of the degree of a PhD degree in
Centre for Earth, Ocean and Atmospheric Sciences

by

Mathew Sebastian

Centre for Earth, Ocean and Atmospheric Sciences
School of Physics

University of Hyderabad
(P.O.) Central University, Gachibowli,
Hyderabad-500 046
Telangana, India

2023

CERTIFICATE

This is to certify that the thesis entitled **"Atmospheric New Particle Formation and Growth in Diverse Environments in India"**, submitted by **Mathew Sebastian** bearing Reg. No. **18ESPE07,** in partial fulfilment of the requirements for the award of the degree of Doctor of Philosophy in **Earth Sciences,** is a bonafide record of the work that has been carried out by him under my supervision and guidance.

The thesis is free from plagiarism and has not been submitted previously, either in part or in full, for the award of any academic degree or diploma to this or any other university or institution.

Further, the student has the following publications before submission of the thesis for adjudication and has produced evidence for the same in the form of the reprint in the relevant area of his research

1. **Sebastian, M.**, Kanawade, V.P., et al., *Observations of particle number size distributions and new particle formation in six Indian locations, Atmospheric Chemistry and Physics,* 22, 2022. *This publication appears in Chapters 3 & 5 of the dissertation*
2. Kanawade, V.P., **Sebastian, M.** and Dasari. P., *New particle formation and growth suppressed during COVID-19 lockdown in urban Hyderabad, Journal of Geophysical Research-Atmospheres,* 127, *2022. This publication appears in Chapter 3 of the dissertation*
3. Kanawade, V.P., **Sebastian, M.**, et al., *Atmospheric new particle formation in India: Current understanding and knowledge gaps, Atmospheric Environment,* 270, 2022. *This publication appears in Chapter 1 of the dissertation*
4. **Sebastian, M.**, Kanawade, V. P., and Pierce, J. R., *Observation of sub-3nm particles and new particle formation at an urban location in India. Atmospheric Environment,* 256, 2021. *This publication appears in Chapter 3 of the dissertation*
5. **Sebastian, M.**, V.P. Kanawade et al., *New particle formation and growth to climate-relevant aerosols at a background remote site in the Western Himalaya, Journal of Geophysical Research-Atmospheres,* 126, 2021. *This publication appears in Chapter 5 of the dissertation*

and has made presentations in the following conferences

1. **Sebastian, M.**, V.P. Kanawade et al., *"Characteristics of size-segregated particle concentrations in an Indian urban location"*, The 21st International Conference On Nucleation & Atmospheric Aerosols (ICNAA), 26–30 June 2023, Brisbane, Australia.
2. **Sebastian, M.**, V.P. Kanawade et al., *"Characteristics of size-segregated particle concentrations in an urban location in India"*, EGU General Assembly, 23–28 April 2023, Vienna, Austria.

3. **Sebastian, M.,** V.P. Kanawade et al., *"Characterisation of particle number size distributions and new particle formation in different Indian locations"*, AGU Fall Meeting, 12–16 Dec 2022, Chicago, USA
4. **Sebastian, M.,** V.P. Kanawade et al., *"Characterisation of particle number size distributions and new particle formation in different Indian locations"*, EGU General Assembly, 23–27 May 2022, Vienna, Austria
5. **Sebastian, M.,** V.P. Kanawade et al., *"New particle formation and growth suppressed during COVID-19 lockdown in urban Hyderabad"*, International Conference on Environmental Science and Engineering, 20–22 Jan 2022, ESED, IIT-Bombay, India
6. **Sebastian, M.,** V.P. Kanawade et al., *"Observation of sub-3nm particles and new particle formation at an urban location in India"*, AGU Fall Meeting 2021, 13–17 Dec. 2021, New Orleans, USA.
7. **Sebastian, M.,** V.P. Kanawade et al., *"Observation of sub-3nm particles and new particle formation at an urban location in India"*, IMS TROPMET, 14–17 Dec. 2020.
8. **Sebastian, M.,** V.P. Kanawade et al., *"New Particle Formation and Growth to Climate-relevant Aerosols at a High-Altitude Site in the Western Himalaya - Ranichauri"*, International Conference on Aerosol Air Quality, Climate Change and Impact on Water Resources and Livelihoods in the Greater Himalayas, 14–16 September 2020, ARIES, Nainital.

Further, the student has passed the following courses towards the fulfilment of the coursework required for a Ph.D.

Course No.	Course	Credits	Pass/Fail
ES801	Earth System Sciences	4	Pass
ES805	Research Methodology	3	Pass
ES806	Mathematics for Earth Sciences	4	Pass
ES807	Interdisciplinary Course	3	Pass
AP811-830	Special paper on a specific research topic	2	Pass
	Total	16	

Supervisor
Dr. Vijay P. Kanawade
UGC-Assistant Professor
Centre for Earth, Ocean & Atmospheric Sciences
University of Hyderabad
Hyderabad-500 046, Telangana, INDIA.

12/12/2023

Head of the Department
Centre for Earth, Ocean & Atmospheric Sciences
University of Hyderabad
Hyderabad-500 046, INDIA.

Dean of School
DEAN
School of Physics
University of Hyderabad
HYDERABAD - 500 046

DECLARATION

I, **Mathew Sebastian,** hereby declare that the thesis entitled " **Atmospheric New Particle Formation and Growth in Diverse Environments in India "** submitted by me under the guidance and supervision of **Dr Vijay P. Kanawade** is a bonafide research work. I also declare that it has not been submitted previously in part or in full to this University or any other University or institution to award any degree or diploma.

Mathew Sebastian
Reg. No. 18ESPE07

Date: 12/12/2023

Dedicated to

My Parents and Teachers,

who have shone the light on my path to the quest for knowledge

Acknowledgements

I express my sincere gratitude to my supervisor Dr. Vijay P. Kanawade for his exceptional mentorship, scholarly insights, and insightful feedback that enriched my doctoral journey. I am always indebted for Dr. Kanawade's unflinching support during difficult moments in my life. I am profoundly grateful for the privilege of being mentored by Dr. Kanawade.

I am grateful to my doctoral committee members, Prof. K. Ashok and Dr. Devleena Mani Tiwari, who gave their insights into every step of my research. Their suggestions and encouragement have immensely helped me to improve my PhD work.

I am thankful to Prof. M. Jayananda, Head, Centre for Earth, Ocean and Atmospheric Sciences, and the former Head, Prof. K. S. Krishna, for providing the facilities and support at the Centre.

I am thankful to the Faculty Members of CEOAS and the PhD scholars for all the fruitful discussions. I also thank the office staff at CEOAS for providing clerical support.

I express my gratitude to my colleagues Abin, Anas, Charan, Feba, Mariya, Poul, Maria, Stella, Varaprasad, and Vikas for their camaraderie and encouraging scientific discussions.

I acknowledge the Institution of Eminence, University of Hyderabad for providing me with financial support, and DST & SERB for financial support towards scientific instruments required for my PhD thesis work.

I am thankful to Collaborators from the National (Space Physics Laboratory-VSSC Thiruvananthapuram, National Physical Laboratory-Delhi, Indian Institute of Tropical Meteorology-Pune, India Meteorological Department, Indian Institute of Technology-Madras, Telangana State Pollution Control Board) and International institutes (Colorado State University-USA, Finnish Meteorological Institute-Finland and Columbia State University-USA) for sharing data, invaluable contributions to research ideas, and unwavering collaborative spirit, all of which have greatly enhanced the depth and breadth of this research endeavour.

I acknowledge the free use of Hybrid Single-Particle Lagrangian Integrated Trajectory (HYSPLIT) simulations from the National Oceanic and Atmospheric Administration (NOAA) Air Resources Laboratory (ARL), National Aeronautics and Space Administration (NASA) and European Satellite data and reanalysis data from Copernicus Open Access Hub.

I sincerely thank my friends and family who generously helped me both in my hometown and at the University. Their selfless actions contributed a lot to my Ph. D. journey.

Finally, I am deeply indebted to my parents and sister, whose constant support and inspiration have been the bedrock of my academic pursuits.

Mathew Sebastian

Contents

	Page No.
Table of Contents	i
List of figures	iv
List of tables	x
Abbreviations	xii
List of publications	xiv
List of National/International Conferences/Symposiums/Workshops attended	xv
Abstract	1
Chapter 1. Introduction	2
1.1 Basics of atmospheric aerosols	2
1.1.1 Atmospheric aerosols	2
1.1.2 Types of aerosols	3
1.1.3 Properties of aerosols	5
1.1.4 Effect of aerosols on climate	6
1.2 Atmospheric new particle formation and growth	7
1.2.1 Aerosol nucleation mechanisms	11
1.2.2 Identification of atmospheric new particle formation events	13
1.3 Literature survey	14
1.3.1 Current understanding of new particle formation in India	14
1.3.2 Critical knowledge gaps and motivation	23
1.4 Objectives of the study	25
1.5 Outline of the thesis	26
Chapter 2. Data and Methods	28
2.1 Measurement sites and instrumental setup	28
2.2 Measurements of particle number size distributions	33
2.2.1 nano Condensation Nucleus Counter	33
2.2.2 Scanning Mobility Particle Sizer	35
2.2.3 Differential Mobility Particle Sizer	36
2.2.4 Wide Range Aerosol Spectrometer	36
2.3 Meteorological and trace gases measurements	36
2.4 HYSPLIT simulations and ERA5 reanalysis data	37
2.4.1 HYSPLIT trajectory model	37
2.4.2. ERA5	37
2.5 Satellite data	38
2.5.1 OMI	38
2.5.2 TROPOMI	38
2.6 Data analysis techniques and procedures	39

2.6.1 Size-segregated particle number concentration 39
2.6.2 Classification of new particle formation events 39
2.6.3 Particle formation and growth rate calculations 43
2.6.4 Condensation sink and coagulation sink calculations 44
2.6.5 Calculation of sulfuric acid proxy concentrations 45
2.6.6 Spatial extent of new particle formation events 46
2.6.7 Survival probability of newly formed particles 47
2.6.8 Estimating new particle formation contribution to cloud condensation nuclei production from new particle formation 48

Chapter 3. Characterization of sub-3nm particles and new particle formation 49
3.1 Introduction 49
3.2 Data analysis methods 50
3.3 Results and discussions 50
3.3.1 Characteristics of size-segregated particles number concentration 50
3.3.2 Formation and growth rates of sub-3nm particles in Hyderabad 54
3.3.3 Role of sulfuric acid and other condensable species in aerosol formation and growth 56
3.3.4 COVID-19 lockdown a case study 59
3.3.5 Characteristics of particle number size distributions and new particle formation events 67
3.4 Summary 77

Chapter 4. Influence of airmass history on new particle formation events 78
4.1 Introduction 78
4.2 Data analysis methodology 80
4.3 Results and discussions 82
4.3.1 The frequency of occurrence of different event types 82
4.3.2 Characteristics of new particle formation events 83
4.3.3 Characteristics of airmass trajectories during NPF and non-event days 86
4.3.4 Spatial extent of NPF events 90
4.4 Summary 90

Chapter 5. New particle formation and growth to climate-relevant aerosols 92
5.1 Introduction 92
5.2 Data analysis methodology 93
5.3 Results and discussions 94
5.3.1 Event identification and classification 94
5.3.2 New particle formation event to cloud condensation nuclei production 96
5.3.2.1 Survival Probability of newly formed particles 97
5.3.2.2 Increase in cloud condensation nuclei concentrations 100
5.4 Summary 103

Chapter 6. Summary and Future Scope **105**
6.1 Summary 105
6.2 Future scope 107

Bibliography 109

List of Figures

Chapter 1 **Page No.**

Figure 1.1 The blue arrows represent solar radiation, and the grey arrows represent terrestrial radiation and The brown arrow denotes the significance of couplings between the surface and the cloud layer (IPCC, 2013). 6

Figure 1.2 Thermodynamic representation of aerosol nucleation. A nucleation barrier of height $G*$ exists. The critical cluster size $Rp*$ is defined by the maximum of the barrier (Curtius, 2006). 9

Figure 1.3 Illustration of the nucleation and subsequent growth process involved in atmospheric binary homogeneous nucleation of H_2SO_4 and H_2O (Kulmala et al., 2013) . 10

Figure 1.4 Diurnal evolution of the particle number size distributions during NPF event exhibiting the 'banana' curve at Hyderabad. The white '+' sign denotes mode diameter and black '+' denotes nucleation mode particle number concentration. 14

Figure 1.5 Geographic locations of various measurement sites from different environments across globe (Kerminen et al., 2018). 15

Figure 1.6 Geographic distribution of sites where observations of new particle formation were reported in India. The superscript number indicates the number of studies reported at the specific site. Different colors indicate the various atmospheric environments such as urban (Delhi, Kanpur, Pune, and Hyderabad), semi-urban (Dibrugarh, Gual Pahari, Solapur), semi-urban-coastal (Trivandrum), semi-rural (Gadanki), mountain semi-rural (Mahabaleshwar), mountain background (Ranichauri and Mukteshwar), mountain remote (Ooty and Hanle), and cruise (North Indian Ocean). The filled contours indicate the climatological mean aerosol optical depth from the MODIS AQUA sensor (Remer et al., 2008) , highlighting the nature of the site. 16

Figure 1.7 Association between site-specific particle formation rate and growth rate as a function of condensation sink. The marker colours indicate the type of the measurement sites, and the marker size is proportional to the condensation sink (the smallest and the biggest marker corresponds to the condensation sink of 0.001 s^{-1} and 0.05 s^{-1}, respectively). RNC: Ranichauri, MUK: Mukteshwar, MBL: Mahabaleshwar, GDN: Gadanki, SLP: Solapur, HYD: Hyderabad KNP: Kanpur, PUN: Pune, DEL: Delhi, and ICARB: cruise in North Indian Ocean. 22

Chapter 2

Figure 2.1 The geographical location of measurement sites on the surface elevation map. Measurement sites such as Ranichauri (RNC), Mukteshwar (MUK), Mahabaleshwar (MBL), Hyderabad (HYD), 28

Thiruvananthapuram (TVM), and Delhi (DEL) are shown by the red plus sign. The global 1-arcsecond (30-m) SRTM digital surface elevation data is obtained from the United States Geological Survey (https://dds.cr.usgs.gov/srtm/version2_1/SRTM30/).

Figure 2.2 Aerosol Physics Laboratory (inside and outside view) at the Earth Sciences Building, University of Hyderabad, INDIA. 30

Figure 2.3 (a) Scatter plot of sub-3nm number concentrations ($N_{sub\text{-}3nm}$) with and without the diffusion dryer (DD). (b) Size dependent percentage loss in particles in the diffusion dryer. Bin1, Bin2, Bin3, Bin4, Bin5 and Bin6 indicates six size bins; 1.2-1.4, 1.4-1.6, 1.6-1.8, 1.8-2.0, 2.0-2.2 and 2.2-3.0 nm, respectively. 34

Figure 2.4 Time evolution of the particle number size distributions on a typical (a) Type-I NPF&G event, (b) Type-II NPF event, (c) Type-III non-event, and (d) Type-IV unidentified event day at Hyderabad. The particle number size distribution in the size range from 1.2 to 3.0 nm and 10 to 514 nm were obtained using the nCNC and SMPS, respectively. 41

Figure 2.5 Temporal evolution of particle number size distributions (filled contour), particle mode diameter (blue plus symbol), and BC mass concentrations (thick black line) for a typical Type-I NPF events (a, b), Type-II NPF events (c, d), Type-III non-event (e) and Type-IV unidentified event (f) days at Ranichauri. 43

Figure 2.6 Size-segregated particle growth rate calculation by fitting a first-order polynomial regression to time evolution of particle mode diameter. White circles denote the particle mode diameter and the black line denotes the fitted curve. 44

Chapter 3

Figure 3.1 Time evolution of particle number-size distributions in the size range of 1.25 to 2.8 nm from nCNC and 10-514 nm from SMPS during 1 April 2019 to 7 December 2022. 51

Figure 3.2 Monthly percentage of occurrence of NPF, non-event polluted and undefined events days based on total valid observations days at Hyderabad from 1 April 2019 to 7 December 2022. 52

Figure 3.3 Size-segregated particle number concentrations in the (a) cluster, (b) nucleation, (c) Aitken and (d) accumulation modes on NPF event days, non-event days and polluted days during winter (DJF), pre-monsoon (MAM), monsoon (JJAS) and post-monsoon (ON). 53

Figure 3.4 Correlation between $PM_{2.5}$ concentration and particle number concentration in each mode during (a) winter (DJF), (b) pre-monsoon (MAM), (c) monsoon (JJAS) and (d) post-monsoon (ON) 54

Figure 3.5 (a) Box-whisker plots of $J_{1.2}$, $J_{1.4}$, $J_{1.6}$, $J_{1.8}$, and $J_{2.0}$. The blue dot indicates the mean, the horizontal line indicates the median, the top and bottom of box indicate 25^{th} and 75^{th} percentiles, respectively, and the top and 55

bottom whisker indicate 5th and 95th percentiles, respectively and (b) the median diurnal variation of $J_{1.2}$, $J_{1.4}$, $J_{1.6}$, $J_{1.8}$, and $J_{2.0}$ for Type-I NPF&G (thick lines) and Type-II NPF (dashed lines) event days.

Figure 3.6 The median diurnal variation of $J_{1.2}$, $J_{1.4}$, $J_{1.6}$, $J_{1.8}$, and $J_{2.0}$ for Type-I NPF&G (thick lines) and Type-II NPF (dashed lines) event days. 55

Figure 3.7 Scatter plot of hourly averaged $J_{1.4}$ versus $N_{sub\text{-}3nm}$as a function of $[H_2SO_4]_{proxy}$ for Type-I (open circle) and Type-II (plus sign) events in Hyderabad. The data pertaining to $J_{1.4}$, $N_{sub\text{-}3nm,}$ and $[H_2SO_4]_{proxy}$ were taken as the average between 6:00 AM to 2:00 PM. The mean values of $J_{1.4}$, $N_{sub\text{-}3nm}$, and $[H_2SO_4]_{proxy}$ for other sites in diverse environments listed in Table 2 are also plotted for comparison: Nanjing (filled and open diamond for spring and winter seasons, respectively), Shanghai (filled circle, winter) Beijing (filled square, spring), Brookhaven (filled upward triangle, spring), and Kent (filled downward triangle, winter).* indicates winter-time measurements. The colour scale shows the concentration of $[H_2SO_4]_{proxy}$. 56

Figure 3.8 Spatial distribution of percentage difference in TROPOMI-retrieved (a) tropospheric NO_2 column and (b) HCHO column between LCD and BAU time periods. The measurement site, Hyderabad, is shown by the open square symbol. Three-day air mass backward trajectories starting at 11:30 a.m. local time during (a) BAU and (b) LCD time periods are also shown. 60

Figure 3.9 Time evolution of particle number size distributions in the size range of 1.2–3.0 nm from nCNC and 10–514 nm from SMPS during (a) BAU and (b) LCD time periods (15 April–31 May). 60

Figure 3.10 The percentage of days of event type during BAU and LCD in the same time period 61

Figure 3.11 Median diurnal variation of (a–e) size-segregated particle number concentrations, (f) total condensation sink (CS_{TOT}), (g) total coagulation sink ($CoagS_{TOT}$), and (h) total aerosol mass for NPF&G (line connected by plus symbol) and non-events (line connected by open circle) during BAU (blue) and LCD (red). Mann-Whitney *U*-test showed statistically significant differences ($p << 0.05$) for all variables between BAU and LCD except for sub-3 nm particles during non-event event days ($p = 0.063$). 62

Figure 3.12 Box-whisker plot of NPF&G characteristics during BAU and LCD; (a) $N_{sub\text{-}3nm}$, (b) N_{NUC}, (c) N_{AIT}, (d) N_{ACCU}, (e) N_{TOT}, (f) CS_{TOT}, (g) $CoagS_{TOT}$, (h) M_{TOT}, (i) $GR_{sub\text{-}3nm}$, (j) $J_{1.5nm,}$ (k) $GR_{10\text{-}25nm}$, and (l) J_{10nm}. The black square symbol indicates the mean, the horizontal line indicates the median, the bottom and top of the box indicate 25th and 75th percentile values, respectively, and the bottom and top of the whisker indicate the 10th and 90th percentile values, respectively. 63

Figure 3.13 Median diurnal variation of (a) sulfur dioxide, (b) ammonia, (c) oxides of nitrogen, (d) ozone, (e) carbon monoxide, (f) $PM_{2.5}$, (g) T/B ratio, and (h) X/B ratio for NPF&G and non-events during BAU and LCD. 65

Figure 3.14 Median diurnal variation of (a) temperature, (b) relative humidity, (c) wind speed, (d) wind direction, and (e) solar radiation for NPF&G and non-events during BAU and LCD. 66

Figure 3.15 (a) Annual and (b-g) seasonal median particle number size distributions at all the sites. The solid line indicates the median, and the light-colored shading indicates 25^{th} and 75^{th} percentile distributions. The blue line and shading indicate winter (DJF), red line and shading indicate pre-monsoon (MAM), green line and shading indicate monsoon (JJAS), and grey line and shading indicate post-monsoon season (ON). Note that the y-axis scale is different for the DEL site. 69

Figure 3.16 Histogram of the relative occurrence of Aitken mode particle number concentrations at the sites. The concentration bins are logarithmically spaced in the x-axis, and the y-axis shows the relative occurrence of values in each bin compared to the total number of valid observations. The black, blue, red, green, and grey lines indicate all data, winter (DJF), pre-monsoon (MAM), monsoon (JJAS), and post-monsoon (ON), respectively. n indicates the number of 10 minutes averaged valid data points. Note that measurements are from different time periods for each site (refer to Table 2.1). 72

Figure 3.17 Histogram of the relative occurrence of accumulation mode particle number concentrations at the sites. The concentration bins are logarithmically spaced in the x-axis, and the y-axis shows the relative occurrence of values in each bin compared to the total number of valid observations. The black, blue, red, green, and grey lines indicate all data, winter (DJF), pre-monsoon (MAM), monsoon (JJAS), and post-monsoon (ON), respectively. n indicates the number of 10 minutes averaged valid data points. Note that measurements are from different time periods for each site (refer to Table 2.1). 73

Figure 3.18 Monthly percentage of occurrence of NPF, non-event, and undefined events days based on total valid observations days at all the sites. The blue, red, green, and grey colored thick lines indicate winter, pre-monsoon, monsoon, and post-monsoon months. Note that measurements are from different time periods for each site (refer to Table 2.1). 75

Figure 3.19 Scatter plot of the particle formation rate and the growth rate as a function of condensation sink at each site. The condensation sink at the start of the event (CS_{onset}) is taken as a one-hour average CS just before the start of the NPF event. The lowest nucleation mode detectable size at each site is shown in the bracket. Note that measurements are from different time periods for each site (refer to Table 2.1). 76

Chapter 4

Figure 4.1	Time-series of (a) particle number size distributions and (b) $N_{>25nm}$ and N_{TOT} for the entire time period (1 April 2019 – 31 March 2022).	81
Figure 4.2	Monthly percentage of occurrence of event types in Hyderabad.	83
Figure 4.3	Scatter plot of hourly averaged CS versus GR for the observed NPF events in Hyderabad (symbols, filled magenta box for dry winter, plus for pre-monsoon and open circle for monsoon). The mean values of CS and GR Hyderabad (blue), Beijing (red), and Usti nad Labem (green) are also plotted for comparison.	85
Figure 4.4	Airmass 3-day backward trajectories starting at 500 m above ground at 6 UTC (11:30 AM local time) during (a) ONDJF, (b) MAM, and (c) JJAS months for NPF events (blue trajectories) and non-events (red trajectories). The measurement site is shown by the open square box.	86
Figure 4.5	Percentage occurrence of air mass trajectory altitude as a function of backward time for (a) ONDJF, (b) MAM, and (c) JJAS months for observed NPF events (top panel) and non-events (bottom panel) based on air mass backward trajectories starting at 500 m above ground at 6 UTC (11:30 AM local time).	87
Figure 4.6	Averaged latitude-pressure cross-section of vertical velocity over longitude bins 76 - 82 °E with the measurement site centered for observed (a) NPF events and (b) non-events for dry winter months (ONDJF).	88
Figure 4.7	Same as Figure 4.6, but for pre-monsoon months (MAM)	88
Figure 4.8	Same as Figure 4.6, but for summer monsoon months (JJAS).	88
Figure 4.9	Averaged LTS for observed (a) NPF events, (b) non-events, and (c) difference (a-b) for dry winter months (ONDJF).	89
Figure 4.10	Same as Figure 4.9, but for pre-monsoon months (MAM)	89
Figure 4.11	Same as Figure 4.9, but for summer monsoon months (JJAS).	89
Figure 4.12	The spatial extent of the observed NPF events for (a) ONDJF, (b) MAM, and (c) JJAS months. The measurement site Hyderabad is shown by the asterisk sign. The contour line is the line of the same distance (in km) from the measurement site. The number in each pixel indicates trajectory duration (in hours).	90

Chapter 5

Figure 5.1	Particle number size distribution data coverage (% of days/month) at the sites. The values in the bracket indicate total data coverage. The blue, red, green, and grey colored thick lines indicate winter (DJF), pre-	93

monsoon (MAM), monsoon (JJAS), and post-monsoon (ON). Note that measurements are from different time periods for each site (refer to Table 2.1).

Figure 5.2 The diurnal-seasonal median particle number size distributions at all the sites; a) Ranichauri, b) Mukteshwar, c) Mahabaleshwar, d) Hyderabad, e) Thiruvananthapuram, and f) Delhi. Note that measurements are from different time periods for each site (refer to Table 2.1). 96

Figure 5.3 Survival probability of newly formed particles to 50 nm (SP50) and 100 nm (SP100). 97

Figure 5.4 Cumulative probability distributions of survival probability to 50 nm (SP50) and 100 nm (SP100) and formation rates of 50 nm (J50) and 100 nm (J100) particles for the NPF events at a) Ranichauri, b) Mukteshwar, c) Mahabaleshwar, d) Hyderabad, e) Thiruvananthapuram, and f) Delhi. 99

Figure 5.5 Box-whisker plot of absolute increase in CCN concentrations for (a) 50 nm and (b) 100 nm particles and percentage increase in CCN concentrations for (c) 50 nm and (d) 100 nm in six diverse locations based on the observed NPF and non-event events. The filled square indicates the mean, the horizontal line indicates the median, the top and bottom of the box indicate 25^{th} and 75^{th} percentile values, and the top and bottom whiskers indicate 10^{th} and 90^{th} percentile values. Note that measurements are from different time periods for each site (refer to Table 2.1), therefore the comparison between the sites is not feasible. 102

List of Tables

Chapter 1 **Page No.**

Table 1.1 Summary of measurement sites (name and type), measurement parameters (time, instrument, and size range) and key NPF characteristics [NPF frequency, formation rate (J_{NUC}), growth rate (GR) and condensation sink (CS)] in diverse environments of India. 20

Chapter 2

Table 2.1 Details of the measurement sites and particle number size distribution measurements considered. 33

Table 2.2 Summary of criteria used for classifying event types based on nCNC and SMPS observations in Hyderabad. NPF&G indicates new particle formation and growth. 40

Table 2.3 Summary of criteria used for classifying event types in Ranichauri. 42

Chapter 3

Table 3.1 Summary of averaged (6:00 AM to 2:00 PM local time) sub-3nm particle number concentrations ($N_{sub\text{-}3nm}$), formation rate of 1.4 nm particles ($J_{1.4}$), growth rate of sub-3nm particles ($GR_{sub\text{-}3nm}$), total growth rate (GR), sulfuric acid concentration proxy ($[H_2SO_4]_{proxy}$), total consternation sink (CS_{TOT}) and total coagulation sink ($CoagS_{TOT}$) for Type-I and Type-II NPF events in Hyderabad and various other sites in diverse environments. ±indicates standard deviation. 58

Table 3.2 Parameters of the modes identified for the description of median particle number size distributions are shown in Figure 3. N, Dp and σ are the number concentration, geometric mean diameter and the standard deviation of the distribution. 70

Table 3.3 Number of valid observation days, number of NPF days (percentage), number of non-event days (percentage), mean formation rates and mean growth of particles at all six sites in India. ± indicates standard deviation. 74

Chapter 4

Table 4.1 Summary of criteria used for classifying different event types. 82

Table 4.2 Summary of averaged (9:00 a.m. to 4:00 p.m. local time) formation rate of 10 nm particles (J_{10}), the growth rate of particles from 10-25 nm diameter ($GR_{10\text{-}25}$), total condensation sink (CS), $[H_2SO_4]_{proxy}$, growth rate due to $[H_2SO_4]$ alone and the percentage contribution of growth rate due to $[H_2SO_4]$ alone to $GR_{10\text{-}25}$ for the observed NPF events. ± indicates standard deviation. 84

Chapter 5

Table 5.1	Number of valid observation days, number of NPF days (percentage), number of non-event days (percentage), mean formation rates and mean growth of particles at all six sites in India. ± indicates standard deviation.	94
Table 5.2	Summary of survival probability and formation rate of 50 nm and 100 nm particles at diverse locations.	98

Abbreviations

AOD	:	Aerosol Optical Depth
amsl	:	above mean sea level
BAU	:	Business-as-usual
BC	:	Black Carbon
CCN	:	Cloud Condensation Nuclei
CO	:	Carbon Monoxide
CO_2	:	Carbon Dioxide
CoagS	:	Coagulation Sink
CPC	:	Condensation Particle Counter
CS	:	Condensation Sink
DEG	:	diethylene glycol
DEL	:	Delhi
DMA	:	Differential Mobility Analyser
DMPS	:	Differential Mobility Particle Sizer
ECMWF	:	European Centre for Medium-Range Weather Forecasts
ERA5	:	ECMWF Re-Analysis 5
FMI	:	Finnish Meteorological Institute
GAW	:	Global Atmospheric Watch
GDAS	:	Global Data Assimilation System
GR	:	Growth rate
H_2SO_4	:	Sulfuric Acid
HCHO	:	Formaldehyde
HYD	:	Hyderabad
HYSPLIT	:	Hybrid Single Particle Lagrangian Integrated Trajectory
IFS	:	Integrated Forecasting System
IMD	:	India Meteorological Department
J	:	Formation rate
LCD	:	Lockdown
LDS	:	lowest detectable size
lpm	:	litre per minute
LTS	:	Lower Tropospheric Stability
LTW	:	Lower Tropospheric Stability
MBL	:	Mahabaleshwar
MUK	:	Mukteshwar
N_2	:	Nitrogen
N_2O	:	Nitrous Oxide
NAIS	:	Neutral Air Ion Spectrometer
N_{CCNmax}	:	maximum CCN concentration during the event
$N_{CCNprior}$	:	CCN concentration before the event
nCNC	:	nano Condensation Nucleus Counter
NH_3	:	Ammonia
NO_2	:	Nitrogen dioxide
NO_x	:	Nitrogen oxides
NPF	:	New Particle Formation

NPF&G	:	New Particle Formation and Growth
O_3	:	Ozone
OMI	:	Ozone Monitoring Instrument
OPC	:	Optical Particle Counter
PM_{10}	:	Particulate matter less than 10 microns in size
$PM_{2.5}$	:	Particulate matter less than 2.5 micron in size
PNSD	:	Particle Number Size Distribution
PSM	:	Particle Size Magnifier
RH	:	Relative Humidity
RNC	:	Ranichauri
SMPS	:	Scanning Mobility Particle Sizer
SO_2	:	Sulfur dioxide
SOA	:	Secondary Organic Aerosols
SP	:	Survival Probability
SR	:	Solar radiation
SSA	:	Single Scattering Albedo
T	:	Temperature
TROPOMI	:	TROPOspheric Monitoring Instrument
TVM	:	Trivandrum
VOC	:	Volatile Organic Compounds
WD	:	Wind speed
WMO	:	World Meteorological Organization
WRAS	:	Wide Range Aerosol Spectrometer
WS	:	Wind Speed
ΔG	:	Gibbs free energy

List of publications

Publications from the Ph.D. thesis

1. **Sebastian, M.,** Kanawade, V.P., et al., *Observations of particle number size distributions and new particle formation in six Indian locations, Atmospheric Chemistry and Physics,* 22, 2022. [IF: 7.197].

2. Kanawade, V.P., **Sebastian, M.** and Dasari. P., *New particle formation and growth suppressed during COVID-19 lockdown in urban Hyderabad*, *Journal of Geophysical Research–Atmospheres,* 127*, 2022.* [IF: 5.217]

3. Kanawade, V.P., **Sebastian, M.**, et al., *Atmospheric new particle formation in India: Current understanding and knowledge gaps*, *Atmospheric Environment,* 270, 2022. [IF: 5.755]

4. **Sebastian, M.,** Kanawade, V. P., and Pierce, J. R., *Observation of sub-3nm particles and new particle formation at an urban location in India*. *Atmospheric Environment,* 256, 2021. [IF: 5.755]

5. **Sebastian, M.,** V.P. Kanawade et al., *New particle formation and growth to climate-relevant aerosols at a background remote site in the Western Himalaya*, *Journal of Geophysical Research–Atmospheres,* 126, 2021. [IF: 5.271]

Publications related to the Ph. D. thesis topic

1. Kohl, M., Lelieveld, J., Chowdhury, S., Ehrhart, S., Sharma, D., Cheng, Y., Tripathi, S. N., **Sebastian, M.,** Pandithurai, G., Wang, H., and Pozzer, A., *Numerical simulation and evaluation of global ultrafine particle concentrations at the Earth's surface, Atmospheric Chemistry and Physics*., 23, 2023. [IF: 7.197]

List of National Conferences/Symposiums attended

1. **Sebastian, M.,** V.P. Kanawade et al., *"Characteristics of size-segregated particle concentrations in an Indian urban location",* The 21st International Conference on Nucleation & Atmospheric Aerosols (ICNAA), 26-30 June 2023, Brisbane (Poster presentation)

2. **Sebastian, M.,** V.P. Kanawade et al., *"Characteristics of size-segregated particle concentrations in an urban location in India",* EGU General Assembly, 23-28 April 2023, Vienna (Oral presentation)

3. **Sebastian, M.,** V.P. Kanawade et al., *"Characterisation of particle number size distributions and new particle formation in different Indian locations",* AGU Fall Meeting, 12-16 Dec 2022, Chicago (Oral presentation – Hybrid mode)

4. **Sebastian, M.,** V.P. Kanawade et al., *"Characterisation of particle number size distributions and new particle formation in different Indian locations",* EGU General Assembly, 23-27 May 2022, Vienna (Oral presentation)

5. **Sebastian, M.,** V.P. Kanawade et al., "*New particle formation and growth suppressed during COVID-19 lockdown in urban Hyderabad",* International Conference on Environmental Science and Engineering, 20 – 22 Jan 2022, ESED, IIT-Bombay (Oral presentation – Hybrid mode)

6. **Sebastian, M.,** V.P. Kanawade et al., *"Observation of sub-3nm particles and new particle formation at an urban location in India",* AGU Fall meeting 2021, 13 - 17 Dec. 2021, New Orleans (Poster presentation – Hybrid mode)

7. **Sebastian, M.,** V.P. Kanawade et al., *"Observation of sub-3nm particles and new particle formation at an urban location in India"*, IMS TROPMET, 14 – 17 Dec. 2020 (Oral presentation – Hybrid mode)

8. **Sebastian, M.,** V.P. Kanawade et al., *"New Particle Formation and Growth to Climate-relevant Aerosols at a High-Altitude Site in the Western Himalaya – Ranichauri",* International Conference on Aerosol Air Quality, Climate Change and Impact on Water Resources and Livelihoods in the Greater Himalayas, 14-16 September 2020, ARIES, Nainital (Oral presentation – Hybrid mode)

Abstract

Aerosols, tiny suspended solid or liquid particles, are ubiquitous in the atmosphere. Aerosols are directly emitted to the atmosphere from a variety of natural and anthropogenic sources and produced via physical and/or chemical transformation in the atmosphere. Gas-to-particle (GTP) conversion, commonly referred to as new particle formation (NPF) which is the greatest source of new particles to the terrestrial atmosphere. The newly formed particles grow in size via condensation of gaseous vapours and can grow to cloud condensation nuclei (CCN)-active sizes (>50-100 nanometer diameter), and thereby can affect Earth's radiation budget and hydrological cycle. While NPF and growth have extensively been studied in the USA, Europe and China, it has been poorly studied in India. Here, we have used particle number size distribution measurements to characterize and examine NPF and growth in diverse geographical locations in India. Using state-of-the-art techniques, we provided direct observational evidence of neutral sub-3nm particle formation and growth from an urban location in India. We found that sulfuric acid plays a key role in the formation of sub-3nm particles, but sulfuric acid does not explain the total observed growth of nucleation mode particles. This indicates that other condensable vapours such as low-volatile organic compounds, ammonia, and/or amines are important for the growth of newly formed particles in the atmosphere. We further illustrated that NPF is not inhibited at high pre-existing particles in Hyderabad. It seemed to us that the balance between aerosol precursor concentration and pre-existing particle loading decides when an NPF event would trigger in the polluted boundary layer. The COVID-19 lockdown case study revealed that the reduction in primary anthropogenic emissions did not inhibit the formation of sub-3nm particles, but the NPF and growth event frequency was three-fold lower during the lockdown than the Business-as-usual time period, possibly due to lower condensable vapours and reduced photochemical activities. Our results show a strong spatiotemporal heterogeneity in the evolution of aerosols in India based on long term measurements of particle number size distributions from six diverse geographical locations in India (Ranichauri, Mukteshwar, Delhi, Mahabaleshwar, Hyderabad, and Trivandrum). NPF events were commonly observed during the pre-monsoon season (March through May) in all locations and less frequently during monsoon (June through September) owing to wet scavenging of aerosol precursors and reduced photochemical activity under cloudy conditions. The critical analyses of air mass history revealed that the air mass source region is not a deciding factor for the occurrence of an NPF event. The modification of air mass as it travels in the atmosphere and local to regional scale meteorological conditions determines when NPF will occur in the atmosphere. Our analyses further showed that an NPF event occurs over a spatial scale of a few 100's kilometres and a temporal scale of 1-2 days. We also examined the fraction of newly formed particles growing to CCN-active sizes in six geographical locations in India. Overall, half of the newly formed particles were found to grow to CCN-active size with large variability from rural to urban locations (~30% to 60%). While sufficient knowledge of the characteristics of NPF events and aerosol growth has evolved over the last decade in India, the chemistry driving NPF and its linkage to CCN production are poorly studied in India and elsewhere. NPF processes have critical importance to climate studies because the fraction of ambiguity in radiative forcing comes from CCN production that itself stems from the uncertainties in NPF and aerosol growth processes together with spatiotemporal heterogeneity in the primary emissions. Therefore, it is crucial to develop a superior process-level understanding of NPF and aerosol growth in the atmosphere.

Chapter 1

Introduction

1.1 Basics of atmospheric aerosols

1.1.1 Atmospheric aerosols

Atmospheric aerosols, tiny solid particles or liquid droplets suspended in the atmosphere, affect air quality, weather, human health, and the Earth's climate and hydrological cycle (IPCC, 2013; Seinfeld et al., 2016). Aerosol particle size covers a wide range from nanometer to 10's of micrometres (John, 2011; Tripathi et al., 1988). Aerosols are directly emitted to the atmosphere from both natural and anthropogenic sources. Natural sources of aerosols consist of volcanic eruptions, wildfires, dust storms, and sea spray. On the other hand, anthropogenic sources encompass various human activities such as industrial activities, vehicle emissions, agricultural practices, and construction. Aerosols are composed of organic matter, nitrate, sulfate, ammonium, black carbon, mineral dust, and other substances. The variability in the composition, size, and concentration of these particles exerts a significant influence on their atmospheric behaviour. Aerosols alter the Earth's radiation budget by scattering or absorbing solar radiation referred to as aerosol direct effect, thereby influencing the amount of energy that reaches the Earth's surface and the lower layers of the atmosphere. Aerosols, such as sulfate particles or sea spray, tend to reflect solar radiation into the atmosphere, resulting in a cooling effect at the Earth's surface, while aerosols, such as black carbon, tend to absorb the sunlight, resulting in the heating of the surrounding atmosphere (Hansen et al., 2000; Partanen et al., 2012; Zhang et al., 2008a). Aerosols further alter the cloud properties via the activation of cloud condensation nuclei (CCN) referred to as the aerosol indirect effect (Albrecht, 1989; Clarke et al., 1998; Haywood and Boucher, 2000; Lohmann and Feichter, 2005; Twomey, 1977; Wang and Penner, 2009). Only a fraction of aerosol acts as CCN depending on the size and chemical composition of aerosols that serve as surfaces for water vapour to condense upon, leading to the formation of cloud droplets. The abundance and size distribution of CCNs have a significant impact on cloud droplet size, cloud albedo, precipitation patterns, and thereby hydrological cycle (Barthlott et al., 2022; Han et al., 1998). Certain aerosols can also act as ice nuclei, facilitating ice crystal formation within cold clouds (Ladino et al., 2017).

These interactions introduce substantial intricacy to the dynamics of clouds and can affect precipitation patterns and climate at both regional and global scales.

The quality of air is an additional crucial concern linked to atmospheric aerosols. Submicron aerosol particles, particularly those with a diameter less than 2.5 micrometres ($PM_{2.5}$), can efficiently penetrate the human respiratory system upon inhalation, thereby presenting potential hazards to human well-being (Apte et al., 2015; Chowdhury et al., 2018; Xing et al., 2016). Prolonged exposure to elevated levels of $PM_{2.5}$ is highly correlated with various respiratory and cardiovascular ailments. The investigation of atmospheric aerosols encompasses a synergistic integration of in-situ observations, aircraft measurements, satellite observations, controlled laboratory experiments, and sophisticated computational simulations. These methodologies are crucial to acquiring comprehensive data regarding the properties, distribution, dynamics, and transport of aerosols to quantify their climatic impact. Atmospheric aerosols are complex and ever-changing constituents of the Earth's atmosphere that have a significant impact on weather, climate, air quality, and human well-being. The complex interplay between solar radiation, aerosols, and clouds significantly impacts the Earth's energy equilibrium and overall ecological health. As our comprehension of aerosol dynamics advances, it becomes progressively imperative to formulate methodologies for mitigating their influence on the environment and human populations.

1.1.2 Types of aerosols

Atmospheric aerosols, microscopic particles suspended in the air, are classified based on size, chemical composition, location, and sources. Based on size, they are divided into cluster mode, nucleation mode, Aitken mode, accumulation mode, and coarse mode particles (Seinfeld and Pandis, 1998). Cluster mode particles, with diameters of 1-3 nm, result from gas-to-particle conversion processes (Kulmala et al., 2014; Lee et al., 2019). Nucleation mode particles, spanning 3-25 nm, mostly consist of secondary aerosols and primary aerosols like vehicular emissions (as small as 7 nm) (Giechaskiel et al., 2022; Karjalainen et al., 2014; Kulmala et al., 2001; Rönkkö et al., 2017). Aitken mode particles (25-100 nm) consist of both primary emissions or secondary productions or both (Yue et al., 2009). Accumulation mode particles cover the size range of 100-1000 nm. Aerosols with a diameter greater than 1000 nm referred to as coarse mode particles, typically originate from mechanical activities such as aerodynamic resuspension and abrasion.

Based on source type, aerosols are categorised as primary and secondary aerosols. Primary aerosols are particles directly emitted into the atmosphere from various natural or anthropogenic sources (Seinfeld and Pandis, 2006). Secondary aerosols form in the atmosphere through chemical reactions involving precursor gases undergoing a gas-to-particle conversion or condensation of vapour onto pre-existing particles (Kerminen et al., 2018; Kulmala et al., 2001; Kulmala et al., 2004). Based on chemical composition, aerosols are broadly classified as organic, sulfate, nitrate, ammonium, chloride, and black/brown carbon. Sulfate, nitrate and ammonium are inorganic aerosols (Finlayson-Pitts and Pitts, 2000; Manisalidis et al., 2020) while organic aerosols are carbon-containing particles in the atmosphere originating from plants, combustion, and industrial emissions. Primary organic aerosols (POA) are referred to as directly emitted hydrocarbon compounds from various primary sources such as vehicle exhaust and biomass burning (Jimenez et al., 2009). Secondary organic aerosols (SOAs) are formed from the oxidation of volatile or semi-volatile organic compounds. SOA is a major component of atmospheric organic aerosols. About 50% of the fine aerosol mass is composed of organic aerosols with SOA fraction ranging from 65 to 95%. (Hallquist et al., 2009; Zhang et al., 2007). Aerosols are also composed of metallic elements like lead, mercury, potassium, copper, nickel, cadmium, etc. (Chen et al., 2015; Nriagu, 1989; Pacyna, 1998). Further, biological aerosols also constitute a major fraction of aerosols namely bacteria, fungi, and pollen and they can impact cloud formation processes and affect human health (Kim et al., 2018; Krishnamoorthy et al., 2020; Madelin, 1994). Desert or wind-blown dust and marine sea salt aerosols constitute the largest fraction of total aerosol mass (Schiffer et al., 2018). Volcanic eruptions are also a significant source of aerosols to the upper troposphere and lower stratosphere, mainly consisting of ash and sulfate particles (Aubry et al., 2021; d'Almeida, 1989; Kloss et al., 2020; Prasad et al., 2019). Based on locations, aerosols can also be classified as tropospheric and stratospheric aerosols. The residence time of tropospheric aerosols vary from a few hours to a week based on their location within the troposphere, and removal mechanism while, stratospheric aerosols have a life time of about a year and mainly from volcanic eruptions that release a huge mass of ash, dust and precursor gases such as SO_2. The upper atmosphere is also the source of aerosols to the lower atmosphere such as meteoric dust (Padma Kumari et al., 2005).

1.1.3 Properties of aerosols

Briefly, the *physical properties* such as size, shape, density, charge and hygroscopicity can influence aerosol evolution in the atmosphere and in turn influence cloud properties, air quality, and climate. Therefore, it is crucial to quantify aerosols to reduce current uncertainties in aerosols effect on climate. For instance, a wide size range of aerosols with four orders of magnitude difference between the smallest and the largest particles decides their mobility, behaviour, and residence time in the atmosphere (Seinfeld and Pandis, 2016). The shape of aerosols is directly linked to their interactions with solar radiation (Li et al., 2022; Lohmann and Feichter, 2005). Aerosols also exist in diverse shapes including spherical, irregular, or elongated. Aerosols can also carry electrical charges and are subject to distinct characteristics which can impact atmospheric dispersion (Dépée et al., 2021). The hygroscopicity of aerosols determines their ability to absorb water vapour and grow in size and therefore act as CCN for cloud formation processes and thereby have effects on the hydrological cycle, radiative forcing and climate (IPCC, 2013; Pöhlker et al., 2023; Singh et al., 2023). The *chemical properties* of aerosols include organic composition (vegetation, combustion, and industrial emissions), inorganic components (sulfate, nitrate, ammonium, chloride, and metallic elements like lead and mercury), biological content (bacteria, fungi, and pollen) carbon content (black/brown carbon) and trace gases (NO_X, SO_2, CO, O_3 etc.). The *optical properties* of aerosols include scattering, absorption, extinction, single scattering albedo (SSA), asymmetry parameter and aerosol optical depth (AOD). These properties play a critical role in determining their impact on climate, visibility, and radiative processes. Depending on the particle size, aerosols scatter radiation by Mie or Rayleigh scattering (Mie, 1908; Young, 1982). Absorption of radiation by aerosols warms the atmosphere (Jacobson, 2001). Aerosol extinction causes a reduction in the intensity of light and thereby affects visibility. The asymmetry parameter characterizes the angular distribution of scattered light and influences the direction of scattered light and cloud radiative properties (Marshall et al., 1995; Zege and Kokhanovsky, 1994). AOD quantifies the total optical thickness of aerosols in a vertical column which is crucial for analysing aerosol loading and radiative forcing (Holben et al., 1998; McClatchey et al., 1972). The *dynamical properties* of aerosols constitute nucleation, condensation, coagulation and sedimentation/settling/deposition. These properties determine the microphysical behaviour of aerosols in the atmosphere. Nucleation refers to the molecular cluster formation via aggregation of the same or different gaseous molecules in the atmosphere (Seinfeld and Pandis, 1998).

Condensation of aerosol precursor gases via diffusion onto aerosol surfaces causes aerosol growth (Brock and Suck, 1982). Coagulation refers to the collision and sticking of the same or different sizes of aerosol particles facilitated by turbulent air motions, particularly for polydisperse aerosol size distributions (Wexler et al., 1994). Aerosols can settle on surfaces due to gravitational forces depending on the size and density of the particle (Seinfeld and Pandis, 2016). Precipitation is responsible for more than 80% of aerosol removal from the atmosphere by wet scavenging (Ohata et al., 2016). The evolution of atmospheric aerosols is determined by all these processes which occur simultaneously.

1.1.4 Effect of aerosols on climate

Aerosols significantly influence the Earth's climate (Chlek and Coakley, 1974). They scatter sunlight back into space, exerting a cooling effect while a fraction of aerosols (e.g. black carbon) absorb light in the atmosphere, thereby warming the atmosphere. The net climate influence depends on aerosol type, concentration, and location and their complex interactions with clouds (IPCC, 2013).

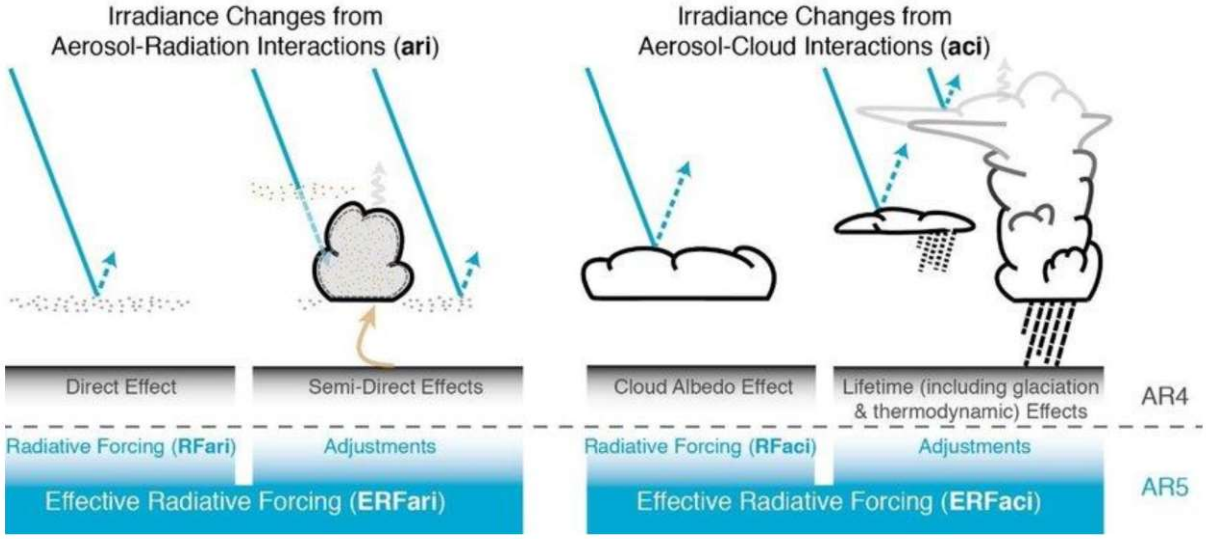

Figure 1.1 Schematic depicting aerosol-cloud-radiation interaction. Blue and grey arrows indicate solar and terrestrial radiation, respectively. The brown arrow indicate the couplings between the surface and the cloud (IPCC, 2013).

Aerosol direct effects

Aerosols scatter and absorb shortwave and longwave radiation referred to as aerosol direct effects (Forster et al., 2007). Aerosol direct effects can vary according to their spatio-temporal distribution,

humidity, and wavelength of light (Haywood and Boucher, 2000). Depending upon the aerosol type, they either scatter or absorb, in turn, it will have either a cooling or warming effect on the atmosphere; For instance, sulfate, dust, and sea salt aerosols tend to scatter the sunlight, thereby increasing Earth's albedo leading to cooling effect. (Charlson et al., 1992) while aerosols such as black carbon (soot) and other organic aerosols tend to absorb the sunlight, thereby warming the atmosphere.

Aerosol indirect effects

Aerosols have indirect effects on the Earth's climate through via activation of CCN. A fraction of aerosols have the potential to as act as CCN and ice nuclei, which can affect the cloud's macro- and micro-physical properties and thereby cloud radiative forcing, hydrological cycle and climate. The aerosol indirect effect is primarily divided into two categories: the first indirect effect (Twomey effect) and the second indirect effect (Albrecht effect). Increased concentrations of aerosol particles with limited amount of moisture, increases the number of cloud droplets but reduce in size. This leads to a greater reflection of sunlight by clouds (higher cloud albedo) which tends to cool the climate regionally. This is the first indirect effect (Ramaswamy et al., 2001) or the Twomey effect (Twomey, 1977) or the cloud albedo effect (Lohmann and Feichter, 2005). The reduced cloud droplets lead to a reduction of efficiency in precipitation. This also implies that it will take longer for the clouds to grow up to a precipitable size causing an increase in cloud lifetime. This will have a cooling effect known as the Albrecht effect or the second indirect effect (Albrecht, 1989).

Aerosol semi-direct effects

Absorbing aerosols in an atmospheric layer above the ground can warm the air around them, preventing water vapour from condensing and evaporation from existing cloud droplets. This will lead to a reduction in cloud cover and also increase the atmospheric stability and reduce? convection. This effect of absorbing aerosols and reducing cloud cover is known as a semi-direct effect (Ackerman et al., 2000; Hansen et al., 1997).

1.2 Atmospheric new particle formation and growth

Secondary aerosols are formed in the atmosphere through chemical reactions involving precursor gases via gas-to-particle conversion (Friedlander, 1977), involving precursor gaseous such as

sulfuric acid, amines, ammonia, and organics (Clement and Ford, 1999; Erupe et al., 2011; Glasoe et al., 2015; Jen et al., 2014; Juozaitis et al., 1996; Kulmala et al., 2002; Kurtén et al., 2008; Yu, 2006b). Newly formed nanometer-size clusters further grow in large sizes in the atmosphere over time referred to as NPF events. NPF event occurs everywhere in the terrestrial atmosphere (Kulmala et al., 2004; Manninen et al., 2010), including the free troposphere (Rose et al., 2017; Tröstl et al., 2016b; Xiao et al., 2023), urban (Crumeyrolle et al., 2023; Deng et al., 2021; Sebastian et al., 2021a), rural (Creamean et al., 2011; Jeong et al., 2010; Kanawade et al., 2012; Kanawade et al., 2014a), mountainous (Kivekäs et al., 2009; Sebastian et al., 2021b; Venzac et al., 2008), marine (Kompalli et al., 2020; O'Dowd et al., 2002) and polar regions (Baccarini et al., 2020; Dall´Osto et al., 2017; Jokinen et al., 2018; Schmale and Baccarini, 2021). NPF is a two-step process (Kulmala et al., 2013; Zhang et al., 2010). The first step is gas-to-particle conversion (aerosol nucleation) where the gas phase precursors aggregate to form a stable cluster. The second step comprises the growth of these nano clusters to larger sizes by condensational growth. NPF is a regional event occurring over a spatial scale of a few hundred kilometres and a temporal scale of 1 to 2 days (Dal Maso et al., 2007; Hussein et al., 2009; Kulmala et al., 2012a). NPF is the greatest source of particle numbers in the terrestrial atmosphere (Makkonen et al., 2012; Spracklen et al., 2010). These newly formed particles are subject to coagulation loss to pre-existing large-size particles in the atmosphere (Lehtinen et al., 2007). However, the newly formed particles can survive to grow bigger by condensation of volatile/semi-volatile vapours onto their surface to reach Atiken to accumulation mode sizes (Kerminen et al., 2012). In urban areas, the NPF process can thus contribute to reduced visibility and haze formation (Guo et al., 2014; Kulmala et al., 2022). Previous studies have revealed that NPF substantially degrades regional air quality and significantly contributes to the total $PM_{2.5}$ mass (Guo et al., 2014; Kulmala et al., 2022; Kulmala et al., 2021).

Nucleation refers to the formation of tiny molecular clusters from precursor gases undergoing a phase transition involving collision and aggregation of gaseous molecules. This process results in simultaneous decrease of both enthalpy and entropy of the thermodynamic system ($\Delta H < 0$ and $\Delta S < 0$). Before the phase transition becomes spontaneous, a free-energy barrier ($\Delta G = \Delta H - T\Delta S > 0$) needs to be overcome. Nucleation is driven by changes in the Gibbs free energy (ΔG), a thermodynamic parameter that accounts for the balance between the cohesive forces attracting

molecules and the thermal energy that tends to disperse them. The thermodynamics of nucleation is given by the following equation where the change in Gibbs free energy is represented as a function of the radius (R_p) of the nucleating particle.

$$\Delta G = -\frac{4}{3}\pi R_p^3 \frac{kT}{v_l} \ln S + 4\pi R_p^2 \sigma \tag{1.1}$$

where S is the saturation ratio, T is the temperature, k is the Boltzmann constant, σ is the surface tension, and v_l is the volume occupied per molecule. Figure 1.1 shows the visual representation of Eq. 1.1.

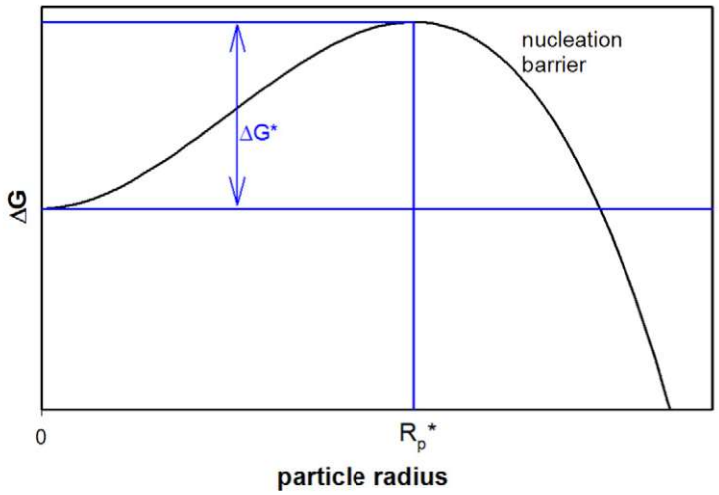

Figure 1.2 Thermodynamic representation of aerosol nucleation. A nucleation barrier of height ΔG^* exists. The critical cluster size R_p^* is defined by the maximum of the barrier (Curtius, 2006).

The value of S will be greater than unity as long as the system is in supersaturation. Thus, the initial term on the right-hand side of the equation will carry a negative value. This is the driving force for the condensation of gaseous molecules and the increase in particle size. For small R_p, the second term is more important in the beginning. During the particle formation process, there is a requirement to construct a new surface (with an area $4\pi R_p^2$), which costs surface energy. At the initial stage, the magnitude of surface energy is bigger than the energy gained during the transition from the gaseous phase to the particle phase. Consequently, a significant energy barrier is present for small particle radii (R_p), obstructing gas nucleation. This occurs despite the gas phase being supersaturated in relation to the equilibrium pressure of the flat surface. The Gibbs free energy curve shows a distinct energy barrier that must be overcome for nucleation to occur (Figure 1.2). The position of the peak of the barrier denotes the critical radius. The size of the critical cluster

depends on factors like temperature, pressure, and the chemical composition of precursor molecules. Once a cluster has reached the size of the critical cluster, the droplet remains in existence and will increase in size through the process of condensation of additional gas phase molecules. For clusters of small sizes that are below the critical size, the probability of a molecule evaporating off the cluster is higher than the probability of another molecule condensing onto it, due to energetic considerations. In the majority of instances, these clusters will disintegrate into individual gas molecules again. However, there exists a probabilistic likelihood that occasionally a group of molecules will accumulate to such an extent that it attains a size significant enough to surpass the critical cluster size to overcome the energy barrier (Curtius, 2006). The Gibbs free energy curve helps identify the critical cluster size, which is essential for nucleation to proceed. Once the critical cluster size is reached, aerosol particles can grow by the condensation of additional molecules onto their surfaces, eventually reaching sizes relevant to atmospheric processes (Kerminen et al., 2018).

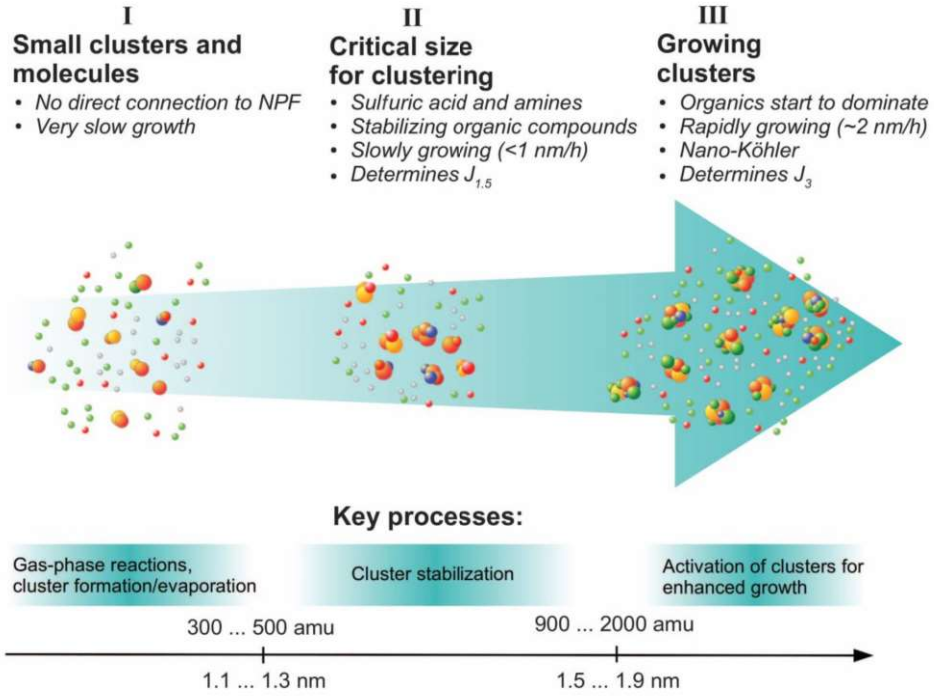

Figure 1.3 Illustration of the nucleation and subsequent growth process involved in atmospheric binary homogeneous nucleation of H_2SO_4 and H_2O (Kulmala et al., 2013).

Sulfuric acid acts as the essential precursor for the process of nucleation (Sipilä et al., 2010). Due to the low vapour pressure of sulfuric acid under standard atmospheric conditions, it acts as the dominant nucleation species (Sipilä et al., 2010; Zhang et al., 2012). It functions as a crucial catalyst by reducing the energy barrier for the condensation of various molecules, including water vapour and ammonia, onto its surface. This phenomenon results in the formation of stable clusters that have the potential to grow into larger aerosol particles. However, H_2SO_4 alone fails to explain the observed particle growth (Riccobono et al., 2012; Riipinen et al., 2012). The sulfuric acid concentration in the gas phase is too low ($<5\times10^7$ molecules cm^{-3}) to allow stable clusters to grow to observable sizes larger than 2.5 nm before undergoing coagulation with existing particles (Kulmala et al., 2000). Such concentrations of sulfuric acid are not sufficient to explain the observed particle growth rates in the atmosphere. This indicates the potential role of other condensable vapors such as NH_3, amines and low-volatility organic gases. The concentration of low-volatility organics and semi-volatile organics is ~2–20 times higher than H_2SO_4 over continental regions (Yu, 2011). Nonetheless, these species, which are more plentiful in the gas phase compared to sulfuric acid, will play a major role in the growth of newly formed particles. In certain geographical areas, the process of organic condensation is responsible for a significant portion of the overall rate of aerosol growth (Kuang et al., 2009; Riipinen et al., 2011). The process of coagulation growth of nucleated particles can also take place when small nuclei of similar size interact with each other. However, it is important to note that the rate of coagulation growth is significantly slower compared to condensation growth and is often disregarded (Dal Maso et al., 2002; Stolzenburg et al., 2005).

1.2.1 Aerosol nucleation mechanisms

Several mechanisms have been proposed to explain observed NPF events in the atmosphere (Ball et al., 1999; Benson et al., 2009; Cai et al., 2023; Curtius, 2006; Dawson et al., 2012; Duplissy et al., 2016; Herb et al., 2011; Jimenez et al., 2009; Jokinen et al., 2018; Kanawade and Tripathi, 2006; Korhonen et al., 1999; Kulmala et al., 2002; Lehtipalo et al., 2016; Lehtipalo et al., 2018; Lovejoy et al., 2004; Metzger et al., 2010; Nilsson and Kulmala, 1998; Schobesberger et al., 2013; Sihto et al., 2006; Sipilä et al., 2010; Tröstl et al., 2016a; Vehkamäki et al., 2002; Yu, 2006a, b; Yu and Turco, 2000; Zhang et al., 2010). A high saturation vapour pressure of a substance means it is volatile, i.e., molecules will easily escape from its surface and do not stick back easily on the

surface so for creating a molecular cluster, we need a vapour with the lowest saturated vapour pressure. Sulfuric acid has the lowest saturated vapour pressure compared to water and other substances and therefore nucleation usually starts with sulfuric acid, which can also cluster with other vapours such as ammonia, amines and volatile organic compounds to create new particles in the atmosphere.

Ambient observations (Erupe et al., 2010; McMurry et al., 2005; Sebastian et al., 2021a) and laboratory experimental (Benson et al., 2009) demonstrated that aerosol nucleation initiates with sulfuric acid. binary homogeneous nucleation (BHN) involves the aggregation of two same or different gaseous molecules such as BHN of H_2SO_4-H_2O system (Hanson and Lovejoy, 2006; Noppel et al., 2001; Vehkamäki et al., 2002) or sulfuric acid clustering with organics (Kürten et al., 2014; Schobesberger et al., 2013; Zhang et al., 2004). Binary nucleation involving the combination of sulfuric acid and dimethylamine (DMA) has also been widely acknowledged as a dominant process in the polluted continental boundary layers (Cai et al., 2023; Erupe et al., 2011; Silva et al., 2008).

Ternary homogenous nucleation (THN) involves three gaseous molecules such as H_2SO_4-H_2O-NH_3 wherein a base molecule stabilizes and enhances the growth of the newly formed particle (Benson et al., 2009; Korhonen et al., 1999; Kulmala et al., 2002; Napari et al., 2002; Yu, 2006b). THN of H_2SO_4-H_2O-NH_3 is thought to be important mainly in the boundary layer but THN is hampered by insufficient laboratory data (Merikanto et al., 2007) and does not work in all locations worldwide. Ammonia has the ability to lower the partial pressure of sulfuric acid, thereby stabilizing the critical embryo (Scott and Cattell, 1979). Kurtén et al. (2008) demonstrated that amines might have a more notable impact than ammonia in the formation of neutral and ion-induced nucleation involving sulfuric acid-water clusters in the Earth's atmosphere, even though such occurrences are infrequently observed in the atmosphere. Amines such as dimethylamine results in particle formation rates that can provide a plausible explanation for the observations made in the atmosphere across a wide range of sulfuric acid concentrations(Almeida et al., 2013; Glasoe et al., 2015; Kurtén et al., 2008). The THN of H_2SO_4-H_2O-organic acids is another mechanism but tested for only selected organics such as isoprene, monoterpenes and formic acid (Zhang et al., 2004) which is a poorly understood mechanism. Ion-induced nucleation involves the formation of

nanoparticles from gaseous molecules by the condensation of vapours onto positive or negative ions (Eichkorn et al., 2002; Lee et al., 2003; Yu and Turco, 2000). These ions are typically in the form in the atmosphere from of cosmic rays or ionizing radiation from radioactive decay. Ion-induced nucleation begins with the ionization of molecules in the atmosphere by high-energy particles, such as cosmic rays. These ions initiate the condensation of neutral molecules, like sulfuric acid and water vapour, around them. Ions provide an attractive surface for the attachment of these molecules, enabling the formation of stable clusters. It has been proposed that the process of NPF through ion-induced nucleation can take place in certain favourable atmospheric conditions such as These conditions include low temperature, high relative humidity, high rate of ion production, and low concentrations of preexisting particles (Laakso et al., 2002). Upper tropospheric and lower stratospheric regions with high ion-production rates from galactic cosmic rays, low temperatures, and small surface areas of pre-existing aerosols contribute to the prevalence of the ion-induced nucleation process as the primary mechanism NPF (Lee et al., 2003; Lovejoy et al., 2004). Nucleation is also induced by iodine species in marine environments where the presence of enhanced biological emissions during low tides and ocean upwelling or sea-ice melting conditions plays a role (Finkenzeller et al., 2023; O'Dowd and Hoffmann, 2005; O'Dowd et al., 2002).

1.2.2 Identification of new particle formation events

The measurement of particle number size distributions has critical importance in characterizing the number, size, surface area, volume, and evolution of atmospheric aerosols. Direct measurements of particle number size distribution starting from a size of a few nanometers to 1 μm are essential to study NPF. Particle number size distributions are modulated by the dynamic properties of aerosols (Seinfeld and Pandis, 2016). Detection of NPF events involves monitoring the temporal changes in particle number size distribution. It can be observed as the emergence of new aerosol particles in the lower spectrum of the measured particle number size distribution. The newly formed particles below 25 nm in diameter grows rapidly into sizes that can be measured using aerosol measurement instruments such as nCNC, SMPS, WRAS and NAIS (Grimm and Eatough, 2009; Vanhanen et al., 2011; Wiedensohler et al., 2012). These particles continue to grow within the measurement range of the instruments due to the condensation of vapours. Over several hours, the particle number concentration gradually decreases as a result of coagulation and mixing with

other air masses. The occurrences of particle formation and subsequent growth can be represented as 'banana' curves in the temporal evolution of particle number size distribution. These curves manifest as two-dimensional contour plots depicting the relationship among particle number concentration, time, and particle diameter (Figure 1.4). There are also algorithms developed to identify the 'banana' curves and NPF events from the particle number size distributions (Heintzenberg et al., 2007).

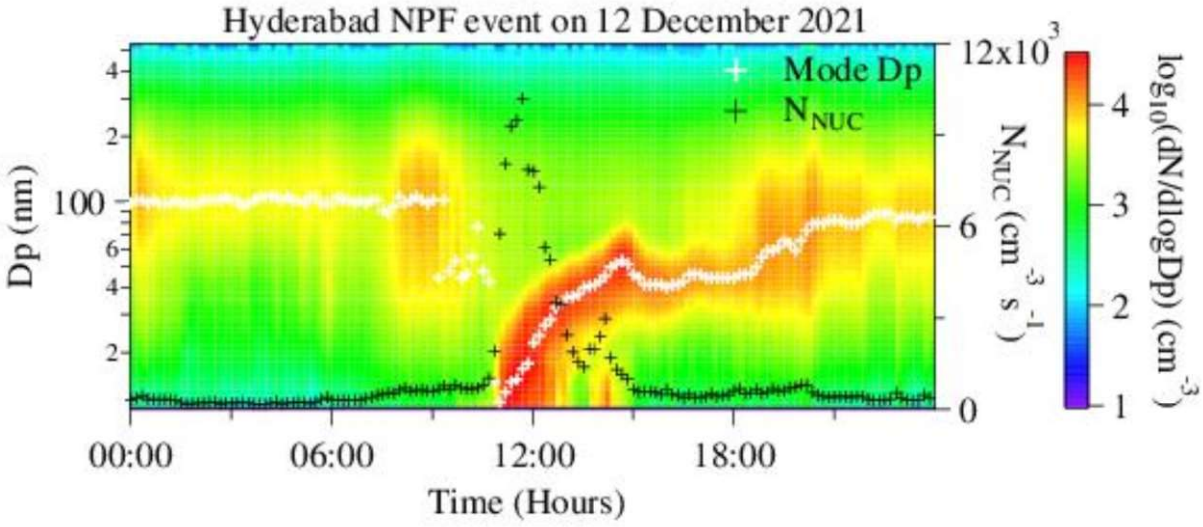

Figure 1.4 Diurnal evolution of the particle number size distributions during NPF event exhibiting the 'banana' curve at Hyderabad. The white '+' sign denotes mode diameter and the black '+' denotes nucleation mode particle number concentration.

1.3 Literature survey

1.3.1 Current understanding of new particle formation in India

NPF was first reported by Aitken (1897) and it has been widely investigated topic in the field of aerosol science (Curtius, 2006; Kanawade et al., 2021; Kulmala and Kerminen, 2008; Kulmala et al., 2016; Kulmala et al., 2014; Kulmala et al., 2012b; Kulmala et al., 2004; Nieminen et al., 2018; Wang et al., 2017). Figure 1.5 shows the locations of various measurement sites from different environments across the globe, but not all locations from where NPF has been reported globally. NPF events have been widely reported from diverse geographical environments globally such as urban (Almeida et al., 2006; Dunn et al., 2004; Hussein et al., 2004; Kanawade et al., 2022; Sebastian et al., 2021a; Stolzenburg et al., 2005; Wu et al., 2008; Yu et al., 2016), semi-urban (Babu et al., 2016; He et al., 2021; Kanawade et al., 2012; O'Dowd and Hoffmann, 2005; Olin et

al., 2022; Peltola et al., 2022; Pikridas et al., 2012; Shen et al., 2016a; Wang et al., 2013; Yu et al., 2014), coastal and marine (Babu et al., 2016; Clarke et al., 1998; He et al., 2021; Jokinen et al., 2018; Kompalli et al., 2020; O'Dowd and Hoffmann, 2005; O'Dowd et al., 2002; Olin et al., 2022; Peltola et al., 2022; Pikridas et al., 2012; Shen et al., 2016a; Yu et al., 2014), rural-background (Hakala et al., 2019; Jeong et al., 2010; Kammer et al., 2018; Kanawade et al., 2014a; Shen et al., 2016b; Wang et al., 2013), mountainous and high-altitude (Boulon et al., 2010; Casquero-Vera et al., 2020; Creamean et al., 2011; Foucart et al., 2018; Hallar et al., 2011; Rose et al., 2015; Sellegri et al., 2019), forest (Andreae et al., 2022; Jung et al., 2013; Junninen et al., 2022; Kanawade et al., 2011; Lee et al., 2016; Mäkelä et al., 2001; Ristovski et al., 2010; Zhao et al., 2022), ice caps and polar regions (Bianchi et al., 2021; Dall´Osto et al., 2017; Venzac et al., 2008), middle and upper troposphere (Kanawade and Tripathi, 2006; Liu et al., 2023), and also in cloud outflows (Clarke et al., 1998; Kim et al., 2013).

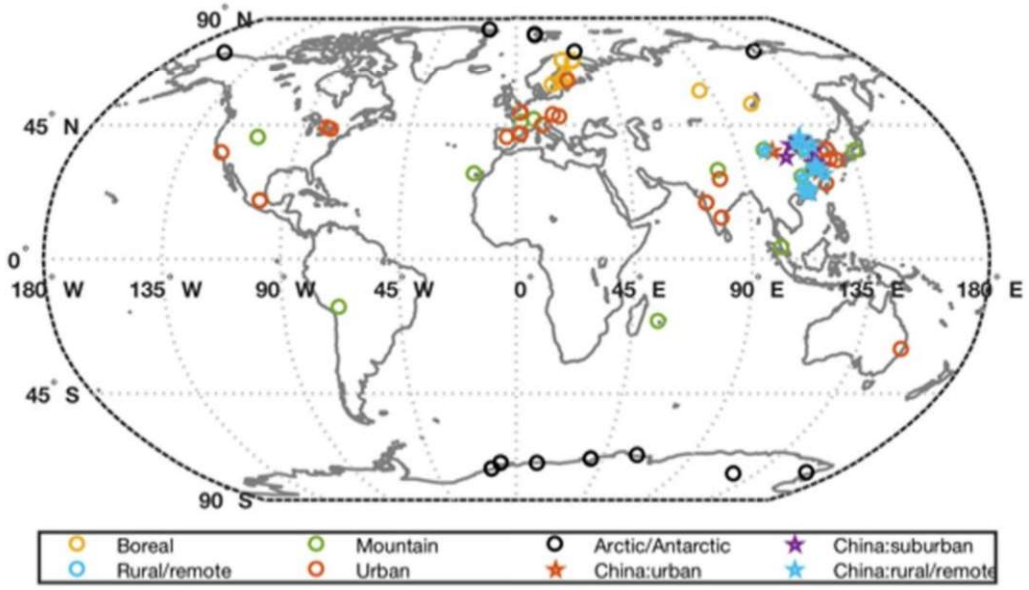

Figure 1.5 Geographical locations of measurement sites in diverse environments. This includes 183 sites that have been reported in the scientific literature (Kerminen et al., 2018).

Overall, NPF has been poorly studied in then Indian context. Table 1.1 presents a comprehensive overview of the locations from where NPF has been reported in India and summarises NPF characteristics in those locations. NPF was reported as a part of independent field campaigns during different seasons of the year as well as using longterm continuous measurements. Hence, the comparison of NPF frequency and its characteristics between sites even with similar

environments is not viable. Because the meteorological conditions and air mass history strongly affect the occurrence of NPF (Kanawade et al., 2012; Stanier et al., 2004b). The comparison is only possible between similar environments and seasons, if they exist. (Bousiotis et al., 2021) showed that the occurrence of NPF is influenced to a greater extent by meteorological conditions in rural areas when compared to urban areas. Further, diverse technologies and configurations were used to measure particle number size distributions, and therefore the characteristics of NPF.

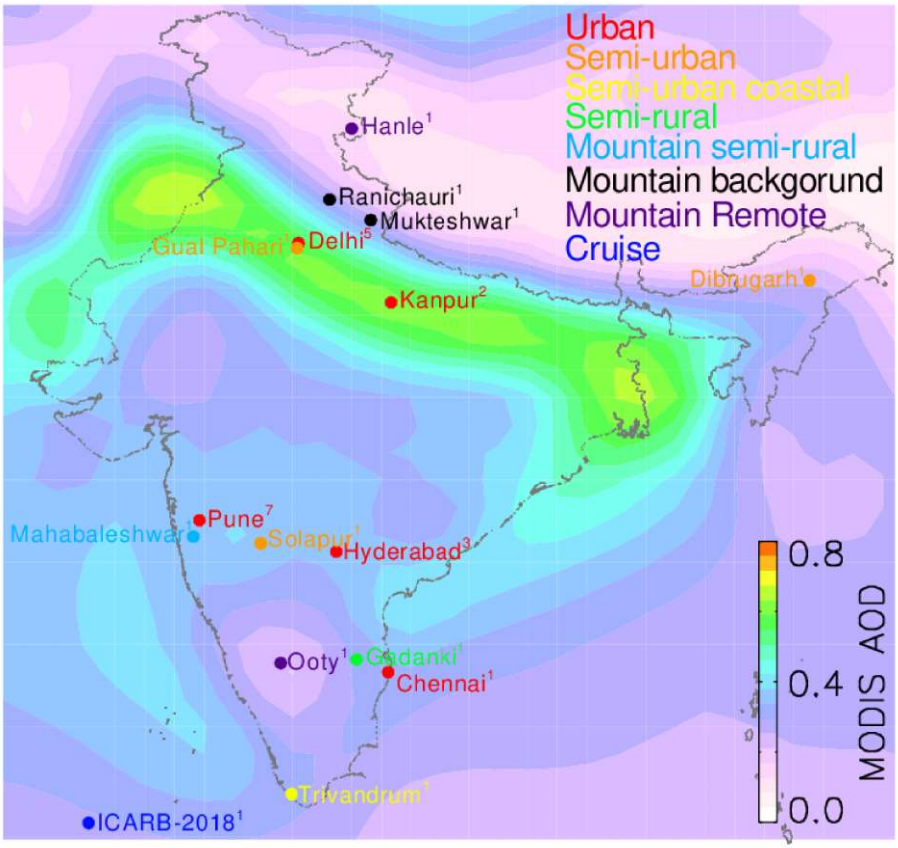

Figure 1.6. Geographic distribution of sites where observations of new particle formation were reported in India. The superscript number indicates the number of studies reported at the specific site. Different colors indicate the various atmospheric environments such as urban (Delhi, Kanpur, Pune, and Hyderabad), semi-urban (Dibrugarh, Gual Pahari, Solapur), semi-urban-coastal (Trivandrum), semi-rural (Gadanki), mountain semi-rural (Mahabaleshwar), mountain background (Ranichauri and Mukteshwar), mountain remote (Ooty and Hanle), and cruise (North Indian Ocean). The filled contours indicate the climatological mean aerosol optical depth from the MODIS AQUA sensor (Remer et al., 2008), highlighting the nature of the site.

To date, NPF events have been reported from 15 continental measurement sites (28 articles) in India (Figure 1.6). NPF events have been documented in various environments across India,

encompassing urban locations such as Delhi, Kanpur, Hyderabad, and Pune (Chate and Devara, 2005; Kamra et al., 2015; Kanawade et al., 2022; Kanawade et al., 2020b; Kanawade et al., 2014c; Mönkkönen et al., 2005; Nepolian et al., 2021; Sarangi et al., 2015; Sebastian et al., 2021a; Sebastian et al., 2022; Siingh et al., 2018; Siingh et al., 2013; Yadav et al., 2021), semi-urban such as Dibrugarh, Gual Pahari and Solapur (Das et al., 2023; Hyvärinen et al., 2010; Varghese et al., 2020), semi-urban coastal, Thiruvananthapuram (Babu et al., 2016; Kompalli et al., 2014; Sebastian et al., 2022), semi-rural, Gadanki (Kanawade et al., 2014a), mountain semi-rural, Mahabaleshwar (Leena et al., 2017; Sebastian et al., 2022), mountain backgrounds such as Ranichauri and Mukteshwar (Neitola et al., 2011; Sebastian et al., 2021b; Sebastian et al., 2022), mountain remote such as Hanle and Ooty (Kompalli et al., 2018; Moorthy et al., 2011), and ocean cruise in the North Indian Ocean (Kompalli et al., 2020). Out of these studies, only four studies used one year or more continuous observations of particle/ion number size distributions to examine NPF characteristics such as the mountain background sites in Western Himalaya, Mukteshwar (2180 m amsl) (Neitola et al., 2011) and Ranichauri (1930 m amsl) (Sebastian et al., 2021b), semi-urban, Gual Pahari (Hyvärinen et al., 2010), and a tropical urban site, Pune (Siingh et al., 2018). NPF was infrequently observed at Ranichauri, accounting for only 8.4% of the total days of observation, with the highest occurrence frequency of NPF during the spring season (Sebastian et al., 2021b). Mukteshwar also showed the highest NPF event occurrence during spring/pre-monsoon (Neitola et al., 2011). The observed highest frequency of NPF during the spring season was linked to the evolution of the planetary boundary layer (PBL) above the altitude of the measurement site, which facilitated the transport of nearby low-altitude pollution reaching up to the measuremtn site. Concuurently, the frequency of ccurence of NPF events in Pune was also highest in pre-monsoon/spring season Overall, there findings are analogous compared to those observed in rural to urban areas across the globe (Kanawade et al., 2012; Kerminen et al., 2018; Kulmala et al., 2004; Sellegri et al., 2019; Shen et al., 2011; Stanier et al., 2004a).

The frequency of occurrence of NPF events exhibited significant variation across the locations in India (Table 1.1). During spring/pre-monsoon and winter seasons, the NPF frequency ranged from 14% to 82% and 8.4% to 70% in India. The large variability could be attributed to non-uniform and the absence of long-term measurements. Hence, the long-term continuous simultaneous measurements of particle number size distributions in diverse geographical locations are essential

for ascertaining the seasonal variation in the frequency of NPF and its characteristics which are currently lacking in India. Quantification of NPF has critical importance to air quality and climate. For instance, Kanawade et al. (2022) showed that the frequency of occurrence of NPF was three-fold lower during the COVID-19 enforced lockdown (April-May, 2020) as compared to the business-as-usual time period (April-May, 2019) due to low precursor vapour concentration under reduced anthropogenic activities, while NPF was inhibited during severe air pollution episode in November 2016 in New Delhi due to large pre-existing particles (Kanawade et al., 2020a). This indicates that the balance between aerosol precursor and pre-existing particles decides when NPF would trigger in the urban atmosphere. However, they found that aerosol growth rates were exceptionally very high (30 nm h^{-1}). Gunthe et al. (2021) showed that the excessive ammonia in Delhi triggers the partitioning of hydrochloric acid into aerosol water and thereby enhances aerosol water uptake through co-condensation, leading to haze and fog formation. The primary organic vapours from biomass burning are also found to intensify nocturnal nanoparticle growth in Delhi in winter under favourable atmospheric conditions (Mishra et al., 2023).

Globally, studies show that urban areas are becoming a hotspot of NPF despite the notion that NPF is inhibited under high pre-existing particles in heavily polluted atmospheres (Kulmala et al., 2017; Yu et al., 2017). For instance, the mean condensation sink during NPF events in Kanpur (Kanawade et al., 2014c), Hyderabad (Sebastian et al., 2021a), Pune (Murugavel and Chate, 2009) and Delhi (Mönkkönen et al., 2005) were approximately 2-10 times higher than that observed in mountain background (Neitola et al., 2011; Sebastian et al., 2021b) and semi-rural locations (Kanawade et al., 2014a). Interestingly, these values are lower by an order of magnitude compared to values reported in Chinese megacities such as Beijing and Shanghai, which reached as high as 0.1 s^{-1} (Xiao et al., 2015). Until now, only three studies have established an association between NPF and precursor gaseous concentrations in India (Kanawade et al., 2014a; Kanawade et al., 2014c; Sebastian et al., 2021a), highlighting the role of SO_2 or sulfuric acid in NPF. The particle growth rates due to sulfuric acid alone accounted only for 5-65% of the total observed growth rates in Hyderabad (Sebastian et al., 2021a), implying the possible involvement of other condensable vapours, such as volatile organic compounds or ammonia or amines, in particle growth(Sebastian et al., 2021a). However, NPF events were seldom observed under lower precursor gaseous

concentrations, such as SO2 in the semi-rural environment of Gadanki (Kanawade et al., 2014a). This further supports the potential involvement of sulfuric acid in the initial phases of NPF events.

Table 1.1 Summary of measurement sites (name and type), measurement parameters (time, instrument, and size range) and key NPF characteristics [NPF frequency, formation rate (J_{NUC}), growth rate (GR) and condensation sink (CS)] in diverse environments of India.

Site Name	Site Type	Measurement periods	Instrument	Size range	NPF freq. (% days)	J_{NUC} (cm^{-3} s^{-1})	GR (nm h^{-1})	CS (10^{-3} s^{-1})	Reference
Delhi	Urban	Oct–Nov 2002	DMPS	3–800 nm	57.1	J_3, 7.3±3.9	14.9±1.8	57.5±8.8[a]	(Mönkkönen et al., 2005)
		Nov–Dec 2011	SMPS	9-425 nm	ND	ND	3.9	ND	(Sarangi et al., 2015)
		Nov 2011–Jan 2013	SMPS	5.14-1000 nm	28.1	J_5, 0.13	3.8[h]	20.8[a]	(Sebastian et al., 2022)
Pune	Urban	Dec 1997	EEA	13-750 nm	ND	J_{13}, 2.3	0.3-1.0[b]	60.0	(Chate and Devara, 2005)
		Nov–Dec 2005	SMPS	20–600 nm	ND	ND	17.0±1.9	71±4	(Murugavel and Chate, 2009)
		Apr–May 2010	NAIS	0.46–50 nm	36.2	ND	7.8±1.7[c]	ND	(Siingh et al., 2013)
		Apr–May 2012	SMPS	4–750 nm	26.6	J_5, 7.2±3.3	6.5±1.2	16.2±7.1	(Kanawade et al., 2014c)
		Mar–May 2012	NAIS+SMPS	3.85–47.8 nm	14	J_5, 6.8±3.4	7.4±1.4[c]	6.6±1.5	(Kamra et al., 2015)
		Mar 2010–Dec 2012	NAIS	0.36–47.1 nm	74.3	ND	3.2 -11.6[c]	ND	(Siingh et al., 2018)
Kanpur	Urban	Apr–May 2013	SMPS	13.8–685 nm	14	J_5, 1.5±1.0	8.7±3.2	33.3±8.7	(Kanawade et al., 2014c)
		Mar–Apr 2013	SMPS	4.45–736.5 nm	82	ND	3.2-6.7	ND	(Kanawade et al., 2020b)
Hyderabad	Urban	Apr–Jun 2019	nCNC SMPS	1–3 nm 10–514 nm	26.7	$J_{1.4}$, 30.7±73.6 J_{10}, 2.3±5.1	2.2±1.7[d] 4.9±3.2[e]	17.0±16.5	(Sebastian et al., 2021a)
		Apr 2019–Mar 2020	SMPS	10–514 nm	16.3	J_{10},0.13	5.7[e]	10.9[a]	(Sebastian et al., 2022)
		March–May 2019	nCNC SMPS	1–3 nm 10–514 nm	47	$J_{1.5}$,36.8±56.9 J_{10}, 3.7±3.6	ND	ND	(Kanawade et al., 2022)
		March–May 2020			15	$J_{1.5}$, 24.3±19.2 J_{10}, 0.5±0.4	ND	ND	
Gual Pahari	Semi-urban	Dec 2007-Jan 2010	DMPS	4-850 nm	70	ND	ND	ND	(Hyvärinen et al., 2010)
Solapur	Semi-urban	Aug 2018–Jan 2019	SMPS	15–700 nm	19	J_{15}, 2.8±2.9	5.0±73.5[f]	16.4±6	(Varghese et al., 2020)
Dibrugrah	Semi-urban	Nov-Dec 2016	SMPS	10.2–333.8	6.5	–	17.17	7.2±2.9	(Das et al., 2023)
Trivandrum	Urban-coastal	May–Jun 2009	SMPS	10–875 nm	ND	ND	0.1-10[e]	6.0-10.0[a]	(Kompalli et al., 2014)
		Jan–Dec 2013	SMPS+APS	15 nm–15 µm	ND	ND	7.4±2.9[g]	10.0-30.0[a]	(Babu et al., 2016)
		Jan 2013–Jan 2014	SMPS	14.6–661.2nm	16.6	J_{16}, 0.01	1.0[k]	22.3[a]	(Sebastian et al., 2022)
Gadanki	Semi-rural	May–Jul 2012	WRAS	5 nm–32 µm	6.3	J_5, 1.2±2.3	4.1±2.0[h]	7.1±4.6	(Kanawade et al., 2014a)

Mahabaleshwar	Mountain semi-rural	Oct–Nov 2014	WRAS	5 nm–32 µm	8.4	J_5, 1.1±0.2	1.4±0.4[h]	15.4±2.6	(Leena et al., 2017)
		Mar 2015–Mar 2016	WRAS	5.14–1000 nm	5.9	J_5, 0.04	4.7[h]	9.4 [a]	(Sebastian et al., 2022)
Mukteshwar	Mountain background	Nov 2005–Jan 2010	DMPS	10–800 nm	11.2	J_{15}, 0.4	2.4[j]	7.4±4.3	(Neitola et al., 2011)
		Jan 2012–Dec 2013	DMPS	10.1–757 nm	2.9	J_{10}, 0.04	2.5[e]	9.3[a]	(Sebastian et al., 2022)
Ranichauri	Mountain background	Dec 2016–Sep 2018	DMPS	10–800 nm	3.6	J_{10}, 0.2±0.2	6.7±3.8[e]	8.6±5.8	(Sebastian et al., 2021b; Sebastian et al., 2022)
Hanle	Mountain remote	Aug 2010	SMPS	16–1364 nm	ND	ND	0.1-20.0[i]	ND	(Kompalli et al., 2014)
ICARB-2018	Cruise	Jan 2018–Feb 2018	SMPS	10–414 nm	ND	J_{10}, 1.9±0.9	14.4±13.1[e]	19.8±55.0	(Kompalli et al., 2020)

'ND' indicates no data

[a]CS prior to NPF event

Particle growth rates of [b]13-25nm, [c]negative ions (3.85-25nm), [d]Sub-3nm, [e]10-25nm, [f]15-30nm, [g]15-100nm, [h]5-25nm, [i]16-25nm,[j]10-800nm,[k]14-25nm

DMPS: Differential Mobility Particle Sizer; EEA: Electrical Aerosol Analyzer; SMPS: Scanning Mobility Particle Sizer; NAIS: Neutral Air-Ion Spectrometer; nCNC: nano Condensation Nucleus Counter; WRAS: Wide Range Aerosol Spectrometer; APS: Aerosol Particle Sizer

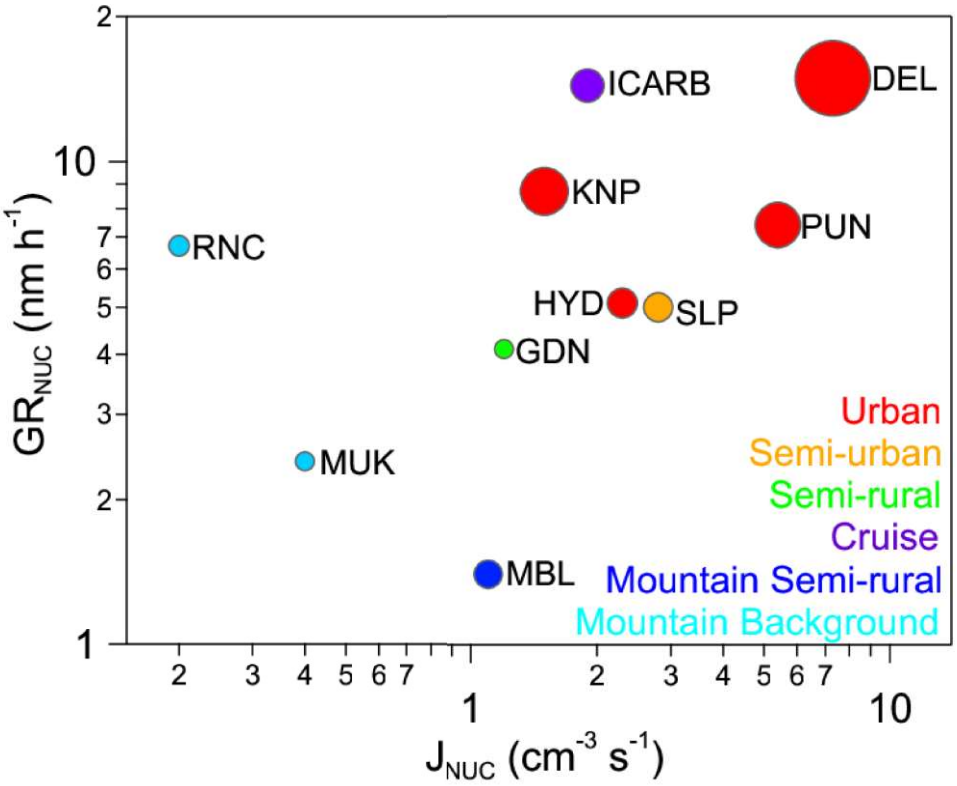

Figure 1.7. Association between site-specific particle formation rate and growth rate as a function of condensation sink. The marker colors indicate the type of the measurement sites, and the marker size is proportional to the condensation sink (the smallest and the biggest marker correspond to the condensation sink of 0.001 s^{-1} and 0.05 s^{-1}, respectively). RNC: Ranichauri, MUK: Mukteshwar, MBL: Mahabaleshwar, GDN: Gadanki, SLP: Solapur, HYD: Hyderabad KNP: Kanpur, PUN: Pune, DEL: Delhi, and ICARB: cruise in North Indian Ocean (Kanawade et al., 2021).

The particle formation rate and growth rate are two characteristic properties of NPF events. The particle formation rate and the particle growth rate together determine the strength of an individual NPF event. Considering 28 studies from diverse locations in India, the particle growth rate varied from 0.1 nm h^{-1} (Hanle) to 30 nm h^{-1} (Delhi). The particle formation rate determined for the lowest detectable size of the instruments employed in diverse locations (1.4, 3, 5, 10, and 15 nm) varied from 0.2 to 36.8 particles cm^{-3} s^{-1}. The documented rates of particle formation and growth align with the observed range at diverse locations globally (Nieminen et al., 2018). In general, we observed a positive association between the particle formation rate and growth rate (Figure 1.7). The observed association is expected which is influenced by the gas-phase production rates of low-volatility vapours (Xiao et al., 2021; Zhang et al., 2012). The first ambient observation of an NPF event was reported by Chate and Devara (2005) from Pune. Later, Mönkkönen et al. (2005) reported NPF and its characteristics based on two months of

particle number size distribution measurements from Delhi and illustrated that NPF events occur under high solar radiation and low condensation sink conditions Furthermore, charged and neutral particle number size distributions have also been measured using NAIS (diameter range of 0.8 to 42 nm) from India, but the formation rate of sub-2nm charged clusters has not been reported until recently (Kamra et al., 2015; Nepolian et al., 2021; Siingh et al., 2018; Siingh et al., 2013), while it has been widely reported from other parts of the world (Kulmala et al., 2012b; Manninen et al., 2010). The formation rate of neutral sub-3nm clusters was also recently reported from Hyderabad (Kanawade et al., 2022; Sebastian et al., 2021a), which provided the first-ever ambient observation-based evidence of sub-3nm particles. While the bursts of sub-3nm particles were observed frequently, only 50% of sub-3nm bursts were accompanied by the subsequent growth of particles into larger sizes with a distinctive 'banana' shaped aerosol growth, indicative of the regional NPF event. This suggests that newly formed particles in the sub-3nm size range do not always grow to large sizes detected by aerosol instruments with the lowest detectable size greater than 3 nm (SMPS or DMPS). (Sebastian et al., 2021a). There are currently only two studies investigating the fraction of newly formed particles growing to CCN-active sizes in India (Sebastian et al., 2021b; Sebastian et al., 2022). Overall, about half of the newly formed particles survived to grow to CCN-active sizes considering diverse locations in India. However, there were no simultaneous measurements of CCN concentrations during these studies to estimate uncertainties in the CCN production estimates from NPF events, except one study reporting high potential of NPF for CCN formation and thus cloud droplet formation under the influence of sulfur plume from the power plant during COVID-19 enforced lockdown (Singh et al., 2023). Therefore, the long-term continuous simultaneous measurements of particle number size distributions and CCN concentration are required to better understand the linkages between NPF events and CCN production.

1.3.2 Critical knowledge gaps and motivation

The complex interaction among atmospheric aerosols, climate, and air quality has received considerable scientific interest in recent decades. One of the fundamental elements of aerosol investigation revolves around the phenomenon of NPF. However, it is important to note that there exist notable gaps in knowledge pertaining specifically to India, despite significant advancements in aerosol science on a global scale. The presence of these gaps poses a challenge in achieving a thorough comprehension of NPF processes, the factors that drive them, and the resulting consequences for human health, air quality, and climate. The intricate interplay

between the country's emissions, meteorological conditions, and regional dynamics hinders the research on NPF in the absence of state-of-the-art techniques.

Long-term observations that encompass spatial and seasonal variability are imperative for quantifying the impacts of NPF events. The unavailability of highly spatially and temporally resolved measurements of aerosol number size distribution poses a challenge in identifying spatial and temporal patterns in the occurrence of NPF. In the Indian context, numerous researchers have carried out measurements of particle number size distributions over different time scales such as campaign mode and long-term observations (e.g., Hyvärinen et al., 2010; Kanawade et al., 2014b; Kompalli et al., 2018; Komppula et al., 2009; Laj et al., 2020; Shika et al., 2020; Tripathi et al., 1988; Tripathi et al., 2006), but most of these studies were not NPF focused. It is worth noting that the particle number size distributions provide insights into the evolution of aerosols in the atmosphere, and thus NPF processes, but it does not provide any insight into the chemical species responsible for cluster formation and subsequent growth. Therefore, the chemical composition of nucleated particles in the sub-3nm size range and subsequent growth is crucial to quantifying NPF events which are currently lacking.

of the recent technological advancements have facilitated the detection of gaseous precursors and nanoclusters in the atmosphere (Kulmala et al., 2014). The quadrupole and High-Resolution Time of Flight Mass Spectrometry (HR-ToF-MS) have been used as detectors, enabling the determination of mass-to-charge ratio values of approximately 2000. The chemical composition of atmospheric clusters/ions has been quantified using the Chemical Ionization – Atmospheric Pressure Ionization – Time of Flight mass spectrometer. (CI-APi-ToF, Jokinen et al., 2012). The cluster-chemical ionization mass spectrometer (CIMS) has also been designed to detect neutral molecular clusters in the atmosphere (Zhao et al., 2010). Additionally, it has been utilized for the identification of specific gaseous precursors like sulfuric acid (Zheng et al., 2011) as well as ammonia and amines (Hanson et al., 2011; You et al., 2014). Direct observations of the chemical composition of nucleation mode particles have been conducted using a thermal desorption chemical ionization mass spectrometer (Smith et al., 2005) as well as a nano aerosol mass spectrometer (Wang et al., 2006). The recent progress in aerosol instrumentation has enabled the direct detection of the chemical composition of sub-3nm particles (Kulmala et al., 2012b). None of these cutting-edge instruments are presently available in India to examine the chemistry driving NPF events in diverse locations, considering the spatial heterogeneity in aerosol and its precursor emissions, in India.

In the Indian context, previous studies predominantly focused on investigating the NPF characteristics and factors influencing NPF events. These factors include aerosol and meteorological characteristics (Hyvärinen et al., 2010; Kanawade et al., 2014c; Komppula et al., 2009), meteorological properties (Hyvärinen et al., 2010; Kanawade et al., 2014c; Komppula et al., 2009), solar radiation (Kanawade et al., 2014c; Moorthy et al., 2011), aerosol precursors such as SO_2 (Kanawade et al., 2014a; Mönkkönen et al., 2005; Sebastian et al., 2021a; Varghese et al., 2020), dynamics of the local coastal atmospheric boundary layer circulation (Babu et al., 2016) and the remaining studies examined NPF in a general context (Das et al., 2023; e.g., Kamra et al., 2015; Leena et al., 2017; Neitola et al., 2011; Siingh et al., 2018; Siingh et al., 2013). Kanawade et al. (2020b) used a high-resolution time-of-flight aerosol mass spectrometer (HR-ToF-AMS) to evaluate the chemical composition of sub-micron particles during observed NPF events in Kanpur. They observed that during NPF events, the growth of sub-micron particles was mostly supported by the condensation of low-volatility organic molecules. They also found that during NPF events, the sub-micron particles contained high signal intensities of organic molecules containing nitrogen.

In summary, there exist several knowledge gaps in NPF processes and feedback in India. The major knowledge gaps in NPF research in India include; i) chemical mechanisms driving NPF in diverse environments, ii) the fraction of newly formed particles that grow to CCN-active sizes, iii) the relative contributions of anthropogenic and biogenic VOCs to NPF, iv) the relative role of NPF to haze formation and v) uncertainties in aerosol-cloud interactions associated with NPF processes and therefore radiative forcing.

1.4 Objectives of the study

With this motivation, the following objectives are addressed in this thesis using the available research infrastructure;

1. Elucidation of sub-3nm particles and new particle formation events
2. Influence of airmass history and meteorological conditions on new particle formation
3. Contribution of new particle formation and growth to climate-relevant aerosols

1.5 Outline of the thesis

The thesis comprises a comprehensive set of seven chapters in all.

Chapter 1

The fundamental concepts related to atmospheric aerosols are introduced in the first chapter. First, atmospheric aerosols, their sources (primary emission and secondary formation), and their significance to air quality, weather and climate studies are briefly outlined. Next, the secondary formation of aerosols via gas-to-particle conversion referred to as aerosol nucleation or new particle formation (NPF) is discussed followed by condensation and coagulation processes. The chapter also provides a comprehensive and detailed literature survey, particularly in the Indian context identifying key knowledge gaps. The objectives of the thesis are developed from these knowledge gaps based on the existing observational infrastructure.

Chapter 2

This chapter provides a detailed overview of the instruments, data products, models and methodologies used in the thesis. Briefly, Particle number size distributions (PNSDs) were measured with the scanning mobility particle sizer (SMPS), differential mobility particle sizer (DMPS), nano condensation nucleus counter (nCNC), and wide range aerosol spectrometer (WRAS). We also used meteorological parameters such as temperature, relative humidity, solar radiation, wind speed and direction from an automatic weather station (AWS) to examine the meteorological influence on NPF. We used black carbon mass concentrations from the Aethalometer (AE-33) as a marker of anthropogenic plumes and trace gases such as oxides of nitrogen (NO_x), sulfur dioxide (SO_2), carbon monoxide (CO), ozone (O_3) and volatile organic compounds (benzene, toluene, xylene) data. SO_2 was also used to calculate sulfuric acid proxy concentrations ($[H_2SO_4]_{proxy}$). The chapter also outlines analysis procedures/methodologies adopted to address the proposed objectives.

Chapter 3

This chapter addresses the first objective of the thesis. Briefly, the chapter present the first direct observation-based evidence of sub-3 nm neutral aerosol particles, their format and growth rates and their association with sulfuric acid proxy concentrations (Sebastian et al., 2021a). This is the first-ever observation-based evidence of the role of H_2SO_4 in sub-3nm particles in India. Further, this chapter also characterizes new particle formation events based

on at least one year of asynchronous data of Prtile number size distribution data from six continental locations in India (Sebastian et al., 2022). We have further utilised the measurements conducted during the COVID-19 lockdown to detect and attribute the influence of anthropogenic emissions on NPF events (Kanawade et al., 2022). Lastly, the chapter also highlights the spatiotemporal variability in particle number size distributions in India.

Chapter 4

This chapter addresses the second objective of the thesis. Here, we have investigated the influence of airmass history on the occurrence of NPF based on 3 years of particle number size distribution data from Hyderabad. We performed the analysis of the ratio of condensation sink and growth rate and the HYSPLIT model calculated air mass back trajectories. Further, we have also calculated the spatial extent of NPF events at the site.

Chapter 5

This chapter addresses the third objective of the thesis. Briefly, we used two different methodologies to investigate the linkages between NPF events and CCN formation. The survival probability of 50 nm and 100 nm was calculated at a mountain background location, Ranichauri, in the Western Himalayas (Sebastian et al., 2021b). The further modified methodology given by (Kerminen et al., 2012) to remove the contribution of background CCN formation during an NPF event and used in six different locations in India to examine the contribution of newly formed particles to CCN production. (Sebastian et al., 2022).

Chapter 6

This chapter presents the major novel findings, particularly in the Indian context, from the thesis. This chapter outlines the future scope based on the findings reported in this thesis.

Chapter 2

Data and Methods

2.1 Measurement sites and instrumental setup

In this thesis, we have used ambient observations of particle size distributions from six different geographical environments in India, such as Hyderabad – urban, Ranichauri- mountain background, Mukteshwar-mountain background, Delhi - urban, Mahabaleshwar- mountain semi-rural, and Thiruvananthapuram – coastal urban, while our primary focus has been on measurements from the Hyderabad City. Figure 2.1 shows the geographical location of six measurement sites on a surface elevation map. The description of each measurement site along with the instrumental set-up are described below.

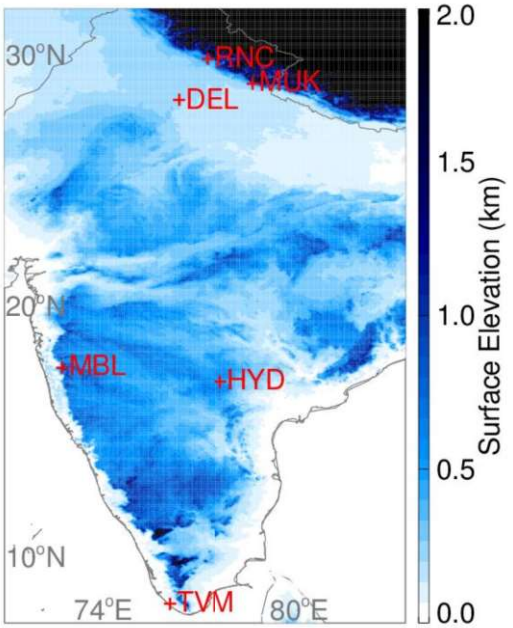

Figure 2.1. The geographical location of measurement sites on the surface elevation map. Measurement sites such as Ranichauri (RNC), Mukteshwar (MUK), Mahabaleshwar (MBL), Hyderabad (HYD), Thiruvananthapuram (TVM), and Delhi (DEL) are shown by the red plus sign. The global 1-arcsecond (30-m) SRTM digital surface elevation data is obtained from the United States Geological Survey (https://dds.cr.usgs.gov/srtm/version2_1/SRTM30/).

The measurement site of Hyderabad is located on the University of Hyderabad campus (HYD). The University of Hyderabad campus is located to the west of Hyderabad city centre (17.46 ^{o}N, 78.32 ^{o}E; ~542 m above mean sea level). HYD is the sixth most populous urban agglomeration in India, located on the Deccan Plateau in India. As per the Census of India (2011), the

population of the Hyderabad urban agglomeration is approximately 6.7 million. Particle number size distributions are measured at the Earth Sciences building, situated within the University of Hyderabad campus, encompassed by sparse forested vegetation spanning a distance of 1 km, except for a few academic structures. The nearest heavy traffic road, the old Hyderabad-Mumbai highway is located approximately 1 km to the east of the particle measurement site. Various air pollutants and meteorological parameters were measured at the Telangana State Pollution Control Board air quality monitoring station situated at the roof-top of the Main Administration building within the University of Hyderabad campus about 1 km to the east of the particle measurement site and 100 m from the Hyderabad-Mumbai highway. In the pre-monsoon season, which spans from March to May, Hyderabad experiences hot weather with temperatures frequently exceeding 30 ^{o}C and relative humidity of about 50% (Kaskaoutis et al., 2009). The summer monsoonal rain typically arrives in mid-June and provides sporadic rains during the season (June through September) with a total annual rainfall 803 mm (IMD, 2020). The annual mean mass concentration of particulate matter with diameters smaller than 2.5 μm ($PM_{2.5}$) is 51 ± 23 μg m^{-3} (Sreekanth et al., 2018).

The particle measurement site is equipped with two instruments for ambient aerosol measurements; AIRMODUS nano Condensation Nucleus Counter (nCNC) and the TSI Scanning Mobility Particle Sizer (SMPS). nCNC measures particle number size distributions in the size range from 1 - 3 nm and SMPS in the size range of 10 - 514 nm. The SMPS consisted of an electrostatic classifier (Model 3082) with a long-differential mobility analyzer (LDMA, Model 3081A) and a butanol condensation particle counter (CPC, Model 3772). The scanning cycle of the SMPS was 300 seconds, yielding a particle number size distribution every 5 minutes. nCNC consisted of an A10 particle size magnifier (PSM) and an A20 condensation particle counter (CPC). The scanning cycle of nCNC was 240 seconds, yielding a particle number size distribution every 4 minutes. More details of nCNC and SMPS are given in Sections 2.2.1 and 2.2.2, respectively. We have used continuous measurements from nCNC and SMPS over 44 months (April 2019 – December 2022) from Hyderabad to address different objectives of the thesis. Further, we have developed an ambient custom-built air inline aerosol flow system as the best practice for ambient aerosol measurements (Figure 2.2). Ambient air was brought to the air-conditioned room through an electrically grounded stainless-steel tube pipe with a length of 5 meters and an inner diameter of 4 inches at a fixed flow rate of 110 litres per minute (lpm) with an air blower (Make: Vents, Model: VSM 125). The stainless-steel pipe was covered with asbestos sheets to avoid condensation within the stainless-steel pipe inside

the air conditioning room. The outdoor inlet of the inline system is designed in an inverted 'U-shape' to avoid rainwater going inside the inline sampling system. The ambient air sample was then drawn to different instruments inside the air-conditioning laboratory with a sample tube length of less than 25 cm to avoid particle losses within the aerosol sampling tubes.

Figure 2.2. Aerosol Physics Laboratory at the Earth Sciences Building, University of Hyderabad, INDIA. (a) Inside view and (b) outside view.

Ranichauri is a village situated in the Tehri-Garhwal district of Uttarakhand state, located on the southern slope of the Western Himalayas. The location of measurement site (30.2°N, 78.25°E; ~2200 m amsl) is positioned on a solitary hilltop, situated on the premises of the College of Forestry in Ranichauri. The location is a Climate Monitoring station, which is overseen by the India Meteorological Department (IMD) as part of the Global Atmospheric Watch (GAW) initiative of the World Meteorological Organization (WMO). There are no major anthropogenic activities in the proximity of the measurement site, thereby qualifying it as a mountain background observatory. Ranichauri is geographically situated at a distance of approximately 70 km to the south of Rishikesh, 100 km to the southeast of Srinagar city, and 100 km to the west of Dehradun city. The region's topography exhibits heterogeneity in the distribution of forests, agricultural land, orchards, and human settlements of small size. The diurnal maximum temperature ranges from 9.4 to 27.2 degrees Celsius and the average precipitation is about 1274 mm annually (Upadhyay et al., 2015). The annual mean black carbon (BC) mass concentrations at Ranichauri measurement site is $1.4 \pm 1.1 \mu g\ m^{-3}$, indicative of the high altitude background site (Kumar et al., 2020). Ranichauri also experiences forest fires during the pre-monsoon (March through May) season with slightly elevated BC mass concentrations. Here, we have used 21 months (December 2016 – September 2018) of continuous particle number size distribution measurements to address one of the objectives of the thesis. At the Ranichauri site, sample air was drawn inside trough a stainless-steel inlet tube

of about 2 m length and dried to less than 40% relative humidity with a Nafion dryer. Measurements of particle number size distributions were obtained using a custom-build Differential Mobility Particle Sizer (DMPS). Details of the instrument are given in Section 2.2.3. Measurements of BC mass concentrations were conducted using the Aethalometer (model AE-33) (Magee Scientific, 2016) which was deployed as part of the IMD national network for BC monitoring (Kumar et al., 2020). The details of the instruments are described in Section 2.3.

Mukteshwar observation site (MUK, 29.43° N, 79.62° E, 2180 m amsl) is located in the Nainital district of Uttarakhand state on the southern slope of the Central Himalaya. The Mukteshwar village is situated 3 km to the northeast of the measurement site at a similar altitude with ~800 inhabitants (Census of India, 2011). MUK is a mountain background site, with an annual mean BC mass concentration of 0.9 μg m^{-3}. The town of Almora (1650 m amsl, 34,000 inhabitants) is located about 16 km to the north, Nainital (1960 m amsl, 41000 inhabitants) is located about 25 km to the southwest, and the city of Haldwani (424 m amsl, 150,000 inhabitants) is located at about 32 km to the southwest to MUK. Delhi, the major metropolitan city (215 m amsl, 16.8 million inhabitants), is located approximately 250 km to the southwest. The systematic measurements of aerosol properties have been conducted at MUK since 2005 in Indo-Finnish cooperation with the Finnish Meteorological Institute (Hooda et al., 2018 and references therein). Here, we have used two years (January 2012 to December 2013) of particle number size distribution measurements in the size range of 10 nm to 757 nm obtained using DMPS (details of the instrument are described in Section 2.2.3). The air sampling procedure was similar to that of the RNC observation site. More details of the site and aerosol sampling can be found in Hyvärinen et al. (2009).

Delhi observation site (DEL, 28.64° N, 77.17° E, 215 m amsl) is located at CSIR-National Physical Laboratory (NPL). Delhi, India's national capital and largest metropolitan city in South Asia, is located in the northwestern Indo-Gangetic Plain (IGP) in northern India. Delhi city has a population of 16.8 million, with a population density of 11,320 km^{-2} (Census of India, 2011). The Great Indian Desert (Thar Desert) is located to the southwest, with hot central plains to the south, and hilly regions to the north and east of Delhi. Long-range transported air masses often influence Delhi's air quality from the northwest anthropogenic sources (agricultural residue burning from Punjab and Haryana in October-November) and southwest natural sources (dust storms from Thar and Arabian Peninsula in April-June) (Kanawade et al., 2020a; Srivastava et

al., 2014). Here we have used particle number size distributions in the size range of 5.14 nm to 1000 nm from November 2011 to January 2013 from GRIMM Wide Range Aerosol Spectrometer (WRAS). More description of the instrument is given in Section 2.2.4. The WRAS system draws ambient air through a stainless-steel inlet tube with an integrated Nafion drier to dry the aerosol samples. A detailed description of the site and aerosol sampling is given elsewhere (Jose et al., 2021).

Mahabaleshwar observation site (MBL, 17.92° N, 73.65° E; 1378 m amsl) is located in the small town named Mahabaleshwar in the forested Western Ghats range in the Satara district of Maharashtra State. A High-Altitude Cloud Physics Laboratory (HACPL) was established by the Indian Institute of Tropical Meteorology (IITM), Pune, in 2012, to study monsoon clouds in this region. HACPL site details are found elsewhere (Anil Kumar et al., 2021). Mahabaleshwar town is a tourist attraction consisting of dense vegetation, residential houses, hotels, and a rural market. Pune city is located about 100 km to the north, Mumbai city is located approximately 250 km to the northwest, and Satara city is located approximately 50 km to the southeast of Mahabaleshwar. Measurements of particle number size distributions were carried out using the GRIMM-WRAS system. More description of the instrument is given in Section 2.2.4. Here, we used particle number size distributions in the size range of 5.14 nm to 1000 nm from March 2015 to March 2016.

Thiruvananthapuram (Trivandrum) observation site (TVM, 8.55° N, 76.97°E, 3 m amsl) is a tropical semi-urban coastal city with a population of ~1 million (Census of India, 2011), located on the southwestern coast of the Indian peninsular. The observations were carried out at the Space Physics Laboratory (SPL) within the Thumba Equatorial Rocket Launching Station, which is about 500 m to the east of the Arabian Sea coast and 10 km northwest of the urban area of Thiruvananthapuram. The experimental site is free from major industrial or urban activities (Babu et al., 2016). TVM site is a part of the Aerosol Radiative Forcing over India (ARFI) project network of the Indian Space Research Organisation - Geosphere-Biosphere Program (ISRO-GBP). Measurements of particle number size distributions in size range from 14.6 nm to 661.2 nm were made using TSI SMPS, which consists of an electrostatic classifier with an LDMA (3081) and a water-based CPC (3786) from January 2013 to January 2014. The ambient air was sampled from a height of 3 m above the ground level through a manifold inlet fitted with a PM_{10} size cut impactor at a 16.67 lpm flow rate. Subsequently, the flow was distributed among various aerosol instruments connected with electrically conductive tubing.

To restrict high relative humidity conditions, a diffusion dryer (Make: TSI, Model: 3062) employing silica gel was used. More details about the site and prevailing meteorology are described in Babu et al. (2016).

Table 2.1. Details of the measurement sites and particle number size distribution measurements considered.

Site Name	Site code	Site type	Instrument	Size range (nm)	Time resolution (minutes)	Time Period
Hyderabad	HYD	Urban	SMPS	10.9 – 514	5	04/2019 – 12/2022
			nCNC	1 - 3	5	04/2019 – 12/2022
Delhi	DEL	Urban	WRAS	5.14 – 1000	5	11/2011 – 01/2013
Thiruvananthapuram	TVM	Coastal Semi-urban	SMPS	14.6 – 661.2	5	01/2013 – 01/2014
Ranichauri	RNC	Mountain background	DMPS	10.1 – 757	10	12/2016 – 09/2018
Mukteshwar	MUK	Mountain background	DMPS	10.1 – 757	5	01/2012 – 12/2013
Mahabaleshwar	MBL	Mountain semi-rural	WRAS	5.14 – 1000	4	03/2015 – 03/2016
Delhi	DEL	Urban	WRAS	5.14 – 1000	5	11/2011 – 01/2013

2.2 Measurements of particle number size distributions

2.2.1 nano Condensation Nucleus Counter (nCNC)

nCNC was used to measure the sub-3nm particle number concentrations. The nCNC unit consisted of a A10 PSM (Particle Size Magnifier) and A20 butanol CPC (Condensation Particle Counter). Details of the A10 PSM are described by Vanhanen et al. (2011). Briefly, diethylene glycol (DEG) supersaturation, which defines the lowest detectable size, is created by turbulently mixing heated saturator air with cooler sample air in the mixing chamber. The cut-off size of the PSM then can be varied by changing the mixing ratio of the saturator and sample air. Thus, nCNC was operated in a continuous scanning mode with a saturator flow rate of 0.1 to 1.3 lpm with an upward ramp (0.1 to 1.3 lpm) automatically followed by a downward ramp (1.3 to 0.1 lpm) with a time step of 1 second, resulting in a cycle of 240 seconds. The measured total particle number concentration above a certain cut-off diameter as a function of the saturator flow rate was used to invert the particle number size distributions. Several inversion techniques have been proposed such as a step-wise method, the Gaussian-shaped kernel function method (Lehtipalo et al., 2014), the Hagen and Alofs (H&A) method (Hagen and Alofs, 1983) and the expectation-maximization (EM) algorithm (Maher and Laird, 1985). Lehtipalo et al. (2014) illustrated that the Gaussian-shaped kernel function method works well for ambient measurements. Chan et al. (2020) tested the feasibility of four inversion methods (stepwise, kernel, Hagen–Alofs, and expectation-maximization) was assessed to determine their effectiveness in inverting the particle number size distribution from the raw scanning particles

data obtained from the PSM. Chan et al., (2002) found that the expectation-maximization (EM) algorithm exhibits greater robustness and achieves the highest levels of accuracy and stability. Here, we used the Gaussian-shaped kernel function method and the expectation-maximization algorithms.

Previous studies showed that the relative humidity of the sample air and the chemical composition of the sampled particles affect the smallest detectable size of the particle counters operated with DEG (Kangasluoma et al., 2014). The nCNC system was equipped with a custom-built diffusion dryer to maintain a relative humidity of less than 40%. However, the detection efficiency may be affected by the thermal motion of ultrafine particles, resulting in their loss within the sampling line (Vanhanen et al., 2011). Particle losses in the diffusion dryer were quantified by performing consecutive ambient air measurements with and without the diffusion dryer. Our experiments showed that about 10% of the total particles are lost in the diffusion dryer (Figure 2.3).

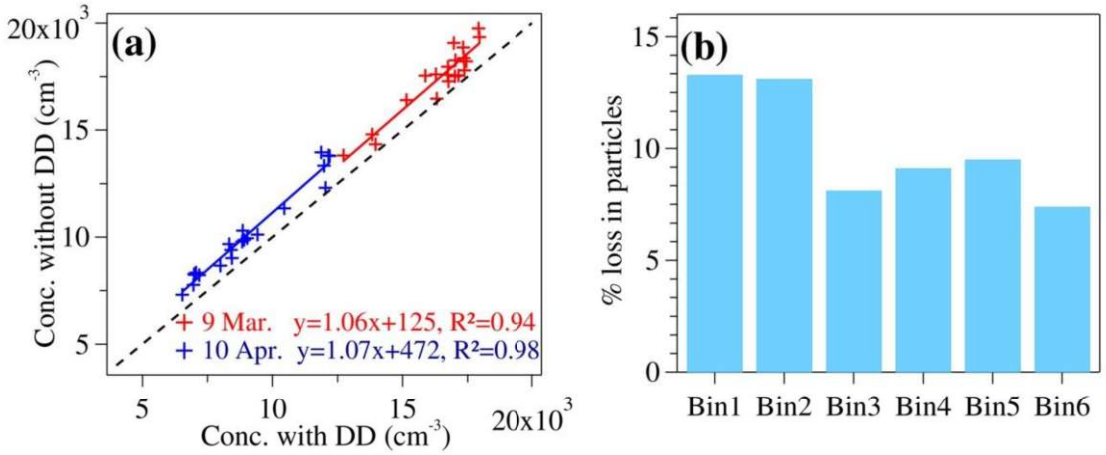

Figure 2.3 (a) Scatter plot of sub-3nm number concentrations ($N_{sub\text{-}3nm}$) with and without the diffusion dryer (DD). (b) Size-dependent percentage loss in particles in the diffusion dryer. Bin1, Bin2, Bin3, Bin4, Bin5 and Bin6 indicate six size bins; 1.2-1.4, 1.4-1.6, 1.6-1.8, 1.8-2.0, 2.0-2.2 and 2.2-3.0 nm, respectively.

2.2.2 Scanning Mobility Particle Sizer (SMPS)

The SMPS measures aerosol number size distribution in the wide size range (1 nm to 10's of µm) depending upon the combination of detection and counting techniques. The system consists of three units; an electrostatic classifier, DMA and CPC. The electrostatic classifier classifies charged particles according to their mobility in an electric field using a DMA. The electrical mobility of the particles is proportional to the number of charges on the particles and inversely proportional to the particle size. The particles entering the classifier are neutralized

using a radioactive source giving the particles a Fuchs equilibrium charge distribution. The charged particles then pass through the DMA where they are subjected to an electric field. This field exerts an electrical force on the particles, causing them to move through the gas in which they are suspended. The electric field strength and the particle's charge-to-mass ratio determine the electrical mobility of a charged particle. The trajectory of charged particles in a DMA is influenced by an electric field. The DMA consists of an inner cylinder connected to a power supply (10 to 10,000 VDC) with either a negative or positive charge and an outer grounded cylinder. This creates an axially homogeneous electric field inside the DMA. Negatively charged particles are repelled towards and deposited on the outer wall, while neutral particles exit with the excess air. Positively charged particles move towards the negatively charged element. Only particles with specific electrical mobility can pass through an open slit near the DMA exit. By adjusting the DMA voltage, the electrical mobility and corresponding particle size can be selected. When the inner cylinder is connected to a positive power supply, negatively charged particles are selected instead of positively charged particles. Upon exiting the DMA, electrically charged particles are categorized based on their electrical mobility. The particles exiting out of the DMA are then transferred to a CPC where the particles are counted. Particles are subjected to growth within a CPC through the process of vaporization of a working fluid (typically butanol, isopropyl alcohol, or water). When the gaseous phase surrounding the particles attains a particular level of supersaturation, the vapour initiates the process of condensation onto the particles. The quantification of supersaturation magnitude directly influences the lower limit of particle detection for the CPC. Once condensational growth is attained, CPC functions similarly to optical particle counters where particles are directed through the focal point of a laser beam, causing the beam to scatter which will then be detected by sensors.

2.2.3 Differential Mobility Particle Sizer (DMPS)

The DMPS works on a similar principle as an SMPS. DMPS was used at Ranichauri and Mukteshwar sites to obtain the particle number size distribution in the size range of 10 nm to 800 nm in 30 size bins. The DMPS consisted of a Vienna-type Differential Mobility Analyser (DMA) that classifies the charged particles according to their electrical mobility and a TSI 3772 CPC that counts particles of the selected mobility. The instrument provides a full scan of particle number size distribution every 10 minutes. The DMPS operated with an inlet flow rate of 1 lpm and a sheath air flow rate of 5 lpm. Diffusional losses in the inlet and inside the DMPS

instrument were considered in the data inversion. The inversion method was identical to that presented by Wiedensohler et al. (2012), for the Finnish Meteorological Institute (FMI) DMPS.

2.2.4 Wide Range Aerosol Spectrometer (WRAS)

The WRAS system provides the particle number size distribution in a size range spanning from 5.5 nm to 32 μm, in 72 size bins. The WRAS system is comprised of an SMPS equipped with a CPC (SMPS+C; CPC model 5.400) and a light scattering optical particle counter (OPC; GRIMM EDM 180). The SMPS+C, which includes a DMA, is utilized to assess the distribution of particle sizes within the electrical mobility size range of 5 to 350 nm. This is achieved by incrementally adjusting the DMA voltage, allowing for measurement in 45 distinct channels. By incrementally adjusting the DMA voltage, it is possible to achieve a particle number size distribution within the range of 5.5 nm to 350 nm, as measured by electric mobility diameters. The GRIMM OPC operates by utilizing the principle of light scattering to analyze individual particles. The light that has been dispersed in various directions is detected using a photodiode and the signals undergo amplification and are subsequently classified into 31 distinct size channels. The measurement involves determining the distribution of particle sizes (based on optical diameters) within the range of 250 nm to 32 μm. The two datasets obtained from SMPS+C and OPC are synchronized and merged using the GRIMM software. The sampling probe utilizes a Nafion dryer to control the relative humidity level to around 40%. The comprehensive elucidation and fundamental concept of the equipment are explained in Grimm and Eatough (2009).

2.3 Meteorological and trace gases measurements

Air pollutants and meteorological parameters measurements were made at the rooftop of the Main Administration building of the University of Hyderabad located within the campus. $PM_{2.5}$ mass concentrations were measured using the principle of β-ray attenuation. The measuring range spanned from 0 to 1000 μg m^{-3}, and the flow rate during the measurement was set at 16.7 lpm. SO_2 was measured utilizing the UV fluorescence methodology. CO was measured utilizing a non-dispersive infrared (NDIR) technique employing a gas-filter correlation method. NO_2 and NH_3 were measured using the Chemiluminescence technique O_3 was measured using a UV-photometric technique. VOCs such as Benzene, Xylene, and Toluene were measured using the gas chromatographic separation technique coupled with a photoionization detector. The wind speed and direction were measured using an ultrasonic-type sensor, which possesses a precision of 1.2 m s^{-1} and 1°, respectively. The air temperature was quantified utilizing a thermistor-based

sensor possessing a precision of ±0.2° C. The measurement of relative humidity was conducted utilizing a capacitive-type sensor, which possesses an accuracy of ±3%. Global solar radiation in the wavelength range of 0.3 - 4 μm was measured using a pyranometer of the silicon photodiode type.

We also used an AE-33 Aethalometer to measure BC mass concentrations from the Ranichauri site. Aethalometer measures light attenuation at 7 wavelengths. The BC mass concentrations are derived at a wavelength of 880 nm using a mass absorption cross-Section (MAC) value of 7.77 m^2 g^{-1} (Petzold et al., 2013) with the maximum absorption due to black carbon than other aerosols at this wavelength (Drinovec et al., 2015). More details of BC measurement and correction can be found in Drinovec et al. (2015).

2.4 HYSPLIT simulations and ERA5 reanalysis data

2.4.1 HYSPLIT trajectory model

Air mass source at different measurement sites was calculated using the NOAA ARL PC-version Hybrid Single-Particle Lagrangian Integrated Trajectory (HYSPLIT) model (Draxler and Rolph, 2010). We calculated the hourly three-day air mass backward trajectories starting at 500 m above the ground level at each site using gridded wind fields from the Global Data Assimilation System (GDAS), which has a spatial resolution of 1° × 1° longitude by latitude and a time resolution of 1 hour (Kanamitsu, 1989). Aerosols have a lifetime of about seven days in the lower troposphere, but NPF events have a temporal extent of 1-2 days and a spatial extent of a few hundred kilometres, this was the reason for choosing a three-day window for calculating air mass backward trajectory in this analysis in the context of NPF events.

2.4.2 ERA5

The ECMWF Re-Analysis 5 (ERA5) is the fifth-generation reanalysis product of the European Centre for Medium Range Weather Forecasts (ECMWF) which provides global climate and weather data since 1940 (Hersbach et al., 2023). Here, model results and observations from all over the world are combined to provide a complete and consistent global dataset. It uses the Integrated Forecasting System (IFS) Cy41r2 (Hersbach et al., 2020). For data assimilation, 4D-Var is used at 12-hour windows from 09 UTC to 21 UTC and 21 UTC to 09 UTC. Though ERA5 provides data from 1940 till 5 days behind real time, after rigorous quality checks, realistically, they provide the final release two to three months later. Here, we have used the ERA5 hourly data on pressure from the Climate Data Store (Hersbach et al., 2023).

Temperature and vertical velocity data were used from 2018 to 2021 and on pressure levels ranging from 1000 hPa to 500 hPa. The provided data was in a regular latitude-longitude grid with a horizontal resolution of 0.25° × 0.25°. Further, Lower Tropospheric Stability (LTS) was calculated by a simple linear equation showing the difference between the potential temperature at 700 hPa and the surface ($LTS = \Theta_{700} - \Theta_{surface}$). The potential temperature was calculated following the Poisson equation and ERA temperature data.

2.5 Satellite data

2.5.1 OMI

The Ozone Monitoring Instrument (OMI) instrument is a spectrometer installed on the NASA Aura satellite that operates in the ultraviolet-visible range of the electromagnetic spectrum (Levelt et al., 2018; Levelt et al., 2006). The offers significantly enhanced ground resolution, measuring 13 km × 24 km. The OMI NO_2 algorithm utilizes Level-1B calibrated radiance and irradiance data from the visible channel (350–500 nm with 0.63 nm spectral resolution) to derive measurements of NO_2 column amounts, including total, tropospheric, and stratospheric concentrations. The Level 2 (L-2) NO_2 product (OMI NO_2) comprises measurements of stratospheric, tropospheric, and total vertical column densities. The algorithm utilizes a series of steps to achieve its objectives. Initially, it uses a spectral fitting algorithm to compute NO_2 slant column densities. The slant column is a measurement that quantifies the total amount of a trace gas present along the average path of photons originating from the Sun, passing through the atmosphere, and reaching the satellite. The NO_2 slant column amounts are subsequently integrated with stratospheric and tropospheric air mass factors in order to calculate vertical column densities (Lamsal et al., 2021).

2.5.2 TROPOMI

The TROPOspheric Monitoring Instrument (TROPOMI), which is installed on the Sentinel-5 Precursor (S-5P) satellite launched in October 2017, operates in a low-Earth polar orbit and has a wide coverage area of 2600 km. This allows for daily monitoring of the entire globe (Veefkind et al., 2012). The TROPOMI instrument is composed of four spectrometers that span the shortwave-ultraviolet-visible-near infrared-infrared wavelengths. These spectrometers have a spectral resolution of 450 - 650 nm in the ultraviolet-visible range. The TROPOMI instrument possesses a notable nadir spatial resolution of 3.5 km × 7 km, which underwent an enhancement to 3.5 km × 5.5 km in August 2019. Additionally, it exhibits a commendable signal-to-noise ratio. The NO_2 retrieval algorithm is based on the DOMINO v2, which is a data product of the

Dutch OMI developed by the Royal Netherlands Meteorological Institute (KNMI) (Boersma et al., 2007). The retrieval algorithm for formaldehyde (HCHO) is based on the OMI QA4ECV product retrieval algorithm (De Smedt et al., 2018), utilizing the Differential Optical Absorption Spectroscopy (DOAS) method. The NO_2 product exhibits a strong correlation ($R \approx 0.68$) with measurements obtained from both aircraft and ground-based sources (Griffin et al., 2019). The average bias of the NO_2 product ranges from -15% to 30%. The correlation between the HCHO product and Multi-Axis DOAS (MAX-DOAS) measurements is strong ($R \approx 0.88$), as well as with Fourier-Transform InfraRed (FTIR) measurements ($R \approx 0.91$) (Vigouroux et al., 2020). The mean bias of the HCHO product ranges from -26% to 30.8%. Here, we used TROPOMI Level 2-pixel data that met the following criteria: (i) a quality assurance value exceeding 0.5, (ii) a solar zenith angle below 65^0, and (iii) a cloud fraction below 0.2. Additionally, we excluded NO_2 column concentrations less than 5.6×10^{14} molecules cm^{-2} and HCHO column concentrations less than 1.0×10^{15} molecules cm^{-2}, which represents the detection limit.

2.6 Data analysis techniques and procedures

2.6.1 Size-segregated particle number concentration

Atmospheric aerosols encompass a broad spectrum of sizes, ranging from sub-3nm particles to particles larger than 10 μm. The particle number size distribution is usually segregated into different modes based on the particle size, such as the cluster mode (consisting of particles with a diameter smaller than 3 nm), the nucleation mode (comprising particles with diameters ranging from 3 to 25 nm), the Aitken mode (encompassing particles with diameters ranging from 25 to 100 nm), the accumulation mode (comprised of particles with diameters ranging from 100 to 1000 nm) and the coarse mode (particles with diameter greater than 1000 nm). We have performed comprehensive analyses of particle number size distributions such as time evolution of particle number size distributions, size-segregated particle number concentrations, total mass, surface area and volume concentrations, and particle mode diameter (the particle diameter corresponding to the peak concentration of each particle number size distribution).

2.6.2 Classification of new particle formation events

In this thesis, the valid observation days were classified into three types of events: NPF event, non-event, and undefined/unidentified event using visual inspection of the particle number size distributions following the methodology given by Dal Maso et al. (2005). A day was classified as an NPF event day with the presence of a distinctly new mode of particles with a diameter smaller than 25 nm and steady growth in diameter of this new mode such that the particle

number size distributions display a noontime 'banana' shaped aerosol growth. A day without any evidence of a distinctly new mode of particle diameter smaller than 25 nm was identified as a non-event day. All the remaining, which were not possible to classify as any one of the above two event types, were categorised as undefined/unidentified event days. We modified the above classification methodology further to identify event subtypes for characterising NPF events in a particular location. Specifically, NPF events were classified by visually inspecting nCNC and SMPS measured particle number size distributions following Dal Maso et al. (2005) and Yu et al. (2016) methodologies and further modified to identify four types (e.g. in Hyderabad) as given in Table 2.2.

Table 2.2 Summary of criteria used for classifying event types based on nCNC and SMPS observations in Hyderabad. NPF&G indicates new particle formation and growth.

Event Type	**nCNC criteria**	**SMPS criteria**
Type-I (NPF&G)	Significant burst of sub-3 nm particles	Particle mode diameter smaller than 25 nm showed steady growth in size for at least 6 hours, thus particle number size distributions appeared as a 'banana' shape
Type-II (NPF)	Significant burst of sub-3 nm particles	Particle mode diameter did not show a steady 'banana' shaped aerosol growth
Type-III (non-event)	No significant increase in sub-3 nm particles	No distinct change in particle mode diameter during the day
Type-IV (unidentified)	Abrupt occurrence of sub-3 nm particles	Unable to identify whether it is one of the above events

The NPF&G events displayed bursts of sub-3nm particles and the particle mode diameter smaller than 25 nm showed steady growth in size for at least 6 hours, thus particle number size distributions displayed a 'banana' shaped aerosol-growth referred to as conventional NPF&G event. A typical NPF&G event is shown in Figure 2.4a. The days with bursts of sub-3nm particles, but the absence of steady growth in the particle mode diameter smaller than 25 nm were classified as an NPF event. A typical NPF event is shown in Figure 2.4b. Note that it was not possible to ascertain whether the sub-3nm particles grew up to 10 nm as the particle number size distribution between 4 nm and 10 nm was not possible to measure due to the unavailability of instruments covering this size range. The days with no or insignificant increase in sub-3nm particles and nucleation mode particle number concentrations (10 - 25 nm) are classified as non-event days. A typical non-event day is shown in Figure 2.4c. Those days that could not be

categorized into any of the above event days are referred to as unidentified events (Figure 2.4d). Days with only SMPS data that showed NPF&G or NPF event features were put into respective event types. Days with only nCNC data did not show significant particle bursts and were classified as non-event events. The rest of the days were not put into any of these types and were not considered in the analysis.

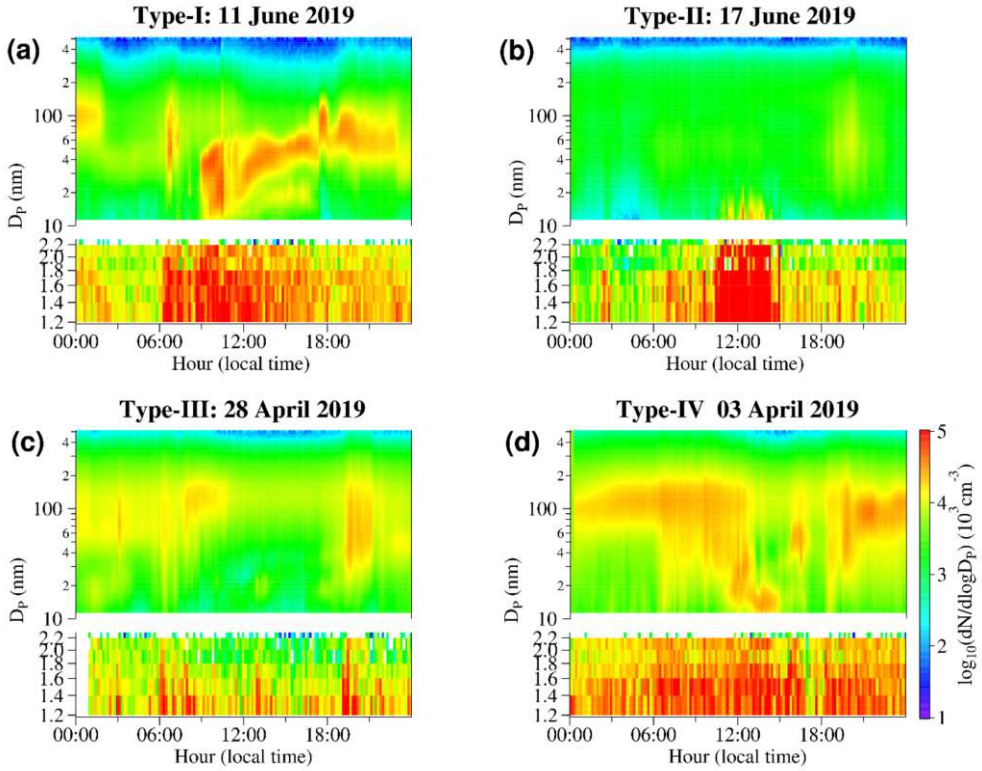

Figure 2.4 Time evolution of the particle number size distributions on a typical (a) Type-I NPF&G event, (b) Type-II NPF event, (c) Type-III non-event, and (d) Type-IV unidentified event day at Hyderabad. The particle number size distribution in the size range from 1.2 to 3.0 nm and 10 to 514 nm were obtained using the nCNC and SMPS, respectively.

Additionally, we used black carbon mass concentrations to classify an NPF event into two sub-classes in Ranichauri namely, cleaner and polluted events. The criteria used for classifying different event types in Ranichauri are summarized in Table 2.3.

Table 2.3 Summary of criteria used for classifying event types in Ranichauri.

Event type	Subtype	Features
Type-I NPF event	Ia (cleaner)	A new mode of particles smaller than 25 nm in size is visible with a steady growth in the particle size for at least 6 hours. GR and J_{10} can be calculated. No or insignificant simultaneous increase in BC mass concentrations with the particle mode diameter.
	Ib (polluted)	Same as Type-Ia, but with a significant simultaneous increase in BC mass concentrations.
Type-II NPF event	IIa (cleaner)	A new mode of particles smaller than 25 nm is absent referred to as an Aitken-mode growth event. GR and J_{10} cannot be calculated. No or insignificant simultaneous increase in BC concentrations with the particle mode diameter.
	IIb (polluted)	Same as Type-IIa, but with a significant simultaneous increase in BC ass concentrations.
Type-III non-event		No distinct change in particle mode diameter during the course of the day
Type-IV unidentified		Difficult to identify whether it is one of the above event types.

Type-I NPF events were identified by the presence of a distinctly new mode of particles with diameters smaller than 25 nm and with steady growth in diameter of this new mode for at least 6 hours such that particle number size distributions display a 'banana' shaped aerosol growth. Type-I NPF events were further classified into two sub-types: Ia and Ib, based on BC mass concentrations. Type-Ia NPF event showed no or insignificant simultaneous increase in BC mass concentrations with the new mode of particles, implying a cleaner NPF event (Figure 2.5a). The Type-Ib NPF event showed a significant simultaneous increase in BC mass concentrations with the new mode of particles, implying a polluted event (Figure 2.5b). Type-II NPF events were similar to Type-I NPF events except that the particle mode diameter was larger than 25 nm. Such events are observed when the air mass with NPF reaches the measurement site after the particles have already grown larger than 25 nm diameter, referred to as Aitken-mode growth events. Type-II NPF events were also classified into two sub-types: IIa (cleaner) and IIb (polluted), similar to Type-I NPF events. Type-IIa NPF events showed no or insignificant simultaneous increase in BC mass concentrations, implying a cleaner event (Figure 2.5c) while Type-IIb NPF events showed a simultaneous increase in BC concentrations, implying a polluted event (Figure 2.5d). The days with no evidence of distinct change in particle mode diameter were identified as Type-III non-event (Figure 2.5e). Those days, which were

difficult to classify as any one of the above categories, were categorised as Type-IV unidentified event days (Figure 2.5f).

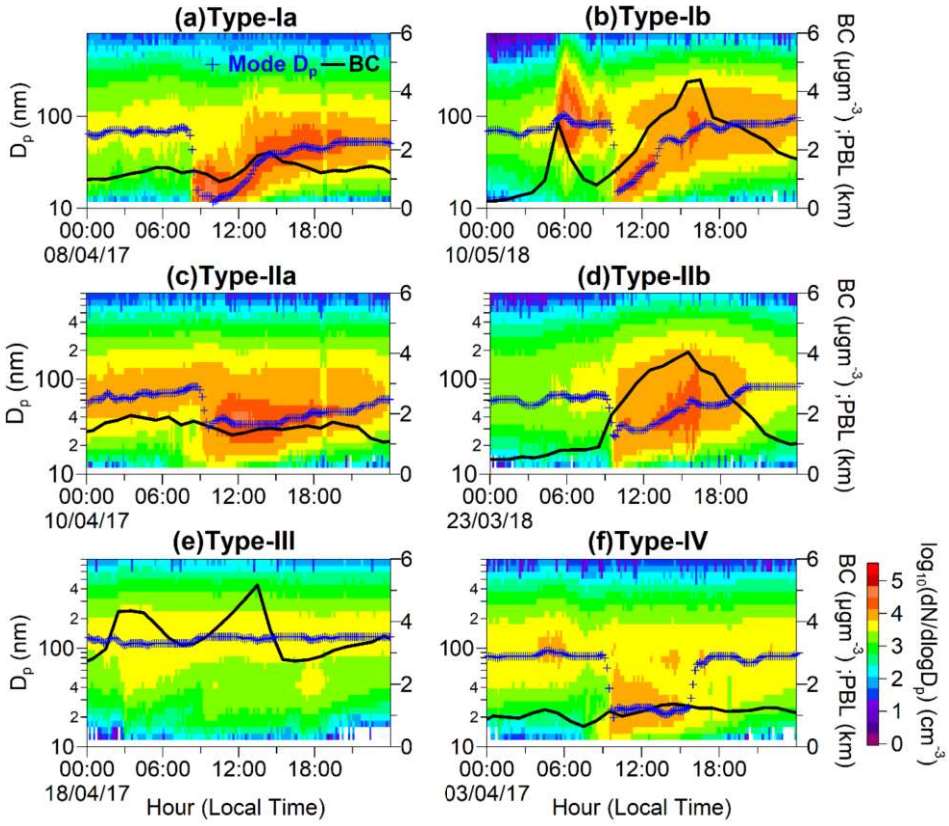

Figure 2.5. Temporal evolution of particle number size distributions (filled contour), particle mode diameter (blue plus symbol), and BC mass concentrations (thick black line) for typical Type-I NPF events (a, b), Type-II NPF events (c, d), Type-III non-event (e) and Type-IV unidentified event (f) days at Ranichauri.

2.6.3 Particle formation and growth rate calculations

Growth rate (GR) of particles is mathematically expressed as the derivative of the diameter, Dp, with respect to time, t, which quantifies the rate at which the particle size is increasing.

$$GR = \frac{\Delta D_p}{\Delta t} = \frac{D_{p2} - D_{p1}}{t_2 - t_1} \quad (2.1)$$

where d_{p1} and d_{p2} represent the particle diameters at times t_1 and t_2, respectively.

The growth rate of sub-3nm particles ($GR_{sub\text{-}3nm}$) was determined by the maximum concentration method following Lehtinen and Kulmala (2003), modified and updated by Makkonen et al. (2012). Briefly, the representative diameter is taken as the midpoint of the measured size bin. First, the time evolution of particle number concentrations in each size bin

is plotted and the normal distribution is fitted to the area around the maximum concentrations. The peak times for each size bin are then identified and plotted against the midpoint of the measured size bin to calculate the growth rate of sub-3nm particles by a linear least-squares fit. The size-segregated GRs were also calculated by fitting a first-order polynomial regression line to the temporal changes in the particle mode diameter of the observed particle number size distributions and calculating the slope of the line as shown in Figure 2.6.

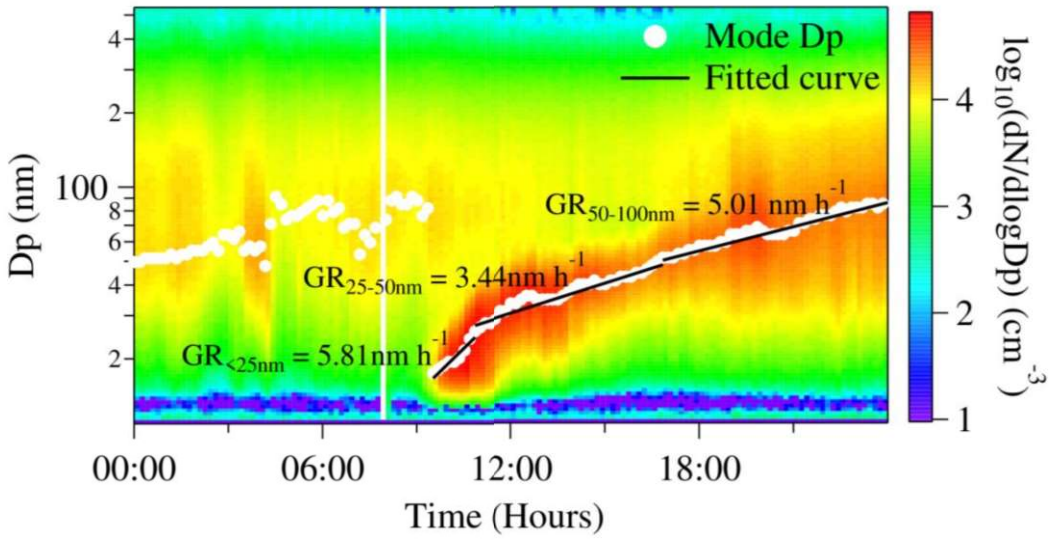

Figure 2.6 Size-segregated particle growth rate calculation by fitting a first-order polynomial regression to the time evolution of particle mode diameter. White circles denote the particle mode diameter and the black line denotes the fitted curve.

The net flux of clusters growing past a certain diameter, D_p, is defined as the nucleation rate $\left(J_{D_p}\right)$ and was calculated following Kulmala et al. (2012b) methodology,

$$J_{D_p} = \frac{dN_{D_p}}{dt} + CoagS_{D_p} \cdot N_{D_p} + \frac{GR}{\Delta D_p} \cdot N_{D_p} \quad (2.2)$$

where N_{D_p} and $CoagS_{D_p}$ are the number of concentrations and coagulation sink of particles in the size range $[D_p, D_p + \Delta D_p]$, respectively.

2.6.4 Condensation sink and coagulation sink calculations

The coagulation sink (CoagS) determines how rapidly nanometer-size aerosol particles are removed through coagulation to pre-existing particles and it was calculated using the methodology of Kerminen et al. (2001) as,

$$CoagS_{D_p} = \sum_{D_p}^{D'_p} K(D_p, D'_p).N_{D'_p} \quad (2.3)$$

where $K(d_p, d'_p)$ is the coagulation coefficient of particle sizes D_p and D'_p.

The condensation sink (CS) determines the ability of the particle number size distribution to remove condensable vapours from the atmosphere and it was calculated following Kulmala et al. (2001) as,

$$CS = 4\pi D. \sum_{D'_p} \beta_{m,D'_p}.D'_p.N_{D'_p} \quad (2.4)$$

where D is the diffusion coefficient of the condensing vapour (assumed to be H_2SO_4, 0.104 cm^2 s^{-1}) and β_m represents a transition regime correction calculated by

$$\beta_m = \frac{1+K_n}{1+1.677K_n+1.333K_n^2} \quad (2.5)$$

where K_n is the Knudsen number given by $K_n = 2\lambda/D_p$ where λ is the mean free path.

Mean free path λ is calculated by

$$\lambda = \frac{\mu\sqrt{\pi}}{\rho\sqrt{2RT}} \quad (2.6)$$

where μ is the fluid viscosity, ρ is the fluid density, T is the absolute temperature, and R (8.314 J $mol^{-1}K^{-1}$) is the gas constant.

2.6.5 Calculation of sulfuric acid proxy concentrations

So far, several investigators have developed a proxy for H_2SO_4 concentrations (Dada et al., 2020; Lu et al., 2019; Petäjä et al., 2009). *Petäjä et al.*, (2009) developed an H_2SO_4 proxy using its source from reactions between SO_2 and OH and its loss by condensation sink. *Lu et al.*, (2019) developed a daytime proxy specifically for relatively high condensation sink. More recently, *Dada et al.*, (2020) developed a new proxy that takes into account the production of gaseous H_2SO_4 from reactions between SO_2 and OH and stabilized Criegee intermediates reactions (monoterpene and ozone), and its losses due to condensation sink and molecular cluster formation. However, we do not have measurements of monoterpenes and hydroxyl (OH) radicals. Therefore, we have calculated a proxy for H_2SO_4 ($[H_2SO_4]_{proxy}$) using the methodology of Mikkonen et al. (2011),

$$[H_2SO_4] = 8.21 \times 10^{-3}. k. Radiation. [SO_2]^{0.62}. (CS. RH)^{-0.13} \quad (2.7)$$

where k is the reaction coefficient (1.0349). The solar radiation (or season) dependence makes this proxy the more robust and best predictive of H_2SO_4 for a wide range of atmospheric conditions.

We have also calculated the growth rate due to H_2SO_4 alone (GR_{H2SO4}) following (Seinfeld and Pandis, 2006) as,

$$GR_{\mathrm{H_2SO_4}} = \frac{3600\times10^{9}.M_S.c^{-\alpha}.([\mathrm{H_2SO_4}]-[\mathrm{H_2SO_4}]_{eq}).W_R}{(2\rho/10^{3}).6.022\times10^{23}} \quad (2.8)$$

$$c^{-\alpha} = \left(\frac{8\times10^{3}.R.T}{\pi.M_S}\right)^{1/2}$$

where $M_s$and c are the molecular weight (98 g mol^{-1}) and mean speed (m s^{-1}) of H_2SO_4 molecules, respectively. α is the mass transfer coefficient which is taken as unity here and $[H_2SO_4]_{eq}$ (molecules cm^{-1}) is the equilibrium concentration of H_2SO_4 (usually $[H_2SO_4]$ >>$[H_2SO_4]_{eq}$). W_R is the ratio of the wet H_2SO_4 particle diameter at a certain RH to the dry H_2SO_4 particle diameter. ρ is the particle density (1.2 g cm^{-3}), R is the universal gas constant (8.314 J mol^{-1} K^{-1}) and T is the air temperature.

2.6.6 Spatial extent of new particle formation events

We used hourly calculated backward air mass trajectories to calculate the spatial extent of the observed NPF events at the University of Hyderabad campus site following the methodology followed by Hussein et al. (2009). For this approach, we first identified the starting time and the time span for each of the NPF events. Then the back trajectories were calculated for every hour till the end of the event throughout the time span of the event. The length of the individual trajectories (in hours) is determined by the number of time steps taken. For example, for an event starting at 08:00 am, the one-hour back trajectory is calculated starting at 08:00 am. For the next hour i.e., 09:00 am, the back trajectory is calculated for 2 hours. Similarly, a three-hour back trajectory will be calculated for 11:00 am. This will be continued till the end (time span) of the event. Further, the percentage occurrences of calculated back trajectories in 0.5°×0.625° sized grids were plotted along the duration of trajectory in each grid.

2.6.7 Survival probability of newly formed particles

Newly formed particles are subject to their loss to large pre-existing particles by scavenging or coagulation. Therefore, the fate of newly formed particles to grow up to the CCN active sizes depends upon several factors such as the abundance of pre-existing particles, precursor vapour concentration, and atmospheric and dynamical (clouds, convection, subsidence, etc.) conditions. For summertime arctic clouds, thee particles as small as 20 nm may activate as CCN (Korhonen et al., 2008; Leaitch et al., 2016), while in typical ambient in-cloud supersaturations, 50 nm and 100 nm are considered as a good proxy for CCN concentration (Kerminen et al., 2012) at approximately 1.0% and 0.2% supersaturation for stratiform clouds, respectively. Here, we have calculated the newly formed particle survival probabilities to 50 nm (SP50) and 100 nm (SP100) size following the methodology given by Pierce and Adams (2007) and first applied to ambient observations by Westervelt et al. (2013). Briefly, SP is the ratio of particle fluxes at the initial size and the CCN-active sizes (typically 50 nm and 100 nm particles). The survival probability from initial size m to n (in our case, 10 to 50 nm and 10 to 100 nm) is calculated by the following equation:

$$SP_{m,n} = \prod_{k=m}^{n-1} exp\left(-\frac{\tau_{k,k+1}^{cond}}{\tau_{k}^{coag}}\right) \quad (2.9)$$

where τ^{cond} is the condensational growth time scale required for a particle to grow to a size of interest. τ^{coag} is the inverse of the coagulation sink for a given size range. The formation rates of CCN-active particles (i.e., 50 nm and 100 nm) are calculated as, $J_{50} = J_{10} \times SP50$ and $J_{100} = J_{10} \times SP100$. J_{10} is the formation rate of a 10 nm particle. While this methodology does not consider aerosol composition and mixing state, the particles larger than 50 nm will serve as CCN under typical supersaturations. Because, the aerosol size plays a major role in the aerosols ability to act as CCN rather than its composition (Dusek et al., 2006).

The calculation of survival probabilities for particles 50 nm and 100 nm is subject to several uncertainties. Initially, the primary particles have the potential to influence particle number concentrations ranging from 10 to 25 nm, consequently impacting the observed nucleation rate. The utilization of two distinct growth rates exclusively for two specific size intervals (10-25 nm and 25-100 nm) could potentially introduce a bias that results in higher survival probabilities than initially anticipated. which are described elsewhere in Westervelt et al. (2013). However, Westervelt et al. (2013) systematically examined the uncertainty associated with survival probability through the utilization of two distinct methodologies. The first approach, as outlined

in the aforementioned study, was employed. The second method, as elucidated by Kuang et al. (2009) involved defining the survival probability as the ratio of N_{100} to N_3 for a specific growth trajectory. Westervelt et al. (2013) also demonstrated that the two methods exhibit substantial similarity in terms of survival probabilities.

2.6.8 Estimating cloud condensation nuclei production from new particle formation

The increase in CCN concentrations from any given NPF event can be estimated by comparing the CCN concentration before the event ($N_{CCNprior}$) and the maximum CCN concentration during the event (N_{CCNmax}) following the methodology developed by Kerminen et al. (2012), which we modified further to remove the contribution from primary/background particles to CCN concentrations. In typical ambient in-cloud supersaturations, the total number of particles from 50 nm to >100 nm can be considered as a proxy for CCN concentrations assuming fixed chemical composition (Kerminen et al., 2012; Westervelt et al., 2013). $N_{CCNprior}$ was chosen to be a one-hour average concentration of particles larger than 50 nm (and 100 nm) just before the start of the NPF event. The start of the NPF event is the time when nucleation mode particle number concentrations increase rapidly during an NPF event. N_{CCNmax} was taken as a maximum one-hour average concentration of particles larger than 50 nm (and 100 nm) during the event. The N_{CCNmax} is not the best representation of CCN concentration after the NPF event because it is not possible to estimate the end of an NPF event. However, it gives a rough estimate of the observed maximum number of primary and secondary particles present in the atmosphere during an event (Kerminen et al., 2012). For non-event days, the seasonally averaged start of the NPF event time was chosen to calculate $N_{CCNprior}$. N_{CCNmax} on non-event days was taken similarly to NPF event days, as a maximum one-hour average concentration of particles larger than 50 nm (and 100 nm). Therefore, the second term in Eq. (2) introduces the approximate CCN concentrations from processes other than NPF. Then, the absolute increase in CCN concentration from NPF is calculated as given below,

$$\text{CCN increase} = (N_{CCNmax} - N_{CCNprior})_{NPFevent} - (N_{CCNmax} - N_{CCNprior})_{non\text{-}events} \quad (2.10)$$

The first term on the right-hand side in Eq. (2) indicates the CCN increase during an NPF event, while the second term indicates the CCN increase during a non-event. However the atmospheric condition on non-event days is generally different from NPF event days; therefore, the calculated increase in CCN concentrations from NPF may be imprecise.

Chapter 3

Characterization of sub-3nm particles and new particle formation events

3.1 Introduction

Atmospheric aerosols affect air quality, visibility, weather, climate and human health (IPCC, 2013; Lelieveld et al., 2015). NPF is the greatest source of particle numbers in the atmosphere (Kanawade et al., 2021; Kulmala, 2003; Kulmala et al., 2013; Kulmala et al., 2004). These newly formed particles can grow up to>50-100 nm (Kulmala et al., 2004; Westervelt et al., 2013) and thereby contribute significantly to the CCN population (Kerminen et al., 2012; Pierce et al., 2012; Sebastian et al., 2021b; Sebastian et al., 2022). Ultrafine particles (particles diameter < 100 nm) dominate the total number concentration but constitute only a small fraction of the total aerosols, especially in urban locations (von Bismarck-Osten et al., 2013; Wehner et al., 2004; Wu et al., 2008; Zhou et al., 2020). The characteristics of particle number size distributions are governed by the balance between NPF, condensation onto pre-existing particles, evaporation of particles, coagulation, and sedimentation, their characterisation is essential (IPCC, 2013).

Several studies have analysed the characteristics of particle number size distributions and size-segregated particle number concentrations across the world (Asmi et al., 2011; Cai et al., 2020; Dominick et al., 2018; Sebastian et al., 2022; Wehner et al., 2004; Zhou et al., 2020). Recent advancements in instrumentation, including the nano condensation nucleus counter (nCNC) and neutral cluster and air ion spectrometers (NAISs), have enabled us to measure sub-3 nm particles and ions. NPF starts with the formation of stable 1–3 nm molecular clusters (McMurry et al., 2011). Aerosol nucleation usually starts with sulfuric acid and other condensable vapours, such as amines, ammonia, and low-volatility organics condense to form stable clusters before re-evaporating (Kulmala, 2003; Kulmala and Kerminen, 2008; Sipilä et al., 2010),. Despite intensive measurements over the last decade, the sources (natural and anthropogenic) and chemical composition of atmospheric sub-3 nm particles and their precursor vapours in diverse environments worldwide remain poorly quantified (Kontkanen et al., 2017; Rose et al., 2015; Xiao et al., 2015). In the Indian context, only three studies have linked new particle formation

to precursor gas concentration (Kanawade et al., 2014a; Kanawade et al., 2014c; Sebastian et al., 2021a) and only two studies have shown observational evidence of neutral sub-3 nm particles (Kanawade et al., 2022; Sebastian et al., 2021a). Frequency of occurrence of new particle formation events, particle formation and growth rates, occurrence frequency of new particle formation events have been reported by several studies in India (Babu et al., 2016; Chate and Devara, 2005; Kamra et al., 2015; Kanawade et al., 2022; Kanawade et al., 2014a; Kanawade et al., 2014b; Kanawade et al., 2014c; Kompalli et al., 2014; Kompalli et al., 2020; Leena et al., 2017; Mönkkönen et al., 2005; Murugavel and Chate, 2009; Neitola et al., 2011; Sebastian et al., 2021a; Sebastian et al., 2021b; Siingh et al., 2013; Varghese et al., 2020). This chapter provides a comprehensive approach to identifying the characteristics of particle number size distribution, size-segregated particle number concentrations and new particle formation events in diverse locations in India with a focus on measurements from Hyderabad.

3.2 Data analysis methods

In this study, we utilized particle number size distributions acquired from SMPS and nCNC over a period of 43 months at the Hyderabad site to investigate variability in size-segregated particle number concentrations (Section 2.1). We considered mainly four particle size regimes such as cluster mode (sub-3nm), nucleation mode (3-25nm), Aitken mode (25-100nm) and accumulation mode (100-1000nm). We further classified the valid observation days into broad four categories such as NPF event, non-event, polluted event and undefined event days. Then, we present size-segregated particle formation rate in the sub-3nm size range, variability in different characteristics of event types. The association between the sub-3nm particle number concentrations and the formation rate as a function of the calculated sulfuric acid proxy is also presented. We further illustrate NPF characteristics during the COVID-19 enforced lockdown and compare that with the Buissness-as-usual time period as a case study. Lastly, we present comprehensive analyses of particle size distributions and NPF characteristics from six diverse geographical environments in India to investigate spatial variability in particle number size distributions and NPF characteristics.

3.3 Results and discussion

3.3.1 Characteristics of size-segregated particle number concentration

In this study, we have used long-term particle number size distribution data from April 2019 to December 2022 (43 months) from the site of Hyderabad for this study. Figure 3.1 displays the temporal evolution of the particle number size distributions from nCNC and SMPS at the site.

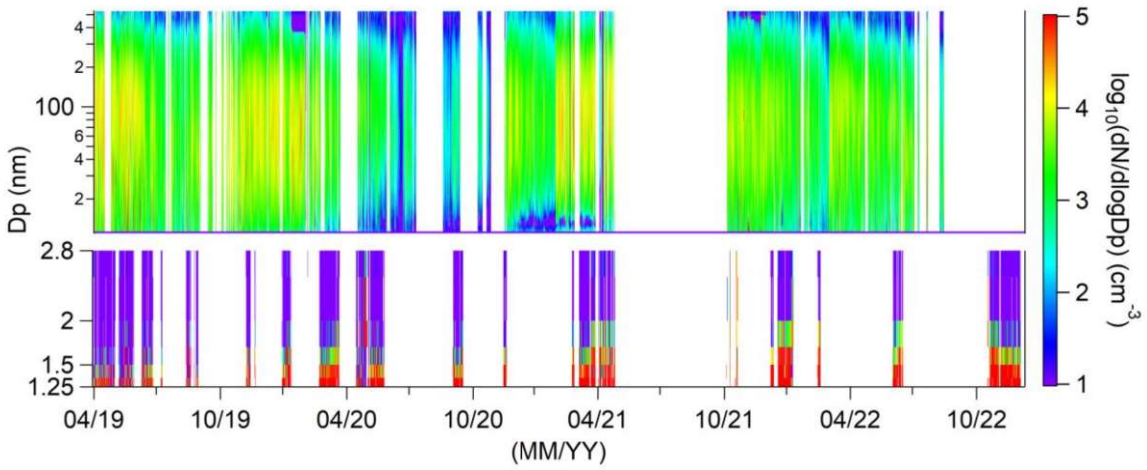

Figure 3.1 Time evolution of particle number size distributions in the size range of 1.25 to 2.8 nm from nCNC and 10-514 nm from SMPS from 1 April 2019 to 7 December 2022.

Figure 3.2 depicts the monthly frequency of NPF events, non-events, polluted events and undefined events. The occurrence of the NPF is most prevalent during pre-monsoon (MAM) The increased NPF frequency in pre-monsoon (MAM) is linked to increased solar radiation and therefore photochemically active atmosphere to facilitate NPF processes (Berland et al., 2017; Juozaitis et al., 1996; Kulmala and Kerminen, 2008; Olin et al., 2020; Zilli Vieira and Koutrakis, 2021). The elevated boundary layer height during pre-monsoon (MAM) offers sufficient air dilution thereby lowering the condensation sink (which is one of the critical factors determining the triggering of aerosol nucleation in a polluted boundary layer). NPF events occurred less frequently during winter (DJF) owing to less active photochemistry under reduced solar radiation which further results in a shallow boundary layer height. The shallow boundary layer increases the accumulation of aerosol precursor and pre-existing particles close to the surface which inhibits NPF under highly polluted conditions (Kerminen and Kulmala, 2002; Kuang et al., 2010). The NPF frequency is lower during the monsoon (JJAS)season owing to the wet scavenging of aerosol precursors and reduced photochemistry under consistent cloud conditions (Kanawade et al., 2014a).

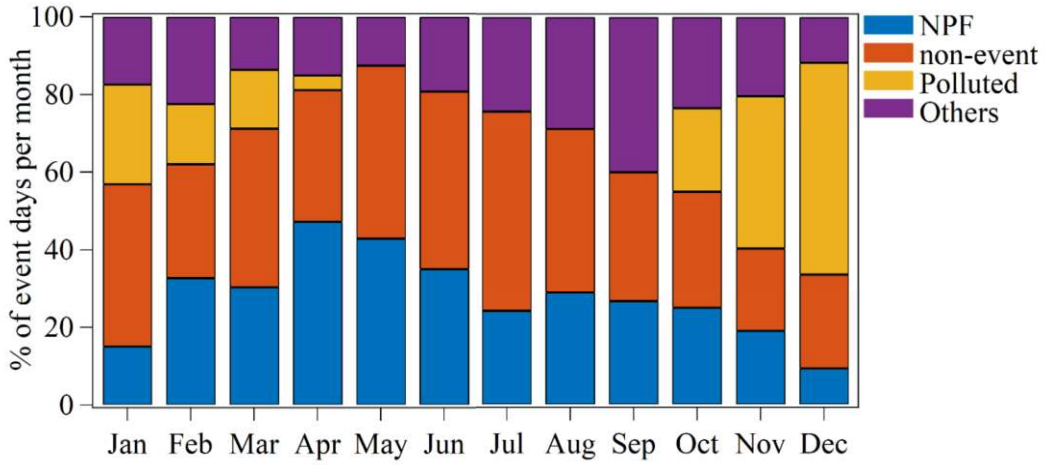

Figure 3.2 Monthly percentage of occurrence of NPF, non-event polluted and undefined events days based on total valid observations days at Hyderabad from 1 April 2019 to 7 December 2022.

Our study further analyses the seasonal attributes of size-segregated particle number concentrations. It was seen that the cluster mode particles dominate the particle number concentration during all seasons and event types (Figure 3.3). This means that cluster formation is active even under pollution which is also seen in other urban sites (Deng et al., 2020; Yu et al., 2016). As we do not have observations of particle number size distribution in the 3-10nm size range (which falls in the nucleation mode size range), the nucleation mode number concentrations are less than that of the Aitken mode particle number concentration. Nucleation mode particle number concentration was the highest for NPF event days among the event types. It was the highest during pre-monsoon (MAM) season which is attributed frequent occurrence of NPF events. Within a season, non-events have the lowest particle number concentration for nucleation, Aitken and accumulation modes.

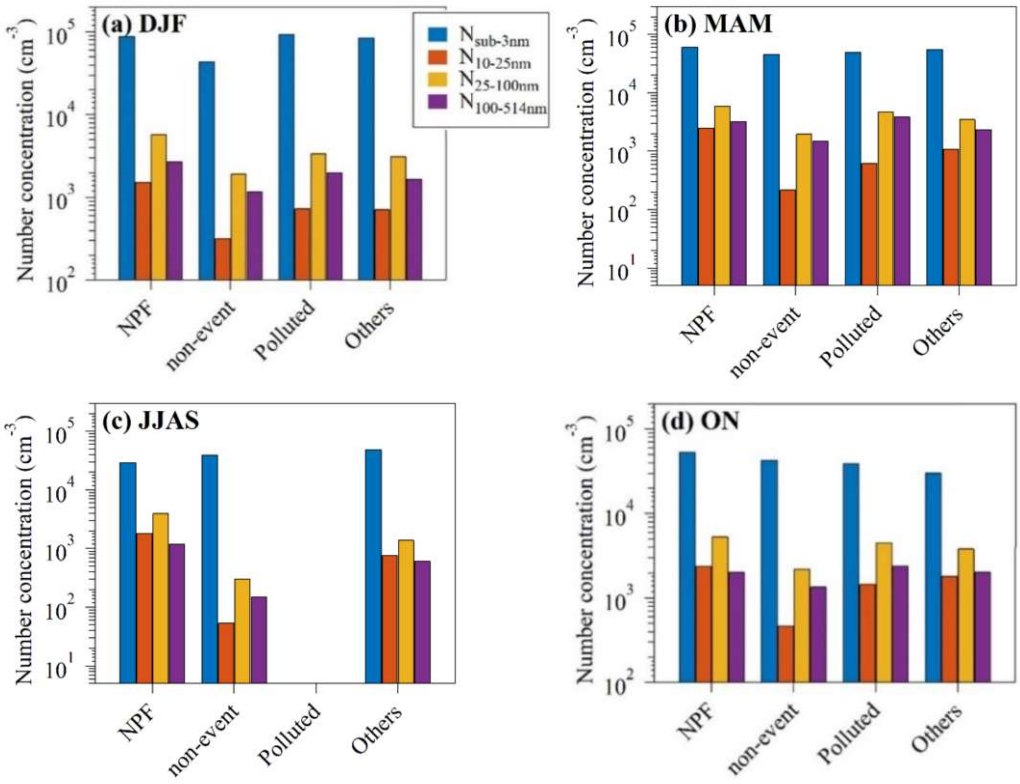

Figure 3.3 The median size-segregated particle number concentrations during (a) winter (DJF), (b) pre-monsoon (MAM), (c) monsoon (JJAS) and (d) post-monsoon (ON) on the NPF, non-events and polluted days.

Figure 3.4 shows the correlation between $PM_{2.5}$ and particle number concentrations for each particle mode. This analysis will be instrumental in determining the effects of aerosol loading on particle concentrations across different size segregations. It can be seen from Figure 3.4a that cluster mode particle concentration and $PM_{2.5}$ concentrations are positively correlated during winter (DJF) and pre-monsoon (MAM). This indicates that an inhibition of cluster mode particle formation was not observed under conditions of high pre-existing particle concentration. Whereas, there exists a negative correlation between nucleation mode particle concentrations and $PM_{2.5}$ during winter (DJF) and pre-monsoon (MAM). This suggests that the nucleation mode particle number concentrations are influenced by the pre-existing aerosol loading. This also adds to the fact not all the particle cluster modes undergo growth to reach nucleation mode size as observed in previous studies at the site (Kanawade et al., 2022; Sebastian et al., 2021a). Similar events with particles not growing beyond 30nm were observed elsewhere in the urban location of Nanjing (Yu et al., 2016). There is a positive correlation between $PM_{2.5}$ and Aitken and accumulation mode, suggesting that NPF plays a substantial role in contributing to the number concentrations of Aitken and accumulation mode particles.

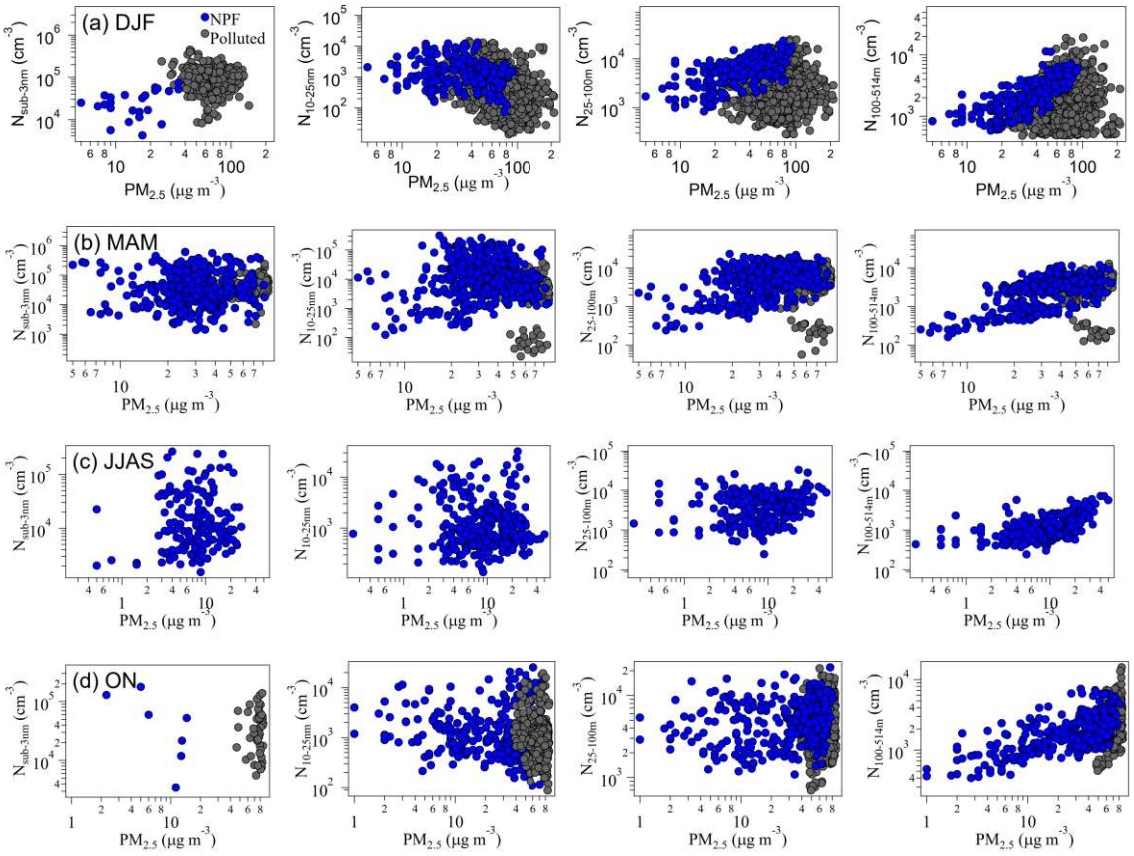

Figure 3.4 Correlation between $PM_{2.5}$ concentration and particle number concentration for each particle mode for (a) winter (DJF), (b) pre-monsoon (MAM), (c) monsoon (JJAS) and (d) post-monsoon (ON)

3.3.2 Formation and growth rates of sub-3nm particles in Hyderabad

In this study, we report the formation and growth rates of sub-3nm particles from India for the first time. We have calculated different attributes of the observed Type-I and Type-II events, including the rate at which particles of each size bin are formed, the number concentration of sub-3nm particles ($N_{sub\text{-}3nm}$), the growth rate of sub-3nm particles ($GR_{sub\text{-}3nm}$), the growth rate of nucleation mode particles ($GR_{10\text{-}25nm}$), the proxy concentration of H_2SO_4, the coagulation sink of sub-3nm ($CoagS_{sub\text{-}3nm}$), and the overall condensation sink (CS). Figure 3.5 shows the box-whisker plots representing the formation rates of individual size bins within the inverted particle number size distribution obtained from the nCNC. In Figure 3.5, the observed rates of formation for larger-size bins are lower than those of smaller-size bins, which can be attributed to the occurrence of coagulation losses during the process of particle growth. The rate of particle formation in the smallest size bin (1.1-1.3 nm) is one order greater than that in the largest size bin (2.2-3.0 nm). The particle formation rates observed for Type-II events were found to be approximately twice as high as those for Type-I events, as shown in Figure 3.5. It is worth

noting that despite the higher formation rates, the particles in Type-II events did not exhibit further growth.

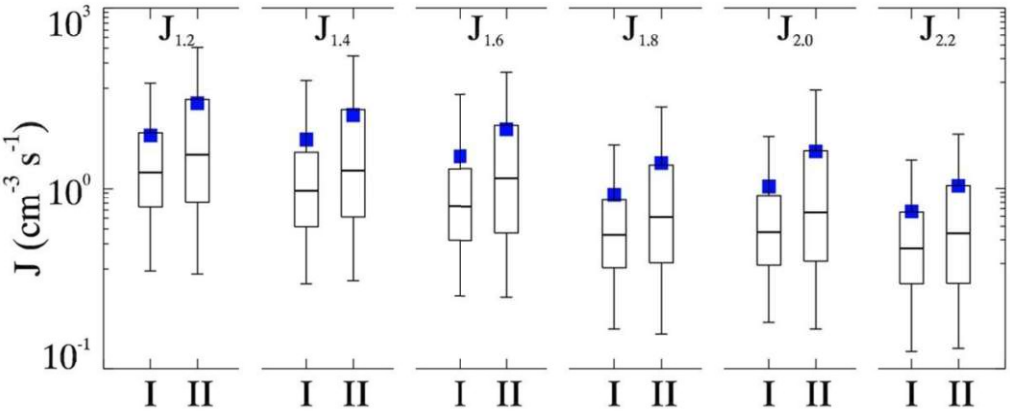

Figure 3.5 Box-whisker plots of $J_{1.2}$, $J_{1.4}$, $J_{1.6}$, $J_{1.8}$, and $J_{2.0}$. The blue dot indicates the mean, the horizontal line indicates the median, the top and bottom of the box indicate 25th and 75th percentiles, respectively, and the top and bottom whisker indicate the 5th and 95th percentiles, respectively

Figure 3.6 displays the median diurnal variation of particle formation rate across various size bins. The mean rate of formation exhibited a continuous upward trend following the onset of sunrise, following the dilution of the atmosphere on the elevation of the boundary layer. The formation rates reach their maximum point during the local mid-day hours. Later, the formation rates subsequently decline to background levels by sunset. The formation rate of particles in the largest size bin (2.2-3.0 nm) is lower by one order. The formation rates of Type-II NPF events were two times higher as compared to Type-I NPF&G events.

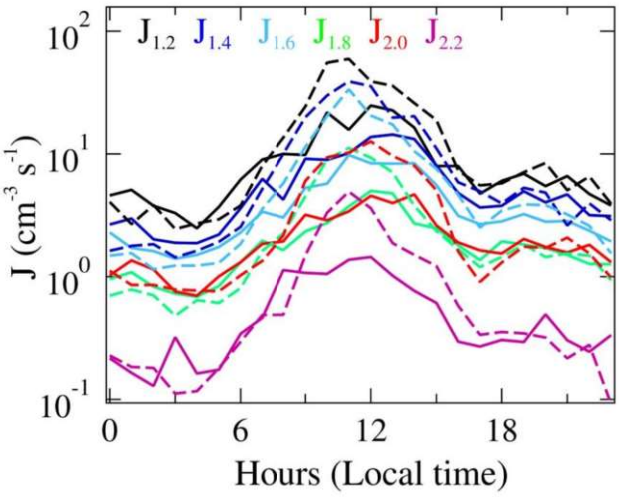

Figure 3.6 The median diurnal variation of $J_{1.2}$, $J_{1.4}$, $J_{1.6}$, $J_{1.8}$, and $J_{2.0}$ for Type-I NPF&G (thick lines) and Type-II NPF (dashed lines) event days.

3.3.3 Role of sulfuric acid and other condensable species in aerosol formation and growth

Figure 3.7 shows the strong association between $J_{1.4}$, $N_{sub\text{-}3nm}$, and $[H_2SO_4]_{proxy}$ indicating the crucial role of H_2SO_4 in particle nucleation in the region of Hyderabad. Sulfuric acid has been recognized as the primary contributor to particle nucleation (Almeida et al., 2013; Erupe et al., 2011; Kirkby et al., 2011; Riipinen et al., 2007; Schobesberger et al., 2013; Sipilä et al., 2010; Weber et al., 1996). The sub-3nm particle concentration and formation rates are higher with a higher sulfuric acid concentration in general. The correlation between $N_{sub\text{-}3nm}$, $J_{1.4}$, and $[H_2SO_4]_{proxy}$ is similar for both Type-I and Type-II events, suggesting that $[H_2SO_4]$ was not a major cause for the difference between Type-I and Type-II event days. Sulfuric acid is also known for its crucial role in particle growth as well (Kulmala and Kerminen, 2008; Vakkari et al., 2015; Wehner et al., 2005; Yu et al., 2017; Yue et al., 2010). Nevertheless, the sole presence of H_2SO_4 does not explain the observed growth rates of nucleated particles to larger sizes (Riccobono et al., 2012; Riipinen et al., 2012). The particle growth rate attributed to H_2SO_4 was determined following the methodology used by Erupe et al. (2010). We observed that H_2SO_4 contributed to 5-65% of the overall observed growth for particles larger than 10 nm on Type-I event days. This finding is in association with previous studies (Erupe et al., 2010; Yli-Juuti et al., 2016).

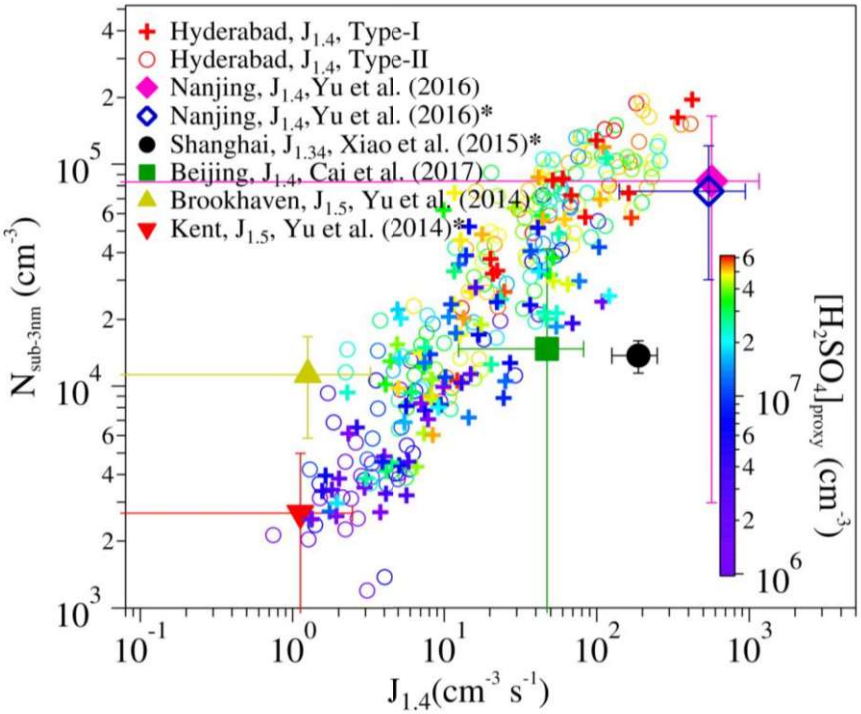

Figure 3.7 Scatter plot of hourly averaged $J_{1.4}$ versus $N_{sub\text{-}3nm}$as a function of $[H_2SO_4]_{proxy}$ for Type-I (open circle) and Type-II (plus sign) events in Hyderabad. The data pertaining to $J_{1.4}$, $N_{sub\text{-}3nm}$, and $[H_2SO_4]_{proxy}$ were taken as the average between 6:00 AM to 2:00 PM. The mean

values of $J_{1.4}$, $N_{sub\text{-}3nm}$, and $[H_2SO_4]_{proxy}$ for other sites in diverse environments listed in Table 2 are also plotted for comparison: Nanjing (filled and open diamond for spring and winter seasons, respectively), Shanghai (filled circle, winter) Beijing (filled square, spring), Brookhaven (filled upward triangle, spring), and Kent (filled downward triangle, winter).* indicates winter-time measurements. The colour scale shows the concentration of $[H_2SO_4]_{proxy}$.

The mean and standard deviation of $J_{1.4}$ and $N_{sub\text{-}3nm}$ for the diverse range of previously studied sites (Table 3.1) are also plotted for comparison. While $N_{sub\text{-}3nm}$ in Hyderabad was approximately half of that in Nanjing (China) (Yu et al., 2016), it was approximately 2-3 times higher than those in Beijing (China) (Cai et al., 2017) and Shanghai (China) (Xiao et al., 2015), both of which are urban areas. $N_{sub\text{-}3nm}$ at Hyderabad was found to be ten times higher than that observed at semi-rural Kent (USA) (Yu et al., 2014) and San Pietro (Po Valley, Italy) (Kontkanen et al., 2016), which are considered to be cleaner sites. During Type-I NPF&G event days, the $J_{1.4}$ value ranged from 0.7 cm^{-3} s^{-1} to 145.1 cm^{-3} s^{-1} (5^{th} to 95^{th} percentiles), with an average of 30.7±73.6 cm^{-3} s^{-1}. The $J_{1.4}$ value in Hyderabad was a magnitude lower compared to Nanjing and Shanghai (Xiao et al., 2015). However, it was found to be similar to the $J_{1.4}$ value observed in Beijing (Cai et al., 2018). Conversely, the $J_{1.4}$ value in Hyderabad was one magnitude higher than that of cleaner locations such as Brookhaven, Kent, and Hyytiala (Finland) (Makkonen et al., 2012; Yu et al., 2014). The mean growth rates of sub-3nm particles $GR_{sub\text{-}3nm}$ were found to be similar for both Type-I (2.2±1.7 nm h^{-1}) and Type-II (2.0±1.4 nm h^{-1}) events suggesting similar levels of vapours that condense to form new particles and facilitate their initial growth. These values were comparable with other sites listed in Table 3.1. The average rate of growth in the size range of 10-25 nm for Type-I NPF&G event days was determined to be 4.9±3.2 nm h^{-1} which is similar to other sites in Table 3.1. The mean $CoagS_{TOT}$ values for Type-I (3.0×10^{-4} s^{-1}) and Type-II (3.2×10^{-4} s^{-1}) events exhibited similar results. Additionally, the calculated CS_{TOT} values were found to be similar for both Type-I (1.6×10^{-2} s^{-1}) and Type-II (1.8×10^{-2} s^{-1}) events. These suggest that the differences observed between the two event types cannot be attributed to variations in pre-existing aerosol concentrations. Based on the preceding discourse, it can be inferred that neither $[H_2SO_4]$, $CoagS_{sub\text{-}3nm}$, nor CS contributed to the hindered particle growth observed in Type-II NPF occurrences.

Table 3.1 Summary of averaged (6:00 AM to 2:00 PM local time) sub-3nm particle number concentrations ($N_{sub\text{-}3nm}$), formation rate of 1.4 nm particles ($J_{1.4}$), growth rate of sub-3nm particles ($GR_{sub\text{-}3nm}$), total growth rate (GR), sulfuric acid concentration proxy ($[H_2SO_4]_{proxy}$), total consternation sink (CS_{TOT}) and total coagulation sink ($CoagS_{TOT}$) for Type-I and Type-II NPF events in Hyderabad and various other sites in diverse environments. ±indicates standard deviation.

Site Location	Site Type	Time period	$N_{sub\text{-}3nm}$ (10^3 cm^{-3})	J (cm^{-3} s^{-1})	$GR_{sub\text{-}3nm}$ (nm h^{-1})	GR (nm h^{-1})	$[H_2SO_4]_{proxy}$ (10^7 cm^{-3})	CS (10^{-2} s^{-1})	$CoagS_{TOT}$ (10^{-4} s^{-1})	Reference
Type-I (NPF&G)	Urban	Apr.– Jun.2019	25.3±35.7	$J_{1.4}$,30.7±73.6	2.2±1.7	$GR_{10\text{-}25}$, 4.9±3.2	2.5±2.0[c]	1.6±0.8[e]	3.4±1.5[e]	This study
Nanjing, China	Urban	May. – Jun. 2014	83.3±80.3	$J_{1.4}$, 566±592	3.6	$GR_{3\text{-}20}$, 8.2	3.9[c]	1.9[f]	-	(Yu et al., 2016)
Nanjing, China	Urban	Dec. 2014 – Mar. 2015	75±45	$J_{1.4}$, 543±402	5.8	$GR_{3\text{-}20}$, 7.2	3.5[c]	3.1[f]	-	(Yu et al., 2016)
Shanghai, China	Urban	Nov. 2013 – Jan. 2014	13.6±2.3	$J_{1.34}$, 188±62.2	1.9±3.1	$GR_{7\text{-}20}$, 11.4	3.7[d]	6.0[g]	-	(Xiao et al., 2015)
Beijing, China	Urban	Mar. – Apr. 2016	14.6±26.6	$J_{1.5}$,47.2±34.7	2.4	2.3[b]	-	2.7[h]	-	(Cai et al., 2017)
Brookhaven, USA	Coastal	Jul. – Aug. 2011	11.2±5.4	$J_{1.5}$, 1.3±2.0	-	$GR_{3\text{-}10}$, 1.6	1.2[d]	0.5[i]	-	(Yu et al., 2014)
Kent, USA	Semi-rural	Dec. 2011 – Jan. 2012	2.7±2.3	$J_{1.5}$, 1.1±1.4	-	$GR_{3\text{-}10}$, 3.7	2.1[d]	0.8[i]	-	(Yu et al., 2014)
Hyytiala, Finland	Forest-rural	Oct. 2010 – Sep. 2011	-	$J_{1.5}$, 1.4	1.4[a]	$GR_{3\text{-}25}$, 3.3	-	-	-	(Makkonen et al., 2012)
San Pietro, Italy	Rural	Jun. – Jul. 2012	8.0[a]	$J_{1.6}$,45[a]	4.3[a]	$GR_{7\text{-}20}$, 7.2	-	1.1[j]	-	(Kontkanen et al., 2016)

"-" indicates no data; [a]for combined positive and negative ion clusters from NAIS; [b]mean growth rate; [c]H_2SO_4 proxy calculated from Mikkonen et al. (2011) ;[d]in-situ measured H_2SO_4; CS calculated for particle size range from [e]10-514 nm; [f]3-750nm; [g]3-615nm; [h]3-10000nm; [i]5-3000nm; [j]3-600 nm.

3.3.4 COVID-19 Lockdown case study

On December 31, 2019, the first case of Corona virus (CoV) was reported to WHO in Wuhan, China, and the outbreak of CoV was labelled a global hazard to public health by WHO. This novel CoV was named Coronavirus disease 2019 (COVID-19) on 11 February 2020 (Sohrabi et al., 2020) and declared a pandemic on March 11, 2020, owing to its rapid global spread and related fatality. the Government of India implemented nationwide lockdown from 24 March to 31 May, 2020, resulting in a considerable reduction in primary emissions. The mass concentrations in major cities worldwide were lowered by 11%-58% as a result of reduced primary emissions during the lockdown (Chauhan and Singh, 2020). India saw a 43% decrease in $PM_{2.5}$ mass concentrations across 22 cities (Sharma et al., 2020). Conversely, Le et al. (2020) reported unexpectedly extremely high PM levels during the COVID-19 lockdown owing to high relative humidity causing heterogeneous chemistry, stable atmospheric conditions, and incessant emissions sources such as electricity generation industries resulting in severe haze formation in Northern China. In Beijing, the reduced anthropogenic activity permitted stronger secondary chemical transformation, resulting the more secondary formation of organic aerosols (Sun et al., 2020).

During COVID-19 lockdown, two opposing effects can be expected for NPF&G. The reduction in primary emissions may result in lower levels of possible nucleating vapours such as SO_2 (Kulmala et al., 2013), ammonia, (Kirkby et al., 2011; Wang et al., 2020), amines (Almeida et al., 2013; Yu et al., 2012), VOCs (Schobesberger et al., 2013; Tröstl et al., 2016a), which can inhibit NPF&G occurrence. On the other hand, the reduction in pre-existing aerosol particles as a result of lockdown, which act as condensation and coagulation sinks for precursor vapours and nucleated particles, can increase NPF&G occurrence (Zhang et al., 2012). While one study in Beijing (Peking University) found similarity in occurrence of NPF&G between 2019 (business-as-usual year) and 2020 (lockdown year) in the same period (Tang et al., 2021), another study found enhancement in NPF&G events in Beijing (China Meteorological Administration) (Shen et al., 2021). A study in India found a lower frequency of NPF occurrences during the COVID-19 lockdown in Delhi (Yadav et al., 2021).

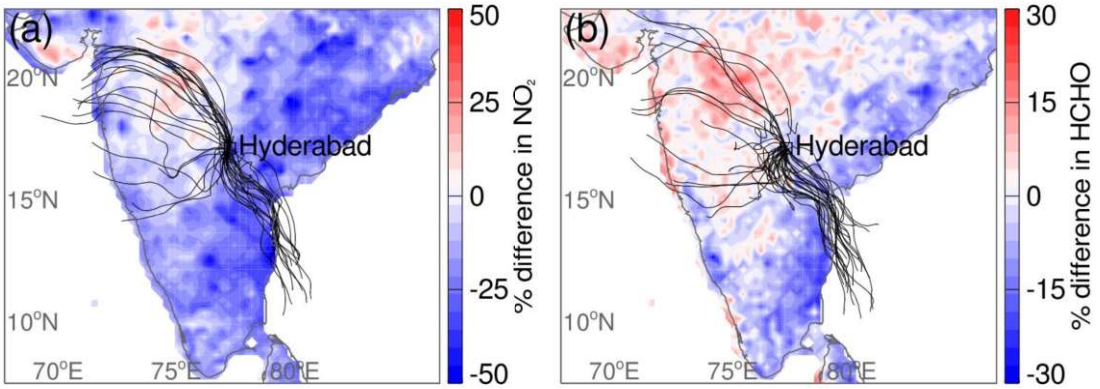

Figure 3.8. Spatial distribution of percentage difference in TROPOMI-retrieved (a) tropospheric NO_2 column and (b) HCHO column between LCD and BAU time periods. The measurement site, Hyderabad, is shown by the open square symbol. Three-day air mass backward trajectories starting at 11:30 a.m. local time during (a) BAU and (b) LCD time periods are also shown.

We investigated the NPF&G characteristics (e.g., frequency, formation rate, growth rate, etc.) in Hyderabad, India, using particle number size distribution measurements from the COVID-19 lockdown (15 April - 31 May 2020, hereafter referred to as LCD) and the previous business-as-usual year (15 April - 31 May 2019, hereafter referred to as BAU). Figure 3.8 depicts the location of Hyderabad on a regional map, as well as the averaged percentage difference in the TROPOMI retrieved NO_2 and HCHO column between the LCD and BAU time periods. When compared to BAU time periods, NO_2 and HCHO concentrations were reduced by 10%-30% during LCD. Hyderabad had air masses from the northwest and southeast, with the southeast being more frequent during LCD than BAU.

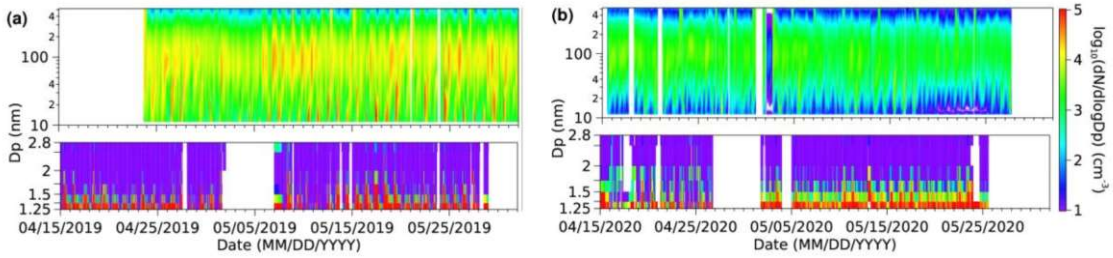

Figure 3.9. Time evolution of particle number size distributions in the size range of 1.2–3.0 nm from nCNC and 10–514 nm from SMPS during (a) BAU and (b) LCD time periods (15 April–31 May).

Figure 3.9 depicts the time evolution of particle size distributions in the 1.2-3.0 nm range from nCNC and 10-514 nm range from SMPS under BAU and LCD in the same time period (15 April to 31 May). This time period was chosen to demonstrate the impact of anthropogenic emission reductions caused by the lockdown. There is a clear gradient in particle size

distributions between BAU and LCD, with 5%-98% lower particle number concentrations during LCD. The time evolution of particle number size distributions demonstrated that NPF events occurred more frequently under BAU than during LCD. Almost every day during the BAU and LCD time periods, particle bursts in the sub-3 nm size range were seen which was also seen in our previous study during spring and early monsoon (April–June) (Sebastian et al., 2021a). only half of the observed particle burst events (NPF) demonstrated particle growth to greater sizes (>10 nm), indicating a regional NPF&G event (Sebastian et al., 2021a). It was seen that sulfuric acid concentrations, sub-3 nm growth rates, condensation sink, sub-3 nm coagulation sink, and atmospheric conditions were all the same between NPF and NPF&G event days.

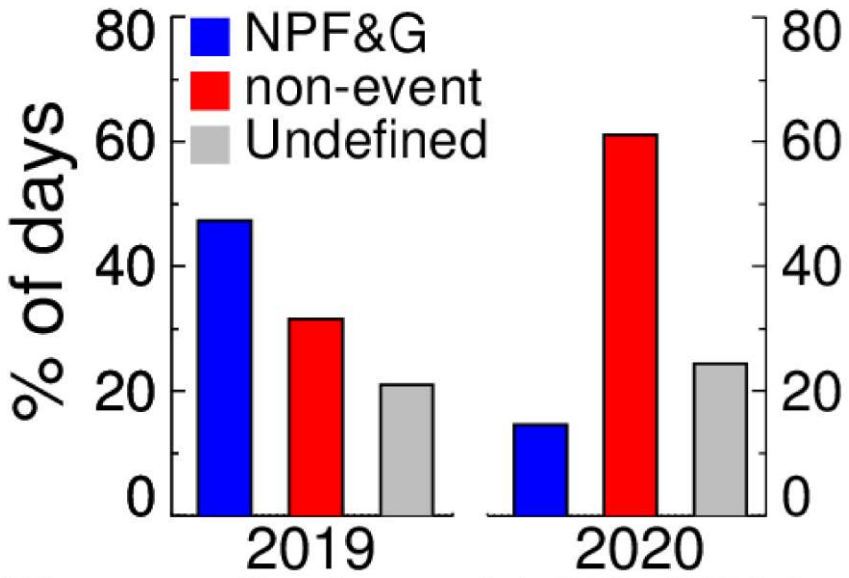

Figure 3.10. The percentage of days of event type during BAU and LCD in the same time period

Figure 3.10 depicts the percentage of days of each event category during the BAU and LCD time periods. The valid observation days for BAU and LCD were 38 and 41, respectively. During BAU and LCD, NPF&G events occurred on 18 (47%) and 6 (15%) of the total valid observation days, respectively. Non-events occurred on 12 (32%) and 25 (61%) and undefined events occurred on 8 (21%) and 10 (24%) days, respectively during BAU and LCD. The frequency of occurrence of NPF&G events was three-fold lower under the primary emission reductions during LCD compared to BAU. The NPF&G is influenced by a variety of elements, including the location's topography, pre-existing particles, the availability of nucleating and condensable vapours, and micro-meteorological circumstances (Nieminen et al., 2018). Some

of these aspects are discussed further below in order to explain the lower frequency of NPF&G events during LCD.

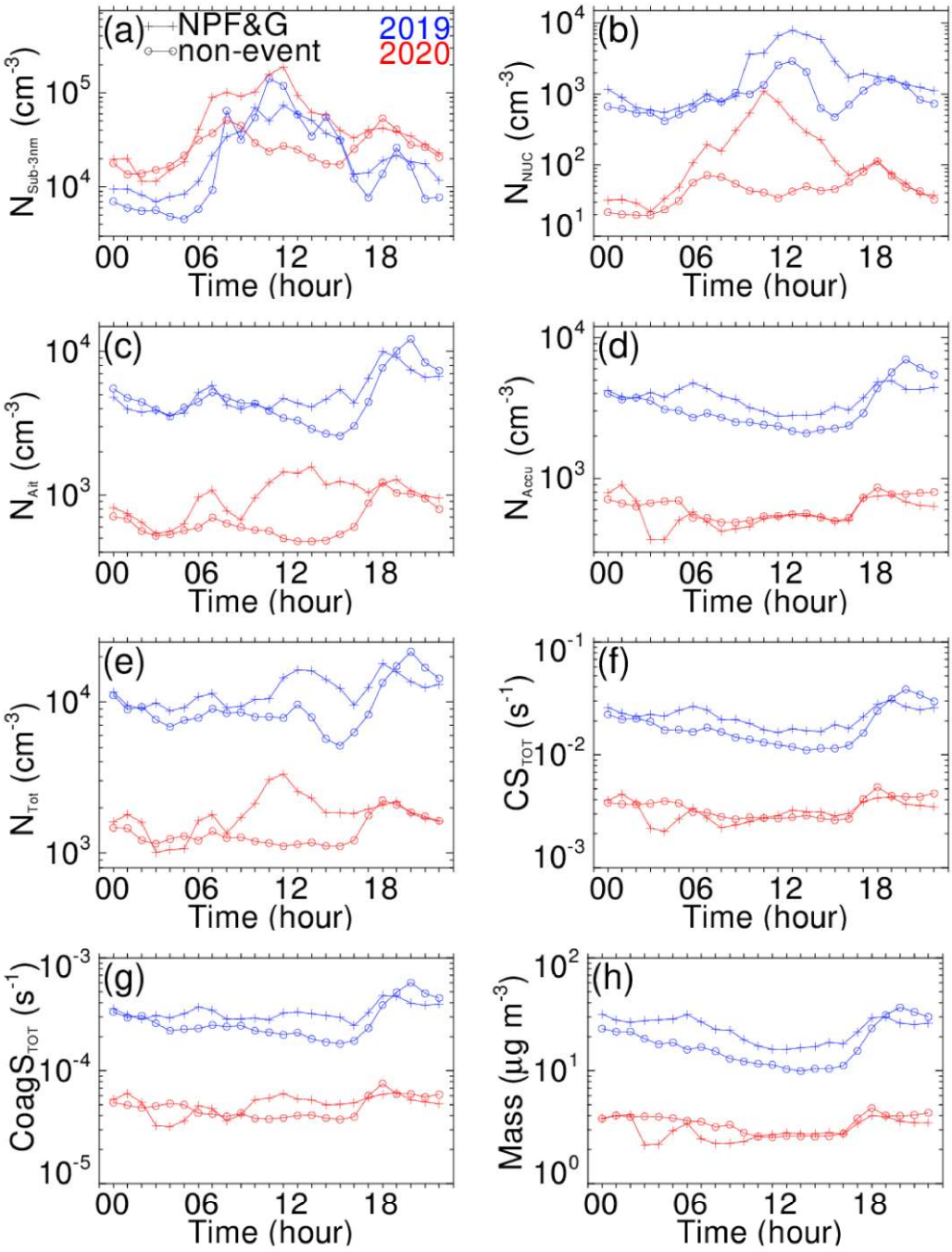

Figure 3.11. Median diurnal variation of (a–e) size-segregated particle number concentrations, (f) total condensation sink (CS_{TOT}), (g) total coagulation sink ($CoagS_{TOT}$), and (h) total aerosol mass for NPF&G (line connected by plus symbol) and non-events (line connected by open circle) during BAU (blue) and LCD (red). Mann-Whitney *U*-test showed statistically significant differences ($p << 0.05$) for all variables between BAU and LCD except for sub-3 nm particles during non-event event days ($p = 0.063$).

It was seen that $N_{sub\text{-}3nm}$ concentrations were consistent between NPF&G and non-event days as well as between BAU and LCD time periods (Figure 3.11a). This suggests that the reduction in primary anthropogenic emissions (aerosol precursors) during LCD at this site did not limit particle formation. However, on most days throughout LCD, these newly formed particles did not grow larger than 10 nm. N_{NUC} concentrations were greater on NPF&G event days than on non-event days during both BAU and LCD. were higher on NPF&G event days than non-event days both during BAU and LCD. Furthermore, N_{NUC} were nearly an order of magnitude lower under LCD than during BAU (Figure 3.11b). N_{AIT}, N_{ACCU}, N_{TOT}, CS_{TOT}, $CoagS_{TOT}$ and total aerosol mass concentrations were similarly lower under LCD than during BAU (Figures 3.11c-5h).

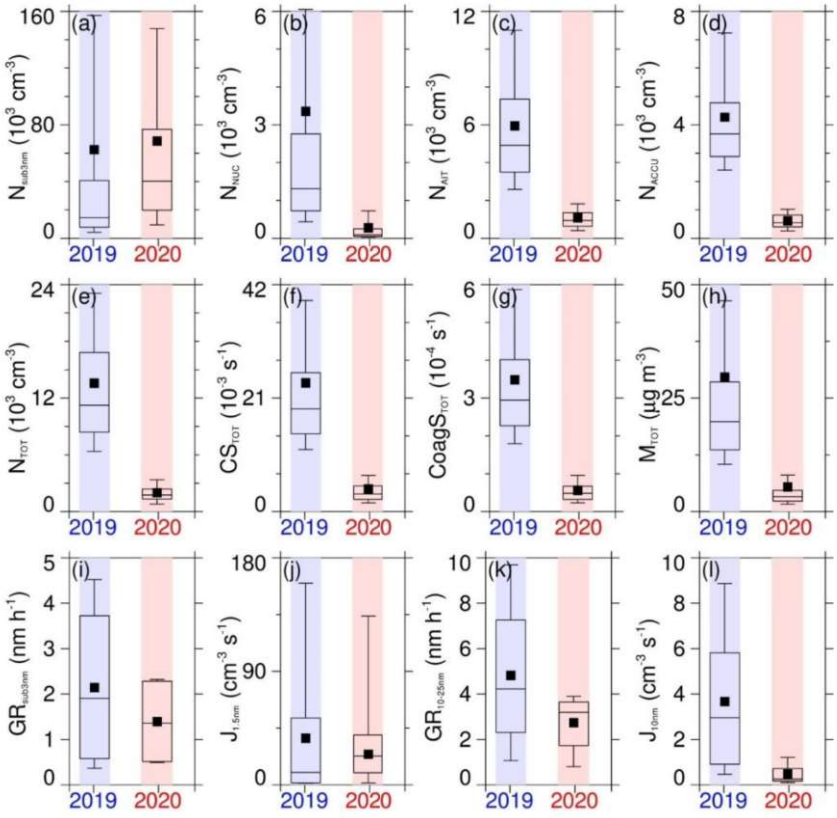

Figure 3.12. Box-whisker plot of NPF&G characteristics during BAU and LCD; (a) $N_{sub\text{-}3nm}$, (b) N_{NUC}, (c) N_{AIT}, (d) N_{ACCU}, (e) N_{TOT}, (f) CS_{TOT}, (g) $CoagS_{TOT}$, (h) M_{TOT}, (i) $GR_{sub\text{-}3nm}$, (j) $J_{1.5nm}$, (k) $GR_{10\text{-}25nm}$, and (l) J_{10nm}. The black square symbol indicates the mean, the horizontal line indicates the median, the bottom and top of the box indicate 25th and 75th percentile values, respectively, and the bottom and top of the whisker indicate the 10th and 90th percentile values, respectively.

Figure 3.12 depicts an analysis examination of several NPF&G parameters during the BAU and LCD time periods. The variability in sub-3nm particle number concentrations was similar

between BAU and LCD (Figure 3.12a). Sub-3nm particle growth rates were marginally lower under LCD than during BAU (Figure 3.12i). $GR_{10\text{-}25nm}$ was two times lower during LCD than during BAU (Figure 3.12k). The mean $J_{1.5}$ ranged from 1.34 to 178.1 cm^{-3} s^{-1}, with a mean value of 36.85±6.9 cm^{-3} s^{-1} during BAU, which is close to LCD time periods (24.3±19.2 cm^{-3} s^{-1}). In general, the mean formation rates of sub-3nm particles were similar between BAU and LCD, whereas J_{10} was nearly 85% lower during LCD (0.5±0.4 particles cm^{-3} s^{-1}) compared to BAU (3.7±3.6 cm^{-3} s^{-1}). The size-segregated particle number concentrations, coagulation sink, condensation sink, and total mass were much lower under LCD than during BAU (Figure 3.12b-h). Figure 3.13 depicts the median diurnal variations of air pollutants including NH_3, SO_2, carbon monoxide (CO), NO_x, O_3, and $PM_{2.5}$, and ratios of aromatic hydrocarbons such as xylene to benzene ratio (X/B) and toluene to benzene ratio (T/B). SO_2 concentrations were similar between NPF&G and non-event days during LCD and BAU (Figure 3.13a), supporting our finding of similar sub-3nm particle formation and growth rates (Figure 3.12). Because, sulfuric acid, produced by SO_2 oxidation, clusters with other vapours like ammonia, amines, and organics for particle formation (Almeida et al., 2013; Kirkby et al., 2011; Schobesberger et al., 2013; Yu et al., 2012) and growth (Vakkari et al., 2015; Yue et al., 2010). NH_3 concentrations were slightly lower during LCD than BAU, especially on NPF&G event days (Figure 3.13b).

Interestingly, LCD had somewhat higher but less variable daytime NOx values than BAU. Photochemical reactions from NOx yield O_3, which was higher than LCD during BAU. While NPF&G events had higher O_3 than non-events during BAU, they had lower O_3 during LCD. CO and $PM_{2.5}$ concentrations were considerably lower under LCD than BAU, as expected. Benzene, toluene, and xylene, which are precursors to secondary organic aerosols, are common in urban air (Molteni et al., 2018). The toluene to benzene ratio (T/B) indicates traffic emissions if it lies between 1.5 and 3.0 (Khoder, 2007; Lee et al., 2002). Industrial emissions are indicated by T/B ratios above 4.5 (Tiwari et al., 2010). The xylene-to-benzene ratio (X/B) indicates the photochemical age of the air mass (Zhang et al., 2008b) X/B ratio values less than 3.0 indicates aged plumes (Tiwari et al., 2010). During BAU, the T/B ratio values were well within the range of 1.5 – 3.0 on both NPF&G and non-event days, indicating traffic-dominated emission sources. During LCD, they sharply increased, indicating emission sources from essential services like power plants and petrochemical industries. The X/B ratio was around 0.5 on NPF&G and non-event days during BAU and LCD, indicating aged air mass plumes at the site. A recent study observed fast secondary inorganic aerosol formation (mainly nitrate, >80%) in

aged Shanghai plumes during the lockdown, but regional transit limited atmospheric new particle formation and growth (Chang et al., 2020). The above discussion shows that sub-3nm particle formation was not limited by the reduction in primary anthropogenic emissions during LCD, but regional NPF&G events were reduced, possibly due to lower condensable vapour concentrations from decreased primary emissions (e.g., vehicular emissions). NPF&G is also greatly influenced by atmospheric conditions (Kanawade et al., 2012; Stanier et al., 2004a), as discussed below.

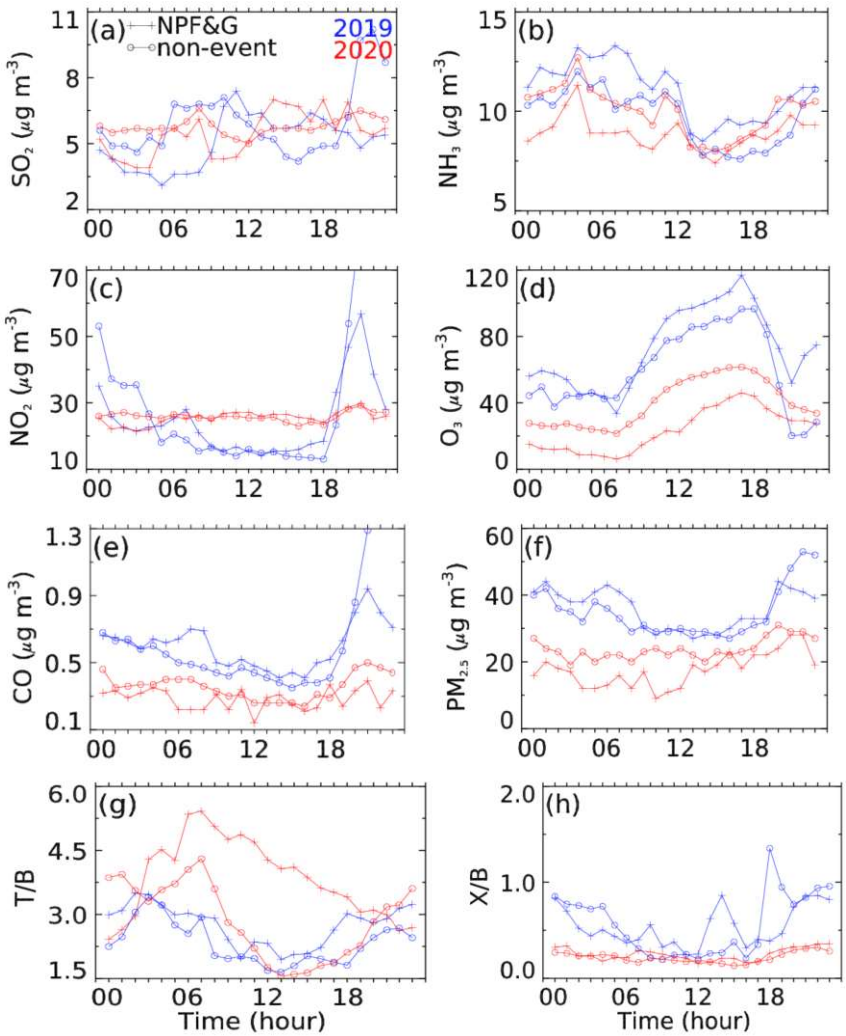

Figure 3.13. Median diurnal variation of (a) sulfur dioxide, (b) ammonia, (c) oxides of nitrogen, (d) ozone, (e) carbon monoxide, (f) $PM_{2.5}$, (g) T/B ratio, and (h) X/B ratio for NPF&G and non-events during BAU and LCD.

The median diurnal variation in temperature, relative humidity, wind speed, wind direction, and solar radiation is shown in Figure 3.14. LCD had 5-7° C lower air temperature than BAU. At lower temperatures, oxidation is low and gas phase highly oxygenated products for condensational growth are low (Stolzenburg et al., 2018), reducing LCD particle growth. On

NPF&G event days during LCD, RH was 3-6% higher than BAU. LCD and BAU NPF&G events may not have been affected by this minor difference. NPF&G event days during BAU had slightly higher wind speed than LCD. Pushpawela et al. (2019) found that high wind speed removes pre-existing particles in urban areas, enhancing NPF&G. LCD and BAU had similar wind and sun radiation on NPF&G event days. The above discussion suggests that lower temperature and wind speed may have reduced NPF&G frequency at this site during LCD.

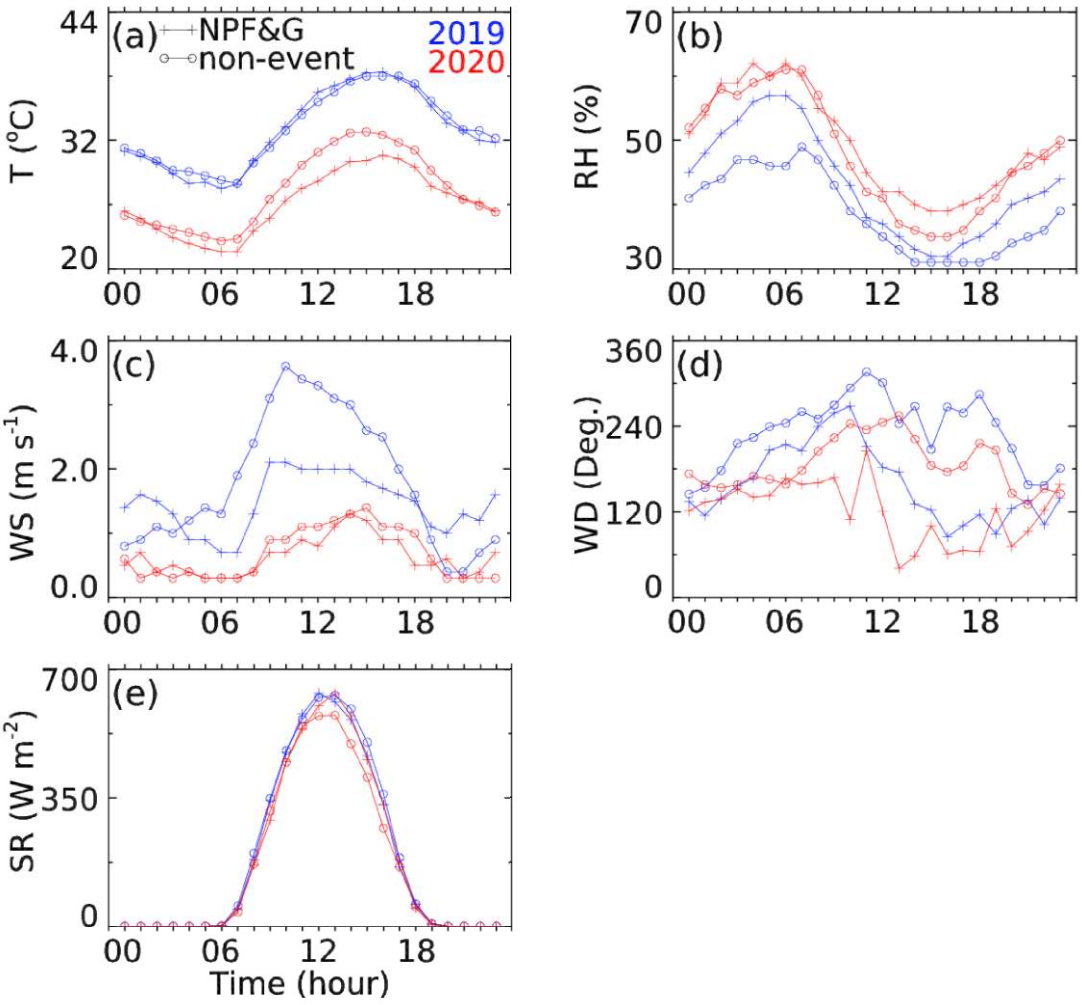

Figure 3.14. Median diurnal variation of (a) temperature, (b) relative humidity, (c) wind speed, (d) wind direction, and (e) solar radiation for NPF&G and non-events during BAU and LCD.

A study also showed the reduction of about 70% of ultrafine particle number concentrations at an urban background site in Pittsburgh, Pennsylvania during lockdown when compared with the mean value based on 15 years (Saha et al., 2018). Another study on two sites (urban background and coastal) in Southern Italy based on long-term (2015-2019) and 2020 in the

same periods also showed 6–53% and 2–17% reductions in nucleation mode and Aitken mode particle number concentrations during lockdown, respectively (Dinoi et al., 2021). In an urban environment (Raleigh, NC, USA), the COVID-19 lockdown reduced particle concentrations between 10 and 40 nm by 32% (Zimmerman et al., 2020). We also found 85% reductions in ultrafine particle number concentrations in Hyderabad. On the contrary, a recent study in Himalayan coniferous forests in India found that greater O_3 concentration boosted the photochemical oxidation of biogenic VOCs, doubling secondary organic production during the COVID-19 shutdown (Chatterjee et al., 2021). Recent studies from China also indicated increased secondary aerosol formation during COVID-19 lockdowns with reduced anthropogenic emissions (Huang et al., 2021; Le et al., 2020; Shen et al., 2021; Sun et al., 2020; Zhong et al., 2021).

Due to active photochemistry and high solar radiation, NPF&G events frequently occur in spring (March-April-May) (Birmili et al., 2000). However, NPF&G occurrence was reduced by three-fold during LCD than BAU. NPF normally begins with SO_2+OH in most settings. However, sulfuric acid clusters need NH_3, ELVOCs, and air to stabilize (Kirkby et al., 2016; Sipilä et al., 2016). Condensable vapours from VOC oxidation reactions with O_3 and OH contribute to particle growth (Paasonen et al., 2018), but the lower temperature by about 5-7^o C implicates the reduced levels of OH and thus sulfuric acid and other condensable vapour production during lockdown. This shows that weather variations can also affect concentrations of chemical species required for NPF&G The lower O_3 and OH contents reduce the production of low-volatility organic vapours for particle growth by condensation, preventing regional NPF&G occurrences.

3.3.5 Characteristics of particle number size distributions and new particle formation events

In this section, we will be analysing the characteristics of particle number size distribution and new particle formation in six locations in India (Ranichauri (RNC), Mukteshwar (MUK), Mahabaleshwar (MBL), Hyderabad (HYD), Thiruvananthapuram (TVM), and Delhi (DEL)) to identify the characteristics of particle number size distributions. Among the urban areas (HYD, TVM, and DEL), TVM exhibits the highest mode diameter which is often attributed to the presence of marine air masses that carry high moisture and coarse sea salt aerosols (Babu et al., 2016) (Figure 3.15a). The highest particle number size distribution is observed during the pre-

monsoon season (MAM) at mountain background sites RNC and MUK (Figure 3.15b-c). The median particle number size distribution of particles at HYD exhibits its highest values during the pre-monsoon (MAM) and post-monsoon (ON) periods attributed to new particle formation (Figure 3.15e). The particle number size distribution exhibits a consistent decrease during the monsoon season, which is due to wet scavenging. At the DEL, the mode diameter of particle number size distributions is the highest during the winter (DJF) season which is due to the shallow boundary layer height, stagnant atmospheric conditions, and elevated emission rates of aerosol precursors (Kanawade et al., 2020a). The observed patterns of strong seasonality in particle number size distributions are in resemblance to previous findings from India (Gani et al., 2020; Hooda et al., 2018; Kanawade et al., 2014b; Komppula et al., 2009). We have also calculated the modal parameters for all the curves in Figure 3.15 and listed in Table 3.2. These parameters will be of great benefit in modelling the seasonal particle number size distributions at different types of locations in India.

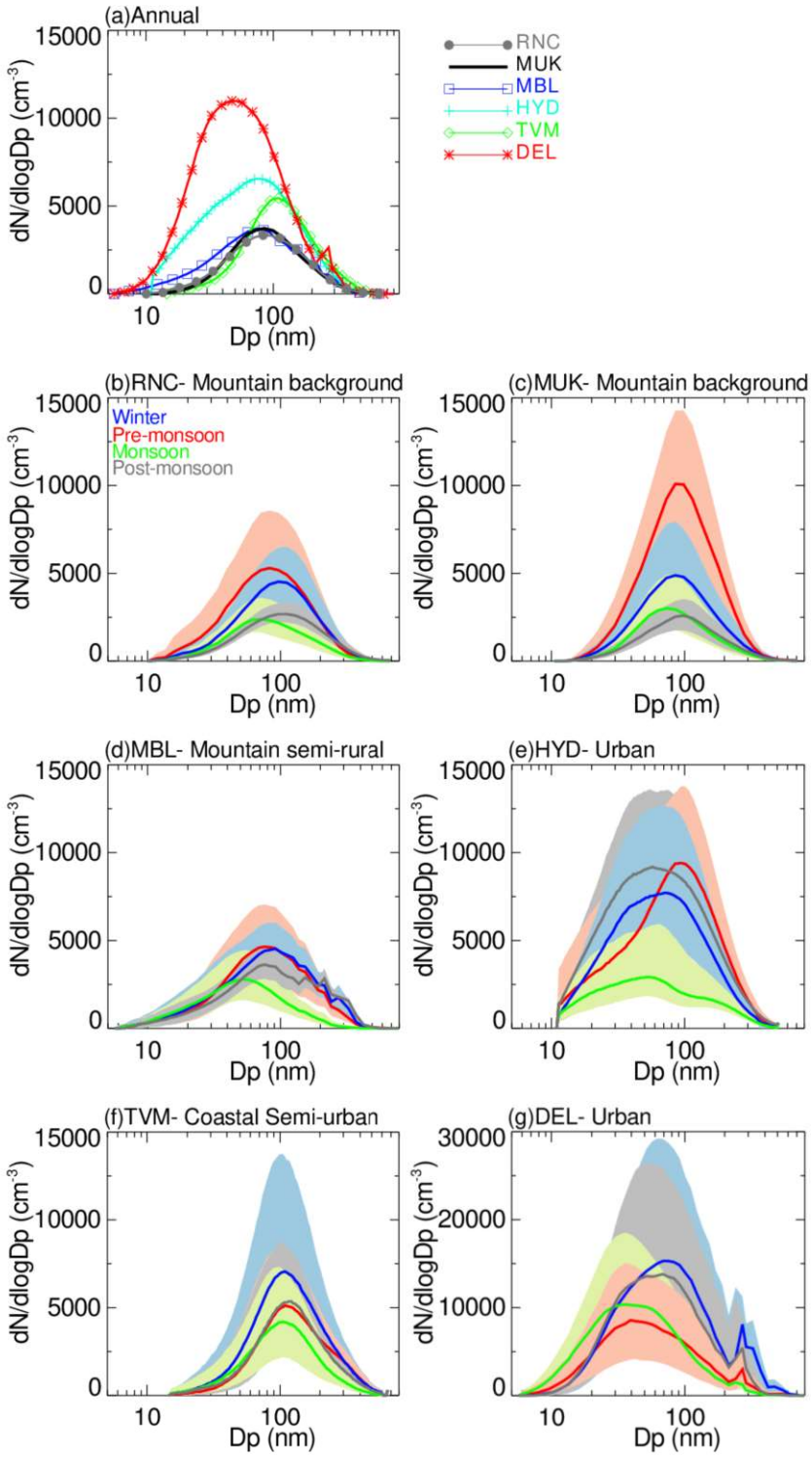

Figure 3.15 (a) Annual and (b-g) seasonal median particle number size distributions at all the sites. The solid line indicates the median, and the light-colored shading indicates the 25th and 75th percentile distributions. The blue line and shading indicate winter (DJF), red line and shading indicate pre-monsoon (MAM), green line and shading indicate monsoon (JJAS), and grey line and shading indicate post-monsoon season (ON). Note that the y-axis scale is different for the DEL site.

Table 3.2 Parameters of the modes identified for the description of median particle number size distributions are shown in Figure 3.15. N, Dp and σ are the number concentration, geometric mean diameter and the standard deviation of the distribution.

	Uni-modal			**Bi-modal**					
Site	N (cm^{-3})	Dp (nm)	σ	N_1 (cm^{-3})	Dp_1 (nm)	σ_1	N_2 (cm^{-3})	Dp_2 (nm)	σ_2
Annual									
RNC	2555	87.5	2.0	591	49.3	1.9	1963	101.8	1.9
DEL	9670	50.9	2.2	8237	44.9	2.0	1465	121.3	1.9
HYD	6401	63.4	2.5	2097	27.3	1.8	4186	90.0	1.9
MBL	3166	74.2	2.3	3104	72.9	2.2	48	197.3	1.2
MUK	2573	85.5	1.9	301	65.1	1.5	2276	90.5	1.9
TVM	3463	111.2	1.8	3379	109.6	1.8	85	330.8	1.3
Winter									
RNC	3205	94.6	1.9	876	53.0	1.9	2357	109.2	1.8
DEL	13555	68.7	2.3	12878	65.9	2.1	678	298.0	1.2
HYD	7314	61.1	2.3	3165	33.9	1.8	3990	95.2	1.8
MBL	3817	84.4	2.3	4877	100.2	2.6	789	319.4	0.6
MUK	3374	86.0	1.9	3344	85.5	1.9	28	256.0	1.2
TVM	4437	113.2	1.8	4266	110.6	1.8	169	320.0	1.3
Pre-Monsoon									
RNC	4012	81.2	2.0	2721	64.6	1.9	1280	118.7	1.7
DEL	7708	49.8	2.3	4622	35.8	1.9	3093	96.0	2.1
HYD	7726	82.0	2.2	1858	24.5	1.8	6007	98.7	1.8
MBL	3702	78.6	2.1	5034	100.5	2.4	1342	228.3	0.5
MUK	6488	91.1	1.8	1748	62.5	1.9	4760	101.4	1.7
TVM	3241	122.4	1.8	2933	115.3	1.7	282	313.0	1.3
Monsoon									
RNC	1774	78.4	2.0	85	58.3	1.3	1693	81.1	2.0
DEL	9336	40.2	2.2	5059	27.4	1.9	4194	66.8	1.9
HYD	3141	49.2	2.8	2844	45.4	2.5	210	196.9	1.4
MBL	2187	50.3	2.1	1960	47.8	2.3	255	58.9	1.4
MUK	1984	79.4	1.9	1765	73.9	1.7	223	199.5	1.5
TVM	2603	103.4	1.8	1565	93.5	2.1	1109	110.1	1.6
Post-Monsoon									
RNC	2072	102.0	2.0	441	52.0	1.8	1629	118.7	1.9
DEL	12152	60.6	2.2	11881	59.5	2.1	286	263.9	1.1
HYD	9949	58.7	2.5	9335	57.5	2.5	123	157.5	1.3
MBL	3277	88.5	2.4	2937	79.4	2.2	289	237.6	1.3
MUK	1782	93.7	1.9	1743	93.3	2.0	50	99.0	1.2
TVM	3176	117.5	1.8	3099	116.2	1.7	86	360.7	1.3

To infer the spatial and temporal heterogeneity in particle number concentrations, we have calculated the relative frequency of number concentrations of size-segregated particles (Figures 3.16 and 3.17). The mountain background sites RNC and MUK exhibit a comparable seasonality in the histograms of number concentration for Aitken mode particles with the highest concentration observed during the pre-monsoon (MAM). This is attributed to the frequent occurrence of new particle formation at these mountain sites these mountain-background sites during the season. Aitken mode particle concentration is the lowest during monsoon (JJAS) and post-monsoon (ON) seasons due to wet-scavenging. The urban environments of HYD, TVM, and DEL exhibit distinct variations in the seasonal patterns observed in the histograms of Aitken mode particle number concentrations. DEL exhibits the highest concentrations of Aitken mode particles during the winter (DJF) and post-monsoon (ON) seasons. On the other hand, TVM experiences the highest particle concentrations during winter (DJF). HYD has similar number concentrations during the winter (DJF), pre-monsoon (MAM), and post-monsoon (ON) seasons. The elevated Aitken mode number concentrations observed during winter (DJF) in urban areas can be attributed to the stagnant atmospheric conditions prevailing during this time. Figure 3.17a-f displays the histograms depicting the relative occurrence of accumulation mode particle number concentrations at all 6 sites. The number concentration histograms of accumulation mode particles at MUK exhibit similarities to those of Aitken mode particles. MBL has similar histograms of accumulation mode number concentrations during the winter (DJF), pre-monsoon (MAM), and post-monsoon (ON) seasons, with the lowest concentrations observed during the monsoon (JJAS) season. This decrease in concentrations during the monsoon can be attributed to the wet scavenging. RNC shows a similar number concentration histograms for accumulation mode particles during winter (DJF) and pre-monsoon (MAM) seasons, as opposed to exhibiting dissimilar histograms for Aitken mode particles. Among the urban sites, DEL exhibits the highest concentrations of accumulation mode particles during the post-monsoon (ON) and winter (DJF) seasons. TVM and HYD show the highest concentrations of accumulation mode particles during the winter (DJF) and post-monsoon (ON) seasons, respectively. The variation in the seasonal patterns observed in the histograms of Aitken and accumulation mode particle concentrations can be attributed to variations in atmospheric conditions, including prevailing synoptic air masses, mesoscale processes such as atmospheric boundary layer dynamics, and particle removal processes.

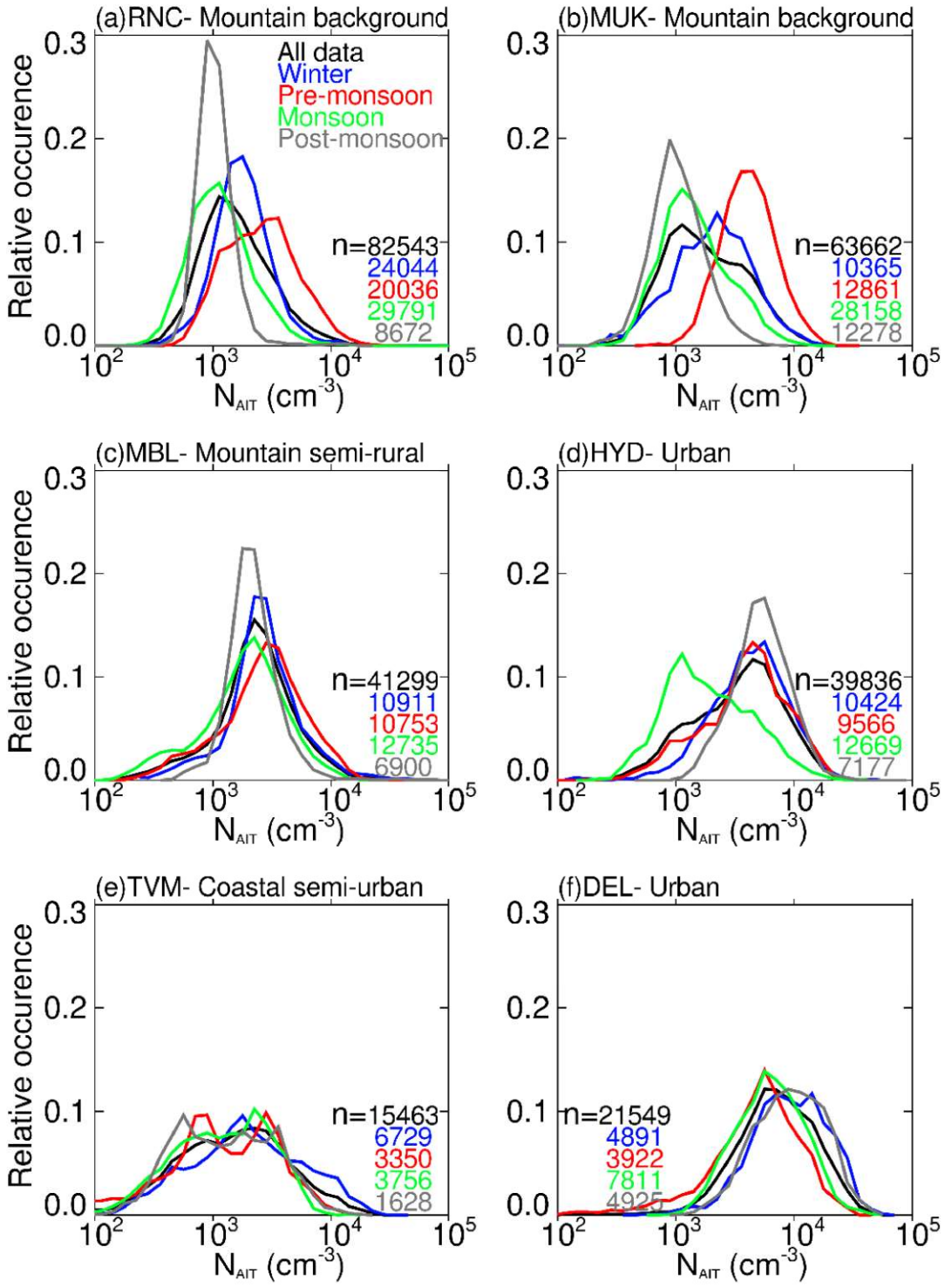

Figure 3.16 Histogram of the relative occurrence of Aitken mode particle number concentrations at the sites. The concentration bins are logarithmically spaced in the x-axis, and the y-axis shows the relative occurrence of values in each bin compared to the total number of valid observations. The black, blue, red, green, and grey lines indicate all data, winter (DJF), pre-monsoon (MAM), monsoon (JJAS), and post-monsoon (ON), respectively. n indicates the number of 10-minute averaged valid data points. Note that measurements are from different time periods for each site (refer to Table 2.1).

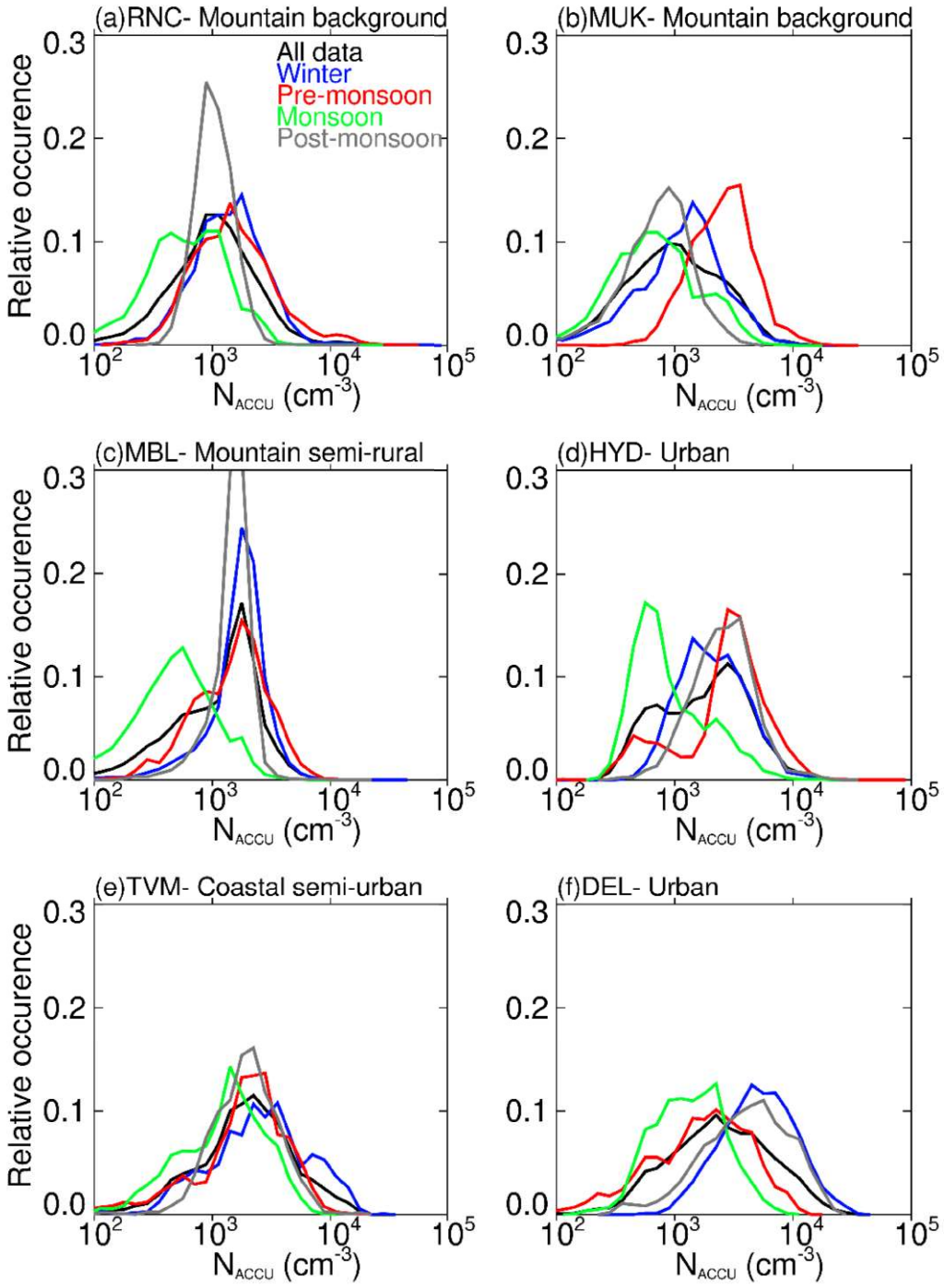

Figure 3.17 Histogram of the relative occurrence of accumulation mode particle number concentrations at the sites. The concentration bins are logarithmically spaced in the x-axis, and the y-axis shows the relative occurrence of values in each bin compared to the total number of valid observations. The black, blue, red, green, and grey lines indicate all data, winter (DJF), pre-monsoon (MAM), monsoon (JJAS), and post-monsoon (ON), respectively. n indicates the number of 10-minute averaged valid data points. Note that measurements are from different time periods for each site (refer to Table 2.1).

Table 3.3 Number of valid observation days, number of NPF days (percentage), number of non-event days (percentage), mean formation rates and mean growth of particles at all six sites in India. ± indicates standard deviation.

Site	valid observation days	NPF days	non-event days	J_{LDS} (cm^{-1} s^{-1})	$GR_{LDS\text{-}25\ nm}$ ($nm\ h^{-1}$)
RNC	586	21 (3.9%)	493 (83.7%)	0.11±0.05	6.3±2.4
MUK	440	13 (2.9%)	321 (73.1%)	0.04±0.02	2.5±1.6
MBL	281	16 (5.9%)	188 (66.1%)	0.04±0.02	4.7±3.0
HYD	270	38 (16.3%)	124 (44.8%)	0.13±0.11	5.7±3.6
TVM	133	23 (16.6%)	55 (41.4%)	0.007±0.005	1.1±1.1
DEL	139	39 (28.1%)	30 (21.1%)	0.13±0.10	3.7±2.1

The valid days of observation were categorized into three distinct types: NPF event day, non-event day, and undefined event day by visually inspecting contour plots of particle number size distributions following the methodology given by (Dal Maso et al., 2005). NPF frequently occurs in the pre-monsoon (MAM) and infrequently during winter (DJF) (Dal Maso et al., 2005; Kanawade et al., 2012; Nieminen et al., 2018). NPF events were also observed frequently during thermal winter (Kulmala et al., 2004; Pikridas et al., 2012) and fall (September, October, and November) (Rodríguez et al., 2005). These studies suggest that the occurrence of NPF events does not follow a universal pattern. Figure 3.18 shows the distribution of NPF event, non-event, and undefined event days. The frequencies of NPF occurrence at all six sites are documented in . The frequency of NPF is the highest during the pre-monsoon (MAM) season when compared to other seasons. Mountain-background sites (RNC and MUK) showed the lowest frequent occurrence of NPF throughout the year, with average annual frequencies of 3.9% and 2.9% respectively. We observed highest frequency of NPF events during the pre-monsoon (MAM) season at these sites which was also observed in previous studies (Neitola et al., 2011; Sebastian et al., 2021b). The upward movement of the planetary boundary layer to the elevation of the measurement site, facilitates the transport of aerosol precursors from nearby polluted regions at lower altitudes (Hooda et al., 2018; Raatikainen et al., 2014). NPF occurs at a lower frequency at RNC and MUK compared to MBL and the high-altitude sites in Europe (Nieminen et al., 2018). NPF is the most frequent in DEL during pre-monsoon (MAM) (63.8%) followed by HYD (28.4%) and MBL (15.9%). TVM coastal semi-urban site experiences frequent NPF events due to the influence of continental air masses. NPF occurred with the highest frequency during post-monsoon (ON) in TVM which is attributed to the mixing of different air masses resulting from the combined influence of mesoscale land-sea breeze

circulation and local atmospheric boundary layer (ABL) dynamics (Babu et al., 2016). The occurrence of NPF at rural sites is influenced by meteorological conditions (solar radiation and relative humidity) but in urban areas, the occurrence of NPF is more closely associated with higher concentrations of precursor gases and the decrease in pre-existing particle concentration by dilution (Bousiotis et al., 2021; Kanawade et al., 2020b; Kanawade et al., 2014c; Kulmala et al., 2021). This suggests that the ratio of precursor concentration to pre-existing particles is a crucial factor in the occurrence of NPF.

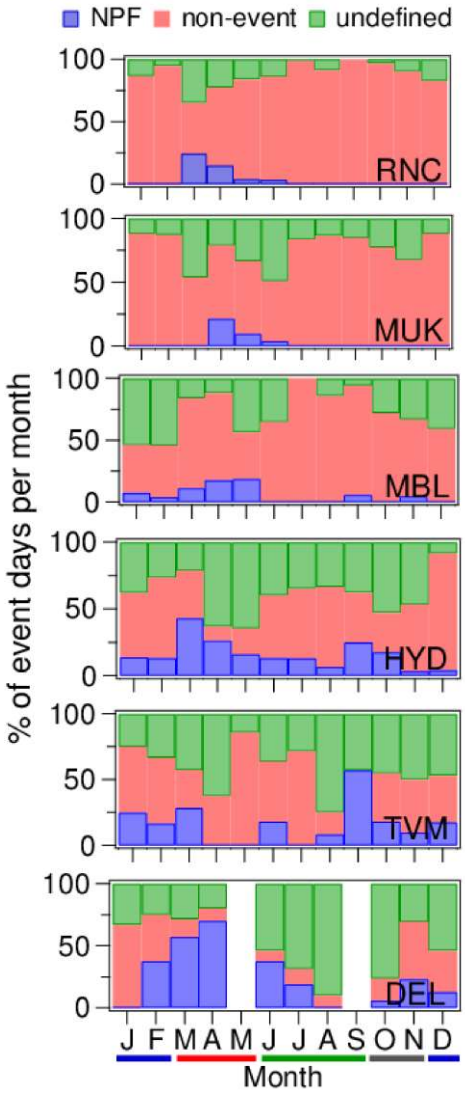

Figure 3.18 Monthly percentage of occurrence of NPF, non-event, and undefined events days based on total valid observation days at all the sites. The thick blue, red, green, and grey lines indicate winter (DJF), pre-monsoon (MAM), monsoon (JJAS), and post-monsoon (ON) months. Note that measurements are from different time periods for each site (refer to Table 2.1).

The scatter plot illustrating the relationship between the J_{SDS} and the $GR_{SDS-25nm}$ identifies a positive correlation (Pearson correlation coefficients of 0.48, 0.78, 0.85, 0.33, 0.68, and 0.18 at RNC, MUK, MBL, HYD, TVM, and DEL, respectively) between them (Figure 3.19). The average condensation sink at the onset of the NPF events observed at urban sites (16.1×10^{-3} s^{-1}) was found to be twice as high as that observed at mountain sites (7.9×10^{-3} s^{-1}). A similar result was observed in Kanpur where higher concentrations of pre-existing particles in Kanpur, as compared to Pune, inhibited the particle formation rates (Kanawade et al., 2014c). The large scatter of data points in Figure 3.19 suggest the varying factors influencing NPF events, such as aerosol nucleation mechanisms (Dunne et al., 2016), the availability of condensable vapours (Kirkby et al., 2011; Schobesberger et al., 2015), and atmospheric conditions (Bousiotis et al., 2021). The average rates of particle formation and growth for each of the six locations are presented in Table 3.3. Across all observed locations, the growth rate of $GR_{SDS-25nm}$ during NPF events exhibited a range of 0.2 to 17.2 nm h^{-1}. In various environments in India and other locations, J_{SDS} and $GR_{SDS-25nm}$ exhibit values that fall within the wide range of observations (Kerminen et al., 2018; Kulmala et al., 2004).

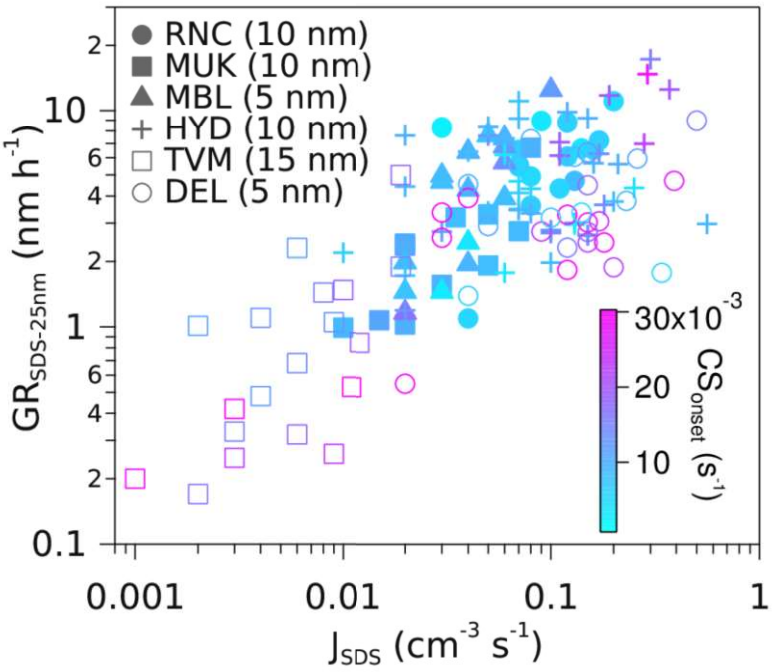

Figure 3.19 Scatter plot of the particle formation rate and the growth rate as a function of the condensation sink at each site. The condensation sink at the start of the event (CSonset) is taken as a 1 h average CS just before the start of the NPF event. The smallest detectable size (SDS) of the nucleation mode at each site is shown in the bracket. Note that measurements are from different time periods for each site (refer to Table 2.1).

3.4 Summary

This chapter presents the first observational evidence of sub-3nm aerosol particles in India, emphasizing their seasonal characteristics and new particle formation events. The study focuses on size-segregated particle number concentration across different modes, revealing that cluster mode particles constitute the majority of the total particle number concentration. The study expands to six sites across diverse Indian environments, highlighting variations in particle number size distributions and NPF characteristics. Urban areas like TVM stand out due to marine air masses influencing larger mode diameters and inflow of continental air masses providing low-volatile vapours for nucleation during late monsoon. Mountain sites experience higher particle number concentrations in pre-monsoon (MAM) owing to the frequent occurrence of NPF events. Winter (DJF) experiences the least NPF occurrences, particularly at mountain background sites (RNC and MUK). High solar insolation and an elevated boundary layer explain the frequent occurrence of NPF during pre-monsoon (MAM) at mountain background sites. A case study of the COVID-19 lockdown showed that the reduction in primary anthropogenic emissions did not inhibit the formation of sub-3nm particles, but the frequency of occurrence of the NPF and growth events was three-fold lower during the lockdown as compared to the Bussiness-as-usual time periods. The spatial variability in particle number size distributions reflects diverse aerosol loading processes, with Aitken mode concentrations highest in pre-monsoon (MAM) at mountain sites and in winter (DJF) at urban sites. Regional new particle formation significantly influences atmospheric particle evolution, modulating particle size distributions, particularly at mountain background sites unaffected by local aerosol emissions. Notably, new particle formation events have a significant impact on particle size distribution, especially in mountain-background sites, emphasizing the intricate interplay of environmental factors and geographical influences on particle formation and distribution in diverse Indian regions.

Chapter 4

Influence of airmass history on new particle formation events

4.1 Introduction

Atmospheric NPF events have been observed in diverse environments globally such as rural/remote, polluted, coastal/marine, agricultural/forested, mountainous, free troposphere, and cloud outflow, more frequently within the atmospheric boundary layer (Andreae et al., 2022; Kanawade et al., 2021; Kerminen et al., 2018; Kulmala et al., 2004; Lee et al., 2019; Nieminen et al., 2018; O'Dowd and Hoffmann, 2005; Olin et al., 2022; Sellegri et al., 2019; Xiao et al., 2021; Zhang et al., 2012). NPF is a non-linear dynamical process and its occurrence is strongly dependent on several factors such as the nature of geographical location and surroundings, the nature and magnitude of precursor gases, the abundance of pre-existing particles, atmospheric condition (temperature, relative humidity, wind speed, solar radiation), and prevailing dynamical conditions (low/high-pressure system and synoptic-scale circulations) (Babu et al., 2016; Clarke et al., 1998; Kerminen et al., 2018; Kompalli et al., 2020; Kulmala et al., 2012b; Pierce et al., 2014; Raes, 1995; Wang et al., 2017; Xiao et al., 2021). Our understanding of NPF events is largely based on determining the particle formation and growth rates from ambient measurements of particle number size distribution together with precursor vapours (Kulmala et al., 2012b) and subsequent efforts to reproduce those rates using models aided by laboratory experiments, to help interpret field measurements. While our knowledge of the driving factors of NPF has increased significantly over the past years (Kulmala et al., 2014; Kulmala et al., 2012b; Xiao et al., 2021; Zhang et al., 2012), the process-level understanding of physical or chemical transformation is still uncertain. Further, the stationary measurements are subject to the advection of air masses with varying origins over inhomogeneous surfaces as air masses travel in the atmosphere. The inhomogeneity in the surroundings of the stationary measurement site in terms of factors affecting the NPF can significantly modulate the particle number size distributions that cannot be explained by local atmospheric conditions even with the knowledge of locally contributing factors (Kivekäs et al., 2016).. Because the spatial surroundings of the stationary measurement site may not always be homogenous, particularly in anthropogenic urban settings. This can lead to ambiguity in the

estimation of NPF-induced modulation in particle number size distributions and the production of CCN-sizes particles which cannot be explained by locally affecting factors. Therefore, the process-level knowledge generated based on the stationary measurement site in remote open areas may not be applicable to the measurement site with significant spatial heterogeneity in the surroundings. Therefore, the particle number size distributions and NPF events can spatially differ within the anthropogenically influenced areas, and may not serve as the representative of the stationary site. This motivated to examine the role of the advection of air masses on the occurrence of NPF events at an anthropogenically influenced stationary measurement site, Hyderabad.

Several investigators showed that the origin of the air mass is important for characterizing aerosol properties of a measurement site (Brock et al., 2021; Dey et al., 2004; Nair et al., 2007; Satheesh et al., 2006; Shika et al., 2020; Tripathi et al., 2006; Tunved et al., 2005), which indicates that the occurrence of NPF events may also be influenced by air mass origin (Benson et al., 2008; Dada et al., 2022; Hakala et al., 2022; Kalkavouras et al., 2021; Kanawade et al., 2012; Nilsson et al., 2001; Rose et al., 2015; Sogacheva et al., 2007). Hakala et al. (2022) showed that NPF events occur in the cleaner air masses but the cleaner air mass mixing with anthropogenic emissions favours the growth of nucleated particles to large-sized particles in Beijing. The transport pathways and evolution of the boundary layer can substantially alter the volume of dilution for precursor gas and aerosol concentrations in the advected air mass which can enhance or reduce aerosol formation and growth (Huang et al., 2020). During winter, temperature inversions can inhibit the increase in boundary layer height, leading to the enhanced accumulation of pollution in close proximity to the surface (Kanawade et al., 2020a; Petäjä et al., 2016), which significantly deteriorates the dilution, thereby reducing aerosol formation. On the contrary, Mishra et al. (2023) revealed the rapid nocturnal particle growth (NPG) under the influence of biomass burning emissions, cold temperatures, high relative humidity, and shallow boundary layer height, while the daytime particle formation was completely absent in Delhi. This suggests that little or no vertical mixing inhibits the NPF, while the vertical mixing of precursor gases and particles in the residual layer favours particle formation (Hodshire et al., 2016). Babu et al. (2016) hypothesized that turbulent mixing of the pristine surface layer and precursor-laden residual layer results in the dilution of pre-existing particles which could trigger NPF under favourable conditions. Wu et al. (2007) also showed that NPF events occurred infrequently during summertime in North China Plain under the influence of stagnant and polluted air masses. The incursion of cold air masses associated with

a stagnant high-pressure system is also shown to favour the occurrence of NPF in Eastern China (Shen et al., 2018). Pierce et al. (2014) also found that NPF occurs frequently under the synoptic conditions associated with high-pressure systems and large-scale subsidence that causes clear sky conditions. Dada et al. (2022) illustrated that two-day intrusion caused drastic changes in the particle number size distribution, chemical composition, and particle hygroscopicity which resulted in extreme aerosol concentrations in the Arctic.

Previous studies show that stronger subsidence of free tropospheric air masses into the atmospheric boundary layer contributes to an increased ultrafine particle number concentrations mainly by two pathways; 1) the free troposphere can act as a reservoir for condensable vapours including those that emerged from convective outflows and can facilitate NPF (Clarke, 1993; Clarke and Kapustin, 2002; Clarke et al., 1998; Raes, 1995) and 2) during subsidence, the mixing of contrasting air masses can result in micro-scale variations in thermodynamic variables and thereby causing local supersaturation of precursor vapours which can trigger NPF events(Babu et al., 2016; Covert et al., 1996; Nilsson and Kulmala, 1998; Nilsson et al., 2001; Wehner et al., 2010). Later, Clarke et al. (2013) showed that the free troposphere acts as a significant source of CCN for the equatorial Pacific marine boundary layer. Recently, Kompalli et al. (2020) showed that nucleation mode particles formed in the free troposphere possibly entrained into the atmospheric boundary layer over the northern Indian Ocean through continental outflow. In the Indian context, except for two studies (Babu et al., 2016; Kompalli et al., 2020), the influence of free tropospheric air mass intrusion into the atmospheric boundary layer NPF events is mysterious. Here, we hypothesized that the free tropospheric air intrusion-induced dilution of polluted boundary layer air reduces condensation sink (the scavenging of condensing vapours by pre-existing large particles) to promote NPF in the polluted boundary layer during the dry winter season (ONDJF).

4.2 Data analysis methodology

Here, we have used measurements of particle number size distribution carried out at the University of Hyderabad campus site for the period from 1 April 2019 to 31 March 2022. The details of the measurement technique and site are described in Chapter 2 (Section. The methodologies used for the calculation of particle growth rate and condensation sink are detailed in Chapter 2 (Section 2.6.1.4). In order to predict the occurrence of NPF, we used the ratio of particle scavenging loss rate to particle growth (ratio of CS to GR). In megacities, it was seen that NPF occurred when the ratio of CS (10^{-4} s^{-1}) to GR (nm h^{-1}) was above 50 (Chu

et al., 2019). Whereas, in moderately polluted conditions, NPF occurred when the ratio was less than 50 (Kulmala et al., 2017). Following this methodology, we performed analyses based on long-term continuous measurements.

The multi-scale offline lagrangian particle dispersion models are the Numerical Atmospheric-dispersion Modelling Environment (NAME) (Jones et al., 2007), the Stochastic Time-Inverted Lagrangian Transport (STILT) (Lin et al., 2003), the Hybrid Signle-Particle Lagrangian Integrated Trajectory (HYSPLIT) model (Stein et al., 2015), and the FELXible PARTicle (FLEXPART) model (Stohl et al., 2005; Stohl et al., 1998) to simulate the transport and turbulent mixing of gases and aerosols in the atmosphere. Here, we used the HYSPLIT model to calculate hourly three-day air mass backward trajectories starting at 500 m above the ground from Hyderabad (17.46 ^{o}N, 78.32 ^{o}E). Additionally, we have calculated the spatial extent of NPF events following the methodology given by Hussein et al. (2009) which is detailed in Chapter 2 (Section 2.6.3). We have also used the (ERA5) climate data products such as vertical velocity and temperature profiles (for calculating potential temperature to determine lower tropospheric stability), the details of which are given in Chapter 2, Section 2.4.2.

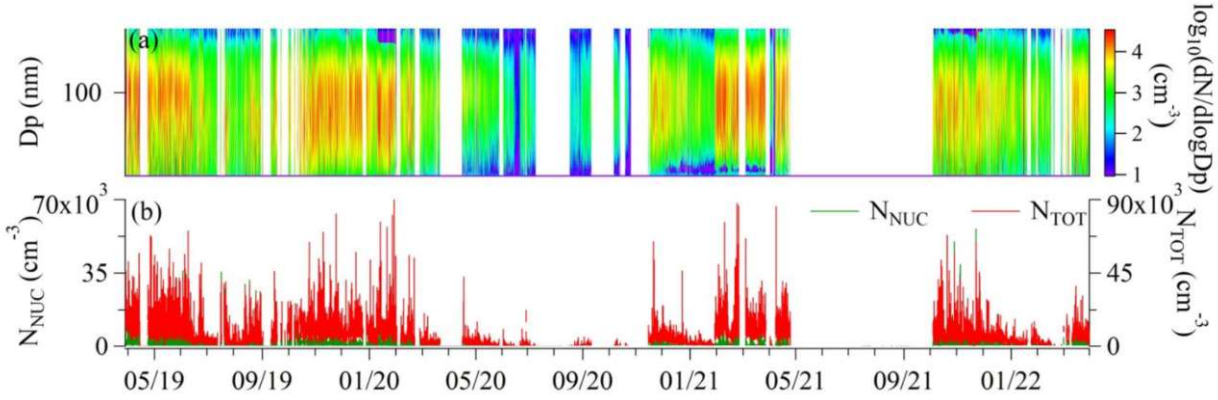

Figure 4.1 Time-series of (a) particle number size distributions and (b) $N_{>25nm}$ and N_{TOT} for the entire time period (1 April 2019 – 31 March 2022)

4.3 Results and discussions

4.3.1 The frequency of occurrence of different event types

Table 4.1. Summary of criteria used for classifying different event types.

Event Type	SMPS criteria
NPF	An abrupt increase in nucleation mode particles (sub-25 nm) with evidence of steady growth in the particle size for at least 6 hours, thus particle number size distributions appearing as conventional noon-time 'banana' shape. Particle mode diameter is less than 25 nm so that the growth rate and formation rate of particles can be calculated.
non-events	No increase in nucleation mode particles (sub-25nm) and particle mode diameter (absence of growth) during the day.
undefined	All the remaining days don't satisfy either of the above two criteria, mostly due to airmass inhomogeneities resulting in broken 'banana' shape, particle bursts without growth (volcano/apple), Aitken mode growth primary emission induced growth, etc.

Table 4.1 summarises the criteria used for the classification of different event types. Out of 665 valid observation days during the study period, NPF events occurred on 218 days (32.8%), which is globally comparable to NPF frequencies observed from long-term measurements with at least one full year of data (Kanawade et al., 2012; Kerminen et al., 2018; Kulmala et al., 2004). Out of 665 valid observation days, non-events were observed on 292 days (42.9%) and undefined events were observed on 155 days (24.3%). Figure 4.2 shows the monthly percentage occurrence of different event types in Hyderabad. NPF frequency was the highest in the pre-monsoon (MAM) season (41.8%) and the lowest in the winter (DJF) season (28.1%). The frequency of occurrence of NPF in the monsoon (JJAS) and post-monsoon (ON) was relatively similar (30.1% and 32.0%, respectively). The lowest NPF frequency in the winter (DJF) season can be attributed to shallow boundary layer-induced high pre-existing particles (high condensation sink for precursor and condensing vapours), while the highest NPF frequency in the pre-monsoon (MAM) season can be attributed to high photochemical activities (high solar radiation) and uplifted boundary layer leading to dilution of the air (low condensation sink).

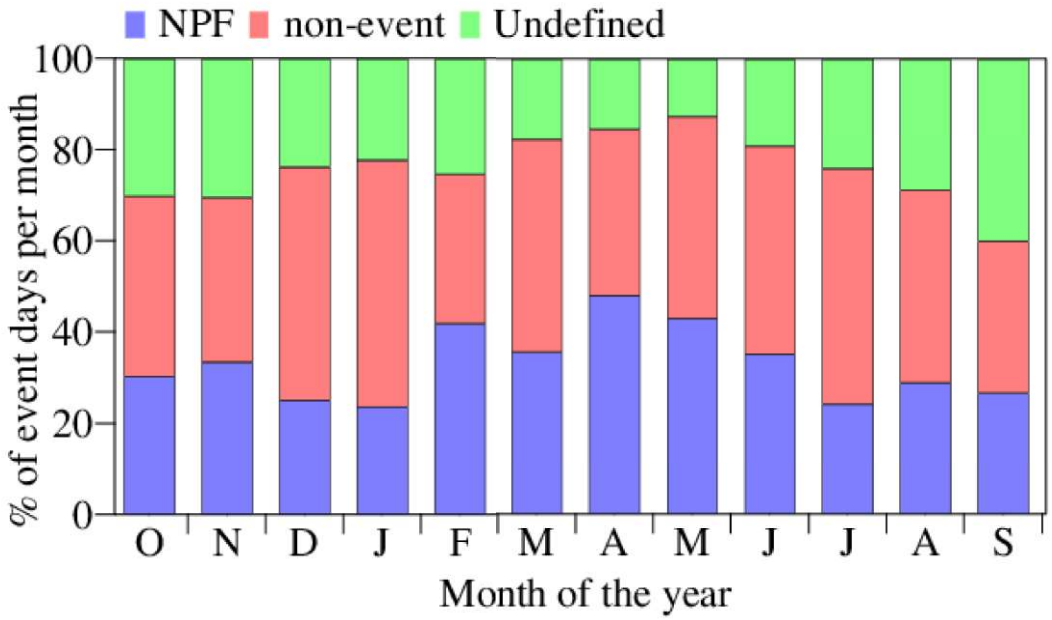

Figure 4.2 Monthly percentage of occurrence of event types in Hyderabad.

4.3.2 Characteristics of new particle formation events

A summary of the basic parameters characterising NPF is given in Table 4.2. Here, we will summarise and discuss the formation rate, growth rate, condensation sink, and source rate of condensation vapours and their contribution to the total observed growth rate. We did not use measurements of particle number size distributions using nCNC system down to ~ 1 nm in this study due to the unavailability of simultaneous and continuous data, therefore we rely on the particle formation rate of larger size, in this case, 10 nm. The formation rate of 10 nm particles based on the observed NPF events days ranged from 0.04 to 11.18 cm^{-3} s^{-1}, with a mean and standard deviation of 2.06±1.65 cm^{-3} s^{-1}, while the particle growth rates ranged from 1.10 to 14.16 nm h^{-1}, with a mean and standard deviation of 5.5±2.7 nm h^{-1}. The mean values of the particle formation rate and growth rate of nucleation mode particles are within the observed range in diverse locations globally (Kanawade et al., 2021; Kerminen et al., 2018; Nieminen et al., 2018).

Table 4.2 Summary of averaged (9:00 a.m. to 4:00 p.m. local time) formation rate of 10 nm particles (J_{10}), the growth rate of particles from 10-25 nm diameter (GR_{10-25}), total condensation sink (CS), $[H_2SO_4]_{proxy}$, growth rate due to $[H_2SO_4]$ alone and the percentage contribution of growth rate due to $[H_2SO_4]$ alone to GR_{10-25} for the observed NPF events. ± indicates standard deviation.

Month	J_{10} (cm^{-3} s^{-1})	GR_{10-25} (nm h^{-1})	CS (10^{-3} s^{-1})	$[H_2SO_4]_{proxy}$ (10^7 molecules cm^{-3})	$GR_{[H2SO4]}$ (nm h^{-1})	Contribution of $[H_2SO_4]$ to GR_{10-25} (%)
Jan	1.34±0.71	3.0±1.2	8.8±5.2	1.35±0.50	0.60±0.30	20.7±5.2
Feb	1.02±0.59	5.5±2.6	11.7±8.5	1.45±0.54	0.62±0.35	14.3±9.4
Mar	1.89±1.18	6.2±3.4	12.5±7.2	1.37±0.37	0.56±0.29	10.4±4.0
Apr	2.61±2.16	6.7±2.2	18.3±5.8	1.33±0.46	0.57±0.31	8.9±4.0
May	2.89±2.07	6.5±2.7	13.1±7.7	1.75±0.42	0.77±0.36	15.6±10.2
Jun	2.67±3.69	6.5±1.8	6.0±4.5	1.09±0.43	0.44±0.29	6.4±3.3
Jul	1.78±0.14	4.3±1.1	9.6±0.9	0.72±0.14	0.27±0.11	6.6±1.6
Aug	1.94±1.99	4.6±2.3	5.3±3.2	0.68±0.18	0.28±0.15	6.0±4.3
Sep	2.36±2.72	5.4±2.6	7.4±3.9	0.53±0.15	0.23±0.09	5.1±2.5
Oct	3.07±1.78	6.3±2.7	10.4±3.9	1.50±0.55	0.58±0.35	12.4±9.3
Nov	2.41±2.58	5.4±2.8	9.9±1.6	1.80±0.55	0.64±0.38	13.9±11.1
Dec	0.75±0.22	6.0±2.0	8.0±2.3	1.72±0.50	0.68±0.37	11.7±3.7
Mean	2.06±1.65	5.5±2.7	10.1±4.6	1.27±0.40	12.4±8.3	11.7±3.7

The high to severe air pollution conditions in India and developing nations make them quite different for NPF studies compared to Western countries. Generally, low pre-existing particles (low condensation sink) favour particle formation and growth, which is not the case in India. The particle formation, growth rates, and condensation sink were the highest in Delhi (winter, subtropical environment) as compared to the formation and growth rates of particles in Pune (pre-monsoon/spring, tropical environment) at a much lower condensation sink (Kanawade et al., 2021). The higher pre-existing particles in severely polluted environments (e.g. Delhi) indicate the precursor-laden air, which can enhance the formation and growth rates of particles if NPF precedes. This suggests that the balance between the volume of pre-existing particles and precursor vapours decides when the NPF will take place in the polluted boundary layer. The spread of the novel 2019 Coronavirus (COVID-19) enforced lockdown provided a unique opportunity to study the influence of heavy air pollution on NPF. Several investigators showed enhanced levels of secondary particulate matter and also the frequency of occurrence of NPF events in China during the COVID-19 enforced lockdown (He et al., 2021; Sun et al., 2020), while the frequency of occurrence of NPF&G events was significantly lower during the COVID-19 lockdown as compared to the business-as-usual time periods in India (Kamra et al., 2022; Kanawade et al., 2022; Yadav et al., 2021). Interestingly, Shen et al. (2016c) found the highest NPF event frequency coincided with improved air quality during the APEC meeting in

2015 in Beijing, indicating the improved air quality in China may experience more frequent NPF events in the future, unlike India.

The occurrence of NPF events in Hyderabad was determined using the ratio of the scavenging loss rate to growth rate of particles (ratio of CS to GR). Figure 4.3 shows the relationship between CS and GR for different seasons for Hyderabad and mean and standard deviation values for Beijing, Ustl nad Labem, and Hyderabad. CS is much higher in Beijing than in Hyderabad and Usti nad Labem, while GR values appear to be comparable between the sites. NPF seems to occur frequently in all seasons in Hyderabad when the CS (10^4 s^{-1}) to GR (nm h^{-1}) ratio was less than 50 and rarely in the winter (DJF) season when the CS (10^4 s^{-1}) to GR (nm h^{-1}) ratio was between 50 and 100. As opposed to this observation, megacities in China witnessed NPF occurrences when the CS (10^4 s^{-1}) to GR (nm h^{-1}) ratio was above 50 (Chu et al., 2019). Whereas in cleaner and moderately polluted environments, NPF occurred when the ratio was below 50 (Kulmala et al., 2017). This suggests that the NPF events are more frequent in India under moderately polluted conditions as opposed to China, indicating that different pathways of particle formation and growth may be active in these countries, owing to dissimilar climatic conditions and spatiotemporal heterogeneity in anthropogenic emission.

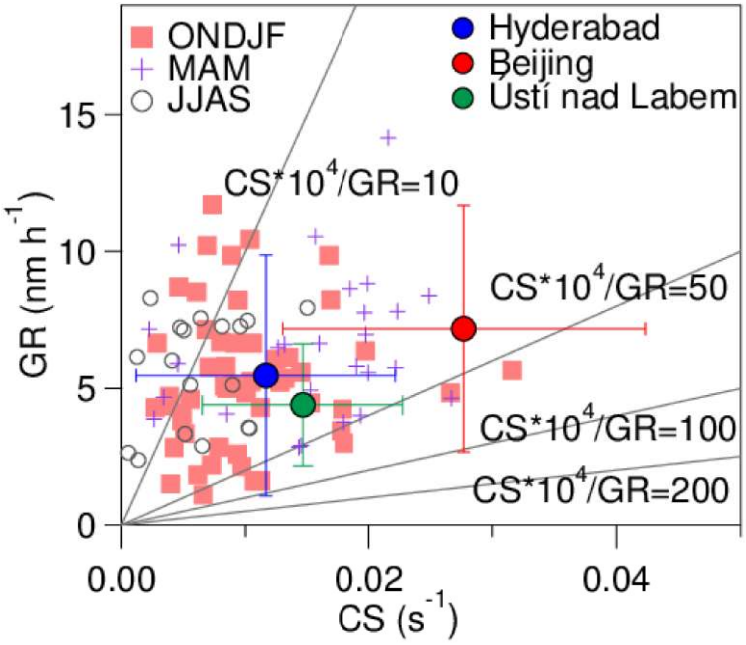

Figure 4.3 Scatter plot of hourly averaged CS versus GR for the observed NPF events in Hyderabad (symbols, filled magenta box for dry winter (DJF), plus for pre-monsoon (MAM) and open circle for monsoon). The mean values of CS and GR Hyderabad (blue), Beijing (red), and Usti nad Labem (green) are also plotted for comparison.

4.3.3. Characteristics of airmass trajectories during NPF and non-event days

While the atmospheric aerosol particles have a relatively short lifetime in the lower atmosphere (~7 days), the particle observations can be significantly affected by the advection air masses over a specific measurement site. Air mass backward trajectories have been utilized to examine the influence of long-range transported air masses and the associated source regions on the observed aerosol properties. Figure 4.4 shows air mass backward trajectories, starting at 500 m above the surface at 6:00 UTC (11:30 am local time) during different seasons for NPF events and non-events days. It is quite obvious that the course of the airmass backward trajectory is relatively the same between NPF and non-events days suggesting that the source of the air mass is not a critical factor for determining the occurrence of NPF. It also appears that air mass backward trajectories associated with NPF events are more dispersed as compared to non-events days. This suggests that the occurrence of NPF is linked to the modification of air mass in the atmosphere as it is advected over an inhomogeneous surface.

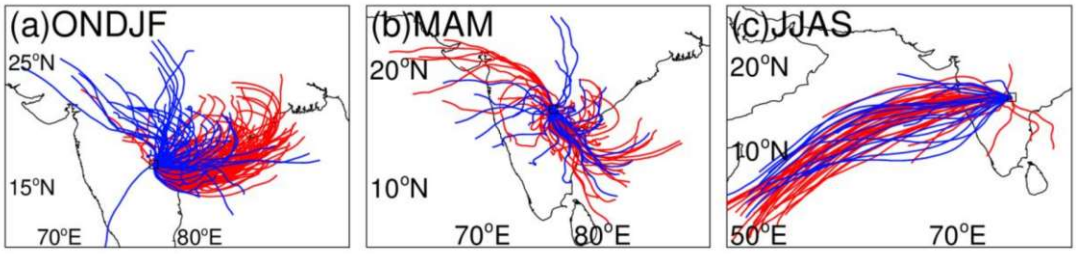

Figure 4.4 Airmass 3-day backward trajectories starting at 500 m above ground at 6 UTC (11:30 AM local time) during (a) ONDJF, (b) MAM, and (c) JJAS months for NPF events (blue trajectories) and non-events (red trajectories). The measurement site is shown by the open square box.

While air mass trajectory cluster analysis can reveal the influence of typical environments on the observed aerosol and atmospheric conditions (Fleming et al., 2012; Nilsson et al., 2001; Tunved et al., 2004), the observed relationships are generally affected by inhomogeneous surroundings (Tunved et al., 2005) and do not explain temporal variations. The mixing of contrasting air masses over inhomogeneous surroundings can cause local-to-regional scale variations in gases, aerosols, and thermodynamic variables via turbulent mixing. Therefore, we next find the percentage of trajectories advecting at a specific altitude along its path as a function of backward time for observed NPF events and non-event days during different seasons (Figure 4.5). While air mass generally advected within the atmospheric boundary layer before it reaches the measurement site, a large fraction of air mass trajectories appears to be intruding from the free troposphere to the atmospheric boundary layer approximately a day

before the NPF event day during the dry winter season (ONDJF). This can create vertical turbulent mixing of gases and aerosols in the vicinity of the measurement site. The shallower boundary layer (enormous amount of precursor vapours and pre-existing particles), temperature inversion-induced stagnant conditions (low ventilation), and lower solar radiation (low photochemical activity) typically inhibit the wintertime NPF in urban areas, but our analysis reveals that NPF still occurs in winter under unfavourable atmospheric conditions.

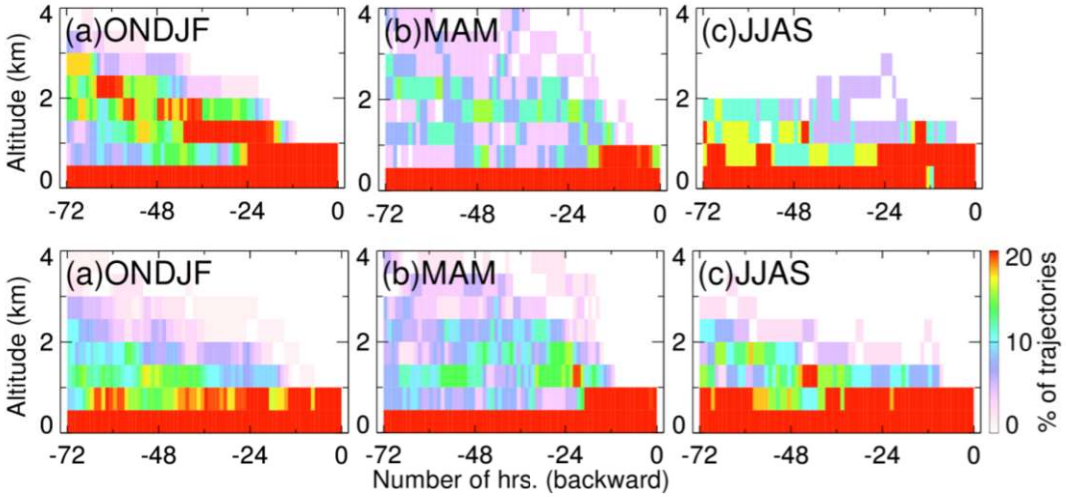

Figure 4.5 Percentage occurrence of air mass trajectory altitude as a function of backward time for (a) ONDJF, (b) MAM, and (c) JJAS months for observed NPF events (top panel) and non-events (bottom panel) based on air mass backward trajectories starting at 500 m above ground at 6 UTC (11:30 AM local time).

Manoj et al. (2019) showed that the contribution of free tropospheric aerosols to columnar aerosol loading is increasing over India, particularly during the wintertime. This underlines the possible role of synoptic conditions associated with subsidence and thus, large-scale pressure systems. This can provide clear-sky sunny conditions which can facilitate NPF. Previous studies showed that NPF often occurs under the synoptic conditions associated with, large-scale high-pressure systems and subsidence, but only under the influence of continental polluted air flow (Kompalli et al., 2020; Pierce et al., 2014). Figure 4.6 shows the averaged latitude-pressure cross-Section of vertical velocity (negative values indicate subsidence) over the longitude bins 76 – 82 °E with the measured site centred for observed NPF events (95 days) and non-events (189 days). It turns out that NPF events are favoured under stronger subsidence conditions associated with the presence of large-scale high-pressure systems during dry winter (ONDJF). As opposed, the synoptic conditions for the rest of the year (MAM and JJAS months, Figures

4.7 and 4.8) indicate that the occurrence of NPF events is not linked to large-scale high-pressure systems associated with subsidence.

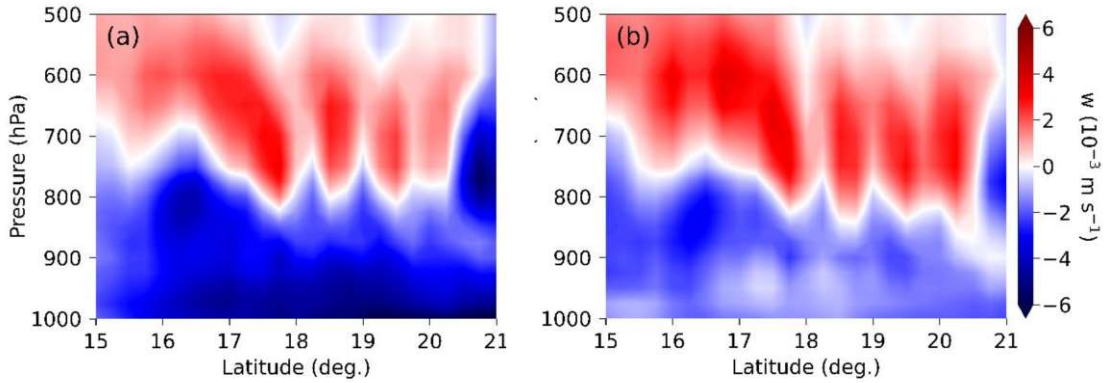

Figure 4.6 Averaged latitude-pressure cross-Section of vertical velocity over longitude bins 76 - 82 °E with the measurement site centered for observed (a) NPF events and (b) non-events for dry winter (ONDJF).

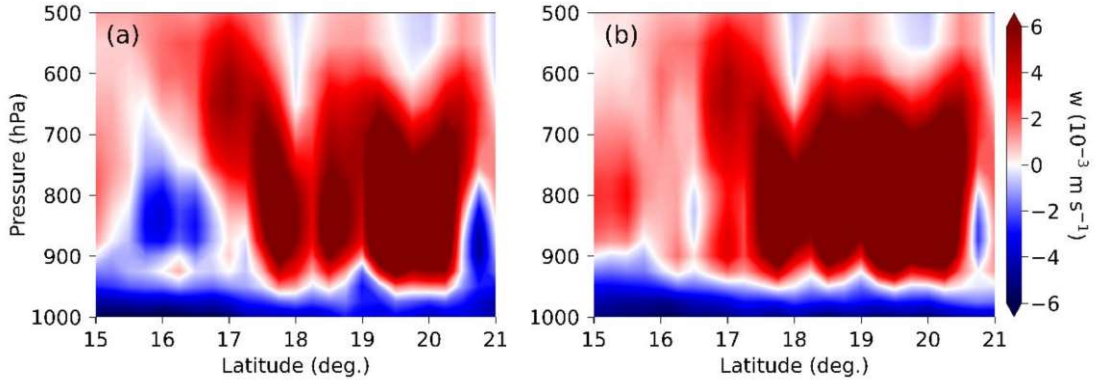

Figure 4.7 Same as Figure 4.6, but for pre-monsoon (MAM)

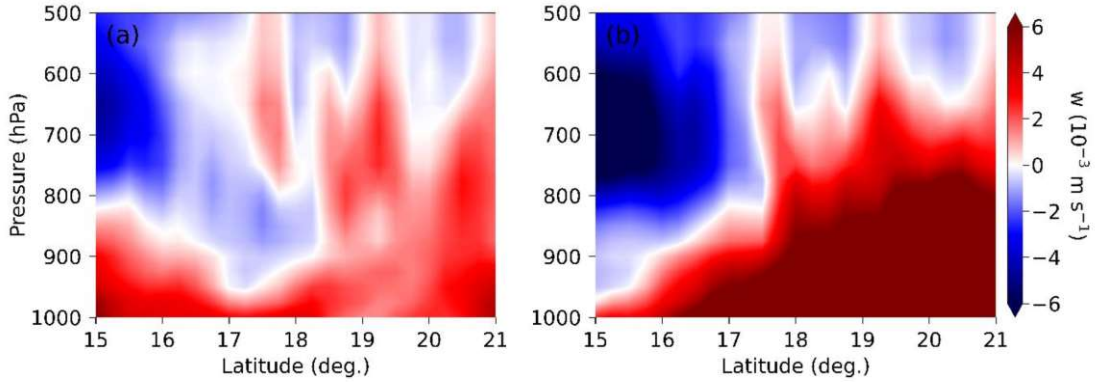

Figure 4.8 Same as Figure 4.6, but for summer monsoon (JJAS).

The high-pressure systems are associated with stable atmospheric conditions with subsiding dry air. The LTS, which is defined as the potential temperature difference between the surface and 700 hPa, is a remarkable indicator of the low-cloud fraction on the seasonal scale (Klein and Hartmann, 1993). We analyzed LTS for the observed NPF events and non-events. Figure 4.9 shows the averaged LTS for observed NPF events and non-events and the difference between them. The robust presence of stable atmospheric conditions for the observed NPF events compared to non-events and the positive difference in the LTS during the dry winter (ONDJF) further substantiate our findings above. In contrast, the difference in the LTS during MAM and JJAS months is negative indicating that stable atmospheric conditions are not necessary criteria for the occurrence of NPF during these months (Figures 4.10 and 4.11).

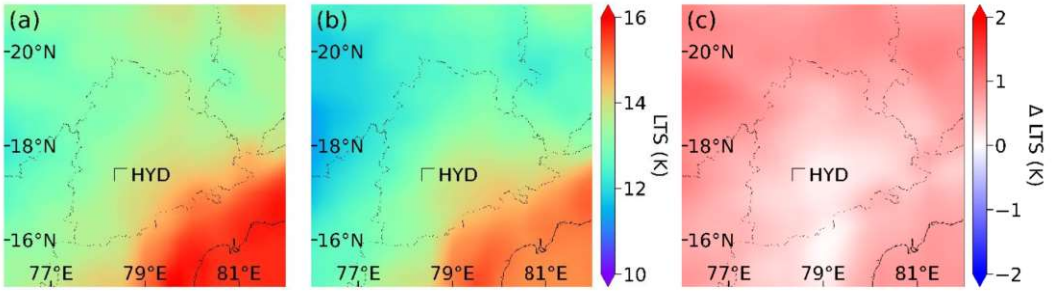

Figure. 4.9 Averaged LTS for observed (a) NPF events, (b) non-events, and (c) difference (a-b) for dry winter months (ONDJF).

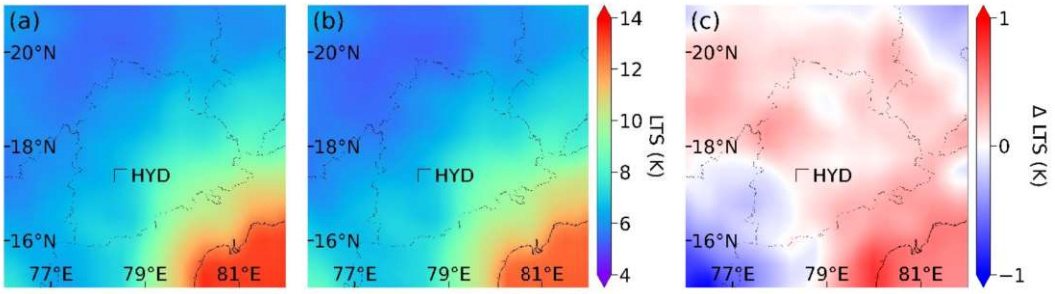

Figure 4.10 Same as Figure 4.9, but for pre-monsoon (MAM)

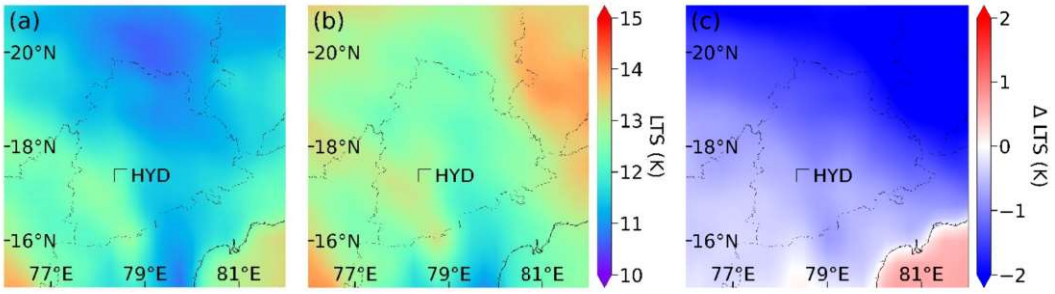

Figure 4.11 Same as Figure 4.9, but for summer monsoon (JJAS).

4.3.4 Spatial extent of NPF events

The spatial extent of an NPF event indicates the regionality of the occurrence of NPF processes in the atmosphere. There are typically two approaches widely used to determine the spatial extent of an NPF event. The first and most expensive approach is based on simultaneous measurements of particle number size distributions across a broad size range at multiple stationary sites (Dal Maso et al., 2007; Jeong et al., 2010; Wehner et al., 2007), and the second is based on the air mass backward trajectories (Crippa and Pryor, 2013; Hussein et al., 2009; Vana et al., 2004). While the regional NPF typically occurs over a spatial scale of a few 100 kilometres, the second approach surprisingly uses only airmass backward trajectories from the stationary measurement site. The fact that newly formed particles are still growing with the air mass as advected further downwind of the stationary measurement site, the airmass forward trajectories should also be utilized to obtain the exact spatial extent of an NPF event. Here, we examined the spatial extent of the observed NPF events based on the methodology given by (Hussein et al., 2009). The detailed methodology to calculate the spatial scale of an NPF event is explained in Chapter 2 (Section 2.6.3). Briefly, we tracked the hourly calculated air mass back trajectories starting at the average NPF start time (10: 00 am local time) and traced them back in the upwind direction where NPF was possibly triggered. All these locations and time data points were stored, gridded, and then plotted in Figure 4.12. It turns out that NPF occurs on a spatial scale of about 300-500 km.

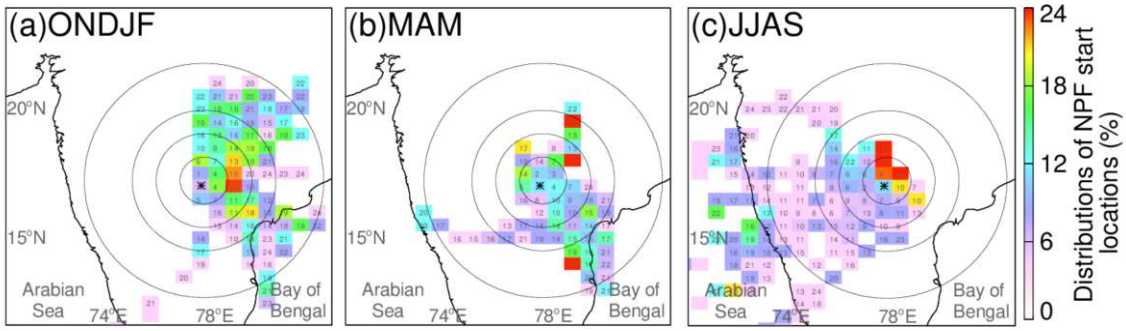

Figure 4.12 The spatial extent of the observed NPF events for (a) ONDJF, (b) MAM, and (c) JJAS months. The measurement site Hyderabad is shown by the asterisk sign. The contour line is the line of the same distance (in km) from the measurement site. The number in each pixel indicates trajectory duration (in hours).

4.4 Summary

NPF is the greatest source of particle numbers, but they need to grow to a larger size to become climatically active or to contribute significantly to the total aerosol mass concentrations. In addition, NPF may contribute to the formation of severe pollution conditions. To our

understanding, NPF in the atmosphere relies largely on the measurements of particle number size distribution carried out at stationary measurement sites. NPF often occurs in homogenously mixed air masses, and therefore air mass movements and the results advection of precursor gases and particles from inhomogeneous surroundings can add considerable complexities in quantifying NPF rates. Here, the main focus is on demonstrating the significant impact that air mass history can have on NPF in an urban polluted environment. We used long-term (2019-2022) continuous measurements of particle number size distributions from an urban site. We show that NPF events occur frequently in pre-monsoon (MAM). Overall, NPF occurs 30% of the days annually at the University of Hyderabad campus site. The highest frequency of NPF was observed on clear-sky sunny conditions while the lowest frequency was observed on cloudy shallow boundary layer conditions. We find that the occurrence of NPF is not air mass origin dependent. It turns out that the air mass history as it advected in the atmosphere matters the most. We illustrate that NPF events are more frequent under moderately polluted conditions in India and it seems to be inhibited in heavy to severely polluted environments. The intrusion of air mass trajectories from the free troposphere to the atmospheric boundary layer appears to be a triggering factor for NPF during the dry winter (ONDJF). Analyses of vertical velocity and LTS revealed that the synoptic conditions associated with the large-scale pressure systems and subsidence can provide clear-sky sunny conditions which can facilitate NPF during the dry winter (ONDJF), unlike the rest of the year. We further find that the spatial extent of NPF is about 300-500 km.

Chapter 5

New particle formation and growth to climate-relevant aerosols

5.1 Introduction

A fraction of aerosols acts as CCN, depending on the size and composition of aerosol particles and atmospheric supersaturation. Therefore, aerosols have the potential to influence cloud properties via their indirect effect, which in turn impacts Earth's radiative balance and hydrological cycle (IPCC, 2023). As demonstrated in this thesis, NPF is the greatest source of particle numbers to the atmosphere and therefore can be considered the major source of CCN in the troposphere. However, there is limited observational evidence to quantify the fraction of newly formed particles contributing to CCN formation in the atmosphere.

Previous field observations and computational simulations conducted across the globe have consistently shown a significant increase in CCN concentrations resulting from NPF (Gordon et al., 2017; Kalivitis et al., 2015; Kerminen et al., 2018; Kerminen et al., 2012; Merikanto et al., 2009; Pierce et al., 2012; Pierce et al., 2014; Rose et al., 2017; Sihto et al., 2011; Tröstl et al., 2016b; Westervelt et al., 2014; Westervelt et al., 2013; Wiedensohler et al., 2009; Yu et al., 2020). Merikanto et al. (2009) found that about 45% of the newly formed particles from NPF events can be attributed to lower tropospheric CCN concentrations worldwide, at a supersaturation of 0.2%. Westervelt et al. (2014) also observed that NPF events contribute by about 50% of boundary layer CCN concentrations at a supersaturation of 0.2%, with an estimated uncertainty range of 49% - 78% (uncertainty due to the choice of the specific nucleation scheme). In contrast, the global model GLOMAP simulation in conjunction with 15 European ground-based measurement sites revealed that the CCN concentrations were influenced by mechanisms other than nucleation at over ten sites (Reddington et al., 2011). This was mainly attributed to the increased coagulation and condensation sinks of ultrafine particles which weakens the response of CCN particles in the boundary layer, resulting in a decrease in ultrafine particle growth by condensation, preventing them from reaching CCN-active sizes (Kuang et al., 2009; Pierce and Adams, 2007). This points to the survival probability of newly formed particles to CCN-active sizes against coagulation by pre-existing particles. Tröstl et al.

(2016b) demonstrated that a small portion of particles less than 50 nm experienced growth beyond 90 nm (50–100 particles cm^{-3}), even over several days. Therefore, to better understand atmospheric NPF and to quantify its contribution to the boundary layer CCN budget, highly-resolved spatiotemporal observational data in diverse environments globally aided with aerosol model simulations are crucial.

5.2 Data analysis methodology

For this analysis, we have used asynchronous long-term particle number size distribution data from all six diverse locations which are described in detail in Chapter 2 Section 2.1. These sites include Ranichauri (RNC), Mukteshwar (MUK), Mahabaleshwar (MBL), Hyderabad (HYD), Thiruvananthapuram (TVM), and Delhi (DEL). The data coverage for particle number size distribution is more than 60% at the RNC, MUK, MBL, and HYD sites. However, the data coverage at TVM was 34%, and at DEL, it was 47%, indicating a lower level of coverage at these locations (Figure 5.1). Here, we have used two methodologies to identify the growth of newly formed particles to the sizes of climate-relevant aerosols. The first methodology as described in Chapter 2 (Section 2.6.4) calculated the survival probability of newly formed particles to climate-relevant sizes following Pierce and Adams (2007). The second methodology calculated the increase in CCN concentration from an NPF event which is described in Chapter 2 (Section 2.6.5) following Kerminen et al. (2012) and further modified. The findings from this chapter are reported in (Sebastian et al., 2021b; Sebastian et al., 2022).

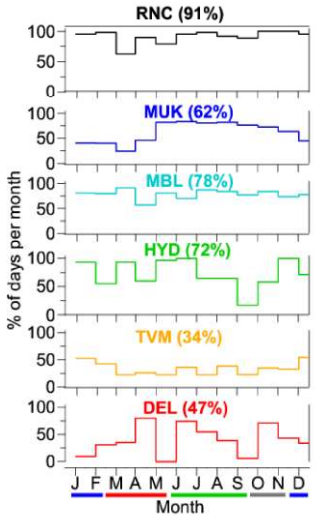

Figure 5.1. Particle number size distribution data coverage (% of days/month) at the sites. The values in the bracket indicate total data coverage. The blue, red, green, and grey colored thick lines indicate winter (DJF), pre-monsoon (MAM), monsoon (JJAS), and post-monsoon (ON). Note that measurements are from different time periods for each site (refer to Table 2.1).

5.3 Results and Discussions

5.3.1 Event identification and classification

The percentage distribution of NPF, non-event, and undefined event days based on valid observation days across all 6 sites in presented in Chapter 3 (Figure 3.18). At RNC, out of 586 valid observation days, NPF events occurred on 21 days (3.9%), with 493 (83.7%) classified as non-event days. At MUK, among 440 valid observation days, NPF events occurred on 13 days (2.9%), with 321 (73.1%) non-event days. MBL, with 281 valid observation days, saw NPF events on 16 days (5.9%), while 188 (66.1%) days were non-event days. HYD, with 270 valid observation days, experienced NPF events on 38 days (16.3%), and 124 (44.8%) days were non-event days. TVM, out of 133 valid observation days, had NPF events on 23 days (16.6%), and 55 (41.4%) days were non-event days. Out of 139 valid observation days in DEL, NPF events occurred on 39 days (28.1%), with 30 (21.1%) non-event days. The frequencies of NPF occurrence at all sites are detailed in Table 5.1.

Table 5.1. Number of valid observation days, number of NPF days (percentage), number of non-event days (percentage), mean formation rates and mean growth of particles at all six sites in India. ± indicates standard deviation.

Site	valid observation days	NPF days	non-event days
RNC	586	21 (3.9%)	493 (83.7%)
MUK	440	13 (2.9%)	321 (73.1%)
MBL	281	16 (5.9%)	188 (66.1%)
HYD	270	38 (16.3%)	124 (44.8%)
TVM	133	23 (16.6%)	55 (41.4%)
DEL	139	39 (28.1%)	30 (21.1%)

Overall, NPF occurrence is highest in pre-monsoon (MAM) compared to other seasons, except for an exception at TVM, where the highest frequency occurs in late monsoon (September). This anomaly is attributed to a mixing of contrasting air masses influenced by mesoscale sea-land breeze dynamics (Babu et al., 2016). The Western Himalayan mountain-background sites (RNC and MUK) exhibit the lowest annual mean NPF frequency (3.9% and 2.9%, respectively), with the highest seasonal frequency in pre-monsoon (MAM). This aligns with previous studies indicating infrequent NPF at these sites (Neitola et al., 2011; Sebastian et al., 2021b). DEL exhibits the highest pre-monsoon (MAM) NPF frequency (63.8%), followed by

HYD (28.4%) and MBL (15.9%) which was also seen in other urban sites in India (Kanpur and Pune) (Kanawade et al., 2014c)

Figure 5.2 illustrates the contour plot of average particle number size distributions evolving over a day for each season at all the sites. The mountain background sites, RNC and MUK, experience daytime new particle formation in pre-monsoon (MAM), while winter (DJF), monsoon (JJAS) and post-monsoon (ON) show the lowest concentrations of nucleation mode particles. MBL experiences new particle formation in winter (DJF), pre-monsoon (MAM), and post-monsoon (ON). Conversely, urban sites (HYD, TVM, and DEL) display the highest particle concentrations during morning and evening peak traffic hours, alongside daytime NPF, as indicated by the average seasonal contour plot. We have considered the increase in particle concentration during evening peak traffic when exploring the frequency of new particle formation occurrence and its impact on CCN concentrations.

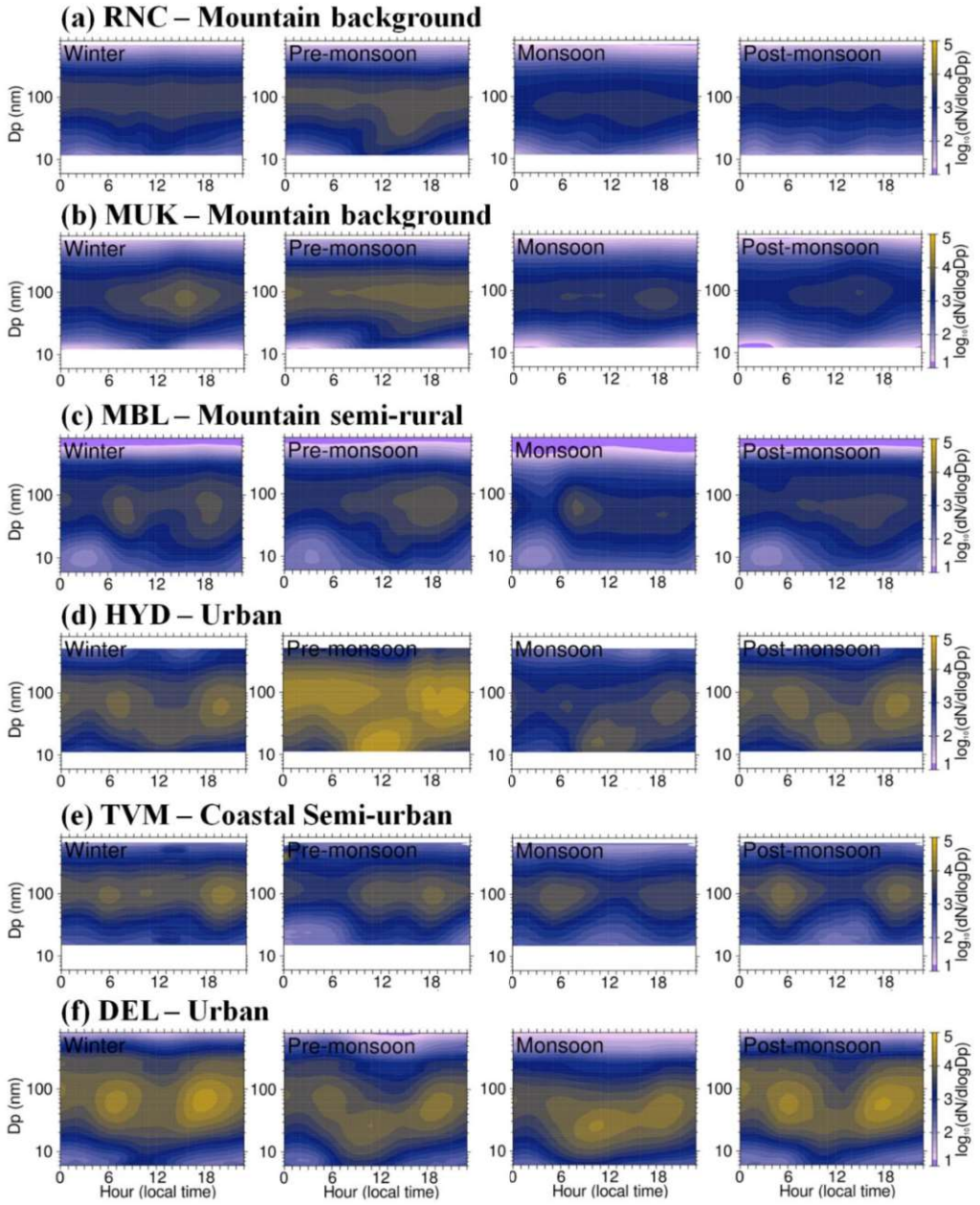

Figure 5.2. The diurnal-seasonal median particle number size distributions at all the sites; a) Ranichauri, b) Mukteshwar, c) Mahabaleshwar, d) Hyderabad, e) Thiruvananthapuram, and f) Delhi. Note that measurements are from different time periods for each site (refer to Table 2.1).

5.3.2 New particle formation to cloud condensation nuclei production

Here, we have used two methodologies as explained in Chapter 2. Briefly, we have calculated the newly formed particle survival probabilities to 50 nm (SP50) and 100 nm (SP100) size following the methodology given by Pierce and Adams (2007) and first applied to ambient observations by Westervelt et al. (2013). SP is the ratio of particle fluxes at the initial size and

the CCN-active sizes (typically 50 nm and 100 nm particles). We also calculated the increase in CCN concentrations from any given NPF event can be estimated by comparing the CCN concentration before the event ($N_{CCNprior}$) and the maximum CCN concentration during the event (N_{CCNmax}) following the methodology developed by Kerminen et al. (2012), which we modified further to remove the contribution from primary/background particles to CCN concentrations.

5.3.2.1. Survival Probability of newly formed particles

The survival probabilities of newly formed particles to 50 nm (SP50) and to 100 nm (SP100) calculated using the methodology described in Section 2.6.4 are discussed here. SP50 values were found to be in a range of 42% to 98% with a mean and standard deviation of 86 ± 11% and SP100 in a range of 12% to 95%, with a mean and standard deviation of 59 ± 20% when considering all six sites of study (Figure 5.3). Mountain background sites, RNC and MUK, show a lower SP50 (82% and 85%, respectively) as compared to urban sites. Both SP50 and SP100 are seen to be the highest for DEL when compared to other sites with a mean of 91 ± 6% and 72 ± 9% respectively. The percentage of newly formed particles surviving from 50 nm to 100 nm was higher for urban sites HYD (73%) and DEL (79%). Whereas it was comparatively low for mountain background sites such as RNC (64%), MUK (66%) and MBL (60%). Table 5.2 presents survival probabilities (SP) and formation rates (J) of particles of 50 nm and 100 nm in diameter at all six sites and a concise global overview of these values.

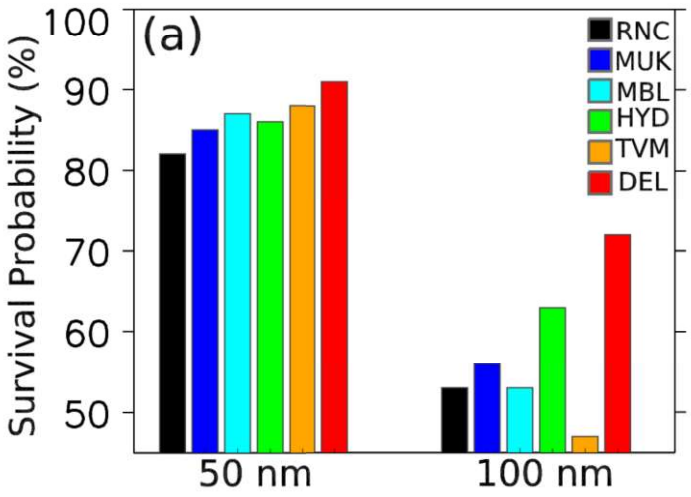

Figure 5.3 Survival probability of newly formed particles to 50 nm (SP50) and 100 nm (SP100).

Table 5.2 Summary of survival probability and formation rate of 50 nm and 100 nm particles at diverse locations.

Location	SP50 (%)	SP100 (%)	J50 (cm^{-3} s^{-1})	J100 (cm^{-3} s^{-1})	Reference
RNC	82±18	53±32	0.08±0.05	0.05±0.04	
MUK	85±15	56±20	0.05±0.04	0.04±0.03	
MBL	87±11	53±24	0.06±0.04	0.04±0.03	This study
HYD	86±9	63±18	0.13±0.10	0.09±0.08	
TVM	88±5	47±19	0.01±0.01	0.01±0.01	
DEL	91±6	72±9	0.16±0.10	0.12±0.07	
Egbert, Canada	33	19	0.039	0.022	Pierce et al. (2014)
Pittsburgh, USA	37	2.4	0.11	0.006	Westervelt et al. (2013)
Atlanta, USA	67	3.7	0.177	0.006	Westervelt et al. (2013)
St. Louis, USA	46	1.8	1.6	0.046	Westervelt et al. (2013)
Hyytiälä, Finalnd	55	2.6	0.23	0.004	Westervelt et al. (2013)
Po Valley, Itlay	34	4.4	0.39	0.34	Westervelt et al. (2013)
Mt. Tai, China	10-140	5-40	-	-	(Zhu et al., 2020)

Based on the measured average particle growth rates, the measured particles of 10 nm size take about 4 to 6 hours to reach the size of 50 nm. The average SP50 value at mountain background sites RNC and MUK are almost two-fold compared to the value reported for a forest site at low altitude namely Egbert, Ontario, Canada which was (33%) (Pierce et al., 2014). However, the average value of SP50 at RNC and MUK was comparable to the observed range at all four urban sites (31-80%) (Westervelt et al., 2013). We also calculated the formation rates of particles of size 50 nm and 100 nm in this study by multiplying J10 with their respective survival probabilities for all six sites. Figure 5.4 depicts the average cumulative probability distribution functions for the survival probability of particles measuring 50 nm and 100 nm (SP50 and SP100) as well as the formation rates of 50 nm and 100 nm particles (J50 and J100) specifically for NPF events from 6 sites. The mountain background sites, RNC and MUK, exhibit J50 values of 0.08±0.05 and 0.05±0.04 cm^{-3} s^{-1}, respectively. This is less as compared to urban sites such as HYD and DEL (0.13±0.10 and 0.16±0.10 cm^{-3} s^{-1}). J100 also possesses a similar trend where the values are higher for urban sites as compared to mountain background sites. For mountain background sites, J50 is about two-fold higher than the observed value (0.039 cm^{-3} s^{-1}) at a low altitude location in Egbert, Ontario, Canada. (Pierce et al., 2014), while it was five-fold lower than that observed in a highly polluted site, Po Valley (0.39 cm^{-3} s^{-1}) (Westervelt et al., 2013). While the mean J100 is approximately 2-3 times higher than that observed at the low altitude site in Egbert, Ontario, Canada (0.02 cm^{-3} s^{-1}) (Pierce et al., 2014), it was almost ten-fold lower than that observed in the Po Valley (0.34 cm^{-3} s^{-1}) (Westervelt et al., 2013).

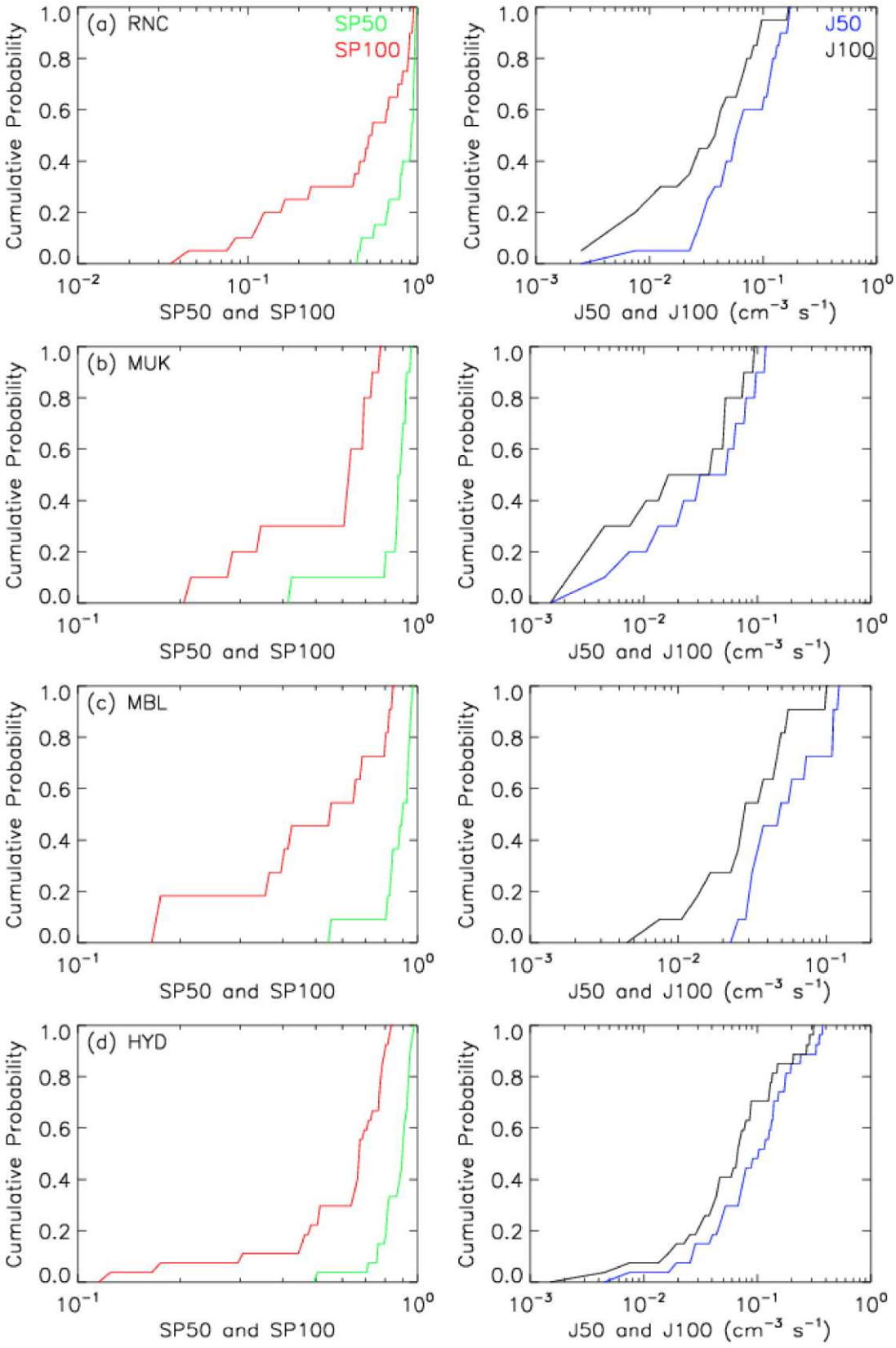
(a) RNC
SP50
SP100
J50
J100
(b) MUK
(c) MBL
(d) HYD
Cumulative Probability
SP50 and SP100
J50 and J100 (cm^{-3} s^{-1})

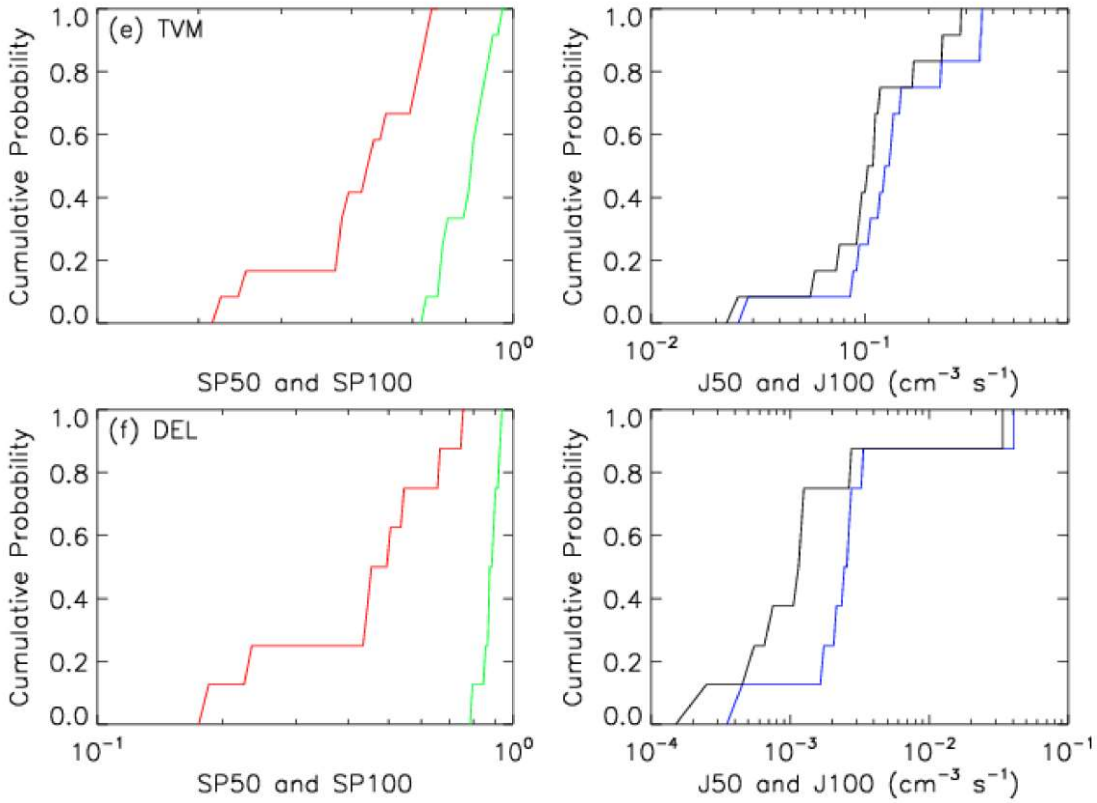

Figure 5.4 Cumulative probability distributions of survival probability to 50 nm (SP50) and 100 nm (SP100) and formation rates of 50 nm (J50) and 100 nm (J100) particles for the NPF events at a) Ranichauri, b) Mukteshwar, c) Mahabaleshwar, d) Hyderabad, e) Thiruvananthapuram, and f) Delhi.

5.3.2.2 Increase in cloud condensation nuclei concentrations

In order to reach climatically relevant sizes, the newly formed particles must undergo sufficient growth through the condensation of vapours while avoiding simultaneous loss to pre-existing particles. Because the freshly formed particles are small and exhibit high diffusivity (Vehkamäki and Riipinen, 2012). Based on the observed range of particle growth rates across all sites (0.2 to 17.3 nm h^{-1}), the newly formed particles may take from a few hours to 1-2 days to reach CCN-active sizes (>50-100 nm). Further, it is difficult to distinguish observationally between CCN that come from NPF and those that result from the primary emissions and the growth of primary particles Kerminen et al. (2012) proposed a methodology to estimate the increase in CCN concentrations during NPF events. We modified the methodology to exclude CCN that originated from the direct primary emissions and the growth of primary particles. Figure 5.5 shows the box-whisker plot of the absolute and percentage increase in CCN concentrations of 50 nm and 100 nm in size in diverse locations.

The observed increase in CCN_{50} varied from 0.168×10^3 cm^{-3} per event to 5.2×10^3 cm^{-3} per event, with a median value of 2.7×10^3 cm^{-3} per event, while the increase in CCN_{100} ranged from 0.02×10^3 cm^{-3} per event to 1.9×10^3 cm^{-3} per event, with a median value of 1.0×10^3 cm^{-3} per event. The observed increase in CCN_{50} and CCN_{100} in the free tropospheric high altitude site, Chacaltaya (5240 m above mean sea level, Bolivia) with 5.1×10^3 cm^{-3} per event for 50 nm and 1.5×10^3 cm^{-3} for 100 nm (Rose et al., 2017) is two times higher than RNC. The observed median increases in CCN_{50} and CCN_{100} at RNC and MUK are similar to the values reported at Botsalano in South Africa. Specifically, the median increase at RNC is 2.3×10^3 cm^{-3} per event for CCN_{50} and 0.9×10^3 cm^{-3} per event for CCN_{100}, while at MUK it is 2.9×10^3 cm^{-3} per event for CCN_{50} and 0.9×10^3 cm^{-3} per event for CCN_{100}. These values are approximately three-fold higher than the reported values at a remote continental site in Finland, where the median increase is 1.0×10^3 cm^{-3} per event for CCN_{50} and 0.2×10^3 cm^{-3} per event for CCN_{100} (Kerminen et al., 2012). Considering all NPF events observed in urban areas, the increase in CCN_{50} varied from 0.08×10^3 cm^{-3} per event to 9.4×10^3 cm^{-3} per event, with a median value of 4.3×10^3 cm^{-3} per event. Similarly, the increase in CCN_{100} ranged from 0.03×10^3 cm^{-3} per event to 4.9×10^3 cm^{-3} per event, with a median value of 1.2×10^3 cm^{-3} per event. The median increase in CCN_{50} and CCN_{100} is lower by a factor of two when compared with observations at the San Pietro Capofiume station, Po Valley, with the increase in CCN_{50} and CCN_{100} 7.3×10^3 cm^{-3} per event and 2.4×10^3 cm^{-3} per event, respectively (Laaksonen et al., 2005). Amongst locations, Delhi showed elevated background concentrations of CCN_{50} and CCN_{100}. To precisely estimate the atmospheric CCN budget and the contribution of newly formed particles via NPF processes, Kerminen et al. (2012) emphasized the need to incorporate both NPF events and non-event days in the analysis. Hence, our modified methodology employed here offers the most accurate representation of the increase in CCN concentrations during an NPF event.

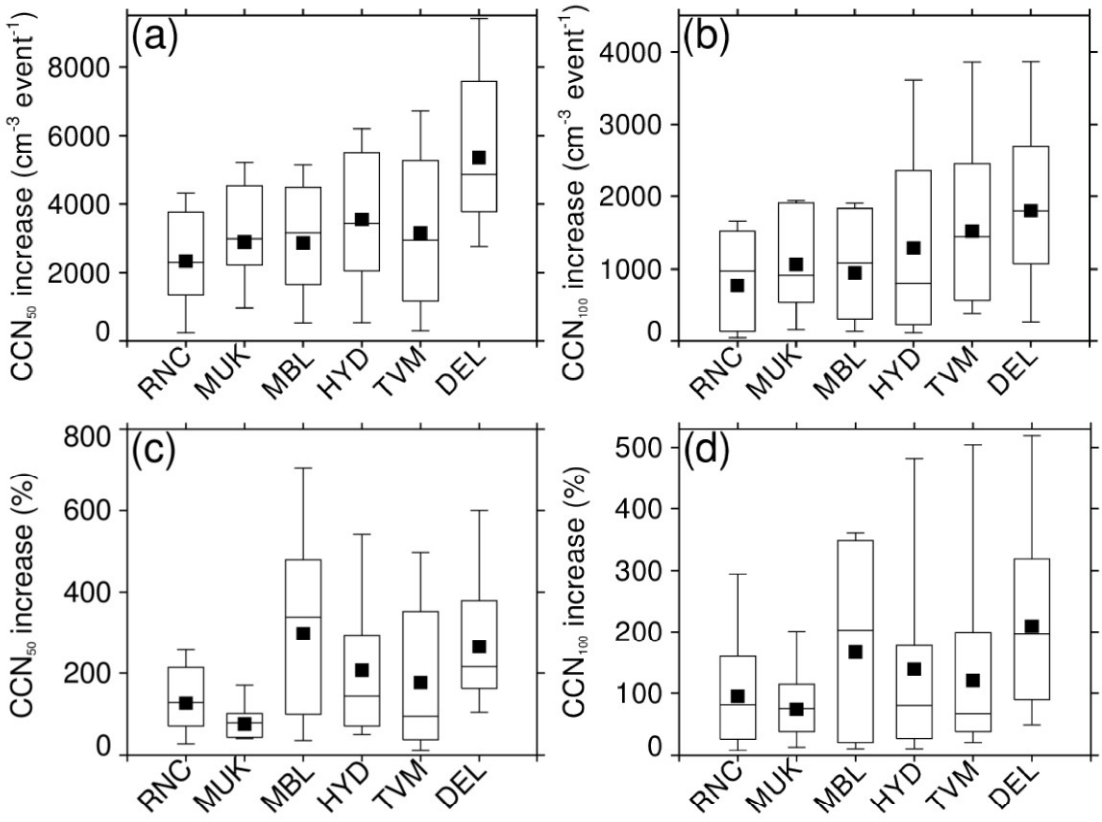

Figure 5.5 Box-whisker plot of absolute increase in CCN concentrations for (a) 50 nm and (b) 100 nm particles and percentage increase in CCN concentrations for (c) 50 nm and (d) 100 nm in six diverse locations based on the observed NPF and non-event events. The filled square indicates the mean, the horizontal line indicates the median, the top and bottom of the box indicate 25th and 75th percentile values, and the top and bottom whiskers indicate 10th and 90th percentile values. Note that measurements are from different time periods for each site (refer to Table 2.1), therefore the comparison between the sites is not feasible.

NPF is expected to be more favoured in locations with low pre-existing particles (low condensation sink) such as RNC, MUK and MBL, while NPF is expected to be less favoured in highly polluted urban environments due to high pre-existing particles (high condensation sink) such as HYD, TVM, and DEL. Nevertheless, NPF events occur more frequently in polluted environments in India and China, accompanied by high particle growth rates (Yu et al., 2017). Guo et al. (2014) revealed that NPF significantly enhances the formation of winter-time haze in Beijing. Kulmala et al. (2021) further demonstrated that more than 65% of the haze particles resulted from NPF events in Beijing. Observation sites located at altitudes exceeding 1000 meters above mean sea level (amsl) have experienced elevated levels of condensation sinks and associated precursor gases that are essential for the initiation of nucleation and early growth processes (Sellegri et al., 2019). Hence, the presence of low condensation sinks may not be the requisite for particle nucleation and early growth, as long as there are high rates of vapour

production. The elevated pre-existing particle concentration is also suggestive of air mass containing a significant amount of precursor vapours. However, when the concentration of the condensation sink reaches a significant level, it hinders the process of particle nucleation or early cluster growth. It may be interesting to note that about 50% of the sub-3nm particle burst events in Hyderabad did not show subsequent growth for particles 10nm and above, indicating the unavailability of vapours for condensational growth such as VOCs (Sebastian et al., 2021a). Rose et al. (2017) showed that the occurrence of NPF was more frequent in the boundary layer (48%) compared to the free troposphere (39%) conditions at Chacaltaya mountain in Bolivia. They further found the highest potential for CCN formation for NPF events those were originated in the boundary layer (67%) than those that originated in the free troposphere (53%). Sellegri et al. (2019) carried out a comprehensive analysis CCN concentrations resulting from NPF events. They showed that the production of CCN was the highest in a highly polluted region, San Pietro Capofiume in the Po Valley(7.3×10^3 cm^{-3}) (Laaksonen et al., 2005) while high-altitude locations exhibit lower CCN production from NPF events (Kerminen et al., 2012; Rose et al., 2017). Our findings are consistent with previous research indicating the more increase in CCN concentrations in urban areas (HYD, TVM, and DEL) as compared to high altitude mountainous regions (RNC, MUK, and MBL) in India. The individual newly formed particle under physical transformation to eventually reach to CCN-active size, though it is not possible to track its journey in the atmosphere. This poses a significant challenge in accurately estimating the CCN concentrations resulting from a specific NPF event. Based on the preceding discussion, the aforementioned findings provide valuable insights regarding the potential contribution of newly formed particles to CCN budget.

5.4 Summary

In this chapter, we present the first-ever estimates of the survival probability of newly formed particles to climate-relevant aerosols from different locations in India. We further present the absolute and percentage increase in CCN concentrations due to NPF processes. We further modified the methodology given by Kerminen et al. (2012) to eliminate the potential influence of primary CCN concentrations on the total CCN budget. This allowed us to obtain the most accurate estimation of the increase in CCN concentrations during NPF events. Briefly, we found that the newly formed particle survival probability to 50 nm size ranged from 44 to 98%, with a mean and standard deviation of 82 ± 18%, and the mean survival probability to 100 nm was 53 ± 32%. The mean formation rates of 50 nm and 100 nm particles were 0.08 cm^{-3} s^{-1} and 0.05 cm^{-3} s^{-1}, respectively. Overall mountain-background locations showed the lowest increase in

CCN concentrations than low-altitude urban polluted locations. Our findings highlight the importance of the efficiency of NPF events for producing CCN, which is a critical basis of aerosol indirect effects. We highlight that the mechanisms behind NPF and the factors that determine their ability to act as CCN need to be studied through on-site field observations, utilizing the latest state-of-the-art advancements in aerosol, CCN, and precursor gas measurement techniques, in conjunction with modeling efforts, to be able to interpret field observations. Furthermore, the incorporation of chemical data and measurements of CCN concentrations into the current observations of particle number size distributions would yield novel insights into the connections between NPF and CCN in both pristine and polluted environments.

Chapter 6

Summary and Future Scope

6.1 Summary

Much has been learned over the last five decades about the effects of atmospheric aerosols on weather, air quality, human health, and climate, and it is becoming clear that aerosols are of significant societal and economical importance. While atmospheric aerosol direct effects are sufficiently characterized, aerosol-induced changes in cloud macro- and micro-physical properties are still inadequately illustrated in global climate models to make reliable future climate predictions. New particle formation, as a result of gas-to-particle conversion, is an important phenomenon associated with atmospheric aerosols, that significantly affect cloud condensation nuclei production in the troposphere, and thereby directly affect cloud properties and this climate and hydrological cycle. Despite extensive research on new particle formation or aerosol nucleation based on field measurements, laboratory experiments, theoretical calculations and modelling efforts, significant knowledge gaps persist globally, especially in the Indian context. These knowledge gaps range from the process-level understanding of new particle formation to its diverse impacts on human health, atmospheric chemistry, weather, and climate. For instance, there is only limited information on detailed molecular-scale processes of aerosol nucleation and the role of a variety of chemical species in aerosol gas-phase and particle (secondary organic aerosol, SOA) chemistry in different environments in India. The understanding and deconvolving of the nucleation and growth processes that govern NPF is, therefore, of utmost importance to reduce current uncertainties in CCN formation estimates, and thereby cloud-adjustments due to aerosols in climate models for precise future climate predictions. Most of the studies on aerosol nucleation have focused on temperate regions where distinct and definitive seasonal variations in climatic conditions can be observed. However, such studies in tropical regions are still extremely limited, where the climatic conditions are much different, especially in associating atmospheric aerosol nucleation and cloud condensation nuclei. The objectives of the thesis are designed to overcome some of these shortcomings to better understand the microphysical behaviour of atmospheric aerosols in diverse environments of India.

In this study, we reported the first direct observational evidence of neutral sub-3nm particles in India. Our observations showed that a pool of sub-3nm particles is often present in the atmosphere, but how fast these clusters grow or are scavenged will determine whether NPF (aerosol nucleation and growth) will be detected in the atmosphere. We observed that only half of these events showed newly formed molecular clusters growing past 10 nm diameter size showing a conventional banana-shaped aerosol growth, which is an indicator of the regional NPF event. We have also used long-term continuous (43 months) observations to examine characteristics of size-segregated particle number concentrations in Hyderabad. It was observed that the cluster mode particles dominate the particle number concentration. We observed that cluster mode particle formation was not inhibited under conditions of high pre-existing particle concentration. We found that NPF events can significantly modulate the shape of particle number size distributions and CCN concentrations in India.

We further investigated the influence of air mass history on new particle formation events in Hyderabad. Our analyses showed that air mass origin is not the deciding factor for the occurrence of the new particle formation in Hyderabad city. Instead, it appears that the local and regional modification of the air mass plays a decisive role in determining the occurrence of new particle formation. We observed that new particle formation events are influenced by subsidence during winter in Hyderabad, which facilitates air dilution and reduces pre-existing particle concentration (lower condensation sink). We also observed that the new particle formation events occurred in Hyderabad over a spatial scale of about 300-50 km.

We further provided observational evidence that newly formed particles grow to cloud condensation nuclei (CCN)-active sizes (i.e., >20-100 nm in diameter), first of its kind in the Indian context. We performed the analysis using at least 1 year of asynchronous particle number size distribution data from six distinct environments in India. It found that the survival probability of newly formed particles to 50 nm sizes was in the range of 42% to 98% and that of SP100 in the range of 12% to 95% among the sites. Urban sites showed a greater survival probability compared to mountain background sites. The absolute increase in CCN concentrations from NPF events showed that NPF contribution to CCN concentration is higher in urban areas as compared to mountain background sites. Our estimates indicate that a significant fraction of nucleated particles grow larger than 100 nm, and thus constitute an important source of CCN for cloud formations. These findings highlight the importance of the efficiency of nucleation events for producing CCN, which is a critical basis of aerosol indirect

effects. Thus, the knowledge of size, number concentration, particle formation, and growth and their efficiency of conversion to active-CCN would help in reducing uncertainties in CCN estimation in the regional and climate models.

6.2 Future scope

New particle formation events often occur frequently in cleaner environments under low background aerosol concentrations globally, but the highly polluted regions in developing countries like India and China are becoming hot spots of new particle formation events, even at very high pre-existing particles. Hence, the improved process-level understanding of new particle formation in polluted atmosphere has crucial significance for air quality, human health, weather and climate studies. This work highlights the following major recommendations for future work in the Indian context.

- Creating a highly spatially and temporally resolved particle number size distribution measurement network in India which is an important parameter to elucidate the evolution of aerosols in the atmosphere and to develop a superior process-level understanding of aerosol properties. Further, deployment of recently developed technologically advanced state-of-the-art aerosols measurements such as Chemical Ionization Atmospheric Pressure Interface Time of Flight Mass Spectrometer (CI-APi-TOF-MS) or Porton Transfer Reaction Mass Spectrometer (PTRMS) or other mass spectrometric techniques for the real-time identification and quantification of gas-phase and particle-phase compounds in the air.

- There is utmost need to put forth dedicated efforts to measure aerosol metrics (number concentration, emission rate, and size distribution) to reduce current uncertainties in governing equations of aerosol chemical and/or physical transformation processes in the models.

- It is also imperative to develop adequate capacity with synergy between observations and modelling research, to develop better understanding of key aerosol phenomenon such as secondary organic/inorganic aerosol (SOA/SIA) formation and NPF-CCN linkages or aerosol growth alongside quantifying primary aerosol emissions in the current models to reduce uncertainties to accurately predict future climate.

- The role of monsoon dynamics on new particle formation in the middle and upper troposphere under anticyclonic circulation may also examined considering the Indian monsoon is one the largest monsoon systems globally

The complex cocktail of primary emissions and secondary formation further adds complexity to understanding NPF and its interaction with boundary layer dynamics and feedback. Therefore, the long-term, continuous, and comprehensive observational networks will remove the potential discrepancies that result from short-term and dissimilar observations. Therefore, it is imperative to initiate efforts to establish collaborative endeavours among researchers, policymakers, and stakeholders to bridge these gaps and unveil valuable insights into the complex non-linear NPF and related processes in India.

Bibliography

Ackerman, A.S., Toon, O.B., Stevens, D.E., Heymsfield, A.J., Ramanathan, V., Welton, E.J. (2000) Reduction of Tropical Cloudiness by Soot. 288, 1042-1047.

Aitken, J.A. (1897) On some nuclei of cloudy condensation. Transactions of the Royal Society XXXIX.

Albrecht, B.A. (1989) Aerosols, Cloud Microphysics, and Fractional Cloudiness. 245, 1227-1230.

Almeida, J., Schobesberger, S., Kurten, A., Ortega, I.K., Kupiainen-Maatta, O., Praplan, A.P., Adamov, A., Amorim, A., Bianchi, F., Breitenlechner, M., David, A., Dommen, J., Donahue, N.M., Downard, A., Dunne, E., Duplissy, J., Ehrhart, S., Flagan, R.C., Franchin, A., Guida, R., Hakala, J., Hansel, A., Heinritzi, M., Henschel, H., Jokinen, T., Junninen, H., Kajos, M., Kangasluoma, J., Keskinen, H., Kupc, A., Kurten, T., Kvashin, A.N., Laaksonen, A., Lehtipalo, K., Leiminger, M., Leppa, J., Loukonen, V., Makhmutov, V., Mathot, S., McGrath, M.J., Nieminen, T., Olenius, T., Onnela, A., Petaja, T., Riccobono, F., Riipinen, I., Rissanen, M., Rondo, L., Ruuskanen, T., Santos, F.D., Sarnela, N., Schallhart, S., Schnitzhofer, R., Seinfeld, J.H., Simon, M., Sipila, M., Stozhkov, Y., Stratmann, F., Tome, A., Trostl, J., Tsagkogeorgas, G., Vaattovaara, P., Viisanen, Y., Virtanen, A., Vrtala, A., Wagner, P.E., Weingartner, E., Wex, H., Williamson, C., Wimmer, D., Ye, P., Yli-Juuti, T., Carslaw, K.S., Kulmala, M., Curtius, J., Baltensperger, U., Worsnop, D.R., Vehkamaki, H., Kirkby, J. (2013) Molecular understanding of sulphuric acid-amine particle nucleation in the atmosphere. Nature 502, 359-363.

Almeida, S.M., Pio, C.A., Freitas, M.C., Reis, M.A., Trancoso, M.A. (2006) Source apportionment of atmospheric urban aerosol based on weekdays/weekend variability: evaluation of road re-suspended dust contribution. Atmospheric Environment 40, 2058-2067.

Andreae, M.O., Andreae, T.W., Ditas, F., Pöhlker, C. (2022) Frequent new particle formation at remote sites in the subboreal forest of North America. Atmos. Chem. Phys. 22, 2487-2505.

Anil Kumar, V., Hazra, A., Pandithurai, G., Kulkarni, G., Mohan, G.M., Mukherjee, S., Leena, P.P., Patil, R.D., Prasad, D.S.V.V.D. (2021) Atmospheric ice nucleating particle measurements and parameterization representative for Indian region. Atmospheric Research 253, 105487.

Apte, J.S., Marshall, J.D., Cohen, A.J., Brauer, M. (2015) Addressing Global Mortality from Ambient PM2.5. Environmental Science & Technology 49, 8057-8066.

Asmi, A., Wiedensohler, A., Laj, P., Fjaeraa, A.M., Sellegri, K., Birmili, W., Weingartner, E., Baltensperger, U., Zdimal, V., Zikova, N., Putaud, J.P., Marinoni, A., Tunved, P., Hansson, H.C., Fiebig, M., Kivekäs, N., Lihavainen, H., Asmi, E., Ulevicius, V., Aalto, P.P., Swietlicki, E., Kristensson, A., Mihalopoulos, N., Kalivitis, N., Kalapov, I., Kiss, G., de Leeuw, G., Henzing, B., Harrison, R.M., Beddows, D., O'Dowd, C., Jennings, S.G., Flentje, H., Weinhold, K., Meinhardt, F., Ries, L., Kulmala, M. (2011) Number size distributions and seasonality of submicron particles in Europe 2008–2009. Atmos. Chem. Phys. 11, 5505-5538.

Aubry, T.J., Staunton-Sykes, J., Marshall, L.R., Haywood, J., Abraham, N.L., Schmidt, A. (2021) Climate change modulates the stratospheric volcanic sulfate aerosol lifecycle and radiative forcing from tropical eruptions. Nature Communications 12, 4708.

Babu, S.S., Kompalli, S.K., Moorthy, K.K. (2016) Aerosol number size distributions over a coastal semi urban location: Seasonal changes and ultrafine particle bursts. Science of The Total Environment 563–564, 351-365.

Baccarini, A., Karlsson, L., Dommen, J., Duplessis, P., Vüllers, J., Brooks, I.M., Saiz-Lopez, A., Salter, M., Tjernström, M., Baltensperger, U., Zieger, P., Schmale, J. (2020) Frequent new particle formation over the high Arctic pack ice by enhanced iodine emissions. Nature Communications 11, 4924.

Ball, S.M., Hanson, D.R., Eisele, F.L., McMurry, P.H. (1999) Laboratory studies of particle nucleation: Initial results for H2SO4, H2O, and NH3 vapors. 104, 23709-23718.

Barthlott, C., Zarboo, A., Matsunobu, T., Keil, C. (2022) Importance of aerosols and shape of the cloud droplet size distribution for convective clouds and precipitation. Atmos. Chem. Phys. 22, 2153-2172.

Benson, D.R., Erupe, M.E., Lee, S.-H. (2009) Laboratory-measured H2SO4-H2O-NH3 ternary homogeneous nucleation rates: Initial observations. Geophysical Research Letters 36.

Benson, D.R., Li-Hao, Y., Shan-Hu, L., Campos, T.L., Rogers, D.C., Jensen, J. (2008) The effects of airmass history on new particle formation in the free troposphere: case studies. Atmos. Chem. Phys. 8, 3015-3024.

Berland, K., Rose, C., Pey, J., Culot, A., Freney, E., Kalivitis, N., Kouvarakis, G., Cerro, J.C., Mallet, M., Sartelet, K., Beckmann, M., Bourriane, T., Roberts, G., Marchand, N., Mihalopoulos, N., Sellegri, K. (2017) Spatial extent of new particle formation events over the Mediterranean Basin from multiple ground-based and airborne measurements. Atmos. Chem. Phys. 17, 9567-9583.

Bianchi, F., Junninen, H., Bigi, A., Sinclair, V.A., Dada, L., Hoyle, C.R., Zha, Q., Yao, L., Ahonen, L.R., Bonasoni, P., Buenrostro Mazon, S., Hutterli, M., Laj, P., Lehtipalo, K., Kangasluoma, J., Kerminen, V.M., Kontkanen, J., Marinoni, A., Mirme, S., Molteni, U., Petäjä, T., Riva, M., Rose, C., Sellegri, K., Yan, C., Worsnop, D.R., Kulmala, M., Baltensperger, U., Dommen, J. (2021) Biogenic particles formed in the Himalaya as an important source of free tropospheric aerosols. Nature Geoscience 14, 4-9.

Birmili, W., Wiedensohler, A., Plass-Dülmer, C., Berresheim, H. (2000) Evolution of newly formed aerosol particles in the continental boundary layer: A case study including OH and H2SO4 measurements. 27, 2205-2208.

Boersma, K.F., Eskes, H.J., Veefkind, J.P., Brinksma, E.J., van der A, R.J., Sneep, M., van den Oord, G.H.J., Levelt, P.F., Stammes, P., Gleason, J.F., Bucsela, E.J. (2007) Near-real time retrieval of tropospheric NO₂ from OMI. Atmos. Chem. Phys. 7, 2103-2118.

Boulon, J., Sellegri, K., Venzac, H., Picard, D., Weingartner, E., Wehrle, G., Collaud Coen, M., Bütikofer, R., Flückiger, E., Baltensperger, U., Laj, P. (2010) New particle formation and ultrafine charged aerosol climatology at a high altitude site in the Alps (Jungfraujoch, 3580 m a.s.l., Switzerland). Atmos. Chem. Phys. 10, 9333-9349.

Bousiotis, D., Brean, J., Pope, F.D., Dall'Osto, M., Querol, X., Alastuey, A., Perez, N., Petäjä, T., Massling, A., Nøjgaard, J.K., Nordstrøm, C., Kouvarakis, G., Vratolis, S., Eleftheriadis, K., Niemi, J.V., Portin, H., Wiedensohler, A., Weinhold, K., Merkel, M., Tuch, T., Harrison, R.M.

(2021) The effect of meteorological conditions and atmospheric composition in the occurrence and development of new particle formation (NPF) events in Europe. Atmos. Chem. Phys. 21, 3345-3370.

Brock, C.A., Froyd, K.D., Dollner, M., Williamson, C.J., Schill, G., Murphy, D.M., Wagner, N.J., Kupc, A., Jimenez, J.L., Campuzano-Jost, P., Nault, B.A., Schroder, J.C., Day, D.A., Price, D.J., Weinzierl, B., Schwarz, J.P., Katich, J.M., Wang, S., Zeng, L., Weber, R., Dibb, J., Scheuer, E., Diskin, G.S., DiGangi, J.P., Bui, T., Dean-Day, J.M., Thompson, C.R., Peischl, J., Ryerson, T.B., Bourgeois, I., Daube, B.C., Commane, R., Wofsy, S.C. (2021) Ambient aerosol properties in the remote atmosphere from global-scale in situ measurements. Atmos. Chem. Phys. 21, 15023-15063.

Brock, J.R., Suck, S.H. (1982) AEROSOL DYNAMICS. Aerosol Science and Technology 2, 200-213.

Cai, J., Chu, B., Yao, L., Yan, C., Heikkinen, L.M., Zheng, F., Li, C., Fan, X., Zhang, S., Yang, D., Wang, Y., Kokkonen, T.V., Chan, T., Zhou, Y., Dada, L., Liu, Y., He, H., Paasonen, P., Kujansuu, J.T., Petäjä, T., Mohr, C., Kangasluoma, J., Bianchi, F., Sun, Y., Croteau, P.L., Worsnop, D.R., Kerminen, V.M., Du, W., Kulmala, M., Daellenbach, K.R. (2020) Size-segregated particle number and mass concentrations from different emission sources in urban Beijing. Atmos. Chem. Phys. 20, 12721-12740.

Cai, R., Yang, D., Ahonen, L.R., Shi, L., Korhonen, F., Ma, Y., Hao, J., Petäjä, T., Zheng, J., Kangasluoma, J., Jiang, J. (2018) Data inversion methods to determine sub-3 nm aerosol size distributions using the particle size magnifier. Atmos. Meas. Tech. 11, 4477-4491.

Cai, R., Yang, D., Fu, Y., Wang, X., Li, X., Ma, Y., Hao, J., Zheng, J., Jiang, J. (2017) Aerosol surface area concentration: a governing factor in new particle formation in Beijing. Atmos. Chem. Phys. 17, 12327-12340.

Cai, R., Yin, R., Li, X., Xie, H.-B., Yang, D., Kerminen, V.-M., Smith, J.N., Ma, Y., Hao, J., Chen, J., Kulmala, M., Zheng, J., Jiang, J., Elm, J. (2023) Significant contributions of trimethylamine to sulfuric acid nucleation in polluted environments. npj Climate and Atmospheric Science 6, 75.

Casquero-Vera, J.A., Lyamani, H., Dada, L., Hakala, S., Paasonen, P., Román, R., Fraile, R., Petäjä, T., Olmo-Reyes, F.J., Alados-Arboledas, L. (2020) New particle formation at urban and high-altitude remote sites in the south-eastern Iberian Peninsula. Atmos. Chem. Phys. 20, 14253-14271.

Census of India, (2011) Provisional population totals: rural-urban distribution Volume 2, Issue 1 of Census of India, 2011, India. India: Office of the

Registrar General & Census Commissioner.

Chan, T., Cai, R., Ahonen, L.R., Liu, Y., Zhou, Y., Vanhanen, J., Dada, L., Chao, Y., Liu, Y., Wang, L., Kulmala, M., Kangasluoma, J. (2020) Assessment of particle size magnifier inversion methods to obtain the particle size distribution from atmospheric measurements. Atmos. Meas. Tech. 13, 4885-4898.

Chang, Y., Huang, R., Ge, X., Huang, X., Hu, J., Duan, Y., Zou, Z., Liu, X., Lehmann, M.F. (2020) Puzzling Haze Events in China During the Coronavirus (COVID-19) Shutdown. Geophysical Research Letters 47, e2020GL088533.

Charlson, R.J., Schwartz, S.E., Hales, J.M., Cess, R.D., Coakley, J.A., Hansen, J.E., Hofmann, D.J. (1992) Climate Forcing by Anthropogenic Aerosols. 255, 423-430.

Chate, D.M., Devara, P.C.S. (2005) Growth Properties of Sub-Micron Aerosols during Cold Season in India. Aerosol and Air Quality Research 5, 127-140.

Chatterjee, A., Mukherjee, S., Dutta, M., Ghosh, A., Ghosh, S.K., Roy, A. (2021) High rise in carbonaceous aerosols under very low anthropogenic emissions over eastern Himalaya, India: Impact of lockdown for COVID-19 outbreak. Atmospheric Environment 244, 117947.

Chauhan, A., Singh, R.P. (2020) Decline in PM2.5 concentrations over major cities around the world associated with COVID-19. Environmental Research 187, 109634.

Chen, P., Bi, X., Zhang, J., Wu, J., Feng, Y. (2015) Assessment of heavy metal pollution characteristics and human health risk of exposure to ambient PM2.5 in Tianjin, China. Particuology 20, 104-109.

Chlek, P., Coakley, J.A. (1974) Aerosols and Climate. 183, 75-77.

Chowdhury, S., Dey, S., Smith, K.R. (2018) Ambient PM2.5 exposure and expected premature mortality to 2100 in India under climate change scenarios. Nature Communications 9, 318.

Chu, B., Kerminen, V.M., Bianchi, F., Yan, C., Petäjä, T., Kulmala, M. (2019) Atmospheric new particle formation in China. Atmos. Chem. Phys. 19, 115-138.

Clarke, A.D. (1993) Atmospheric nuclei in the Pacific midtroposphere: Their nature, concentration, and evolution. 98, 20633-20647.

Clarke, A.D., Freitag, S., Simpson, R.M.C., Hudson, J.G., Howell, S.G., Brekhovskikh, V.L., Campos, T., Kapustin, V.N., Zhou, J. (2013) Free troposphere as a major source of CCN for the equatorial pacific boundary layer: long-range transport and teleconnections. Atmos. Chem. Phys. 13, 7511-7529.

Clarke, A.D., Kapustin, V.N. (2002) A Pacific Aerosol Survey. Part I: A Decade of Data on Particle Production, Transport, Evolution, and Mixing in the Troposphere %J Journal of the Atmospheric Sciences. 59, 363-382.

Clarke, A.D., Varner, J.L., Eisele, F., Mauldin, R.L., Tanner, D., Litchy, M. (1998) Particle production in the remote marine atmosphere: Cloud outflow and subsidence during ACE 1. 103, 16397-16409.

Clement, C.F., Ford, I.J. (1999) Gas-to-particle conversion in the atmosphere: I. Evidence from empirical atmospheric aerosols. Atmospheric Environment 33, 475-487.

Covert, D.S., Kapustin, V.N., Bates, T.S., Quinn, P.K. (1996) Physical properties of marine boundary layer aerosol particles of the mid-Pacific in relation to sources and meteorological transport. 101, 6919-6930.

Creamean, J.M., Ault, A.P., Ten Hoeve, J.E., Jacobson, M.Z., Roberts, G.C., Prather, K.A. (2011) Measurements of Aerosol Chemistry during New Particle Formation Events at a Remote Rural Mountain Site. Environmental Science & Technology 45, 8208-8216.

Crippa, P., Pryor, S.C. (2013) Spatial and temporal scales of new particle formation events in eastern North America. Atmospheric Environment 75, 257-264.

Crumeyrolle, S., Kontkanen, J.S.S., Rose, C., Velazquez Garcia, A., Bourrianne, E., Catalfamo, M., Riffault, V., Tison, E., Ferreira de Brito, J., Visez, N., Ferlay, N., Auriol, F., Chiapello, I. (2023) Measurement report: Atmospheric new particle formation at a peri-urban site in Lille, northern France. Atmos. Chem. Phys. 23, 183-201.

Curtius, J. (2006) Nucleation of atmospheric aerosol particles. Comptes Rendus Physique 7, 1027-1045.

d'Almeida, G.A., (1989) Desert Aerosol: Characteristics and Effects on Climate, in: Leinen, M., Sarnthein, M. (Eds.), Paleoclimatology and Paleometeorology: Modern and Past Patterns of Global Atmospheric Transport. Springer Netherlands, Dordrecht, pp. 311-338.

Dada, L., Angot, H., Beck, I., Baccarini, A., Quéléver, L.L.J., Boyer, M., Laurila, T., Brasseur, Z., Jozef, G., de Boer, G., Shupe, M.D., Henning, S., Bucci, S., Dütsch, M., Stohl, A., Petäjä, T., Daellenbach, K.R., Jokinen, T., Schmale, J. (2022) A central arctic extreme aerosol event triggered by a warm air-mass intrusion. Nature Communications 13, 5290.

Dada, L., Ylivinkka, I., Baalbaki, R., Li, C., Guo, Y., Yan, C., Yao, L., Sarnela, N., Jokinen, T., Daellenbach, K.R., Yin, R., Deng, C., Chu, B., Nieminen, T., Wang, Y., Lin, Z., Thakur, R.C., Kontkanen, J., Stolzenburg, D., Sipilä, M., Hussein, T., Paasonen, P., Bianchi, F., Salma, I., Weidinger, T., Pikridas, M., Sciare, J., Jiang, J., Liu, Y., Petäjä, T., Kerminen, V.M., Kulmala, M. (2020) Sources and sinks driving sulfuric acid concentrations in contrasting environments: implications on proxy calculations. Atmos. Chem. Phys. 20, 11747-11766.

Dal Maso, M., Kulmala, M., Lehtinen, K.E.J., Mäkelä, J.M., Aalto, P., O'Dowd, C.D. (2002) Condensation and coagulation sinks and formation of nucleation mode particles in coastal and boreal forest boundary layers. Journal of Geophysical Research: Atmospheres 107, PAR 2-1-PAR 2-10.

Dal Maso, M., Kulmala, M., Riipinen, I., Wagner, R., Hussein, T., Aalto, P.P., Lehtinen, K.E.J. (2005) Formation and growth of fresh atmospheric aerosols: eight years of aerosol size distribution data from SMEAR II, Hyytiälä, Finland. Boreal Env. Res. 10, 323-336.

Dal Maso, M., Sogacheva, L., P., A.P., RIiipinen, I., Komppula, M., Tunved, P., Korhonen, L., Suur-uski, V., Hirsikko, A., Kurten, T., Kerminen, V.-M., Lihavainen, H., Viisanen, Y., Hansson, H.-C., Kulmala, M. (2007) Aerosol size distribution measurements at four Nordic field stations: identification, analysis and trajectory analysis of new particle formation bursts. 59, 350-361.

Dall´Osto, M., Beddows, D.C.S., Tunved, P., Krejci, R., Ström, J., Hansson, H.C., Yoon, Y.J., Park, K.-T., Becagli, S., Udisti, R., Onasch, T., O´Dowd, C.D., Simó, R., Harrison, R.M. (2017) Arctic sea ice melt leads to atmospheric new particle formation. Scientific Reports 7, 3318.

Das, B., Pathak, B., Chutia, L., Subba, T., Bhuyan, P.K., (2023) Genesis of New Particle Formation Events in a Semi-Urban Location in Eastern Himalayan Foothills, Atmosphere.

Dawson, M.L., Varner, M.E., Perraud, V., Ezell, M.J., Gerber, R.B., Finlayson-Pitts, B.J. (2012) Simplified mechanism for new particle formation from methanesulfonic acid, amines, and water via experiments and ab initio calculations. Proceedings of the National Academy of Sciences 109, 18719-18724.

De Smedt, I., Theys, N., Yu, H., Danckaert, T., Lerot, C., Compernolle, S., Van Roozendael, M., Richter, A., Hilboll, A., Peters, E., Pedergnana, M., Loyola, D., Beirle, S., Wagner, T., Eskes, H., van Geffen, J., Boersma, K.F., Veefkind, P. (2018) Algorithm theoretical baseline for formaldehyde retrievals from S5P TROPOMI and from the QA4ECV project. Atmos. Meas. Tech. 11, 2395-2426.

Deng, C., Cai, R., Yan, C., Zheng, J., Jiang, J. (2021) Formation and growth of sub-3 nm particles in megacities: impact of background aerosols. Faraday Discussions 226, 348-363.

Deng, C., Fu, Y., Dada, L., Yan, C., Cai, R., Yang, D., Zhou, Y., Yin, R., Lu, Y., Li, X., Qiao, X., Fan, X., Nie, W., Kontkanen, J., Kangasluoma, J., Chu, B., Ding, A., Kerminen, V.M., Paasonen, P., Worsnop, D.R., Bianchi, F., Liu, Y., Zheng, J., Wang, L., Kulmala, M., Jiang, J. (2020) Seasonal Characteristics of New Particle Formation and Growth in Urban Beijing. Environmental Science & Technology 54, 8547-8557.

Dépée, A., Lemaitre, P., Gelain, T., Monier, M., Flossmann, A. (2021) Laboratory study of the collection efficiency of submicron aerosol particles by cloud droplets – Part II: Influence of electric charges. Atmos. Chem. Phys. 21, 6963-6984.

Dey, S., Tripathi, S.N., Singh, R.P., Holben, B.N. (2004) Influence of dust storms on the aerosol optical properties over the Indo-Gangetic basin. 109.

Dinoi, A., Gulli, D., Ammoscato, I., Calidonna, C.R., Contini, D. (2021) Impact of the Coronavirus Pandemic Lockdown on Atmospheric Nanoparticle Concentrations in Two Sites of Southern Italy. Atmosphere 12, 352.

Dominick, D., Wilson, S.R., Paton-Walsh, C., Humphries, R., Guérette, E.-A., Keywood, M., Kubistin, D., Marwick, B. (2018) Characteristics of airborne particle number size distributions in a coastal-urban environment. Atmospheric Environment 186, 256-265.

Draxler, R.R., Rolph, G.D. (2010) HYSPLIT—HYbrid Single-Particle Lagrangian Integrated Trajectory Model. . Available online: http://ready.arl.noaa.gov/HYSPLIT.php.

Drinovec, L., Močnik, G., Zotter, P., Prévôt, A.S.H., Ruckstuhl, C., Coz, E., Rupakheti, M., Sciare, J., Müller, T., Wiedensohler, A., Hansen, A.D.A. (2015) The "dual-spot" Aethalometer: an improved measurement of aerosol black carbon with real-time loading compensation. Atmos. Meas. Tech. 8, 1965-1979.

Dunn, M.J., Jiménez, J.-L., Baumgardner, D., Castro, T., McMurry, P.H., Smith, J.N. (2004) Measurements of Mexico City nanoparticle size distributions: Observations of new particle formation and growth. Geophysical Research Letters 31, n/a-n/a.

Dunne, E.M., Gordon, H., Kürten, A., Almeida, J., Duplissy, J., Williamson, C.J., Ortega, I.K., Pringle, K.J., Adamov, A., Baltensperger, U., Barmet, P., Benduhn, F., Bianchi, F., Breitenlechner, M., Clarke, A., Curtius, J., Dommen, J., Donahue, N.M., Ehrhart, S., Flagan, R.C., Franchin, A., Guida, R., Hakala, J., Hansel, A., Heinritzi, M., Jokinen, T., Kangasluoma, J., Kirkby, J., Kulmala, M., Kupc, A., Lawler, M.J., Lehtipalo, K., Makhmutov, V., Mann, G.,

Mathot, S., Merikanto, J., Miettinen, P., Nenes, A., Onnela, A., Rap, A., Reddington, C.L.S., Riccobono, F., Richards, N.A.D., Rissanen, M.P., Rondo, L., Sarnela, N., Schobesberger, S., Sengupta, K., Simon, M., Sipilä, M., Smith, J.N., Stozkhov, Y., Tomé, A., Tröstl, J., Wagner, P.E., Wimmer, D., Winkler, P.M., Worsnop, D.R., Carslaw, K.S. (2016) Global atmospheric particle formation from CERN CLOUD measurements. 354, 1119-1124.

Duplissy, J., Merikanto, J., Franchin, A., Tsagkogeorgas, G., Kangasluoma, J., Wimmer, D., Vuollekoski, H., Schobesberger, S., Lehtipalo, K., Flagan, R.C., Brus, D., Donahue, N.M., Vehkamäki, H., Almeida, J., Amorim, A., Barmet, P., Bianchi, F., Breitenlechner, M., Dunne, E.M., Guida, R., Henschel, H., Junninen, H., Kirkby, J., Kürten, A., Kupc, A., Määttänen, A., Makhmutov, V., Mathot, S., Nieminen, T., Onnela, A., Praplan, A.P., Riccobono, F., Rondo, L., Steiner, G., Tome, A., Walther, H., Baltensperger, U., Carslaw, K.S., Dommen, J., Hansel, A., Petäjä, T., Sipilä, M., Stratmann, F., Vrtala, A., Wagner, P.E., Worsnop, D.R., Curtius, J., Kulmala, M. (2016) Effect of ions on sulfuric acid-water binary particle formation: 2. Experimental data and comparison with QC-normalized classical nucleation theory. 121, 1752-1775.

Dusek, U., Frank, G.P., Hildebrandt, L., Curtius, J., Schneider, J., Walter, S., Chand, D., Drewnick, F., Hings, S., Jung, D., Borrmann, S., Andreae, M.O. (2006) Size Matters More Than Chemistry for Cloud-Nucleating Ability of Aerosol Particles. Science 312, 1375-1378.

Eichkorn, S., Wohlfrom, K.H., Arnold, F., Busen, R. (2002) Massive positive and negative chemiions in the exhaust of an aircraft jet engine at ground-level: mass distribution measurements and implications for aerosol formation. Atmospheric Environment 36, 1821-1825.

Erupe, M.E., Benson, D.R., Li, J., Young, L.H., Verheggen, B., Al-Refai, M., Tahboub, O., Cunningham, V., Frimpong, F., Viggiano, A.A., Lee, S.H. (2010) Correlation of Aerosol Nucleation Rate with Sulfuric Acid and Ammonia in Kent Ohio: An Atmospheric Observation. J. Geophys. Res. 115.

Erupe, M.E., Viggiano, A.A., Lee, S.H. (2011) The effect of trimethylamine on atmospheric nucleation involving H2SO4. Atmos. Chem. Phys. 11, 4767-4775.

Finkenzeller, H., Iyer, S., He, X.C., Simon, M., Koenig, T.K., Lee, C.F., Valiev, R., Hofbauer, V., Amorim, A., Baalbaki, R., Baccarini, A., Beck, L., Bell, D.M., Caudillo, L., Chen, D., Chiu, R., Chu, B., Dada, L., Duplissy, J., Heinritzi, M., Kemppainen, D., Kim, C., Krechmer, J., Kürten, A., Kvashnin, A., Lamkaddam, H., Lee, C.P., Lehtipalo, K., Li, Z., Makhmutov, V., Manninen, H.E., Marie, G., Marten, R., Mauldin, R.L., Mentler, B., Müller, T., Petäjä, T., Philippov, M., Ranjithkumar, A., Rörup, B., Shen, J., Stolzenburg, D., Tauber, C., Tham, Y.J., Tomé, A., Vazquez-Pufleau, M., Wagner, A.C., Wang, D.S., Wang, M., Wang, Y., Weber, S.K., Nie, W., Wu, Y., Xiao, M., Ye, Q., Zauner-Wieczorek, M., Hansel, A., Baltensperger, U., Brioude, J., Curtius, J., Donahue, N.M., Haddad, I.E., Flagan, R.C., Kulmala, M., Kirkby, J., Sipilä, M., Worsnop, D.R., Kurten, T., Rissanen, M.P., Volkamer, R. (2023) The gas-phase formation mechanism of iodic acid as an atmospheric aerosol source. Nature Chemistry 15, 129-135.

Finlayson-Pitts, B., Pitts, Jr. (2000) Chemistry of Upper and Lower Atmosphere.

Fleming, Z.L., Monks, P.S., Manning, A.J. (2012) Review: Untangling the influence of air-mass history in interpreting observed atmospheric composition. Atmospheric Research 104-105, 1-39.

Forster, P., Ramaswamy, V., Artaxo, P., Berntsen, T., Betts, R., Fahey, D.W., Haywood, J., Lean, J., Lowe, D.C., Myhre, G., Nganga, J., Prinn, R., Raga, G., Schulz, M., Van Dorland, R. (2007) Changes in Atmospheric Constituents and in Radiative Forcing. In: Climate Change 2007: The Physical Science Basis, Contribution of Working Group I to the Fourth Assessment Report of the Intergovernmental Panel on Climate Change, edited by: Solomon, S., Qin, D., Manning, M., Chen, Z., Marquis, M., Averyt, K. B., Tignor, M., and Miller, H. L., Cambridge University

Press, Cambridge, United Kingdom and New York, NY, USA, 2007.

Foucart, B., Sellegri, K., Tulet, P., Rose, C., Metzger, J.M., Picard, D. (2018) High occurrence of new particle formation events at the Maïdo high-altitude observatory (2150 m), Réunion (Indian Ocean). Atmos. Chem. Phys. 18, 9243-9261.

Friedlander, S.K. (1977) Smoke, Dust and Haze: Fundamentals of Aerosol Behaviour.

Gani, S., Bhandari, S., Patel, K., Seraj, S., Soni, P., Arub, Z., Habib, G., Hildebrandt Ruiz, L., Apte, J.S. (2020) Particle number concentrations and size distribution in a polluted megacity: the Delhi Aerosol Supersite study. Atmos. Chem. Phys. 20, 8533-8549.

Giechaskiel, B., Melas, A., Martini, G., Dilara, P., Ntziachristos, L. (2022) Revisiting Total Particle Number Measurements for Vehicle Exhaust Regulations. 13, 155.

Glasoe, W.A., Volz, K., Panta, B., Freshour, N., Bachman, R., Hanson, D.R., McMurry, P.H., Jen, C. (2015) Sulfuric acid nucleation: An experimental study of the effect of seven bases. Journal of Geophysical Research: Atmospheres 120, 1933-1950.

Gordon, H., Kirkby, J., Baltensperger, U., Bianchi, F., Breitenlechner, M., Curtius, J., Dias, A., Dommen, J., Donahue, N.M., Dunne, E.M., Duplissy, J., Ehrhart, S., Flagan, R.C., Frege, C., Fuchs, C., Hansel, A., Hoyle, C.R., Kulmala, M., Kürten, A., Lehtipalo, K., Makhmutov, V., Molteni, U., Rissanen, M.P., Stozkhov, Y., Tröstl, J., Tsagkogeorgas, G., Wagner, R., Williamson, C., Wimmer, D., Winkler, P.M., Yan, C., Carslaw, K.S. (2017) Causes and importance of new particle formation in the present-day and preindustrial atmospheres. Journal of Geophysical Research: Atmospheres 122, 8739-8760.

Griffin, D., Zhao, X., McLinden, C.A., Boersma, F., Bourassa, A., Dammers, E., Degenstein, D., Eskes, H., Fehr, L., Fioletov, V., Hayden, K., Kharol, S.K., Li, S.-M., Makar, P., Martin, R.V., Mihele, C., Mittermeier, R.L., Krotkov, N., Sneep, M., Lamsal, L.N., Linden, M.t., Geffen, J.v., Veefkind, P., Wolde, M. (2019) High-Resolution Mapping of Nitrogen Dioxide With TROPOMI: First Results and Validation Over the Canadian Oil Sands. 46, 1049-1060.

Grimm, H., Eatough, D.J. (2009) Aerosol Measurement: The Use of Optical Light Scattering for the Determination of Particulate Size Distribution, and Particulate Mass, Including the Semi-Volatile Fraction. Journal of the Air & Waste Management Association 59, 101-107.

Gunthe, S.S., Liu, P., Panda, U., Raj, S.S., Sharma, A., Darbyshire, E., Reyes-Villegas, E., Allan, J., Chen, Y., Wang, X., Song, S., Pöhlker, M.L., Shi, L., Wang, Y., Kommula, S.M., Liu, T., Ravikrishna, R., McFiggans, G., Mickley, L.J., Martin, S.T., Pöschl, U., Andreae,

M.O., Coe, H. (2021) Enhanced aerosol particle growth sustained by high continental chlorine emission in India. Nature Geoscience 14, 77-84.

Guo, S., Hu, M., Zamora, M.L., Peng, J., Shang, D., Zheng, J., Du, Z., Wu, Z., Shao, M., Zeng, L., Molina, M.J., Zhang, R. (2014) Elucidating severe urban haze formation in China. 111, 17373-17378.

Hagen, D.E., Alofs, D.J. (1983) Linear Inversion Method to Obtain Aerosol Size Distributions from Measurements with a Differential Mobility Analyzer. Aerosol Science and Technology 2, 465-475.

Hakala, S., Alghamdi, M.A., Paasonen, P., Vakkari, V., Khoder, M.I., Neitola, K., Dada, L., Abdelmaksoud, A.S., Al-Jeelani, H., Shabbaj, I.I., Almehmadi, F.M., Sundström, A.M., Lihavainen, H., Kerminen, V.M., Kontkanen, J., Kulmala, M., Hussein, T., Hyvärinen, A.P. (2019) New particle formation, growth and apparent shrinkage at a rural background site in western Saudi Arabia. Atmos. Chem. Phys. 19, 10537-10555.

Hakala, S., Vakkari, V., Bianchi, F., Dada, L., Deng, C., Dällenbach, K.R., Fu, Y., Jiang, J., Kangasluoma, J., Kujansuu, J., Liu, Y., Petäjä, T., Wang, L., Yan, C., Kulmala, M., Paasonen, P. (2022) Observed coupling between air mass history, secondary growth of nucleation mode particles and aerosol pollution levels in Beijing. Environmental Science: Atmospheres 2, 146-164.

Hallar, A.G., Lowenthal, D.H., Chirokova, G., Borys, R.D., Wiedinmyer, C. (2011) Persistent daily new particle formation at a mountain-top location. Atmospheric Environment 45, 4111-4115.

Hallquist, M., Wenger, J.C., Baltensperger, U., Rudich, Y., Simpson, D., Claeys, M., Dommen, J., Donahue, N.M., George, C., Goldstein, A.H., Hamilton, J.F., Herrmann, H., Hoffmann, T., Iinuma, Y., Jang, M., Jenkin, M.E., Jimenez, J.L., Kiendler-Scharr, A., Maenhaut, W., McFiggans, G., Mentel, T.F., Monod, A., Prévôt, A.S.H., Seinfeld, J.H., Surratt, J.D., Szmigielski, R., Wildt, J. (2009) The formation, properties and impact of secondary organic aerosol: current and emerging issues. Atmos. Chem. Phys. 9, 5155-5236.

Han, Q., Rossow, W.B., Chou, J., Welch, R.M. (1998) Global Survey of the Relationships of Cloud Albedo and Liquid Water Path with Droplet Size Using ISCCP. Journal of Climate 11, 1516-1528.

Hansen, J., Sato, M., Ruedy, R. (1997) Radiative forcing and climate response. 102, 6831-6864.

Hansen, J., Sato, M., Ruedy, R., Lacis, A., Oinas, V. (2000) Global warming in the twenty-first century: An alternative scenario. Proceedings of the National Academy of Sciences 97, 9875-9880.

Hanson, D.R., Lovejoy, E.R. (2006) Measurement of the Thermodynamics of the Hydrated Dimer and Trimer of Sulfuric Acid. The Journal of Physical Chemistry A 110, 9525-9528.

Hanson, D.R., McMurry, P.H., Jiang, J., Tanner, D., Huey, L.G. (2011) Ambient Pressure Proton Transfer Mass Spectrometry: Detection of Amines and Ammonia. Environmental Science & Technology 45, 8881-8888.

Haywood, J., Boucher, O. (2000) Estimates of the direct and indirect radiative forcing due to tropospheric aerosols: A review. 38, 513-543.

He, X.C., Tham, Y.J., Dada, L., Wang, M., Finkenzeller, H., Stolzenburg, D., Iyer, S., Simon, M., Kürten, A., Shen, J., Rörup, B., Rissanen, M.P., Schobesberger, S., Baalbaki, R., Wang, D.S., Koenig, T.K., Jokinen, T., Sarnela, N., Beck, L.J., Almeida, J., Amanatidis, S., Amorim, A., Ataei, F., Baccarini, A., Bertozzi, B., Bianchi, F., Brilke, S., Caudillo, L., Chen, D., Chiu, R., Chu, B., Dias, A., Ding, A., Dommen, J., Duplissy, J., El Haddad, I., Gonzalez Carracedo, L., Granzin, M., Hansel, A., Heinritzi, M., Hofbauer, V., Junninen, H., Kangasluoma, J., Kemppainen, D., Kim, C., Kong, W., Krechmer, J.E., Kvashin, A.N., Laitinen, T., Lamkaddam, H., Lee, C.P., Lehtipalo, K., Leiminger, M., Li, Z., Makhmutov, V., Manninen, H.E., Marie, G., Marten, R., Mathot, S., Mauldin, R.L., Mentler, B., Möhler, O., Müller, T., Nie, W., Onnela, A., Petäjä, T., Pfeifer, J., Philippov, M., Ranjithkumar, A., Saiz-Lopez, A., Salma, I., Scholz, W., Schuchmann, S., Schulze, B., Steiner, G., Stozhkov, Y., Tauber, C., Tomé, A., Thakur, R.C., Väisänen, O., Vazquez-Pufleau, M., Wagner, A.C., Wang, Y., Weber, S.K., Winkler, P.M., Wu, Y., Xiao, M., Yan, C., Ye, Q., Ylisirniö, A., Zauner-Wieczorek, M., Zha, Q., Zhou, P., Flagan, R.C., Curtius, J., Baltensperger, U., Kulmala, M., Kerminen, V.M., Kurtén, T., Donahue, N.M., Volkamer, R., Kirkby, J., Worsnop, D.R., Sipilä, M. (2021) Role of iodine oxoacids in atmospheric aerosol nucleation. Science 371, 589-595.

Heintzenberg, J., Wehner, B., Birmili, W. (2007) 'How to find bananas in the atmospheric aerosol': new approach for analyzing atmospheric nucleation and growth events. 59, 273-282.

Herb, J., Nadykto, A.B., Yu, F. (2011) Large ternary hydrogen-bonded pre-nucleation clusters in the Earth's atmosphere. Chemical Physics Letters 518, 7-14.

Hersbach, H., Bell, B., Berrisford, P., Biavati, G., Horányi, A., Muñoz Sabater, J., Nicolas, J., Peubey, C., Radu, R., Rozum, I., Schepers, D., Simmons, A., Soci, C., Dee, D., Thépaut, J.-N. (2023) ERA5 hourly data on pressure levels from 1940 to present. Copernicus Climate Change Service (C3S) Climate Data Store (CDS)

Hersbach, H., Bell, B., Berrisford, P., Hirahara, S., Horányi, A., Muñoz-Sabater, J., Nicolas, J., Peubey, C., Radu, R., Schepers, D., Simmons, A., Soci, C., Abdalla, S., Abellan, X., Balsamo, G., Bechtold, P., Biavati, G., Bidlot, J., Bonavita, M., De Chiara, G., Dahlgren, P., Dee, D., Diamantakis, M., Dragani, R., Flemming, J., Forbes, R., Fuentes, M., Geer, A., Haimberger, L., Healy, S., Hogan, R.J., Hólm, E., Janisková, M., Keeley, S., Laloyaux, P., Lopez, P., Lupu, C., Radnoti, G., de Rosnay, P., Rozum, I., Vamborg, F., Villaume, S., Thépaut, J.-N. (2020) The ERA5 global reanalysis. 146, 1999-2049.

Hodshire, A.L., Lawler, M.J., Zhao, J., Ortega, J., Jen, C., Yli-Juuti, T., Brewer, J.F., Kodros, J.K., Barsanti, K.C., Hanson, D.R., McMurry, P.H., Smith, J.N., Pierce, J.R. (2016) Multiple new-particle growth pathways observed at the US DOE Southern Great Plains field site. Atmos. Chem. Phys. 16, 9321-9348.

Holben, B.N., Eck, T.F., Slutsker, I., Tanré, D., Buis, J.P., Setzer, A., Vermote, E., Reagan, J.A., Kaufman, Y.J., Nakajima, T., Lavenu, F., Jankowiak, I., Smirnov, A. (1998) AERONET—A Federated Instrument Network and Data Archive for Aerosol Characterization. Remote Sensing of Environment 66, 1-16.

Hooda, R.K., Kivekäs, N., O'Connor, E.J., Collaud Coen, M., Pietikäinen, J.-P., Vakkari, V., Backman, J., Henriksson, S.V., Asmi, E., Komppula, M., Korhonen, H., Hyvärinen, A.-P., Lihavainen, H. (2018) Driving Factors of Aerosol Properties Over the Foothills of Central Himalayas Based on 8.5 Years Continuous Measurements. Journal of Geophysical Research: Atmospheres 123, 13,421-413,442.

Huang, X., Ding, A., Gao, J., Zheng, B., Zhou, D., Qi, X., Tang, R., Wang, J., Ren, C., Nie, W., Chi, X., Xu, Z., Chen, L., Li, Y., Che, F., Pang, N., Wang, H., Tong, D., Qin, W., Cheng, W., Liu, W., Fu, Q., Liu, B., Chai, F., Davis, S.J., Zhang, Q., He, K. (2021) Enhanced secondary pollution offset reduction of primary emissions during COVID-19 lockdown in China. National Science Review 8.

Huang, X., Ding, A., Wang, Z., Ding, K., Gao, J., Chai, F., Fu, C. (2020) Amplified transboundary transport of haze by aerosol–boundary layer interaction in China. Nature Geoscience 13, 428-434.

Hussein, T., Junninen, H., Tunved, P., Kristensson, A., Dal Maso, M., Riipinen, I., Aalto, P.P., Hansson, H.C., Swietlicki, E., Kulmala, M. (2009) Time span and spatial scale of regional new particle formation events over Finland and Southern Sweden. Atmos. Chem. Phys. 9, 4699-4716.

Hussein, T., Puustinen, A., Aalto, P.P., Mäkelä, J.M., Hämeri, K., Kulmala, M. (2004) Urban aerosol number size distributions. Atmos. Chem. Phys. 4, 391-411.

Hyvärinen, A.P., Lihavainen, H., Komppula, M., Panwar, T.S., Sharma, V.P., Hooda, R.K., Viisanen, Y. (2010) Aerosol measurements at the Gual Pahari EUCAARI station: preliminary results from in-situ measurements. Atmos. Chem. Phys. 10, 7241-7252.

Hyvärinen, A.P., Lihavainen, H., Komppula, M., Sharma, V.P., Kerminen, V.-M., Panwar, T., Viisanen, Y. (2009) Continuous measurements of optical properties of atmospheric aerosols in Mukteshwar, northern India. Journal of Geophysical Research-Atmospheres 114.

IMD (2020) Observed Rainfall Variability and Changes over Telangana State. Met Monograph No.: ESSO/IMD/HS/Rainfall Variability/25(2020)/49 by IMD, Pune

IPCC, (2013) Climate Change 2013: The Physical Science Basis. Contribution of Working Group I to the Fifth Assessment Report of the Intergovernmental Panel on Climate Change, in: Stocker, T.F., D. Qin, G.-K. Plattner, M. Tignor, S.K. Allen, J. Boschung, A. Nauels, Y. Xia, V. Bex and P.M. Midgley (Ed.), Cambridge, United Kingdom and New York, NY, USA, , p. 1535 pp.

IPCC (2023) Climate Change 2022 – Impacts, Adaptation and Vulnerability: Working Group II Contribution to the Sixth Assessment Report of the Intergovernmental Panel on Climate Change. Cambridge University Press, Cambridge.

Jacobson, M.Z. (2001) Strong radiative heating due to the mixing state of black carbon in atmospheric aerosols. Nature 409, 695-697.

Jen, C.N., McMurry, P.H., Hanson, D.R. (2014) Stabilization of sulfuric acid dimers by ammonia, methylamine, dimethylamine, and trimethylamine. Journal of Geophysical Research: Atmospheres 119, 7502-7514.

Jeong, C.H., Evans, G.J., McGuire, M.L., Chang, R.Y.W., Abbatt, J.P.D., Zeromskiene, K., Mozurkewich, M., Li, S.M., Leaitch, W.R. (2010) Particle formation and growth at five rural and urban sites. Atmos. Chem. Phys. 10, 7979-7995.

Jimenez, J.L., Canagaratna, M.R., Donahue, N.M., Prevot, A.S.H., Zhang, Q., Kroll, J.H., DeCarlo, P.F., Allan, J.D., Coe, H., Ng, N.L., Aiken, A.C., Docherty, K.S., Ulbrich, I.M., Grieshop, A.P., Robinson, A.L., Duplissy, J., Smith, J.D., Wilson, K.R., Lanz, V.A., Hueglin, C., Sun, Y.L., Tian, J., Laaksonen, A., Raatikainen, T., Rautiainen, J., Vaattovaara, P., Ehn, M., Kulmala, M., Tomlinson, J.M., Collins, D.R., Cubison, M.J., E., Dunlea, J., Huffman, J.A., Onasch, T.B., Alfarra, M.R., Williams, P.I., Bower, K., Kondo, Y., Schneider, J., Drewnick, F., Borrmann, S., Weimer, S., Demerjian, K., Salcedo, D., Cottrell, L., Griffin, R., Takami, A., Miyoshi, T., Hatakeyama, S., Shimono, A., Sun, J.Y., Zhang, Y.M., Dzepina, K., Kimmel, J.R., Sueper, D., Jayne, J.T., Herndon, S.C., Trimborn, A.M., Williams, L.R., Wood, E.C., Middlebrook, A.M., Kolb, C.E., Baltensperger, U., Worsnop, D.R. (2009) Evolution of Organic Aerosols in the Atmosphere. 326, 1525-1529.

John, W., (2011) Size Distribution Characteristics of Aerosols, Aerosol Measurement, pp. 41-54.

Jokinen, T., Sipilä, M., Junninen, H., Ehn, M., Lönn, G., Hakala, J., Petäjä, T., Mauldin Iii, R.L., Kulmala, M., Worsnop, D.R. (2012) Atmospheric sulphuric acid and neutral cluster measurements using CI-APi-TOF. Atmos. Chem. Phys. 12, 4117-4125.

Jokinen, T., Sipilä, M., Kontkanen, J., Vakkari, V., Tisler, P., Duplissy, E.M., Junninen, H., Kangasluoma, J., Manninen, H.E., Petäjä, T., Kulmala, M., Worsnop, D.R., Kirkby, J., Virkkula, A., Kerminen, V.M. (2018) Ion-induced sulfuric acid–ammonia nucleation drives particle formation in coastal Antarctica. Science Advances 4, eaat9744.

Jones, A.R., Thomson, D.J., Hort, M., Devenish, B., (2007) The U.K. Met Office's next-generation atmospheric dispersion model, NAME III, in: (Eds), B.C.a.N.A.-L. (Ed.), Air Pollution Modeling and its Application XVII (Proceedings of the 27th NATO/CCMS International Technical Meeting on Air Pollution Modelling and its Application), pp. 580-589.

Jose, S., Mishra, A.K., Lodhi, N.K., Sharma, S.K., Singh, S. (2021) Characteristics of Aerosol Size Distributions and New Particle Formation Events at Delhi: An Urban Location in the Indo-Gangetic Plains. 9.

Jung, J., Miyazaki, Y., Kawamura, K. (2013) Different characteristics of new particle formation between urban and deciduous forest sites in Northern Japan during the summers of 2010–2011. Atmos. Chem. Phys. 13, 51-68.

Junninen, H., Ahonen, L., Bianchi, F., Quéléver, L.L.J., Schallhart, S., Dada, L., Manninen, H.E., Leino, K., Lampilahti, J., Mazon, S.B., Rantala, P., Räty, M., Kontkanen, J., Negri, S., Aliaga, D., Garmash, O., Alekseychik, P., Lipp, H., Tamme, K., Levula, J., Sipilä, M., Ehn, M., Worsnop, D.R., Zilitinkevich, S., Mammarella, I., Rinne, J., Vesala, T., Petäjä, T., Kerminen, V.M., Kulmala, M. (2022) Terpene emissions from boreal wetlands can initiate

stronger atmospheric new particle formation than boreal forests. Communications Earth & Environment 3, 93.

Juozaitis, A., Trakumas, S., Girgždien≐, R., Girgždys, A., Šopauskien≐, D., Ulevičius, V. (1996) Investigations of gas-to-particle conversion in the atmosphere. Atmospheric Research 41, 183-201.

Kalivitis, N., Kerminen, V.M., Kouvarakis, G., Stavroulas, I., Bougiatioti, A., Nenes, A., Manninen, H.E., Petäjä, T., Kulmala, M., Mihalopoulos, N. (2015) Atmospheric new particle formation as a source of CCN in the eastern Mediterranean marine boundary layer. Atmos. Chem. Phys. 15, 9203-9215.

Kalkavouras, P., BougiatiotI, A., Hussein, T., Kalivitis, N., Stavroulas, I., Michalopoulos, P., Mihalopoulos, N., (2021) Regional New Particle Formation over the Eastern Mediterranean and Middle East, Atmosphere.

Kammer, J., Perraudin, E., Flaud, P.M., Lamaud, E., Bonnefond, J.M., Villenave, E. (2018) Observation of nighttime new particle formation over the French Landes forest. Science of The Total Environment 621, 1084-1092.

Kamra, A.K., Siingh, D., Gautam, A.S., Kanawade, V.P., Tripathi, S.N., Srivastava, A.K. (2015) Atmospheric ions and new particle formation events at a tropical location, Pune, India. Quarterly Journal of the Royal Meteorological Society 141, 3140-3156.

Kamra, A.K., Victor, J.N., Siingh, D., Singh, A., Dharmaraj, T. (2022) Changes in the new particle formation and shrinkage events of the atmospheric ions during the COVID-19 lockdown. Urban Climate 44, 101214.

Kanamitsu, M. (1989) Description of the NMC Global Data Assimilation and Forecast System. Weather and Forecasting 4, 335-342.

Kanawade, V., Tripathi, S.N. (2006) Evidence for the role of ion-induced particle formation during an atmospheric nucleation event observed in Tropospheric Ozone Production about the Spring Equinox (TOPSE). Journal of Geophysical Research: Atmospheres 111.

Kanawade, V.P., Benson, D.R., Lee, S.H. (2012) Statistical analysis of 4-year observations of aerosol sizes in a semi-rural continental environment. Atmospheric Environment 59, 30-38.

Kanawade, V.P., Jobson, B.T., Guenther, A.B., Erupe, M.E., Pressley, S.N., Tripathi, S.N., Lee, S.H. (2011) Isoprene suppression of new particle formation in a mixed deciduous forest. Atmos. Chem. Phys. 11, 6013-6027.

Kanawade, V.P., Sebastian, M., Dasari, P. (2022) Reduction in Anthropogenic Emissions Suppressed New Particle Formation and Growth: Insights From the COVID-19 Lockdown. Journal of Geophysical Research: Atmospheres 127, e2021JD035392.

Kanawade, V.P., Sebastian, M., Hooda, R.K., Hyvärinen, A.P. (2021) Atmospheric new particle formation in India: Current understanding, knowledge gaps and future directions. Atmospheric Environment.

Kanawade, V.P., Shika, S., Pöhlker, C., Rose, D., Suman, M.N.S., Gadhavi, H., Kumar, A., Nagendra, S.M.S., Ravikrishna, R., Yu, H., Sahu, L.K., Jayaraman, A., Andreae, M.O., Pöschl,

U., Gunthe, S.S. (2014a) Infrequent occurrence of new particle formation at a semi-rural location, Gadanki, in tropical Southern India. Atmospheric Environment 94, 264-273.

Kanawade, V.P., Srivastava, A.K., Ram, K., Asmi, E., Vakkari, V., Soni, V.K., Varaprasad, V., Sarangi, C. (2020a) What caused severe air pollution episode of November 2016 in New Delhi? Atmospheric Environment 222, 117125.

Kanawade, V.P., Tripathi, S.N., Bhattu, D., Shamjad, P.M. (2014b) Sub-micron particle number size distributions characteristics at an urban location, Kanpur, in the Indo-Gangetic Plain. Atmospheric Research 147–148, 121-132.

Kanawade, V.P., Tripathi, S.N., Chakraborty, A., Yu, H. (2020b) Chemical Characterization of Sub-micron Aerosols during New Particle Formation in an Urban Atmosphere. Aerosol and Air Quality Research 20, 1294-1305.

Kanawade, V.P., Tripathi, S.N., Siingh, D., Gautam, A.S., Srivastava, A.K., Kamra, A.K., Soni, V.K., Sethi, V. (2014c) Observations of new particle formation at two distinct Indian subcontinental urban locations. Atmospheric Environment 96, 370-379.

Kangasluoma, J., Kuang, C., Wimmer, D., Rissanen, M.P., Lehtipalo, K., Ehn, M., Worsnop, D.R., Wang, J., Kulmala, M., Petäjä, T. (2014) Sub-3 nm particle size and composition dependent response of a nano-CPC battery. Atmos. Meas. Tech. 7, 689-700.

Karjalainen, P., Pirjola, L., Heikkilä, J., Lähde, T., Tzamkiozis, T., Ntziachristos, L., Keskinen, J., Rönkkö, T. (2014) Exhaust particles of modern gasoline vehicles: A laboratory and an on-road study. Atmospheric Environment 97, 262-270.

Kaskaoutis, D.G., Badarinath, K.V.S., Kumar Kharol, S., Rani Sharma, A., Kambezidis, H.D. (2009) Variations in the aerosol optical properties and types over the tropical urban site of Hyderabad, India. 114.

Kerminen, V.-M., Kulmala, M. (2002) Analytical formulae connecting the “real” and the “apparent” nucleation rate and the nuclei number concentration for atmospheric nucleation events. Journal of Aerosol Science 33, 609-622.

Kerminen, V.M., Chen, X., Vakkari, V., Petäjä, T., Kulmala, M., Bianchi, F. (2018) Atmospheric new particle formation and growth: review of field observations. Environmental Research Letters 13, 103003.

Kerminen, V.M., Paramonov, M., Anttila, T., Riipinen, I., Fountoukis, C., Korhonen, H., Asmi, E., Laakso, L., Lihavainen, H., Swietlicki, E., Svenningsson, B., Asmi, A., Pandis, S.N., Kulmala, M., Petäjä, T. (2012) Cloud condensation nuclei production associated with atmospheric nucleation: a synthesis based on existing literature and new results. Atmos. Chem. Phys. 12, 12037-12059.

Kerminen, V.M., Pirjola, L., Kulmala, M. (2001) How significantly does coagulation scavenging limit atmospheric particle production? Journal of Geophysical Research 106, 24119-24126.

Khoder, M.I. (2007) Ambient levels of volatile organic compounds in the atmosphere of Greater Cairo. Atmospheric Environment 41, 554-566.

Kim, K.H., Kabir, E., Jahan, S.A. (2018) Airborne bioaerosols and their impact on human health. J Environ Sci (China) 67, 23-35.

Kim, Y., Yoon, S.-C., Kim, S.-W., Kim, K.-Y., Lim, H.-C., Ryu, J. (2013) Observation of new particle formation and growth events in Asian continental outflow. Atmospheric Environment 64, 160-168.

Kirkby, J., Curtius, J., Almeida, J., Dunne, E., Duplissy, J., Ehrhart, S., Franchin, A., Gagne, S., Ickes, L., Kurten, A., Kupc, A., Metzger, A., Riccobono, F., Rondo, L., Schobesberger, S., Tsagkogeorgas, G., Wimmer, D., Amorim, A., Bianchi, F., Breitenlechner, M., David, A., Dommen, J., Downard, A., Ehn, M., Flagan, R.C., Haider, S., Hansel, A., Hauser, D., Jud, W., Junninen, H., Kreissl, F., Kvashin, A., Laaksonen, A., Lehtipalo, K., Lima, J., Lovejoy, E.R., Makhmutov, V., Mathot, S., Mikkila, J., Minginette, P., Mogo, S., Nieminen, T., Onnela, A., Pereira, P., Petaja, T., Schnitzhofer, R., Seinfeld, J.H., Sipila, M., Stozhkov, Y., Stratmann, F., Tome, A., Vanhanen, J., Viisanen, Y., Vrtala, A., Wagner, P.E., Walther, H., Weingartner, E., Wex, H., Winkler, P.M., Carslaw, K.S., Worsnop, D.R., Baltensperger, U., Kulmala, M. (2011) Role of sulphuric acid, ammonia and galactic cosmic rays in atmospheric aerosol nucleation. Nature 476, 429-433.

Kirkby, J., Duplissy, J., Sengupta, K., Frege, C., Gordon, H., Williamson, C., Heinritzi, M., Simon, M., Yan, C., Almeida, J., Tröstl, J., Nieminen, T., Ortega, I.K., Wagner, R., Adamov, A., Amorim, A., Bernhammer, A.-K., Bianchi, F., Breitenlechner, M., Brilke, S., Chen, X., Craven, J., Dias, A., Ehrhart, S., Flagan, R.C., Franchin, A., Fuchs, C., Guida, R., Hakala, J., Hoyle, C.R., Jokinen, T., Junninen, H., Kangasluoma, J., Kim, J., Krapf, M., Kürten, A., Laaksonen, A., Lehtipalo, K., Makhmutov, V., Mathot, S., Molteni, U., Onnela, A., Peräkylä, O., Piel, F., Petäjä, T., Praplan, A.P., Pringle, K., Rap, A., Richards, N.A.D., Riipinen, I., Rissanen, M.P., Rondo, L., Sarnela, N., Schobesberger, S., Scott, C.E., Seinfeld, J.H., Sipilä, M., Steiner, G., Stozhkov, Y., Stratmann, F., Tomé, A., Virtanen, A., Vogel, A.L., Wagner, A.C., Wagner, P.E., Weingartner, E., Wimmer, D., Winkler, P.M., Ye, P., Zhang, X., Hansel, A., Dommen, J., Donahue, N.M., Worsnop, D.R., Baltensperger, U., Kulmala, M., Carslaw, K.S., Curtius, J. (2016) Ion-induced nucleation of pure biogenic particles. Nature 533, 521-526.

Kivekäs, N., Carpman, J., Roldin, P., Leppä, J., O'Connor, E., Kristensson, A., Asmi, E. (2016) Coupling an aerosol box model with one-dimensional flow: a tool for understanding observations of new particle formation events. Tellus B: Chemical and Physical Meteorology 68, 29706.

Kivekäs, N., Sun, J., Zhan, M., Kerminen, V.-M., Hyvärinen, A., Komppula, M., Viisanen, Y., Hong, N., Zhang, Y., Kulmala, M., Zhang, X.C., Deli, G., Lihavainen, H. (2009) Long term particle size distribution measurements at Mount Waliguan, a high-altitude site in inland China. Atmos. Chem. Phys. 9, 5461-5474.

Klein, S.A., Hartmann, D.L. (1993) The Seasonal Cycle of Low Stratiform Clouds %J Journal of Climate. 6, 1587-1606.

Kloss, C., Sellitto, P., Legras, B., Vernier, J.-P., Jégou, F., Venkat Ratnam, M., Suneel Kumar, B., Lakshmi Madhavan, B., Berthet, G. (2020) Impact of the 2018 Ambae Eruption on the Global Stratospheric Aerosol Layer and Climate. 125, e2020JD032410.

Kompalli, S.K., Babu, S.S., Moorthy, K.K., Gogoi, M.M., Nair, V.S., Chaubey, J.P. (2014) The formation and growth of ultrafine particles in two contrasting environments: a case study. Ann. Geophys. 32, 817-830.

Kompalli, S.K., Babu, S.S., Udayasoorian, C., Jayabalakrishnan, R.M. (2018) Role of anthropogenic emissions and meteorology on ultrafine particle bursts over a high altitude site in Western Ghats during pre-monsoon. Journal of Atmospheric and Solar-Terrestrial Physics 179, 378-388.

Kompalli, S.K., Nair, V.S., Jayachandran, V., Gogoi, M.M., Babu, S.S. (2020) Particle number size distributions and new particle formation events over the northern Indian Ocean during continental outflow. Atmospheric Environment 238, 117719.

Komppula, M., Lihavainen, H., Hyvärinen, A.P., Kerminen, V.-M., Panwar, T.S., Sharma, V.P., Viisanen, Y. (2009) Physical properties of aerosol particles at a Himalayan background site in India. Journal of Geophysical Research: Atmospheres 114, n/a-n/a.

Kontkanen, J., Järvinen, E., Manninen, H.E., Lehtipalo, K., Kangasluoma, J., Decesari, S., Gobbi, G.P., Laaksonen, A., Petäjä, T., Kulmala, M. (2016) High concentrations of sub-3nm clusters and frequent new particle formation observed in the Po Valley, Italy, during the PEGASOS 2012 campaign. Atmos. Chem. Phys. 16, 1919-1935.

Kontkanen, J., Lehtipalo, K., Ahonen, L., Kangasluoma, J., Manninen, H.E., Hakala, J., Rose, C., Sellegri, K., Xiao, S., Wang, L., Qi, X., Nie, W., Ding, A., Yu, H., Lee, S., Kerminen, V.-M., Petäjä, T., Kulmala, M. (2017) Measurements of sub-3 nm particles using a particle size magnifier in different environments: from clean mountain top to polluted megacities. Atmos. Chem. Phys. 17, 2163-2187.

Korhonen, H., Carslaw, K.S., Spracklen, D.V., Ridley, D.A., Ström, J. (2008) A global model study of processes controlling aerosol size distributions in the Arctic spring and summer. 113.

Korhonen, P., Kulmala, M., Laaksonen, A., Viisanen, Y., McGraw, R., Seinfeld, J.H. (1999) Ternary nucleation of H2SO4, NH3, and H2O in the atmosphere. 104, 26349-26353.

Krishnamoorthy, S., Muthalagu, A., Priyamvada, H., Akkal, S., Valsan, A.E., Raghunathan, R., Kanawade, V.P., Gunthe, S.S. (2020) On distinguishing the natural and human-induced sources of airborne pathogenic viable bioaerosols: characteristic assessment using advanced molecular analysis. SN Applied Sciences 2, 1162.

Kuang, C., McMurry, P.H., McCormick, A.V. (2009) Determination of cloud condensation nuclei production from measured new particle formation events. Geophysical Research Letters 36, n/a-n/a.

Kuang, C., Riipinen, I., Sihto, S.L., Kulmala, M., McCormick, A.V., McMurry, P.H. (2010) An improved criterion for new particle formation in diverse atmospheric environments. Atmos. Chem. Phys. 10, 8469-8480.

Kulmala, M. (2003) How Particles Nucleate and Grow. Science 302, 1000-1001.

Kulmala, M., Cai, R., Stolzenburg, D., Zhou, Y., Dada, L., Guo, Y., Yan, C., Petäjä, T., Jiang, J., Kerminen, V.M. (2022) The contribution of new particle formation and subsequent growth to haze formation. Environmental Science: Atmospheres 2, 352-361.

Kulmala, M., Dada, L., Daellenbach, K.R., Yan, C., Stolzenburg, D., Kontkanen, J., Ezhova, E., Hakala, S., Tuovinen, S., Kokkonen, T.V., Kurppa, M., Cai, R., Zhou, Y., Yin, R., Baalbaki, R., Chan, T., Chu, B., Deng, C., Fu, Y., Ge, M., He, H., Heikkinen, L., Junninen, H., Liu, Y., Lu, Y., Nie, W., Rusanen, A., Vakkari, V., Wang, Y., Yang, G., Yao, L., Zheng, J., Kujansuu, J., Kangasluoma, J., Petäjä, T., Paasonen, P., Järvi, L., Worsnop, D.R., Ding, A., Liu, Y., Wang, L., Jiang, J., Bianchi, F., Kerminen, V.M. (2021) Is reducing new particle formation a plausible solution to mitigate particulate air pollution in Beijing and other Chinese megacities? Faraday Discussions 226, 334-347.

Kulmala, M., Dal Maso, M., Mäkelä, J.M., Pirjola, L., Väkevä, M., Aalto, P., Miikkulainen, P., Hämeri, K., O'Dowd, C.D. (2001) On the formation, growth and composition of nucleation mode particles. Tellus 53.

Kulmala, M., Kerminen, V.-M. (2008) On the formation and growth of atmospheric nanoparticles. Atmospheric Research 90, 132-150.

Kulmala, M., Kerminen, V.M., Petäjä, T., Ding, A., Wang, L. (2017) Atmospheric Gas-to-Particle Conversion: why NPF events are observed in megacities? Faraday Discuss. 200.

Kulmala, M., Kontkanen, J., Junninen, H., Lehtipalo, K., Manninen, H.E., Nieminen, T., Petäjä, T., Sipilä, M., Schobesberger, S., Rantala, P., Franchin, A., Jokinen, T., Järvinen, E., Äijälä, M., Kangasluoma, J., Hakala, J., Aalto, P.P., Paasonen, P., Mikkilä, J., Vanhanen, J., Aalto, J., Hakola, H., Makkonen, U., Ruuskanen, T., Mauldin, R.L., Duplissy, J., Vehkamäki, H., Bäck, J., Kortelainen, A., Riipinen, I., Kurtén, T., Johnston, M.V., Smith, J.N., Ehn, M., Mentel, T.F., Lehtinen, K.E.J., Laaksonen, A., Kerminen, V.M., Worsnop, D.R. (2013) Direct Observations of Atmospheric Aerosol Nucleation. Science 339, 943-946.

Kulmala, M., Korhonen, P., Napari, I., Karlsson, A., Berresheim, H., O'Dowd, C.D. (2002) Aerosol formation during PARFORCE: Ternary nucleation of H2SO4, NH3, and H2O. Journal of Geophysical Research: Atmospheres 107, PAR 15-11-PAR 15-11.

Kulmala, M., Luoma, K., Virkkula, A., Petäjä, T., Paasonen, P., Kerminen, V.-M., Nie, W., Qi, X., Shen, X.J., Chi, X., Ding, A. (2016) On the mode-segregated aerosol particle number concentration load: contributions of primary and secondary particles in Hyytiälä and Nanjing. Boreal Environ. Res. 21, 319–331.

Kulmala, M., Petäjä, T., Ehn, M., Thornton, J., Sipilä, M., Worsnop, D.R., Kerminen, V.-M. (2014) Chemistry of Atmospheric Nucleation: On the Recent Advances on Precursor Characterization and Atmospheric Cluster Composition in Connection with Atmospheric New Particle Formation. Annual Review of Physical Chemistry 65, 21-37.

Kulmala, M., Petäjä, T., Nieminen, T., Sipilä, M., Manninen, H.E., Lehtipalo, K., Dal Maso, M., Aalto, P.P., Junninen, H., Paasonen, P., Riipinen, I., Lehtinen, K.E.J., Laaksonen, A., Kerminen, V.-M. (2012a) Measurement of the nucleation of atmospheric aerosol particles. Nature Protocols 7, 1651-1667.

Kulmala, M., Petäjä, T., Nieminen, T., Sipilä, M., Manninen, H.E., Lehtipalo, K., Dal Maso, M., Aalto, P.P., Junninen, H., Paasonen, P., Riipinen, I., Lehtinen, K.E.J., Laaksonen, A., Kerminen, V.M. (2012b) Measurement of the nucleation of atmospheric aerosol particles. Nature Protocols 7, 1651-1667.

Kulmala, M., Pirjola, L., Makela, J.M. (2000) Stable sulphate clusters as a source of new atmospheric particles. Nature 404, 66-69.

Kulmala, M., Vehkamäki, H., Petäjä, T., Dal Maso, M., Lauri, A., Kerminen, V.M., Birmili, W., McMurry, P.H. (2004) Formation and growth rates of ultrafine atmospheric particles: a review of observations. Journal of Aerosol Science 35, 143-176.

Kumar, R.R., Soni, V.K., Jain, M.K. (2020) Evaluation of spatial and temporal heterogeneity of black carbon aerosol mass concentration over India using three year measurements from IMD BC observation network. Science of The Total Environment 723, 138060.

Kürten, A., Jokinen, T., Simon, M., Sipilä, M., Sarnela, N., Junninen, H., Adamov, A., Almeida, J., Amorim, A., Bianchi, F., Breitenlechner, M., Dommen, J., Donahue, N.M., Duplissy, J., Ehrhart, S., Flagan, R.C., Franchin, A., Hakala, J., Hansel, A., Heinritzi, M., Hutterli, M., Kangasluoma, J., Kirkby, J., Laaksonen, A., Lehtipalo, K., Leiminger, M., Makhmutov, V., Mathot, S., Onnela, A., Petäjä, T., Praplan, A.P., Riccobono, F., Rissanen, M.P., Rondo, L., Schobesberger, S., Seinfeld, J.H., Steiner, G., Tomé, A., Tröstl, J., Winkler, P.M., Williamson, C., Wimmer, D., Ye, P., Baltensperger, U., Carslaw, K.S., Kulmala, M., Worsnop, D.R., Curtius, J. (2014) Neutral molecular cluster formation of sulfuric acid–dimethylamine observed in real time under atmospheric conditions. Proceedings of the National Academy of Sciences 111, 15019-15024.

Kurtén, T., Loukonen, V., Vehkamäki, H., Kulmala, M. (2008) Amines are likely to enhance neutral and ion-induced sulfuric acid-water nucleation in the atmosphere more effectively than ammonia. Atmos. Chem. Phys. 8, 4095-4103.

Laakso, L., Mäkelä, J.M., Pirjola, L., Kulmala, M. (2002) Model studies on ion-induced nucleation in the atmosphere. 107, AAC 5-1-AAC 5-19.

Laaksonen, A., Hamed, A., Joutsensaari, J., Hiltunen, L., Cavalli, F., Junkermann, W., Asmi, A., Fuzzi, S., Facchini, M.C. (2005) Cloud condensation nucleus production from nucleation events at a highly polluted region. 32.

Ladino, L.A., Korolev, A., Heckman, I., Wolde, M., Fridlind, A.M., Ackerman, A.S. (2017) On the role of ice-nucleating aerosol in the formation of ice particles in tropical mesoscale convective systems. Geophys Res Lett 44, 1574-1582.

Laj, P., Bigi, A., Rose, C., Andrews, E., Lund Myhre, C., Collaud Coen, M., Lin, Y., Wiedensohler, A., Schulz, M., Ogren, J.A., Fiebig, M., Gliß, J., Mortier, A., Pandolfi, M., Petäja, T., Kim, S.W., Aas, W., Putaud, J.P., Mayol-Bracero, O., Keywood, M., Labrador, L., Aalto, P., Ahlberg, E., Alados Arboledas, L., Alastuey, A., Andrade, M., Artíñano, B., Ausmeel, S., Arsov, T., Asmi, E., Backman, J., Baltensperger, U., Bastian, S., Bath, O., Beukes, J.P., Brem, B.T., Bukowiecki, N., Conil, S., Couret, C., Day, D., Dayantolis, W., Degorska, A., Eleftheriadis, K., Fetfatzis, P., Favez, O., Flentje, H., Gini, M.I., Gregorič, A., Gysel-Beer, M., Hallar, A.G., Hand, J., Hoffer, A., Hueglin, C., Hooda, R.K., Hyvärinen, A., Kalapov, I., Kalivitis, N., Kasper-Giebl, A., Kim, J.E., Kouvarakis, G., Kranjc, I., Krejci, R., Kulmala, M., Labuschagne, C., Lee, H.J., Lihavainen, H., Lin, N.H., Löschau, G., Luoma, K., Marinoni, A., Martins Dos Santos, S., Meinhardt, F., Merkel, M., Metzger, J.M., Mihalopoulos, N., Nguyen, N.A., Ondracek, J., Pérez, N., Perrone, M.R., Petit, J.E., Picard, D., Pichon, J.M., Pont, V., Prats, N., Prenni, A., Reisen, F., Romano, S., Sellegri, K., Sharma, S., Schauer, G., Sheridan, P., Sherman, J.P., Schütze, M., Schwerin, A., Sohmer, R., Sorribas, M., Steinbacher,

M., Sun, J., Titos, G., Toczko, B., Tuch, T., Tulet, P., Tunved, P., Vakkari, V., Velarde, F., Velasquez, P., Villani, P., Vratolis, S., Wang, S.H., Weinhold, K., Weller, R., Yela, M., Yus-Diez, J., Zdimal, V., Zieger, P., Zikova, N. (2020) A global analysis of climate-relevant aerosol properties retrieved from the network of Global Atmosphere Watch (GAW) near-surface observatories. Atmos. Meas. Tech. 13, 4353-4392.

Lamsal, L.N., Krotkov, N.A., Vasilkov, A., Marchenko, S., Qin, W., Yang, E.S., Fasnacht, Z., Joiner, J., Choi, S., Haffner, D., Swartz, W.H., Fisher, B., Bucsela, E. (2021) Ozone Monitoring Instrument (OMI) Aura nitrogen dioxide standard product version 4.0 with improved surface and cloud treatments. Atmos. Meas. Tech. 14, 455-479.

Le, T., Wang, Y., Liu, L., Yang, J., Yung, Y.L., Li, G., Seinfeld, J.H. (2020) Unexpected air pollution with marked emission reductions during the COVID-19 outbreak in China. 369, 702-706.

Leaitch, W.R., Korolev, A., Aliabadi, A.A., Burkart, J., Willis, M.D., Abbatt, J.P.D., Bozem, H., Hoor, P., Köllner, F., Schneider, J., Herber, A., Konrad, C., Brauner, R. (2016) Effects of 20–100 nm particles on liquid clouds in the clean summertime Arctic. Atmos. Chem. Phys. 16, 11107-11124.

Lee, S.C., Chiu, M.Y., Ho, K.F., Zou, S.C., Wang, X. (2002) Volatile organic compounds (VOCs) in urban atmosphere of Hong Kong. Chemosphere 48, 375-382.

Lee, S.H., Gordon, H., Yu, H., Lehtipalo, K., Haley, R., Li, Y., Zhang, R. (2019) New Particle Formation in the Atmosphere: From Molecular Clusters to Global Climate. Journal of Geophysical Research: Atmospheres 124, 7098-7146.

Lee, S.H., Reeves, J.M., Wilson, J.C., Hunton, D.E., Viggiano, A.A., Miller, T.M., Ballenthin, J.O., Lait, L.R. (2003) Particle Formation by Ion Nucleation in the Upper Troposphere and Lower Stratosphere. Science 301, 1886-1889.

Lee, S.H., Uin, J., Guenther, A.B., de Gouw, J.A., Yu, F., Nadykto, A.B., Herb, J., Ng, N.L., Koss, A., Brune, W.H., Baumann, K., Kanawade, V.P., Keutsch, F.N., Nenes, A., Olsen, K., Goldstein, A., Ouyang, Q. (2016) Isoprene suppression of new particle formation: Potential mechanisms and implications. Journal of Geophysical Research: Atmospheres 121, 14,621-614,635.

Leena, P.P., A.K., V., Dani, K.K., Sombawne, S.M., Murugavel, P., Pandithurai, G. (2017) Evidence of new particle formation during post monsoon season over a high-altitude site of the Western Ghats, India. Toxicological & Environmental Chemistry 99, 652-664.

Lehtinen, K.E.J., Dal Maso, M., Kulmala, M., Kerminen, V.-M. (2007) Estimating nucleation rates from apparent particle formation rates and vice versa: Revised formulation of the Kerminen–Kulmala equation. Journal of Aerosol Science 38, 988-994.

Lehtinen, K.E.J., Kulmala, M. (2003) A model for particle formation and growth in the atmosphere with molecular resolution in size. Atmos. Chem. Phys. 3, 251-257.

Lehtipalo, K., Kontkanen, J., Kangasluoma, J., Franchin, A., Wimmer, D., Schobesberger, S., Junninen, H., Petäjä, T., Sipilä, M., Worsnop, D., Kulmala, M., Mikkilä, J., Vanhanen, J., Leppä, J. (2014) Methods for determining particle size distribution and growth rates between 1 and 3 nm using the Particle Size Magnifier. Boreal Environment Research 19, 215-236.

Lehtipalo, K., Rondo, L., Kontkanen, J., Schobesberger, S., Jokinen, T., Sarnela, N., Kurten, A., Ehrhart, S., Franchin, A., Nieminen, T., Riccobono, F., Sipila, M., Yli-Juuti, T., Duplissy, J., Adamov, A., Ahlm, L., Almeida, J., Amorim, A., Bianchi, F., Breitenlechner, M., Dommen, J., Downard, A.J., Dunne, E.M., Flagan, R.C., Guida, R., Hakala, J., Hansel, A., Jud, W., Kangasluoma, J., Kerminen, V.-M., Keskinen, H., Kim, J., Kirkby, J., Kupc, A., Kupiainen-Maatta, O., Laaksonen, A., Lawler, M.J., Leiminger, M., Mathot, S., Olenius, T., Ortega, I.K., Onnela, A., Petaja, T., Praplan, A., Rissanen, M.P., Ruuskanen, T., Santos, F.D., Schallhart, S., Schnitzhofer, R., Simon, M., Smith, J.N., Trostl, J., Tsagkogeorgas, G., Tome, A., Vaattovaara, P., Vehkamaki, H., Vrtala, A.E., Wagner, P.E., Williamson, C., Wimmer, D., Winkler, P.M., Virtanen, A., Donahue, N.M., Carslaw, K.S., Baltensperger, U., Riipinen, I., Curtius, J., Worsnop, D.R., Kulmala, M. (2016) The effect of acid-base clustering and ions on the growth of atmospheric nano-particles. Nat Commun 7.

Lehtipalo, K., Yan, C., Dada, L., Bianchi, F., Xiao, M., Wagner, R., Stolzenburg, D., Ahonen, L.R., Amorim, A., Baccarini, A., Bauer, P.S., Baumgartner, B., Bergen, A., Bernhammer, A.-K., Breitenlechner, M., Brilke, S., Buchholz, A., Mazon, S.B., Chen, D., Chen, X., Dias, A., Dommen, J., Draper, D.C., Duplissy, J., Ehn, M., Finkenzeller, H., Fischer, L., Frege, C., Fuchs, C., Garmash, O., Gordon, H., Hakala, J., He, X., Heikkinen, L., Heinritzi, M., Helm, J.C., Hofbauer, V., Hoyle, C.R., Jokinen, T., Kangasluoma, J., Kerminen, V.-M., Kim, C., Kirkby, J., Kontkanen, J., Kürten, A., Lawler, M.J., Mai, H., Mathot, S., Mauldin, R.L., Molteni, U., Nichman, L., Nie, W., Nieminen, T., Ojdanic, A., Onnela, A., Passananti, M., Petäjä, T., Piel, F., Pospisilova, V., Quéléver, L.L.J., Rissanen, M.P., Rose, C., Sarnela, N., Schallhart, S., Schuchmann, S., Sengupta, K., Simon, M., Sipilä, M., Tauber, C., Tomé, A., Tröstl, J., Väisänen, O., Vogel, A.L., Volkamer, R., Wagner, A.C., Wang, M., Weitz, L., Wimmer, D., Ye, P., Ylisirniö, A., Zha, Q., Carslaw, K.S., Curtius, J., Donahue, N.M., Flagan, R.C., Hansel, A., Riipinen, I., Virtanen, A., Winkler, P.M., Baltensperger, U., Kulmala, M., Worsnop, D.R. (2018) Multicomponent new particle formation from sulfuric acid, ammonia, and biogenic vapors. 4, eaau5363.

Lelieveld, J., Evans, J.S., Fnais, M., Giannadaki, D., Pozzer, A. (2015) The contribution of outdoor air pollution sources to premature mortality on a global scale. Nature 525, 367-371.

Levelt, P.F., Joiner, J., Tamminen, J., Veefkind, J.P., Bhartia, P.K., Stein Zweers, D.C., Duncan, B.N., Streets, D.G., Eskes, H., van der A, R., McLinden, C., Fioletov, V., Carn, S., de Laat, J., DeLand, M., Marchenko, S., McPeters, R., Ziemke, J., Fu, D., Liu, X., Pickering, K., Apituley, A., González Abad, G., Arola, A., Boersma, F., Chan Miller, C., Chance, K., de Graaf, M., Hakkarainen, J., Hassinen, S., Ialongo, I., Kleipool, Q., Krotkov, N., Li, C., Lamsal, L., Newman, P., Nowlan, C., Suleiman, R., Tilstra, L.G., Torres, O., Wang, H., Wargan, K. (2018) The Ozone Monitoring Instrument: overview of 14 years in space. Atmos. Chem. Phys. 18, 5699-5745.

Levelt, P.F., Oord, G.H.J.v.d., Dobber, M.R., Malkki, A., Huib, V., Johan de, V., Stammes, P., Lundell, J.O.V., Saari, H. (2006) The ozone monitoring instrument. IEEE Transactions on Geoscience and Remote Sensing 44, 1093-1101.

Li, J., Carlson, B.E., Yung, Y.L., Lv, D., Hansen, J., Penner, J.E., Liao, H., Ramaswamy, V., Kahn, R.A., Zhang, P., Dubovik, O., Ding, A., Lacis, A.A., Zhang, L., Dong, Y. (2022) Scattering and absorbing aerosols in the climate system. Nature Reviews Earth & Environment 3, 363-379.

Lin, J.C., Gerbig, C., Wofsy, S.C., Andrews, A.E., Daube, B.C., Davis, K.J., Grainger, C.A. (2003) A near-field tool for simulating the upstream influence of atmospheric observations: The Stochastic Time-Inverted Lagrangian Transport (STILT) model. 108.

Liu, Y., Su, H., Wang, S., Wei, C., Tao, W., Pöhlker, M.L., Pöhlker, C., Holanda, B.A., Krüger, O.O., Hoffmann, T., Wendisch, M., Artaxo, P., Pöschl, U., Andreae, M.O., Cheng, Y. (2023) Strong particle production and condensational growth in the upper troposphere sustained by biogenic VOCs from the canopy of the Amazon Basin. Atmos. Chem. Phys. 23, 251-272.

Lohmann, U., Feichter, J. (2005) Global indirect aerosol effects: a review. Atmos. Chem. Phys. 5, 715-737.

Lovejoy, E.R., Curtius, J., Froyd, K.D. (2004) Atmospheric ion-induced nucleation of sulfuric acid and water. Journal of Geophysical Research: Atmospheres 109.

Lu, Y., Yan, C., Fu, Y., Chen, Y., Liu, Y., Yang, G., Wang, Y., Bianchi, F., Chu, B., Zhou, Y., Yin, R., Baalbaki, R., Garmash, O., Deng, C., Wang, W., Liu, Y., Petäjä, T., Kerminen, V.M., Jiang, J., Kulmala, M., Wang, L. (2019) A proxy for atmospheric daytime gaseous sulfuric acid concentration in urban Beijing. Atmos. Chem. Phys. 19, 1971-1983.

Madelin, T.M. (1994) Fungal aerosols: A review. Journal of Aerosol Science 25, 1405-1412.

Magee Scientific, (2016) Aethalometer® Model AE33 User Manual - Version 1.54. Aerosol d.o.o., , Ljubljana, Slovenia, pp. 159-195.

Maher, E.F., Laird, N.M. (1985) EM algorithm reconstruction of particle size distributions from diffusion battery data. Journal of Aerosol Science 16, 557-570.

Mäkelä, J.M., Yli-Koivisto, S., Hiltunen, V., Seidl, W., Swietlicki, E., Teinilä, K., Sillanpää, M., Koponen, I.K., Paatero, J., Rosman, K., Hämeri, K. (2001) Chemical composition of aerosol during particle formation events in boreal forest. 2001 53.

Makkonen, R., Asmi, A., Kerminen, V.M., Boy, M., Arneth, A., Hari, P., Kulmala, M. (2012) Air pollution control and decreasing new particle formation lead to strong climate warming. Atmos. Chem. Phys. 12, 1515-1524.

Manisalidis, I., Stavropoulou, E., Stavropoulos, A., Bezirtzoglou, E. (2020) Environmental and Health Impacts of Air Pollution: A Review. 8.

Manninen, H.E., Nieminen, T., Asmi, E., Gagné, S., Häkkinen, S., Lehtipalo, K., Aalto, P., Vana, M., Mirme, A., Mirme, S., Hõrrak, U., Plass-Dülmer, C., Stange, G., Kiss, G., Hoffer, A., Törő, N., Moerman, M., Henzing, B., de Leeuw, G., Brinkenberg, M., Kouvarakis, G.N., Bougiatioti, A., Mihalopoulos, N., O'Dowd, C., Ceburnis, D., Arneth, A., Svenningsson, B., Swietlicki, E., Tarozzi, L., Decesari, S., Facchini, M.C., Birmili, W., Sonntag, A., Wiedensohler, A., Boulon, J., Sellegri, K., Laj, P., Gysel, M., Bukowiecki, N., Weingartner, E., Wehrle, G., Laaksonen, A., Hamed, A., Joutsensaari, J., Petäjä, T., Kerminen, V.-M., Kulmala, M. (2010) EUCAARI ion spectrometer measurements at 12 European sites – analysis of new particle formation events. Atmos. Chem. Phys. 10, 7907-7927.

Manoj, M.R., Satheesh, S.K., Moorthy, K.K., Gogoi, M.M., Babu, S.S. (2019) Decreasing Trend in Black Carbon Aerosols Over the Indian Region. 46, 2903-2910.

Marshall, S.F., Covert, D.S., Charlson, R.J. (1995) Relationship between asymmetry parameter and hemispheric backscatter ratio: implications for climate forcing by aerosols. Applied Optics 34, 6306-6311.

McClatchey, R., Fenn, R., Selby, J., Volz, F., Garing, J. (1972) Optical Properties of the Atmosphere (Third Edition). Environ. Res. Pap. 32, 113.

McMurry, P.H., Fink, M., Sakurai, H., Stolzenburg, M.R., Mauldin III, R.L., Smith, J., Eisele, F., Moore, K., Sjostedt, S., Tanner, D., Huey, L.G., Nowak, J.B., Edgerton, E., Voisin, D. (2005) A criterion for new particle formation in the sulfur-rich Atlanta atmosphere. 110.

McMurry, P.H., Kulmala, M., Worsnop, D.R. (2011) Special Issue on Aerosol Measurements in the 1 nm Range. Aerosol Science and Technology 45, i-i.

Merikanto, J., Napari, I., Vehkamäki, H., Anttila, T., Kulmala, M. (2007) New parameterization of sulfuric acid-ammonia-water ternary nucleation rates at tropospheric conditions. Journal of Geophysical Research: Atmospheres 112.

Merikanto, J., Spracklen, D.V., Mann, G.W., Pickering, S.J., Carslaw, K.S. (2009) Impact of nucleation on global CCN. Atmos. Chem. Phys. 9, 8601-8616.

Metzger, A., Verheggen, B., Dommen, J., Duplissy, J., Prevot, A.S.H., Weingartner, E., Riipinen, I., Kulmala, M., Spracklen, D.V., Carslaw, K.S., Baltensperger, U. (2010) Evidence for the role of organics in aerosol particle formation under atmospheric conditions. Proceedings of the National Academy of Sciences 107, 6646-6651.

Mie, G. (1908) Beiträge zur Optik trüber Medien, speziell kolloidaler Metallösungen. 330, 377-445.

Mikkonen, S., Romakkaniemi, S., Smith, J.N., Korhonen, H., Petäjä, T., Plass-Duelmer, C., Boy, M., McMurry, P.H., Lehtinen, K.E.J., Joutsensaari, J., Hamed, A., Mauldin Iii, R.L., Birmili, W., Spindler, G., Arnold, F., Kulmala, M., Laaksonen, A. (2011) A statistical proxy for sulphuric acid concentration. Atmos. Chem. Phys. 11, 11319-11334.

Mishra, S., Tripathi, S.N., Kanawade, V.P., Haslett, S.L., Dada, L., Ciarelli, G., Kumar, V., Singh, A., Bhattu, D., Rastogi, N., Daellenbach, K.R., Ganguly, D., Gargava, P., Slowik, J.G., Kulmala, M., Mohr, C., El-Haddad, I., Prevot, A.S.H. (2023) Rapid night-time nanoparticle growth in Delhi driven by biomass-burning emissions. Nature Geoscience 16, 224-230.

Molteni, U., Bianchi, F., Klein, F., El Haddad, I., Frege, C., Rossi, M.J., Dommen, J., Baltensperger, U. (2018) Formation of highly oxygenated organic molecules from aromatic compounds. Atmos. Chem. Phys. 18, 1909-1921.

Mönkkönen, P., Koponen, I.K., Lehtinen, K.E.J., Hämeri, K., Uma, R., Kulmala, M. (2005) Measurements in a highly polluted Asian mega city: observations of aerosol number size distribution, modal parameters and nucleation events. Atmos. Chem. Phys. 5, 57-66.

Moorthy, K.K., Sreekanth, V., Chaubey, J.P., Gogoi, M.M., Babu, S.S., Kompalli, S.K., Bagare, S.P., Bhatt, B.C., Gaur, V.K., Prabhu, T.P., Singh, N.S. (2011) Fine and ultrafine particles at a near–free tropospheric environment over the high-altitude station Hanle in the Trans-Himalaya: New particle formation and size distribution. Journal of Geophysical Research: Atmospheres 116, n/a-n/a.

Murugavel, P., Chate, D.M. (2009) Generation and growth of aerosols over Pune, India. Atmospheric Environment 43, 820-828.

Nair, V.S., Moorthy, K.K., Alappattu, D.P., Kunhikrishnan, P.K., George, S., Nair, P.R., Babu, S.S., Abish, B., Satheesh, S.K., Tripathi, S.N., Niranjan, K., Madhavan, B.L., Srikant, V., Dutt, C.B.S., Badarinath, K.V.S., Reddy, R.R. (2007) Wintertime aerosol characteristics over the Indo-Gangetic Plain (IGP): Impacts of local boundary layer processes and long-range transport. 112.

Napari, I., Noppel, M., Vehkamäki, H., Kulmala, M. (2002) Parametrization of ternary nucleation rates for H2SO4-NH3-H2O vapors. Journal of Geophysical Research: Atmospheres 107, AAC 6-1-AAC 6-6.

Neitola, K., Asmi, E., Komppula, M., Hyvärinen, A.P., Raatikainen, T., Panwar, T.S., Sharma, V.P., Lihavainen, H. (2011) New particle formation infrequently observed in Himalayan foothills – why? Atmos. Chem. Phys. 11, 8447-8458.

Nepolian, J.V., Siingh, D., Singh, R.P., Gautam, A.S., Gautam, S. (2021) Analysis of Positive and Negative Atmospheric Air Ions During New Particle Formation (NPF) Events over Urban City of India. Aerosol Science and Engineering 5, 460-477.

Nieminen, T., Kerminen, V.M., Petäjä, T., Aalto, P.P., Arshinov, M., Asmi, E., Baltensperger, U., Beddows, D.C.S., Beukes, J.P., Collins, D., Ding, A., Harrison, R.M., Henzing, B., Hooda, R., Hu, M., Hõrrak, U., Kivekäs, N., Komsaare, K., Krejci, R., Kristensson, A., Laakso, L., Laaksonen, A., Leaitch, W.R., Lihavainen, H., Mihalopoulos, N., Németh, Z., Nie, W., O'Dowd, C., Salma, I., Sellegri, K., Svenningsson, B., Swietlicki, E., Tunved, P., Ulevicius, V., Vakkari, V., Vana, M., Wiedensohler, A., Wu, Z., Virtanen, A., Kulmala, M. (2018) Global analysis of continental boundary layer new particle formation based on long-term measurements. Atmos. Chem. Phys. 18, 14737-14756.

Nilsson, E.D., Kulmala, M. (1998) The potential for atmospheric mixing processes to enhance the binary nucleation rate. 103, 1381-1389.

Nilsson, E.D., Paatero, J., Boy, M. (2001) Effects of air masses and synoptic weather on aerosol formation in the continental boundary layer. Tellus B: Chemical and Physical Meteorology 53, 462-478.

Noppel, M., Vehkamäki, H., Kulmala, M. (2001) An improved model for hydrate formation in sulfuric acid–water nucleation. The Journal of Chemical Physics 116, 218-228.

Nriagu, J.O. (1989) A global assessment of natural sources of atmospheric trace metals. Nature 338, 47-49.

O'Dowd, C.D., Hoffmann, T. (2005) Coastal New Particle Formation: A Review of the Current State-Of-The-Art. Environmental Chemistry 2, 245-255.

O'Dowd, C.D., Jimenez, J.L., Bahreini, R., Flagan, R.C., Seinfeld, J.H., Hämeri, K., Pirjola, L., Kulmala, M., Jennings, S.G., Hoffmann, T. (2002) Marine aerosol formation from biogenic iodine emissions. Nature 417, 632-636.

Ohata, S., Moteki, N., Mori, T., Koike, M., Kondo, Y. (2016) A key process controlling the wet removal of aerosols: new observational evidence. Scientific Reports 6, 34113.

Olin, M., Kuuluvainen, H., Aurela, M., Kalliokoski, J., Kuittinen, N., Isotalo, M., Timonen, H.J., Niemi, J.V., Rönkkö, T., Dal Maso, M. (2020) Traffic-originated nanocluster emission exceeds H2SO4-driven photochemical new particle formation in an urban area. Atmos. Chem. Phys. 20, 1-13.

Olin, M., Okuljar, M., Rissanen, M.P., Kalliokoski, J., Shen, X.J., Dada, L., Lampimäki, M., Wu, Y., Lohila, A., Duplissy, J., Sipilä, M., Petäjä, T., Kulmala, M., Dal Maso, M. (2022) Measurement report: Atmospheric new particle formation in a coastal agricultural site explained with binPMF analysis of nitrate CI-APi-TOF spectra. Atmos. Chem. Phys. 22, 8097-8115.

Paasonen, P., Peltola, M., Kontkanen, J., Junninen, H., Kerminen, V.M., Kulmala, M. (2018) Comprehensive analysis of particle growth rates from nucleation mode to cloud condensation nuclei in boreal forest. Atmos. Chem. Phys. 18, 12085-12103.

Pacyna, J.M. (1998) Source inventories for atmospheric trace metals. Atmosperic Particles 5, 385-423.

Padma Kumari, B., Trigo-Rodríguez, J.M., Londhe, A.L., Jadhav, D.B., Trimbake, H.K. (2005) Optical observations of meteoric dust in the middle atmosphere during Leonid activity in recent years 2001–2003 over India. 32.

Partanen, A.-I., Kokkola, H., Romakkaniemi, S., Kerminen, V.-M., Lehtinen, K.E.J., Bergman, T., Arola, A., Korhonen, H. (2012) Direct and indirect effects of sea spray geoengineering and the role of injected particle size. Journal of Geophysical Research: Atmospheres 117.

Peltola, M., Rose, C., Trueblood, J.V., Gray, S., Harvey, M., Sellegri, K. (2022) New particle formation in coastal New Zealand with a focus on open-ocean air masses. Atmos. Chem. Phys. 22, 6231-6254.

Petäjä, T., Järvi, L., Kerminen, V.M., Ding, A.J., Sun, J.N., Nie, W., Kujansuu, J., Virkkula, A., Yang, X., Fu, C.B., Zilitinkevich, S., Kulmala, M. (2016) Enhanced air pollution via aerosol-boundary layer feedback in China. Scientific Reports 6, 18998.

Petäjä, T., Mauldin, I.R.L., Kosciuch, E., McGrath, J., Nieminen, T., Paasonen, P., Boy, M., Adamov, A., Kotiaho, T., Kulmala, M. (2009) Sulfuric acid and OH concentrations in a boreal forest site. Atmos. Chem. Phys. 9, 7435-7448.

Petzold, A., Ogren, J.A., Fiebig, M., Laj, P., Li, S.M., Baltensperger, U., Holzer-Popp, T., Kinne, S., Pappalardo, G., Sugimoto, N., Wehrli, C., Wiedensohler, A., Zhang, X.Y. (2013) Recommendations for reporting "black carbon" measurements. Atmos. Chem. Phys. 13, 8365-8379.

Pierce, J.R., Adams, P.J. (2007) Efficiency of cloud condensation nuclei formation from ultrafine particles. Atmos. Chem. Phys. 7, 1367-1379.

Pierce, J.R., Leaitch, W.R., Liggio, J., Westervelt, D.M., Wainwright, C.D., Abbatt, J.P.D., Ahlm, L., Al-Basheer, W., Cziczo, D.J., Hayden, K.L., Lee, A.K.Y., Li, S.M., Russell, L.M., Sjostedt, S.J., Strawbridge, K.B., Travis, M., Vlasenko, A., Wentzell, J.J.B., Wiebe, H.A., Wong, J.P.S., Macdonald, A.M. (2012) Nucleation and condensational growth to CCN sizes during a sustained pristine biogenic SOA event in a forested mountain valley. Atmos. Chem. Phys. 12, 3147-3163.

Pierce, J.R., Westervelt, D.M., Atwood, S.A., Barnes, E.A., Leaitch, W.R. (2014) New-particle formation, growth and climate-relevant particle production in Egbert, Canada: analysis from 1 year of size-distribution observations. Atmos. Chem. Phys. 14, 8647-8663.

Pikridas, M., Riipinen, I., Hildebrandt, L., Kostenidou, E., Manninen, H., Mihalopoulos, N., Kalivitis, N., Burkhart, J.F., Stohl, A., Kulmala, M., Pandis, S.N. (2012) New particle formation at a remote site in the eastern Mediterranean. 117.

Pöhlker, M.L., Pöhlker, C., Quaas, J., Mülmenstädt, J., Pozzer, A., Andreae, M.O., Artaxo, P., Block, K., Coe, H., Ervens, B., Gallimore, P., Gaston, C.J., Gunthe, S.S., Henning, S., Herrmann, H., Krüger, O.O., McFiggans, G., Poulain, L., Raj, S.S., Reyes-Villegas, E., Royer, H.M., Walter, D., Wang, Y., Pöschl, U. (2023) Global organic and inorganic aerosol hygroscopicity and its effect on radiative forcing. Nature Communications 14, 6139.

Prasad, P., Raman, M.R., Ratnam, M.V., Ravikiran, V., Madhavan, B.L., Bhaskara Rao, S.V. (2019) Nocturnal, seasonal and intra-annual variability of tropospheric aerosols observed using ground-based and space-borne lidars over a tropical location of India. Atmospheric Environment 213, 185-198.

Pushpawela, B., Jayaratne, R., Morawska, L. (2019) The influence of wind speed on new particle formation events in an urban environment. Atmospheric Research 215, 37-41.

Raatikainen, T., Hyvärinen, A.P., Hatakka, J., Panwar, T.S., Hooda, R.K., Sharma, V.P., Lihavainen, H. (2014) The effect of boundary layer dynamics on aerosol properties at the Indo-Gangetic plains and at the foothills of the Himalayas. Atmospheric Environment 89, 548-555.

Raes, F. (1995) Entrainment of free tropospheric aerosols as a regulating mechanism for cloud condensation nuclei in the remote marine boundary layer. 100, 2893-2903.

Ramaswamy, V., Boucher, O., Haigh, J., Hauglustaine, D., Haywood, J., Myhre, G., Nakajima, T., Shi, G.Y., Solomon, S., (2001) Radiative forcing of climate change, in: Houghton, J.T., Ding, Y., Griggs, D.J., Noguer, M., van der Linden, P.J., Da, X., Maskell, K., Johnson, C.A. (Eds.). Cambridge University Press, Cambridge, United Kingdom, pp. 349-416.

Reddington, C.L., Carslaw, K.S., Spracklen, D.V., Frontoso, M.G., Collins, L., Merikanto, J., Minikin, A., Hamburger, T., Coe, H., Kulmala, M., Aalto, P., Flentje, H., Plass-Dülmer, C., Birmili, W., Wiedensohler, A., Wehner, B., Tuch, T., Sonntag, A., O'Dowd, C.D., Jennings, S.G., Dupuy, R., Baltensperger, U., Weingartner, E., Hansson, H.C., Tunved, P., Laj, P., Sellegri, K., Boulon, J., Putaud, J.P., Gruening, C., Swietlicki, E., Roldin, P., Henzing, J.S., Moerman, M., Mihalopoulos, N., Kouvarakis, G., Ždímal, V., Zíková, N., Marinoni, A., Bonasoni, P., Duchi, R. (2011) Primary versus secondary contributions to particle number concentrations in the European boundary layer. Atmos. Chem. Phys. 11, 12007-12036.

Remer, L.A., Kleidman, R.G., Levy, R.C., Kaufman, Y.J., Tanré, D., Mattoo, S., Martins, J.V., Ichoku, C., Koren, I., Yu, H., Holben, B.N. (2008) Global aerosol climatology from the MODIS satellite sensors. Journal of Geophysical Research: Atmospheres 113.

Riccobono, F., Rondo, L., Sipilä, M., Barmet, P., Curtius, J., Dommen, J., Ehn, M., Ehrhart, S., Kulmala, M., Kürten, A., Mikkilä, J., Paasonen, P., Petäjä, T., Weingartner, E., Baltensperger, U. (2012) Contribution of sulfuric acid and oxidized organic compounds to particle formation and growth. Atmos. Chem. Phys. 12, 9427-9439.

Riipinen, I., Pierce, J.R., Yli-Juuti, T., Nieminen, T., Häkkinen, S., Ehn, M., Junninen, H., Lehtipalo, K., Petäjä, T., Slowik, J., Chang, R., Shantz, N.C., Abbatt, J., Leaitch, W.R., Kerminen, V.M., Worsnop, D.R., Pandis, S.N., Donahue, N.M., Kulmala, M. (2011) Organic condensation: a vital link connecting aerosol formation to cloud condensation nuclei (CCN) concentrations. Atmos. Chem. Phys. 11, 3865-3878.

Riipinen, I., Sihto, S.L., Kulmala, M., Arnold, F., Dal Maso, M., Birmili, W., Saarnio, K., Teinilä, K., Kerminen, V.M., Laaksonen, A., Lehtinen, K.E.J. (2007) Connections between atmospheric sulphuric acid and new particle formation during QUEST III–IV campaigns in Heidelberg and Hyytiälä. Atmos. Chem. Phys. 7, 1899-1914.

Riipinen, I., Yli-Juuti, T., Pierce, J.R., Petäjä, T., Worsnop, D.R., Kulmala, M., Donahue, N.M. (2012) The contribution of organics to atmospheric nanoparticle growth. Nature Geoscience 5, 453-458.

Ristovski, Z.D., Suni, T., Kulmala, M., Boy, M., Meyer, N.K., Duplissy, J., Turnipseed, A., Morawska, L., Baltensperger, U. (2010) The role of sulphates and organic vapours in growth of newly formed particles in a eucalypt forest. Atmos. Chem. Phys. 10, 2919-2926.

Rodríguez, S., Dingenen, V.R., Putaud, J.P., Santos, M.D.S., Roselli, D. (2005) Nucleation and growth of new particles in the rural atmosphere of Northern Italy—relationship to air quality monitoring. Atmospheric Environment 39, 6734-6746.

Rönkkö, T., Kuuluvainen, H., Karjalainen, P., Keskinen, J., Hillamo, R., Niemi, J.V., Pirjola, L., Timonen, H.J., Saarikoski, S., Saukko, E., Järvinen, A., Silvennoinen, H., Rostedt, A., Olin, M., Yli-Ojanperä, J., Nousiainen, P., Kousa, A., Dal Maso, M. (2017) Traffic is a major source of atmospheric nanocluster aerosol. Proceedings of the National Academy of Sciences, 201700830.

Rose, C., Sellegri, K., Moreno, I., Velarde, F., Ramonet, M., Weinhold, K., Krejci, R., Andrade, M., Wiedensohler, A., Ginot, P., Laj, P. (2017) CCN production by new particle formation in the free troposphere. Atmos. Chem. Phys. 17, 1529-1541.

Rose, C., Sellegri, K., Velarde, F., Moreno, I., Ramonet, M., Weinhold, K., Krejci, R., Ginot, P., Andrade, M., Wiedensohler, A., Laj, P. (2015) Frequent nucleation events at the high altitude station of Chacaltaya (5240 m a.s.l.), Bolivia. Atmospheric Environment 102, 18-29.

Saha, P.K., Robinson, E.S., Shah, R.U., Zimmerman, N., Apte, J.S., Robinson, A.L., Presto, A.A. (2018) Reduced Ultrafine Particle Concentration in Urban Air: Changes in Nucleation and Anthropogenic Emissions. Environmental Science & Technology 52, 6798-6806.

Sarangi, B., Aggarwal, S.G., Gupta, P.K. (2015) A Simplified Approach to Calculate Particle Growth Rate Due to Self-Coagulation, Scavenging and Condensation Using SMPS Measurements during a Particle Growth Event in New Delhi. Aerosol and Air Quality Research 15, 166-179.

Satheesh, S.K., Srinivasan, J., Moorthy, K.K. (2006) Spatial and temporal heterogeneity in aerosol properties and radiative forcing over Bay of Bengal: Sources and role of aerosol transport. 111.

Schiffer, J.M., Mael, L.E., Prather, K.A., Amaro, R.E., Grassian, V.H. (2018) Sea Spray Aerosol: Where Marine Biology Meets Atmospheric Chemistry. ACS Central Science 4, 1617-1623.

Schmale, J., Baccarini, A. (2021) Progress in Unraveling Atmospheric New Particle Formation and Growth Across the Arctic. Geophysical Research Letters 48, e2021GL094198.

Schobesberger, S., Franchin, A., Bianchi, F., Rondo, L., Duplissy, J., Kürten, A., Ortega, I.K., Metzger, A., Schnitzhofer, R., Almeida, J., Amorim, A., Dommen, J., Dunne, E.M., Ehn, M., Gagné, S., Ickes, L., Junninen, H., Hansel, A., Kerminen, V.M., Kirkby, J., Kupc, A., Laaksonen, A., Lehtipalo, K., Mathot, S., Onnela, A., Petäjä, T., Riccobono, F., Santos, F.D., Sipilä, M., Tomé, A., Tsagkogeorgas, G., Viisanen, Y., Wagner, P.E., Wimmer, D., Curtius, J., Donahue, N.M., Baltensperger, U., Kulmala, M., Worsnop, D.R. (2015) On the composition of ammonia–sulfuric-acid ion clusters during aerosol particle formation. Atmos. Chem. Phys. 15, 55-78.

Schobesberger, S., Junninen, H., Bianchi, F., Lönn, G., Ehn, M., Lehtipalo, K., Dommen, J., Ehrhart, S., Ortega, I.K., Franchin, A., Nieminen, T., Riccobono, F., Hutterli, M., Duplissy, J., Almeida, J., Amorim, A., Breitenlechner, M., Downard, A.J., Dunne, E.M., Flagan, R.C., Kajos, M., Keskinen, H., Kirkby, J., Kupc, A., Kürten, A., Kurtén, T., Laaksonen, A., Mathot, S., Onnela, A., Praplan, A.P., Rondo, L., Santos, F.D., Schallhart, S., Schnitzhofer, R., Sipilä, M., Tomé, A., Tsagkogeorgas, G., Vehkamäki, H., Wimmer, D., Baltensperger, U., Carslaw, K.S., Curtius, J., Hansel, A., Petäjä, T., Kulmala, M., Donahue, N.M., Worsnop, D.R. (2013) Molecular understanding of atmospheric particle formation from sulfuric acid and large oxidized organic molecules. Proceedings of the National Academy of Sciences 110, 17223-17228.

Scott, W.D., Cattell, F.C.R. (1979) Vapor pressure of ammonium sulfates. Atmospheric Environment (1967) 13, 307-317.

Sebastian, M., Kanawade, V.P., Pierce, J.R. (2021a) Observation of sub-3nm particles and new particle formation at an urban location in India. Atmospheric Environment 256, 118460.

Sebastian, M., Kanawade, V.P., Soni, V., Asmi, E., Westervelt, D.M., Vakkari, V., Hyvärinen, A.P., Pierce, J.R., Hooda, R.K. (2021b) New Particle Formation and Growth to Climate-Relevant Aerosols at a Background Remote Site in the Western Himalaya. Journal of Geophysical Research: Atmospheres 126.

Sebastian, M., Kompalli, S.K., Kumar, V.A., Jose, S., Babu, S.S., Pandithurai, G., Singh, S., Hooda, R.K., Soni, V.K., Pierce, J.R., Vakkari, V., Asmi, E., Westervelt, D.M., Hyvärinen, A.P., Kanawade, V.P. (2022) Observations of particle number size distributions and new particle formation in six Indian locations. Atmos. Chem. Phys. 22, 4491-4508.

Seinfeld, J.H., Bretherton, C., Carslaw, K.S., Coe, H., DeMott, P.J., Dunlea, E.J., Feingold, G., Ghan, S., Guenther, A.B., Kahn, R., Kraucunas, I., Kreidenweis, S.M., Molina, M.J., Nenes, A., Penner, J.E., Prather, K.A., Ramanathan, V., Ramaswamy, V., Rasch, P.J., Ravishankara, A.R., Rosenfeld, D., Stephens, G., Wood, R. (2016) Improving our fundamental understanding of the role of aerosol−cloud interactions in the climate system. Proceedings of the National Academy of Sciences 113, 5781-5790.

Seinfeld, J.H., Pandis, S.N. (1998) Atmospheric chemistry and physics, from air pollution to climate change

John Wiley & Sons, Inc., New York.

Seinfeld, J.H., Pandis, S.N. (2006) Atmospheric Chemistry and Physics: From Air Pollution to Climate Change. John Wiley, New York 2nd ed.

Seinfeld, J.H., Pandis, S.N. (2016) Atmospheric chemistry and physics : From air pollution to climate change, Third edition ed. John Wiley & Sons, Inc. Hoboken, New Jersey, Hoboken, New Jersey.

Sellegri, K., Rose, C., Marinoni, A., Lupi, A., Wiedensohler, A., Andrade, M., Bonasoni, P., Laj, P. (2019) New Particle Formation: A Review of Ground-Based Observations at Mountain Research Stations. Atmosphere 10, 493.

Sharma, S., Zhang, M., Anshika, M., Gao, J., Zhang, H., Kota, S.H. (2020) Effect of restricted emissions during COVID-19 on air quality in India. Science of The Total Environment 728, 138878.

Shen, L., Wang, H., Lü, S., Li, L., Yuan, J., Zhang, X., Tian, X., Tang, Q. (2016a) Observation of aerosol size distribution and new particle formation at a coastal city in the Yangtze River Delta, China. Science of The Total Environment 565, 1175-1184.

Shen, X., Sun, J., Yu, F., Wang, Y., Zhong, J., Zhang, Y., Hu, X., Xia, C., Zhang, S., Zhang, X. (2021) Enhancement of nanoparticle formation and growth during the COVID-19 lockdown period in urban Beijing. Atmos. Chem. Phys. 21, 7039-7052.

Shen, X.J., Sun, J., Kivekäs, N., Kristensson, A., Zhang, X., Zhang, Y., Zhang, L., Fan, R., Qi, X., Ma, Q., Zhou, H. (2018) Spatial distribution and occurrence probability of regional new particle formation events in eastern China. Atmos. Chem. Phys. 18, 587-599.

Shen, X.J., Sun, J., Zhang, X., Zhang, Y., Zhang, L., Fan, R. (2016b) Key features of new particle formation events at background sites in China and their influence on cloud condensation nuclei. Frontiers of Environmental Science & Engineering 10, 5.

Shen, X.J., Sun, J.Y., Zhang, X.Y., Zhang, Y.M., Zhang, L., Fan, R.X., Zhang, Z.X., Zhang, X.L., Zhou, H.G., Zhou, L.Y., Dong, F., Shi, Q.F. (2016c) The influence of emission control on particle number size distribution and new particle formation during China's V-Day parade in 2015. Science of The Total Environment 573, 409-419.

Shen, X.J., Sun, J.Y., Zhang, Y.M., Wehner, B., Nowak, A., Tuch, T., Zhang, X.C., Wang, T.T., Zhou, H.G., Zhang, X.L., Dong, F., Birmili, W., Wiedensohler, A. (2011) First long-term study of particle number size distributions and new particle formation events of regional aerosol in the North China Plain. Atmos. Chem. Phys. 11, 1565-1580.

Shika, S., Gadhavi, H., Suman, M.N.S., Ravikrishna, R., Gunthe, S.S. (2020) Atmospheric aerosol properties at a semi-rural location in southern India: particle size distributions and implications for cloud droplet formation. SN Applied Sciences 2, 1007.

Sihto, S.L., Kulmala, M., Kerminen, V.-M., Dal Maso, M., Petäjä, T., Riipinen, I., Korhonen, H., Arnold, F., Janson, R., Boy, M., Laaksonen, A., Lehtinen, K.E.J. (2006) Atmospheric

sulphuric acid and aerosol formation: implications from atmospheric measurements for nucleation and early growth mechanisms. Atmos. Chem. Phys. 6, 4079-4091.

Sihto, S.L., Mikkilä, J., Vanhanen, J., Ehn, M., Liao, L., Lehtipalo, K., Aalto, P.P., Duplissy, J., Petäjä, T., Kerminen, V.M., Boy, M., Kulmala, M. (2011) Seasonal variation of CCN concentrations and aerosol activation properties in boreal forest. Atmos. Chem. Phys. 11, 13269-13285.

Siingh, D., Gautam, A.S., Buchunde, P.S., Kamra, A.K. (2018) Classification of the new particle formation events observed at a tropical site, Pune, India. Atmospheric Environment 190, 10-22.

Siingh, D., Gautam, A.S., Kamra, A.K., Komsaare, K. (2013) Nucleation events for the formation of charged aerosol particles at a tropical station — Preliminary results. Atmospheric Research 132–133, 239-252.

Silva, P.J., Erupe, M.E., Price, D., Elias, J., G. J. Malloy, Q., Li, Q., Warren, B., Cocker, D.R. (2008) Trimethylamine as Precursor to Secondary Organic Aerosol Formation via Nitrate Radical Reaction in the Atmosphere. Environmental Science & Technology 42, 4689-4696.

Singh, A., Raj, S.S., Panda, U., Kommula, S.M., Jose, C., Liu, T., Huang, S., Swain, B., Pöhlker, M.L., Reyes-Villegas, E., Ojha, N., Vaishya, A., Bigi, A., Ravikrishna, R., Zhu, Q., Shi, L., Allen, J., Martin, S.T., McFiggans, G., Andreae, M.O., Pöschl, U., Coe, H., Bianchi, F., Su, H., Kanawade, V.P., Liu, P., Gunthe, S.S. (2023) Rapid growth and high cloud-forming potential of anthropogenic sulfate aerosol in a thermal power plant plume during COVID lockdown in India. npj Climate and Atmospheric Science 6, 109.

Sipilä, M., Berndt, T., Petäjä, T., Brus, D., Vanhanen, J., Stratmann, F., Patokoski, J., Mauldin, R.L., Hyvärinen, A.P., Lihavainen, H., Kulmala, M. (2010) The Role of Sulfuric Acid in Atmospheric Nucleation. Science 327, 1243-1246.

Sipilä, M., Sarnela, N., Jokinen, T., Henschel, H., Junninen, H., Kontkanen, J., Richters, S., Kangasluoma, J., Franchin, A., Peräkylä, O., Rissanen, M.P., Ehn, M., Vehkamäki, H., Kurten, T., Berndt, T., Petäjä, T., Worsnop, D., Ceburnis, D., Kerminen, V.M., Kulmala, M., O'Dowd, C. (2016) Molecular-scale evidence of aerosol particle formation via sequential addition of HIO(3). Nature 537, 532-534.

Smith, J.N., Moore, K.F., Eisele, F.L., Voisin, D., Ghimire, A.K., Sakurai, H., McMurry, P.H. (2005) Chemical composition of atmospheric nanoparticles during nucleation events in Atlanta. 110.

Sogacheva, L., Hamed, A., Facchini, M.C., Kulmala, M., Laaksonen, A. (2007) Relation of air mass history to nucleation events in Po Valley, Italy, using back trajectories analysis. Atmos. Chem. Phys. 7, 839-853.

Sohrabi, C., Alsafi, Z., O'Neill, N., Khan, M., Kerwan, A., Al-Jabir, A., Iosifidis, C., Agha, R. (2020) World Health Organization declares global emergency: A review of the 2019 novel coronavirus (COVID-19). International journal of surgery (London, England) 76, 71-76.

Spracklen, D.V., Carslaw, K.S., Merikanto, J., Mann, G.W., Reddington, C.L., Pickering, S., Ogren, J.A., Andrews, E., Baltensperger, U., Weingartner, E., Boy, M., Kulmala, M., Laakso, L., Lihavainen, H., Kivekäs, N., Komppula, M., Mihalopoulos, N., Kouvarakis, G., Jennings,

S.G., O'Dowd, C., Birmili, W., Wiedensohler, A., Weller, R., Gras, J., Laj, P., Sellegri, K., Bonn, B., Krejci, R., Laaksonen, A., Hamed, A., Minikin, A., Harrison, R.M., Talbot, R., Sun, J. (2010) Explaining global surface aerosol number concentrations in terms of primary emissions and particle formation. Atmos. Chem. Phys. 10, 4775-4793.

Sreekanth, V., Mahesh, B., Niranjan, K. (2018) Gradients in PM2.5 over India: Five city study. Urban Climate 25, 99-108.

Srivastava, A.K., Soni, V.K., Singh, S., Kanawade, V.P., Singh, N., Tiwari, S., Attri, S.D. (2014) An early South Asian dust storm during March 2012 and its impacts on Indian Himalayan foothills: A case study. Science of The Total Environment 493, 526-534.

Stanier, C.O., Khlystov, A.Y., Pandis, S.N. (2004a) Ambient aerosol size distributions and number concentrations measured during the Pittsburgh Air Quality Study (PAQS). Atmospheric Environment 38, 3275-3284.

Stanier, C.O., Khlystov, A.Y., Pandis, S.N. (2004b) Nucleation Events During the Pittsburgh Air Quality Study: Description and Relation to Key Meteorological, Gas Phase, and Aerosol Parameters Special Issue of Aerosol Science and Technology on Findings from the Fine Particulate Matter Supersites Program. Aerosol Science and Technology 38, 253-264.

Stein, A.F., Draxler, R.R., Rolph, G.D., Stunder, B.J.B., Cohen, M.D., Ngan, F. (2015) NOAA's HYSPLIT Atmospheric Transport and Dispersion Modeling System %J Bulletin of the American Meteorological Society. 96, 2059-2077.

Stohl, A., Forster, C., Frank, A., Seibert, P., Wotawa, G. (2005) Technical note: The Lagrangian particle dispersion model FLEXPART version 6.2. Atmos. Chem. Phys. 5, 2461-2474.

Stohl, A., Hittenberger, M., Wotawa, G. (1998) Validation of the lagrangian particle dispersion model FLEXPART against large-scale tracer experiment data. Atmospheric Environment 32, 4245-4264.

Stolzenburg, D., Fischer, L., Vogel, A.L., Heinritzi, M., Schervish, M., Simon, M., Wagner, A.C., Dada, L., Ahonen, L.R., Amorim, A., Baccarini, A., Bauer, P.S., Baumgartner, B., Bergen, A., Bianchi, F., Breitenlechner, M., Brilke, S., Buenrostro Mazon, S., Chen, D., Dias, A., Draper, D.C., Duplissy, J., El Haddad, I., Finkenzeller, H., Frege, C., Fuchs, C., Garmash, O., Gordon, H., He, X., Helm, J., Hofbauer, V., Hoyle, C.R., Kim, C., Kirkby, J., Kontkanen, J., Kürten, A., Lampilahti, J., Lawler, M., Lehtipalo, K., Leiminger, M., Mai, H., Mathot, S., Mentler, B., Molteni, U., Nie, W., Nieminen, T., Nowak, J.B., Ojdanic, A., Onnela, A., Passananti, M., Petäjä, T., Quéléver, L.L.J., Rissanen, M.P., Sarnela, N., Schallhart, S., Tauber, C., Tomé, A., Wagner, R., Wang, M., Weitz, L., Wimmer, D., Xiao, M., Yan, C., Ye, P., Zha, Q., Baltensperger, U., Curtius, J., Dommen, J., Flagan, R.C., Kulmala, M., Smith, J.N., Worsnop, D.R., Hansel, A., Donahue, N.M., Winkler, P.M. (2018) Rapid growth of organic aerosol nanoparticles over a wide tropospheric temperature range. Proceedings of the National Academy of Sciences 115, 9122-9127.

Stolzenburg, M.R., McMurry, P.H., Sakurai, H., Smith, J.N., Mauldin, R.L., Eisele, F.L., Clement, C.F. (2005) Growth rates of freshly nucleated atmospheric particles in Atlanta. Journal of Geophysical Research: Atmospheres 110, n/a-n/a.

Sun, Y., Lei, L., Zhou, W., Chen, C., He, Y., Sun, J., Li, Z., Xu, W., Wang, Q., Ji, D., Fu, P., Wang, Z., Worsnop, D.R. (2020) A chemical cocktail during the COVID-19 outbreak in Beijing, China: Insights from six-year aerosol particle composition measurements during the Chinese New Year holiday. Science of The Total Environment 742, 140739.

Tang, L., Shang, D., Fang, X., Wu, Z., Qiu, Y., Chen, S., Li, X., Zeng, L., Guo, S., Hu, M. (2021) More significant impacts from new particle formation on haze formation during COVID-19 lockdown. Geophysical Research Letters n/a, e2020GL091591.

Tiwari, V., Hanai, Y., Masunaga, S. (2010) Ambient levels of volatile organic compounds in the vicinity of petrochemical industrial area of Yokohama, Japan. Air Quality, Atmosphere & Health 3, 65-75.

Tripathi, R.M., Khandekar, R.N., Mishra, U.C. (1988) Size distribution of atmospheric aerosols in urban sites in India. Science of The Total Environment 77, 237-244.

Tripathi, S.N., Tare, V., Chinnam, N., Srivastava, A.K., Dey, S., Agarwal, A., Kishore, S., Lal, R.B., Manar, M., Kanawade, V.P., Chauhan, S.S.S., Sharma, M., Reddy, R.R., Gopal, K.R., Narasimhulu, K., Reddy, L.S.S., Gupta, S., Lal, S. (2006) Measurements of atmospheric parameters during Indian Space Research Organization Geosphere Biosphere Programme Land Campaign II at a typical location in the Ganga basin: 1. Physical and optical properties. 111.

Tröstl, J., Chuang, W.K., Gordon, H., Heinritzi, M., Yan, C., Molteni, U., Ahlm, L., Frege, C., Bianchi, F., Wagner, R., Simon, M., Lehtipalo, K., Williamson, C.J., Craven, J.S., Duplissy, J., Adamov, A., Almeida, J., Bernhammer, A.K., Breitenlechner, M., Brilke, S., Dias, A., Ehrhart, S., Flagan, R.C., Franchin, A., Fuchs, C., Guida, R., Gysel, M., Hansel, A., Hoyle, C.R., Jokinen, T., Junninen, H., Kangasluoma, J., Keskinen, H., Kim, J., Krapf, M., Kürten, A., Laaksonen, A., Lawler, M.J., Leiminger, M., Mathot, S., Möhler, O., Nieminen, T., Onnela, A., Petäjä, T., Piel, F.M., Miettinen, P., Rissanen, M.P., Rondo, L., Sarnela, N., Schobesberger, S., Sengupta, K., Sipilä, M., Smith, J.N., Steiner, G., Tomè, A., Virtanen, A., Wagner, A.C., Weingartner, E., Wimmer, D., Winkler, P.M., Ye, P., Carslaw, K.S., Curtius, J., Dommen, J., Kirkby, J., Kulmala, M., Riipinen, I., Worsnop, D.R., Donahue, N.M., Baltensperger, U. (2016a) The role of low-volatility organic compounds in initial particle growth in the atmosphere. Nature 533, 527-531.

Tröstl, J., Herrmann, E., Frege, C., Bianchi, F., Molteni, U., Bukowiecki, N., Hoyle, C.R., Steinbacher, M., Weingartner, E., Dommen, J., Gysel, M., Baltensperger, U. (2016b) Contribution of new particle formation to the total aerosol concentration at the high-altitude site Jungfraujoch (3580 m asl, Switzerland). Journal of Geophysical Research: Atmospheres 121, 11,692-611,711.

Tunved, P., Nilsson, E.D., Hansson, H.-C., Ström, J., Kulmala, M., Aalto, P., Viisanen, Y. (2005) Aerosol characteristics of air masses in northern Europe: Influences of location, transport, sinks, and sources. 110.

Tunved, P., Ström, J., Hansson, H.C. (2004) An investigation of processes controlling the evolution of the boundary layer aerosol size distribution properties at the Swedish background station Aspvreten. Atmos. Chem. Phys. 4, 2581-2592.

Twomey, S.J.J.o.t.a.s. (1977) The influence of pollution on the shortwave albedo of clouds. 34, 1149-1152.

Upadhyay, R.G., Ranjan, R., Negi, P.S. (2015) Climate variability and tredn at Ranichauri (Uttarakhand). Journal of Agrometeorology 17, 241-243.

Vakkari, V., Tiitta, P., Jaars, K., Croteau, P., Beukes, J.P., Josipovic, M., Kerminen, V.-M., Kulmala, M., Venter, A.D., van Zyl, P.G., Worsnop, D.R., Laakso, L. (2015) Reevaluating the contribution of sulfuric acid and the origin of organic compounds in atmospheric nanoparticle growth. Geophysical Research Letters 42, 10,486-410,493.

Vana, M., Kulmala, M., Dal Maso, M., Hõrrak, U., Tamm, E. (2004) Comparative study of nucleation mode aerosol particles and intermediate air ions formation events at three sites. 109.

Vanhanen, J., Mikkilä, J., Lehtipalo, K., Sipilä, M., Manninen, H.E., Siivola, E., Petäjä, T., Kulmala, M. (2011) Particle Size Magnifier for Nano-CN Detection. Aerosol Science and Technology 45, 533-542.

Varghese, M., Leena, P.P., Murugavel, P., Bankar, S., Todekar, K., Chowdhuri, S., Safai, P.D., Malap, N., Konwar, M., Dixit, S., Rao, Y.J., Prabha, T.V. (2020) New particle formation observed from a rain shadow region of the Western Ghats, India. Toxicological & Environmental Chemistry 102, 305-333.

Veefkind, J.P., Aben, I., McMullan, K., Förster, H., de Vries, J., Otter, G., Claas, J., Eskes, H.J., de Haan, J.F., Kleipool, Q., van Weele, M., Hasekamp, O., Hoogeveen, R., Landgraf, J., Snel, R., Tol, P., Ingmann, P., Voors, R., Kruizinga, B., Vink, R., Visser, H., Levelt, P.F. (2012) TROPOMI on the ESA Sentinel-5 Precursor: A GMES mission for global observations of the atmospheric composition for climate, air quality and ozone layer applications. Remote Sensing of Environment 120, 70-83.

Vehkamäki, H., Kulmala, M., Napari, I., Lehtinen, K.E.J., Timmreck, C., Noppel, M., Laaksonen, A. (2002) An improved parameterization for sulfuric acid–water nucleation rates for tropospheric and stratospheric conditions. Journal of Geophysical Research: Atmospheres 107, AAC 3-1-AAC 3-10.

Vehkamäki, H., Riipinen, I. (2012) Thermodynamics and kinetics of atmospheric aerosol particle formation and growth. Chemical Society Reviews 41, 5160-5173.

Venzac, H., Sellegri, K., Laj, P., Villani, P., Bonasoni, P., Marinoni, A., Cristofanelli, P., Calzolari, F., Fuzzi, S., Decesari, S., Facchini, M.-C., Vuillermoz, E., Verza, G.P. (2008) High frequency new particle formation in the Himalayas. Proceedings of the National Academy of Sciences 105, 15666-15671.

Vigouroux, C., Langerock, B., Bauer Aquino, C.A., Blumenstock, T., Cheng, Z., De Mazière, M., De Smedt, I., Grutter, M., Hannigan, J.W., Jones, N., Kivi, R., Loyola, D., Lutsch, E., Mahieu, E., Makarova, M., Metzger, J.M., Morino, I., Murata, I., Nagahama, T., Notholt, J., Ortega, I., Palm, M., Pinardi, G., Röhling, A., Smale, D., Stremme, W., Strong, K., Sussmann, R., Té, Y., van Roozendael, M., Wang, P., Winkler, H. (2020) TROPOMI–Sentinel-5 Precursor formaldehyde validation using an extensive network of ground-based Fourier-transform infrared stations. Atmos. Meas. Tech. 13, 3751-3767.

von Bismarck-Osten, C., Birmili, W., Ketzel, M., Massling, A., Petäjä, T., Weber, S. (2013) Characterization of parameters influencing the spatio-temporal variability of urban particle number size distributions in four European cities. Atmospheric Environment 77, 415-429.

Wang, F., Zhang, Z., Massling, A., Ketzel, M., Kristensson, A. (2013) Particle formation events measured at a semirural background site in Denmark. Environmental Science and Pollution Research 20, 3050-3059.

Wang, M., Kong, W., Marten, R., He, X.-C., Chen, D., Pfeifer, J., Heitto, A., Kontkanen, J., Dada, L., Kürten, A., Yli-Juuti, T., Manninen, H.E., Amanatidis, S., Amorim, A., Baalbaki, R., Baccarini, A., Bell, D.M., Bertozzi, B., Bräkling, S., Brilke, S., Murillo, L.C., Chiu, R., Chu, B., De Menezes, L.-P., Duplissy, J., Finkenzeller, H., Carracedo, L.G., Granzin, M., Guida, R., Hansel, A., Hofbauer, V., Krechmer, J., Lehtipalo, K., Lamkaddam, H., Lampimäki, M., Lee, C.P., Makhmutov, V., Marie, G., Mathot, S., Mauldin, R.L., Mentler, B., Müller, T., Onnela, A., Partoll, E., Petäjä, T., Philippov, M., Pospisilova, V., Ranjithkumar, A., Rissanen, M., Rörup, B., Scholz, W., Shen, J., Simon, M., Sipilä, M., Steiner, G., Stolzenburg, D., Tham, Y.J., Tomé, A., Wagner, A.C., Wang, D.S., Wang, Y., Weber, S.K., Winkler, P.M., Wlasits, P.J., Wu, Y., Xiao, M., Ye, Q., Zauner-Wieczorek, M., Zhou, X., Volkamer, R., Riipinen, I., Dommen, J., Curtius, J., Baltensperger, U., Kulmala, M., Worsnop, D.R., Kirkby, J., Seinfeld, H., El-Haddad, I., Flagan, R.C., Donahue, N.M. (2020) Rapid growth of new atmospheric particles by nitric acid and ammonia condensation. Nature 581, 184-189.

Wang, M., Penner, J.E. (2009) Aerosol indirect forcing in a global model with particle nucleation. Atmos. Chem. Phys. 9, 239-260.

Wang, S., Zordan, C.A., Johnston, M.V. (2006) Chemical Characterization of Individual, Airborne Sub-10-nm Particles and Molecules. Analytical Chemistry 78, 1750-1754.

Wang, Z., Wu, Z., Yue, D., Shang, D., Guo, S., Sun, J., Ding, A., Wang, L., Jiang, J., Guo, H., Gao, J., Cheung, H.C., Morawska, L., Keywood, M., Hu, M. (2017) New particle formation in China: Current knowledge and further directions. Science of The Total Environment 577, 258-266.

Weber, R.J., Marti, J.J., McMurry, P.H., Eisele, F.L., Tanner, D.J., Jefferson, A. (1996) MEASURED ATMOSPHERIC NEW PARTICLE FORMATION RATES: IMPLICATIONS FOR NUCLEATION MECHANISMS. Chemical Engineering Communications 151, 53-64.

Wehner, B., Petäjä, T., Boy, M., Engler, C., Birmili, W., Tuch, T., Wiedensohler, A., Kulmala, M. (2005) The contribution of sulfuric acid and non-volatile compounds on the growth of freshly formed atmospheric aerosols. Geophysical Research Letters 32, n/a-n/a.

Wehner, B., Siebert, H., Ansmann, A., Ditas, F., Seifert, P., Stratmann, F., Wiedensohler, A., Apituley, A., Shaw, R.A., Manninen, H.E., Kulmala, M. (2010) Observations of turbulence-induced new particle formation in the residual layer. Atmos. Chem. Phys. 10, 4319-4330.

Wehner, B., Siebert, H., Stratmann, F., Tuch, T., Wiedensohler, A., Petaja, T., Dal Maso, M., Kulmala, M. (2007) Horizontal homogeneity and vertical extent of new particle formation events. 59, 362-371.

Wehner, B., Wiedensohler, A., Tuch, T.M., Wu, Z.J., Hu, M., Slanina, J., Kiang, C.S. (2004) Variability of the aerosol number size distribution in Beijing, China: New particle formation, dust storms, and high continental background. Geophysical Research Letters 31.

Westervelt, D.M., Pierce, J.R., Adams, P.J. (2014) Analysis of feedbacks between nucleation rate, survival probability and cloud condensation nuclei formation. Atmos. Chem. Phys. 14, 5577-5597.

Westervelt, D.M., Pierce, J.R., Riipinen, I., Trivitayanurak, W., Hamed, A., Kulmala, M., Laaksonen, A., Decesari, S., Adams, P.J. (2013) Formation and growth of nucleated particles into cloud condensation nuclei: model–measurement comparison. Atmos. Chem. Phys. 13, 7645-7663.

Wexler, A.S., Lurmann, F.W., Seinfeld, J.H. (1994) Modelling urban and regional aerosols—I. model development. Atmospheric Environment 28, 531-546.

Wiedensohler, A., Birmili, W., Nowak, A., Sonntag, A., Weinhold, K., Merkel, M., Wehner, B., Tuch, T., Pfeifer, S., Fiebig, M., Fjäraa, A.M., Asmi, E., Sellegri, K., Depuy, R., Venzac, H., Villani, P., Laj, P., Aalto, P., Ogren, J.A., Swietlicki, E., Williams, P., Roldin, P., Quincey, P., Hüglin, C., Fierz-Schmidhauser, R., Gysel, M., Weingartner, E., Riccobono, F., Santos, S., Grüning, C., Faloon, K., Beddows, D., Harrison, R., Monahan, C., Jennings, S.G., O'Dowd, C.D., Marinoni, A., Horn, H.G., Keck, L., Jiang, J., Scheckman, J., McMurry, P.H., Deng, Z., Zhao, C.S., Moerman, M., Henzing, B., de Leeuw, G., Löschau, G., Bastian, S. (2012) Mobility particle size spectrometers: harmonization of technical standards and data structure to facilitate high quality long-term observations of atmospheric particle number size distributions. Atmos. Meas. Tech. 5, 657-685.

Wiedensohler, A., Cheng, Y.F., Nowak, A., Wehner, B., Achtert, P., Berghof, M., Birmili, W., Wu, Z.J., Hu, M., Zhu, T., Takegawa, N., Kita, K., Kondo, Y., Lou, S.R., Hofzumahaus, A., Holland, F., Wahner, A., Gunthe, S.S., Rose, D., Su, H., Pöschl, U. (2009) Rapid aerosol particle growth and increase of cloud condensation nucleus activity by secondary aerosol formation and condensation: A case study for regional air pollution in northeastern China. Journal of Geophysical Research: Atmospheres 114, n/a-n/a.

Wu, Z., Hu, M., Lin, P., Liu, S., Wehner, B., Wiedensohler, A. (2008) Particle number size distribution in the urban atmosphere of Beijing, China. Atmospheric Environment 42, 7967-7980.

Wu, Z., Hu, M., Liu, S., Wehner, B., Bauer, S., Ma ßling, A., Wiedensohler, A., Petäjä, T., Dal Maso, M., Kulmala, M. (2007) New particle formation in Beijing, China: Statistical analysis of a 1-year data set. 112.

Xiao, M., Hoyle, C.R., Dada, L., Stolzenburg, D., Kürten, A., Wang, M., Lamkaddam, H., Garmash, O., Mentler, B., Molteni, U., Baccarini, A., Simon, M., He, X.C., Lehtipalo, K., Ahonen, L.R., Baalbaki, R., Bauer, P.S., Beck, L., Bell, D., Bianchi, F., Brilke, S., Chen, D., Chiu, R., Dias, A., Duplissy, J., Finkenzeller, H., Gordon, H., Hofbauer, V., Kim, C., Koenig, T.K., Lampilahti, J., Lee, C.P., Li, Z., Mai, H., Makhmutov, V., Manninen, H.E., Marten, R., Mathot, S., Mauldin, R.L., Nie, W., Onnela, A., Partoll, E., Petäjä, T., Pfeifer, J., Pospisilova, V., Quéléver, L.L.J., Rissanen, M., Schobesberger, S., Schuchmann, S., Stozhkov, Y., Tauber, C., Tham, Y.J., Tomé, A., Vazquez-Pufleau, M., Wagner, A.C., Wanger, R., Wang, Y., Weitz, L., Wimmer, D., Wu, Y., Yan, C., Ye, P., Ye, Q., Zha, Q., Zhou, X., Amorim, A., Carslaw, K., Curtius, J., Hansel, A., Volkamer, R., Winkler, P.M., Flagan, R.C., Kulmala, M., Worsnop, D.R., Kirkby, J., Donahue, N.M., Baltensperger, U., El Haddad, I., Dommen, J. (2021) The driving factors of new particle formation and growth in the polluted boundary layer. Atmos. Chem. Phys. Discuss. 2021, 1-28.

Xiao, Q., Zhang, J., Wang, Y., Ziemba, L.D., Crosbie, E., Winstead, E.L., Robinson, C.E., DiGangi, J.P., Diskin, G.S., Reid, J.S., Schmidt, K.S., Sorooshian, A., Hilario, M.R.A., Woods, S., Lawson, P., Stamnes, S.A., Wang, J. (2023) New Particle Formation in the Tropical Free Troposphere during CAMP2Ex: Statistics and Impact of Emission Sources, Convective activity, and Synoptic Condition. Atmos. Chem. Phys. Discuss. 2023, 1-34.

Xiao, S., Wang, M.Y., Yao, L., Kulmala, M., Zhou, B., Yang, X., Chen, J.M., Wang, D.F., Fu, Q.Y., Worsnop, D.R., Wang, L. (2015) Strong atmospheric new particle formation in winter in urban Shanghai, China. Atmos. Chem. Phys. 15, 1769-1781.

Xing, Y.F., Xu, Y.H., Shi, M.H., Lian, Y.X. (2016) The impact of PM2.5 on the human respiratory system. J Thorac Dis 8, E69-74.

Yadav, S.K., Kompalli, S.K., Gurjar, B.R., Mishra, R.K. (2021) Aerosol number concentrations and new particle formation events over a polluted megacity during the COVID-19 lockdown. Atmospheric Environment 259, 118526.

Yli-Juuti, T., Tikkanen, O.-P., Manninen, H., Nieminen, T., Kulmala, M. (2016) Analysis of sub-3 nm particle growth in connection with sulfuric acid in boreal forest. BOREAL ENVIRONMENT RESEARCH 21, 287-298.

You, Y., Kanawade, V.P., de Gouw, J.A., Guenther, A.B., Madronich, S., Sierra-Hernández, M.R., Lawler, M., Smith, J.N., Takahama, S., Ruggeri, G., Koss, A., Olson, K., Baumann, K., Weber, R.J., Nenes, A., Guo, H., Edgerton, E.S., Porcelli, L., Brune, W.H., Goldstein, A.H., Lee, S.H. (2014) Atmospheric amines and ammonia measured with a chemical ionization mass spectrometer (CIMS). Atmos. Chem. Phys. 14, 12181-12194.

Young, A.T. (1982) Rayleigh scattering. Physics Today 35, 42-48.

Yu, F. (2006a) Binary H2SO4-H2O homogeneous nucleation based on kinetic quasi-unary nucleation model: Look-up tables. Journal of Geophysical Research: Atmospheres 111.

Yu, F. (2006b) Effect of ammonia on new particle formation: A kinetic H2SO4-H2O-NH3 nucleation model constrained by laboratory measurements. Journal of Geophysical Research: Atmospheres 111.

Yu, F. (2011) A secondary organic aerosol formation model considering successive oxidation aging and kinetic condensation of organic compounds: global scale implications. Atmos. Chem. Phys. 11, 1083-1099.

Yu, F., Luo, G., Nair, A.A., Schwab, J.J., Sherman, J.P., Zhang, Y. (2020) Wintertime new particle formation and its contribution to cloud condensation nuclei in the Northeastern United States. Atmos. Chem. Phys. 20, 2591-2601.

Yu, F., Turco, R.P. (2000) Ultrafine aerosol formation via ion-mediated nucleation. 27, 883-886.

Yu, H., Gannet, H.A., You, Y., Sedlacek, A., Springston, S., Kanawade, V.P., Lee, Y.N., Wang, J., Kuang, C., McGraw, R.L., McCubbin, I., Mikkila, J., Lee, S.-H. (2014) Sub-3 nm particles observed at the coastal and continental sites in the United States. Journal of Geophysical Research: Atmospheres 119, 860-879.

Yu, H., McGraw, R., Lee, S.H. (2012) Effects of amines on formation of sub-3 nm particles and their subsequent growth. Geophysical Research Letters 39, n/a-n/a.

Yu, H., Ren, L., Kanawade, V.P. (2017) New Particle Formation and Growth Mechanisms in Highly Polluted Environments. Current Pollution Reports 3, 245-253.

Yu, H., Zhou, L., Dai, L., Shen, W., Dai, W., Zheng, J., Ma, Y., Chen, M. (2016) Nucleation and growth of sub-3 nm particles in the polluted urban atmosphere of a megacity in China. Atmos. Chem. Phys. 16, 2641-2657.

Yue, D., Hu, M., Wu, Z., Wang, Z., Guo, S., Wehner, B., Nowak, A., Achtert, P., Wiedensohler, A., Jung, J., Kim, Y.J., Liu, S. (2009) Characteristics of aerosol size distributions and new particle formation in the summer in Beijing. Journal of Geophysical Research: Atmospheres 114.

Yue, D.L., Hu, M., Zhang, R.Y., Wang, Z.B., Zheng, J., Wu, Z.J., Wiedensohler, A., He, L.Y., Huang, X.F., Zhu, T. (2010) The roles of sulfuric acid in new particle formation and growth in the mega-city of Beijing. Atmos. Chem. Phys. 10, 4953-4960.

Zege, E.P., Kokhanovsky, A.A. (1994) Analytical solution to the optical transfer function of a scattering medium with large particles. Applied Optics 33, 6547-6554.

Zhang, H., Ma, J., Zheng, Y.J.C.J.A.S. (2008a) The study of global radiative forcing due to black carbon aerosol. 32, 1147-1158.

Zhang, J., Wang, T., Chameides, W.L., Cardelino, C., Blake, D.R., Streets, D.G. (2008b) Source characteristics of volatile organic compounds during high ozone episodes in Hong Kong, Southern China. Atmos. Chem. Phys. 8, 4983-4996.

Zhang, Q., Jimenez, J.L., Canagaratna, M.R., Allan, J.D., Coe, H., Ulbrich, I., Alfarra, M.R., Takami, A., Middlebrook, A.M., Sun, Y.L., Dzepina, K., Dunlea, E., Docherty, K., DeCarlo, P.F., Salcedo, D., Onasch, T., Jayne, J.T., Miyoshi, T., Shimono, A., Hatakeyama, S., Takegawa, N., Kondo, Y., Schneider, J., Drewnick, F., Borrmann, S., Weimer, S., Demerjian, K., Williams, P., Bower, K., Bahreini, R., Cottrell, L., Griffin, R.J., Rautiainen, J., Sun, J.Y., Zhang, Y.M., Worsnop, D.R. (2007) Ubiquity and dominance of oxygenated species in organic aerosols in anthropogenically-influenced Northern Hemisphere midlatitudes. Geophysical Research Letters 34.

Zhang, R., Khalizov, A., Wang, L., Hu, M., Xu, W. (2012) Nucleation and Growth of Nanoparticles in the Atmosphere. Chemical Reviews 112, 1957-2011.

Zhang, R., Suh, I., Zhao, J., Zhang, D., Fortner, E.C., Tie, X., Molina, L.T., Molina, M.J. (2004) Atmospheric New Particle Formation Enhanced by Organic Acids. Science 304, 1487-1490.

Zhang, Y., Liu, P., Liu, X.-H., Jacobson, M.Z., McMurry, P.H., Yu, F., Yu, S., Schere, K.L. (2010) A comparative study of nucleation parameterizations: 2. Three-dimensional model application and evaluation. Journal of Geophysical Research: Atmospheres 115.

Zhao, B., Fast, J., Shrivastava, M., Donahue, N.M., Gao, Y., Shilling, J.E., Liu, Y., Zaveri, R.A., Gaudet, B., Wang, S., Wang, J., Li, Z., Fan, J. (2022) Formation Process of Particles and Cloud Condensation Nuclei Over the Amazon Rainforest: The Role of Local and Remote New-Particle Formation. Geophysical Research Letters 49, e2022GL100940.

Zhao, J., Eisele, F.L., Titcombe, M., Kuang, C., McMurry, P.H. (2010) Chemical ionization mass spectrometric measurements of atmospheric neutral clusters using the cluster-CIMS. Journal of Geophysical Research: Atmospheres 115, n/a-n/a.

Zheng, J., Hu, M., Zhang, R., Yue, D., Wang, Z., Guo, S., Li, X., Bohn, B., Shao, M., He, L., Huang, X., Wiedensohler, A., Zhu, T. (2011) Measurements of gaseous H₂SO₄ by AP-ID-CIMS during CAREBeijing 2008 Campaign. Atmos. Chem. Phys. 11, 7755-7765.

Zhong, H., Huang, R., Chang, Y., Duan, J., Lin, C., Chen, Y. (2021) Enhanced formation of secondary organic aerosol from photochemical oxidation during the COVID-19 lockdown in a background site in Northwest China. Science of The Total Environment 778, 144947.

Zhou, Y., Dada, L., Liu, Y., Fu, Y., Kangasluoma, J., Chan, T., Yan, C., Chu, B., Daellenbach, K.R., Bianchi, F., Kokkonen, T.V., Liu, Y., Kujansuu, J., Kerminen, V.M., Petäjä, T., Wang, L., Jiang, J., Kulmala, M. (2020) Variation of size-segregated particle number concentrations in wintertime Beijing. Atmos. Chem. Phys. 20, 1201-1216.

Zhu, Y., Xue, L., Gao, J., Chen, J., Li, H., Zhao, Y., Guo, Z., Chen, T., Wen, L., Zheng, P., Shan, Y., Wang, X., Wang, T., Yao, X., Wang, W. (2020) Increased new particle yields with largely decreased probability of survival to CCN size at the summit of Mt. Tai under reduced SO2 emissions. Atmos. Chem. Phys. Discuss. 2020, 1-30.

Zilli Vieira, C.L., Koutrakis, P. (2021) The impact of solar activity on ambient ultrafine particle concentrations: An analysis based on 19-year measurements in Boston, USA. Environmental Research 201, 111532.

Zimmerman, A., Petters, M.D., Meskhidze, N. (2020) Observations of new particle formation, modal growth rates, and direct emissions of sub-10 nm particles in an urban environment. Atmos Environ (1994) 242, 117835.

Atmos. Chem. Phys., 22, 4491–4508, 2022
https://doi.org/10.5194/acp-22-4491-2022
© Author(s) 2022. This work is distributed under
the Creative Commons Attribution 4.0 License.

Atmospheric Chemistry and Physics
Open Access
EGU

Observations of particle number size distributions and new particle formation in six Indian locations

Mathew Sebastian[1], Sobhan Kumar Kompalli[2], Vasudevan Anil Kumar[3], Sandhya Jose[4,5], S. Suresh Babu[2], Govindan Pandithurai[3], Sachchidanand Singh[4,5], Rakesh K. Hooda[6], Vijay K. Soni[7], Jeffrey R. Pierce[8], Ville Vakkari[6,9], Eija Asmi[6], Daniel M. Westervelt[10,11], Antti-Pekka Hyvärinen[6], and Vijay P. Kanawade[1]

[1]Centre for Earth, Ocean and Atmospheric Sciences, University of Hyderabad, Hyderabad, India
[2]Space Physics Laboratory, Vikram Sarabhai Space Centre, Thiruvananthapuram, India
[3]Indian Institute of Tropical Meteorology, Ministry of Earth Sciences, Pune, India
[4]CSIR-National Physical Laboratory, Dr. K.S. Krishnan Road, New Delhi, India
[5]Academy of Scientific and Innovative Research (AcSIR), Ghaziabad-201002, India
[6]Finnish Meteorological Institute, Erik Palmenin Aukio 1, Helsinki, Finland
[7]India Meteorological Department, Ministry of Earth Sciences, New Delhi, India
[8]Department of Atmospheric Science, Colorado State University, Fort Collins, CO, USA
[9]Atmospheric Chemistry Research Group, Chemical Resource Beneficiation, North-West University, Potchefstroom, South Africa
[10]Division of Ocean and Climate Physics, Lamont-Doherty Earth Observatory of Columbia University, Palisades, New York, USA
[11]NASA Goddard Institute for Space Studies, New York City, NY, USA

Correspondence: Vijay P. Kanawade (vijaykanawade03@yahoo.co.in)

Received: 24 September 2021 – Discussion started: 25 October 2021
Revised: 28 February 2022 – Accepted: 2 March 2022 – Published: 7 April 2022

Abstract. Atmospheric new particle formation (NPF) is a crucial process driving aerosol number concentrations in the atmosphere; it can significantly impact the evolution of atmospheric aerosol and cloud processes. This study analyses at least 1 year of asynchronous particle number size distributions from six different locations in India. We also analyze the frequency of NPF and its contribution to cloud condensation nuclei (CCN) concentrations. We found that the NPF frequency has a considerable seasonal variability. At the measurement sites analyzed in this study, NPF frequently occurs in March–May (pre-monsoon, about 21 % of the days) and is the least common in October–November (post-monsoon, about 7 % of the days). Considering the NPF events in all locations, the particle formation rate (J_{SDS}) varied by more than 2 orders of magnitude (0.001–0.6 cm^{-3} s^{-1}) and the growth rate between the smallest detectable size and 25 nm ($GR_{SDS\text{-}25\,nm}$) by about 3 orders of magnitude (0.2–17.2 $nm\,h^{-1}$). We found that J_{SDS} was higher by nearly 1 order of magnitude during NPF events in urban areas than mountain sites. GR_{SDS} did not show a systematic difference. Our results showed that NPF events could significantly modulate the shape of particle number size distributions and CCN concentrations in India. The contribution of a given NPF event to CCN concentrations was the highest in urban locations (4.3×10^3 cm^{-3} per event and 1.2×10^3 cm^{-3} per event for 50 and 100 nm, respectively) as compared to mountain background sites (2.7×10^3 cm^{-3} per event and 1.0×10^3 cm^{-3} per event, respectively). We emphasize that the physical and chemical pathways responsible for NPF and factors that control its contribution to CCN production require in situ field observations using recent advances in aerosol and its precursor gaseous measurement techniques.

1 Introduction

Cooling by atmospheric aerosols offsets a significant fraction of the radiative forcing of greenhouse gases (Paasonen et al., 2013) directly by scattering and absorbing solar radiation and indirectly by altering cloud microphysical properties via activation of cloud condensation nuclei (CCN; Rosenfeld et al., 2014; Sarangi et al., 2018). New particle formation (NPF), as a result of gas-to-particle conversion, is the largest source of aerosol numbers to the terrestrial atmosphere (Kulmala et al., 2007; Zhang et al., 2012). While nucleated particles from NPF are initially very small molecular clusters (1–2 nm; Kerminen et al., 2012), these molecular clusters can grow to large sizes within a few hours to a few days and ultimately reach CCN active sizes (> 50–100 nm; Pierce and Adams, 2007; Westervelt et al., 2013). Thus, CCN forms the direct microphysical link between aerosols and clouds and plays a vital role in the hydrological cycle and climate.

In India, several intensive field campaigns such as the Indian Ocean Experiment (INDOEX; Ramanathan et al., 2001), Indian Space Research Organization (ISRO)-Geosphere-Biosphere Programme (GBP)-Land campaign II (Tripathi et al., 2006; Tare et al., 2006), and Integrated Campaign for Aerosols, gases, and Radiation Budget (ICARB; Moorthy et al., 2008; Nair et al., 2020; Kompalli et al., 2020) have measured sub-micron particle number size distributions (PNSDs). There are also short- and long-term field observations of sub-micron PNSDs in a variety of diverse locations in India (Hyvärinen et al., 2010; Kanawade et al., 2014a; Shika et al., 2020; Tripathi et al., 1988; Komppula et al., 2009; Singh et al., 2004; Moorthy et al., 2011; Babu et al., 2016; Kompalli et al., 2018). However, there are sparse studies in India characterizing seasonal variation in PNSDs and number concentrations (Kanawade et al., 2014a; Hyvärinen et al., 2010; Komppula et al., 2009; Hooda et al., 2018; Laj et al., 2020) and atmospheric NPF (Sebastian et al., 2021b; Siingh et al., 2018; Neitola et al., 2011; Moorthy et al., 2011; Kanawade et al., 2014b, c; Kanawade et al., 2020a). The characterization of PNSDs is critical because they are controlled by an evolving balance between NPF, condensation of vapor on pre-existing particles, evaporation of particles, coagulation, and sedimentation (IPCC, 2013). Previous field measurements and modeling studies globally demonstrated a substantial enhancement in CCN number concentrations from nucleation (Yu et al., 2020; Wiedensohler et al., 2009; Sihto et al., 2011; Rose et al., 2017; Tröstl et al., 2016; Kalivitis et al., 2015; Westervelt et al., 2013; Pierce et al., 2012; Pierce et al., 2014; Westervelt et al., 2014; Kerminen et al., 2012; Kerminen et al., 2018; Merikanto et al., 2009; Gordon et al., 2017). For instance, Merikanto et al. (2009) revealed that 45 % of the global low-level CCN at 0.2 % supersaturation originates from nucleation. Westervelt et al. (2014) also found that nucleation contributes to about half of the boundary layer CCN (at supersaturation of 0.2 %), with an estimated uncertainty range of 49 % to 78 %, which is sensitive to the choice of nucleation scheme. In contrast, Reddington et al. (2011), using the global model GLOMAP against ground-based measurements at 15 European sites, found that CCN-sized particle number concentrations were driven by processes other than nucleation at more than 10 sites. They explained that the weakened response of CCN-sized particles to boundary layer nucleation arises from an increase in coagulation and condensation sinks for ultrafine particles, thereby reducing the condensational growth of ultrafine particles to CCN active sizes (Kuang et al., 2009; Pierce and Adams, 2007). Tröstl et al. (2016) also revealed that only a small fraction of total particles of less than 50 nm grew beyond 90 nm (50–100 particles cm^{-3}), even on a timescale of several days. Therefore, to better understand atmospheric NPF and its contribution to the boundary layer CCN budget, we need highly resolved spatiotemporal observational data in diverse environments globally, aided with aerosol model simulations, to help to interpret field observations.

Overall, studies pertinent to the impact of NPF on aerosol–cloud interactions are highly sparse in India. The sources of aerosols, and gaseous precursors required for secondary aerosol formation, depict considerable spatiotemporal heterogeneity over India. Therefore, observational aerosols and precursors data must be synthesized to understand the processes that govern NPF and its contribution to CCN concentrations in different settings of India. The primary objective of this study is to harmonize observational PNSDs data from six diverse locations in India to present analyses of PNSDs, atmospheric NPF, and the contribution of NPF to CCN concentrations.

2 Methods

2.1 Observation sites and aerosol sampling instrumentation

Figure 1 shows the geographical location of measurement sites on the surface elevation map. Table 1 provides details of measurement sites and particle data analyzed in this study.

Ranichauri observation site (RNC; 30.2° N, 78.25° E; ∼ 1930 m above mean sea level, a.m.s.l.) is located in the Tehri–Garhwal district of Uttarakhand state in the southern slope of the western Himalaya. The RNC site is situated on an isolated hilltop within the campus of the College of Forestry in the Ranichauri village. The RNC site is a climate monitoring station managed by the India Meteorological Department (IMD). It is a mountain background remote observatory (Sebastian et al., 2021b) and located about 70 km to the northeast of Rishikesh city, about 100 km to the northwest of the Srinagar city, and about 100 km to the east of Dehradun. Here, particle number size distributions ranging from 10 to 757 nm (30 size bins) are measured using a differential mobility particle sizer (DMPS, Finnish Meteorological Institute assembled) from December 2016 to September 2018 (Sebastian et al., 2021b). The DMPS consisted of a

Table 1. Details of the measurement sites and particle number size distribution measurements analyzed in this study.

Site name	Site code	Site type	Instrument	Size range (nm)	Time resolution (min)	Time period
Ranichauri	RNC	Mountain background	DMPS	10.1–757	10	Dec 2016–Sep 2018
Mukteshwar	MUK	Mountain background	DMPS	10.1–757	5	Jan 2012–Dec 2013
Mahabaleshwar	MBL	Mountain semi-rural	WRAS	5.14–1000	4	Mar 2015–Mar 2016
Hyderabad	HYD	Urban	SMPS	10.9–514	5	Apr 2019–Mar 2020
Thiruvananthapuram	TVM	Semi-urban coastal	SMPS	14.6–661.2	5	Jan 2013–Jan 2014
Delhi	DEL	Urban	WRAS	5.14–1000	5	Nov 2011–Jan 2013

DMPS: differential mobility particle sizer, WRAS: wide-range aerosol spectrometer, SMPS: scanning mobility particle sizer

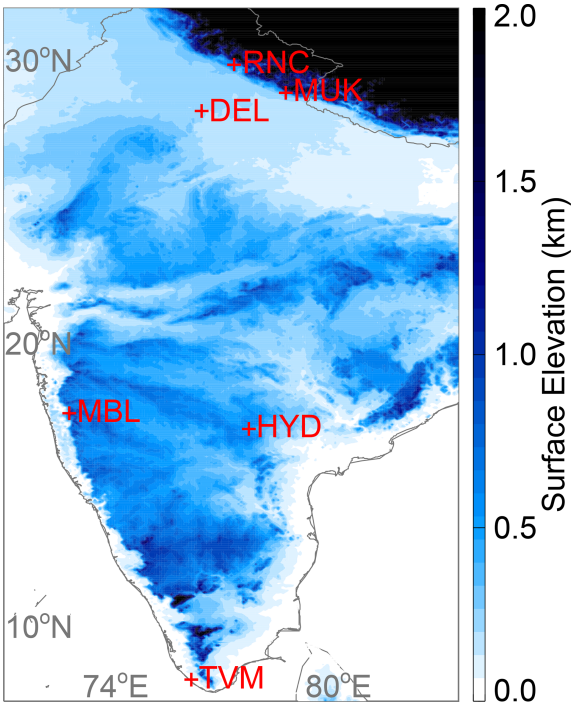

Figure 1. The geographical location of measurement sites on the surface elevation map. Measurement sites such as Ranichauri (RNC), Mukteshwar (MUK), Mahabaleshwar (MBL), Hyderabad (HYD), Thiruvananthapuram (TVM), and Delhi (DEL) are shown by the red plus sign. The global 1 arcsec (30 m) SRTM digital surface elevation data are obtained from the United States Geological Survey (https://www.usgs.gov/centers/eros/science/usgs-eros-archive-digital-elevation-shuttle-radar-topography-mission-srtm-1#overview, last access: July 2018).

Vienna-type differential mobility analyzer (DMA) that classifies the charged particles according to their electrical mobility and a TSI 3772 condensation particle counter (CPC) that counts particles of the selected mobility. The sample air was drawn inside through a stainless-steel inlet tube of about 2 m in length and dried to less than 40 % relative humidity with a Nafion dryer (Perma Pure model MD-700-48). Diffusion losses in the inlet and inside the DMPS instrument were considered in the data inversion. The inversion method was identical to that presented by Wiedensohler et al. (2012) for the Finnish Meteorological Institute (FMI) DMPS.

Mukteshwar observation site (MUK; 29.43° N, 79.62° E, 2180 m a.m.s.l.) is located in the Nainital district of Uttarakhand state in the southern slope of the central Himalaya. The Mukteshwar village is situated 3 km to the northeast of the measurement site, at a similar altitude, with ∼800 inhabitants (Census of India, 2011). MUK can be considered a mountain background site, with an annual mean black carbon (BC) concentration of 0.9 µg m^{-3}. The town of Almora (1650 m a.m.s.l., 34 000 inhabitants) is located at about 16 km to the north, Nainital (1960 m a.m.s.l., 41 000 inhabitants) is located at about 25 km to the southwest, and the city of Haldwani (424 m a.m.s.l., 150 000 inhabitants) is located at about 32 km to the southwest of MUK. Delhi, the major metropolitan city (215 m a.m.s.l., 16.8 million inhabitants), is located approximately 250 km to the southwest. Systematic measurements of aerosol properties have been conducted at MUK since 2005 in Indo-Finnish cooperation with the Finnish Meteorological Institute (Hooda et al., 2018 and references therein). Here, we used only 2 years (January 2012 to December 2013) of measurements of particle number size distributions in the range of 10 to 757 nm (30 size bins). The air sampling procedure was similar to that of RNC. More details of the site and aerosol sampling can be found in Hyvärinen et al. (2009).

Delhi observation site (DEL; 28.64° N, 77.17° E, 215 m a.m.s.l.) is located at CSIR-National Physical Laboratory (NPL). Delhi, India's capital and the largest metropolitan city in South Asia, is located on the northwestern Indo Gangetic Plain (IGP) in northern India. Delhi has a population of 16.8 million, with a population density of 11 320 km^{-2} (Census of India, 2011). The Great Indian Desert (Thar Desert) of Rajasthan state is located to the southwest, hot central plains to the south, and hilly regions to the north and east of Delhi. Long-range transported air masses often influence Delhi's air quality from the northwest (agricultural residue burning from Punjab and Haryana in October–November) and southwest (dust storms from Thar and Arabian Peninsula in April–June; Kanawade et al.,

2020b; Srivastava et al., 2014). A wide-range aerosol spectrometer (WRAS, manufactured by GRIMM, Germany), installed on the second floor of the NPL main building, was used to measure particle number size distributions. WRAS consists of a scanning mobility particle sizer (SMPS) and an environmental dust monitor (EDM). GRIMM-SMPS system consists of a Vienna-type monodisperse differential mobility analyzer (M-DMA). DMA classifies the particle according to their electrical mobility, which is then counted using a CPC. EDM uses an optical particle counter (OPC), which works on the light scattering technology for particle counting, gives the particle number size distribution in the range from 250 nm to 32 µm (Grimm and Eatough, 2009). The WRAS system uses a stainless-steel inlet tube with an integrated Nafion drier to dry the aerosol samples. A detailed description of the site and aerosol sampling is given elsewhere (Jose et al., 2021). Thus, the WRAS system gives the particle number size distribution in the range from 5.5 nm to 32 µm (72 size bins). A detailed description and principle of the instrument are discussed elsewhere (Grimm and Eatough, 2009). In this study, we used particle number size distributions in the range of 5.14 to 1000 nm from November 2011 to January 2013.

Mahabaleshwar observation site (MBL; 17.92° N, 73.65° E; 1378 m a.m.s.l.) is located in a small town named Mahabaleshwar in the forested Western Ghats range in the Satara district of Maharashtra state. In MBL, a High-Altitude Cloud Physics Laboratory (HACPL) was established by the Indian Institute of Tropical Meteorology (IITM), Pune, in 2012, to study monsoon clouds in this region. HACPL site details are found elsewhere (Anil Kumar et al., 2021). Mahabaleshwar town is a tourist attraction consisting of dense vegetation, residential houses, hotels, and a rural market. Pune city is located on the leeward side of the Western Ghats about 100 km to the north, Mumbai is located approximately 250 km to the northwest, and Satara city is located approximately 50 km to the southeast of Mahabaleshwar. Measurements of particle number size distributions were carried out using the GRIMM-WRAS system. A detailed description and principle of the instrument are discussed elsewhere (Grimm and Eatough, 2009). The WRAS has a stainless-steel inlet tube with an integrated Nafion dryer to reduce relative humidity to ∼ 40 %. In this study, we used particle number size distributions in the range of 5.14 to 1000 nm from March 2015 to March 2016.

Hyderabad observation site (HYD; 17.46° N, 78.32° E; 542 m a.m.s.l.), University of Hyderabad, is located in the outskirts of Hyderabad city. HYD details can be found in Sebastian et al. (2021a). Briefly, particle number size distributions in the range from 10.9 to 514 nm (108 size bins) were measured using TSI SMPS, which consists of an electrostatic classifier with a long DMA (TSI LDMA, model 3082) and a butanol CPC (TSI, model 3772), on the second floor of the Earth Sciences building located on the University of Hyderabad campus from April 2019 to March 2020. The scanning cycle of SMPS was 300 s, yielding a particle number size distribution every 5 min.

Thiruvananthapuram (Trivandrum) observation site (TVM; 8.55° N, 76.97° E, 3 m a.m.s.l.) is located in a tropical semi-urban coastal city with a population of ∼ 1 million (Census of India, 2011) on the southwestern coast of the Indian peninsular. The observations were carried out at the Space Physics Laboratory (SPL) within the Thumba Equatorial Rocket Launching Station, which is about 500 m due east of the Arabian Sea coast and 10 km northwest of the urban area of Thiruvananthapuram. The experimental site is free from major industrial or urban activities (Babu et al., 2016). TVM station is a part of the Aerosol Radiative Forcing over India (ARFI) project network of the Indian Space Research Organisation – Geosphere-Biosphere Program (ISRO-GBP). Measurements of particle number size distributions in the range from 14.6 to 661.2 nm (108 size bins) were made using TSI SMPS, which consists of an electrostatic classifier with an LDMA (3081) and a water-based CPC (3786) from January 2013 to January 2014. The ambient air was sampled from a height of 3 m above ground level through a manifold inlet fitted with a PM_{10} size cut impactor at 16.67 L min^{-1} flow rate. Subsequently, the flow was distributed among various aerosol instruments connected with electrically conductive tubing. A diffusion dryer (make: TSI; model: 3062) employing silica gel was used to restrict high relative humidity conditions. More details about the site and prevailing meteorology are described in Babu et al. (2016).

Particle number size distributions are categorized by season. We have defined four seasons as indicated in Table 2. The overall particle number size distribution data coverage was adequate (> 60 %) at the RNC, MUK, MBL, and HYD sites (Fig. 2) for determining the main seasonal and annual features of particle number size distributions and NPF characteristics. The data coverage at TVM (34 %) and DEL (47 %) was lower. We also analyzed the number concentration of three sub-micron aerosol modes: Aitken mode (25–100 nm), accumulation mode (100–514 nm), and total particles (< 514 nm). Figure S1 in the Supplement shows the HYbrid Single-Particle Lagrangian Integrated Trajectory (HYSPLIT, Draxler and Draxler, 2010) calculated 3 d air mass backward trajectories arriving at 500 m above the ground level at all sites for winter, pre-monsoon, monsoon, and post-monsoon seasons. RNC and MUK generally experience a mixture of relatively cleaner free tropospheric air and polluted air from the highly polluted Indo-Gangetic Plain. MBL experiences marine air masses during pre-monsoon and monsoon seasons and continental air masses during post-monsoon and winter. HYD experiences mixed marine and continental air masses from the northeast during post-monsoon and winter seasons and from southeast and west during pre-monsoon and monsoon, respectively. TVM predominantly experiences air masses of marine origin throughout the year, with continental influence during the winter season. DEL mostly experiences air masses from the northwest

Table 2. Seasons are defined in the analysis and average weather conditions.

Season	Months	Comments
Winter	December, January, February	Cold and dry
Pre-monsoon	March, April, May	Hot and dry
Monsoon	June, July, August, September	Warm, humid, and wet
Post-monsoon	October, November	Cool and humid

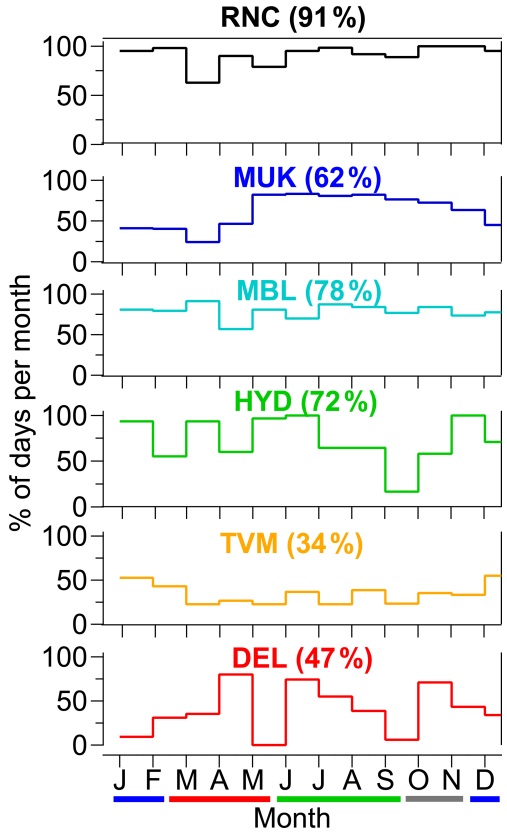

Figure 2. Particle number size distributions data coverage (% of days per month) at the sites. The values in the bracket indicate total data coverage. The thick blue, red, green, and gray lines indicate winter, pre-monsoon, monsoon, and post-monsoon months. Note that measurements are from different time periods for each site (see Table 1).

during pre-monsoon, post-monsoon, and winter seasons and from southeast and southwest during monsoon season.

2.2 New particle formation event classification and features

We classified observation days into three types of events: NPF event day, non-event day, and undefined event day using visual inspection of the particle number size distributions, following the methodology given by Dal Maso et al. (2005). A day was classified as an NPF event day by the presence of a distinctly new mode of particles with a diameter smaller than 25 nm and steady growth in diameter of this new mode such that the particle number size distributions display a noontime "banana" shaped aerosol growth. The particle mode diameter (i.e., the local maximum of the particle number size distribution) was obtained by fitting a log-normal distribution to the measured particle number size distribution. A day without any evidence of a distinctly new mode of particles of diameters smaller than 25 nm was identified as a non-event day. Those days which were difficult to be classified as any one of the above two event types were identified as undefined event days. For NPF events, the particle growth rate was calculated by fitting a first-order polynomial line through growing particle mode diameter between the smallest detectable size (SDS) of the instrument (e.g., 10 nm for RNC) and 25 nm as a function of time and calculating its slope ($GR_{SDS\text{-}25\,nm}$). The formation rate of a particle at the SDS (J_{SDS}) was also found using the simplified approximation of the general dynamic equation (GDE), describing the evolution of the particle number size distribution as given below:

$$J_{SDS} = \frac{dN_{SDS\text{-}25}}{dt} + F_{CoagS} + F_{growth}, \quad (1)$$

where the first term in Eq. (1) is the rate of the change of nucleation mode particle number concentrations, the second term is the coagulation loss of nucleation mode particles, and the third term is the flux out of the size range of SDS-25 nm, i.e., condensational growth (Dal Maso et al., 2005). A direct comparison of J_{SDS} and $GR_{SDS\text{-}25\,nm}$ between the sites is not possible because of the different size ranges covered by the instruments.

2.3 Increase in CCN concentrations from NPF

The increase in CCN concentrations from any given NPF event can be estimated by comparing the CCN concentration before the event ($N_{CCNprior}$) and the maximum CCN concentration during the event (N_{CCNmax}) following the methodology developed by Kerminen et al. (2012), which we modified further. In typical ambient in-cloud supersaturations, the total number of particles from 50 to > 100 nm can be considered as a proxy for CCN concentrations assuming fixed chemical composition (Westervelt et al., 2013; Kerminen et al., 2012). $N_{CCNprior}$ was chosen to be a 1 h average concentration of particles larger than 50 nm (and 100 nm) just before the start of the NPF event. The start of the NPF event is the time when nucleation mode particle number concentrations increase rapidly during an NPF event. N_{CCNmax} was taken as a maximum 1 h average concentration of particles larger than 50 nm (and 100 nm) during the event. The N_{CCNmax} is not the best representation of CCN concentration after the NPF event because it is not possible to estimate the end of an NPF event. However, it gives a rough estimate of the observed maximum number of primary and secondary particles present in the atmosphere during an event (Kerminen et al., 2012). For non-event days, the seasonally averaged start of the NPF

event time was chosen to calculate $N_{CCNprior}$. N_{CCNmax} on non-event days was taken to be similar to NPF event days, as a maximum 1 h average concentration of particles larger than 50 nm (and 100 nm). The second term in Eq. (2) gives approximate CCN concentrations from processes other than NPF. Then, the absolute increase in CCN concentration from NPF is calculated as given below:

$$\text{CCN increase} = (N_{CCNmax} - N_{CCNprior})_{NPFevent} - (N_{CCNmax} - N_{CCNprior})_{non-events}. \quad (2)$$

The first term on the right-hand side in Eq. (2) indicates the CCN increase during an NPF event, while the second term indicates the CCN increase during a non-event. However, the atmospheric condition on non-event days is generally different from NPF event days; therefore, the calculated increase in CCN concentrations from NPF may be imprecise.

3 Results and discussion

3.1 Variability in particle number size distributions and number concentrations

Figure 3 shows the annual and seasonal median and 25th and 75th percentile values of particle number size distributions at all the sites. The thick line represents the median value, whereas the shaded area indicates particle number size distribution between 25th and 75th percentiles. The mountain sites (RNC, MUK, and MBL) all show similar mode diameters, with the lowest concentrations at RNC. Among the urban areas (HYD, TVM, and DEL), TVM has the largest mode diameter, which is frequently influenced by the influx of marine air masses containing high moisture and coarser sea salt aerosols (Fig. 3a; Babu et al., 2016). The peak number concentration of PNSDs is the highest in pre-monsoon (MAM) than in other seasons at the mountain background sites RNC and MUK (Fig. 3b–c), while it was similar in winter and pre-monsoon at MBL (Fig. 3d). These elevated concentrations are accompanied by a smaller mode diameter of the Aitken mode particles. The highest number concentration is attributed to the frequent occurrence of NPF in these locations in pre-monsoon (Sebastian et al., 2021b; Neitola et al., 2011). The contribution of newly formed particles to total particles is also visible in the 75th percentile PNSDs at these sites. The number size distributions of particles were significantly the lowest in monsoon and post-monsoon.

The median number size distribution of particles at HYD is the highest in pre-monsoon and post-monsoon (Fig. 3e). The highest particle number concentrations in pre-monsoon and post-monsoon can be attributed to the frequent occurrence of NPF in these seasons at the site. The influence of NPF is also noticeable in the 75th percentile PNSDs. The PNSD is consistently the lowest in monsoon, attributed to the wet scavenging of particles. The concentrations of Aitken and accumulation mode particles are the highest in winter compared to the other seasons. The mode diameter of PNSDs at TVM is comparatively similar in all seasons (Fig. 3f). At DEL, the mode diameter of PNSDs is the highest in winter compared to the other seasons (Fig. 3g). The shallow boundary layer height, stagnant atmospheric conditions, and high emission rates of aerosol precursors in winter (Kanawade et al., 2020b) allow particles to stay close to the surface and grow larger under high relative humidity and high condensable vapor concentrations. The median PNSD is consistently the lowest in monsoon at TVM due to extensive wet scavenging. The strong seasonality in PNSDs is similar to those reported earlier in India (Hooda et al., 2018; Komppula et al., 2009; Gani et al., 2020; Kanawade et al., 2014a). The uni- and bi-modal parameters of the particle number size distributions presented in Fig. 3 are tabulated in Table S1 in the Supplement.

Figure 4 shows the average observed PNSDs evolving over the day for each season, as a contour plot, at all the sites. For the mountain background sites RNC and MUK, the average seasonal contour plot indicates daytime NPF in pre-monsoon. However, winter, monsoon, and post-monsoon had the lowest concentrations of smaller particles that are not associated with NPF. For MBL, NPF occurred in winter, pre-monsoon, and post-monsoon. For all urban sites (HYD, TVM, and DEL), the average seasonal contour plot indicates the highest concentration of particles in the morning and evening peak traffic hours, in addition to daytime NPF. In Sect. 3.2, we have considered this high particle concentration from evening peak traffic while investigating the frequency of occurrence of NPF and its contribution to CCN concentrations.

Figure 5 shows the box–whisker plot of the seasonal number concentrations of Aitken, accumulation, and total particles at all the sites. The periods of study are different for all the sites, where direct comparison of particle number concentrations is not possible. The median Aitken mode particle number concentrations are the lowest at RNC (1.4×10^3 cm^{-3}) and the highest at DEL (7.1×10^3 cm^{-3}). The median accumulation mode particle number concentrations are the lowest at MUK (0.9×10^3 cm^{-3}) and the highest at DEL (2.4×10^3 cm^{-3}). The total particle number concentrations are the lowest at MUK (2.7×10^3 cm^{-3}) and the highest at DEL (12.5×10^3 cm^{-3}). The median particle number concentrations are about five-fold higher in urban locations (HYD, TVM, and DEL) than mountain sites (RNC, MUK, and MBL). Overall, the size-segregated particle number concentrations show strong seasonal spatial variability, with the lowest concentrations at the mountain sites and the highest at the urban sites. Further, the size-segregated particle number concentrations also show larger variability in each urban location than in the mountain sites. Next, we discuss the seasonality in the number concentration of Aitken, accumulation, and total particles in all locations to understand space- and time-varying heterogeneity in particle number concentrations.

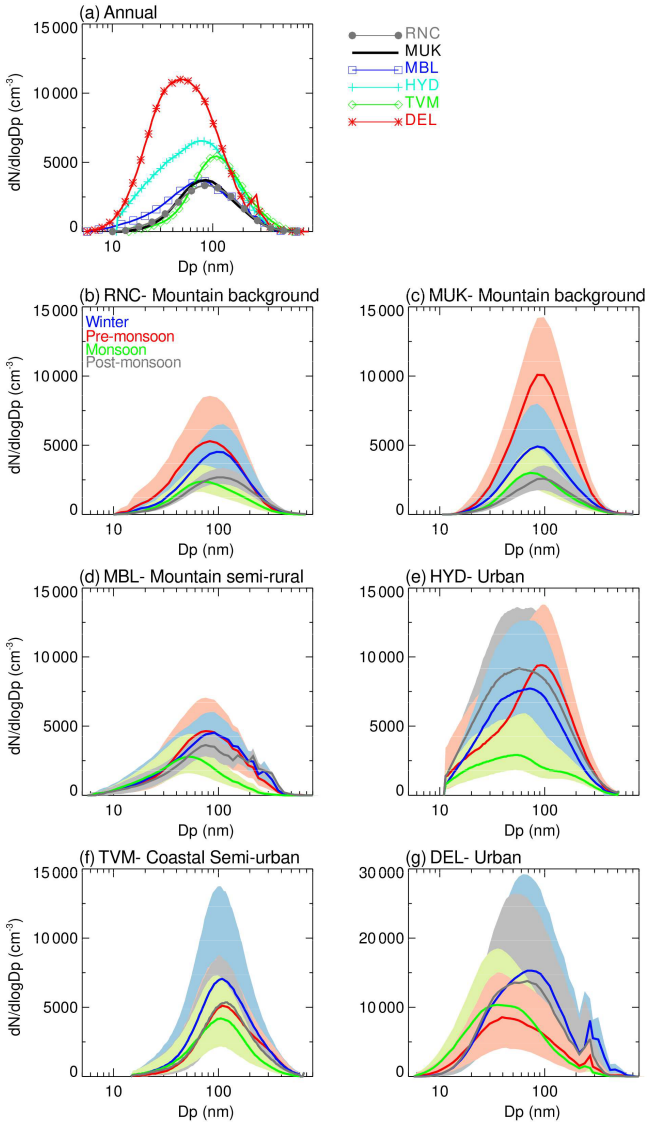

Figure 3. **(a)** Annual and **(b–g)** seasonal median particle number size distributions at all the sites. The solid line indicates the median, and the light-colored shading indicates 25th and 75th percentile distributions. The blue line and shading indicate winter (DJF), red line and shading indicate pre-monsoon (MAM), green line and shading indicate monsoon (JJAS), and gray line and shading indicate post-monsoon season (ON). Note that the *y* axis scale is different for the DEL site. Note that measurements are from different time periods for each site (see Table 1).

The relative occurrence of the number concentrations of size-segregated (Aitken and accumulation) particles was calculated to determine the maximum concentrations of a given particle mode in different seasons at all sites. The histograms of the relative occurrence of Aitken mode particle number concentrations at all the sites are presented in Fig. 6a–f. The mountain background sites RNC and MUK show a similar seasonality in number concentration histograms of Aitken mode particles, with the highest concentrations in the pre-monsoon season. The lowest concentrations are observed in monsoon and post-monsoon due to increased removal of particles by wet scavenging. MBL does not show notable seasonality in the number concentration histograms of Aitken mode particles. HYD, TVM, and DEL are urban environments but show different seasonality in the number concentration histograms of Aitken mode particles. DEL shows the highest Aitken mode particle number concentrations in winter and post-monsoon; TVM shows the highest concentrations in winter. In contrast, HYD shows comparable number concentrations in winter, pre-monsoon, and post-monsoon. The highest Aitken mode number concentrations in pre-monsoon at the mountain background sites are attributed to the high frequency of NPF occurrence in pre-monsoon (see Sect. 3.2.1). The highest Aitken mode number concentrations in winter at the urban sites can be explained by the high pre-existing particle concentration. DEL has the highest concentration of Aitken mode particles during winter owing to the anthropogenic sources and the stagnant atmospheric conditions during the season (Kanawade et al., 2020b). The difference in seasonality in the number concentration histograms of Aitken mode particles can be explained by the differences in the atmospheric conditions (e.g., prevailing synoptic air masses; mesoscale processes such as planetary boundary layer, PBL, dynamics; and particle removal processes) and considerable heterogeneity in aerosol composition (natural versus anthropogenic aerosol emission sources); DEL is representative of a sub-tropical climate, HYD is representative of a tropical climate, and TVM is representative of a tropical coastal climate.

Similar histograms of accumulation mode particles are presented in Fig. 7a–f. The seasonality in accumulation mode particles is slightly different as compared to Aitken mode particles at some sites. RNC shows similar number concentration histograms of accumulation mode particles in winter and pre-monsoon instead of dissimilar histograms for Aitken mode particles. The number concentration histograms of accumulation mode particles at MUK are similar to Aitken mode particles. MBL shows similar number concentration histograms in winter, pre-monsoon, and post-monsoon, with the lowest concentrations in monsoon due to wet scavenging. Among the urban sites, DEL shows the highest accumulation mode concentrations in post-monsoon and winter. TVM and HYD show the highest accumulation mode concentrations in winter and post-monsoon, respectively. The seasonality in total particles was also similar to Aitken mode particles, indicating that they constituted the most considerable fraction of total particles at all the sites (Fig. S2). However, it is difficult to separate a fraction of Aitken or accumulation mode particles that originated from NPF from that of the primary emissions, especially in urban areas where the primary emission rates of aerosols are very high (Thomas et al., 2019). The survival probability of newly formed particles to > 50–100 nm size depends on many factors such as the frequency

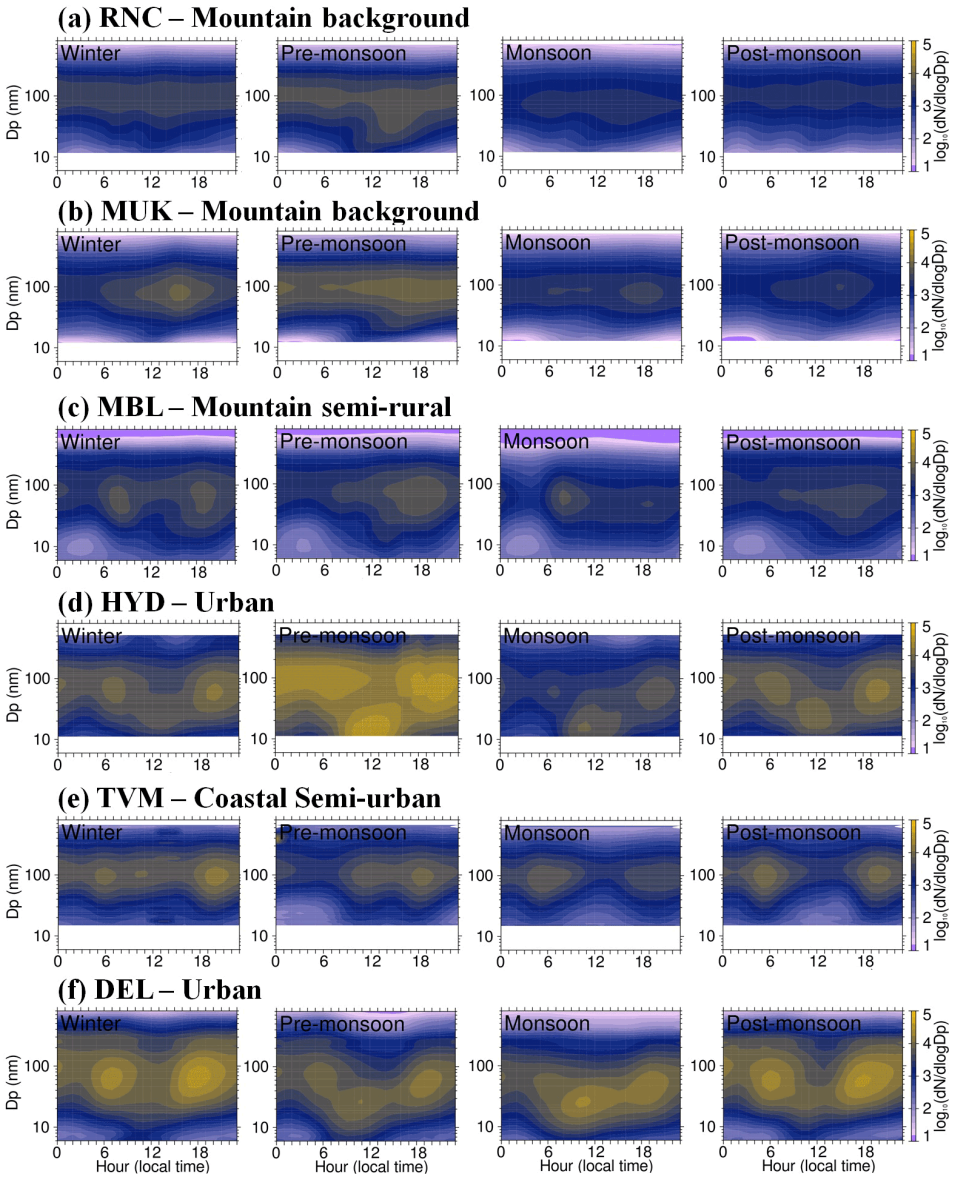

Figure 4. The diurnal–seasonal median particle number size distributions at all the sites: **(a)** Ranichauri, **(b)** Mukteshwar, **(c)** Mahabaleshwar, **(d)** Hyderabad, **(e)** Thiruvananthapuram, and **(f)** Delhi. Note that measurements are from different time periods for each site (see Table 1).

and intensity of the NPF occurrence, availability of condensable vapors, pre-existing particles, and atmospheric conditions. In Sect. 3.2.3, we estimate the absolute increase of CCN concentrations from NPF following the methodology given by Kerminen et al. (2012) and modified to calculate CCN concentrations for any given NPF event.

3.2 New particle formation and its contribution to CCN concentrations

3.2.1 NPF event characteristics

The frequency of occurrence of NPF events, the particle formation rate of nucleation mode particles (J_{SDS}), and the particle growth rate of nucleation mode particles ($GR_{SDS\text{-}25\,nm}$) are typically derived to quantify the NPF (Kerminen et al., 2018; Nieminen et al., 2018; Kulmala et al., 2004). These NPF characteristics are closely associated with aerosol precursor concentrations, pre-existing aerosol particles, and atmospheric conditions. As a result, the frequency of occurrence of NPF events varies from one location to another as well as seasonally. NPF is thought to occur frequently during the spring (pre-monsoon) and rarely during the winter (Kanawade et al., 2012; Dal Maso et al., 2005; Nieminen et al., 2018). However, NPF events were also observed frequently during thermal winter (Kulmala et al., 2004; Pikridas et al., 2012) and fall (September, October, and Novem-

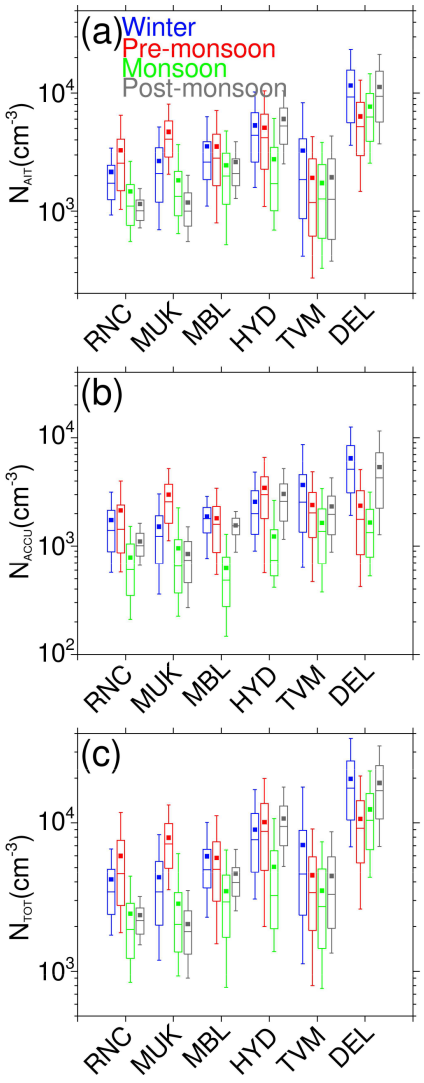

Figure 5. Box–whisker plot of seasonal number concentrations of **(a)** Aitken mode, **(b)** accumulation mode, and **(c)** total particles using the entire data. The blue, red, green, and gray colors indicate winter (DJF), pre-monsoon (MAM), monsoon (JJAS), and post-monsoon (ON) months. The solid square indicates the mean, horizontal line indicates the median, the top and bottom of the box indicate 25th and 75th percentile values, and the top and bottom whiskers indicate 10th and 90th percentile values. Note that measurements are from different time periods for each site (see Table 1).

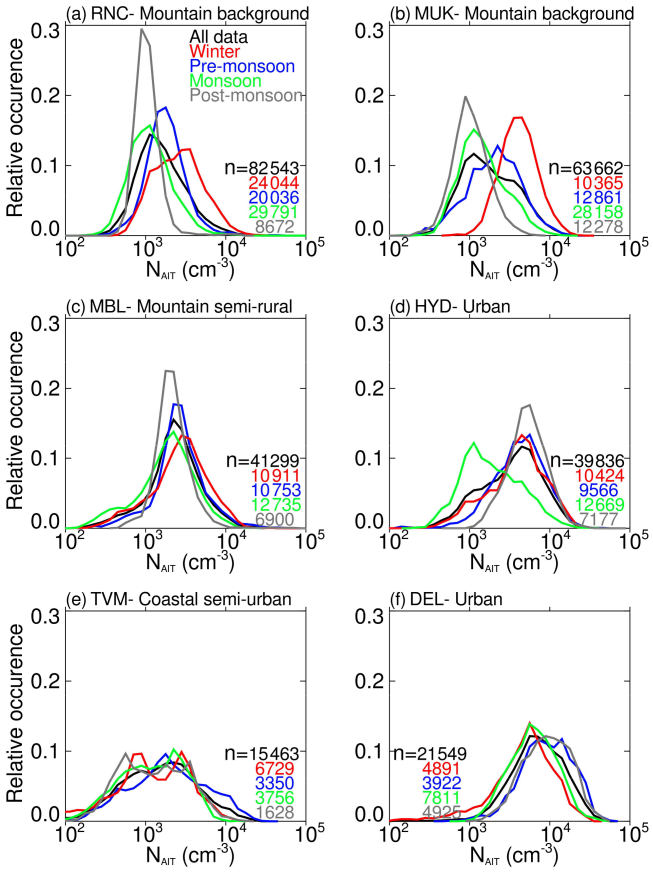

Figure 6. Histogram of the relative occurrence of Aitken mode particle number concentrations at the sites. The concentration bins are logarithmically spaced on the *x* axis, and the *y* axis shows the relative occurrence of values in each bin compared to the total number of valid observations. The black, blue, red, green, and gray lines indicate all data, winter (DJF), pre-monsoon (MAM), monsoon (JJAS), and post-monsoon (ON), respectively. *n* indicates the number of 10 min averaged valid data points. Note that measurements are from different time periods for each site (see Table 1).

ber; Rodríguez et al., 2005). These studies indicate that there is no universal pattern in the occurrence of NPF events. Figure 8 shows the percentage of NPF, non-event, and undefined event days based on valid observation days at all the sites. Out of a total of 586 valid observation days at RNC, NPF events occurred on 21 d (3.9 %), whereas 493 (83.7 %) were non-event days. Out of a total of 440 valid observation days at MUK, NPF events occurred on 13 d (2.9 %), whereas 321 (73.1 %) were non-event days. Out of a total of 281 valid observation days at MBL, NPF events occurred on 16 d (5.9 %), whereas 188 (66.1 %) were non-event days. Out of a total of 270 valid observation days at HYD, NPF events occurred on 38 d (16.3 %), whereas 124 (44.8 %) were non-event days. Out of a total of 133 valid observation days at TVM, NPF events occurred on 23 d (16.6 %), whereas 55 (41.4 %) were non-event days. Out of a total of 139 valid observation days at DEL, NPF events occurred on 39 d (28.1 %), whereas 30 (21.1 %) were non-event days. The frequencies of NPF occurrence at all six sites are tabulated in Table S2.

3.2.2 Particle formation rate and growth rate

Overall, the frequency of occurrence of NPF is the highest in pre-monsoon as compared to other seasons. There is also an exception to this, with the highest frequency of NPF occurrence in the late monsoon (September) at TVM. Babu et al. (2016) reported that NPF events over this site

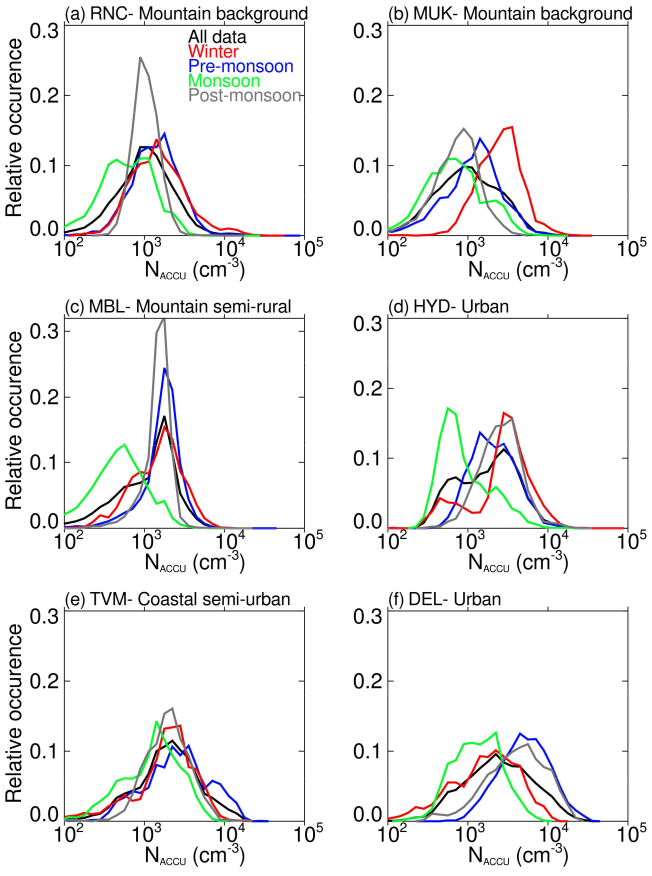

Figure 7. Histogram of the relative occurrence of accumulation mode particle number concentrations at the sites. The concentration bins are logarithmically spaced on the x axis, and the y axis shows the relative occurrence of values in each bin compared to the total number of valid observations. The black, blue, red, green, and gray lines indicate all data, winter (DJF), pre-monsoon (MAM), monsoon (JJAS), and post-monsoon (ON), respectively. n indicates the number of 10 min averaged valid data points. Note that measurements are from different time periods for each site (see Table 1).

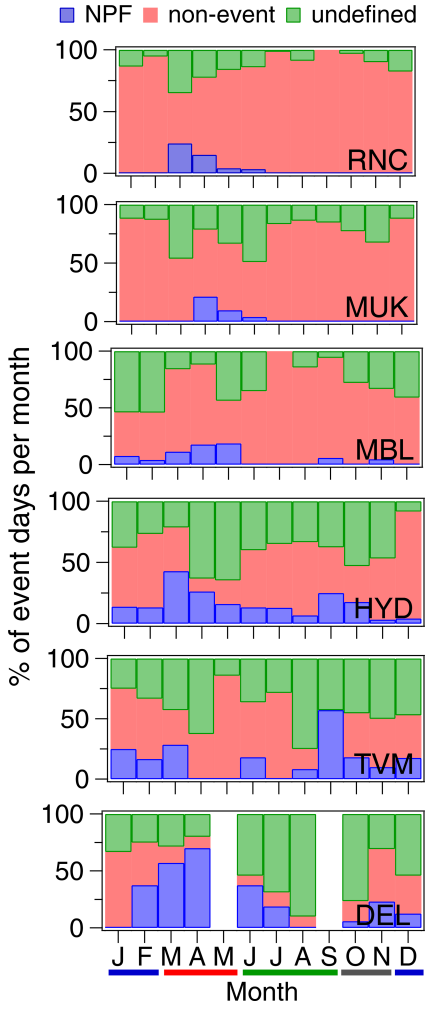

Figure 8. Monthly percentage of occurrence of NPF, non-event, and undefined events days based on total valid observations days at all the sites. The thick blue, red, green, and gray lines indicate winter, pre-monsoon, monsoon, and post-monsoon months. Note that measurements are from different time periods for each site (see Table 1).

occurred due to a mixing of contrasting air masses due to the combined effect of mesoscale land–sea breeze circulation and local ABL dynamics. Though prevailing air masses are oceanic, the wind speeds and total rainfall were lower during September than other monsoonal months. A cleaner synoptic air mass (i.e., lower background concentrations and condensation sink), combined with the occurrence of well-defined mesoscale land–sea breeze transitions and horizontal convergence of contrasting air masses during September, was responsible for the highest NPF frequency. Among the sites, the mountain background sites in the western Himalaya (RNC and MUK) have the lowest annual mean frequency of occurrence of NPF (3.9 % and 2.9 %, respectively), with the highest seasonal frequency of occurrence of NPF in pre-monsoon. Previous studies also showed the infrequent occurrence of NPF at RNC (Sebastian et al., 2021b) and MUK (Neitola et al., 2011), with the highest frequency in pre-monsoon. The highest NPF frequency in pre-monsoon was connected to the PBL lifting up to the measurement site elevation, which appeared to transport aerosol precursors from nearby polluted lower-altitude regions (Hooda et al., 2018; Raatikainen et al., 2014). However, NPF occurred frequently (39 %) at the Nepal Climate Observatory-Pyramid (NCO-P) site in the eastern Himalaya (Venzac et al., 2008). A recent study also observed a very high NPF frequency (69 %) at NCO-P from November to December when cleaner conditions prevailed, with little transportation from the polluted lower-altitude regions (Bianchi et al., 2021). They showed that up-valley winds bring gaseous aerosol precursors to higher altitudes. These precursors are oxidized into compounds of very low volatility and are subsequently converted

into new particles during their transport to the site. The above discussion indicates that the RNC and MUK mountain background sites in the western Himalayas are strikingly different from the NCO-P site in the eastern Himalayas (Bianchi et al., 2021). The annual NPF frequency at RNC and MUK is lower than MBL and the high-altitude sites in Europe (Nieminen et al., 2018). DEL has the highest frequency of occurrence of NPF events in pre-monsoon (63.8 %), followed by HYD (28.4 %) and MBL (15.9 %). The TVM coastal semi-urban site witnesses frequent NPF events under the influence of continental air masses. As the air masses change from continental to mixed or marine origin, the NPF event frequency decreases (Babu et al., 2016). NPF was also observed commonly at other urban sites in India (Kanpur and Pune) under a high source of aerosol precursors when pre-existing particle concentrations reduced sufficiently due to dilution (Kanawade et al., 2020a; Kanawade et al., 2014b). While the severe air pollution episode in Delhi in November 2016 suppressed NPF, co-condensation of vapors of anthropogenic origin along with water onto primary particles assisted rapid particle growth (1.6 to 30.3 nm h^{-1}; Kanawade et al., 2020b). The emission of precursor compounds from traffic and other sources in Beijing, China, also contributed significantly to molecular cluster formation, particle growth, and secondary aerosol mass formation, leading to haze formation under favorable meteorological conditions (Kulmala et al., 2021). In Europe, atmospheric conditions (such as the solar radiation and relative humidity) appear to dictate NPF occurrence at rural sites, whereas the increased concentrations of precursor gases are more important for the occurrence of NPF in urban areas (Bousiotis et al., 2021). This explains why NPF occurs more frequently in urban areas than rural, remote or high-altitude locations (Guo et al., 2020; Nieminen et al., 2018; Sellegri et al., 2019). This also indicates that the balance between the precursor concentration and pre-existing particles plays a vital role in the NPF occurrence. Owing to large spatial heterogeneity in aerosol precursor emissions and background aerosol concentrations in India, the chemical species contributing to aerosol nucleation and growth have not been identified (Kanawade et al., 2021).

Figure 9 shows a scatter plot of the J_{SDS} and the $GR_{SDS\text{-}25\,nm}$ as a function of the condensation sink at each site. A fairly good correlation between J_{SDS} and $GR_{SDS\text{-}25\,nm}$ at each site (Pearson correlation coefficient of 0.48, 0.78, 0.85, 0.33, 0.68, and 0.18 at RNC, MUK, MBL, HYD, TVM, and DEL, respectively) indicates that J_{SDS} and $GR_{SDS\text{-}25\,nm}$ are strongly coupled. The large scatter in data points is a result of important factors influencing the NPF, such as nucleation mechanisms (Dunne et al., 2016), the availability of other condensable vapors that are needed to stabilize molecular clusters containing sulfuric acid (Kirkby et al., 2011; Schobesberger et al., 2015), and atmospheric conditions (Bousiotis et al., 2021). A recent study showed that amines stabilize the nucleating cluster while organics contribute to higher concentrations of condensable vapors, particularly in

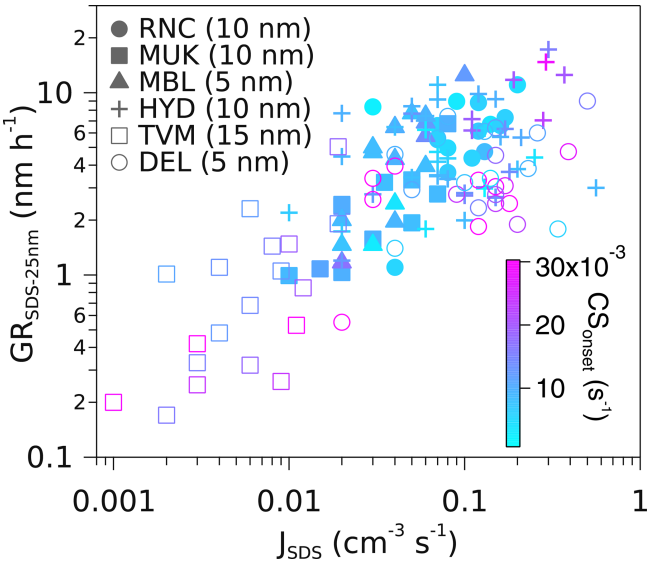

Figure 9. Scatter plot of the particle formation rate and the growth rate as a function of the condensation sink at each site. The condensation sink at the start of the event (CS_{onset}) is taken as a 1 h average CS just before the start of the NPF event. The smallest detectable size (SDS) of the nucleation mode at each site is shown in the bracket. Note that measurements are from different time periods for each site (see Table 1).

urban areas (Xiao et al., 2021). The mean particle formation rates and growth rates for all six sites are tabulated in Table S2. Considering all the sites, $GR_{SDS\text{-}25\,nm}$ during NPF events varied from 0.2 to 17.2 nm h^{-1}. Overall, J_{SDS} and $GR_{SDS\text{-}25\,nm}$ are within the observed large range of values in diverse environments in India and elsewhere (Nieminen et al., 2018; Kerminen et al., 2018; Kulmala et al., 2004). Expectedly, the mean condensation sink at the start of the NPF event is higher at the urban sites than the mountain sites. The mean condensation sink at the urban sites (16.1×10^{-3} s^{-1}) was twice that of the mountain sites (7.9×10^{-3} s^{-1}). A previous study also showed that the higher pre-existing particles at Kanpur than at Pune suppressed the particle formation rate but favored particle growth under high concentrations of condensable vapors (Kanawade et al., 2014b).

3.2.3 Increase in CCN concentrations during NPF events

To reach climatologically relevant sizes, the newly formed particles must grow by condensation while avoiding coagulation removal by pre-existing particles because these freshly formed particles are small and highly diffusive (Vehkamäki and Riipinen, 2012). Based on the observed range of particle growth rates at all the sites (0.2 to 17.3 nm h^{-1}), newly formed particles may take from a few hours to 1–2 d to grow to CCN active sizes (> 50–100 nm). Over such timescales, it is observationally challenging to separate CCN originating

from NPF from those emanating from the growth of small primary particles and direct emissions of CCN active sized particles. The increase in CCN concentrations during any given NPF event was estimated following the methodology developed by Kerminen et al. (2012), which we modified to remove CCN originating from the growth of small primary particles and direct emissions of CCN active sized particles based on non-event days.

Figure 10 shows the box–whisker plot of the absolute increase in CCN concentrations (50 and 100 nm) at all the sites. Considering all NPF events at mountain sites, the increase in CCN_{50} ranged from 0.168×10^3 cm^{-3} to 5.2×10^3 cm^{-3} per event, with a median value of 2.7×10^3 cm^{-3} per event, whereas the increase in CCN_{100} ranged from 0.02×10^3 to 1.9×10^3 cm^{-3} per event, with a median value of 1.0×10^3 cm^{-3} per event. The increases in CCN_{50} and CCN_{100} are about two-fold lower than the free tropospheric site, Chacaltaya (5240 m a.m.s.l., Bolivia), for NPF events that started in the boundary layer (5.1×10^3 and 1.5×10^3 cm^{-3} per event for 50 and 100 nm, respectively; Rose et al., 2017). The median increase in CCN_{50} and CCN_{100}, respectively, at RNC (2.3×10^3 and 0.9×10^3 cm^{-3} per event) and MUK (2.9×10^3 and 0.9×10^3 cm^{-3} per event) are comparable to those reported at Botsalano (2.5×10^3 and 0.8×10^3 cm^{-3} per event; 1420 m a.m.s.l., South Africa), but about three-fold higher than those reported at a remote continental site in Finland (1.0×10^3 and 0.2×10^3 cm^{-3} per event; Kerminen et al., 2012). Considering all NPF events at the urban sites, the CCN_{50} increase ranged from 0.08×10^3 to 9.4×10^3 cm^{-3} per event, with a median value of 4.3×10^3 cm^{-3} per event, whereas CCN_{100} increase ranged from 0.03×10^3 to 4.9×10^3 cm^{-3} per event, with a median value of 1.2×10^3 cm^{-3} per event. These values are about two-fold lower compared to values reported at the station of San Pietro Capofiume, in a polluted region of the Po Valley; 7.3×10^3 and 2.4×10^3 cm^{-3} per event, respectively, for 50 and 100 nm (Laaksonen et al., 2005). High background number concentrations of CCN_{50} and CCN_{100} in Delhi resulted in a smaller relative increase of CCN from NPF during the post-monsoon and winter seasons when compared to the other sites. In order to comprehensively investigate the atmospheric CCN budget and the contribution of NPF to it, Kerminen et al. (2012) pointed out that the analysis should include not only NPF events but also non-event days. Therefore, the modified methodology applied here following Kerminen et al. (2012) provides the best representative of the increase in CCN concentrations for an NPF event.

The sites with low pre-existing particle concentrations (hence, low condensation sink values), high solar radiation, and cooler temperatures at high altitudes (or in the free tropospheric; RNC, MUK, and MBL) should favor NPF with enhanced frequency as compared to near-surface urban environments (HYD, TVM, and DEL) wherein pre-existing particles concentration are high, leading to faster removal of nucleating vapors. However, NPF in polluted environments occurs more often than expected, with enhanced growth rates (Yu et al., 2017). Guo et al. (2014) also reported that NPF leads to winter-time haze formation in Beijing. Kulmala et al. (2021) recently showed that > 65 % of the number concentration of haze particles resulted from NPF in Beijing. The observation sites at altitudes higher than 1000 m a.m.s.l. also favored NPF at the high condensation sinks, and linked precursor gases needed to initiate nucleation and early growth (Sellegri et al., 2019). Therefore, the low condensation sinks are not necessarily required to trigger nucleation and early growth, provided there are high vapor production rates. The high pre-existing particle concentration is also an indication of precursor-laden air. However, when the condensation sink gets very high, it inhibits aerosol nucleation. Further, at Hyderabad, about half of the NPF events did not display aerosol nucleation (sub-3 nm particle formation) with subsequent growth of these particles to larger sizes (> 10 nm), perhaps due to lower organic vapor concentrations (Sebastian et al., 2021a). Rose et al. (2017) also reported a higher frequency of NPF occurrence for boundary layer (48 %) than for free troposphere (39 %) conditions at the Chacaltaya mountain (5240 m a.m.s.l.), Bolivia. Thus potential CCN formation was higher for NPF events initiated in the boundary layer (67 %) than in the free troposphere (53 %). Sellegri et al. (2019) reviewed the CCN concentrations from NPF events in the boundary layer and high-altitude locations. They revealed that the CCN production

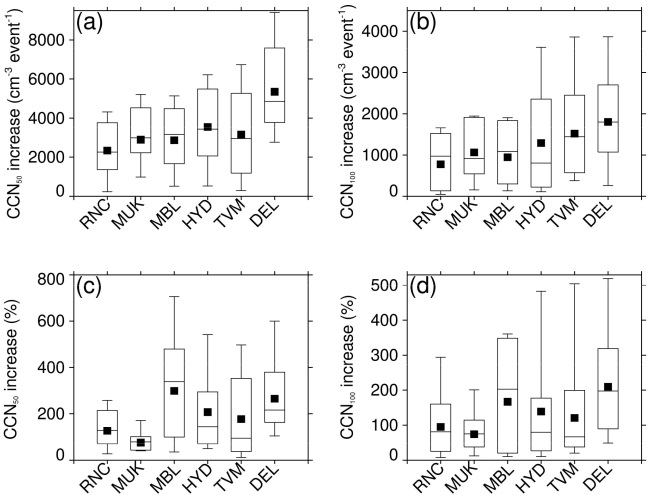

Figure 10. Box–whisker plot of absolute increase in CCN concentrations for **(a)** 50 and **(b)** 100 nm particles and percentage increase in CCN concentrations for **(c)** 50 and **(d)** 100 nm at all the sites based on observed NPF and non-event days. The solid square indicates the mean, the horizontal line indicates the median, the top and bottom of the box indicate 25th and 75th percentile values, and the top and bottom whiskers indicate 10th and 90th percentile values. Note that measurements are from different time periods for each site (see Table 1).

is the highest at San Pietro Capofiume, a polluted region of the Po Valley ($7.3 \times 10^3\,cm^{-3}$; Laaksonen et al., 2005) as compared to high-altitude sites (Rose et al., 2017; Kerminen et al., 2012). Our findings are similar to these studies, showing higher increases in CCN concentrations in urban locations (HYD, TVM, and DEL) compared to mountain locations (RNC, MUK, and MBL) in India. It is not possible to track nucleated particles until they become CCN, and they are always mixed with CCN originating from primary sources. This makes it extremely difficult to estimate CCN arising from a given NPF event. In light of the above discussion, these results offer some insights into potential CCN concentrations originating from NPF.

4 Conclusions

In this study, we used at least 1 year of asynchronous particle number size distribution measurements from six locations in India, consisting of mountain background sites (Ranichauri and Mukteshwar), a mountain semi-rural site (Mahabaleshwar), urban sites (Delhi and Hyderabad), and a semi-urban coastal site (Thiruvananthapuram). The results from this study provide some insights into the processes influencing particle number size distributions and CCN concentrations in different environments (mountain and urban) of India.

We found that the regional NPF was most common in the pre-monsoon (spring) at all the measurement sites, with an exception at TVM, where NPF occurred mostly in the late monsoon season (September), which was linked to the inflow of continental air masses that provided a source of low volatile vapors for nucleation. During pre-monsoon, DEL has the highest frequency of NPF occurrence (63.8 %), followed by HYD (28.4 %) and MBL (15.9 %). NPF was the least common during winter at all the sites, particularly at the mountain background sites (RNC and MUK), which were without a single NPF event. The high solar insolation (active photochemistry) and the elevated boundary layer (efficient ventilation leading to low pre-existing particles near the surface) explain the most frequent occurrence of NPF in the pre-monsoon (spring), but this is not a universal NPF frequency pattern in India or elsewhere globally. We found that J_{SDS} during NPF events tends to increase with increasing anthropogenic influence, and is 1 order of magnitude higher in urban areas ($0.12\,cm^{-3}\,s^{-1}$) than mountain sites ($0.06\,cm^{-3}\,s^{-1}$). We did not find any systematic pattern in $GR_{SDS\text{-}25\,nm}$, with the highest $GR_{SDS\text{-}25\,nm}$ at RNC ($6.3\,nm\,h^{-1}$) and the lowest at TVM ($1.1\,nm\,h^{-1}$). The observed values of the NPF frequency, J_{SDS}, and $GR_{SDS\text{-}25\,nm}$ indicate that regional NPF events can significantly influence the evolution of particles in the atmosphere. We found that NPF modulates the shape of the particle number size distributions significantly, especially at the mountain background sites (RNC and MUK), which are not directly influenced by the local direct emissions of aerosols (traffic and industry). The number size distribution of particles is higher in pre-monsoon at mountain background sites, whereas it is higher in winter at the urban sites, with the exception of HYD. All sites generally show lower concentrations of particles in monsoon due to increased removal by wet scavenging. The histograms of size-segregated particle number concentrations show large variability from one site to another, reflecting the varying contribution of different processes to the total aerosol loading. For instance, the Aitken mode particle concentrations were the highest in pre-monsoon at the mountain background sites (RNC and MUK), whereas they were the highest in winter at the urban sites (HYD, TVM, and DEL). Among the sites, the lowest measured median total particle number concentration was found at MUK ($2.7 \times 10^3\,cm^{-3}$) and the highest at DEL ($12.5 \times 10^3\,cm^{-3}$).

We found that the increase in CCN concentrations during an NPF event is higher in urban locations (4.3×10^3 and $1.2 \times 10^3\,cm^{-3}$ per event for 50 and 100 nm, respectively) compared to mountain background sites (2.7×10^3 and $1.0 \times 10^3\,cm^{-3}$ per event for 50 and 100 nm, respectively). We modified Kerminen and colleagues' approach for removing the potential contribution of primary CCN active particles to give the best possible estimate for the increase in CCN concentrations during a given NPF event. Such analyses should be supplemented by regional model simulations or high spatial resolution measurements of NPF and CCN concentrations.

Code availability. Particle number size distributions data were analyzed in IGOR Pro 8.0. Figure 8 was created in IGOR Pro 8.0, while all other figures were created in IDL 8.0.

Data availability. Particles data will be made available upon a reasonable request to the corresponding author.

Supplement. The supplement related to this article is available online at: https://doi.org/10.5194/acp-22-4491-2022-supplement.

Author contributions. VPK conceived the idea and designed the research. MS and VPK carried out comprehensive data analysis. MS carried out CCN estimation analysis and interpretation with critical input from JRP, VV, and VPK. MS, SKK, VAK, and SJ performed particle size distribution measurements and analysis. MS and VPK wrote the first draft, and MS edited it with critical input from all co-authors.

Competing interests. The contact author has declared that neither they nor their co-authors have any competing interests.

Disclaimer. Publisher's note: Copernicus Publications remains neutral with regard to jurisdictional claims in published maps and institutional affiliations.

Acknowledgements. Vijay P. Kanawade was supported by the Department of Science & Technology (DST)-Science Engineering Research Board (SERB; ECR/2016/001333) and DST-Climate Change Division Program (Aerosol/89/2017). Vijay K. Soni acknowledges the technical support from Sanjay Rawat for maintaining the climate monitoring station at Ranichauri. IITM and HACPL are fully funded by the Ministry of Earth Sciences (MoES), Govt. of India. The data collection at Thiruvananthapuram was carried out under the Aerosol Radiative Forcing over India (ARFI) project of the Indian Space Research Organisation-Geosphere Biosphere Program (ISRO-GBP). Rakesh K. Hooda, Ville Vakkari, Eija Asmi, and Antti-P. Hyvärinen acknowledge Academy of Finland Flagship funding (grant no. 337552). Rakesh K. Hooda and Antti-P. Hyvärinen also acknowledge the team of TERI, Mukteshwar and Ved P. Sharma for technical support. Jeffrey R. Pierce was supported by the Atmospheric System Research program, part of the US Department of Energy's Office of Biological and Environmental Research within the Office of Science, under grant DE-SC0019000.

Financial support. This research has been supported by the Department of Science & Technology (DST)-Science Engineering Research Board (grant no. ECR/2016/001333).

Review statement. This paper was edited by Tuukka Petäjä and reviewed by two anonymous referees.

References

Anil Kumar, V., Hazra, A., Pandithurai, G., Kulkarni, G., Mohan, G. M., Mukherjee, S., Kumar, A. V., Hazra, A., Pandithurai, G., Kulkarni, G., Mohan, G. M., Mukherjee, S., Leena, P. P., Patil, R. D., and Prasad, D. S. V. V. D.: Atmospheric ice nucleating particle measurements and parameterization representative for Indian region, Atmos. Res., 253, 105487, https://doi.org/10.1016/j.atmosres.2021.105487, 2021.

Babu, S. S., Kompalli, S. K., and Moorthy, K. K.: Aerosol number size distributions over a coastal semi urban location: Seasonal changes and ultrafine particle bursts, Sci. Total Environ., 563–564, 351–365, https://doi.org/10.1016/j.scitotenv.2016.03.246, 2016.

Bianchi, F., Junninen, H., Bigi, A., Sinclair, V. A., Dada, L., Hoyle, C. R., Zha, Q., Yao, L., Ahonen, L. R., Bonasoni, P., Buenrostro Mazon, S., Hutterli, M., Laj, P., Lehtipalo, K., Kangasluoma, J., Kerminen, V. M., Kontkanen, J., Marinoni, A., Mirme, S., Molteni, U., Petäjä, T., Riva, M., Rose, C., Sellegri, K., Yan, C., Worsnop, D. R., Kulmala, M., Baltensperger, U., and Dommen, J.: Biogenic particles formed in the Himalaya as an important source of free tropospheric aerosols, Nat. Geosci., 14, 4–9, https://doi.org/10.1038/s41561-020-00661-5, 2021.

Bousiotis, D., Brean, J., Pope, F. D., Dall'Osto, M., Querol, X., Alastuey, A., Perez, N., Petäjä, T., Massling, A., Nøjgaard, J. K., Nordstrøm, C., Kouvarakis, G., Vratolis, S., Eleftheriadis, K., Niemi, J. V., Portin, H., Wiedensohler, A., Weinhold, K., Merkel, M., Tuch, T., and Harrison, R. M.: The effect of meteorological conditions and atmospheric composition in the occurrence and development of new particle formation (NPF) events in Europe, Atmos. Chem. Phys., 21, 3345–3370, https://doi.org/10.5194/acp-21-3345-2021, 2021.

Census of India: Provisional population totals: rural-urban distribution, Vol. 2, Issue 1 of Census of India, 2011, India, India: Office of the Registrar General & Census Commissioner, 2011.

Dal Maso, M., Kulmala, M., Riipinen, I., Wagner, R., Hussein, T., Aalto, P. P., and Lehtinen, K. E. J.: Formation and growth of fresh atmospheric aerosols: eight years of aerosol size distribution data from SMEAR II, Hyytiälä, Finland, Boreal Environ. Res., 10, 323–336, 2005.

Draxler, R. R. and Draxler, G. D.: HYSPLIT – HYbrid Single-Particle Lagrangian Integrated Trajectory Model, http://ready.arl.noaa.gov/HYSPLIT.php (last access: January 2022), 2010.

Dunne, E. M., Gordon, H., Kürten, A., Almeida, J., Duplissy, J., Williamson, C., Ortega, I. K., Pringle, K. J., Adamov, A., Baltensperger, U., Barmet, P., Benduhn, F., Bianchi, F., Breitenlechner, M., Clarke, A., Curtius, J., Dommen, J., Donahue, N. M., Ehrhart, S., Flagan, R. C., Franchin, A., Guida, R., Hakala, J., Hansel, A., Heinritzi, M., Jokinen, T., Kangasluoma, J., Kirkby, J., Kulmala, M., Kupc, A., Lawler, M. J., Lehtipalo, K., Makhmutov, V., Mann, G., Mathot, S., Merikanto, J., Miettinen, P., Nenes, A., Onnela, A., Rap, A., Reddington, C. L. S., Riccobono, F., Richards, N. A. D., Rissanen, M. P., Rondo, L., Sarnela, N., Schobesberger, S., Sengupta, K., Simon, M., Sipilä, M., Smith, J. N., Stozkhov, Y., Tomé, A., Tröstl, J., Wagner, P. E., Wimmer, D., Winkler, P. M., Worsnop, D. R., and Carslaw, K. S.: Global atmospheric particle formation from CERN CLOUD measurements, Science, 354, 1119–1124, https://doi.org/10.1126/science.aaf2649, 2016.

Gani, S., Bhandari, S., Patel, K., Seraj, S., Soni, P., Arub, Z., Habib, G., Hildebrandt Ruiz, L., and Apte, J. S.: Particle number concentrations and size distribution in a polluted megacity: the Delhi Aerosol Supersite study, Atmos. Chem. Phys., 20, 8533–8549, https://doi.org/10.5194/acp-20-8533-2020, 2020.

Gordon, H., Kirkby, J., Baltensperger, U., Bianchi, F., Breitenlechner, M., Curtius, J., Dias, A., Dommen, J., Donahue, N. M., Dunne, E. M., Duplissy, J., Ehrhart, S., Flagan, R. C., Frege, C., Fuchs, C., Hansel, A., Hoyle, C. R., Kulmala, M., Kürten, A., Lehtipalo, K., Makhmutov, V., Molteni, U., Rissanen, M. P., Stozkhov, Y., Tröstl, J., Tsagkogeorgas, G., Wagner, R., Williamson, C., Wimmer, D., Winkler, P. M., Yan, C., and Carslaw, K. S.: Causes and importance of new particle formation in the present-day and preindustrial atmospheres, J. Geophys. Res.-Atmos., 122, 8739–8760, https://doi.org/10.1002/2017jd026844, 2017.

Grimm, H. and Eatough, D. J.: Aerosol Measurement: The Use of Optical Light Scattering for the Determination of Particulate Size Distribution, and Particulate Mass, Including the Semi-Volatile Fraction, J. Air Waste Manage., 59, 101–107, https://doi.org/10.3155/1047-3289.59.1.101, 2009.

Guo, S., Hu, M., Zamora, M. L., Peng, J., Shang, D., Zheng, J., Du, Z., Wu, Z., Shao, M., Zeng, L., Molina, M. J., and Zhang, R.: Elucidating severe urban haze formation

in China, P. Natl. Acad. Sci. USA, 111, 17373–17378, https://doi.org/10.1073/pnas.1419604111, 2014.

Guo, S., Hu, M., Peng, J., Wu, Z., Zamora, M. L., Shang, D., Du, Z., Zheng, J., Fang, X., Tang, R., Wu, Y., Zeng, L., Shuai, S., Zhang, W., Wang, Y., Ji, Y., Li, Y., Zhang, A. L., Wang, W., Zhang, F., Zhao, J., Gong, X., Wang, C., Molina, M. J., and Zhang, R.: Remarkable nucleation and growth of ultrafine particles from vehicular exhaust, P. Natl. Acad. Sci. USA, 117, 3427–3432, https://doi.org/10.1073/pnas.1916366117, 2020.

Hooda, R. K., Kivekäs, N., O'Connor, E. J., Collaud Coen, M., Pietikäinen, J.-P., Vakkari, V., Backman, J., Henriksson, S. V., Asmi, E., Komppula, M., Korhonen, H., Hyvärinen, A.-P., and Lihavainen, H.: Driving Factors of Aerosol Properties Over the Foothills of Central Himalayas Based on 8.5 Years Continuous Measurements, J. Geophys. Res.-Atmos., 123, 13421–413442, https://doi.org/10.1029/2018jd029744, 2018.

Hyvärinen, A. P., Lihavainen, H., Komppula, M., Sharma, V. P., Kerminen, V. M., Panwar, T. S., and Viisanen, Y.: Continuous measurements of optical properties of atmospheric aerosols in Mukteshwar, northern India, J. Geophys. Res.-Atmos., 114, D08207, https://doi.org/10.1029/2008JD011489, 2009.

Hyvärinen, A.-P., Lihavainen, H., Komppula, M., Panwar, T. S., Sharma, V. P., Hooda, R. K., and Viisanen, Y.: Aerosol measurements at the Gual Pahari EUCAARI station: preliminary results from in-situ measurements, Atmos. Chem. Phys., 10, 7241–7252, https://doi.org/10.5194/acp-10-7241-2010, 2010.

IPCC: Climate Change 2013: The Physical Science Basis. Contribution of Working Group I to the Fifth Assessment Report of the Intergovernmental Panel on Climate Change, Cambridge, United Kingdom and New York, NY, USA, 1535 pp., 2013.

Jose, S., Mishra, A. K., Lodhi, N. K., Sharma, S. K., and Singh, S.: Characteristics of Aerosol Size Distributions and New Particle Formation Events at Delhi: An Urban Location in the Indo-Gangetic Plains, Front. Earth Sci., 9, 750111, https://doi.org/10.3389/feart.2021.750111, 2021.

Kalivitis, N., Kerminen, V.-M., Kouvarakis, G., Stavroulas, I., Bougiatioti, A., Nenes, A., Manninen, H. E., Petäjä, T., Kulmala, M., and Mihalopoulos, N.: Atmospheric new particle formation as a source of CCN in the eastern Mediterranean marine boundary layer, Atmos. Chem. Phys., 15, 9203–9215, https://doi.org/10.5194/acp-15-9203-2015, 2015.

Kanawade, V. P., Benson, D. R., and Lee, S.-H.: Statistical analysis of 4-year observations of aerosol sizes in a semi-rural continental environment, Atmos. Environ., 59, 30–38, https://doi.org/10.1016/j.atmosenv.2012.05.047, 2012.

Kanawade, V. P., Tripathi, S. N., Bhattu, D., and Shamjad, P. M.: Sub-micron particle number size distributions characteristics at an urban location, Kanpur, in the Indo-Gangetic Plain, Atmos. Res., 147–148, 121–132, https://doi.org/10.1016/j.atmosres.2014.05.010, 2014a.

Kanawade, V. P., Tripathi, S. N., Siingh, D., Gautam, A. S., Srivastava, A. K., Kamra, A. K., Soni, V. K., and Sethi, V.: Observations of new particle formation at two distinct Indian subcontinental urban locations, Atmos. Environ., 96, 370–379, https://doi.org/10.1016/j.atmosenv.2014.08.001, 2014b.

Kanawade, V. P., Shika, S., Pöhlker, C., Rose, D., Suman, M. N. S., Gadhavi, H., Kumar, A., Nagendra, S. M. S., Ravikrishna, R., Yu, H., Sahu, L. K., Jayaraman, A., Andreae, M. O., Pöschl, U., and Gunthe, S. S.: Infrequent occurrence of new particle formation at a semi-rural location, Gadanki, in tropical Southern India, Atmos. Environ., 94, 264–273, https://doi.org/10.1016/j.atmosenv.2014.05.046, 2014c.

Kanawade, V. P., Tripathi, S. N., Chakraborty, A., and Yu, H.: Chemical Characterization of Sub-micron Aerosols during New Particle Formation in an Urban Atmosphere, Aerosol Air Qual. Res., 20, 1294–1305, https://doi.org/10.4209/aaqr.2019.04.0196, 2020a.

Kanawade, V. P., Srivastava, A. K., Ram, K., Asmi, E., Vakkari, V., Soni, V. K., Varaprasad, V., and Sarangi, C.: What caused severe air pollution episode of November 2016 in New Delhi?, Atmos. Environ., 222, 117125, https://doi.org/10.1016/j.atmosenv.2019.117125, 2020b.

Kanawade, V. P., Sebastian, M., Hooda, R. K., and Hyvärinen, A. P.: Atmospheric new particle formation in India: Current understanding, knowledge gaps and future directions, Atmos. Environ., 270, 118894, https://doi.org/10.1016/j.atmosenv.2021.118894, 2021.

Kerminen, V.-M., Paramonov, M., Anttila, T., Riipinen, I., Fountoukis, C., Korhonen, H., Asmi, E., Laakso, L., Lihavainen, H., Swietlicki, E., Svenningsson, B., Asmi, A., Pandis, S. N., Kulmala, M., and Petäjä, T.: Cloud condensation nuclei production associated with atmospheric nucleation: a synthesis based on existing literature and new results, Atmos. Chem. Phys., 12, 12037–12059, https://doi.org/10.5194/acp-12-12037-2012, 2012.

Kerminen, V.-M., Chen, X., Vakkari, V., Petäjä, T., Kulmala, M., and Bianchi, F.: Atmospheric new particle formation and growth: review of field observations, Environ. Res. Lett., 13, 103003, https://doi.org/10.1088/1748-9326/aadf3c, 2018.

Kirkby, J., Curtius, J., Almeida, J., Dunne, E., Duplissy, J., Ehrhart, S., Franchin, A., Gagne, S., Ickes, L., Kurten, A., Kupc, A., Metzger, A., Riccobono, F., Rondo, L., Schobesberger, S., Tsagkogeorgas, G., Wimmer, D., Amorim, A., Bianchi, F., Breitenlechner, M., David, A., Dommen, J., Downard, A., Ehn, M., Flagan, R. C., Haider, S., Hansel, A., Hauser, D., Jud, W., Junninen, H., Kreissl, F., Kvashin, A., Laaksonen, A., Lehtipalo, K., Lima, J., Lovejoy, E. R., Makhmutov, V., Mathot, S., Mikkila, J., Minginette, P., Mogo, S., Nieminen, T., Onnela, A., Pereira, P., Petaja, T., Schnitzhofer, R., Seinfeld, J. H., Sipila, M., Stozhkov, Y., Stratmann, F., Tome, A., Vanhanen, J., Viisanen, Y., Vrtala, A., Wagner, P. E., Walther, H., Weingartner, E., Wex, H., Winkler, P. M., Carslaw, K. S., Worsnop, D. R., Baltensperger, U., and Kulmala, M.: Role of sulphuric acid, ammonia and galactic cosmic rays in atmospheric aerosol nucleation, Nature, 476, 429–433, 2011.

Kompalli, S. K., Babu, S. S., Udayasoorian, C., and Jayabalakrishnan, R. M.: Role of anthropogenic emissions and meteorology on ultrafine particle bursts over a high altitude site in Western Ghats during pre-monsoon, J. Atmos. Sol.-Terr. Phys., 179, 378–388, https://doi.org/10.1016/j.jastp.2018.09.001, 2018.

Kompalli, S. K., Nair, V. S., Jayachandran, V., Gogoi, M. M., and Babu, S. S.: Particle number size distributions and new particle formation events over the northern Indian Ocean during continental outflow, Atmos. Environ., 238, 117719, https://doi.org/10.1016/j.atmosenv.2020.117719, 2020.

Komppula, M., Lihavainen, H., Hyvärinen, A. P., Kerminen, V.-M., Panwar, T. S., Sharma, V. P., and Viisanen, Y.: Physical properties of aerosol particles at a Himalayan background site in India, J. Geophys. Res.-Atmos., 114, D12202, https://doi.org/10.1029/2008jd011007, 2009.

Kuang, C., McMurry, P. H., and McCormick, A. V.: Determination of cloud condensation nuclei production from measured new particle formation events, Geophys. Res. Lett., 36, L09822, https://doi.org/10.1029/2009gl037584, 2009.

Kulmala, M., Vehkamäki, H., Petäjä, T., Dal Maso, M., Lauri, A., Kerminen, V.-M., Birmili, W., and McMurry, P. H.: Formation and growth rates of ultrafine atmospheric particles: a review of observations, J. Aerosol Sci., 35, 143–176, https://doi.org/10.1016/j.jaerosci.2003.10.003, 2004.

Kulmala, M., Riipinen, I., Sipilä, M., Manninen, H. E., Petäjä, T., Junninen, H., Maso, M. D., Mordas, G., Mirme, A., Vana, M., Hirsikko, A., Laakso, L., Harrison, R. M., Hanson, I., Leung, C., Lehtinen, K. E. J., and Kerminen, V.-M.: Toward Direct Measurement of Atmospheric Nucleation, Science, 318, 89–92, https://doi.org/10.1126/science.1144124, 2007.

Kulmala, M., Dada, L., Daellenbach, K. R., Yan, C., Stolzenburg, D., Kontkanen, J., Ezhova, E., Hakala, S., Tuovinen, S., Kokkonen, T. V., Kurppa, M., Cai, R., Zhou, Y., Yin, R., Baalbaki, R., Chan, T., Chu, B., Deng, C., Fu, Y., Ge, M., He, H., Heikkinen, L., Junninen, H., Liu, Y., Lu, Y., Nie, W., Rusanen, A., Vakkari, V., Wang, Y., Yang, G., Yao, L., Zheng, J., Kujansuu, J., Kangasluoma, J., Petäjä, T., Paasonen, P., Järvi, L., Worsnop, D., Ding, A., Liu, Y., Wang, L., Jiang, J., Bianchi, F., and Kerminen, V.-M.: Is reducing new particle formation a plausible solution to mitigate particulate air pollution in Beijing and other Chinese megacities?, Faraday Discuss., 226, 334–347, https://doi.org/10.1039/D0FD00078G, 2021.

Laaksonen, A., Hamed, A., Joutsensaari, J., Hiltunen, L., Cavalli, F., Junkermann, W., Asmi, A., Fuzzi, S., and Facchini, M. C.: Cloud condensation nucleus production from nucleation events at a highly polluted region, Geophys. Res. Lett., 32, L06812, https://doi.org/10.1029/2004GL022092, 2005.

Laj, P., Bigi, A., Rose, C., Andrews, E., Lund Myhre, C., Collaud Coen, M., Lin, Y., Wiedensohler, A., Schulz, M., Ogren, J. A., Fiebig, M., Gliß, J., Mortier, A., Pandolfi, M., Petäja, T., Kim, S.-W., Aas, W., Putaud, J.-P., Mayol-Bracero, O., Keywood, M., Labrador, L., Aalto, P., Ahlberg, E., Alados Arboledas, L., Alastuey, A., Andrade, M., Artíñano, B., Ausmeel, S., Arsov, T., Asmi, E., Backman, J., Baltensperger, U., Bastian, S., Bath, O., Beukes, J. P., Brem, B. T., Bukowiecki, N., Conil, S., Couret, C., Day, D., Dayantolis, W., Degorska, A., Eleftheriadis, K., Fetfatzis, P., Favez, O., Flentje, H., Gini, M. I., Gregorič, A., Gysel-Beer, M., Hallar, A. G., Hand, J., Hoffer, A., Hueglin, C., Hooda, R. K., Hyvärinen, A., Kalapov, I., Kalivitis, N., Kasper-Giebl, A., Kim, J. E., Kouvarakis, G., Kranjc, I., Krejci, R., Kulmala, M., Labuschagne, C., Lee, H.-J., Lihavainen, H., Lin, N.-H., Löschau, G., Luoma, K., Marinoni, A., Martins Dos Santos, S., Meinhardt, F., Merkel, M., Metzger, J.-M., Mihalopoulos, N., Nguyen, N. A., Ondracek, J., Pérez, N., Perrone, M. R., Petit, J.-E., Picard, D., Pichon, J.-M., Pont, V., Prats, N., Prenni, A., Reisen, F., Romano, S., Sellegri, K., Sharma, S., Schauer, G., Sheridan, P., Sherman, J. P., Schütze, M., Schwerin, A., Sohmer, R., Sorribas, M., Steinbacher, M., Sun, J., Titos, G., Toczko, B., Tuch, T., Tulet, P., Tunved, P., Vakkari, V., Velarde, F., Velasquez, P., Villani, P., Vratolis, S., Wang, S.-H., Weinhold, K., Weller, R., Yela, M., Yus-Diez, J., Zdimal, V., Zieger, P., and Zikova, N.: A global analysis of climate-relevant aerosol properties retrieved from the network of Global Atmosphere Watch (GAW) near-surface observatories, Atmos. Meas. Tech., 13, 4353–4392, https://doi.org/10.5194/amt-13-4353-2020, 2020.

Merikanto, J., Spracklen, D. V., Mann, G. W., Pickering, S. J., and Carslaw, K. S.: Impact of nucleation on global CCN, Atmos. Chem. Phys., 9, 8601–8616, https://doi.org/10.5194/acp-9-8601-2009, 2009.

Moorthy, K. K., Satheesh, S. K., Babu, S. S., and Dutt, C. B. S.: Integrated Campaign for Aerosols, gases and Radiation Budget (ICARB): An overview, J. Earth Syst. Sci., 117, 243–262, https://doi.org/10.1007/s12040-008-0029-7, 2008.

Moorthy, K. K., Sreekanth, V., Prakash Chaubey, J., Gogoi, M. M., Suresh Babu, S., Kumar Kompalli, S., Bagare, S. P., Bhatt, B. C., Gaur, V. K., Prabhu, T. P., and Singh, N. S.: Fine and ultrafine particles at a near–free tropospheric environment over the high-altitude station Hanle in the Trans-Himalaya: New particle formation and size distribution, J. Geophys. Res.-Atmos., 116, D20212, https://doi.org/10.1029/2011jd016343, 2011.

Nair, V. S., Jayachandran, V. N., Kompalli, S. K., Gogoi, M. M., and Babu, S. S.: Cloud condensation nuclei properties of South Asian outflow over the northern Indian Ocean during winter, Atmos. Chem. Phys., 20, 3135–3149, https://doi.org/10.5194/acp-20-3135-2020, 2020.

Neitola, K., Asmi, E., Komppula, M., Hyvärinen, A.-P., Raatikainen, T., Panwar, T. S., Sharma, V. P., and Lihavainen, H.: New particle formation infrequently observed in Himalayan foothills – why?, Atmos. Chem. Phys., 11, 8447–8458, https://doi.org/10.5194/acp-11-8447-2011, 2011.

Nieminen, T., Kerminen, V.-M., Petäjä, T., Aalto, P. P., Arshinov, M., Asmi, E., Baltensperger, U., Beddows, D. C. S., Beukes, J. P., Collins, D., Ding, A., Harrison, R. M., Henzing, B., Hooda, R., Hu, M., Hõrrak, U., Kivekäs, N., Komsaare, K., Krejci, R., Kristensson, A., Laakso, L., Laaksonen, A., Leaitch, W. R., Lihavainen, H., Mihalopoulos, N., Németh, Z., Nie, W., O'Dowd, C., Salma, I., Sellegri, K., Svenningsson, B., Swietlicki, E., Tunved, P., Ulevicius, V., Vakkari, V., Vana, M., Wiedensohler, A., Wu, Z., Virtanen, A., and Kulmala, M.: Global analysis of continental boundary layer new particle formation based on long-term measurements, Atmos. Chem. Phys., 18, 14737–14756, https://doi.org/10.5194/acp-18-14737-2018, 2018.

Paasonen, P., Asmi, A., Petäjä, T., Kajos, M. K., Äijälä, M., Junninen, H., Holst, T., Abbatt, J. P. D., Arneth, A., Birmili, W., van der Gon, H. D., Hamed, A., Hoffer, A., Laakso, L., Laaksonen, A., Richard Leaitch, W., Plass-Dülmer, C., Pryor, S. C., Räisänen, P., Swietlicki, E., Wiedensohler, A., Worsnop, D. R., Kerminen, V.-M., and Kulmala, M.: Warming-induced increase in aerosol number concentration likely to moderate climate change, Nat. Geosci., 6, 438–442, https://doi.org/10.1038/ngeo1800, 2013.

Pierce, J. R. and Adams, P. J.: Efficiency of cloud condensation nuclei formation from ultrafine particles, Atmos. Chem. Phys., 7, 1367–1379, https://doi.org/10.5194/acp-7-1367-2007, 2007.

Pierce, J. R., Leaitch, W. R., Liggio, J., Westervelt, D. M., Wainwright, C. D., Abbatt, J. P. D., Ahlm, L., Al-Basheer, W., Cziczo, D. J., Hayden, K. L., Lee, A. K. Y., Li, S.-M., Russell, L. M., Sjostedt, S. J., Strawbridge, K. B., Travis, M., Vlasenko, A., Wentzell, J. J. B., Wiebe, H. A., Wong, J. P. S., and Macdonald, A. M.: Nucleation and condensational growth to CCN sizes during a sustained pristine biogenic SOA event in a

forested mountain valley, Atmos. Chem. Phys., 12, 3147–3163, https://doi.org/10.5194/acp-12-3147-2012, 2012.

Pierce, J. R., Westervelt, D. M., Atwood, S. A., Barnes, E. A., and Leaitch, W. R.: New-particle formation, growth and climate-relevant particle production in Egbert, Canada: analysis from 1 year of size-distribution observations, Atmos. Chem. Phys., 14, 8647–8663, https://doi.org/10.5194/acp-14-8647-2014, 2014.

Pikridas, M., Riipinen, I., Hildebrandt, L., Kostenidou, E., Manninen, H., Mihalopoulos, N., Kalivitis, N., Burkhart, J. F., Stohl, A., Kulmala, M., and Pandis, S. N.: New particle formation at a remote site in the eastern Mediterranean, Journal geophys. Res.-Atmos., 117, D12205, https://doi.org/10.1029/2012JD017570, 2012.

Raatikainen, T., Hyvärinen, A. P., Hatakka, J., Panwar, T. S., Hooda, R. K., Sharma, V. P., and Lihavainen, H.: The effect of boundary layer dynamics on aerosol properties at the Indo-Gangetic plains and at the foothills of the Himalayas, Atmos. Environ., 89, 548–555, https://doi.org/10.1016/j.atmosenv.2014.02.058, 2014.

Ramanathan, V., Crutzen, P. J., Lelieveld, J., Mitra, A. P., Althausen, D., Anderson, J., Andreae, M. O., Cantrell, W., Cass, G. R., Chung, C. E., Clarke, A. D., Coakley, J. A., Collins, W. D., Conant, W. C., Dulac, F., Heintzenberg, J., Heymsfield, A. J., Holben, B., Howell, S., Hudson, J., Jayaraman, A., Kiehl, J. T., Krishnamurti, T. N., Lubin, D., McFarquhar, G., Novakov, T., Ogren, J. A., Podgorny, I. A., Prather, K., Priestley, K., Prospero, J. M., Quinn, P. K., Rajeev, K., Rasch, P., Rupert, S., Sadourny, R., Satheesh, S. K., Shaw, G. E., Sheridan, P., and Valero, F. P. J.: Indian Ocean Experiment: An integrated analysis of the climate forcing and effects of the great Indo-Asian haze, J. Geophys. Res.-Atmos., 106, 28371–28398, https://doi.org/10.1029/2001JD900133, 2001.

Reddington, C. L., Carslaw, K. S., Spracklen, D. V., Frontoso, M. G., Collins, L., Merikanto, J., Minikin, A., Hamburger, T., Coe, H., Kulmala, M., Aalto, P., Flentje, H., Plass-Dülmer, C., Birmili, W., Wiedensohler, A., Wehner, B., Tuch, T., Sonntag, A., O'Dowd, C. D., Jennings, S. G., Dupuy, R., Baltensperger, U., Weingartner, E., Hansson, H.-C., Tunved, P., Laj, P., Sellegri, K., Boulon, J., Putaud, J.-P., Gruening, C., Swietlicki, E., Roldin, P., Henzing, J. S., Moerman, M., Mihalopoulos, N., Kouvarakis, G., Ždímal, V., Zíková, N., Marinoni, A., Bonasoni, P., and Duchi, R.: Primary versus secondary contributions to particle number concentrations in the European boundary layer, Atmos. Chem. Phys., 11, 12007–12036, https://doi.org/10.5194/acp-11-12007-2011, 2011.

Rodríguez, S., Van Dingenen, R., Putaud, J.-P., Martins-Dos Santos, S., and Roselli, D.: Nucleation and growth of new particles in the rural atmosphere of Northern Italy—relationship to air quality monitoring, Atmospheric Environ., 39, 6734–6746, https://doi.org/10.1016/j.atmosenv.2005.07.036, 2005.

Rose, C., Sellegri, K., Moreno, I., Velarde, F., Ramonet, M., Weinhold, K., Krejci, R., Andrade, M., Wiedensohler, A., Ginot, P., and Laj, P.: CCN production by new particle formation in the free troposphere, Atmos. Chem. Phys., 17, 1529–1541, https://doi.org/10.5194/acp-17-1529-2017, 2017.

Rosenfeld, D., Sherwood, S., Wood, R., and Donner, L.: Climate Effects of Aerosol-Cloud Interactions, Science, 343, 379–380, https://doi.org/10.1126/science.1247490, 2014.

Sarangi, C., Kanawade, V. P., Tripathi, S. N., Thomas, A., and Ganguly, D.: Aerosol-induced intensification of cooling effect of clouds during Indian summer monsoon, Nat. Commun., 9, 3754, https://doi.org/10.1038/s41467-018-06015-5, 2018.

Schobesberger, S., Franchin, A., Bianchi, F., Rondo, L., Duplissy, J., Kürten, A., Ortega, I. K., Metzger, A., Schnitzhofer, R., Almeida, J., Amorim, A., Dommen, J., Dunne, E. M., Ehn, M., Gagné, S., Ickes, L., Junninen, H., Hansel, A., Kerminen, V.-M., Kirkby, J., Kupc, A., Laaksonen, A., Lehtipalo, K., Mathot, S., Onnela, A., Petäjä, T., Riccobono, F., Santos, F. D., Sipilä, M., Tomé, A., Tsagkogeorgas, G., Viisanen, Y., Wagner, P. E., Wimmer, D., Curtius, J., Donahue, N. M., Baltensperger, U., Kulmala, M., and Worsnop, D. R.: On the composition of ammonia–sulfuric-acid ion clusters during aerosol particle formation, Atmos. Chem. Phys., 15, 55–78, https://doi.org/10.5194/acp-15-55-2015, 2015.

Sebastian, M., Kanawade, V. P., and Pierce, J. R.: Observation of sub-3nm particles and new particle formation at an urban location in India, Atmos. Environ., 256, 118460, https://doi.org/10.1016/j.atmosenv.2021.118460, 2021a.

Sebastian, M., Kanawade, V., Soni, V., Asmi, E., Westervelt, D., Vakkari, V., Hyvärinen, A. P., Pierce, J., and Hooda, R.: New Particle Formation and Growth to Climate-Relevant Aerosols at a Background Remote Site in the Western Himalaya, J. Geophys. Res.-Atmos., 126, D033267, https://doi.org/10.1029/2020JD033267, 2021b.

Sellegri, K., Rose, C., Marinoni, A., Lupi, A., Wiedensohler, A., Andrade, M., Bonasoni, P., and Laj, P.: New Particle Formation: A Review of Ground-Based Observations at Mountain Research Stations, Atmosphere, 10, 493, https://doi.org/10.3390/atmos10090493, 2019.

Shika, S., Gadhavi, H., Suman, M. N. S., Ravikrishna, R., and Gunthe, S. S.: Atmospheric aerosol properties at a semi-rural location in southern India: particle size distributions and implications for cloud droplet formation, SN Appl. Sci., 2, 1007, https://doi.org/10.1007/s42452-020-2804-2, 2020.

Sihto, S.-L., Mikkilä, J., Vanhanen, J., Ehn, M., Liao, L., Lehtipalo, K., Aalto, P. P., Duplissy, J., Petäjä, T., Kerminen, V.-M., Boy, M., and Kulmala, M.: Seasonal variation of CCN concentrations and aerosol activation properties in boreal forest, Atmos. Chem. Phys., 11, 13269–13285, https://doi.org/10.5194/acp-11-13269-2011, 2011.

Siingh, D., Gautam, A. S., Buchunde, P., and Kamra, A. K.: Classification of the new particle formation events observed at a tropical site, Pune, India, Atmos. Environ., 190, 10–22, https://doi.org/10.1016/j.atmosenv.2018.07.025, 2018.

Singh, R. P., Dey, S., Tripathi, S. N., Tare, V., and Holben, B.: Variability of aerosol parameters over Kanpur, northern India, J. Geophys. Res.-Atmos., 109, D23206, https://doi.org/10.1029/2004JD004966, 2004.

Srivastava, A. K., Soni, V. K., Singh, S., Kanawade, V. P., Singh, N., Tiwari, S., and Attri, S. D.: An early South Asian dust storm during March 2012 and its impacts on Indian Himalayan foothills: A case study, Sci. Total Environ., 493, 526–534, https://doi.org/10.1016/j.scitotenv.2014.06.024, 2014.

Tare, V., Tripathi, S. N., Chinnam, N., Srivastava, A. K., Dey, S., Manar, M., Kanawade, V. P., Agarwal, A., Kishore, S., Lal, R. B., and Sharma, M.: Measurements of atmospheric parameters during Indian Space Research Organization Geosphere Biosphere Program Land Campaign II at a typical location in the Ganga Basin: 2. Chemical properties, J. Geophys. Res.-Atmos., 111, D23210, https://doi.org/10.1029/2006JD007279, 2006.

Thomas, A., Sarangi, C., and Kanawade, V. P.: Recent Increase in Winter Hazy Days over Central India and the Arabian Sea, Sci. Rep., 9, 17406, https://doi.org/10.1038/s41598-019-53630-3, 2019.

Tripathi, R. M., Khandekar, R. N., and Mishra, U. C.: Size distribution of atmospheric aerosols in urban sites in India, Sci. Total Environ., 77, 237–244, https://doi.org/10.1016/0048-9697(88)90059-9, 1988.

Tripathi, S. N., Tare, V., Chinnam, N., Srivastava, A. K., Dey, S., Agarwal, A., Kishore, S., Lal, R. B., Manar, M., Kanawade, V. P., Chauhan, S. S. S., Sharma, M., Reddy, R. R., Gopal, K. R., Narasimhulu, K., Reddy, L. S. S., Gupta, S., and Lal, S.: Measurements of atmospheric parameters during Indian Space Research Organization Geosphere Biosphere Programme Land Campaign II at a typical location in the Ganga basin: 1. Physical and optical properties, J. Geophys. Res.-Atmos., 111, D23209, https://doi.org/10.1029/2006JD007278, 2006.

Tröstl, J., Herrmann, E., Frege, C., Bianchi, F., Molteni, U., Bukowiecki, N., Hoyle, C. R., Steinbacher, M., Weingartner, E., Dommen, J., Gysel, M., and Baltensperger, U.: Contribution of new particle formation to the total aerosol concentration at the high-altitude site Jungfraujoch (3580 m asl, Switzerland), J. Geophys. Res.-Atmos., 121, 11692–611711, https://doi.org/10.1002/2015jd024637, 2016.

Vehkamäki, H. and Riipinen, I.: Thermodynamics and kinetics of atmospheric aerosol particle formation and growth, Chem. Soc. Rev., 41, 5160–5173, https://doi.org/10.1039/C2CS00002D, 2012.

Venzac, H., Sellegri, K., Laj, P., Villani, P., Bonasoni, P., Marinoni, A., Cristofanelli, P., Calzolari, F., Fuzzi, S., Decesari, S., Facchini, M.-C., Vuillermoz, E., and Verza, G. P.: High frequency new particle formation in the Himalayas, P. Natl. Acad. Sci. USA, 105, 15666–15671, https://doi.org/10.1073/pnas.0801355105, 2008.

Westervelt, D. M., Pierce, J. R., Riipinen, I., Trivitayanurak, W., Hamed, A., Kulmala, M., Laaksonen, A., Decesari, S., and Adams, P. J.: Formation and growth of nucleated particles into cloud condensation nuclei: model–measurement comparison, Atmos. Chem. Phys., 13, 7645–7663, https://doi.org/10.5194/acp-13-7645-2013, 2013.

Westervelt, D. M., Pierce, J. R., and Adams, P. J.: Analysis of feedbacks between nucleation rate, survival probability and cloud condensation nuclei formation, Atmos. Chem. Phys., 14, 5577–5597, https://doi.org/10.5194/acp-14-5577-2014, 2014.

Wiedensohler, A., Cheng, Y. F., Nowak, A., Wehner, B., Achtert, P., Berghof, M., Birmili, W., Wu, Z. J., Hu, M., Zhu, T., Takegawa, N., Kita, K., Kondo, Y., Lou, S. R., Hofzumahaus, A., Holland, F., Wahner, A., Gunthe, S. S., Rose, D., Su, H., and Pöschl, U.: Rapid aerosol particle growth and increase of cloud condensation nucleus activity by secondary aerosol formation and condensation: A case study for regional air pollution in northeastern China, J. Geophys. Res.-Atmos., 114, D00G08, https://doi.org/10.1029/2008jd010884, 2009.

Wiedensohler, A., Birmili, W., Nowak, A., Sonntag, A., Weinhold, K., Merkel, M., Wehner, B., Tuch, T., Pfeifer, S., Fiebig, M., Fjäraa, A. M., Asmi, E., Sellegri, K., Depuy, R., Venzac, H., Villani, P., Laj, P., Aalto, P., Ogren, J. A., Swietlicki, E., Williams, P., Roldin, P., Quincey, P., Hüglin, C., Fierz-Schmidhauser, R., Gysel, M., Weingartner, E., Riccobono, F., Santos, S., Grüning, C., Faloon, K., Beddows, D., Harrison, R., Monahan, C., Jennings, S. G., O'Dowd, C. D., Marinoni, A., Horn, H.-G., Keck, L., Jiang, J., Scheckman, J., McMurry, P. H., Deng, Z., Zhao, C. S., Moerman, M., Henzing, B., de Leeuw, G., Löschau, G., and Bastian, S.: Mobility particle size spectrometers: harmonization of technical standards and data structure to facilitate high quality long-term observations of atmospheric particle number size distributions, Atmos. Meas. Tech., 5, 657–685, https://doi.org/10.5194/amt-5-657-2012, 2012.

Xiao, M., Hoyle, C. R., Dada, L., Stolzenburg, D., Kürten, A., Wang, M., Lamkaddam, H., Garmash, O., Mentler, B., Molteni, U., Baccarini, A., Simon, M., He, X.-C., Lehtipalo, K., Ahonen, L. R., Baalbaki, R., Bauer, P. S., Beck, L., Bell, D., Bianchi, F., Brilke, S., Chen, D., Chiu, R., Dias, A., Duplissy, J., Finkenzeller, H., Gordon, H., Hofbauer, V., Kim, C., Koenig, T. K., Lampilahti, J., Lee, C. P., Li, Z., Mai, H., Makhmutov, V., Manninen, H. E., Marten, R., Mathot, S., Mauldin, R. L., Nie, W., Onnela, A., Partoll, E., Petäjä, T., Pfeifer, J., Pospisilova, V., Quéléver, L. L. J., Rissanen, M., Schobesberger, S., Schuchmann, S., Stozhkov, Y., Tauber, C., Tham, Y. J., Tomé, A., Vazquez-Pufleau, M., Wagner, A. C., Wagner, R., Wang, Y., Weitz, L., Wimmer, D., Wu, Y., Yan, C., Ye, P., Ye, Q., Zha, Q., Zhou, X., Amorim, A., Carslaw, K., Curtius, J., Hansel, A., Volkamer, R., Winkler, P. M., Flagan, R. C., Kulmala, M., Worsnop, D. R., Kirkby, J., Donahue, N. M., Baltensperger, U., El Haddad, I., and Dommen, J.: The driving factors of new particle formation and growth in the polluted boundary layer, Atmos. Chem. Phys., 21, 14275–14291, https://doi.org/10.5194/acp-21-14275-2021, 2021.

Yu, F., Luo, G., Nair, A. A., Schwab, J. J., Sherman, J. P., and Zhang, Y.: Wintertime new particle formation and its contribution to cloud condensation nuclei in the Northeastern United States, Atmos. Chem. Phys., 20, 2591–2601, https://doi.org/10.5194/acp-20-2591-2020, 2020.

Yu, H., Ren, L., and Kanawade, V. P.: New Particle Formation and Growth Mechanisms in Highly Polluted Environments, Current Pollution Reports, 3, 245–253, https://doi.org/10.1007/s40726-017-0067-3, 2017.

Zhang, R., Khalizov, A., Wang, L., Hu, M., and Xu, W.: Nucleation and Growth of Nanoparticles in the Atmosphere, Chem. Rev., 112, 1957–2011, https://doi.org/10.1021/cr2001756, 2012.

Check for updates

JGR Atmospheres

RESEARCH ARTICLE
10.1029/2021JD035392

Key Points:

- Particle number concentrations decreased by about 85% during the COVID-19 enforced lockdown in Hyderabad
- Atmospheric new particle formation and growth suppressed during lockdown
- The reduction in anthropogenic emissions and meteorological variabilities lead to suppressed new particle formation and growth events

Correspondence to:
V. P. Kanawade,
vijaykanawade03@yahoo.co.in

Citation:
Kanawade, V. P., Sebastian, M., & Dasari, P. (2022). Reduction in anthropogenic emissions suppressed new particle formation and growth: Insights from the COVID-19 lockdown. *Journal of Geophysical Research: Atmospheres*, *127*, e2021JD035392. https://doi.org/10.1029/2021JD035392

Received 9 JUN 2021
Accepted 24 DEC 2021

Author Contributions:
Conceptualization: V. P. Kanawade
Data curation: M. Sebastian, P. Dasari
Formal analysis: V. P. Kanawade, M. Sebastian
Funding acquisition: V. P. Kanawade
Investigation: V. P. Kanawade
Methodology: V. P. Kanawade
Project Administration: V. P. Kanawade
Resources: V. P. Kanawade, P. Dasari
Supervision: V. P. Kanawade
Visualization: V. P. Kanawade, M. Sebastian
Writing – original draft: V. P. Kanawade
Writing – review & editing: V. P. Kanawade, M. Sebastian, P. Dasari

© 2022. American Geophysical Union. All Rights Reserved.

Reduction in Anthropogenic Emissions Suppressed New Particle Formation and Growth: Insights From the COVID-19 Lockdown

V. P. Kanawade[1], M. Sebastian[1], and P. Dasari[2]

[1]Centre for Earth, Ocean and Atmospheric Sciences, University of Hyderabad, Hyderabad, India, [2]Telangana State Pollution Control Board, Hyderabad, India

Abstract To control the spread of the novel 2019 Coronavirus (COVID-19), the Government of India enforced nationwide social and transportation restrictions (lockdown) in three phases from the evening of 24 March to 31 May 2020, which resulted in a significant reduction of primary emissions. Here, we performed the analyses of particle number size distribution measurements in the particle size range of 1.2–3 nm and 10–514 nm carried out from 15 April to 31 May 2020 (lockdown, LCD) and compared with measurements from the previous year during the same time period (15 April to 31 May 2019, business-as-usual, BAU) at University of Hyderabad in Hyderabad, India. The number concentrations of sub-3 nm particles were comparable between LCD and BAU, but the number concentrations of particles greater than 10 nm diameter were lower by about 85% during LCD than BAU. It indicates that the reduction in primary anthropogenic emissions did not inhibit the formation of sub-3 nm particles. But the frequency of occurrence of the new particle formation and growth (NPF&G) events was three-fold lower during LCD than BAU. The ratio of formaldehyde to nitrogen dioxide indicated that India falls in a NO_x-limited regime, which reduces ambient ozone concentrations (lower condensable vapors via ozone oxidation of volatile organic compounds). Besides, the lower temperature (lower hydroxyl radical concentration) and lower wind speed during LCD may have contributed to the suppression of NPF&G events. Therefore, we emphasize the need to account for processes and interactions related to NPF&G in formulating particulate pollution mitigation policies in urban environments.

Plain Language Summary To combat the spread of the COVID-19 outbreak, social-economic activities, except essential services (hospitals, community helpers, power plants etc.) phased out during April-May 2020 in India. This unintended country-wide lockdown substantially lowered anthropogenic emissions of air pollutants (particulate matter, oxides of nitrogen, sulfur dioxide, volatile organic compounds, carbon monoxide etc.). We found that the atmospheric new particle formation and growth (NPF&G) was suppressed during lockdown than the business-as-usual time period. The formation of sub-3 nanometer particles frequently occurred, but these freshly-formed particles did not grow beyond 10 nanometer. Under anthropogenic emission reductions, the lower ozone and lower temperature may have inhibited the production of low-volatility condensable vapors for particle growth. These findings underline that air quality improvement can be made by cutting off anthropogenic emissions in the warming anthropogenic future. However, the complex chemistry driving NPF&G requires further investigation to adopt targeted anthropogenic emission mitigation strategies.

1. Introduction

The first case of Corona virus (CoV) was reported to World Health Organization (WHO) Country Office in Wuhan, China, on 31 December 2019 with symptoms of unexplained low respiratory infections. The WHO declared the outbreak of CoV to be a public health emergency of international concern and announced this novel CoV as Coronavirus disease 2019 (COVID-19) on 11 February 2020 (Sohrabi et al., 2020). Later, COVID-19 was declared a pandemic by WHO on 11 March 2020 due to its rapid spread and associated mortality across the globe. The outbreak of COVID-19 has led many countries to close their borders and impose a nationwide lockdown. To tackle the spread of COVID-19, social and transportation restrictions were enforced (referred to as lockdown) that resulted in the shutdown of all the businesses activities, including transportation, educational institutes, social activities, marketplaces, industries, construction and demolition, hotels and restaurants, etc. except the essential services like hospitals, community helpers, power plants, petrochemical industries, etc. As governments across the globe enforced lockdown, satellite images of emission reductions (e.g., nitrogen dioxide, NO_2 and aerosol optical

Table 1
Different Scenarios and Corresponding Time Periods Considered in This Study

Scenarios	Time period
Business-as-usual (BAU)	25 March–31 May 2019
Lockdown (LCD)	25 March–31 May 2020

depth, AOD) have shown that the COVID-19 pandemic has led to improved air quality across the world (Metya et al., 2020; Srivastava et al., 2021). Numerous efforts have been put forth to measure and analyze changes to air pollution and characterize linkages between the pandemic, air pollution, and meteorology (Gunthe et al., 2020; Sathe et al., 2021; Srivastava, 2021).

The government of India also declared the nationwide lockdown on the evening of 24 March 2020 for 21 days (25 March to 14 April 2020) to limit the spread of COVID-19. As infections and deaths due to COVID-19 continued to escalate during the first phase of lockdown, the Government of India extended the lockdown in three phases till 31 May 2020, with conditional relaxation to some regions where COVID-19 spread was contained. The mass concentrations of particulate matter of diameter less than 2.5 μm ($PM_{2.5}$) over major cities across the world reduced by about 11%–58% due to primary emission reductions during COVID-19 lockdown (Chauhan & Singh, 2020). A study over 22 cities across India also showed a 43% reduction in $PM_{2.5}$ mass concentrations (Sharma et al., 2020). There are plenty of reports of concentration changes for common air pollutants (O_3, NO_2, SO_2, PM, etc.). Still, these provide little or no insights into aerosol chemistry and its consequent effects on air quality. Le et al. (2020) reported unexpectedly extremely high PM levels owing to the combination of anomalously high relative humidity promoted heterogeneous aerosol chemistry, stagnant air conditions, and uninterrupted emissions from essential services (e.g., power plants and petrochemical industries) during COVID-19 lockdown, which resulted in severe haze formation in Northern China. Sun et al. (2020) also indicated that the reduced anthropogenic activities facilitated stronger secondary chemical transformation during the lockdown in Beijing, with higher ratios of secondary to primary organic aerosols (OA) and higher sulfur and nitrogen oxidation capacity. Such increased oxidation capacity of aerosol precursors found to enhance aerosol formation and growth rates, with sulfuric acid (H_2SO_4) and organic oxidized vapors increased by about 35% and 133%, respectively, on new particle formation and growth (NPF&G) event days in urban Beijing (Shen et al., 2021). Huang et al. (2021) also reported the elevated formation of secondary particulate matter due to enhanced oxidizing capacity caused by increased O_3 levels and night-time nitrate (NO_3) radical formation. The other study in China also showed that NO_2 concentrations decreased by 46.1%, whereas O_3 concentrations increased by about 47.3% during COVID-19 lockdown (Zhao et al., 2020), indicating the critical role of volatile organic compounds (VOCs) in O_3 formation. The elevated O_3 levels promote SO_2 oxidation into sulfate and VOCs into low volatility vapors which contribute to aerosol nucleation and growth processes (Ehn et al., 2014) and thereby increasing the secondary particulate matter (Huang et al., 2021; Shen et al., 2021; Sun et al., 2020; Zhong et al., 2021). However, the chemistry driving secondary aerosol formation is complex and challenging to disentangle from primary aerosol emissions (Kroll et al., 2020).

As for NPF&G, two opposite effects can be expected during COVID-19 lockdown. The primary emission reduction may decrease the levels of potential nucleating vapors such as SO_2 (Kulmala et al., 2013), ammonia (NH_3) (Kirkby et al., 2011; Wang et al., 2020), amines (Almeida et al., 2013; Yu et al., 2012), VOCs (Schobesberger et al., 2013; Tröstl et al., 2016), which might inhibit the occurrence of NPF&G. On the contrary, the reduced pre-existing aerosol particles due to lockdown, which act as condensation and coagulation sink for precursor vapors and newly formed small clusters, may enhance NPF&G (Zhang et al., 2012). While one study in Beijing (Peking University) showed stable frequencies of NPF&G between 2019 (business-as-usual year) and 2020 (lockdown year) in the same period (Tang et al., 2021), another study showed enhancement in nanoparticle formation and growth in Beijing (China Meteorological Administration) (Shen et al., 2021). In the Indian context, a recent study showed the reduced frequency of NPF occurrence during COVID-19 enforced lockdown in urban Delhi (Yadav et al., 2021). Gkatzelis et al. (2021) also showed that NO_2 and $PM_{2.5}$ concentrations reduced by about 40% over India during COVID-19 lockdown. Hence, it remains unclear whether NPF&G will increase or decrease or remain unchanged under the future reduced anthropogenic emission scenario. Here, we focus on the evolution of particle number size distributions characteristics during COVID-19 lockdown (hereafter referred to as LCD) and compare that with the previous business-as-usual year (hereafter referred to as BAU; Table 1). The main aim of this study is to investigate the differences in NPF&G characteristics (e.g., frequency, formation rate, growth rate etc.) between LCD and BAU time periods and to delineate the impact of COVID-19 lockdown on NPF&G events at an urban location, Hyderabad, in India.

21698996, 2022, 2, Downloaded from https://agupubs.onlinelibrary.wiley.com/doi/10.1029/2021JD035392, Wiley Online Library on [13/12/2023]. See the Terms and Conditions (https://onlinelibrary.wiley.com/terms-and-conditions) on Wiley Online Library for rules of use; OA articles are governed by the applicable Creative Commons License

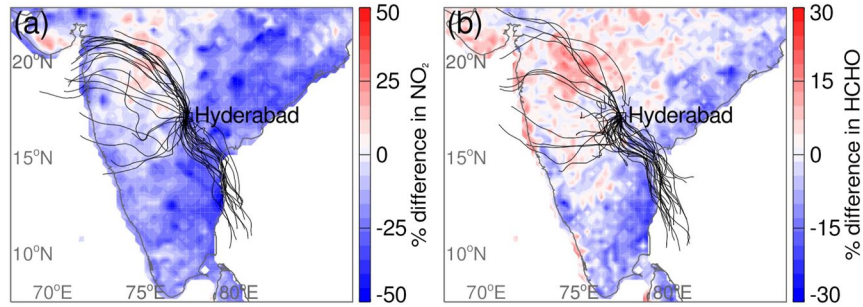

Figure 1. Spatial distribution of percentage difference in TROPOMI-retrieved (a) tropospheric NO_2 column and (b) HCHO column between LCD and BAU time periods. The measurement site, Hyderabad, is shown by the open square symbol. Three-day air mass backward trajectories starting at 11:30 a.m. local time during (a) BAU and (b) LCD time periods are also shown.

2. Materials and Methods

2.1. Measurement Site, HYSPLIT Calculations, and Satellite Data

The particle number size distribution measurements were carried out at the Earth Sciences building in the University of Hyderabad campus (17.46°N, 78.32°E; ~542 m above mean sea level). The measurement site is surrounded by thin forested vegetation in a radius of 1 km, except few academic buildings. The major road, the old Hyderabad-Mumbai highway, with heavy traffic, is located about a kilometer to the east of the measurement site. More information about the site can be found in Sebastian et al. [2021]. The three-day air mass backward trajectories starting at 100 m above the ground level starting at 11:30 a.m. local time were also calculated from the NOAA ARL PC-version Hybrid Single-Particle Lagrangian Integrated Trajectory (HYSPLIT) transport and dispersion model using gridded wind fields from the Global Data Assimilation System (GDAS), which has a spatial resolution of 1° × 1° longitude by latitude and a time resolution of 1 hr (Draxler & Rolph, 2010) to highlight the influence of long-range transported air masses at the site.

The TROPOspheric Monitoring Instrument (TROPOMI), onboard Sentinel-5 Precursor (S-5P) launched in October 2017, is in a low-Earth polar orbit with a swath of 2600 km, resulting in daily global coverage (Veefkind et al., 2012). The TROPOMI instrument consists of four spectrometers covering the UV–VIS–NIR–SWIR wavelength ranges at a spectral resolution of 0.45–0.65 nm in the UV–VIS range. TROPOMI has a high nadir spatial resolution of 3.5 × 7 km, which was upgraded to 3.5 × 5.5 km in August 2019, with a high signal-to-noise ratio. The NO_2 retrieval algorithm is based on the DOMINO v2 (Dutch Ozone Monitoring Instrument NO_2 data products of KNMI for OMI) (Boersma et al., 2011) and QA4ECV (Quality Assurance for Essential Climate Variables) (Boersma et al., 2018) processing systems. The formaldehyde (HCHO) retrieval algorithm is based on the Differential Optical Absorption Spectroscopy (DOAS) method and is directly inherited from the OMI QA4ECV product retrieval algorithm (De Smedt et al., 2018). The NO_2 product correlates well with aircraft and ground-based measurements ($R \cong 0.68$) with mean bias ranging from −15% to 30% (Griffin et al., 2019). The HCHO product correlates highly with Multi-Axis DOAS (MAX-DOAS, $R \cong 0.88$) and Fourier-Transform InfraRed (FTIR, $R \cong 0.91$) measurements with a mean bias ranging from −26% to 30.8% (Vigouroux et al., 2020). Here, we used TROPOMI L2 pixels with (a) quality assurance value greater than 0.5, (b) solar zenith angle less than 65° and (c) cloud fraction less than 0.2. Further, we only consider observations with NO_2 column higher than 5.6×10^{14} molecules/cm^2 and HCHO column higher than 1.0×10^{15} molecules/cm^2 (detection limitation). Figure 1 shows the location of the city of Hyderabad on a regional map showing the averaged percentage difference in TROPOMI retrieved NO_2 and HCHO column between LCD and BAU time periods. NO_2 and HCHO concentrations were lower by 10%–30% during LCD as compared to BAU time periods. Hyderabad experienced air masses from northwest and southeast, with more frequently from the southeast during LCD than BAU.

2.2. Particle Number Size Distribution Measurements From nCNC and SMPS

Particle number size distributions in the size range from 1.2 to 3.0 nm (6 bins) and 10–514 nm (107 bins) were measured using AIRMODUS A11 nano Condensation Nucleus Counter (nCNC) and TSI Scanning Mobility Particle Sizer (SMPS), respectively. A11 nCNC consists of A10 diethylene glycol (DEG) Particle Size Magnifier

21698996, 2022, 2, Downloaded from https://agupubs.onlinelibrary.wiley.com/doi/10.1029/2021JD035392, Wiley Online Library on [13/12/2023]. See the Terms and Conditions (https://onlinelibrary.wiley.com/terms-and-conditions) on Wiley Online Library for rules of use; OA articles are governed by the applicable Creative Commons License

21698996, 2022, 2, Downloaded from https://agupubs.onlinelibrary.wiley.com/doi/10.1029/2021JD035392, Wiley Online Library on [13/12/2023]. See the Terms and Conditions (https://onlinelibrary.wiley.com/terms-and-conditions) on Wiley Online Library for rules of use; OA articles are governed by the applicable Creative Commons License

(PSM) and A20 butanol Condensation Particle Counter (CPC). DEG supersaturation, which defines the smallest detectable size by the PSM, is created by turbulently mixing heated saturator air with cooler sample air in the mixing chamber. The cut-off size of the PSM can then be varied by changing the mixing ratio of the saturator and sample air. Thus, nCNC was operated in a continuous scanning mode with a saturator flow rate of 0.1–1.3 litre per minute (lpm) with an upward ramp (0.1–1.3 lpm) automatically followed by a downward ramp (1.3–0.1 lpm) with a time step of 1 s, resulting in a cycle of 240 s. The instrument was also calibrated using NiCr aerosols from a hot wire aerosol generator. The relative humidity of the sample air and chemical composition of the sampled particles can also affect the smallest detectable size of the particle counters operated with DEG (Kangasluoma et al., 2014). Therefore, the ambient air sample was drawn to the nCNC through a diffusion dryer to maintain relative humidity less than 40%. Ultrafine particles can also be lost inside the diffusion dryer due to their thermal motion affecting the total detection efficiency. The calculated particle losses within the diffusion dryer were less than 10% (Sebastian et al., 2021). Chan et al. (2020) recently assessed four inversion methods (stepwise, kernel, Hagen–Alofs and expectation-maximization) to determine their feasibility to invert the particle number size distribution from the PSM raw scanning data. They found that the expectation-maximization (EM) algorithm (Maher & Laird, 1985) is more robust and has the highest accuracy and stability. Therefore, we used the EM algorithm to obtain the particle number size distribution in the diameter range from 1.2 to 3 nm, with six bins (1.2–1.4, 1.4–1.6, 1.6–1.8, 1.8–2.0, 2.0–2.2, and 2.2–3.0 nm). The sub-3 nm particles may include charged particles, neutral particles, air ions or even big molecules that are activated by the supersaturated vapor in CPCs, and we cannot differentiate between them. For convenience, we refer them to neutrally charged sub-3 nm particles in this study. We also conducted particle number size distribution measurements in the diameter range from 10 to 514 nm using Scanning Mobility Particle Sizer (SMPS). The SMPS consists of an electrostatic classifier (3082) with a long-differential mobility analyzer (LDMA, 3081A) and a butanol CPC (3772). The scanning cycle of the SMPS was 300 s, yielding a particle number size distribution every 5 min. Unfortunately, there were no measurements of particle number size distributions in the diameter between 3 and 10 nm.

2.3. Air Pollutants and Meteorological Parameters

$PM_{2.5}$ concentrations were measured based on the principle of β–ray attenuation with a measuring range of 0–1,000 μg/m^3 and a flow rate of 16.7 lpm. CO was measured using a non-dispersive infra-red technique with a gas-filter correlation method. NO_2 and NH_3 measurements were conducted based on the Chemiluminescence technique. SO_2 was measured based on the UV-Fluorescence technique. O_3 was measured based on UV-photometric technique. Benzene, Xylene and Toluene measurements were based on the principle of gas chromatographic separation and photoionization detector. The wind speed and direction were measured using an ultrasonic-type sensor, with an accuracy of 1.2 m s^{-1} and 1°, respectively. The air temperature was measured using a thermistor-type sensor with an accuracy of ±0.2°C. Relative humidity was measured using a capacitive-type sensor, with an accuracy of ±3%. A silicon photodiode-type pyranometer was used to measure global solar radiation in the wavelength range of 0.3–4 μm. Air pollutants and meteorological measurements were conducted from the roof-top of the Main Administration building within the University of Hyderabad campus.

2.4. Event Classification and Characteristics

New particle formation and growth events were classified by visually inspecting nCNC and SMPS particle number size distributions, following Dal Maso et al. (2005) methodology. An event is referred to as an NPF&G event when there is a rapid increase in number concentrations of sub-3 nm particles (greater than 10,000 particles cm^{-3}) and nucleation mode particles (10–25 nm), and the particle mode diameter smaller than 25 nm showed steady growth in size for at least 6 hr, thus particle number size distributions displaying a "banana-shaped" aerosol-size growth. The days with no/insignificant increase in number concentration of sub-3 nm particles and nucleation mode particles and no distinct change particle mode diameter were classified as non-events. Those days that could not be categorized into any of these two categories were classified as undefined events. These undefined events included mainly broken banana-shaped aerosol growth due to the rapid mixing of different air masses or abrupt increase in nucleation/Aitken mode particles without evidence for particle growth. For the observed NPF&G events, the growth rate of sub-3 nm particles ($GR_{sub\text{-}3nm}$) was determined by the maximum concentration method following Lehtinen and Kulmala (2003), modified and updated by Kulmala et al. (2012). The net flux of clusters growing past a certain diameter, d_p, is defined as the formation rate (J_{d_p}), which was calculated following

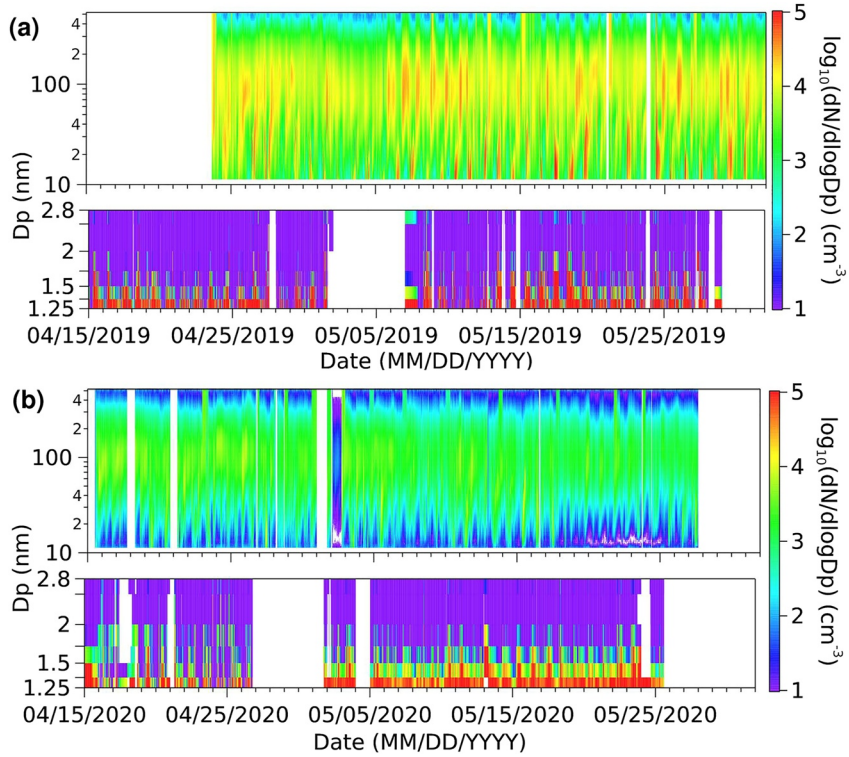

Figure 2. Time evolution of particle number size distributions in the size range of 1.2–3.0 nm from nCNC and 10–514 nm from SMPS during (a) BAU and (b) LCD time periods (15 April–31 May).

Kulmala et al. (2013) methodology. The particle growth rate between 10 and 25 nm ($GR_{10–25\ nm}$) was calculated by fitting a first-order polynomial line through growing particle mode diameter between 10 and 25 nm as a function of time and calculating its slope, following Dal Maso et al. (2005) methodology. The coagulation sink (CoagS) was calculated using the methodology of Kerminen et al. (2001), while the condensation sink (CS) was calculated following Kulmala et al. (2012). More details can be found in Sebastian et al. (2021). The size-segregated particle number concentrations in the sub-3 nm (particle diameter <3 nm, $N_{sub\text{-}3\ nm}$), nucleation mode (10–25 nm, N_{NUC}), Aitken mode (25–100 nm, N_{AIT}), accumulation mode (100–514 nm, N_{ACCU}) and total particles (10–514 nm, N_{TOT}) were also calculated.

3. Results

Figure 2 shows the time evolution of number size distributions of particles in the size range of 1.2–3.0 nm from nCNC and 10–514 nm from SMPS during BAU and LCD in the same time period (15 April to 31 May). This time period was considered to illustrate the influence of anthropogenic emission reductions due to lockdown. The gradient in particle number size distributions between BAU and LCD is evident, with 5%–98% lower particle number concentrations during LCD. The time evolution of particle number size distributions revealed the frequent occurrence of NPF events during the BAU than LCD.

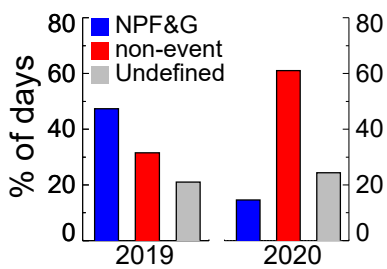

Figure 3. The percentage of days of event type during BAU and LCD in the same time period.

Figure 3 shows the percentage of days of event type during BAU and LCD time periods. BAU and LCD had 38 and 41 valid observation days, respectively. The NPF&G event occurred on 18 days (47%) and 6 days (15%) out of total valid observation days during BAU and LCD, respectively. The non-events occurred on 12 days (32%) and 25 days (61%) out of total valid observation days during BAU and LCD, respectively. The undefined events occurred on 8 days (21%) and 10 days (24%) out of the valid observation days during BAU and LCD, respectively. The frequency of occurrence of NPF&G

21698996, 2022, 2, Downloaded from https://agupubs.onlinelibrary.wiley.com/doi/10.1029/2021JD035392, Wiley Online Library on [13/12/2023]. See the Terms and Conditions (https://onlinelibrary.wiley.com/terms-and-conditions) on Wiley Online Library for rules of use; OA articles are governed by the applicable Creative Commons License

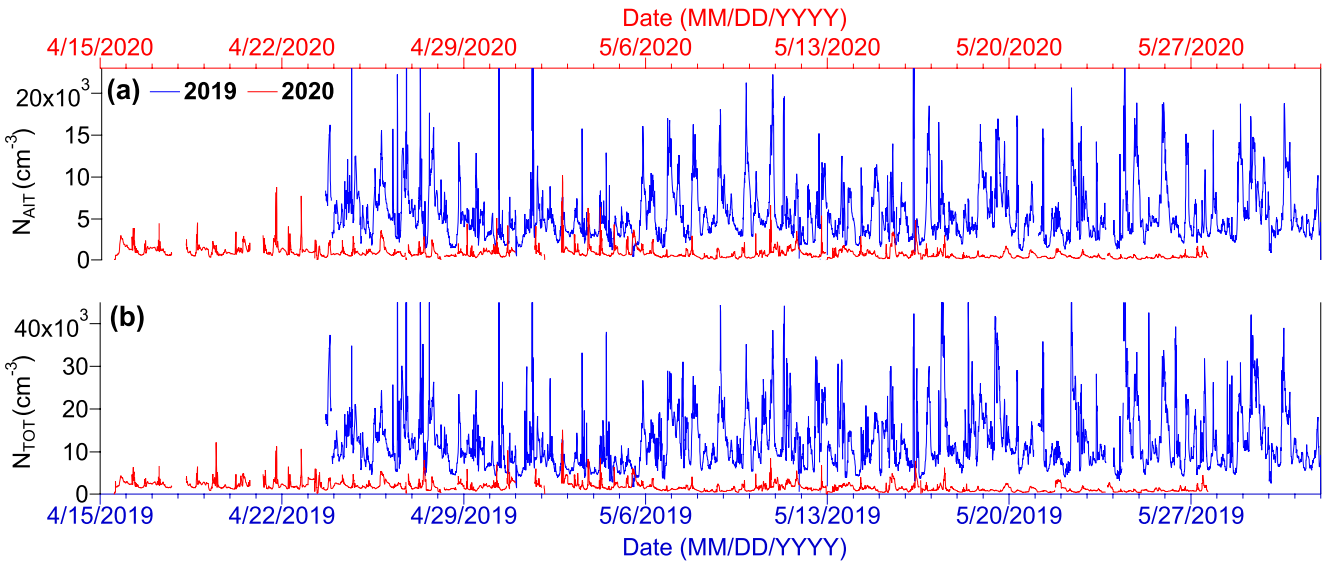

Figure 4. Time evolution of number concentrations of (a) Aitken mode (25–100 nm) particles and (b) total (10–514 nm) particles during BAU (blue) and LCD (red).

events was three-fold lower under the primary emission reductions during LCD compared to BAU. The NPF&G is affected by multiple factors such as the topography of the location, pre-existing particles, availability of nucleating and condensable vapors, and micro-meteorological conditions, with different degrees of importance for these factors among the individual locations (Nieminen et al., 2018). Below we examine some of these factors to explain the reduced frequency of NPF&G events during LCD.

To illustrate the influence of reduced anthropogenic emissions during LCD, the size-segregated particle number concentrations were calculated from nCNC and SMPS; $N_{sub\text{-}3nm}$, N_{NUC}, N_{AIT}, N_{ACCU}, and N_{TOT}. N_{AIT} is derived from primary emissions by fossil fuel, biofuel and wood combustion sources (e.g., vehicles, industry, and residential heating) (Kanawade et al., 2020; Mylläri et al., 2016; Rönkkö et al., 2017; Z. B. Wang et al., 2013) or secondary aerosol formation and growth (Kulmala et al., 2013; R. Zhang et al., 2012) or both. Figure 4a shows the time evolution of the number concentrations of N_{AIT} during BAU and LCD. N_{AIT} showed a significant reduction during LCD, and the variations were below 4,000 particles cm^{-3} compared to >15,000 particles cm^{-3} during BAU. The mean N_{AIT} concentrations were 5,660 and 882 cm^{-3} during BAU and LCD, respectively. Overall, N_{AIT} reduced by approximately 85% during LCD, implying reduced primary anthropogenic emissions or secondary formation or both. The time evolution of number concentrations of N_{TOT} also showed similar reductions (86%) during LCD (Figure 4b), indicating that the air quality was significantly improved due to the primary emission reduction during LCD (Srivastava et al., 2021; Zhang et al., 2021).

New particle formation and growth play a vital role in shaping the particle number size distribution. Particle bursts in the sub-3 nm size range were observed almost all days during BAU and LCD time periods (Figure 2). Our recent study at this site also showed that particle bursts of sub-3 nm frequently occur during spring and early monsoon (April–June) (Sebastian et al., 2021). Still, only half of the observed particle burst events (NPF) showed growth of these particles to larger sizes (>10 nm), which is indicative of the regional NPF&G event (Sebastian et al., 2021). Sebastian et al. (2021) showed that sulfuric acid concentrations, sub-3 nm growth rates, condensation sink, sub-3 nm coagulation sink, and atmospheric conditions were the same between NPF and NPF&G event days. Although wind direction has some differences between the types of events and therefore, *Sebastian and colleagues* hypothesized that the differences in airmass direction and history might have dissimilar organic vapors for condensational growth between the types of events. Surprisingly, $N_{sub\text{-}3nm}$ concentrations were comparable not only between NPF&G and non-event days but also between BAU and LCD time periods (Figure 5a). During BAU NPF&G event days, $N_{sub\text{-}3nm}$ ranged from 25 to 977,502 particles cm^{-3}, with mean and standard deviation (σ) of 62,479 ± 138,687 particles cm^{-3} whereas it ranged from 3900 to 776,583 particles cm^{-3}, with mean and σ of 68,625 ± 95,935 particles cm^{-3} during LCD NPF&G event days. This indicates that particle formation was not limited by the reduction in primary anthropogenic emissions (aerosol precursors) during LCD at this site. However, these newly formed particles did not grow beyond 10 nm on most of the days

21698996, 2022, 2, Downloaded from https://agupubs.onlinelibrary.wiley.com/doi/10.1029/2021JD035392, Wiley Online Library on [13/12/2023]. See the Terms and Conditions (https://onlinelibrary.wiley.com/terms-and-conditions) on Wiley Online Library for rules of use; OA articles are governed by the applicable Creative Commons License

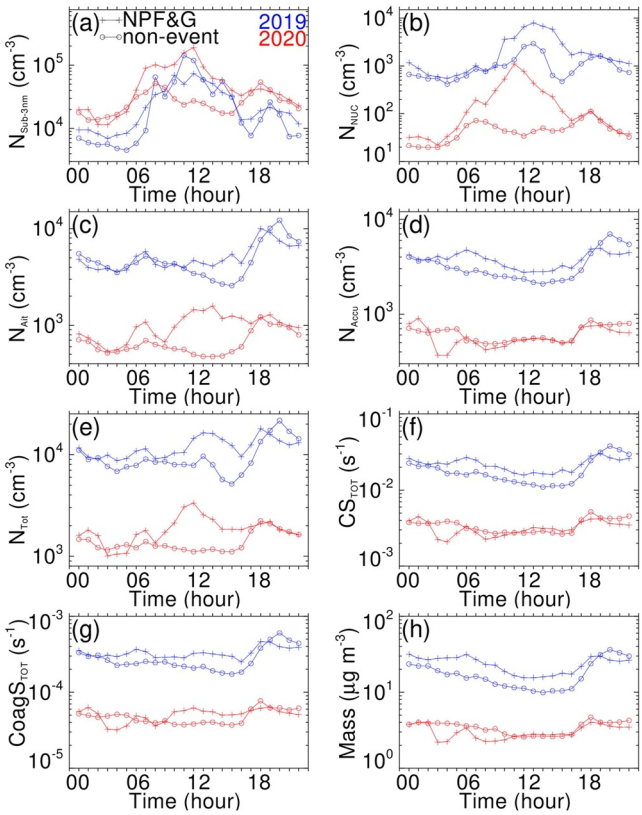

Figure 5. Median diurnal variation of (a–e) size-segregated particle number concentrations, (f) total condensation sink (CS_{TOT}), (g) total coagulation sink ($CoagS_{TOT}$), and (h) total aerosol mass for NPF&G (line connected by plus symbol) and non-events (line connected by open circle) during BAU (blue) and LCD (red). Mann-Whitney *U*-test showed statistically significant differences ($p << 0.05$) for all variables between BAU and LCD except for sub-3 nm particles during non-event event days ($p = 0.063$).

during LCD. The number concentrations of N_{NUC} were higher on NPF&G event days than non-event days both during BAU and LCD. Further, N_{NUC} were lower by about an order of magnitude during LCD than BAU (Figure 5b). Concentrations of N_{AIT}, N_{ACCU}, N_{TOT}, CS_{TOT}, $CoagS_{TOT}$, and aerosol mass were also lower during LCD than BAU (Figures 5c–5h). During BAU NPF&G event days, N_{NUC} ranged from 16 to 48,421 particles cm^{-3}, with mean and σ of 3354 ± 5,397 particles cm^{-3} whereas it ranged from 10 to 10,200 particles cm^{-3}, with mean and σ of 278 ± 683 particles cm^{-3} during LCD. Similarly, N_{AIT} ranged 73 to 36,115 particles cm^{-3}, with mean and σ of 5,942 ± 3711 particles cm^{-3} during BAU whereas it ranged from 67 to 3706 particles cm^{-3}, with mean and σ of 1,084 ± 640 particles cm^{-3} during LCD. The mean concentrations of N_{ACCU} were lower by about 85% during LCD (616 ± 295 particles cm^{-3}) than BAU (4,266 ± 2150 particles cm^{-3}). The total aerosol particles (N_{TOT}) also decreased by about 86% during LCD at this site. As a result, the condensation sink, coagulation sink and aerosol mass values were also reduced by about 86% during LCD compared to BAU. N_{ACCU} was lower during non-event days than NPF&G event days during BAU, but it was similar between a non-event and NPF&G event days during LCD (Figure 5d). The total aerosol mass concentrations were also lower by 85% during LCD than BAU (Figure 5h).

Figure 6 shows a statistical analysis of various NPF&G characteristics during BAU and LCD time periods. The variability in sub-3 nm particle number concentrations was comparable between BAU and LCD (Figure 6a). The size-segregated particle number concentrations, condensation sink, coagulation sink and aerosol mass were significantly lower during LCD than BAU (Figures 6b–6h). The sub-3 nm particles growth rates were slightly lower during LCD than BAU (Figure 6i). $GR_{10–25\ nm}$ was two-fold lower during LCD than BAU (Figure 6k). The mean formation rates of particles of 1.5 nm varied from 1.34 to 178.1 particles cm^{-3} s^{-1}, with mean and σ of 36.8 ± 56.9 particles cm^{-3} s^{-1} during BAU, which is comparable to LCD time periods (24.3 ± 19.2 particles cm^{-3} s^{-1}). The mean formation rates of sub-3 nm particles between BAU and LCD were in general comparable, but J_{10} was lower by about 85% during LCD (0.5 ± 0.4 particles cm^{-3} s^{-1}) as compared to BAU (3.7 ± 3.6 particles cm^{-3} s^{-1}).

We further investigate the potential causes of reduced NPF&G during LCD. Figure 7 shows the median diurnal variations of air pollutants such as SO_2, NH_3, NO_2, O_3, carbon monoxide (CO), and $PM_{2.5}$, and ratios of aromatic hydrocarbons such as toluene to benzene ratio (T/B) and xylene to benzene ratio (X/B). The oxidation of SO_2 produces sulfuric acid, which is the major contributor to nanoparticle formation and growth by clustering with other vapors such as ammonia, amines, or organics (Almeida et al., 2013; J. Kirkby et al., 2011; Schobesberger et al., 2013; Yu et al., 2012) and growth (Vakkari et al., 2015; Yue et al., 2010). SO_2 concentrations were comparable between NPF&G and non-event days both during LCD and BAU (Figure 7a), which further corroborates our finding of similar sub-3 nm particle formation rates and growth rates both during LCD and BAU (Figure 6). NH_3 concentrations were slightly lower during LCD than BAU, particularly on NPF&G event days (Figure 7b). Surprisingly, the daytime NO_2 concentrations were somewhat higher but less variable during LCD than BAU. NO_x undergoes a series of photochemical reactions to produce O_3, which was higher during BAU than LCD. While O_3 was higher on NPF&G events than non-events during BAU, it was lower on NPF&G events than non-events during LCD. As expected, CO and $PM_{2.5}$ concentrations were significantly lower during LCD than BAU. Urban atmospheres often constitute anthropogenic VOCs such as benzene, toluene and xylene, which are essential precursors for secondary organic aerosol formation (Molteni et al., 2018). The toluene to benzene ratio (T/B), with values within the range of 1.5–3.0 can be used as a marker of traffic emission (Khoder, 2007; Lee et al., 2002). The T/B ratio greater than 4.5 indicates industrial-originated emission sources (Tiwari et al., 2010). The xylene to benzene ratio (X/B) is used as an indicator of the photochemical age of an air mass (Zhang et al., 2008), with the ratio values less than 3.0 indicating aged plumes (Tiwari et al., 2010). The T/B ratio values

21698996, 2022, 2, Downloaded from https://agupubs.onlinelibrary.wiley.com/doi/10.1029/2021JD035392, Wiley Online Library on [13/12/2023]. See the Terms and Conditions (https://onlinelibrary.wiley.com/terms-and-conditions) on Wiley Online Library for rules of use; OA articles are governed by the applicable Creative Commons License

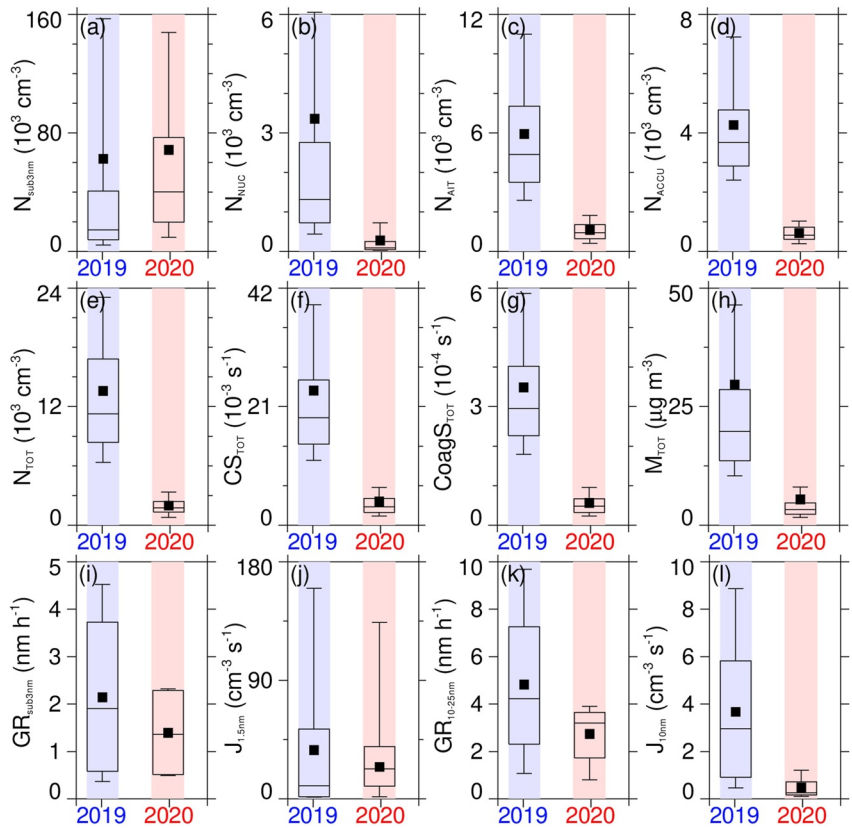

Figure 6. Box-whisker plot of NPF&G characteristics during BAU and LCD; (a) $N_{sub\text{-}3nm}$, (b) N_{NUC}, (c) N_{AIT}, (d) N_{ACCU}, (e) N_{TOT}, (f) CS_{TOT}, (g) $CoagS_{TOT}$, (h) M_{TOT}, (i) $GR_{sub\text{-}3nm}$, (j) $J_{1.5nm}$, (k) $GR_{10\text{-}25nm}$, and (l) J_{10nm}. The black square symbol indicates the mean, the horizontal line indicates the median, the bottom and top of the box indicate 25th and 75th percentile values, respectively, and the bottom and top of the whisker indicate the 10th and 90th percentiles values, respectively.

were well within the range of 1.5–3.0 on both NPF&G and non-event days during BAU, indicating traffic-dominated emission sources, whereas the T/B ratio values sharply increased on NPF&G event days during LCD, indicating emission sources from essential services such as power plants and petrochemical industries. The X/B ratio values were around 0.5 on both NPF&G and non-event days both during BAU and LCD, indicating that this site experiences aged air mass plumes. A recent study found fast secondary inorganic aerosol formation (mostly nitrate, >80%) in aged plumes in Shanghai during the enforced lockdown, but the regional transport hindered atmospheric new particle formation and growth (Chang et al., 2020). It can be concluded from the above discussion that the sub-3 nm particle formation was not limited by the reduction in primary anthropogenic emissions during LCD, but the regional NPF&G events were reduced, perhaps due to the lower concentrations of condensable vapors from decreased primary anthropogenic emissions (e.g., vehicular emissions) during LCD. NPF&G is also strongly modulated by the underlying atmospheric condition (Kanawade et al., 2012; Stanier et al., 2004), which we discuss below.

Figure 8 shows the median diurnal variation in meteorological parameters, such as temperature, relative humidity, wind speed, wind direction and solar radiation. The air temperature was lower by about 5°–7°C during LCD than BAU. The lower temperature corresponds to the low extent of oxidation and thus low yields of highly oxygenated products in the gas-phase for condensational growth (Stolzenburg et al., 2018), leading to reduced particle growth during LCD. The RH was higher by 3%–6% on NPF&G event days during LCD compared to BAU. This relatively minor change may not have contributed to differences that we see between LCD and BAU NPF&G events. The wind speed was slightly higher on NPF&G event days during BAU than LCD. Previous studies showed that high wind speed enhances NPF&G in an urban environment by removing pre-existing particles (Pushpawela et al., 2019). The wind direction and solar radiation on NPF&G event days were comparable between LCD and

21698996, 2022, 2, Downloaded from https://agupubs.onlinelibrary.wiley.com/doi/10.1029/2021JD035392, Wiley Online Library on [13/12/2023]. See the Terms and Conditions (https://onlinelibrary.wiley.com/terms-and-conditions) on Wiley Online Library for rules of use; OA articles are governed by the applicable Creative Commons License

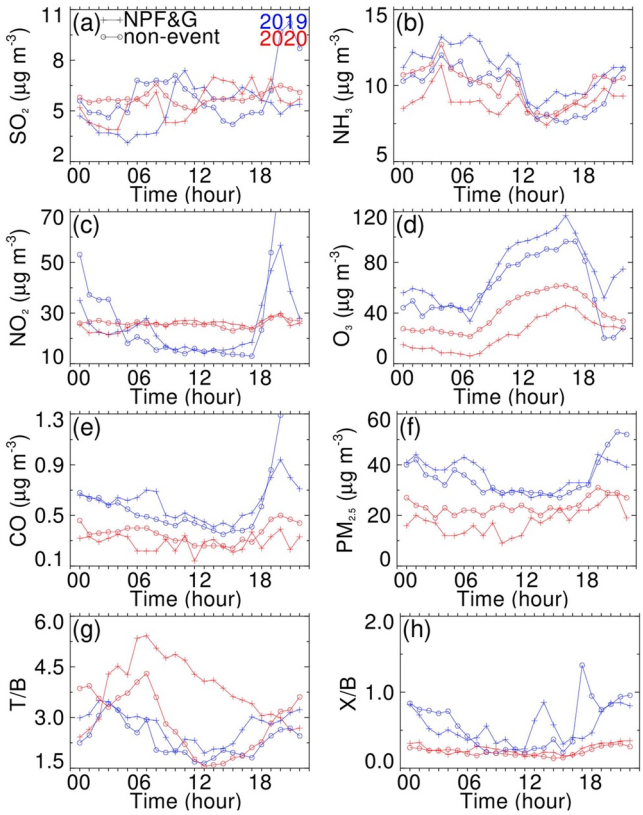

Figure 7. Median diurnal variation of (a) sulfur dioxide, (b) ammonia, (c) nitrogen dioxide, (d) ozone, (e) carbon monoxide, (f) $PM_{2.5}$, (g) T/B ratio, and (h) X/B ratio for NPF&G and non-events during BAU and LCD.

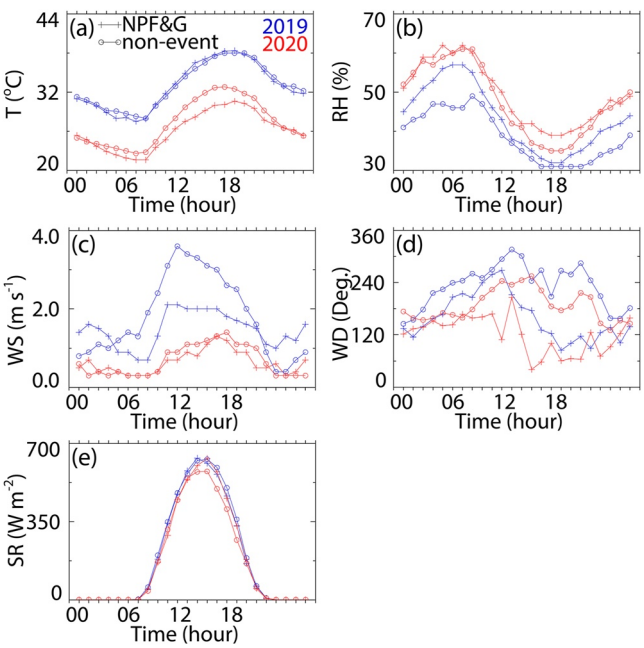

Figure 8. Median diurnal variation of (a) temperature, (b) relative humidity, (c) wind speed, (d) wind direction, and (e) solar radiation for NPF&G and non-events during BAU and LCD.

BAU. From the above discussion, it can be concluded that the lower temperature and lower wind speed may have further contributed to the inhibition of NPF&G at this site during LCD.

4. Discussions

COVID-19 enforced lockdown provided a unique and rare opportunity to detect, attribute, and understand the impacts of anthropogenic emissions on the Earth's atmosphere from regional to global scale (Forster et al., 2020; Kroll et al., 2020; Liu et al., 2020). For instance, Forster et al. (2020) estimated a global cooling of about 0.01 ± 0.005°C by 2030 compared to baseline scenarios due to pandemic-driven anthropogenic emission reductions. Thomas et al. (2021) estimated about 20%–25% reduction in aerosol-induced forcing over the Indo-Gangetic Plain outflow region of the Bay of Bengal owing to COVID-19 imposed lockdown over India. A long-term (15 years) study at an urban background site in Pittsburgh, Pennsylvania, showed about 70% reduction in ultrafine particle number concentrations due to the dramatic reduction in anthropogenic emissions during lockdown (Saha et al., 2018). The study at two sites (urban background and coastal) in Southern Italy based on long-term (2015–2019) and 2020 in the same period also showed 6%–53% and 2%–17% reductions in nucleation mode and Aitken mode particle number concentrations during the lockdown, respectively (Dinoi et al., 2021). The number concentrations of particles between 10 and 40 nm were also reduced by about 32% in an urban environment (Raleigh, NC, USA) during the COVID-19 pandemic (Zimmerman et al., 2020). Concurrently, our analyses also showed about 85% reductions in ultrafine particle number concentrations in Hyderabad.

On the contrary, a recent study in Himalayan coniferous forests in India showed the doubling of secondary organic formation during the COVID-19 lockdown, owing to higher O_3 concentration promoted photochemical oxidation of biogenic VOCs (Chatterjee et al., 2021). Recent studies in China also showed elevated secondary aerosol formation under reduced anthropogenic emissions during COVID-19 lockdowns (Huang et al., 2021; Le et al., 2020; Shen et al., 2021; Sun et al., 2020; Zhong et al., 2021). The response of primary aerosol emissions to COVID-19 lockdown is linear, but the large fraction of aerosols is secondary in nature, produced when gas-phase species react to form products of low volatility to condense into the particle phase (Kroll et al., 2020). Such chemical transformation adds additional complexity to attribute the impact of COVID-19 lockdown on air pollution.

NPF&G frequently occurs during spring (March-April-May) owing to active photochemistry associated with intense solar radiation creating the necessary condition for NPF (Birmili et al., 2000). However, NPF&G was inhibited during the COVID-19 enforced lockdown, with a three-fold lower frequency during LCD than BAU. NPF usually starts with sulfuric acid (SO_2+OH) in most environments. But clusters containing sulfuric acid need to be stabilized by other gaseous compounds like NH_3, extremely low volatile organic compounds (ELVOCs), and air ions (Bianchi et al., 2016; Kirkby et al., 2016; Sipilä et al., 2016). The oxidation reactions of VOCs with O_3 and OH can produce condensable vapors that contribute significantly to particle growth (Paasonen et al., 2018), but the considerably lower temperature (5°–7°C) indicates reduced OH concentrations and thereby low production of sulfuric acid and other condensable vapors during the lockdown. This suggests that meteorological variabilities can also lead to anomalies in the concentrations

21698996, 2022, 2, Downloaded from https://agupubs.onlinelibrary.wiley.com/doi/10.1029/2021JD035392, Wiley Online Library on [13/12/2023]. See the Terms and Conditions (https://onlinelibrary.wiley.com/terms-and-conditions) on Wiley Online Library for rules of use; OA articles are governed by the applicable Creative Commons License

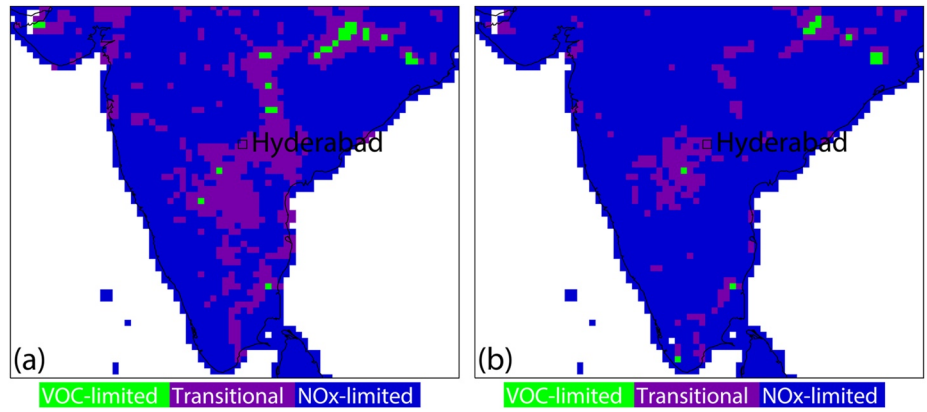

Figure 9. Ozone formation sensitivity in India during (a) BAU and (b) LCD.

of chemical species required for NPF&G. Therefore, the lower O_3 and OH concentrations indicate the reduced production of low volatility organic vapors for particle growth by condensation and thus inhibiting regional NPF&G events.

Le et al. (2020) recently reported remarkably high air pollution levels during the COVID-19 lockdown in northern China. Using synergistic observations analyses and model simulations, *Le and colleagues* showed that nonlinear production chemistry and reduced NO_2 results in enhanced O_3 in urban areas, further increasing the atmospheric oxidizing capacity and facilitating secondary aerosol formation under anomalously high humidity, stagnant airflow and uninterrupted emission from power plants and petrochemical facilities during the lockdown. The ozone sensitivity to the concentrations of VOCs and NO_x is complex and nonlinear (Kroll et al., 2020), and it can be defined by the ratio of HCHO to NO_2 (FNR). An FNR smaller than 2.3 indicates the VOC-limited regime, an FNR higher than 4.2 indicates the NOx-limited regime, and the FNR between 2.3 and 4.2 reflects the transition between the two regimes (Wang et al., 2021). At low NOx concentrations, the O_3 formation varies linearly with NOx and is independent of VOC concentration, referred to as the NOx-limited regime. At low VOC concentrations, the O_3 formation is inversely proportional to NOx and varies linearly with VOC, referred to as a VOC-limited regime for O_3 formation (Sillman et al., 1990). India falls mainly in a NOx-limited regime (Figure 9), which reduces ambient O_3 concentrations. This substantiates our findings of reduced O_3 concentrations at our site. The NOx-limited regime covers more geographical regions over India during the LCD than BAU. This corroborates the previous discussion of the low abundance of condensable vapors for growth of freshly formed particles during LCD than BAU.

5. Conclusions

Here, ambient measurements of particle number size distributions, air pollutants and meteorological parameters were carried out at the University of Hyderabad campus site in Hyderabad, India, between 15 April to 31 May 2020 (LCD) and 15 April to 31 May 2019 (BAU) to investigate the influence of COVID-19 enforced lockdown on NPF&G events. Particle number size distributions were measured in the size range of 1.2–3.0 nm and 10–514 nm. The formation of sub-3 nm particles frequently occurred during LCD and BAU, but the occurrence of the regional NPF&G events was decreased by three-fold during LCD (15% as compared to 47% during BAU of the total valid observation days). The formation rates and growth rates of sub-3 nm particles were comparable between LCD and BAU. The number concentrations of sub-3 nm particles were also comparable between LCD and BAU. But, the number concentrations of nucleation mode, Aitken mode and accumulation mode particles were reduced by approximately 85% on NPF&G event days during LCD than BAU. The ozone sensitivity analysis revealed that India falls mainly in the NOx-limited regime, which reduces ambient O_3 concentrations. Temperature was considerably lower (5°–7°C) during LCD than BAU. Analysis of anthropogenic aromatic hydrocarbons also indicated the reduced emissions of anthropogenic VOCs owing to primary emission reductions (e.g., vehicular) during LCD. Thus, the lower O_3 concentrations and lower temperature can significantly reduce atmospheric oxidation capacity and thus the production of low volatility organic vapors for growth of freshly formed particles and thereby suppressing NPF&G events at this site during LCD.

21698996, 2022, 2, Downloaded from https://agupubs.onlinelibrary.wiley.com/doi/10.1029/2021JD035392, Wiley Online Library on [13/12/2023]. See the Terms and Conditions (https://onlinelibrary.wiley.com/terms-and-conditions) on Wiley Online Library for rules of use; OA articles are governed by the applicable Creative Commons License

21698996, 2022, 2, Downloaded from https://agupubs.onlinelibrary.wiley.com/doi/10.1029/2021JD035392, Wiley Online Library on [13/12/2023]. See the Terms and Conditions (https://onlinelibrary.wiley.com/terms-and-conditions) on Wiley Online Library for rules of use; OA articles are governed by the applicable Creative Commons License

Our observations highlight that the reduced anthropogenic emissions during lockdown favor suppression of NPF&G at this tropical urban site. The secondary formation of aerosols is essentially linked to emission and atmospheric conditions. These linkages are highly nonlinear and challenging to disentangle. The COVID-19 lockdown-induced emission changes provided a unique opportunity to experiment on the future anthropogenic emission reduction scenario and improve our understanding of these linkages and associated air pollution. The secondary aerosol formation exhibits varying changes from one location to another from what has been observed for anthropogenic NO_2 or aerosol emissions. Nonetheless, these and previously published results provide some insight into the chemical nature of the atmosphere and its consequent effects on air quality.

Data Availability Statement

nCNC, SMPS, trace gases, and meteorological data sets are archived at http://dx.doi.org/10.17632/65f8wnkfc9.1.

Acknowledgments
V.P. Kanawade would like to thank the Department of Science & Technology (DST)-SERB Grant (ECR/2016/001333) and Department of Science & Technology–Climate Change Programme Division (Aerosol/89/2017) for financial support to carry out this study. The authors gratefully acknowledge the NOAA Air Resources Laboratory (ARL) for the provision of the HYSPLIT transport and dispersion model used in this publication. The authors acknowledge Copernicus Open Access Hub for the unrestricted access to Sentinel-5P TROPOMI L2 retrieved NO_2 and HCHO column data. The authors thank Abin Thomas for helping with TROPOMI data analysis. The authors also thank three anonymous reviewers and Associate Editor for their constructive comments and suggestions.

References

Almeida, J., Schobesberger, S., Kürten, A., Ortega, I. K., Kupiainen-Määttä, O., Praplan, A. P., et al. (2013). Molecular understanding of sulphuric acid-amine particle nucleation in the atmosphere. *Nature*, *502*(7471), 359–363. https://doi.org/10.1038/nature12663

Bianchi, F., Tröstl, J., Junninen, H., Frege, C., Henne, S., Hoyle, C. R., et al. (2016). New particle formation in the free troposphere: A question of chemistry and timing. *Science*, *352*(6289), 1109–1112. https://doi.org/10.1126/science.aad5456

Birmili, W., Wiedensohler, A., Plass-Dülmer, C., & Berresheim, H. (2000). Evolution of newly formed aerosol particles in the continental boundary layer: A case study including OH and H2SO4 measurements. *Geophysical Research Letters*, *27*(15), 2205–2208. https://doi.org/10.1029/1999GL011334

Boersma, K. F., Eskes, H. J., Dirksen, R. J., van der A, R. J., Veefkind, J. P., Stammes, P., et al. (2011). An improved tropospheric NO_2 column retrieval algorithm for the ozone monitoring instrument. *Atmospheric Measurement Techniques*, *4*(9), 1905–1928. https://doi.org/10.5194/amt-4-1905-2011

Boersma, K. F., Eskes, H. J., Richter, A., De Smedt, I., Lorente, A., Beirle, S., et al. (2018). Improving algorithms and uncertainty estimates for satellite NO_2 retrievals: Results from the quality assurance for the essential climate variables (QA4ECV) project. *Atmospheric Measurement Techniques*, *11*(12), 6651–6678. https://doi.org/10.5194/amt-11-6651-2018

Chan, T., Cai, R., Ahonen, L. R., Liu, Y., Zhou, Y., Vanhanen, J., et al. (2020). Assessment of particle size magnifier inversion methods to obtain the particle size distribution from atmospheric measurements. *Atmospheric Measurement Techniques*, *13*(9), 4885–4898. https://doi.org/10.5194/amt-13-4885-2020

Chang, Y., Huang, R., Ge, X., Huang, X., Hu, J., Duan, Y., et al. (2020). Puzzling haze events in China during the Coronavirus (COVID-19) shutdown. *Geophysical Research Letters*, *47*(12), e2020GL088533. https://doi.org/10.1029/2020GL088533

Chatterjee, A., Mukherjee, S., Dutta, M., Ghosh, A., Ghosh, S. K., & Roy, A. (2021). High rise in carbonaceous aerosols under very low anthropogenic emissions over eastern Himalaya, India: Impact of lockdown for COVID-19 outbreak. *Atmospheric Environment*, *244*, 117947. https://doi.org/10.1016/j.atmosenv.2020.117947

Chauhan, A., & Singh, R. P. (2020). Decline in PM2.5 concentrations over major cities around the world associated with COVID-19. *Environmental Research*, *187*, 109634. https://doi.org/10.1016/j.envres.2020.109634

Dal Maso, M., Kulmala, M., Riipinen, I., & Wagner, R. (2005). Formation and growth of fresh atmospheric aerosols: Eight years of aerosol size distribution data from SMEAR II, Hyytiälä, Finland. *Boreal Environment Research*, *10*, 323–336.

De Smedt, I., Theys, N., Yu, H., Danckaert, T., Lerot, C., Compernolle, S., et al. (2018). Algorithm theoretical baseline for formaldehyde retrievals from S5P TROPOMI and from the QA4ECV project. *Atmospheric Measurement Techniques*, *11*(4), 2395–2426. https://doi.org/10.5194/amt-11-2395-2018

Dinoi, A., Gulli, D., Ammoscato, I., Calidonna, C. R., & Contini, D. (2021). Impact of the coronavirus pandemic lockdown on atmospheric nanoparticle concentrations in two sites of Southern Italy. *Atmosphere*, *12*(3). https://doi.org/10.3390/atmos12030352

Draxler, R. R., & Rolph, G. D. (2010). HYSPLIT—HYbrid Single-particle Lagrangian integrated trajectory model. Retrieved From http://ready.arl.noaa.gov/HYSPLIT.php

Ehn, M., Thornton, J. A., Kleist, E., Sipilä, M., Junninen, H., Pullinen, I., et al. (2014). A large source of low-volatility secondary organic aerosol. *Nature*, *506*(7489), 476–479. https://doi.org/10.1038/nature13032

Forster, P. M., Forster, H. I., Evans, M. J., Gidden, M. J., Jones, C. D., Keller, C. A., et al. (2020). Current and future global climate impacts resulting from COVID-19. *Nature Climate Change*, *10*(10), 913–919. https://doi.org/10.1038/s41558-020-0883-0

Gkatzelis, G. I., Gilman, J. B., Brown, S. S., Eskes, H., Gomes, A. R., Lange, A. C., et al. (2021). The global impacts of COVID-19 lockdowns on urban air pollution: A critical review and recommendations. *Elementa: Science of the Anthropocene*, *9*(1). https://doi.org/10.1525/elementa.2021.00176

Griffin, D., Zhao, X., McLinden, C. A., Boersma, F., Bourassa, A., Dammers, E., et al. (2019). High-resolution mapping of nitrogen dioxide with TROPOMI: First results and validation over the Canadian oil sands. *Geophysical Research Letters*, *46*(2), 1049–1060. https://doi.org/10.1029/2018GL081095

Gunthe, S. S., Swain, B., Patra, S. S., & Amte, A. (2020). On the global trends and spread of the COVID-19 outbreak: Preliminary assessment of the potential relation between location-specific temperature and UV index. *Journal of Public Health*, *30*, 219–228. https://doi.org/10.1007/s10389-020-01279-y

Huang, X., Ding, A., Gao, J., Zheng, B., Zhou, D., Qi, X., et al. (2021). Enhanced secondary pollution offset reduction of primary emissions during COVID-19 lockdown in China. *National Science Review*, *8*(2). https://doi.org/10.1093/nsr/nwaa137

Kanawade, V. P., Benson, D. R., & Lee, S.-H. (2012). Statistical analysis of 4-year observations of aerosol sizes in a semi-rural continental environment. *Atmospheric Environment*, *59*, 30–38. https://doi.org/10.1016/j.atmosenv.2012.05.047

Kanawade, V. P., Tripathi, S. N., Chakraborty, A., & Yu, H. (2020). Chemical characterization of sub-micron aerosols during new particle formation in an urban atmosphere. *Aerosol and Air Quality Research*, *20*(6), 1294–1305. https://doi.org/10.4209/aaqr.2019.04.0196

Kangasluoma, J., Kuang, C., Wimmer, D., Rissanen, M. P., Lehtipalo, K., Ehn, M., et al. (2014). Sub-3 nm particle size and composition dependent response of a nano-CPC battery. *Atmospheric Measurement Techniques*, *7*(3), 689–700. https://doi.org/10.5194/amt-7-689-2014

Kerminen, V.-M., Pirjola, L., & Kulmala, M. (2001). How significantly does coagulation scavenging limit atmospheric particle production? *Journal of Geophysical Research*, *106*, 24119–24125. https://doi.org/10.1029/2001jd000322

Khoder, M. I. (2007). Ambient levels of volatile organic compounds in the atmosphere of Greater Cairo. *Atmospheric Environment*, *41*(3), 554–566. https://doi.org/10.1016/j.atmosenv.2006.08.051

Kirkby, J., Curtius, J., Almeida, J., Dunne, E., Duplissy, J., Ehrhart, S., et al. (2011). Role of sulphuric acid, ammonia and galactic cosmic rays in atmospheric aerosol nucleation. *Nature*, *476*(7361), 429–433. https://doi.org/10.1038/nature10343

Kirkby, J., Duplissy, J., Sengupta, K., Frege, C., Gordon, H., Williamson, C., et al. (2016). Ion-induced nucleation of pure biogenic particles. *Nature*, *533*(7604), 521–526. https://doi.org/10.1038/nature17953

Kroll, J. H., Heald, C. L., Cappa, C. D., Farmer, D. K., Fry, J. L., Murphy, J. G., & Steiner, A. L. (2020). The complex chemical effects of COVID-19 shutdowns on air quality. *Nature Chemistry*, *12*(9), 777–779. https://doi.org/10.1038/s41557-020-0535-z

Kulmala, M., Kontkanen, J., Junninen, H., Lehtipalo, K., Manninen, H. E., Nieminen, T., et al. (2013). Direct observations of atmospheric aerosol nucleation. *Science*, *339*(6122), 943–946. https://doi.org/10.1126/science.1227385

Kulmala, M., Petäjä, T., Nieminen, T., Sipilä, M., Manninen, H. E., Lehtipalo, K., et al. (2012). Measurement of the nucleation of atmospheric aerosol particles. *Nature Protocols*, *7*(9), 1651–1667. https://doi.org/10.1038/nprot.2012.091

Le, T., Wang, Y., Liu, L., Yang, J., Yung, Y. L., Li, G., & Seinfeld, J. H. (2020). Unexpected air pollution with marked emission reductions during the COVID-19 outbreak in China. *Science*, *369*(6504), 702–706. https://doi.org/10.1126/science.abb7431

Lee, S. C., Chiu, M. Y., Ho, K. F., Zou, S. C., & Wang, X. (2002). Volatile organic compounds (VOCs) in urban atmosphere of Hong Kong. *Chemosphere*, *48*(3), 375–382. https://doi.org/10.1016/S0045-6535(02)00040-1

Lehtinen, K. E. J., & Kulmala, M. (2003). A model for particle formation and growth in the atmosphere with molecular resolution in size. *Atmospheric Chemistry and Physics*, *3*(1), 251–257. https://doi.org/10.5194/acp-3-251-2003

Liu, F., Page, A., Strode, S. A., Yoshida, Y., Choi, S., Zheng, B., et al. (2020). Abrupt decline in tropospheric nitrogen dioxide over China after the outbreak of COVID-19. *Science Advances*, *6*(28), eabc2992. https://doi.org/10.1126/sciadv.abc2992

Maher, E. F., & Laird, N. M. (1985). EM algorithm reconstruction of particle size distributions from diffusion battery data. *Journal of Aerosol Science*, *16*(6), 557–570. https://doi.org/10.1016/0021-8502(85)90007-2

Metya, A., Dagupta, P., Halder, S., Chakraborty, S., & Tiwari, Y. K. (2020). COVID-19 lockdowns improve air quality in the South-East Asian regions, as seen by the remote sensing satellites. *Aerosol and Air Quality Research*, *20*(8), 1772–1782. https://doi.org/10.4209/aaqr.2020.05.0240

Molteni, U., Bianchi, F., Klein, F., El Haddad, I., Frege, C., Rossi, M. J., et al. (2018). Formation of highly oxygenated organic molecules from aromatic compounds. *Atmospheric Chemistry and Physics*, *18*(3), 1909–1921. https://doi.org/10.5194/acp-18-1909-2018

Mylläri, F., Asmi, E., Anttila, T., Saukko, E., Vakkari, V., Pirjola, L., et al. (2016). New particle formation in the fresh flue-gas plume from a coal-fired power plant: Effect of flue-gas cleaning. *Atmospheric Chemistry and Physics*, *16*(11), 7485–7496. https://doi.org/10.5194/acp-16-7485-2016

Nieminen, T., Kerminen, V.-M., Petäjä, T., Aalto, P. P., Arshinov, M., Asmi, E., et al. (2018). Global analysis of continental boundary layer new particle formation based on long-term measurements. *Atmospheric Chemistry and Physics*, *18*(19), 14737–14756. https://doi.org/10.5194/acp-18-14737-2018

Paasonen, P., Peltola, M., Kontkanen, J., Junninen, H., Kerminen, V. M., & Kulmala, M. (2018). Comprehensive analysis of particle growth rates from nucleation mode to cloud condensation nuclei in boreal forest. *Atmospheric Chemistry and Physics*, *18*(16), 12085–12103. https://doi.org/10.5194/acp-18-12085-2018

Pushpawela, B., Jayaratne, R., & Morawska, L. (2019). The influence of wind speed on new particle formation events in an urban environment. *Atmospheric Research*, *215*, 37–41. https://doi.org/10.1016/j.atmosres.2018.08.023

Rönkkö, T., Kuuluvainen, H., Karjalainen, P., Keskinen, J., Hillamo, R., Niemi, J. V., et al. (2017). Traffic is a major source of atmospheric nanocluster aerosol. *Proceedings of the National Academy of Sciences*, *114*. https://doi.org/10.1073/pnas.1700830114

Saha, P. K., Robinson, E. S., Shah, R. U., Zimmerman, N., Apte, J. S., Robinson, A. L., & Presto, A. A. (2018). Reduced ultrafine particle concentration in urban air: Changes in nucleation and anthropogenic emissions. *Environmental Science & Technology*, *52*(12), 6798–6806. https://doi.org/10.1021/acs.est.8b00910

Sathe, Y., Gupta, P., Bawase, M., Lamsal, L., Patadia, F., & Thipse, S. (2021). Surface and satellite observations of air pollution in India during COVID-19 lockdown: Implication to air quality. *Sustainable Cities and Society*, *66*, 102688. https://doi.org/10.1016/j.scs.2020.102688

Schobesberger, S., Junninen, H., Bianchi, F., Lonn, G., Ehn, M., Lehtipalo, K., et al. (2013). Molecular understanding of atmospheric particle formation from sulfuric acid and large oxidized organic molecules. *Proceedings of the National Academy of Sciences*, *110*(43), 17223–17228. https://doi.org/10.1073/pnas.1306973110

Sebastian, M., Kanawade, P., & Pierce, J. R. (2021). Observation of sub-3 nm particles and new particle formation at an urban location in India. *Atmospheric Environment*, *256*, 118460. https://doi.org/10.1016/j.atmosenv.2021.118460

Sharma, S., Zhang, M., Anshika, M., Gao, J., Zhang, H., & Kota, S. H. (2020). Effect of restricted emissions during COVID-19 on air quality in India. *Science of the Total Environment*, *728*, 138878. https://doi.org/10.1016/j.scitotenv.2020.138878

Shen, X., Sun, J., Yu, F., Zhang, X., Zhong, J., Zhang, Y., et al. (2021). Enhancement of nanoparticle formation and growth during the COVID-19 lockdown period in urban Beijing. *Atmospheric Chemistry and Physics*, *21*, 70391–70521. https://doi.org/10.5194/acp-21-7039-2021

Sillman, S., Logan, J. A., & Wofsy, S. C. (1990). The sensitivity of ozone to nitrogen oxides and hydrocarbons in regional ozone episodes. *Journal of Geophysical Research*, *95*(D2), 1837–1851. https://doi.org/10.1029/JD095iD02p01837

Sipilä, M., Sarnela, N., Jokinen, T., Henschel, H., Junninen, H., Kontkanen, J., et al. (2016). Molecular-scale evidence of aerosol particle formation via sequential addition of HIO_3. *Nature*, *537*(7621), 532–534. https://doi.org/10.1038/nature19314

Sohrabi, C., Alsafi, Z., O'Neill, N., Khan, M., Kerwan, A., Al-Jabir, A., et al. (2020). World health organization declares global emergency: A review of the 2019 novel coronavirus (COVID-19). *International Journal of Surgery*, *76*, 71–76. https://doi.org/10.1016/j.ijsu.2020.02.034

Srivastava, A. (2021). COVID-19 and air pollution and meteorology-an intricate relationship: A review. *Chemosphere*, *263*, 128297. https://doi.org/10.1016/j.chemosphere.2020.128297

Srivastava, A. K., Bhoyar, P. D., Kanawade, V. P., Devara, P. C. S., Thomas, A., & Soni, V. K. (2021). Improved air quality during COVID-19 at an urban megacity over the Indo-Gangetic Basin: From stringent to relaxed lockdown phases. *Urban Climate*, *36*, 100791. https://doi.org/10.1016/j.uclim.2021.100791

Stanier, C. O., Khlystov, A. Y., & Pandis, S. N. (2004). Ambient aerosol size distributions and number concentrations measured during the Pittsburgh Air Quality Study (PAQS). *Atmospheric Environment*, *38*(20), 3275–3284. https://doi.org/10.1016/j.atmosenv.2004.03.020

21698996, 2022, 2, Downloaded from https://agupubs.onlinelibrary.wiley.com/doi/10.1029/2021JD035392, Wiley Online Library on [13/12/2023]. See the Terms and Conditions (https://onlinelibrary.wiley.com/terms-and-conditions) on Wiley Online Library for rules of use; OA articles are governed by the applicable Creative Commons License

Stolzenburg, D., Fischer, L., Vogel, A. L., Heinritzi, M., Schervish, M., Simon, M., et al. (2018). Rapid growth of organic aerosol nanoparticles over a wide tropospheric temperature range. *Proceedings of the National Academy of Sciences*, *115*(37), 9122–9127. https://doi.org/10.1073/pnas.1807604115

Sun, Y., Lei, L., Zhou, W., Chen, C., He, Y., Sun, J., et al. (2020). A chemical cocktail during the COVID-19 outbreak in Beijing, China: Insights from six-year aerosol particle composition measurements during the Chinese New Year holiday. *Science of the Total Environment*, *742*, 140739. https://doi.org/10.1016/j.scitotenv.2020.140739

Tang, L., Shang, D., Fang, X., Wu, Z., Qiu, Y., Chen, S., et al. (2021). More significant impacts from new particle formation on haze formation during COVID-19 lockdown. *Geophysical Research Letters*, *48*, e2020GL091591. https://doi.org/10.1029/2020GL091591

Thomas, A., Kanawade, V. P., Sarangi, C., & Srivastava, A. K. (2021). Effect of COVID-19 shutdown on aerosol direct radiative forcing over the Indo-Gangetic Plain outflow region of the Bay of Bengal. *Science of the Total Environment*, *782*, 146918. https://doi.org/10.1016/j.scitotenv.2021.146918

Tiwari, V., Hanai, Y., & Masunaga, S. (2010). Ambient levels of volatile organic compounds in the vicinity of petrochemical industrial area of Yokohama, Japan. *Air Quality, Atmosphere & Health*, *3*(2), 65–75. https://doi.org/10.1007/s11869-009-0052-0

Tröstl, J., Chuang, W. K., Gordon, H., Heinritzi, M., Yan, C., Molteni, U., et al. (2016). The role of low-volatility organic compounds in initial particle growth in the atmosphere. *Nature*, *533*(7604), 527–531. https://doi.org/10.1038/nature18271

Vakkari, V., Tiitta, P., Jaars, K., Croteau, P., Beukes, J. P., Josipovic, M., et al. (2015). Reevaluating the contribution of sulfuric acid and the origin of organic compounds in atmospheric nanoparticle growth. *Geophysical Research Letters*, *42*, 10–486. https://doi.org/10.1002/2015gl066459

Veefkind, J. P., Aben, I., McMullan, K., Förster, H., de Vries, J., Otter, G., et al. (2012). TROPOMI on the ESA Sentinel-5 precursor: A GMES mission for global observations of the atmospheric composition for climate, air quality and ozone layer applications. *Remote Sensing of Environment*, *120*, 70–83. https://doi.org/10.1016/j.rse.2011.09.027

Vigouroux, C., Langerock, B., Bauer Aquino, C. A., Blumenstock, T., Cheng, Z., De Mazière, M., et al. (2020). TROPOMI–Sentinel-5 Precursor formaldehyde validation using an extensive network of ground-based Fourier-transform infrared stations. *Atmospheric Measurement Techniques*, *13*(7), 3751–3767. https://doi.org/10.5194/amt-13-3751-2020

Wang, M., Kong, W., Marten, R., He, X.-C., Chen, D., Pfeifer, J., et al. (2020). Rapid growth of new atmospheric particles by nitric acid and ammonia condensation. *Nature*, *581*(7807), 184–189. https://doi.org/10.1038/s41586-020-2270-4

Wang, W., van der A, R., Ding, J., van Weele, M., & Cheng, T. (2021). Spatial and temporal changes of the ozone sensitivity in China based on satellite and ground-based observations. *Atmospheric Chemistry and Physic*, *21*(9), 7253–7269. https://doi.org/10.5194/acp-21-7253-2021

Wang, Z. B., Hu, M., Yue, D. L., He, L. Y., Huang, X., Yang, Q., et al. (2013). New particle formation in the presence of a strong biomass burning episode at a downwind rural site in PRD, China. *Tellus B: Chemical and Physical Meteorology*, *65*(1), 19965. https://doi.org/10.3402/tellusb.v65i0.19965

Yadav, S. K., Kompalli, S. K., Gurjar, B. R., & Mishra, R. K. (2021). Aerosol number concentrations and new particle formation events over a polluted megacity during the COVID-19 lockdown. *Atmospheric Environment*, *259*, 118526. https://doi.org/10.1016/j.atmosenv.2021.118526

Yu, H., McGraw, R., & Lee, S.-H. (2012). Effects of amines on formation of sub-3 nm particles and their subsequent growth. *Geophysical Research Letters*, *39*(2). https://doi.org/10.1029/2011gl050099

Yue, D. L., Hu, M., Zhang, R. Y., Wang, Z. B., Zheng, J., Wu, Z. J., et al. (2010). The roles of sulfuric acid in new particle formation and growth in the mega-city of Beijing. *Atmospheric Chemistry and Physics*, *10*(10), 4953–4960. https://doi.org/10.5194/acp-10-4953-2010

Zhang, J., Wang, T., Chameides, W. L., Cardelino, C., Blake, D. R., & Streets, D. G. (2008). Source characteristics of volatile organic compounds during high ozone episodes in Hong Kong, Southern China. *Atmospheric Chemistry and Physics*, *8*(16), 4983–4996. https://doi.org/10.5194/acp-8-4983-2008

Zhang, M., Katiyar, A., Zhu, S., Shen, J., Xia, M., Ma, J., et al. (2021). Impact of reduced anthropogenic emissions during COVID-19 on air quality in India. *Atmospheric Chemistry and Physics*, *21*(5), 4025–4037. https://doi.org/10.5194/acp-21-4025-2021

Zhang, R., Khalizov, A., Wang, L., Hu, M., & Xu, W. (2012). Nucleation and growth of nanoparticles in the atmosphere. *Chemical Reviews*, *112*(3), 1957–2011. https://doi.org/10.1021/cr2001756

Zhao, Y., Zhang, K., Xu, X., Shen, H., Zhu, X., Zhang, Y., et al. (2020). Substantial changes in nitrogen dioxide and ozone after excluding meteorological impacts during the COVID-19 outbreak in mainland China. *Environmental Science and Technology Letters*, *7*(6), 402–408. https://doi.org/10.1021/acs.estlett.0c00304

Zhong, H., Huang, R., Chang, Y., Duan, J., Lin, C., & Chen, Y. (2021). Enhanced formation of secondary organic aerosol from photochemical oxidation during the COVID-19 lockdown in a background site in Northwest China. *Science of the Total Environment*, *778*, 144947. https://doi.org/10.1016/j.scitotenv.2021.144947

Zimmerman, A., Petters, M. D., & Meskhidze, N. (2020). Observations of new particle formation, modal growth rates, and direct emissions of sub-10 nm particles in an urban environment. *Atmospheric Environment*, *242*, 117835. https://doi.org/10.1016/j.atmosenv.2020.117835

21698996, 2022, 2, Downloaded from https://agupubs.onlinelibrary.wiley.com/doi/10.1029/2021JD035392, Wiley Online Library on [13/12/2023]. See the Terms and Conditions (https://onlinelibrary.wiley.com/terms-and-conditions) on Wiley Online Library for rules of use; OA articles are governed by the applicable Creative Commons License

Atmospheric Environment 270 (2022) 118894

Contents lists available at ScienceDirect

Atmospheric Environment

journal homepage: www.elsevier.com/locate/atmosenv

Atmospheric new particle formation in India: Current understanding and knowledge gaps

Vijay P. Kanawade [a,*], Mathew Sebastian [a], Rakesh K. Hooda [b], Antti-Pekka Hyvärinen [b]

[a] Centre for Earth, Ocean, and Atmospheric Sciences, University of Hyderabad, Hyderabad, India
[b] Finnish Meteorological Institute, Erik Palmenin Aukio 1, Helsinki, Finland

HIGHLIGHTS

- We synthesized the current understanding of atmospheric new particle formation in India.
- Very little is known on physiochemical processes driving new particle formation in India.
- We identified the critical knowledge gaps on new particle formation in India.

ARTICLE INFO

Keywords:
Gas-to-particle conversion
New particle formation
Chemical mechanisms
Haze
Formation
Air quality

ABSTRACT

Atmospheric new particle formation (NPF), via gas-to-particle conversion, is the largest source of aerosol numbers to the terrestrial atmosphere. NPF produces about half of the present-day cloud condensation nuclei (CCN), thus significantly influencing cloud properties and Earth's energy budget. But, observations of NPF are scarce globally, particularly in India. The first-ever evidence of NPF in India was reported in 2005. To the best of our knowledge, there are only 22 published papers to date based on independent field campaigns and long-term field observations in India. These studies reported the key characteristics of NPF, such as frequency of occurrence of NPF, particle formation rate, growth rate, and atmospheric conditions influencing NPF. Very little is known about the chemical mechanisms responsible for NPF in India because field observations using state-of-the-art instruments (e.g., CI-APi-TOF, EESI-TOF) are not available for real-time identification and quantification of gas-phase and particle-phase compounds in the air. Therefore, this review focuses on the observed characteristics of NPF in different environments and identifies critical knowledge gaps for future NPF studies in India. We recommend a measurement network of aerosol and precursor concentrations in different environments using the recently developed state-of-the-art instruments aided with regional model simulations, incorporated with the nucleation schemes based on the laboratory experiments (CLOUD), to interpret field measurements.

1. Introduction

Atmospheric new particle formation (NPF) refers to the formation of secondary aerosols from gaseous vapours that undergo gas-to-particle (GTP) conversion (Friedlander, 1977). NPF starts with the formation of a thermodynamically stable cluster (diameter <3 nm) from multi-component systems, which then grows to detectable size in the atmosphere (Kulmala et al., 2000; Zhang, 2010). NPF often occurs over a spatial scale of a few hundreds of kilometres and at a temporal scale of 1–2 days (Kulmala et al., 2012). Over such a spatio-temporal scale, the freshly-formed particles can essentially grow to cloud condensation nuclei (CCN) active sizes (diameter >50–100 nm). However, the competition of condensational growth and coagulation scavenging determines the fate of these tiny particles, first to grow to nucleation mode (<25 nm) and Aitken mode sizes and then up to CCN active-sizes (Kerminen et al., 2004). The fraction of newly-formed particles that grow to CCN active-sizes, where they affect climate directly by scattering or absorbing solar radiation or indirectly by influencing cloud properties (Albrecht, 1989; Twomey, 1977), vary significantly around the world (Kuang et al., 2009; Sebastian et al., 2021b; Westervelt et al., 2014). Atmospheric observations show that about 10%–60% of the NPF events lead to significant CCN production depending upon the location (Asmi et al., 2011; Kerminen et al., 2018; Kuang et al., 2009; Laakso et al., 2013; Rose et al., 2017; Sebastian et al., 2021b; Yu et al., 2014;

* Corresponding author.
E-mail address: vijaykanawade03@yahoo.co.in (V.P. Kanawade).

https://doi.org/10.1016/j.atmosenv.2021.118894
Received 8 July 2021; Received in revised form 6 October 2021; Accepted 8 December 2021
Available online 10 December 2021
1352-2310/© 2021 Elsevier Ltd. All rights reserved.

Yue et al., 2011). Global modelling simulations also showed that NPF produces about half of the global CCN in the troposphere (Merikanto et al., 2009; Spracklen et al., 2008; Westervelt et al., 2014; Yu and Luo, 2009), with an estimated uncertainty range of 38–66% (Gordon et al., 2017). Such large uncertainties in the contribution of NPF to the global CCN budget, which, together with our limited understanding of aerosol-cloud interactions, can hinder the accurate estimation of radiative forcing by atmospheric aerosols. The fact that NPF is a highly non-linear dynamic process; its connection to boundary layer dynamics and haze formation in highly polluted conditions is also largely unknown (Kulmala et al., 2021). Therefore, the study of atmospheric NPF in different environments has become critically important.

GTP conversion is thought to start with sulfuric acid (H_2SO_4) in most environments, but clusters containing H_2SO_4 need to be stabilized by other gaseous compounds like ammonia (NH_3), amines, extremely low volatile organic compounds (ELVOCs) and air ions (Bianchi et al., 2016; Kirkby et al., 2016; Sipilä et al., 2016). The highly oxygenated organic molecules (HOMs) with exceedingly low vapour pressure are also involved in the GTP conversion (Bianchi et al., 2021; Ehn et al., 2014; Pospisilova et al., 2020; Riccobono et al., 2014; Schobesberger et al., 2013) or the multi-component system involving H_2SO_4 and HOMs, NH_3, amines or iodine was also shown to closely reproduce observed particle formation and growth rates (Baccarini et al., 2020; Lehtipalo et al., 2018), but their relative roles remain unclear. Several investigators indicated that condensation of organic vapours becomes more critical with growing particle size (e.g., Bonn et al., 2008; Metzger et al., 2010; Riipinen et al., 2012; Stolzenburg et al., 2018). The small clusters formed solely of ELVOCs can grow efficiently via the ion-induced nucleation pathway (Kirkby et al., 2016). Further, atmospheric ions produced by galactic cosmic rays (GCR) facilitate aerosol nucleation and growth, ultimately impacting CCN concentrations and cloud properties (Carslaw et al., 2002; Usoskin and Kovaltsov, 2008). The aerosol microphysical model incorporated with parameterised ion-induced nucleation elucidated that the ion mechanism is an important source of sub-10 nm particles in the middle and upper troposphere (Kanawade and Tripathi, 2006). Yu et al. (2018) recently developed a comprehensive kinetic H_2SO_4-H_2O-NH_3 ternary ion-mediated nucleation (TIMN) model with thermodynamic data derived from both quantum chemical calculations and laboratory experiments which predicted nucleation rates in good agreement with CLOUD experiments. In fact, a pool of sub-3nm neutral/charged clusters is often present in the atmosphere (Kulmala et al., 2007; Lehtipalo et al., 2011; Sebastian et al., 2021a), but how fast these clusters grow or are scavenged will determine whether NPF will be detected in the atmosphere. Nevertheless, the reduced evaporation rates of clusters due to stabilising agents and increasing particle growth rates boosted by the additional vapours are needed for notable atmospheric NPF (Kulmala et al., 2017).

NPF is commonly quantified by three key characteristics; the frequency of occurrence of NPF, the particle formation rate, and the particle growth rate. These characteristics are strongly coupled to aerosol precursors, pre-existing aerosol particles, and atmospheric conditions. The frequency of occurrence of NPF varies from one location to another as well as seasonally. NPF is thought to occur frequently during spring (March-April-May) and rarely during the winter (December-January-February) (Birmili et al., 2003; Dal Maso et al., 2005; Kanawade et al., 2012; Nieminen et al., 2018; Shen et al., 2011; Wu et al., 2008). Although, NPF events were also observed frequently during the winter (Kulmala et al., 2004; Lee et al., 2008; Pikridas et al., 2012) and fall (September-October-November) (Rodríguez et al., 2005). Therefore, there is not a universal pattern in the frequency of occurrence of NPF. For the observed regional NPF events, the typical formation rate of 3 nm particles varied from 0.01 to 100 particles cm^{-3} s^{-1}, although the values up to 10^4 particle cm^{-3} s^{-1} were also observed in industrial plumes and coastal regions (Kulmala et al., 2004). The typical particle growth rates were observed to vary in the range from 0.1 to 20 nm h^{-1} (Kuang et al., 2009; Kulmala et al., 2004), with some exceptional values as high as 200 nm h^{-1} in coastal regions (Nieminen et al., 2018; O'Dowd et al., 2000). The availability of condensable vapour alone does not determine the number or mass that reaches larger size because self-coagulation and coagulation scavenging can also significantly affect the particle number size distribution. The self-coagulation increases the mean size of the particle mode and simultaneously decreases the total particle number concentrations of this mode. In contrast, the coagulation scavenging does not considerably increase the size of the growing mode (Kerminen et al., 2018). All the above driving factors and characteristics have been studied extensively in field observations and laboratory experiments, but their relative roles are uncertain in different atmospheric conditions, especially with regard to the chemical species driving NPF (Bianchi et al., 2016; Bzdek and Johnston, 2010; Kulmala et al., 2014).

India is a rapidly developing country with regional hotspots of high anthropogenic aerosol loading coinciding with regions of high population density, urbanization, and industrialization. Numerous studies have revealed an increasing trend in anthropogenic aerosols over India (Babu et al., 2013; Dey and Di Girolamo, 2011; Hooda et al., 2018; Moorthy et al., 2013; Ramachandran et al., 2012; Srivastava, 2017; Thomas et al., 2019). Further, sulfur dioxide (SO_2) and nitrogen dioxide (NO_2), markers of anthropogenic emissions, have also increased by more than 100% and 50%, respectively, from 2005 to 2015 over India (Krotkov et al., 2016). While newly-formed particles can rapidly be scavenged by the high pre-existing particles (Kulmala et al., 2017), NPF has frequently been reported in the polluted boundary layer in India (Kanawade et al., 2020b; Kanawade et al., 2014c; Mönkkönen et al., 2005) and elsewhere worldwide (e.g., Kontkanen et al., 2017; Xiao et al., 2021; Yu et al., 2017; Yu et al., 2016). On the other hand, the recent studies under the reduction of primary emissions in urban areas (Delhi and Hyderabad) during COVID-19 enforced lockdown showed the reduced frequency of the occurrence of NPF (Kanawade et al., 2020a,b; Yadav et al., 2021). This indicates that the balance between precursor gaseous compounds and pre-existing particles decide when NPF will be detected in the polluted boundary layer (Gani et al., 2020; Hyvärinen et al., 2010). The higher pre-existing particles indicate precursor-laden air, but they inhibit aerosol nucleation when the condensation sink is unusually high.

The methods used for determining, analyzing, and interpreting NPF have been detailed elsewhere (e.g., Kerminen et al., 2018; Kulmala et al., 2012), which is out of the scope of this study. Kulmala et al. (2012) highlighted the state-of-the-art instrumentations, best practices, and other currently used tools to investigate NPF. Surprisingly, some of these technological advancements are presently not deployed in India to elucidate NPF, particularly gas-phase and particle-phase chemistry driving NPF. This resulted in significant knowledge gaps in NPF research in India. To the best of our knowledge, there are only 22 published papers illustrating various characteristics and driving factors of NPF (Sebastian et al., 2021a and references therein). But, the direct observational evidence of chemical species contributing to particle formation and growth and the chemical mechanisms driving atmospheric NPF in India are unknown. Therefore, this review is intended to highlight the current understanding and the critical knowledge gaps in NPF in India.

2. Measurement techniques used to study NPF in India

Atmospheric aerosol measurements can be achieved with a variety of techniques and from different platforms to measure physical (optical and dynamical) and chemical properties. The measurement of particle number size distributions has critical importance in characterizing the number, size, surface area, volume, and evolution of aerosols in the atmosphere. In practice, the direct measurements of particle number size distribution in the size range from a few nanometers to 1 μm are usually used to study NPF, which facilitates the quantification of NPF. Quantitative methods have also been developed to derive NPF characteristics from particle number size distribution measurements such as NPF frequency, particle formation rates, and growth rates (Dal Maso et al., 2005; Kulmala et al., 2004). The particle formation rate and

growth rate together quantify the strength of the NPF event. We below briefly discuss different measurement techniques used in India so far.

The differential and scanning mobility particle sizer (DMPS and SMPS, respectively) have been used to measure the particle number size distributions and have proved to be versatile in their use (Komppula et al., 2009; Wiedensohler et al., 2012). Compared to the DMPS, the SMPS gives particle number size distribution with a much higher temporal resolution, though operating with similar hardware. Mobility particle sizers are based on the principle of the mobility of a charged particle in an electric field. The particles entering the system are neutralized (using a radioactive source) such that they have a Fuchs equilibrium charge distribution. Then the widely used differential mobility analyzer (DMA) is used to classify particles according to their electrical mobility. These monodisperse particles of a given size are then counted by a condensation particle counter (CPC). In CPC, vapour from a working fluid (e.g., water or butanol) condenses onto the particles so that they grow in size and can be optically counted. The advanced SMPS using diethylene glycol (DEG)-CPC can also measure particles down to ~1 nm (Jiang et al., 2011). A typical instrument measuring particle number size distribution thus consists of a neutralizer, an electrostatic classifier, and a counter. The major advantages of mobility particle sizers are their ease of portability and significantly low power consumption. They can also be used to produce monodisperse aerosol distribution for calibrating and testing other particle instruments (e.g., CCN counter). The Aerodynamic Particle Sizer (APS) has also been used in combination with the SMPS system to obtain particle number size distribution in the wide size range (~5 nm to >10 μm). The wide range aerosol spectrometer (WRAS) is also used to obtain particle number size distributions in a wide particle size range of 5 nm–32 μm, using a combination of two technologies such as the SMPS with butanol CPC for nanoparticles and the environmental dust monitor (EDM) 180 for the large particles. The nano Condensation Nucleus Counter (nCNC Vanhanen et al., 2011) has recently been deployed in India to make observations of particle number size distributions in the size range of 1–4 nm in the urban atmosphere of Hyderabad (Sebastian et al., 2021a). The nCNC consists of a saturator flow region, a mixing section where the sample air mixes with the saturated DEG vapours and a growth section where the particles in the sample air grow with the supersaturated DEG vapours condensing onto them. First, DEG is used to grow particles, and then these particles are further grown and counted by a butanol CPC (bPCP). The nCNC can work in the scanning mode by changing the mixing ratio of the saturator and sample air to obtain particle size down to 1.2 nm. The major benefits of nCNC include its sensitivity down to ~1 nm and can detect both electrically charged and neutral particles. The charged particle number size distributions are measured with a neutral air ion spectrometer (NAIS). The measurement principle of NAIS is based on unipolar charging of the sampled particles and their subsequent detection with the electrical mobility analyzer (Mirme et al., 2007). NAIS can provide positive and negative ion distributions over a wide range of electrical mobility of 3.16–0.001 $cm^2\ V^{-1}\ s^{-1}$, corresponding to a mobility diameter range of 0.8–47 nm (Mirme and Mirme, 2013). Fig. 1 shows the geographic distribution of sites where NPF has been reported, at least once, in India, which constitutes continental India and adjoining marine areas such as the Arabian Sea, the Indian Ocean and the Bay of Bengal.

3. NPF classification schemes

The conventional classification scheme developed by Dal Maso et al. (2005) categorises a day as an NPF event, non-event or undefined, by analyzing particle number size distributions and visually inspecting them. An NPF event day displays a distinct new mode of particles with diameters smaller than 25 nm followed by the subsequent steady growth of this new mode for at least 6 h such that the particle number size

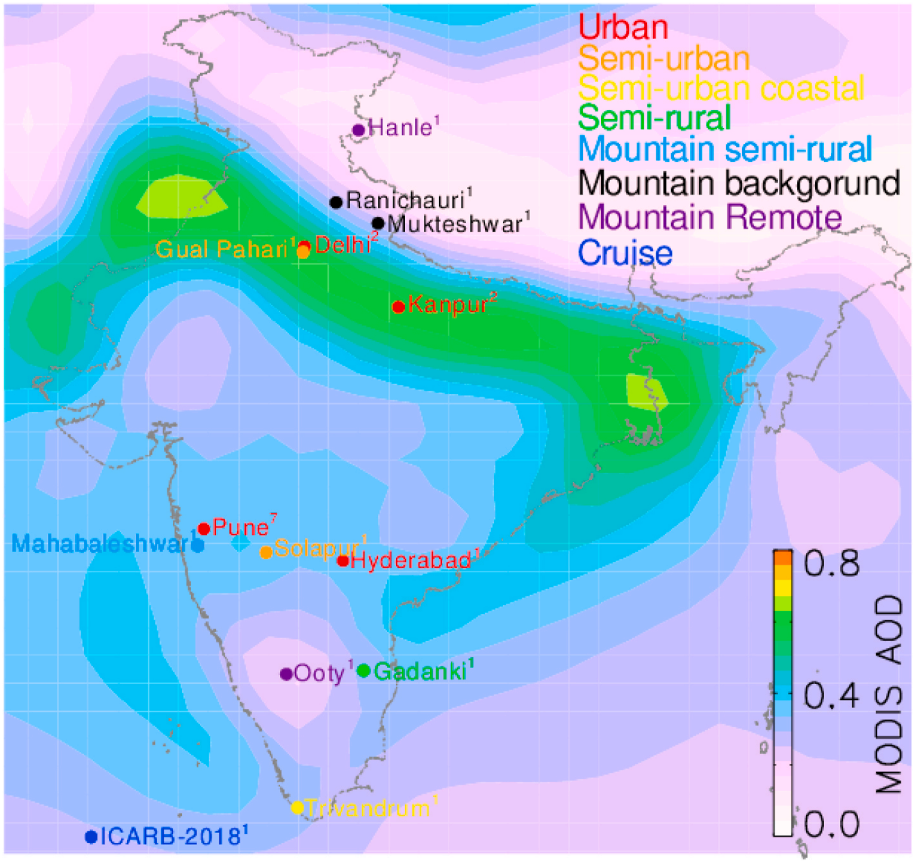

Fig. 1. Geographic distribution of sites where observations of new particle formation were reported in India. The superscript number indicates the number of studies reported at the specific site. Different colours indicate the various atmospheric environments such as urban (Delhi, Kanpur, Pune, and Hyderabad), semi-urban (Gual Pahari and Solapur), semi-urban-coastal (Trivandrum), semi-rural (Gadanki), mountain semi-rural (Mahabaleshwar), mountain background (Ranichauri and Mukteshwar), mountain remote (Ooty and Hanle), and cruise (North Indian Ocean). The filled contours indicate the climatological mean aerosol optical depth from the MODIS AQUA sensor (Remer et al., 2008), highlighting the nature of the site. (For interpretation of the references to colour in this figure legend, the reader is referred to the Web version of this article.)

distributions display a "banana-shaped" aerosol-size growth. The appearance of the "banana-shaped" curve indicates that this phenomenon is taking place over a distance of a few hundreds of kilometres in radius and is thus referred to as a regional NPF event. Typical regional NPF events from the mountain background (Mukteshwar) and polluted (Hyderabad) sites are shown in Fig. 2. NPF events are also classified as regional events, transported events, and particle bursts based on observed characteristics of sub-3nm and nucleation mode particles (Dada et al., 2018). An NPF event day can further be classified in sub-categories such as strong, moderate and weak based on the net rate of increase in nuclei mode particles ($dN_{10}/dt > 15000\ cm^{-3}\ h^{-1}$), ($4000\ cm^{-3}\ h^{-1} > dN_{10}/dt < 15000\ cm^{-3}\ h^{-1}$) and ($<4000\ cm^{-3}\ h^{-1}$), respectively (Stanier et al., 2004b) or cleaner and polluted NPF event based on anthropogenic tracer data such as black carbon (Sebastian et al., 2021b) or distinct data features. NPF events have also been classified by visually inspecting ion concentrations versus time plots into truncated-banana, hump, apple, mixed and rain-induced types (Manninen et al., 2010; Vana et al., 2008). A non-event typically shows higher particle number concentrations at sizes larger than nucleation mode (<25 nm) without any evidence of a distinct change in particle mode diameter. A day that shows particle bursts in nucleation mode, but no growth or broken aerosol growth or growth of Aitken mode (>25 nm) particles or remain unexplained is classified as an undefined event. Undefined events have also been further classified in different sub-categories such as pollution-related, ultrafine-mode peaks, Aitken-mode peaks etc., based on sulfur dioxide and nitrogen dioxide data (Buenrostro Mazon et al., 2009; Kanawade et al., 2014c). The above criteria have been used for the classification of NPF events in India.

4. Current understanding of NPF in India

Table 1 summarises measurement sites where NPF has been reported, various measurement parameters, and key NPF characteristics. NPF was reported from independent field campaigns spanned over different times (season) of the year and also long-term continuous measurements. Therefore, the comparison between sites of even similar environments cannot be made. One also needs to note that NPF studies discussed here use different technologies and setups to measure particle number size distributions and report NPF characteristics for varying particle size and/or the range of size. Further, the meteorological conditions, such as temperature, relative humidity and wind speed, can also significantly affect NPF (Birmili and Wiedensohler, 2000; Kanawade et al., 2012; Stanier et al., 2004b). A recent study showed that the meteorological condition is a more important factor in NPF occurrence at rural sites as compared to urban sites (Bousiotis et al., 2021). Still, the analysis of reported values of NPF frequency, particle formation rate, growth rate and condensation sink allowed us to draw general inferences on the current understanding of NPF in India.

The first quantity derived to quantify NPF in different environments and seasons is the frequency of occurrence of NPF. It is crucial to know how frequently NPF occurs. NPF often starts after the sunrise and diminishes by sunset in most cases, owing to the important role of photochemistry in NPF (Kerminen et al., 2018; Kulmala et al., 2004), although there are also exceptions of the sustained growth over several days (An et al., 2019; Pierce et al., 2012) and nighttime NPF (Kammer et al., 2018; Lee et al., 2008; Rose et al., 2018; Salimi et al., 2017).

Until now, NPF events have been reported in diverse environments of India, including urban sites such as Delhi, Kanpur, Hyderabad and Pune (Chate and Devara, 2005; Kamra et al., 2015; Kanawade et al., 2020b; Kanawade et al., 2014c; Mönkkönen et al., 2005; Nepolian et al., 2021; Sarangi et al., 2015; Sebastian et al., 2021a; Siingh et al., 2013, 2018; Yadav et al., 2021), semi-urban such as Gual Pahari and Solapur (Hyvärinen et al., 2010; Varghese et al., 2020), semi-urban coastal, Thiruvananthapuram (Babu et al., 2016; Kompalli et al., 2014), semi-rural, Gadanki (Kanawade et al., 2014a), mountain semi-rural, Mahabaleshwar (Leena et al., 2017), mountain backgrounds such as Ranichauri and Mukteshwar (Neitola et al., 2011; Sebastian et al., 2021b), mountain remote such as Hanle and Ooty (Kompalli et al., 2018; Moorthy et al., 2011), and ocean cruise (North Indian Ocean, Kompalli et al., 2020). Out of published studies to date, only four studies are based on more than 2-years of continuous observations of particle/ion number size distributions reporting NPF frequency; the mountain background sites in Western Himalaya, Mukteshwar (surface elevation, 2180 m amsl) (Neitola et al., 2011) and Ranichauri (1930 m amsl) (Sebastian et al., 2021b), semi-urban, Gual Pahari (Hyvärinen et al., 2010), and a tropical urban site, Pune (Siingh et al., 2018). NPF rarely occurred at Ranichauri (8.4% of the total observation days), with the highest NPF frequency during spring (Sebastian et al., 2021b). Neitola et al. (2011) also showed that NPF events occur sporadically at Mukteshwar, with the highest frequency of NPF occurrence in the spring/pre-monsoon. The highest frequency during spring at these sites was connected to the uplifting of the planetary boundary layer (PBL) to the elevation of the measurement site, which appeared to transport aerosol precursors from nearby polluted lower-altitude regions. The NPF frequently occurred at a tropical urban site, Pune (74.3%), with the highest frequency during spring. These findings, in general, are consistent with those found in rural to urban locations worldwide (Kanawade et al., 2012; Nieminen et al., 2018; Shen et al., 2011; Stanier et al., 2004a). But, Bianchi et al. (2021) observed a very high NPF frequency (69%) at Nepal Climate Observatory-Pyramid (NCO-P) during November–December 2014 when cleaner conditions prevail, with little transport from the polluted lower-altitude regions. They showed that up-valley winds bring gaseous aerosol precursors to higher altitudes which are oxidized into compounds of very low volatility and subsequently converted to aerosol particles during their transport to the site. The remaining 17 NPF studies were conducted as independent campaign field observations, about 10 NPF studies were conducted in the spring-summer season, and the remaining seven were conducted in the fall-winter season (Table 1). At these sites, the NPF frequency varied greatly from 14% (Pune) to 82% (Kanpur) in spring and from 8.4% (Mahabaleshwar) to 70% (Gual Pahari) in winter. It is clear that there is no common pattern in the NPF frequency at the sites in India. Therefore, the long-term continuous

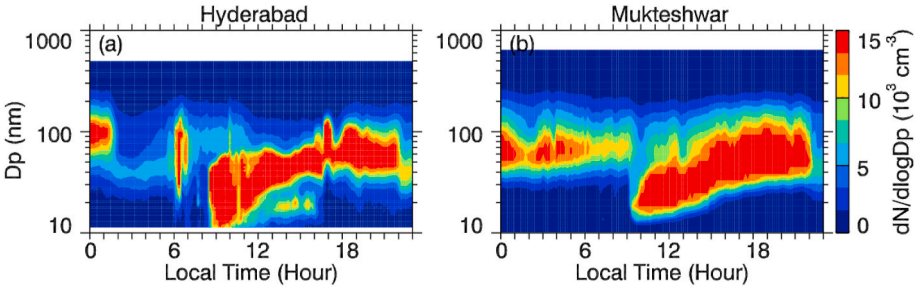

Fig. 2. Example of a typical regional NPF event as measured by (a) scanning mobility particle sizer in Hyderabad on June 11, 2019 and (b) differential mobility particle sizer in Mukteshwar on April 24, 2012.

Table 1
Summary of measurement sites (name and type), measurement parameters (time period, instrument, and size range) and key NPF characteristics [NPF frequency, formation rate (J_{NUC}), growth rate (GR) and condensation sink (CS)] in diverse environments of India.

Site Name	Site Type	Measurement periods	Instrument	Size range	NPF frequency (% days)	J_{NUC} (cm^{-3} s^{-1})	GR (nm h^{-1})	CS (10^{-3} s^{-1})	Reference
Delhi	Urban	Oct–Nov 2002	DMPS	3–800 nm	57.1	J_3, 7.3 ± 3.9	14.9 ± 1.8	57.5 ± 8.8[a]	Mönkkönen et al. (2005)
		Nov–Dec 2011	SMPS	9–425 nm	ND	ND	3.9	ND	Sarangi et al. (2015)
Pune	Urban	Dec 1997	EEA	13–750 nm	ND	J_{13}, 2.3	0.3–1.0[b]	60.0	Chate and Devara (2005)
		Nov–Dec 2005	SMPS	20–600 nm	ND	ND	17.0 ± 1.9	71 ± 4	Murugavel and Chate (2009)
		Apr–May 2010	NAIS	0.46–50 nm	36.2	ND	7.8 ± 1.7[c]	ND	Siingh et al. (2013)
		Apr–May 2012	SMPS	4–750 nm	26.6	J_5, 7.2 ± 3.3	6.5 ± 1.2	16.2 ± 7.1	Kanawade et al. (2014c)
		Mar–May 2012	NAIS+SMPS	3.85–47.8 nm	14	J_5, 6.8 ± 3.4	7.4 ± 1.4[c]	6.6 ± 1.5	Kamra et al. (2015)
		Mar 2010–Dec 2012	NAIS	0.36–47.1 nm	74.3	ND	3.2–11.6[c]	ND	Siingh et al. (2018)
Kanpur	Urban	Apr–May 2013	SMPS	13.8–685 nm	14	J_5, 1.5 ± 1.0	8.7 ± 3.2	33.3 ± 8.7	Kanawade et al. (2014c)
		Mar–Apr 2013	SMPS	4.45–736.5 nm	82	ND	3.2–6.7	ND	(Kanawade et al., 2020b)
Hyderabad	Urban	Apr–Jun 2019	nCNC SMPS	1–3 nm 10–514 nm	26.7	$J_{1.4}$, 30.7 ± 73.6 J_{10}, 2.3 ± 5.1	2.2 ± 1.7[d] 4.9 ± 3.2[e]	17.0 ± 16.5	Sebastian et al. (2021a)
Gual Pahari	Semi-urban	Dec 2007–Jan 2010	DMPS	4–850 nm	70	ND	ND	ND	Hyvärinen et al. (2010)
Solapur	Semi-urban	Aug 2018–Jan 2019	SMPS	15–700 nm	19	J_{15}, 2.8 ± 2.9	5.0 ± 73.5[f]	16.4 ± 6	Varghese et al. (2020)
Trivandrum	Urban-coastal	May–Jun 2009	SMPS	10–875 nm	ND	ND	0.1–10[e]	6.0–10.0[a]	Kompalli et al. (2014)
		Jan–Dec 2013	SMPS+APS	15 nm–15 μm	ND	ND	7.4 ± 2.9[g]	10.0–30.0[a]	Babu et al. (2016)
Gadanki	Semi-rural	May–Jul 2012	WRAS	5 nm–32 μm	6.3	J_5, 1.2 ± 2.3	4.1 ± 2.0[h]	7.1 ± 4.6	Kanawade et al. (2014a)
Mahabaleshwar	Mountain semi-rural	Oct–Nov 2014	WRAS	5 nm–32 μm	8.4	J_5, 1.1 ± 0.2	1.4 ± 0.4[h]	15.4 ± 2.6	Leena et al. (2017)
Mukteshwar	Mountain background	Nov 2005–Jan 2010	DMPS	10–800 nm	11.2	J_{15}, 0.4	2.4[j]	7.4 ± 4.3	Neitola et al. (2011)
Ranichauri	Mountain background	Dec 2016–Sep 2018	DMPS	10–800 nm	8.4	J_{10}, 0.2 ± 0.2	6.7 ± 3.8[e]	8.6 ± 5.8	Sebastian et al. (2021b)
Hanle	Mountain remote	Aug 2010	SMPS	16–1364 nm	ND	ND	0.1–20.0[i]	ND	Kompalli et al. (2014)
ICARB-2018	Cruise	Jan 2018–Feb 2018	SMPS	10–414 nm	ND	J_{10}, 1.9 ± 0.9	14.4 ± 13.1[e]	19.8 ± 55.0	Kompalli et al. (2020)

'ND' indicates no data.
[a]CS prior to NPF event.
Particle growth rates of [b]13-25nm, [c]negative ions (3.85-25nm),[d]Sub-3nm, [e]10-25nm, [f]15-30nm, [g]15-100nm, [h]5-25nm, [i]16-25nm,[j]10-800nmDMPS: Differential Mobility Particle Sizer; EEA: Electrical Aerosol Analyzer; SMPS: Scanning Mobility Particle Sizer; NAIS: Neutral Air-Ion Spectrometer; nCNC: nano Condensation Nucleus Counter; WRAS: Wide Range Aerosol Spectrometer; APS: Aerosol Particle Sizer.

measurements of particle number size distributions are indispensable to determine the seasonality in the NPF frequency.

The strength of an individual NPF event is characterised by the formation rate of new particles and the growth rate of these newly formed particles to larger sizes. In India, Chate and Devara (2005) were the first to report evidence of new particle formation and growth during calm and cold nights (Dec. 1997) from a polluted city, Pune. They reported key NPF characteristics such as the formation rate, growth rate and condensation sink, although based on only a few days of nighttime observations. Later, Mönkkönen et al. (2005) reported NPF and its characteristics based on two months of particle number size distributions measurements (Oct.–Nov., 2002) from a polluted city, Delhi. They showed that NPF events occurred when solar radiation was the most intense and the condensation sink reduced enough to trigger aerosol nucleation. The formation rate of 3 nm particles ranged from 3.3 to 13.9 particles cm^{-3} s^{-1}, with a mean and standard deviation (σ) of 7.3 ± 3.9 particles cm^{-3} s^{-1}, whereas the particle growth rate ranged from 11.6 to 18.1 nm h^{-1}, with a mean and σ of 14.9 ± 1.8 nm h^{-1}. The particle formation rate and growth rate are comparable to those observed in China (Chu et al., 2019). Guo et al. (2014) illustrated a case with NPF followed by continuous growth leading to haze formation in Beijing, China. In India, the contribution of NPF to haze formation and air quality remains unexplored. Although, Kanawade et al. (2020a) recently reported that NPF was suppressed during the severe air pollution episode of November 2016 in New Delhi, with an exceptionally high particle growth rate of up to 30 nm h^{-1}. To date, there are only three NPF observational studies from Delhi, despite the fact that the world air quality report 2018 recently marked Delhi as "world air pollution capital".

The high pre-existing particles are expected to prevent NPF in a heavily polluted atmosphere, but urban areas are becoming a hotspot of NPF, especially in developing countries like India and China (Kulmala et al., 2017; Yu et al., 2017). For instance, the mean condensation sink values during NPF events were 0.017 s^{-1}, 0.033 s^{-1}, 0.057 s^{-1} and 0.071 s^{-1} in Hyderabad (Sebastian et al., 2021a), Kanpur (Kanawade et al., 2014c), Delhi (Mönkkönen et al., 2005) and Pune (Murugavel and Chate, 2009), respectively, which are approximately 2–10 times higher than that observed in semi-rural (Kanawade et al., 2014a) and mountain

background locations (Neitola et al., 2011; Sebastian et al., 2021b). Although, these values are slightly lower than Chinese megacities, such as Beijing and Shanghai, where the condensation sink was reported to be as high as 0.1 s^{-1} (Xiao et al., 2015).

In urban areas (Hyderabad and Kanpur), NPF was associated with sulfuric acid concentrations (Kanawade et al., 2014c; Sebastian et al., 2021a), but the particle growth rate due to sulfuric acid alone was accounted for only 5–65% of the total observed growth in Hyderabad. This suggested the potential role of condensable vapours other than sulfuric acid (e.g., organic compounds) in particle growth (Sebastian et al., 2021a). NPF in the semi-rural environment (Gadanki) infrequently occurred due to lower precursor gaseous (SO_2 and NO_2) concentrations (Kanawade et al., 2014a). Only these three studies so far have linked NPF, though indirectly and in the absence of analytical techniques listed above, to precursor gaseous concentrations in India. NAIS gives particle and ion size distribution in a diameter range of 0.8–47 nm, but the formation rate of sub-2 nm ion clusters are surprisingly not reported in India (Kamra et al., 2015; Nepolian et al., 2021; Siingh et al., 2013, 2018), which is otherwise widely reported elsewhere worldwide (Gagné et al., 2011; Yan et al., 2018). The formation rate of 3 nm, 5 nm, 10 nm and 15 nm particles have been reported from diverse environments in India (e.g., Kompalli et al., 2014; Leena et al., 2017; Mönkkönen et al., 2005; Neitola et al., 2011). The formation rate of neutral clusters as small as 1.4 nm has also been reported recently (Sebastian et al., 2021a). The formation rate of 1.4 nm particles ($J_{1.4}$) varied from 0.7 particles cm^{-3} s^{-1} to 145.1 particles cm^{-3} s^{-1} (5th to 95th percentiles) with a mean and σ of 30.7 ± 73.6 particles cm^{-3} s^{-1} (Sebastian et al., 2021a), which is comparable to that of urban Beijing, China (Cai et al., 2017). It is worth mentioning that a recent study developed a coupled computational fluid dynamic (CFD)-aerosol dynamics model to simulate the formation and growth of nanoparticles from glowing wire (Ghosh et al., 2020), which can be applicable in case of direct emission of nanoparticles from vehicular exhaust, fires and industrial chimneys.

.

Up to now, NPF events have been reported from 12 continental measurement sites (22 articles) in India. Based on these 22 studies, we found that the mean growth rate was lowest at Hanle (0.1 nm h^{-1}) and the highest at Delhi (30 nm h^{-1}). The mean particle formation rates were derived for the lowest detection limits of the instruments used at different sites (1.4, 3, 5, 10 and 15 nm). The mean values of the particle formation rates varied from 0.2 to 30.7 particles cm^{-3} s^{-1}, which is within the observed range in diverse locations globally (e.g., Nieminen et al., 2018). Overall, the site-specific particle formation rate and growth rate were positively correlated (Pearson correlation coefficient of 0.49, Fig. 3), which is expected as these rates depend on gas-phase production rates of low-volatility vapours, driven by the source and atmospheric condition, for particle formation and growth (Kulmala and Kerminen, 2008; Xiao et al., 2021; Zhang et al., 2012). Generally, low pre-existing aerosol loading (i.e., condensation sink) favours higher particle formation and growth rates, which is not the case here. For instance, Delhi (winter) reported the highest particle formation and growth rates at higher condensation sink, while Pune (spring/pre-monsoon) reported similar rates but at a lower condensation sink. There are two possibilities why the particle formation and growth rates are different between two similar environments. First, Delhi and Pune are representative of sub-tropical and tropical environments, respectively, and thus have different atmospheric conditions. Secondly, the higher pre-existing particles in Delhi indicate precursor-laden air, which can enhance particle formation and growth rates if NPF precedes. The contradictory particle formation and growth rates have also been reported elsewhere worldwide, even in similar environments and seasons and are, therefore, a subject of scientific debate. It is because the particle formation rate, growth rate and condensation sink are affected by multiple factors (topography of the location, background aerosol concentration, nucleating vapour, availability of condensable vapours, boundary layer dynamics and associated atmospheric conditions including temperature, relative humidity, wind speed and solar radiation) with different degrees of importance for these factors among the individual locations (Nieminen et al., 2018).

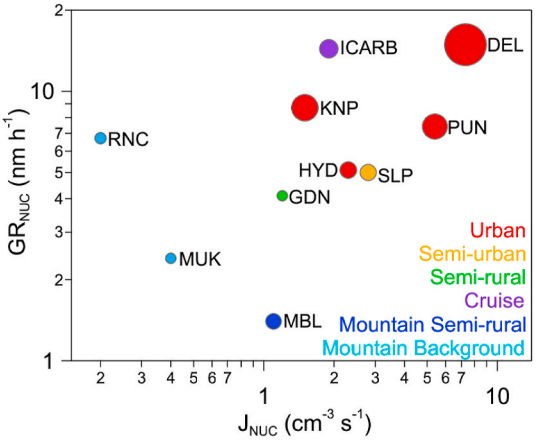

Fig. 3. Association between site-specific particle formation rate and growth rate as a function of condensation sink. The marker colours indicate the type of the measurement sites, and the marker size is proportional to the condensation sink (the smallest and the biggest marker corresponds to the condensation sink of 0.001 s^{-1} and 0.05 s^{-1}, respectively). RNC: Ranichauri, MUK: Mukteshwar, MBL: Mahabaleshwar, GDN: Gadanki, SLP: Solapur, HYD: Hyderabad KNP: Kanpur, PUN: Pune, DEL: Delhi, and ICARB: cruise in North Indian Ocean. (For interpretation of the references to colour in this figure legend, the reader is referred to the Web version of this article.)

Until recently, there were no observations of a neutral sub-3nm size regime in India, where stable cluster formation and early growth occur (Sebastian et al., 2021a). Our recent study showed that the sub-3nm particle formation frequently occurs in Hyderabad, but only half of these events were followed by a "banana-shaped" aerosol growth to larger sizes, indicating a regional NPF event. While we did not have direct observations of organic vapours, we hypothesized and illustrated that the differences in the abundance of condensable organics caused the differences in particle growth/survival to a larger size (Sebastian et al., 2021a). We recommended future studies using state-of-the-art techniques for gas- and particle-phase quantification and detection to validate our hypothesis and initiated our efforts in this direction. Further, our recent study, for the first time in India, linked NPF to climate-relevant aerosols by estimating the survival probability of newly-formed particles to CCN-active sizes (i.e.,>50–100 nm) based on long-term continuous measurements of particle number size distribution (Sebastian et al., 2021b). We found that ~60% of the particles surviving to 50 nm survived to 100 nm, making the overall survival probability of 100 nm to about 53%. The long-term continuous measurements of particle number size distributions alongside CCN concentrations are critical for better understanding NPF and CCN linkages, which is currently hampered by the scarcity of observations in India and elsewhere worldwide.

5. Critical knowledge gaps in NPF in India

In India, several investigators have conducted both short- and long-term measurements of particle number size distributions (e.g., Hyvärinen et al., 2010; Kanawade et al., 2014b; Kompalli et al., 2018; Komppula et al., 2009; Laj et al., 2020; Shika et al., 2020; Tripathi et al., 1988; Tripathi et al., 2006). But they did not explicitly study atmospheric NPF. Scanning mobility particle sizer in combination with nano-DMA or Wide Range Aerosol Spectrometer has been used in India to reach particle size of 3–5 nm diameter, but atmospheric NPF is still scarcely studied. Firstly, the particle number size distributions in the sub-3nm diameter size range, where initial cluster formation and growth occur, are

primarily required for characterizing NPF. Secondly, particle number size distribution shows us how NPF proceeds, but they do not give any information on the chemical species involved in cluster formation and subsequent growth to detectable large sizes. The direct measurement of sub-3nm-sized molecular clusters and the development of analytical methods capable of detecting and characterizing the small amount of matter in newly-formed particles are required for elucidating NPF. Although the measurements of neutral and charged sub-3nm clusters are currently available in India from two locations (Hyderabad and Pune, respectively), the identification and quantification of gas-phase and particle-phase compounds in nanoparticles, and thus the chemistry driving NPF is unknown in India.

Numerous recent advancements based on mass spectrometry have made it possible to detect gaseous precursors (Kulmala et al., 2014). Either quadrupole or High-Resolution Time of Flight Mass Spectrometry (HR-ToF-MS) has been used as a detector, giving mass to charge ratio up to ~2000. The chemical composition of atmospheric clusters/ions has been measured with the Chemical Ionization – Atmospheric Pressure Ionization – Time of Flight mass spectrometer (CI-APi-ToF, Jokinen et al., 2012). The cluster-Chemical Ionization Mass Spectrometer has also been developed for detecting neutral molecular clusters in the atmosphere (Zhao et al., 2010) or specific gaseous precursors such as sulfuric acid (Zheng et al., 2011) or ammonia and amines (Hanson et al., 2011; You et al., 2014; Zheng et al., 2015). Further direct observations of the chemical composition of nucleation mode particles have also been made with thermal desorption chemical ionization mass spectrometer (TDCIMS, Smith et al., 2005) and with nano aerosol mass spectrometer (NAMS, Wang et al., 2006). Surprisingly, none of the above state-of-the-art instruments is currently available in India to detect the chemical composition of small molecular clusters. Nevertheless, the recent advancements in aerosol instrumentation have made it possible to directly detect the chemical composition of sub-3nm particles (Kulmala et al., 2012).

While the key NPF characteristics (frequency, formation rate, and growth rate) and atmospheric conditions influencing NPF have adequately been reported from different environments in India, the chemical mechanisms driving NPF at a given atmospheric condition are unknown to date. Because to unravel the fundamental mechanisms driving NPF, in-situ field measurement of various aerosol precursors (sulfuric acid, amines, ammonia, highly oxygenated organic compounds etc.) and chemical characterization of nanoparticles down to the smallest particle diameter (e.g., sub-10 nm) are essential. The field observations of particle number size distribution and chemical composition aided with aerosol microphysical modelling incorporated with aerosol nucleation schemes based on laboratory experiments (e.g., CLOUD) are also crucial to interpreting field observations. In India, previous studies primarily examined the role of different factors in NPF. These factors included solar radiation (Kanawade et al., 2014c; Moorthy et al., 2011), aerosol precursors such as sulfur dioxide (Kanawade et al., 2014a; Mönkkönen et al., 2005; Sebastian et al., 2021a; Varghese et al., 2020), aerosol and meteorological properties (Hyvärinen et al., 2010; Kanawade et al., 2014c; Komppula et al., 2009), dynamics of the local coastal atmospheric boundary layer circulation (Babu et al., 2016), and the remaining studies characterised NPF in general (e.g., Kamra et al., 2015; Leena et al., 2017; Neitola et al., 2011; Siingh et al., 2018; Siingh et al., 2013). None of the 22 published papers till-date presented the potential chemical species contributing to aerosol nucleation and growth in India, except two recent studies (Kanawade et al., 2020b; Sebastian et al., 2021a). Kanawade et al. (2020b) used a high-resolution time-of-flight aerosol mass spectrometer (HR-ToF-AMS) to assess chemical changes in the sub-micron particles formed during the observed NPF events in a heavily polluted city, Kanpur. They found that the condensation of low-volatility organic species mainly facilitated the growth of sub-micron particles during NPF events. Further, they found high signal intensities of nitrogen-containing organic compounds in the sub-micron particles during the observed NPF events. On the other hand, Sebastian et al. (2021a) calculated the H_2SO_4 proxy and the growth rate due to H_2SO_4 alone for the observed NPF events in a polluted city, Hyderabad. They showed that the calculated sulfuric acid proxy positively correlated with the formation rate of 1.4 nm particles, indicating the potential role of H_2SO_4 in aerosol nucleation. But, the calculated growth rate due to H_2SO_4 alone failed to explain the observed growth rates of nucleation mode particles, indicating the potential contribution of other condensable species such as organic vapours.

Further, NPF studies in India are sporadic at different locations and typically included measurements of preliminary datasets such as particle number size distributions, trace gases, and meteorological parameters. The use of the state-of-the-art instruments is extremely limited, especially for explicitly measuring specific gaseous aerosol precursors and chemical composition at the molecular level (e.g., EESI-TOF and CI-APi-TOF). Besides, there are currently only four studies reporting more than two years of continuous particle number size distribution measurements. Thus, very little is known about the processes leading to NPF in India. A comprehensive approach is needed to understand how NPF will contribute to India's haze formation and CCN production. Together with primary emission reductions, the way forward is to make long-term, continuous, and comprehensive observations of aerosol particles (mass, number size distribution, chemical composition, etc.), precursor gases (SO_2, NO_x, VOCs, H_2SO_4, NH_3, etc.) and atmospheric oxidants (O_3, HO_x, NO_3, Criegee intermediates, etc.) (Kulmala, 2015). The regional aerosol microphysical model incorporated with different nucleation schemes from laboratory experiments can support interpreting field measurements. With a network of such observations, we will be able to understand the interactions and feedbacks associated with primary and secondary aerosol production. Therefore, to develop a better understanding of air quality-climate interactions and feedbacks related to NPF; we recommend addressing the following, yet largely open knowledge gaps on NPF in India; 1) the chemical mechanisms driving NPF in different environments, 2) the contribution of newly-formed particles via GTP and associated NPF processes to CCN production, 3) to quantify the relative contribution of anthropogenic and biogenic volatile organic compounds to NPF and 4) the relative importance of NPF to haze formation and air quality-climate interactions.

This indeed motivated us to recapitulate the current understanding of NPF to boost observational networks using state-of-the-art techniques in India. The complex cocktail of primary emissions and secondary formation further adds complexity to understanding NPF and its interaction with boundary layer dynamics and feedbacks. Therefore, the long-term, continuous, and comprehensive observational networks will remove the potential discrepancies that result from short-term and dissimilar observations.

Declaration of competing interest

The authors declare that they have no known competing financial interests or personal relationships that could have appeared to influence the work reported in this paper.

Acknowledgements

This study was supported by the Institute of Eminence-University of Hyderabad (sanction no. UoH/IoE/RC1/RC1-20-014). RKH and APH acknowledge the Academy of Finland Flagship funding (grant no. 337552). The authors are thankful to the reviewers for their critical and constructive comments and suggestions.

References

Albrecht, B.A., 1989. Aerosols, cloud microphysics, and fractional cloudiness. Science 245, 1227–1230.

An, Z., Huang, R.-J., Zhang, R., Tie, X., Li, G., Cao, J., Zhou, W., Shi, Z., Han, Y., Gu, Z., Ji, Y., 2019. Severe haze in northern China: a synergy of anthropogenic emissions and atmospheric processes. Proc. Natl. Acad. Sci. U.S.A. 116, 8657–8666.

Asmi, E., Kivekäs, N., Kerminen, V.M., Komppula, M., Hyvärinen, A.P., Hatakka, J., Viisanen, Y., Lihavainen, H., 2011. Secondary new particle formation in Northern Finland Pallas site between the years 2000 and 2010. Atmos. Chem. Phys. 11, 12959–12972.

Babu, S.S., Kompalli, S.K., Moorthy, K.K., 2016. Aerosol number size distributions over a coastal semi urban location: seasonal changes and ultrafine particle bursts. Sci. Total Environ. 563–564, 351–365.

Babu, S.S., Manoj, M.R., Moorthy, K.K., Gogoi, M.M., Nair, V.S., Kompalli, S.K., Satheesh, S.K., Niranjan, K., Ramagopal, K., Bhuyan, P.K., Singh, D., 2013. Trends in aerosol optical depth over Indian region: potential causes and impact indicators. J. Geophys. Res.: Atmos. 118 (11), 711–794, 806.

Baccarini, A., Karlsson, L., Dommen, J., Duplessis, P., Vüllers, J., Brooks, I.M., Saiz-Lopez, A., Salter, M., Tjernström, M., Baltensperger, U., Zieger, P., Schmale, J., 2020. Frequent new particle formation over the high Arctic pack ice by enhanced iodine emissions. Nat. Commun. 11, 4924.

Bianchi, F., Junninen, H., Bigi, A., Sinclair, V.A., Dada, L., Hoyle, C.R., Zha, Q., Yao, L., Ahonen, L.R., Bonasoni, P., Buenrostro Mazon, S., Hutterli, M., Laj, P., Lehtipalo, K., Kangasluoma, J., Kerminen, V.M., Kontkanen, J., Marinoni, A., Mirme, S., Molteni, U., Petäjä, T., Riva, M., Rose, C., Sellegri, K., Yan, C., Worsnop, D.R., Kulmala, M., Baltensperger, U., Dommen, J., 2021. Biogenic particles formed in the Himalaya as an important source of free tropospheric aerosols. Nat. Geosci. 14, 4–9.

Bianchi, F., Tröstl, J., Junninen, H., Frege, C., Henne, S., Hoyle, C.R., Molteni, U., Herrmann, E., Adamov, A., Bukowiecki, N., Chen, X., Duplissy, J., Gysel, M., Hutterli, M., Kangasluoma, J., Kontkanen, J., Kürten, A., Manninen, H.E., Münch, S., Peräkylä, O., Petäjä, T., Rondo, L., Williamson, C., Weingartner, E., Curtius, J., Worsnop, D.R., Kulmala, M., Dommen, J., Baltensperger, U., 2016. New particle formation in the free troposphere: A question of chemistry and timing. Science 352 (6289), 1109–1112. https://doi.org/10.1126/science.aad5456.

Birmili, W., Berresheim, H., Plass-Dülmer, C., Elste, T., Gilge, S., Wiedensohler, A., Uhrner, U., 2003. The Hohenpeissenberg aerosol formation experiment (HAFEX): a long-term study including size-resolved aerosol, H_2SO_4, OH, and monoterpenes measurements. Atmos. Chem. Phys. 3, 361–376.

Birmili, W., Wiedensohler, A., 2000. New particle formation in the continental boundary layer: meteorological and gas phase parameter influence. Geophys. Res. Lett. 27, 3325–3328.

Bonn, B., Kulmala, M., Riipinen, I., Sihto, S.-L., Ruuskanen, T.M., 2008. How biogenic terpenes govern the correlation between sulfuric acid concentrations and new particle formation. J. Geophys. Res.: Atmos. 113.

Bousiotis, D., Brean, J., Pope, F.D., Dall'Osto, M., Querol, X., Alastuey, A., Perez, N., Petäjä, T., Massling, A., Nøjgaard, J.K., Nordstrøm, C., Kouvarakis, G., Vratolis, S., Eleftheriadis, K., Niemi, J.V., Portin, H., Wiedensohler, A., Weinhold, K., Merkel, M., Tuch, T., Harrison, R.M., 2021. The effect of meteorological conditions and atmospheric composition in the occurrence and development of new particle formation (NPF) events in Europe. Atmos. Chem. Phys. 21, 3345–3370.

Buenrostro Mazon, S., Riipinen, I., Schultz, D.M., Valtanen, M., Dal Maso, M., Sogacheva, L., Junninen, H., Nieminen, T., Kerminen, V.M., Kulmala, M., 2009. Classifying previously undefined days from eleven years of aerosol-particle-size distribution data from the SMEAR II station, Hyytiälä, Finland. Atmos. Chem. Phys. 9, 667–676.

Bzdek, B.R., Johnston, M.V., 2010. New particle formation and growth in the troposphere. Anal. Chem. 82, 7871–7878.

Cai, R., Yang, D., Fu, Y., Wang, X., Li, X., Ma, Y., Hao, J., Zheng, J., Jiang, J., 2017. Aerosol surface area concentration: a governing factor in new particle formation in Beijing. Atmos. Chem. Phys. 17, 12327–12340.

Carslaw, K.S., Harrison, R.G., Kirkby, J., 2002. Cosmic Rays Clouds Clim. 298, 1732–1737.

Chate, D.M., Devara, P.C.S., 2005. Growth properties of sub-micron aerosols during cold season in India. Aerosol Air Qual. Res. 5, 127–140.

Chu, B., Kerminen, V.M., Bianchi, F., Yan, C., Petäjä, T., Kulmala, M., 2019. Atmospheric new particle formation in China. Atmos. Chem. Phys. 19, 115–138.

Dada, L., Chellapermal, R., Buenrostro Mazon, S., Paasonen, P., Lampilahti, J., Manninen, H.E., Junninen, H., Petäjä, T., Kerminen, V.M., Kulmala, M., 2018. Refined classification and characterization of atmospheric new-particle formation events using air ions. Atmos. Chem. Phys. 18, 17883–17893.

Dal Maso, M., Kulmala, M., Riipinen, I., Wagner, R., 2005. Formation and growth of fresh atmospheric aerosols: eight years of aerosol size distribution data from SMEAR II. Hyytiälä, Finland. Boreal Environ. Res. 10, 323–336.

Dey, S., Di Girolamo, L., 2011. A decade of change in aerosol properties over the Indian subcontinent. Geophys. Res. Lett. 38.

Ehn, M., Thornton, J.A., Kleist, E., Sipila, M., Junninen, H., Pullinen, I., Springer, M., Rubach, F., Tillmann, R., Lee, B., Lopez-Hilfiker, F., Andres, S., Acir, I.-H., Rissanen, M., Jokinen, T., Schobesberger, S., Kangasluoma, J., Kontkanen, J., Nieminen, T., Kurten, T., Nielsen, L.B., Jorgensen, S., Kjaergaard, H.G., Canagaratna, M., Maso, M.D., Berndt, T., Petaja, T., Wahner, A., Kerminen, V.-M., Kulmala, M., Worsnop, D.R., Wildt, J., Mentel, T.F., 2014. A large source of low-volatility secondary organic aerosol. Nature 506, 476–479.

Friedlander, S.K., 1977. Smoke, Dust and Haze: Fundamentals of Aerosol Behaviour. John Wiley & Sons.

Gagné, S., Lehtipalo, K., Manninen, H.E., Nieminen, T., Schobesberger, S., Franchin, A., Yli-Juuti, T., Boulon, J., Sonntag, A., Mirme, S., Mirme, A., Hõrrak, U., Petäjä, T., Asmi, E., Kulmala, M., 2011. Intercomparison of air ion spectrometers: an evaluation of results in varying conditions. Atmos. Meas. Tech. 4, 805–822.

Gani, S., Bhandari, S., Patel, K., Seraj, S., Soni, P., Arub, Z., Habib, G., Hildebrandt Ruiz, L., Apte, J.S., 2020. Particle number concentrations and size distribution in a polluted megacity: the Delhi Aerosol Supersite study. Atmos. Chem. Phys. 20, 8533–8549.

Ghosh, K., Tripathi, S.N., Joshi, M., Mayya, Y.S., Khan, A., Sapra, B.K., 2020. Particle formation from vapors emitted from glowing wires: theory and experiments. Aerosol. Sci. Technol. 54, 243–261.

Gordon, H., Kirkby, J., Baltensperger, U., Bianchi, F., Breitenlechner, M., Curtius, J., Dias, A., Dommen, J., Donahue, N.M., Dunne, E.M., Duplissy, J., Ehrhart, S., Flagan, R.C., Frege, C., Fuchs, C., Hansel, A., Hoyle, C.R., Kulmala, M., Kürten, A., Lehtipalo, K., Makhmutov, V., Molteni, U., Rissanen, M.P., Stozkhov, Y., Tröstl, J., Tsagkogeorgas, G., Wagner, R., Williamson, C., Wimmer, D., Winkler, P.M., Yan, C., Carslaw, K.S., 2017. Causes and importance of new particle formation in the present-day and preindustrial atmospheres. J. Geophys. Res.: Atmos. 122, 8739–8760.

Guo, S., Hu, M., Zamora, M.L., Peng, J., Shang, D., Zheng, J., Du, Z., Wu, Z., Shao, M., Zeng, L., Molina, M.J., Zhang, R., 2014. Elucidating severe urban haze formation in China. Proc. Natl. Acad. Sci. U.S.A. 111, 17373–17378.

Hanson, D.R., McMurry, P.H., Jiang, J., Tanner, D., Huey, L.G., 2011. Ambient pressure proton transfer mass spectrometry: detection of amines and ammonia. Environ. Sci. Technol. 45, 8881–8888.

Hooda, R.K., Kivekäs, N., O'Connor, E.J., Collaud Coen, M., Pietikäinen, J.-P., Vakkari, V., Backman, J., Henriksson, S.V., Asmi, E., Komppula, M., Korhonen, H., Hyvärinen, A.-P., Lihavainen, H., 2018. Driving factors of aerosol properties over the foothills of central himalayas based on 8.5 years. Continuous Meas. 123 (13), 421-413,442.

Hyvärinen, A.P., Lihavainen, H., Komppula, M., Panwar, T.S., Sharma, V.P., Hooda, R.K., Viisanen, Y., 2010. Aerosol measurements at the Gual Pahari EUCAARI station: preliminary results from in-situ measurements. Atmos. Chem. Phys. 10, 7241–7252.

Jiang, J., Chen, M., Kuang, C., Attoui, M., McMurry, P.H., 2011. Electrical mobility spectrometer using a diethylene glycol condensation particle counter for measurement of aerosol size distributions down to 1 nm. Aerosol. Sci. Technol. 45, 510–521.

Jokinen, T., Sipilä, M., Junninen, H., Ehn, M., Lönn, G., Hakala, J., Petäjä, T., Mauldin Iii, R.L., Kulmala, M., Worsnop, D.R., 2012. Atmospheric sulphuric acid and neutral cluster measurements using CI-APi-TOF. Atmos. Chem. Phys. 12, 4117–4125.

Kammer, J., Perraudin, E., Flaud, P.M., Lamaud, E., Bonnefond, J.M., Villenave, E., 2018. Observation of nighttime new particle formation over the French Landes forest. Sci. Total Environ. 621, 1084–1092.

Kamra, A.K., Siingh, D., Gautam, A.S., Kanawade, V.P., Tripathi, S.N., Srivastava, A.K., 2015. Atmospheric ions and new particle formation events at a tropical location, Pune, India. Q. J. R. Meteorol. Soc. 141, 3140–3156.

Kanawade, V.P., Benson, D.R., Lee, S.-H., 2012. Statistical analysis of 4-year observations of aerosol sizes in a semi-rural continental environment. Atmos. Environ. 59, 30–38.

Kanawade, V.P., Shika, S., Pöhlker, C., Rose, D., Suman, M.N.S., Gadhavi, H., Kumar, A., Nagendra, S.M.S., Ravikrishna, R., Yu, H., Sahu, L.K., Jayaraman, A., Andreae, M.O., Pöschl, U., Gunthe, S.S., 2014a. Infrequent occurrence of new particle formation at a semi-rural location, Gadanki, in tropical Southern India. Atmos. Environ. 94, 264–273.

Kanawade, V.P., Srivastava, A.K., Ram, K., Asmi, E., Vakkari, V., Soni, V.K., Varaprasad, V., Sarangi, C., 2020a. What caused severe air pollution episode of November 2016 in New Delhi? Atmos. Environ. 222, 117125.

Kanawade, V.P., Tripathi, S.N., Chakraborty, A., Yu, H., 2020b. Chemical characterization of sub-micron aerosols during new particle formation in an urban atmosphere. Aerosol Air Qual. Res. 20, 1294–1305.

Kanawade, V.P., Tripathi, S.N., 2006. Evidence for the role of ion-induced particle formation during an atmospheric nucleation event observed in Tropospheric Ozone Production about the Spring Equinox (TOPSE). J. Geophys. Res.: Atmos. 111.

Kanawade, V.P., Tripathi, S.N., Bhattu, D., Shamjad, P.M., 2014b. Sub-micron particle number size distributions characteristics at an urban location, Kanpur, in the Indo-Gangetic Plain. Atmos. Res. 147–148, 121–132.

Kanawade, V.P., Tripathi, S.N., Siingh, D., Gautam, A.S., Srivastava, A.K., Kamra, A.K., Soni, V.K., Sethi, V., 2014c. Observations of new particle formation at two distinct Indian subcontinental urban locations. Atmos. Environ. 96, 370–379.

Kerminen, V.-M., Chen, X., Vakkari, V., Petäjä, T., Kulmala, M., Bianchi, F., 2018. Atmospheric new particle formation and growth: review of field observations. Environ. Res. Lett. 13, 103003.

Kerminen, V.-M., Lehtinen, K.E.J., Anttila, T., Kulmala, M., 2004. Dynamics of atmospheric nucleation mode particles: a timescale analysis. Tellus B 56, 135–146.

Kirkby, J., Duplissy, J., Sengupta, K., Frege, C., Gordon, H., Williamson, C., Heinritzi, M., Simon, M., Yan, C., Almeida, J., Tröstl, J., Nieminen, T., Ortega, I.K., Wagner, R., Adamov, A., Amorim, A., Bernhammer, A.-K., Bianchi, F., Breitenlechner, M., Brilke, S., Chen, X., Craven, J., Dias, A., Ehrhart, S., Flagan, R.C., Franchin, A., Fuchs, C., Guida, R., Hakala, J., Hoyle, C.R., Jokinen, T., Junninen, H., Kangasluoma, J., Kim, J., Krapf, M., Kürten, A., Laaksonen, A., Lehtipalo, K., Makhmutov, V., Mathot, S., Molteni, U., Onnela, A., Peräkylä, O., Piel, F., Petäjä, T., Praplan, A.P., Pringle, K., Rap, A., Richards, N.A.D., Riipinen, I., Rissanen, M.P., Rondo, L., Sarnela, N., Schobesberger, S., Scott, C.E., Seinfeld, J.H., Sipilä, M., Steiner, G., Stozhkov, Y., Stratmann, F., Tomé, A., Virtanen, A., Vogel, A.L., Wagner, A.C., Wagner, P.E., Weingartner, E., Wimmer, D., Winkler, P.M., Ye, P., Zhang, X., Hansel, A., Dommen, J., Donahue, N.M., Worsnop, D.R., Baltensperger, U., Kulmala, M., Carslaw, K.S., Curtius, J., 2016. Ion-induced nucleation of pure biogenic particles. Nature 533, 521–526.

Kompalli, S.K., Babu, S.S., Moorthy, K.K., Gogoi, M.M., Nair, V.S., Chaubey, J.P., 2014. The formation and growth of ultrafine particles in two contrasting environments: a case study. Ann. Geophys. 32, 817–830.

Kompalli, S.K., Babu, S.S., Udayasoorian, C., Jayabalakrishnan, R.M., 2018. Role of anthropogenic emissions and meteorology on ultrafine particle bursts over a high altitude site in Western Ghats during pre-monsoon. J. Atmos. Sol. Terr. Phys. 179, 378–388.

Kompalli, S.K., Nair, V.S., Jayachandran, V., Gogoi, M.M., Babu, S.S., 2020. Particle number size distributions and new particle formation events over the northern Indian Ocean during continental outflow. Atmos. Environ. 238, 117719.
Komppula, M., Lihavainen, H., Hyvärinen, A.P., Kerminen, V.M., Panwar, T.S., Sharma, V.P., Viisanen, Y., 2009. Physical properties of aerosol particles at a Himalayan background site in India. J. Geophys. Res.: Atmos. 114.
Kontkanen, J., Lehtipalo, K., Ahonen, L., Kangasluoma, J., Manninen, H.E., Hakala, J., Rose, C., Sellegri, K., Xiao, S., Wang, L., Qi, X., Nie, W., Ding, A., Yu, H., Lee, S., Kerminen, V.M., Petäjä, T., Kulmala, M., 2017. Measurements of sub-3 nm particles using a particle size magnifier in different environments: from clean mountain top to polluted megacities. Atmos. Chem. Phys. 17, 2163–2187.
Krotkov, N.A., McLinden, C.A., Li, C., Lamsal, L.N., Celarier, E.A., Marchenko, S.V., Swartz, W.H., Bucsela, E.J., Joiner, J., Duncan, B.N., Boersma, K.F., Veefkind, J.P., Levelt, P.F., Fioletov, V.E., Dickerson, R.R., He, H., Lu, Z., Streets, D.G., 2016. Aura OMI observations of regional SO_2 and NO_2 pollution changes from 2005 to 2015. Atmos. Chem. Phys. 16, 4605–4629.
Kuang, C., McMurry, P.H., McCormick, A.V., 2009. Determination of cloud condensation nuclei production from measured new particle formation events. Geophys. Res. Lett. 36.
Kulmala, M., 2015. Atmospheric chemistry: China's choking cocktail. Nature 526, 497–499.
Kulmala, M., Dada, L., Daellenbach, K.R., Yan, C., Stolzenburg, D., Kontkanen, J., Ezhova, E., Hakala, S., Tuovinen, S., Kokkonen, T.V., Kurppa, M., Cai, R., Zhou, Y., Yin, R., Baalbaki, R., Chan, T., Chu, B., Deng, C., Fu, Y., Ge, M., He, H., Heikkinen, L., Junninen, H., Liu, Y., Lu, Y., Nie, W., Rusanen, A., Vakkari, V., Wang, Y., Yang, G., Yao, L., Zheng, J., Kujansuu, J., Kangasluoma, J., Petäjä, T., Paasonen, P., Järvi, L., Worsnop, D., Ding, A., Liu, Y., Wang, L., Jiang, J., Bianchi, F., Kerminen, V.-M., 2021. Is reducing new particle formation a plausible solution to mitigate particulate air pollution in Beijing and other Chinese megacities? Faraday Discuss 226, 334–347.
Kulmala, M., Kerminen, V.-M., 2008. On the growth of atmospheric nanoparticles. Atmos. Res. 90, 132–150.
Kulmala, M., Kerminen, V.-M., Petäjä, T., Ding, A., Wang, L., 2017. Atmospheric Gas-to-Particle Conversion: why NPF events are observed in megacities? Faraday Discuss 200, 271–288.
Kulmala, M., Petäjä, T., Ehn, M., Thornton, J., Sipilä, M., Worsnop, D.R., Kerminen, V.M., 2014. Chemistry of atmospheric nucleation: on the recent advances on precursor characterization and atmospheric cluster composition in connection with atmospheric new particle formation. Annu. Rev. Phys. Chem. 65, 21–37.
Kulmala, M., Petäjä, T., Nieminen, T., Sipilä, M., Manninen, H.E., Lehtipalo, K., Dal Maso, M., Aalto, P.P., Junninen, H., Paasonen, P., Riipinen, I., Lehtinen, K.E.J., Laaksonen, A., Kerminen, V.-M., 2012. Measurement of the nucleation of atmospheric aerosol particles. Nat. Protoc. 7, 1651–1667.
Kulmala, M., Pirjola, L., Makela, J.M., 2000. Stable sulphate clusters as a source of new atmospheric particles. Nature 404, 66–69.
Kulmala, M., Riipinen, I., Sipilä, M., Manninen, H.E., Petäjä, T., Junninen, H., Maso, M. D., Mordas, G., Mirme, A., Vana, M., Hirsikko, A., Laakso, L., Harrison, R.M., Hanson, I., Leung, C., Lehtinen, K.E.J., Kerminen, V.-M., 2007. Toward direct measurement of atmospheric nucleation. Science 318, 89–92.
Kulmala, M., Vehkamäki, H., Petäjä, T., Dal Maso, M., Lauri, A., Kerminen, V.M., Birmili, W., McMurry, P.H., 2004. Formation and growth rates of ultrafine atmospheric particles: a review of observations. J. Aerosol Sci. 35, 143–176.
Laakso, L., Merikanto, J., Vakkari, V., Laakso, H., Kulmala, M., Molefe, M., Kgabi, N., Mabaso, D., Carslaw, K.S., Spracklen, D.V., Lee, L.A., Reddington, C.L., Kerminen, V. M., 2013. Boundary layer nucleation as a source of new CCN in savannah environment. Atmos. Chem. Phys. 13, 1957–1972.
Laj, P., Bigi, A., Rose, C., Andrews, E., Lund Myhre, C., Collaud Coen, M., Lin, Y., Wiedensohler, A., Schulz, M., Ogren, J.A., Fiebig, M., Gliß, J., Mortier, A., Pandolfi, M., Petäja, T., Kim, S.W., Aas, W., Putaud, J.P., Mayol-Bracero, O., Keywood, M., Labrador, L., Aalto, P., Ahlberg, E., Alados Arboledas, L., Alastuey, A., Andrade, M., Artíñano, B., Ausmeel, S., Arsov, T., Asmi, E., Backman, J., Baltensperger, U., Bastian, S., Bath, O., Beukes, J.P., Brem, B.T., Bukowiecki, N., Conil, S., Couret, C., Day, D., Dayantolis, W., Degorska, A., Eleftheriadis, K., Fetfatzis, P., Favez, O., Flentje, H., Gini, M.I., Gregorič, A., Gysel-Beer, M., Hallar, A. G., Hand, J., Hoffer, A., Hueglin, C., Hooda, R.K., Hyvärinen, A., Kalapov, I., Kalivitis, N., Kasper-Giebl, A., Kim, J.E., Kouvarakis, G., Kranjc, I., Krejci, R., Kulmala, M., Labuschagne, C., Lee, H.J., Lihavainen, H., Lin, N.H., Löschau, G., Luoma, K., Marinoni, A., Martins Dos Santos, S., Meinhardt, F., Merkel, M., Metzger, J.M., Mihalopoulos, N., Nguyen, N.A., Ondracek, J., Pérez, N., Perrone, M. R., Petit, J.E., Picard, D., Pichon, J.M., Pont, V., Prats, N., Prenni, A., Reisen, F., Romano, S., Sellegri, K., Sharma, S., Schauer, G., Sheridan, P., Sherman, J.P., Schütze, M., Schwerin, A., Sohmer, R., Sorribas, M., Steinbacher, M., Sun, J., Titos, G., Toczko, B., Tuch, T., Tulet, P., Tunved, P., Vakkari, V., Velarde, F., Velasquez, P., Villani, P., Vratolis, S., Wang, S.H., Weinhold, K., Weller, R., Yela, M., Yus-Diez, J., Zdimal, V., Zieger, P., Zikova, N., 2020. A global analysis of climate-relevant aerosol properties retrieved from the network of Global Atmosphere Watch (GAW) near-surface observatories. Atmos. Meas. Tech. 13, 4353–4392.
Lee, S.-H., Young, L.-H., Benson, D.R., Suni, T., Kulmala, M., Junninen, H., Campos, T.L., Rogers, D.C., Jensen, J., 2008. Observations of nighttime new particle formation in the troposphere. J. Geophys. Res.: Atmos. 113.
Leena, P.P., Anil Kumar, V., Dani, K.K., Sombawne, S.M., Murugavel, P., Pandithurai, G., 2017. Evidence of new particle formation during post monsoon season over a high-altitude site of the Western Ghats, India. Toxicol. Environ. Chem. 99, 652–664.
Lehtipalo, K., Sipilä, M., Junninen, H., Ehn, M., Berndt, T., Kajos, M.K., Worsnop, D.R., Petäjä, T., Kulmala, M., 2011. Observations of nano-CN in the nocturnal boreal forest. Aerosol. Sci. Technol. 45, 499–509.
Lehtipalo, K., Yan, C., Dada, L., Bianchi, F., Xiao, M., Wagner, R., Stolzenburg, D., Ahonen, L.R., Amorim, A., Baccarini, A., Bauer, P.S., Baumgartner, B., Bergen, A., Bernhammer, A.-K., Breitenlechner, M., Brilke, S., Buchholz, A., Mazon, S.B., Chen, D., Chen, X., Dias, A., Dommen, J., Draper, D.C., Duplissy, J., Ehn, M., Finkenzeller, H., Fischer, L., Frege, C., Fuchs, C., Garmash, O., Gordon, H., Hakala, J., He, X., Heikkinen, L., Heinritzi, M., Helm, J.C., Hofbauer, V., Hoyle, C.R., Jokinen, T., Kangasluoma, J., Kerminen, V.-M., Kim, C., Kirkby, J., Kontkanen, J., Kürten, A., Lawler, M.J., Mai, H., Mathot, S., Mauldin, R.L., Molteni, U., Nichman, L., Nie, W., Nieminen, T., Ojdanic, A., Onnela, A., Passananti, M., Petäjä, T., Piel, F., Pospisilova, V., Quéléver, L.L.J., Rissanen, M.P., Rose, C., Sarnela, N., Schallhart, S., Schuchmann, S., Sengupta, K., Simon, M., Sipilä, M., Tauber, C., Tomé, A., Tröstl, J., Väisänen, O., Vogel, A.L., Volkamer, R., Wagner, A.C., Wang, M., Weitz, L., Wimmer, D., Ye, P., Ylisirniö, A., Zha, Q., Carslaw, K.S., Curtius, J., Donahue, N.M., Flagan, R.C., Hansel, A., Riipinen, I., Virtanen, A., Winkler, P.M., Baltensperger, U., Kulmala, M., Worsnop, D.R., 2018. Multicomponent new particle formation from sulfuric acid, ammonia, and biogenic vapors. Sci. Adv. 4 eaau5363.
Manninen, H.E., Nieminen, T., Asmi, E., Gagné, S., Häkkinen, S., Lehtipalo, K., Aalto, P., Vana, M., Mirme, A., Mirme, S., Hõrrak, U., Plass-Dülmer, C., Stange, G., Kiss, G., Hoffer, A., Töró, N., Moerman, M., Henzing, B., de Leeuw, G., Brinkenberg, M., Kouvarakis, G.N., Bougiatioti, A., Mihalopoulos, N., O'Dowd, C., Ceburnis, D., Arneth, A., Svenningsson, B., Swietlicki, E., Tarozzi, L., Decesari, S., Facchini, M.C., Birmili, W., Sonntag, A., Wiedensohler, A., Boulon, J., Sellegri, K., Laj, P., Gysel, M., Bukowiecki, N., Weingartner, E., Wehrle, G., Laaksonen, A., Hamed, A., Joutsensaari, J., Petäjä, T., Kerminen, V.M., Kulmala, M., 2010. EUCAARI ion spectrometer measurements at 12 European sites – analysis of new particle formation events. Atmos. Chem. Phys. 10, 7907–7927.
Merikanto, J., Spracklen, D.V., Mann, G.W., Pickering, S.J., Carslaw, K.S., 2009. Impact of nucleation on global CCN. Atmos. Chem. Phys. 9, 8601–8616.
Metzger, A., Verheggen, B., Dommen, J., Duplissy, J., Prevot, A.S.H., Weingartner, E., Riipinen, I., Kulmala, M., Spracklen, D.V., Carslaw, K.S., Baltensperger, U., 2010. Evidence for the role of organics in aerosol particle formation under atmospheric conditions. Proc. Natl. Acad. Sci. U.S.A. 107, 6646–6651.
Mirme, A., Tamm, E., Mordas, G., Vana, M., Uin, J., Mirme, S., Bernotas, T., Laakso, L., Hirsikko, A., Kulmala, M., 2007. A wide-range multi-channel air ion spectrometer. Boreal Environ. Res. 12, 247–264.
Mirme, S., Mirme, A., 2013. The mathematical principles and design of the NAIS – a spectrometer for the measurement of cluster ion and nanometer aerosol size distributions. Atmos. Meas. Tech. 6, 1061–1071.
Mönkkönen, P., Koponen, I.K., Lehtinen, K.E.J., Hämeri, K., Uma, R., Kulmala, M., 2005. Measurements in a highly polluted Asian mega city: observations of aerosol number size distribution, modal parameters and nucleation events. Atmos. Chem. Phys. 5, 57–66.
Moorthy, K.K., Babu, S.S., Manoj, M.R., Satheesh, S.K., 2013. Buildup of aerosols over the Indian region. Geophys. Res. Lett. 40, 1011–1014.
Moorthy, K.K., Sreekanth, V., Prakash, C.J., Gogoi, M.M., Suresh, B.S., Kompalli, S.K., Bagare, S.P., Bhatt, B.C., Gaur, V.K., Prabhu, T.P., Singh, N.S., 2011. Fine and ultrafine particles at a near–free tropospheric environment over the high-altitude station Hanle in the Trans-Himalaya: new particle formation and size distribution. J. Geophys. Res.: Atmos. 116.
Murugavel, P., Chate, D.M., 2009. Generation and growth of aerosols over Pune, India. Atmos. Environ. 43, 820–828.
Neitola, K., Asmi, E., Komppula, M., Hyvärinen, A.P., Raatikainen, T., Panwar, T.S., Sharma, V.P., Lihavainen, H., 2011. New particle formation infrequently observed in Himalayan foothills – why? Atmos. Chem. Phys. 11, 8447–8458.
Nepolian, J.V., Siingh, D., Singh, R.P., Gautam, A.S., Gautam, S., 2021. Analysis of positive and negative atmospheric air ions during new particle formation (NPF) events over urban city of India. Aerosol Sci. Eng. 5, 460–477. https://doi.org/10.1007/s41810-021-00115-4.
Nieminen, T., Kerminen, V.M., Petäjä, T., Aalto, P.P., Arshinov, M., Asmi, E., Baltensperger, U., Beddows, D.C.S., Beukes, J.P., Collins, D., Ding, A., Harrison, R. M., Henzing, B., Hooda, R., Hu, M., Hõrrak, U., Kivekäs, N., Komsaare, K., Krejci, R., Kristensson, A., Laakso, L., Laaksonen, A., Leaitch, W.R., Lihavainen, H., Mihalopoulos, N., Németh, Z., Nie, W., O'Dowd, C., Salma, I., Sellegri, K., Svenningsson, B., Swietlicki, E., Tunved, P., Ulevicius, V., Vakkari, V., Vana, M., Wiedensohler, A., Wu, Z., Virtanen, A., Kulmala, M., 2018. Global analysis of continental boundary layer new particle formation based on long-term measurements. Atmos. Chem. Phys. 18, 14737–14756.
O'Dowd, C., Hoell, C., Becker, E., 2000. PARFORCE intensive $eld campaign results: particle concentration and low tide Finnish Association for Aerosol Research. Rep. Ser. Aerosol Sci. 22–27.
Pierce, J.R., Leaitch, W.R., Liggio, J., Westervelt, D.M., Wainwright, C.D., Abbatt, J.P.D., Ahlm, L., Al-Basheer, W., Cziczo, D.J., Hayden, K.L., Lee, A.K.Y., Li, S.M., Russell, L. M., Sjostedt, S.J., Strawbridge, K.B., Travis, M., Vlasenko, A., Wentzell, J.J.B., Wiebe, H.A., Wong, J.P.S., Macdonald, A.M., 2012. Nucleation and condensational growth to CCN sizes during a sustained pristine biogenic SOA event in a forested mountain valley. Atmos. Chem. Phys. 12, 3147–3163.
Pikridas, M., Riipinen, I., Hildebrandt, L., Kostenidou, E., Manninen, H., Mihalopoulos, N., Kalivitis, N., Burkhart, J.F., Stohl, A., Kulmala, M., Pandis, S.N., 2012. New particle formation at a remote site in the eastern Mediterranean. J. Geophys. Res.: Atmos. 117.
Pospisilova, V., Lopez-Hilfiker, F.D., Bell, D.M., El Haddad, I., Mohr, C., Huang, W., Heikkinen, L., Xiao, M., Dommen, J., Prevot, A.S.H., Baltensperger, U., Slowik, J.G., 2020. On the fate of oxygenated organic molecules in atmospheric aerosol particles. Sci. Adv. 6, eaax8922.
Ramachandran, S., Kedia, S., Srivastava, R., 2012. Aerosol optical depth trends over different regions of India. Atmos. Environ. 49, 338–347.

Remer, L.A., Kleidman, R.G., Levy, R.C., Kaufman, Y.J., Tanré, D., Mattoo, S., Martins, J. V., Ichoku, C., Koren, I., Yu, H., Holben, B.N., 2008. Global Aerosol Climatology from the MODIS Satellite Sensors, vol. 113.

Riccobono, F., Schobesberger, S., Scott, C.E., Dommen, J., Ortega, I.K., Rondo, L., Almeida, J., Amorim, A., Bianchi, F., Breitenlechner, M., David, A., Downard, A., Dunne, E.M., Duplissy, J., Ehrhart, S., Flagan, R.C., Franchin, A., Hansel, A., Junninen, H., Kajos, M., Keskinen, H., Kupc, A., Kürten, A., Kvashin, A.N., Laaksonen, A., Lehtipalo, K., Makhmutov, V., Mathot, S., Nieminen, T., Onnela, A., Petäjä, T., Praplan, A.P., Santos, F.D., Schallhart, S., Seinfeld, J.H., Sipilä, M., Spracklen, D.V., Stozhkov, Y., Stratmann, F., Tomé, A., Tsagkogeorgas, G., Vaattovaara, P., Viisanen, Y., Vrtala, A., Wagner, P.E., Weingartner, E., Wex, H., Wimmer, D., Carslaw, K.S., Curtius, J., Donahue, N.M., Kirkby, J., Kulmala, M., Worsnop, D.R., Baltensperger, U., 2014. Oxidation products of biogenic emissions contribute to nucleation of atmospheric particles. Science 344, 717–721.

Riipinen, I., Yli-Juuti, T., Pierce, J.R., Petäjä, T., Worsnop, D.R., Kulmala, M., Donahue, N.M., 2012. The contribution of organics to atmospheric nanoparticle growth. Nat. Geosci. 5, 453–458.

Rodríguez, S., Van Dingenen, R., Putaud, J.-P., Martins-Dos Santos, S., Roselli, D., 2005. Nucleation and growth of new particles in the rural atmosphere of Northern Italy—relationship to air quality monitoring. Atmos. Environ. 39, 6734–6746.

Rose, C., Sellegri, K., Moreno, I., Velarde, F., Ramonet, M., Weinhold, K., Krejci, R., Andrade, M., Wiedensohler, A., Ginot, P., Laj, P., 2017. CCN production by new particle formation in the free troposphere. Atmos. Chem. Phys. 17, 1529–1541.

Rose, C., Zha, Q., Dada, L., Yan, C., Lehtipalo, K., Junninen, H., Mazon, S.B., Jokinen, T., Sarnela, N., Sipilä, M., Petäjä, T., Kerminen, V.-M., Bianchi, F., Kulmala, M., 2018. Observations of biogenic ion-induced cluster formation in the atmosphere. Sci. Adv. 4, eaar5218.

Salimi, F., Rahman, M.M., Clifford, S., Ristovski, Z., Morawska, L., 2017. Nocturnal new particle formation events in urban environments. Atmos. Chem. Phys. 17, 521–530.

Sarangi, B., Aggarwal, S.G., Gupta, P.K., 2015. A simplified approach to calculate particle growth rate due to self-coagulation, scavenging and condensation using SMPS measurements during a particle growth event in New Delhi. Aerosol Air Qual. Res. 15, 166–179.

Schobesberger, S., Junninen, H., Bianchi, F., Lönn, G., Ehn, M., Lehtipalo, K., Dommen, J., Ehrhart, S., Ortega, I.K., Franchin, A., Nieminen, T., Riccobono, F., Hutterli, M., Duplissy, J., Almeida, J., Amorim, A., Breitenlechner, M., Downard, A. J., Dunne, E.M., Flagan, R.C., Kajos, M., Keskinen, H., Kirkby, J., Kupc, A., Kürten, A., Kurtén, T., Laaksonen, A., Mathot, S., Onnela, A., Praplan, A.P., Rondo, L., Santos, F.D., Schallhart, S., Schnitzhofer, R., Sipilä, M., Tomé, A., Tsagkogeorgas, G., Vehkamäki, H., Wimmer, D., Baltensperger, U., Carslaw, K.S., Curtius, J., Hansel, A., Petäjä, T., Kulmala, M., Donahue, N.M., Worsnop, D.R., 2013. Molecular understanding of atmospheric particle formation from sulfuric acid and large oxidized organic molecules. Proc. Natl. Acad. Sci. U.S.A. 110, 17223–17228.

Sebastian, M., Kanawade, V.P., Pierce, J.R., 2021a. Observation of sub-3nm particles and new particle formation at an urban location in India. Atmos. Environ. 256, 118460.

Sebastian, M., Kanawade, V.P., Soni, V.K., Asmi, E., Westervelt, D.M., Vakkari, V., Hyvärinen, A.-P., Pierce, J.R., Hooda, R.K., 2021b. New particle formation and growth to climate-relevant aerosols at a background remote site in the western Himalaya. J. Geophys. Res.: Atmos. 126, e2020JD033267.

Shen, X.J., Sun, J.Y., Zhang, Y.M., Wehner, B., Nowak, A., Tuch, T., Zhang, X.C., Wang, T.T., Zhou, H.G., Zhang, X.L., Dong, F., Birmili, W., Wiedensohler, A., 2011. First long-term study of particle number size distributions and new particle formation events of regional aerosol in the North China Plain. Atmos. Chem. Phys. 11, 1565–1580.

Shika, S., Gadhavi, H., Suman, M.N.S., Ravikrishna, R., Gunthe, S.S., 2020. Atmospheric aerosol properties at a semi-rural location in southern India: particle size distributions and implications for cloud droplet formation. SN Appl. Sci. 2, 1007.

Siingh, D., Gautam, A.S., Buchunde, P.S., Kamra, A.K., 2018. Classification of the new particle formation events observed at a tropical site, Pune, India. Atmos. Environ. 190, 10–22.

Siingh, D., Gautam, A.S., Kamra, A.K., Komsaare, K., 2013. Nucleation events for the formation of charged aerosol particles at a tropical station — preliminary results. Atmos. Res. 132–133, 239–252.

Sipilä, M., Sarnela, N., Jokinen, T., Henschel, H., Junninen, H., Kontkanen, J., Richters, S., Kangasluoma, J., Franchin, A., Peräkylä, O., Rissanen, M.P., Ehn, M., Vehkamäki, H., Kurten, T., Berndt, T., Petäjä, T., Worsnop, D., Ceburnis, D., Kerminen, V.-M., Kulmala, M., O'Dowd, C., 2016. Molecular-scale evidence of aerosol particle formation via sequential addition of HIO3. Nature 537, 532–534.

Smith, J.N., Moore, K.F., Eisele, F.L., Voisin, D., Ghimire, A.K., Sakurai, H., McMurry, P. H., 2005. Chemical composition of atmospheric nanoparticles during nucleation events in Atlanta. J. Geophys. Res.: Atmos. 110.

Spracklen, D.V., Carslaw, K.S., Kulmala, M., Kerminen, V.-M., Sihto, S.-L., Riipinen, I., Merikanto, J., Mann, G.W., Chipperfield, M.P., Wiedensohler, A., Birmili, W., Lihavainen, H., 2008. Contribution of particle formation to global cloud condensation nuclei concentrations. Geophys. Res. Lett. 35 (n/a-n/a).

Srivastava, R., 2017. Trends in aerosol optical properties over South Asia. Int. J. Climatol. 37, 371–380.

Stanier, C.O., Khlystov, A.Y., Pandis, S.N., 2004a. Ambient aerosol size distributions and number concentrations measured during the Pittsburgh Air Quality Study (PAQS). Atmos. Environ. 38, 3275–3284.

Stanier, C.O., Khlystov, A.Y., Pandis, S.N., 2004b. Nucleation events during the pittsburgh air quality study: description and relation to key meteorological, gas phase. Aerosol. Sci. Technol. 38, 253–264.

Stolzenburg, D., Fischer, L., Vogel, A.L., Heinritzi, M., Schervish, M., Simon, M., Wagner, A.C., Dada, L., Ahonen, L.R., Amorim, A., Baccarini, A., Bauer, P.S., Baumgartner, B., Bergen, A., Bianchi, F., Breitenlechner, M., Brilke, S., Buenrostro Mazon, S., Chen, D., Dias, A., Draper, D.C., Duplissy, J., El Haddad, I., Finkenzeller, H., Frege, C., Fuchs, C., Garmash, O., Gordon, H., He, X., Helm, J., Hofbauer, V., Hoyle, C.R., Kim, C., Kirkby, J., Kontkanen, J., Kürten, A., Lampilahti, J., Lawler, M., Lehtipalo, K., Leiminger, M., Mai, H., Mathot, S., Mentler, B., Molteni, U., Nie, W., Nieminen, T., Nowak, J.B., Ojdanic, A., Onnela, A., Passananti, M., Petäjä, T., Quéléver, L.L.J., Rissanen, M.P., Sarnela, N., Schallhart, S., Tauber, C., Tomé, A., Wagner, R., Wang, M., Weitz, L., Wimmer, D., Xiao, M., Yan, C., Ye, P., Zha, Q., Baltensperger, U., Curtius, J., Dommen, J., Flagan, R.C., Kulmala, M., Smith, J.N., Worsnop, D.R., Hansel, A., Donahue, N.M., Winkler, P.M., 2018. Rapid growth of organic aerosol nanoparticles over a wide tropospheric temperature range. Proc. Natl. Acad. Sci. U.S.A. 115, 9122–9127.

Thomas, A., Sarangi, C., Kanawade, V.P., 2019. Recent increase in winter hazy days over Central India and the Arabian Sea. Sci. Rep. 9, 17406.

Tripathi, R.M., Khandekar, R.N., Mishra, U.C., 1988. Size distribution of atmospheric aerosols in urban sites in India. Sci. Total Environ. 77, 237–244.

Tripathi, S.N., Tare, V., Chinnam, N., Srivastava, A.K., Dey, S., Agarwal, A., Kishore, S., Lal, R.B., Manar, M., Kanawade, V.P., Chauhan, S.S.S., Sharma, M., Reddy, R.R., Gopal, K.R., Narasimhulu, K., Reddy, L.S.S., Gupta, S., Lal, S., 2006. Measurements of atmospheric parameters during Indian space research organization geosphere biosphere programme land campaign II at a typical location in the ganga basin: 1. Physical and optical properties. J. Geophys. Res.: Atmos. 111.

Twomey, S., 1977. The influence of pollution on the shortwave albedo of clouds. J. Atmos. Sci. 34, 1149–1152.

Usoskin, I.G., Kovaltsov, G.A., 2008. Cosmic rays and climate of the Earth: possible connection. Compt. Rendus Geosci. 340, 441–450.

Vana, M., Ehn, M., Petäjä, T., Vuollekoski, H., Aalto, P., de Leeuw, G., Ceburnis, D., O'Dowd, C.D., Kulmala, M., 2008. Characteristic features of air ions at Mace Head on the west coast of Ireland. Atmos. Res. 90, 278–286.

Vanhanen, J., Mikkilä, J., Lehtipalo, K., Sipilä, M., Manninen, H.E., Siivola, E., Petäjä, T., Kulmala, M., 2011. Particle size magnifier for nano-CN detection. Aerosol. Sci. Technol. 45, 533–542.

Varghese, M., Leena, P.P., Murugavel, P., Bankar, S., Todekar, K., Chowdhuri, S., Safai, P. D., Malap, N., Konwar, M., Dixit, S., Rao, Y.J., Prabha, T.V., 2020. New particle formation observed from a rain shadow region of the Western Ghats, India. Toxicol. Environ. Chem. 102, 305–333.

Wang, S., Zordan, C.A., Johnston, M.V., 2006. Chemical characterization of individual, airborne sub-10-nm particles and molecules. Anal. Chem. 78, 1750–1754.

Westervelt, D.M., Pierce, J.R., Adams, P.J., 2014. Analysis of feedbacks between nucleation rate, survival probability and cloud condensation nuclei formation. Atmos. Chem. Phys. 14, 5577–5597.

Wiedensohler, A., Birmili, W., Nowak, A., Sonntag, A., Weinhold, K., Merkel, M., Wehner, B., Tuch, T., Pfeifer, S., Fiebig, M., Fjäraa, A.M., Asmi, E., Sellegri, K., Depuy, R., Venzac, H., Villani, P., Laj, P., Aalto, P., Ogren, J.A., Swietlicki, E., Williams, P., Roldin, P., Quincey, P., Hüglin, C., Fierz-Schmidhauser, R., Gysel, M., Weingartner, E., Riccobono, F., Santos, S., Grüning, C., Faloon, K., Beddows, D., Harrison, R., Monahan, C., Jennings, S.G., O'Dowd, C.D., Marinoni, A., Horn, H.G., Keck, L., Jiang, J., Scheckman, J., McMurry, P.H., Deng, Z., Zhao, C.S., Moerman, M., Henzing, B., de Leeuw, G., Löschau, G., Bastian, S., 2012. Mobility particle size spectrometers: harmonization of technical standards and data structure to facilitate high quality long-term observations of atmospheric particle number size distributions. Atmos. Meas. Tech. 5, 657–685.

Wu, Z., Hu, M., Lin, P., Liu, S., Wehner, B., Wiedensohler, A., 2008. Particle number size distribution in the urban atmosphere of Beijing, China. Atmos. Environ. 42, 7967–7980.

Xiao, M., Hoyle, C.R., Dada, L., Stolzenburg, D., Kürten, A., Wang, M., Lamkaddam, H., Garmash, O., Mentler, B., Molteni, U., Baccarini, A., Simon, M., He, X.C., Lehtipalo, K., Ahonen, L.R., Baalbaki, R., Bauer, P.S., Beck, L., Bell, D., Bianchi, F., Brilke, S., Chen, D., Chiu, R., Dias, A., Duplissy, J., Finkenzeller, H., Gordon, H., Hofbauer, V., Kim, C., Koenig, T.K., Lampilahti, J., Lee, C.P., Li, Z., Mai, H., Makhmutov, V., Manninen, H.E., Marten, R., Mathot, S., Mauldin, R.L., Nie, W., Onnela, A., Partoll, E., Petäjä, T., Pfeifer, J., Pospisilova, V., Quéléver, L.L.J., Rissanen, M., Schobesberger, S., Schuchmann, S., Stozhkov, Y., Tauber, C., Tham, Y. J., Tomé, A., Vazquez-Pufleau, M., Wagner, A.C., Wanger, R., Wang, Y., Weitz, L., Wimmer, D., Wu, Y., Yan, C., Ye, P., Ye, Q., Zha, Q., Zhou, X., Amorim, A., Carslaw, K., Curtius, J., Hansel, A., Volkamer, R., Winkler, P.M., Flagan, R.C., Kulmala, M., Worsnop, D.R., Kirkby, J., Donahue, N.M., Baltensperger, U., El Haddad, I., Dommen, J., 2021. The driving factors of new particle formation and growth in the polluted boundary layer. Atmos. Chem. Phys. Discuss. 2021, 1–28.

Xiao, S., Wang, M.Y., Yao, L., Kulmala, M., Zhou, B., Yang, X., Chen, J.M., Wang, D.F., Fu, Q.Y., Worsnop, D.R., Wang, L., 2015. Strong atmospheric new particle formation in winter in urban Shanghai, China. Atmos. Chem. Phys. 15, 1769–1781.

Yadav, S.K., Kompalli, S.K., Gurjar, B.R., Mishra, R.K., 2021. Aerosol number concentrations and new particle formation events over a polluted megacity during the COVID-19 lockdown. Atmos. Environ. 259, 118526.

Yan, C., Dada, L., Rose, C., Jokinen, T., Nie, W., Schobesberger, S., Junninen, H., Lehtipalo, K., Sarnela, N., Makkonen, U., Garmash, O., Wang, Y., Zha, Q., Paasonen, P., Bianchi, F., Sipilä, M., Ehn, M., Petäjä, T., Kerminen, V.M., Worsnop, D.R., Kulmala, M., 2018. The role of H_2SO_4-NH_3 anion clusters in ion-induced aerosol nucleation mechanisms in the boreal forest. Atmos. Chem. Phys. 18, 13231–13243.

You, Y., Kanawade, V.P., de Gouw, J.A., Guenther, A.B., Madronich, S., Sierra-Hernández, M.R., Lawler, M., Smith, J.N., Takahama, S., Ruggeri, G., Koss, A., Olson, K., Baumann, K., Weber, R.J., Nenes, A., Guo, H., Edgerton, E.S., Porcelli, L., Brune, W.H., Goldstein, A.H., Lee, S.H., 2014. Atmospheric amines and ammonia measured with a chemical ionization mass spectrometer (CIMS). Atmos. Chem. Phys. 14, 12181–12194.

Yu, F., Luo, G., 2009. Simulation of particle size distribution with a global aerosol model: contribution of nucleation to aerosol and CCN number concentrations. Atmos. Chem. Phys. 9, 7691–7710.
Yu, F., Nadykto, A.B., Herb, J., Luo, G., Nazarenko, K.M., Uvarova, L.A., 2018. H2SO4–H2O–NH3 ternary ion-mediated nucleation (TIMN): kinetic-based model and comparison with CLOUD measurements. Atmos. Chem. Phys. 18, 17451–17474.
Yu, H., Ortega, J., Smith, J.N., Guenther, A.B., Kanawade, V.P., You, Y., Liu, Y., Hosman, K., Karl, T., Seco, R., Geron, C., Pallardy, S.G., Gu, L., Mikkilä, J., Lee, S.-H., 2014. New particle formation and growth in an isoprene-dominated ozark forest: from sub-5 nm to CCN-active sizes. Aerosol. Sci. Technol. 48, 1285–1298.
Yu, H., Ren, L., Kanawade, V.P., 2017. New particle formation and growth mechanisms in highly polluted environments. Current Pollution Rep. 3, 245–253.
Yu, H., Zhou, L., Liang, D., Shen, W., Dai, W., Zheng, J., Ma, Y., Chen, M., 2016. Nucleation and growth of sub-3 nm particles in the polluted urban atmosphere of a megacity in China. Atmos. Chem. Phys. 16, 2641–2657.
Yue, D.L., Hu, M., Zhang, R.Y., Wu, Z.J., Su, H., Wang, Z.B., Peng, J.F., He, L.Y., Huang, X.F., Gong, Y.G., Wiedensohler, A., 2011. Potential contribution of new particle formation to cloud condensation nuclei in Beijing. Atmos. Environ. 45, 6070–6077.
Zhang, R., 2010. Getting to the critical Nucleus of aerosol formation. Science 328, 1366–1367.
Zhang, R., Khalizov, A., Wang, L., Hu, M., Xu, W., 2012. Nucleation and growth of nanoparticles in the atmosphere. Chem. Rev. 112, 1957–2011.
Zhao, J., Eisele, F.L., Titcombe, M., Kuang, C., McMurry, P.H., 2010. Chemical ionization mass spectrometric measurements of atmospheric neutral clusters using the cluster-CIMS. J. Geophys. Res.: Atmos. 115 (n/a-n/a).
Zheng, J., Hu, M., Zhang, R., Yue, D., Wang, Z., Guo, S., Li, X., Bohn, B., Shao, M., He, L., Huang, X., Wiedensohler, A., Zhu, T., 2011. Measurements of gaseous H_2SO_4 by AP-ID-CIMS during CAREBeijing 2008 campaign. Atmos. Chem. Phys. 11, 7755–7765.
Zheng, J., Ma, Y., Chen, M., Zhang, Q., Wang, L., Khalizov, A.F., Yao, L., Wang, Z., Wang, X., Chen, L., 2015. Measurement of atmospheric amines and ammonia using the high-resolution time-of-flight chemical ionization mass spectrometry. Atmos. Environ. 102, 249–259.

Atmospheric Environment 256 (2021) 118460

Contents lists available at ScienceDirect

Atmospheric Environment

journal homepage: www.elsevier.com/locate/atmosenv

Observation of sub-3nm particles and new particle formation at an urban location in India

Mathew Sebastian [a], Vijay P. Kanawade [a,*], Jeffrey R. Pierce [b]

[a] Centre for Earth, Ocean and Atmospheric Sciences, University of Hyderabad, Hyderabad, India
[b] Department of Atmospheric Sciences, Colorado State University, Colorado, USA

HIGHLIGHTS

- Direct observation-based evidence of sub-3nm aerosol particles in India.
- The formation of sub-3nm particles occurred on about 63.9% of the total observation days.
- About 58% of the sub-3nm particle formation events did not show banana-shaped aerosol size growth.

GRAPHICAL ABSTRACT

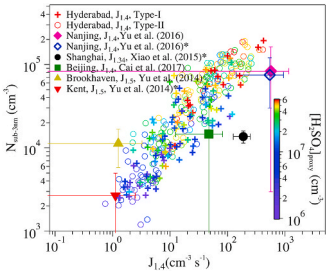

ARTICLE INFO

Keywords:
Formation rate
Growth rate
Sub-3nm particles
Urban environment

ABSTRACT

The formation of aerosol particles with diameters smaller than 3 nm (sub-3nm) is the dominant source of particle number in the atmosphere. But, observations of sub-3nm particles are scarce globally, particularly in India. Here, we present the direct observational evidence of sub-3nm particles in India. Simultaneous observations of particle size distributions in the size range from 1.2 to 3 nm and from 10 to 514 nm were made at an urban location, Hyderabad, in India during April–June 2019. New particle formation (NPF, the formation of sub-3nm particles) occurred frequently (63.9% of the total observation days). However, only 26.7% of the days displayed sub-3nm particle formation with subsequent growth of these particles to larger sizes (>10 nm), which is indicative of the regional NPF and growth (NPF&G) events, and these events had a formation rate of particles of diameter 1.4 nm ($J_{1.4}$) of 30.7 ± 73.6 $cm^{-3}s^{-1}$. The rest of the NPF event days had a higher $J_{1.4}$ of 58.3 ± 99.2 $cm^{-3}s^{-1}$, but the particles did not grow larger than 10 nm. Both NPF&G and NPF days had similar sulfuric acid concentrations, sub-3nm growth rates, condensation sink, and sub-3nm coagulation sink values. The wind speed and solar radiation were also similar on NPF&G and NPF days, but temperature, relative humidity, and wind direction had some differences between the types of events as explained by airmass back trajectory calculations. While organic vapors were not measured in this study, we hypothesize that the differences in airmass direction and history might have dissimilar organic vapors for condensational growth between the types of events, which determine when NPF events include subsequent growth to larger sizes.

* Corresponding author.
E-mail address: vijaykanawade03@yahoo.co.in (V.P. Kanawade).

https://doi.org/10.1016/j.atmosenv.2021.118460
Received 7 February 2021; Received in revised form 29 April 2021; Accepted 4 May 2021
Available online 7 May 2021
1352-2310/© 2021 Elsevier Ltd. All rights reserved.

1. Introduction

Atmospheric aerosol particles play a critical role in a variety of processes in our lives including weather, climate, public health, and haze formation (Chowdhury et al., 2018; Huang et al., 2014; IPCC, 2013; Kanawade et al., 2020a; Lelieveld et al., 2015). Aerosols are either directly emitted to the atmosphere from a variety of natural or anthropogenic sources (Paasonen et al., 2016) or formed from vapors that undergo gas-to-particle conversion (referred to as new particle formation, NPF). The small molecular clusters formed from NPF can further grow to sizes where they may act as cloud condensation nuclei (CCN) (larger than 50–100 nm in diameter, depending on the cloud) by vapor condensation and coagulation (Kuang et al., 2009; Pierce and Adams, 2007). NPF occurs almost everywhere in the terrestrial troposphere from mixed layer close to the surface to the upper troposphere (Kerminen et al., 2018; Kulmala et al., 2004b). Recent studies highlighted that a majority of the NPF events (42%) starts in the residual layer and these newly formed particles may be entrained into the growing mixed layer, where they continue to grow in size (Lampilahti et al., 2020; Nicholas et al., 2019). NPF has been estimated to produce about 54% of CCN in the troposphere in the present day with an estimated uncertainty range of 45–85% (Gordon et al., 2017). Such large uncertainties in the CCN formation, owing to our limited understanding of NPF and growth to CCN-active sizes, can hamper accurate estimation of the indirect forcing by aerosols and thereby future climate predictions (IPCC, 2013).

Atmospheric NPF starts with the formation and activation of 1–3 nm diameter clusters hereafter referred to as sub-3nm particles ($N_{sub\text{-}3nm}$) (McMurry et al., 2011). The sub-3nm particles form when sulfuric acid (H_2SO_4) and other condensable vapors (low-volatility organics, ammonia, amines, and water) collide to form stable clusters before re-evaporating (Kulmala and Kerminen, 2008). Ions from galactic cosmic rays and the radioactive decay of terrestrial elements also aid in the formation of small clusters in the lower and middle atmosphere (Jokinen et al., 2012; Kanawade and Tripathi, 2006; Kirkby et al., 2011; Turco et al., 1998). The stable critical cluster in the size range of 1.5–2.0 nm is either activated by condensation of low-volatility organic vapors once they have overcome the Kelvin barrier (Donahue et al., 2011; Kulmala et al., 2004a) or by heterogeneous reactions between the clusters and organic vapor (Wang et al., 2010). These small clusters are highly susceptible to coagulational scavenging by larger aerosols (Kuang et al., 2010; Westervelt et al., 2014). Thus, the competition between condensational growth and coagulation determines whether these small clusters will grow to become a CCN (Lehtipalo et al., 2016; Pierce and Adams, 2007; Seinfeld and Pandis, 1998). Recent advancements in aerosol instrumentation have led it possible to directly detect the number concentration and chemical composition of sub-3nm particles. These technological advancements include condensation particle counters (e.g. DEG-SMPS, CPCb, PH-CPC, Jiang et al., 2011; Kulmala et al., 2007a; Sipilä et al., 2009), particle size magnifier (PSM, Vanhanen et al., 2011), neutral air ion spectrometer (NAIS, Mirme and Mirme, 2013), Atmospheric Pressure interface Time-Of-Flight mass spectrometer (APi-TOF, Junninen et al., 2010), Chemical Ionization Atmospheric Pressure interface Time-Of-Flight mass spectrometer (CI-APi-TOF, Jokinen et al., 2012), and cluster-chemical ionization mass spectrometer (Cluster-CIMS, Zhao et al., 2010). Observations of sub-3nm particle number concentrations in the boreal forest, Finland showed that a pool of sub-2nm neutral clusters is always present (Kulmala et al., 2007b; Lehtipalo et al., 2011) and size-resolved growth rates increase linearly with the particle size from 1 nm to 5 nm (Kulmala et al., 2013; Lehtipalo et al., 2014). Similar results were also observed at two different sites in the USA (Atlanta and Boulder) based on de-coupling method to measure size- and time-dependent growth rates of sub-5nm particles (Kuang et al., 2012). But, the growth of sub-3nm particles to CCN-active sizes in the urban environment of Nanjing, China was limited by high anthropogenic precursors (Yu et al., 2016). A recent study elucidated the complex interactions between biogenic and anthropogenic vapors wherein oxides of nitrogen (NO_x) inhibits particle formation, while highly oxygenated molecules (HOMs), H_2SO_4 and ammonia together enhance particle formation (Lehtipalo et al., 2018). While field observations and modeling studies indicated that low-volatility organic vapors contribute significantly to the growth of nanoparticles (Barsanti et al., 2009; Paasonen et al., 2010; Riipinen et al., 2012; Smith et al., 2008, 2010; Yu et al., 2012), the relative contribution of different precursors to the growth of 1–5 nm particles varies greatly with atmospheric conditions (Riipinen et al., 2012).

Until now, the sources (natural and anthropogenic) and chemical composition of atmospheric sub-3nm particles and their precursors in diverse environments globally are mostly unknown, despite extensive measurements over the last decade (Kontkanen et al., 2017; Rose et al., 2015; Sulo et al., 2021; Xiao et al., 2015). Further, the contribution of neutral particles/clusters and ions to the total population of sub-3nm particles is also uncertain. The concentration of background aerosols and their precursors both are high in polluted environments, especially in developing countries like India and China. In China, despite extensive studies in the past 15 years using state-of-the-art instruments, the frequent occurrence of NPF at high aerosol loading conditions is mysterious (Chu et al., 2019). On the other hand, in India, there are only about 16 studies that have investigated NPF characteristics (frequency, particle growth and formation rates, diurnality, seasonality and meteorological influence on NPF). These studies used a Differential Mobility Particle Sizer (DMPS) (Hyvärinen et al., 2010; Komppula et al., 2009; Mönkkönen et al., 2005; Neitola et al., 2011; Sebastian et al., 2021), a Scanning Mobility Particle Sizer (SMPS) (Babu et al., 2016; Kanawade et al., 2014b, 2014c, 2020b; Kompalli et al., 2014; Moorthy et al., 2011; Murugavel and Chate, 2009), or a Wide Range Aerosol Spectrometer (WARS) (Kanawade et al., 2014a; Leena et al., 2017) to report particle size distributions down to 3 nm in diameter. The NAIS (Mirme et al., 2010) has also been used to study concentrations of positively and negatively charged particles in the size range of 1–40 nm (Kamra et al., 2015; Siingh et al., 2013). But none of the above previous studies in India have reported direct observation based evidence of neutral sub-3nm particles. Here, we provide the first, to the best of our knowledge, observation based evidence of neutral sub-3nm particles in India. The days with the formation of sub-3nm particles followed by subsequent growth to larger sizes (NPF&G) occurred less frequently than those days with the formation of sub-3nm particles without subsequent growth in particle size (NPF). We investigate the differences between the days with NPF&G and the days with NPF only and compare our observations to studies performed in other diverse locations.

2. Material and methods

2.1. Site description

The measurement site, the University of Hyderabad campus, is located to the west of Hyderabad urban city (17.46 ^{o}N, 78.32 ^{o}E; ~542 m above mean sea level), which is the sixth most populous urban agglomeration in India, located on the Deccan Plateau in India. According to the Census of India (2011), the population of Hyderabad urban agglomeration is about 6.7 million. The annual mean mass concentration of particulate matter with diameters smaller than 2.5 μm ($PM_{2.5}$) is 51 ± 23 μg m^{-3}, which is five times higher than the World Health Organization (WHO) recommended threshold value (10 μg m^{-3}) (Sreekanth et al., 2018). Fig. 1 shows the location of the Hyderabad city on a regional map showing averaged Ozone Monitoring Instrument (OMI) retrieved cloud screened tropospheric nitrogen dioxide (NO_2) column over the time period from April to June 2019 as a marker of combustion emissions indicating its urban nature. The direction of air masses arriving at Hyderabad was calculated using the NOAA ARL PC-version Hybrid Single-Particle Lagrangian Integrated Trajectory (HYSPLIT) transport and dispersion model (Draxler and Draxler, 2010). The two-day air mass backward trajectories starting at 500 m above the

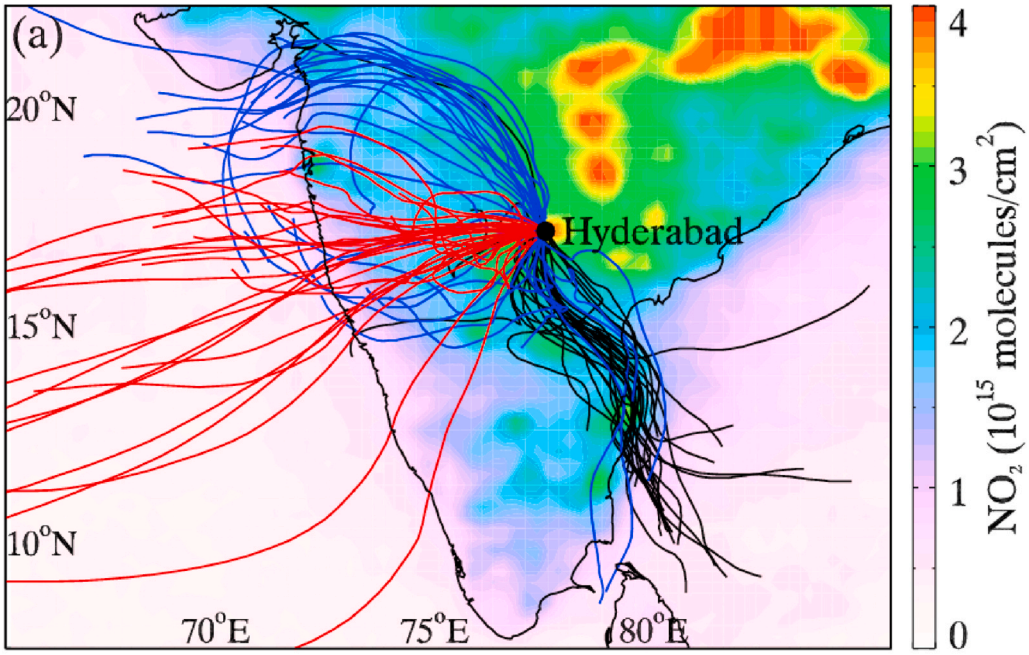

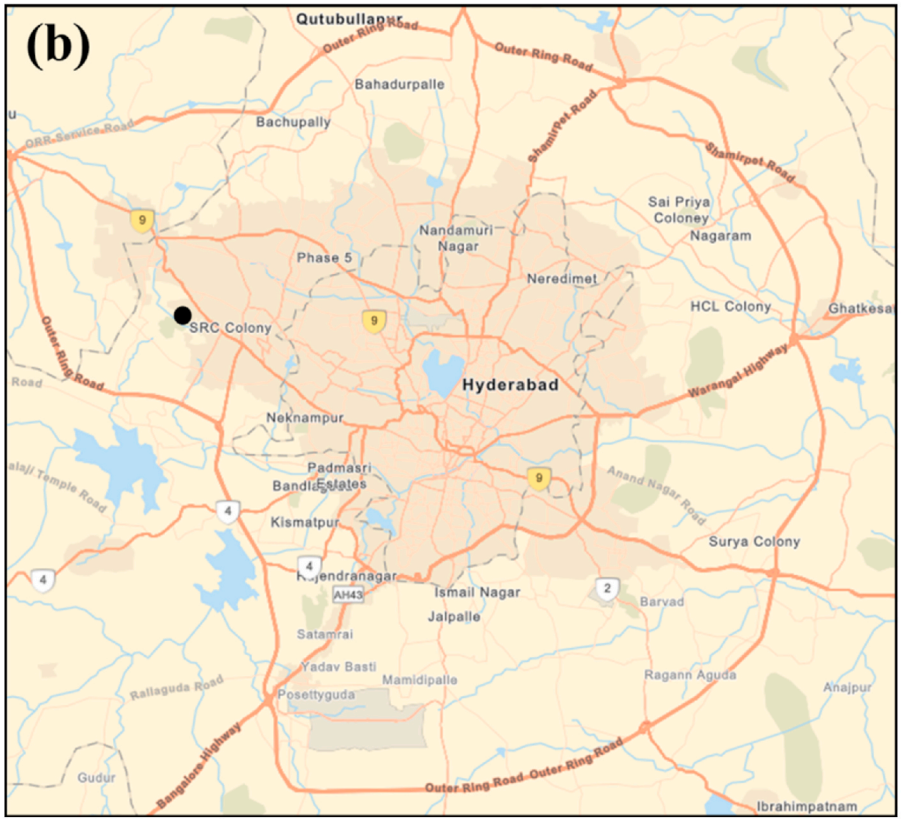

Fig. 1. (a) The spatial distribution of OMI-retrieved tropospheric nitrogen dioxide (NO_2) tropospheric column averaged over April–June 2019. The measurement site, Hyderabad, is shown by black dot symbol. Colored thin lines (black, blue and red) show HYSPLIT calculated 48 h air mass backward trajectories, starting at 8:30 a.m. local time at 500 m above the ground level at the measurement site, for different months (April, May, and June, respectively). (b) Street-map of Hyderabad city showing University of Hyderabad campus site by black dot, created at www.arcgis.com. (For interpretation of the references to colour in this figure legend, the reader is referred to the Web version of this article.)

ground level were calculated using gridded wind fields from the Global Data Assimilation System (GDAS), which has a spatial resolution of 1° × 1° longitude by latitude and a time resolution of 1 h (Kanamitsu, 1989). Hyderabad experiences a mixture of clean marine and polluted continental air masses during the pre-monsoon season (March through May). The observations were made at the Earth Sciences building located in the University of Hyderabad campus from 30 March to June 25, 2019. The site is surrounded by thin forested vegetation in a radius of 1 km, except few academic buildings. The nearest busy road, the old Hyderabad-Mumbai highway, is located about a kilometer to the east of the measurement site. During the pre-monsoon season (March through May), the weather over Hyderabad is generally hot (temperatures frequently exceeding over 30 °C) and dry (relative humidity less than 50%) (Kaskaoutis et al., 2009), and summer monsoonal rain arrives in mid-June. Hence, our observations mark the transition from the pre-monsoon season to the monsoon season.

2.2. Measurements of sub-3nm particles and particle size distributions

Sub-3nm particles were measured using A11 nCNC (AIRMODUS Oy, Finland), which consists of A10 Particle Size Magnifier (PSM) and A20 butanol Condensation Particle Counter (bCPC). In-depth details of the A10 PSM are described by Vanhanen et al. (2011). Briefly, diethylene glycol (DEG) supersaturation, which defines the lowest detectable size, is created by turbulently mixing heated saturator air with cooler sample air in the mixing chamber. The cut-off size of the PSM then can be varied by changing the mixing ratio of the saturator and sample air. Thus, nCNC was operated in a continuous scanning mode with a saturator flow rate of 0.1–1.3 litre per minute (lpm) with an upward ramp (0.1–1.3 lpm) automatically followed by a downward ramp (1.3–0.1 lpm) with a time step of 1 s, resulting in a cycle of 240 s.

The nCNC system is housed in an air-conditioned room to attain a stable room temperature. The instrument was calibrated using NiCr aerosols from a hot wire aerosol generator. Previous studies showed that the relative humidity of the sample air and chemical composition of the sampled particles affect the smallest detectable size of the particle counters operated with DEG (Kangasluoma et al., 2013, 2014). To prevent this issue, ambient air was brought to the air-conditioned room through an electrically grounded stainless steel stack (5 m long and 4 inch inner diameter) at a fixed flow rate of 110 lpm with a blower (Make: Vents, Model: VSM 125). The ambient air sample was then drawn to the nCNC through a custom-built diffusion dryer to maintain relative humidity less than 40%. Ultrafine particles can also be lost inside the sampling line due to their thermal motion affecting the total detection efficiency (Vanhanen et al., 2011). We calculated particle losses within the diffusion dryer by conducting sequential ambient air measurements with and without the diffusion dryer and found that less than 10% of the particles were lost in the diffusion dryer (Fig. S1 (a)). The nCNC was run at different fixed saturation flow rates with and without diffusion dryer to identify the percentage loss of particles at different sizes. The size dependent percentage loss in particles in the diffusion dryer is shown in Fig. S1(b). It was seen that there was a loss of 13.3% of particles at the lowest measured size (1.2–1.4 nm) and 7.4% at the largest size (2.2–3.0 nm). The measured total particle number concentration above a certain cut-off diameter as a function of the saturator flow rate was used to invert the particle size distribution. Several inversion techniques have been proposed such as step-wise method, Gaussian-shaped kernel function method (Lehtipalo et al., 2014), the Hagen and Alofs (H&A) method (Hagen and Alofs, 1983) and the expectation-maximization (EM) algorithm (Hagen and Alofs, 1983; Maher and Laird, 1985). Lehtipalo et al. (2014) recently illustrated that the Gaussian-shaped kernel function method works well for ambient measurements. Therefore, we used the Gaussian-shaped kernel function method to invert the raw scanning data to the particle size distribution in the size range from 1.2 to 3 nm, with 6 bins (1.2–1.4, 1.4–1.6, 1.6–1.8, 1.8–2.0, 2.0–2.2 and 2.2–3.0 nm). The sub-3nm particles may include charged particles, neutral particles, air ions or even big molecules that are activated by the supersaturated vapor in CPCs, and we cannot differentiate between them. For convenience, we refer them to neutrally charged sub-3nm particles in this study. In addition, we conducted simultaneous measurements of particle size distributions in the size range from 10 to 514 nm using TSI Scanning Mobility Particle Sizer (SMPS) which consists of an electrostatic classifier (Model 3082) with a long-differential mobility analyzer (LDMA, Model 3081 A) and a butanol CPC (Model 3772). The scanning cycle of the SMPS was 300 s, yielding a particle size distribution every 5 min. Sulfur dioxide (SO_2) was measured with a pulsed UV-fluorescence analyzer (Thermo Environmental). We also used meteorological parameters such as temperature, relative humidity (RH), wind speed, wind direction and solar radiation from the Automatic Weather Station at the site.

2.3. Classification of NPF events

NPF events were classified by visually inspecting nCNC and SMPS particle size distributions, following Dal Maso et al. (2005) and (Yu et al., 2016) methodologies, and further modified to identify four types (Table 1). The Type-I NPF&G events displayed significant bursts of sub-3nm particles in nCNC and the particle mode diameter smaller than 25 nm showed a steady growth in size for at least 6 h in SMPS, thus particle size distributions displaying a banana shape (e.g. Fig. 4a). The days with significant particle burst on sub-3nm particles in nCNC, but the absence of steady growth in SMPS were classified as Type-II NPF events (e.g. Fig. 4b). It was not possible to ascertain whether the particles continuously grew up to 10 nm as the aerosol size distribution between 4 nm and 10 nm was not measured. The days with no or insignificant increase in sub-3nm particles and nucleation mode particle number concentrations (10–25 nm) are classified as Type-III non-event days. Those days which could not be categorized into any of the above event types are referred to as Type-IV unidentified events. Type-IV events mostly consisted of events with large fluctuations in the particle size distributions, broken banana-shaped aerosol-size growth and/or noisy data as a result of abrupt mixing of different airmasses or any other unknown cause. nCNC measurements were not available during 1–7 May and 28 May - 9 June whereas SMPS measurements were not available during 14–23 April. Some of these days with only SMPS data showed Type-I or Type-II event features and were put into respective event Types. Some of the days with only nCNC data did not show significant particle bursts and were classified as Type-III events. The rest of the days were not put into any of these Types and were not considered in the analysis.

For the observed Type-I NPF&G events, the growth rate of sub-3nm particles ($GR_{sub\text{-}3nm}$) was determined by the maximum concentration method following Lehtinen and Kulmala (2003), modified and updated by Kulmala et al. (2012). Briefly, the representative diameter is taken as the midpoint of the measured size bin. First, the time evolution of particle number concentrations in each size bin is plotted and the normal distribution is fitted to the area around the maximum concentrations. The peak times for each size bin are then identified and plotted against the midpoint of the measured size bin to calculate the growth rate of sub-3nm particles by a linear least-squares fit.

The net flux of clusters growing past a certain diameter, d_p, is defined as the formation rate (J_{d_p}) and was calculated following Kulmala et al. (2012) methodology as,

$$J_{d_p} = \frac{dN_{d_p}}{\mathrm{dt}} + CoagS_{d_p} \cdot N_{d_p} + \frac{\mathrm{GR}_{\mathrm{sub-3nm}}}{\Delta \mathrm{d_p}} \cdot N_{d_p}$$

where N_{d_p} and $CoagS_{d_p}$ are the number concentration and coagulation sink of particles in the size range $[\mathrm{d_p}, \mathrm{d_p} + \Delta \mathrm{d_p}]$, respectively.

The coagulation sink (CoagS) determines how rapidly nanometer-size aerosol particles are removed through coagulation to pre-existing

Table 1
Summary of criteria used for classifying new particle formation based on nCNC and SMPS observations.

Event type	nCNC criteria	SMPS criteria
Type-I (NPF&G)	Significant burst of sub-3 nm particles	Particle mode diameter smaller than 25 nm showed a steady growth in size for at least 6 h, thus particle size distributions appearing as a banana shape
Type-II (NPF)	Significant burst of sub-3 nm particles	Particle mode diameter did not show a steady banana-shaped aerosol growth
Type-III (non-event)	No significant increase in sub-3 nm particles	No distinct change in particle mode diameter during the course of the day
Type-IV (unidentified)	Abrupt occurrence of sub-3 nm particles	Unable to identify whether it is one of the above events

particles and it was calculated using the methodology of Kulmala et al. (2012) as,

$$CoagS_{d_p} = \sum_{d_p}^{d'_p} K(d_p, d'_p).N_{d'_p}$$

where $K(d_p, d'_p)$ is the coagulation coefficient of particle sizes $d_p$and d'_p.

The condensation sink (CS) determines the ability of the particle size distribution to remove condensable vapors from the atmosphere and it was calculated following Kulmala et al. (2012) as,

$$CS = 4\pi D.\sum_{d'_p} \beta_{m,d'_p}.d'_p.N_{d'_p}$$

where D is the diffusion coefficient of the condensing vapor (assumed to be H_2SO_4, 0.104 cm^2 s^{-1}) and β_m represents a transition regime correction calculated by

$$\beta_m = \frac{1 + Kn}{1 + 1.677Kn + 1.333Kn^2}$$

where Knis the Knudsen number given by $Kn = 2\lambda/d_p$ where λis the mean free path.

Several investigators have developed a proxy for H_2SO_4 (Dada et al., 2020; Lu et al., 2019; Petäjä et al., 2009). Petäjä et al. (2009) developed a H_2SO_4 proxy in Hyytiala, Southern Finland using its source from reactions between SO_2 and OH and its loss by condensation sink. Lu et al. (2019) developed a daytime proxy based on measurements in Beijing, China specifically for relatively high condensation sink. More recently, Dada et al. (2020) developed a new proxy that takes into account the production of gaseous H_2SO_4 from reactions between SO_2 and OH and stabilized Criegee intermediates reactions (monoterpene and ozone), and its losses due to condensaiton sink and molecular cluster formaiton. However, we do not have measurements of monoterpenes and hydroxyl (OH) radicals. Therefore, we have calculated a proxy for H_2SO_4 ($[H_2SO_4]_{proxy}$) using the methodology of Mikkonen et al. (2011) as,

$$[H_2SO_4] = 8.21 \times 10^{-3}.k.Radiation.[SO_2]^{0.62}.(CS.RH)^{-0.13}$$

where k is the reaction coefficient (1.03495). The lower radiation (or season) dependence makes this proxy the more robust and best predictive H_2SO_4 proxy for a wide range of atmospheric conditions.

We have also calculated the growth rate due to H_2SO_4 alone (GR_{H2SO4}) following Erupe et al. (2010) as,

$$GR_{H_2SO_4} = \frac{3600 \times 10^9.M_s.c^{-\alpha}.([H_2SO_4] - [H_2SO_4]_{eq}).W_R}{(2\rho/10^3).6.022 \times 10^{23}}$$

$$c^{-\alpha} = \left(\frac{8 \times 10^3.R.T}{\pi.M_s}\right)^{1/2}$$

where $M_s$and c are the molecular weight (98 g mol^{-1}) and mean speed (m s^{-1}) of H_2SO_4, respectively. α is the mass transfer coefficient which is taken as unity here and $[H_2SO_4]_{eq}$ (molecules cm^{-1}) is the equilibrium concentration of H_2SO_4 (usually $[H_2SO_4] \gg [H_2SO_4]_{eq}$). $W_R$is the ratio of the wet H_2SO_4 diameter at a certain RH to dry H_2SO_4 particle diameter. ρ is the particle density (1200 kg m^{-3}), R the universal gas constant (8.314 J mol^{-1} K^{-1}) and T is the temperature.

3. Results and discussion

Fig. 2 shows the time evolution of particle size distribution from nCNC and SMPS for the entire study period. The number concentrations of sub-3nm particles occurred frequently, and subsequently, these freshly nucleated particles grew to larger sizes, showing typical banana-shaped particle size growth in the SMPS data. Fig. 3 shows the percentage of days of the occurrence of different types of events. Out of a total of 86 observation days, events with sustained sub-3nm concentrations above 10,000 particles cm^{-3} occurred on 55 days (63.9%), out of which Type-I NPF&G events occurred on 23 days (26.7%) and Type-II NPF events were observed on 32 days (37.2%). About 13 days (15.1%) showed no evidence for NPF (Type-III) and 7 days (8.1%) had unidentified features (Type-IV).

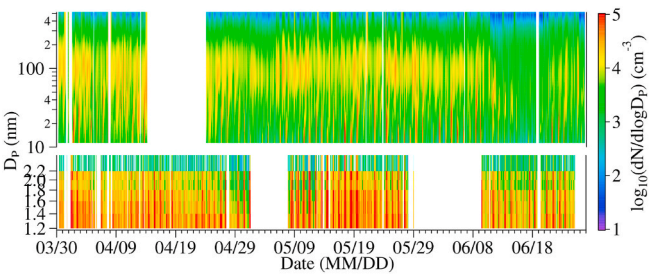

Fig. 2. Time-evolution of 10 min averaged particle size distributions from nCNC (1.2–3.0 nm) and SMPS (10–514 nm) from 30 March to June 25, 2019.

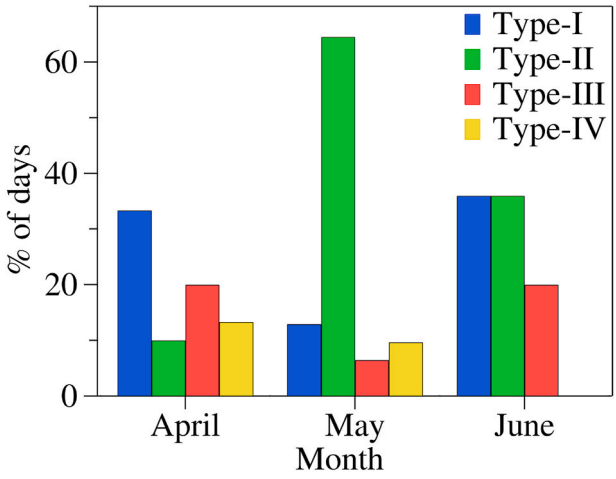

Fig. 3. The monthly percentage of occurrence of different type of event days.

Fig. 4 shows the diurnal pattern of typical Type-I, Type-II and Type-III event days. Both Type-I and Type-II event days display a large increase of sub-3nm particle number concentrations after sunrise (particle number concentrations greater than 10,000 particles cm^{-3}). For the typical Type-I event (Fig. 4a), a simultaneous increase in sub-3nm particles and nucleation mode particles in the diameter range from 10 nm to 25 nm at about 9:00 a.m. local time followed by the growth of these particles to larger sizes was observed. However, for the typical Type-II event (Fig. 4b), there was a significant increase in sub-3nm particles but the particle size distributions did not show any banana-shaped aerosol growth at all. The typical Type-III non-event day (Fig. 4c) did not show any significant increase of sub-3nm particles or aerosol growth.

We then examined various characteristics of the observed Type-I and Type-II events, such as the formation rate of particles of each size bin, $N_{sub\text{-}3nm}$, $GR_{sub\text{-}3nm}$, mean growth rate (GR), $[H_2SO_4]_{proxy}$, coagulation sink of sub-3nm particles ($CoagS_{sub\text{-}3nm}$), and total condensation sink (CS). Fig. 5a shows the box-whisker plots of formation rates of each of the size bins of the inverted particle size distribution from nCNC. In Fig. 5a, the formation rates for larger size bins are lower than those of smaller size bins, likely due to coagulational losses during the particle growth. The formation rate of particles in the smallest size bin (1.1–1.3 nm) is higher by one order of magnitude than the largest size bin (2.2–3.0 nm). Particle formation rates for Type-II events were approximately twice as high as Type-I events (Fig. 5a), even though the particles in the Type-II events did not continue to grow. Fig. 5b shows the

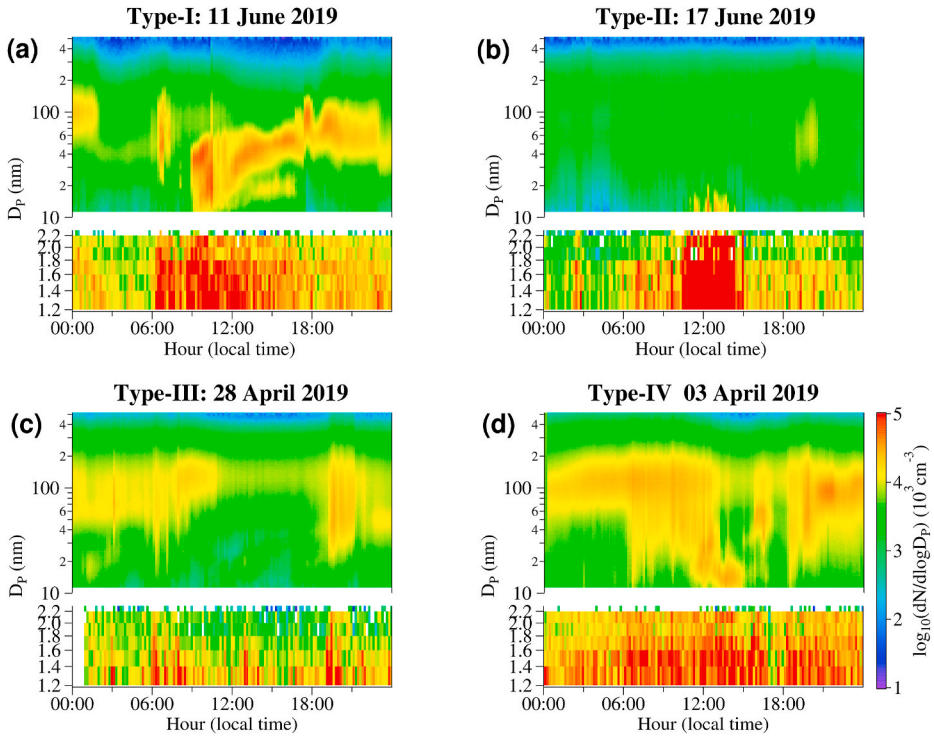

Fig. 4. Time evolution of the particle size distributions of typical (a) Type-I, (b) Type-II, (c) Type-III, and (d) Type-IV event days at Hyderabad. The size distribution in the size range from 1.2 to 3.0 nm and 10–514 nm were obtained using the nCNC and SMPS, respectively.

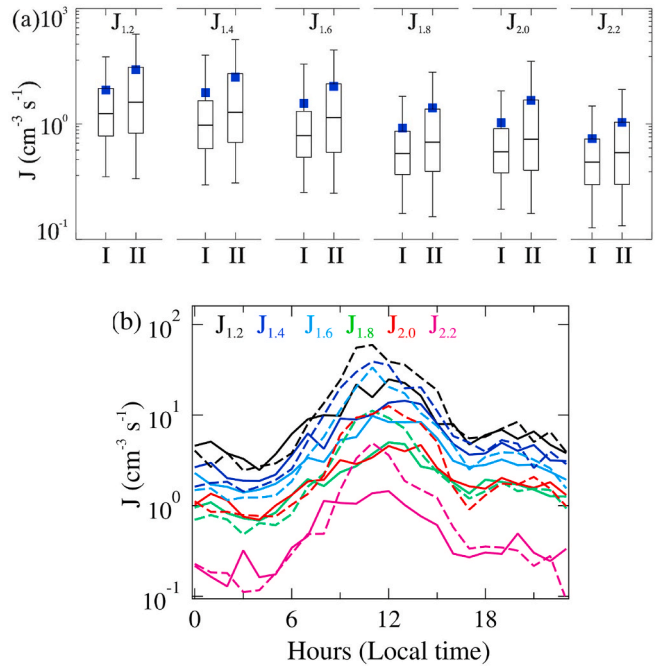

Fig. 5. (a) Box-whisker plots of $J_{1.2}$, $J_{1.4}$, $J_{1.6}$, $J_{1.8}$, and $J_{2.0}$. The blue dot indicates the mean, horizontal line indicates the median, top and bottom of box indicate 25th and 75th percentiles, respectively, and top and bottom whisker indicate 5th and 95th percentiles, respectively and (b) the median diurnal variation of $J_{1.2}$, $J_{1.4}$, $J_{1.6}$, $J_{1.8}$, and $J_{2.0}$ for Type-I NPF&G (thick lines) and Type-II NPF (dashed lines) event days. (For interpretation of the references to colour in this figure legend, the reader is referred to the Web version of this article.)

averaged diurnal variation of particle formation rate of different size bins. The average formation rate monotonically increased after sunrise, peaking around local noontime, and then dropping to pre-sunrise values

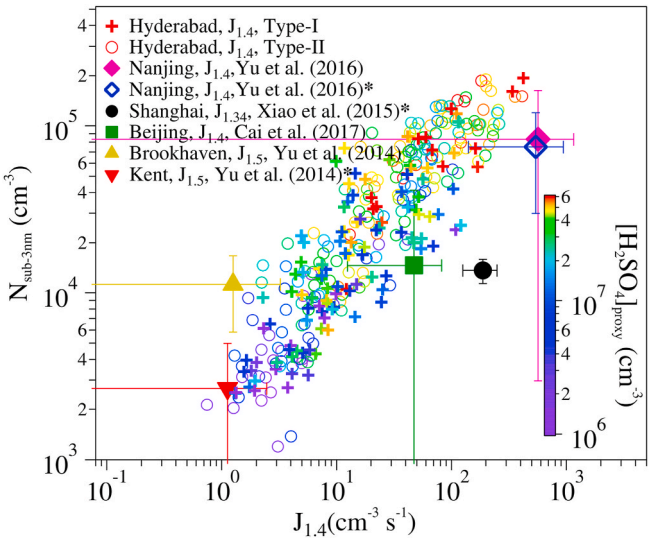

Fig. 6. Scatter plot of hourly averaged $J_{1.4}$ versus $N_{sub\text{-}3nm}$as a function of $[H_2SO_4]_{proxy}$ for Type-I (open circle) and Type-II (plus sign) events in Hyderabad. The data pertaining to $J_{1.4}$, $N_{sub\text{-}3nm,}$ and $[H_2SO_4]_{proxy}$ were taken as the average between 6:00 a.m. to 2:00 p.m. The mean values of $J_{1.4}$, $N_{sub\text{-}3nm}$, and $[H_2SO_4]_{proxy}$ for other sites in diverse environments listed in Table 2 are also plotted for comparison: Nanjing (filled and open diamond for spring and winter seasons, respectively), Shanghai (filled circle, winter) Beijing (filled square, spring), Brookhaven (filled upward triangle, spring), and Kent (filled downward triangle, winter).* indicates winter-time measurements. The colour scale shows the concentration of $[H_2SO_4]_{proxy}$. (For interpretation of the references to colour in this figure legend, the reader is referred to the Web version of this article.)

after sunset.

Fig. 6 shows a scatter plot of hourly averaged $J_{1.4}$ versus $N_{sub\text{-}3nm}$ of Type-I and Type-II events as a function of $[H_2SO_4]_{proxy}$ in Hyderabad. The mean and standard deviation of $J_{1.4}$ and $N_{sub\text{-}3nm}$ for the diverse range of previously studied sites (Table 2) are also plotted for comparison. The strong association among $J_{1.4}$, $N_{sub\text{-}3nm}$, and $[H_2SO_4]_{proxy}$ indicates the key role of H_2SO_4 in particle nucleation in Hyderabad. The sub-3nm particle concentration and formation rates are higher with a higher sulfuric acid concentration in general. The mean $N_{sub\text{-}3nm}$ concentration was higher by about a factor of two for Type-II event days (49.1 ± 56.2 cm^{-3}) as compared to Type-I event days (25.3 ± 35.7 cm^{-3}) (Fig. S2a). Further, the association between $N_{sub\text{-}3nm}$, $J_{1.4}$, and $[H_2SO_4]_{proxy}$ are similar for Type-I and Type-II events indicating that the $[H_2SO_4]$ was not the major cause for differences between Type-I and Type-II event days. The averaged nucleation mode particle number concentration ($N_{10\text{–}25nm}$) was also similar between Type-I and Type-II events (Fig. S2b). The averaged Aitken mode particle number concentration ($N_{25\text{–}100nm}$) was higher by a factor of 1.4 on Type-I NPF&G event days than Type-II NPF events (Fig. S2c) indicating that newly formed particles grow to large sizes significantly on Type-I events days. The accumulation mode particle number concentrations were similar between Type-I NPF&G and Type-II NPF event days (Fig. S2d) because newly formed particles on Type-I NPF&G event days did not grow beyond 100 nm in diameter. Therefore, the total surface area of particles, SA_{TOT} was similar between Type-I and Type-II event days (Fig. S2h). Further, the mean sulfuric acid concentrations were $(2.5 \pm 2.0) \times 10^7$ cm^{-3} and $(2.9 \pm 1.9) \times 10^7$ cm^{-3} for Type-I and Type-II events, respectively, which were nearly the same (Fig. S2e).

Table 2 summarizes the averaged (6:00 a.m. to 2:00 p.m. local time) characteristics of Type-I and Type-II events observed in Hyderabad and also provides these statistics for the other locations from previous studies. $N_{sub\text{-}3nm}$ concentrations were lower by about a factor of two in Hyderabad than in Nanjing (Yu et al., 2016), whereas they were higher by a factor of about 2–3 than Beijing (Cai et al., 2017) and Shanghai (Xiao et al., 2015), which are all urban locations. $N_{sub\text{-}3nm}$ concentrations at Hyderabad was an order of magnitude higher than that of Kent (Yu et al., 2014) and San Pietro (Kontkanen et al., 2016), which are comparatively cleaner sites. On Type-I NPF&G event days, $J_{1.4}$ varied from 0.7 cm^{-3} s^{-1} to 145.1 cm^{-3} s^{-1} (5th to 95th percentiles) with a mean and standard deviation of 30.7 ± 73.6 cm^{-3} s^{-1}, whereas on Type-II NPF event days, it varied from 0.7 cm^{-3} s^{-1} to 276.6 cm^{-3} s^{-1}with a mean and standard deviation of 58.3 ± 99.2 cm^{-3} s^{-1}. $J_{1.4}$ in Hyderabad was lower by an order of magnitude than in urban Nanjing and Shanghai, China (Xiao et al., 2015; Yu et al., 2016), whereas it was comparable to that of urban Beijing, China (Cai et al., 2018) and one order of magnitude higher than that of a relatively pristine atmosphere of coastal Brookhaven, USA, semi-rural Kent, USA, and forest-rural Hyytiala, Finland (Kulmala et al., 2012; Yu et al., 2014). The mean sub-3nm particle growth rates in Hyderabad were similar to that of other studies mentioned in Table 2. The mean growth rate in the size range 10–25 nm for Type-I NPF&G event days was found to be 4.9 ± 3.2 nm h^{-1}, which is also within the observed range in other locations (Table 2). Growth rate beyond 10 nm for Type-II events were not possible to be calculated as the particles did not grow beyond 10 nm. The mean total CS in the size range from 10 to 514 nm (CS_{TOT}) in Hyderabad was lower by a factor of 1.2–3 than other urban sites in China, but a direct comparison between Hyderabad and other sites cannot be established as the total CS was calculated for varying particle size ranges in respective sites.

The mean sub-3nm particle growth rates were found to be comparable between Type-I (2.2 ± 1.7 nm h^{-1}) and Type-II (2.0 ± 1.4 nm h^{-1}) events, indicating the similar levels of condensing vapors for nucleation

Table 2
Summary of averaged (6:00 a.m. to 2:00 p.m. local time) sub-3nm particle number concentrations ($N_{sub\text{-}3nm}$), formation rate of 1.4 nm particles ($J_{1.4}$), growth rate of sub-3nm particles ($GR_{sub\text{-}3nm}$), total growth rate (GR), sulfuric acid concentration proxy ($[H_2SO_4]_{proxy}$), total consternation sink (CS_{TOT}) and total coagulation sink ($CoagS_{TOT}$) for Type-I and Type-IINPF events in Hyderabad and various other sites in diverse environments. ±indicates standard deviation.

Site location	Site type	Time period	$N_{sub\text{-}3nm}$ (10^3 cm^{-3})	J (cm^{-3} s^{-1})	$GR_{sub\text{-}3nm}$ (nm h^{-1})	GR (nm h^{-1})	$[H_2SO_4]_{proxy}$ (10^7 cm^{-3})	CS (10^{-2} s^{-1})	$CoagS_{TOT}$ (10^{-4} s^{-1})	Reference
Type-I (NPF&G)	Urban	Apr–Jun.2019	25.3 ± 35.7	$J_{1.4}$,30.7 ± 73.6	2.2 ± 1.7	$GR_{10\text{-}25}$, 4.9 ± 3.2	2.5 ± 2.0[c]	1.6 ± 0.8[e]	3.4 ± 1.5[e]	This study
Type-II (NPF)	Urban	Apr–Jun. 2019	49.1 ± 56.2	$J_{1.4}$,58.3 ± 99.2	2.0 ± 1.4	–	2.9 ± 1.9[c]	1.8 ± 2.5[e]	3.2 ± 2.8[e]	This study
Nanjing, China	Urban	May.–Jun. 2014	83.3 ± 80.3	$J_{1.4}$, 566 ± 592	3.6	$GR_{3\text{-}20}$, 8.2	3.9[c]	1.9[f]	–	Yu et al. (2016)
Nanjing, China	Urban	Dec. 2014–Mar. 2015	75 ± 45	$J_{1.4}$, 543 ± 402	5.8	$GR_{3\text{-}20}$, 7.2	3.5[c]	3.1[f]	–	Yu et al. (2016)
Shanghai, China	Urban	Nov. 2013–Jan. 2014	13.6 ± 2.3	$J_{1.34}$, 188 ± 62.2	1.9 ± 3.1	$GR_{7\text{-}20}$, 11.4	3.7[d]	6.0[g]	–	Xiao et al. (2015)
Beijing, China	Urban	Mar.–Apr. 2016	14.6 ± 26.6	$J_{1.5}$,47.2 ± 34.7	2.4	2.3[b]	–	2.7[h]	–	Cai et al. (2017)
Brookhaven, USA	Coastal	Jul.–Aug. 2011	11.2 ± 5.4	$J_{1.5}$, 1.3 ± 2.0	–	$GR_{3\text{-}10}$, 1.6	1.2[d]	0.5[i]	–	Yu et al. (2014)
Kent, USA	Semi-rural	Dec. 2011–Jan. 2012	2.7 ± 2.3	$J_{1.5}$, 1.1 ± 1.4	–	$GR_{3\text{-}10}$, 3.7	2.1[d]	0.8[i]	–	Yu et al. (2014)
Hyytiala, Finland	Forest-rural	Oct. 2010–Sep. 2011	–	$J_{1.5}$, 1.4	1.4[a]	$GR_{3\text{-}25}$, 3.3	–	–	–	Kulmala et al. (2012)
San Pietro, Italy	Rural	Jun.–Jul. 2012	8.0[a]	$J_{1.6}$,45[a]	4.3[a]	$GR_{7\text{-}20}$, 7.2	–	1.1[j]	–	Kontkanen et al. (2016)

"-" indicates no data.
[a] For combined positive and negative ion clusters from NAIS.
[b] Mean growth rate.
[c] H_2SO_4 proxy calculated from Mikkonen et al. (2011).
[d] In-situ measured H_2SO_4; CS calculated for particle size range from.
[e] 10-514 nm.
[f] 3-750 nm.
[g] 3-615 nm.
[h] 3-10000 nm.
[i] 5-3000 nm.
[j] 3-600 nm.

and early growth of freshly formed particles during Type-I and Type-II events. Sulfuric acid is attributed to be the major contributor in particle nucleation by clustering with vapors (e.g. H_2O, NH_3 or organics) (Almeida et al., 2013; Erupe et al., 2011; Kirkby et al., 2011; Riipinen et al., 2007; Schobesberger et al., 2013; Sipilä et al., 2010; Weber et al., 1996) and growth (Kulmala and Kerminen, 2008; Vakkari et al., 2015; Wehner et al., 2005; Yu et al., 2017; Yue et al., 2010). However, H_2SO_4 alone fails to explain the growth at larger sizes (Riccobono et al., 2012; Riipinen et al., 2012). The particle growth rate due to H_2SO_4 was calculated following Erupe et al. (2010), and it accounted for 5–65% of the total observed growth for sizes larger than 10 nm on Type-I event days in this study (although it can explain all of the sub-3nm growth on both Type-I and Type-II days and this growth rate from H_2SO_4 was similar between the two types of days). This result is in-line with previous studies from diverse environments (Erupe et al., 2010; Yli-Juuti et al., 2016). This incomplete growth by sulfuric acid indicates the potential role of other condensable vapors in the particle growth. The mean $CoagS_{TOT}$ for Type-I (3.4×10^{-4} s^{-1}) and Type-II (3.2×10^{-4} s^{-1}) events were also comparable (Fig. S2f). These similar values indicate that differences in the CoagS were not the cause of Type-II events being different from the Type-I events. Further, CS_{TOT} was also comparable between Type-I (1.6×10^{-2} s^{-1}) and Type-II (1.8×10^{-2} s^{-1}) events (Fig. S2g) further indicating that the pre-existing aerosol concentrations were also not responsible for the differences between the event types. It can be concluded from the above discussion that neither [H_2SO_4], nor $CoagS_{sub\text{-}3nm}$, nor CS was the cause for the inhibited particle growth during Type-II NPF events. We further continue to investigate the potential differences between Type-I NPF&G and Type-II NPF events below in order to understand why NPF only sometimes appears to have particles survive.

Fig. S3 shows the diurnal variation in meteorological parameters, such as relative humidity, absolute temperature, wind speed, wind direction, solar radiation, and rainfall. There is strong diurnal variation in median RH ranging from 32 to 68%. The median RH is lower by ~3% throughout the day on Type-II NPF events than Type-I NPF&G events, which may be driven by temperature differences. The median temperature at the site varied from 24 to 38 °C on a diurnal basis during the period of study, which was higher by ~2 °C throughout the day on Type-II NPF events than Type-I NPF&G events, which may create differences in organic condensation between the days, which we discuss further below. Wind speed at the site appears similar for all Types of events. Fig. S3d shows that the wind direction shifts from south-west to south-east on Type-I NPF&G event days at around noontime whereas it remains south-west on Type-II NPF event days. It is possible that air mass from a particular direction is causing the lack of growth in the Type-II NPF events. This wind-direction shift in the Type-I NPF&G events could be indicative of an air-mass shift; however, it is the Type-I NPF&G events that have continuous, "banana-shaped" growth that requires a generally continuous homogeneous air mass. Hence, there is no clear evidence of regular air-mass shifts in either the Type-I or Type-II events. Related to the wind direction differences, we calculated airmass back trajectories for Type-I and Type-II event days using HYSPLIT model (Fig. 7). The airmass back trajectories were initiated at 08:30 a.m. and 2:30 p.m. local time at an altitude of 500 m above ground level. Type-I events occurred mostly in airmass from the west and south, while Type-II NPF events occurred mostly with the air masses arriving from the north-west and west of Hyderabad (a few from the south). While there is much overlap between the back trajectories of the two Types, it is possible that the differences that do exist may contribute to a difference in chemical species that may contribute to particle growth (discussed below). Solar radiation at the site peaks to ~600 Wm^{-2} around 12:00 p.m. local time and follows a similar pattern for all three Types of events diurnally with Type-III events having a slightly lower maximum during noon (Fig. S3e). There were only a few rainfall events during the period of observation and instruments were switched off during heavy rains. Hence, the meteorological parameters such as temperature, relative humidity, wind speed, and solar radiation were all comparable, except wind direction, between the Type-I and Type-II event days, which we explore more below.

While we do not have direct observations of organic species in this study, we hypothesize that differences in the abundance of condensable organics on Type-I NPF&G and Type–II NPF days may be contributing to the differences in particle growth/survival. The gas-phase oxidation of volatile organic compounds plays a crucial role in particle growth. The concentration of low volatility organics and semi-volatile organics are ~2–20 times higher than [H_2SO_4] over continental regions (Yu, 2011).

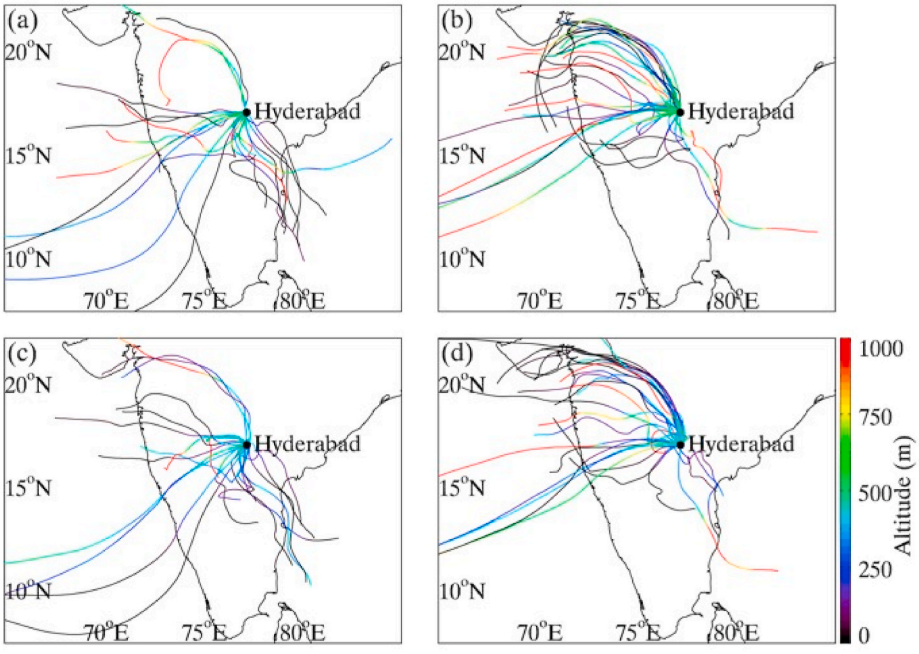

Fig. 7. HYSPLIT-calculated 48-h air mass backward trajectories starting at 500 m above the ground level as a function of altitude (a) starting at 8:30 a.m. local time for Type-I events, (b) Type-II events, (c) starting at 2:30 p.m. local time for Type-I events, and (d) Type-II events.

Patoulias et al. (2014) illustrated that low volatile organics play a crucial role in the early growth stage along with sulfuric acid, and semi-volatile organics contribute greatly once the particles have grown to larger sizes. The early (sub-3nm) growth rates were also similar on both Types of events, which may be due to the similar [H_2SO_4]. Furthermore, our estimated growth rate due to [H_2SO_4] is similar to the early growth rates, implying that [H_2SO_4] was responsible for most of this growth. Type-I NPF&G event days had double the growth rate for particles larger than 10 nm compared to the sub-3nm growth rate, from which we can infer that other species, such as semi-volatile organics accelerated the growth at the larger sizes. If Type-II NPF days did not have these condensable vapors, the early growth rates would not accelerate, making the newly formed particles more susceptible to coagulational losses.

We see two potential reasons why the organic vapors may be different between the days. First, the airmass back trajectories and wind directions were somewhat different, on average, between the two types of days, which may lead to air masses with different condensable species concentrations. Secondly, the temperatures were, on average, about 2° higher on Type-II NPF days than Type-I NPF&G days. Higher temperatures correspond to higher saturation vapor concentrations of gas phase species, causing condensable organics to be more volatile, leading to slower growth rates, especially at smaller sizes. However, this temperature difference is relatively minor, so it is unclear if it can explain much of the differences between the two Types of events.

4. Conclusions

We present direct observation-based evidence of sub-3nm aerosol particles from an urban location, Hyderabad, in India. Formation of sub-3nm particles occurred frequently in Hyderabad (63.9% of the total 86 observation days) with only 26.7% of all the days showing nucleation in sub-3nm size range followed by a "banana-shaped" particle growth to larger sizes, thus indicating a complete Type-I NPF&G event. About 37.2% of the total days had nucleation with no growth for particle sizes larger than 10 nm (Type-II NPF events). Type-I NPF&G events had a formation rate ($J_{1.4}$) of 30.7 ± 73.6 cm^{-3} s^{-1} and Type-II NPF event days had 58.3 ± 99.2 $cm^{-3}s^{-1}$. Sub-3 nm particle concentrations for Type-I NPF&G and Type-II NPF events were 25.3 ± 35.7 cm^{-3} and 49.1 ± 56.2 cm^{-3}, respectively. Furthermore, the formation rates and related values were all in the range of prior studies across diverse environments. Though the formation rates were higher for Type-II NPF events, the particles did not grow beyond 10 nm. Moreover, different characteristics of the early formation and growth of the two Types of events ([H_2SO_4], sub-3nm coagulation sink, condensation sink, and the sub-3nm growth rates) were all similar. The sub-3nm particle number concentrations were also well correlated with the calculated sulfuric acid proxy indicating that sulfuric acid may have played an important role in the formation of sub-3nm particles at Hyderabad, in-line with other studies (Kulmala et al., 2013; Yu et al., 2014, 2016). But, it is also possible that other compounds e.g. low-volatile organic compounds or ammonia might have also played a significant role in the formation and growth of sub-3nm particles (Barsanti et al., 2009; Lehtipalo et al., 2018; Riipinen et al., 2012; Tröstl et al., 2016). Amongst meteorological conditions, it appeared that the differences in airmass direction and history may have dissimilar aerosol precursor species available for growth between different Types of events. Observations in diverse environments ranging from urban to remote continental areas concluded that the growth is dominated by the condensation of organic compounds and sulfuric acid (Kerminen et al., 2018). Long-term observations of sub-3nm particles in the boreal forest also indicated that sulfuric acid and highly oxygenated molecules and their dimers play a significant role in new particle formation (Sulo et al., 2021). Thus, we hypothesize that the growth of sub-3nm particles on the Type-II NPF event days might have been inhibited by a low abundance of organic vapors in the airmass arriving at the site.

A future study using a suite of state-of-the-art instruments for gas-phase and aerosol composition measurements is required to test our hypothesis. Further, long-term observations are crucial to investigate the frequency, intensity and seasonal timing of sub-3nm particle formation and growth at our site to investigate contributions of newly formed particles to the total aerosol loading and related weather (fog, haze and cloud formation) and health effects.

CRediT authorship contribution statement

Mathew Sebastian: Data curation, Software, Formal analysis, Methodology, Writing – original draft. **Vijay P. Kanawade:** Conceptualization, Funding acquisition, Investigation, Methodology, Project administration, Supervision, Writing – original draft, Writing – review & editing. **Jeffrey R. Pierce:** Investigation, Methodology, Writing – review & editing.

Declaration of competing interest

The authors declare that they have no known competing financial interests or personal relationships that could have appeared to influence the work reported in this paper.

Acknowledgments and data availability

VPK would like to thank, Department of Science & Technology (DST) – Climate Change Programme Division (Aerosol/89/2017) and DST-Science and Engineering Research Board (SERB) (ECR/2016/001333) for funding support. JRP was supported by the US Department of Energy's Atmospheric System Research, an Office of Science, Office of Biological and Environmental Research program, under grant DE-SC0019000. Authors acknowledge P. Dasari, Telangana Pollution Control Board (TSPCB) for providing meteorological and SO_2 data from Hyderabad University site. The authors gratefully acknowledge the NOAA Air Resources Laboratory (ARL) for the provision of the HYSPLIT transport and dispersion model used in this publication. Authors also acknowledge Abin Thomas for helping us with HYSPLIT model runs and discussions. The authors also thank the anonymous reviewers for their many insightful comments and suggestions. nCNC raw particle number concentrations and SMPS datasets are archived at https://doi.org/10.17632/hrh6mpkyrs.1.

Appendix A. Supplementary data

Supplementary data to this article can be found online at https://doi.org/10.1016/j.atmosenv.2021.118460.

References

Almeida, J., Schobesberger, S., Kurten, A., Ortega, I.K., Kupiainen-Maatta, O., Praplan, A. P., Adamov, A., Amorim, A., Bianchi, F., Breitenlechner, M., David, A., Dommen, J., Donahue, N.M., Downard, A., Dunne, E., Duplissy, J., Ehrhart, S., Flagan, R.C., Franchin, A., Guida, R., Hakala, J., Hansel, A., Heinritzi, M., Henschel, H., Jokinen, T., Junninen, H., Kajos, M., Kangasluoma, J., Keskinen, H., Kupc, A., Kurten, T., Kvashin, A.N., Laaksonen, A., Lehtipalo, K., Leiminger, M., Leppa, J., Loukonen, V., Makhmutov, V., Mathot, S., McGrath, M.J., Nieminen, T., Olenius, T., Onnela, A., Petaja, T., Riccobono, F., Riipinen, I., Rissanen, M., Rondo, L., Ruuskanen, T., Santos, F.D., Sarnela, N., Schallhart, S., Schnitzhofer, R., Seinfeld, J. H., Simon, M., Sipila, M., Stozhkov, Y., Stratmann, F., Tome, A., Trostl, J., Tsagkogeorgas, G., Vaattovaara, P., Viisanen, Y., Virtanen, A., Vrtala, A., Wagner, P. E., Weingartner, E., Wex, H., Williamson, C., Wimmer, D., Ye, P., Yli-Juuti, T., Carslaw, K.S., Kulmala, M., Curtius, J., Baltensperger, U., Worsnop, D.R., Vehkamaki, H., Kirkby, J., 2013. Molecular understanding of sulphuric acid-amine particle nucleation in the atmosphere. Nature 502, 359–363.

Babu, S.S., Kompalli, S.K., Moorthy, K.K., 2016. Aerosol number size distributions over a coastal semi urban location: seasonal changes and ultrafine particle bursts. Sci. Total Environ. 563–564, 351–365.

Barsanti, K.C., McMurry, P.H., Smith, J.N., 2009. The potential contribution of organic salts to new particle growth. Atmos. Chem. Phys. 9, 2949–2957.

Cai, R., Yang, D., Ahonen, L.R., Shi, L., Korhonen, F., Ma, Y., Hao, J., Petäjä, T., Zheng, J., Kangasluoma, J., Jiang, J., 2018. Data inversion methods to determine sub-3 nm

aerosol size distributions using the particle size magnifier. Atmospheric Measurement and Techniques 11, 4477–4491.
Cai, R., Yang, D., Fu, Y., Wang, X., Li, X., Ma, Y., Hao, J., Zheng, J., Jiang, J., 2017. Aerosol surface area concentration: a governing factor in new particle formation in Beijing. Atmos. Chem. Phys. 17, 12327–12340.
Census of India, 2011. India, Registrar General. Census of India, 2011. Provisional Population Totals, India. Paper 1 (2011).
Chowdhury, S., Dey, S., Smith, K., 2018. Ambient PM2.5 exposure and expected premature mortality to 2100 in India under climate change scenarios. Nat. Commun. 9, 318.
Chu, B., Kerminen, V.M., Bianchi, F., Yan, C., Petäjä, T., Kulmala, M., 2019. Atmospheric new particle formation in China. Atmos. Chem. Phys. 19, 115–138.
Dada, L., Ylivinkka, I., Baalbaki, R., Li, C., Guo, Y., Yan, C., Yao, L., Sarnela, N., Jokinen, T., Daellenbach, K.R., Yin, R., Deng, C., Chu, B., Nieminen, T., Wang, Y., Lin, Z., Thakur, R.C., Kontkanen, J., Stolzenburg, D., Sipilä, M., Hussein, T., Paasonen, P., Bianchi, F., Salma, I., Weidinger, T., Pikridas, M., Sciare, J., Jiang, J., Liu, Y., Petäjä, T., Kerminen, V.M., Kulmala, M., 2020. Sources and sinks driving sulfuric acid concentrations in contrasting environments: implications on proxy calculations. Atmos. Chem. Phys. 20, 11747–11766.
Dal Maso, M., Kulmala, M., Riipinen, I., Wagner, R., 2005. Formation and growth of fresh atmospheric aerosols: eight years of aerosol size distribution data from SMEAR II, Hyytiälä, Finland. Boreal Environ. Res. 10, 323–336.
Donahue, N.M., Trump, E.R., Pierce, J.R., Riipinen, I., 2011. Theoretical constraints on pure vapor-pressure driven condensation of organics to ultrafine particles. Geophysocal Research Letters 38, L16801.
Draxler, R.R., Draxler, G.D., 2010. HYSPLIT—HYbrid Single-Particle Lagrangian Integrated Trajectory Model. http://ready.arl.noaa.gov/HYSPLIT.php.
Erupe, M.E., Benson, D.R., Li, J., Young, L.-H., Verheggen, B., Al-Refai, M., Tahboub, O., Cunningham, V., Frimpong, F., Viggiano, A.A., Lee, S.-H., 2010. Correlation of aerosol nucleation rate with sulfuric acid and ammonia in kent Ohio: an atmospheric observation. J. Geophys. Res. 115, D23216.
Erupe, M.E., Viggiano, A.A., Lee, S.H., 2011. The effect of trimethylamine on atmospheric nucleation involving H2SO4. Atmos. Chem. Phys. 11, 4767–4775.
Gordon, H., Kirkby, J., Baltensperger, U., Bianchi, F., Breitenlechner, M., Curtius, J., Dias, A., Dommen, J., Donahue, N.M., Dunne, E.M., Duplissy, J., Ehrhart, S., Flagan, R.C., Frege, C., Fuchs, C., Hansel, A., Hoyle, C.R., Kulmala, M., Kürten, A., Lehtipalo, K., Makhmutov, V., Molteni, U., Rissanen, M.P., Stozkhov, Y., Tröstl, J., Tsagkogeorgas, G., Wagner, R., Williamson, C., Wimmer, D., Winkler, P.M., Yan, C., Carslaw, K.S., 2017. Causes and importance of new particle formation in the present-day and preindustrial atmospheres. J. Geophys. Res.: Atmosphere 122, 8739–8760.
Hagen, D.E., Alofs, D.J., 1983. Linear inversion method to obtain aerosol size distributions from measurements with a differential mobility analyzer. Aerosol. Sci. Technol. 2, 465–475.
Huang, R.-J., Zhang, Y., Bozzetti, C., Ho, K.-F., Cao, J.-J., Han, Y., Daellenbach, K.R., Slowik, J.G., Platt, S.M., Canonaco, F., Zotter, P., Wolf, R., Pieber, S.M., Bruns, E.A., Crippa, M., Ciarelli, G., Piazzalunga, A., Schwikowski, M., Abbaszade, G., Schnelle-Kreis, J., Zimmermann, R., An, Z., Szidat, S., Baltensperger, U., Haddad, I.E., Prévôt, A.H., 2014. High secondary aerosol contribution to particulate pollution during haze events in China. Nature 514, 218–222.
Hyvärinen, A.P., Lihavainen, H., Komppula, M., Panwar, T.S., Sharma, V.P., Hooda, R.K., Viisanen, Y., 2010. Aerosol measurements at the Gual Pahari EUCAARI station: preliminary results from in-situ measurements. Atmos. Chem. Phys. 10, 7241–7252.
IPCC, 2013. Climate Change 2013:The Physical Science Basis. Contribution of Working Group I to the Fifth Assessment Report of the Intergovernmental Panel on Climate Change. Cambridge University Press, Cambridge, United Kingdom and New York, NY, USA.
Jiang, J., Chen, M., Kuang, C., Attoui, M., McMurry, P.H., 2011. Electrical mobility spectrometer using a diethylene glycol condensation particle counter for measurement of aerosol size distributions down to 1 nm. Aerosol. Sci. Technol. 45, 510–521.
Jokinen, T., Sipilä, M., Junninen, H., Ehn, M., Lönn, G., Hakala, J., Petäjä, T., Mauldin Iii, R.L., Kulmala, M., Worsnop, D.R., 2012. Atmospheric sulphuric acid and neutral cluster measurements using CI-APi-TOF. Atmos. Chem. Phys. 12, 4117–4125.
Junninen, H., Ehn, M., Petäjä, T., Luosujärvi, L., Kotiaho, T., Kostiainen, R., Rohner, U., Gonin, M., Fuhrer, K., Kulmala, M., Worsnop, D.R., 2010. A high-resolution mass spectrometer to measure atmospheric ion composition. Atmospheric Measurement and Techniques 3, 1039–1053.
Kamra, A.K., Siingh, D., Gautam, A.S., Kanawade, V.P., Tripathi, S.N., Srivastava, A.K., 2015. Atmospheric ions and new particle formation events at a tropical location, Pune, India. Q. J. R. Meteorol. Soc. 141, 3140–3156.
Kanamitsu, M., 1989. Description of the NMC global data assimilation and forecast system. Weather Forecast. 4, 335–342.
Kanawade, V.P., Shika, S., Pöhlker, C., Rose, D., Suman, M.N.S., Gadhavi, H., Kumar, A., Nagendra, S.M.S., Ravikrishna, R., Yu, H., Sahu, L.K., Jayaraman, A., Andreae, M.O., Pöschl, U., Gunthe, S.S., 2014a. Infrequent occurrence of new particle formation at a semi-rural location, Gadanki, in tropical Southern India. Atmos. Environ. 94, 264–273.
Kanawade, V.P., Srivastava, A.K., Ram, K., Asmi, E., Vakkari, V., Soni, V.K., Varaprasad, V., Sarangi, C., 2020a. What caused severe air pollution episode of November 2016 in New Delhi? Atmos. Environ. 222, 117125.
Kanawade, V.P., Tripathi, S.N., 2006. Evidence for the role of ion-induced particle formation during an atmospheric nucleation event observed in Tropospheric Ozone Production about the Spring Equinox (TOPSE). J. Geophys. Res.: Atmosphere 111, D02209.
Kanawade, V.P., Tripathi, S.N., Bhattu, D., Shamjad, P.M., 2014b. Sub-micron particle number size distributions characteristics at an urban location, Kanpur, in the Indo-Gangetic Plain. Atmos. Res. 147–148, 121–132.
Kanawade, V.P., Tripathi, S.N., Chakraborty, A., Yu, H., 2020b. Chemical characterization of sub-micron aerosols during new particle formation in an urban atmosphere. Aerosol and Air Quality Research 20, 1294–1305.
Kanawade, V.P., Tripathi, S.N., Siingh, D., Gautam, A.S., Srivastava, A.K., Kamra, A.K., Soni, V.K., Sethi, V., 2014c. Observations of new particle formation at two distinct Indian subcontinental urban locations. Atmos. Environ. 96, 370–379.
Kangasluoma, J., Junninen, H., Lehtipalo, K., Mikkilä, J., Vanhanen, J., Attoui, M., Sipilä, M., Worsnop, D., Kulmala, M., Petäjä, T., 2013. Remarks on ion generation for CPC detection efficiency studies in sub-3-nm size range. Aerosol. Sci. Technol. 47, 556–563.
Kangasluoma, J., Kuang, C., Wimmer, D., Rissanen, M.P., Lehtipalo, K., Ehn, M., Worsnop, D.R., Wang, J., Kulmala, M., Petäjä, T., 2014. Sub-3 nm particle size and composition dependent response of a nano-CPC battery. Atmospheirc Measuremen and Techniques 7, 689–700.
Kaskaoutis, D., Badarinath, K., Kharol, S., Sharma, A., Kambezidis, H., 2009. Variations in the aerosol optical properties and types over the tropical urban site of Hyderabad, India. J. Geophys. Res.: Atmosphere 114, D22204.
Kerminen, V.-M., Chen, X., Vakkari, V., Petäjä, T., Kulmala, M., Bianchi, F., 2018. Atmospheric new particle formation and growth: review of field observations. Environ. Res. Lett. 13, 103003.
Kirkby, J., Curtius, J., Almeida, J., Dunne, E., Duplissy, J., Ehrhart, S., Franchin, A., Gagne, S., Ickes, L., Kurten, A., Kupc, A., Metzger, A., Riccobono, F., Rondo, L., Schobesberger, S., Tsagkogeorgas, G., Wimmer, D., Amorim, A., Bianchi, F., Breitenlechner, M., David, A., Dommen, J., Downard, A., Ehn, M., Flagan, R.C., Haider, S., Hansel, A., Hauser, D., Jud, W., Junninen, H., Kreissl, F., Kvashin, A., Laaksonen, A., Lehtipalo, K., Lima, J., Lovejoy, E.R., Makhmutov, V., Mathot, S., Mikkila, J., Minginette, P., Mogo, S., Nieminen, T., Onnela, A., Pereira, P., Petaja, T., Schnitzhofer, R., Seinfeld, J.H., Sipila, M., Stozhkov, Y., Stratmann, F., Tome, A., Vanhanen, J., Viisanen, Y., Vrtala, A., Wagner, P.E., Walther, H., Weingartner, E., Wex, H., Winkler, P.M., Carslaw, K.S., Worsnop, D.R., Baltensperger, U., Kulmala, M., 2011. Role of sulphuric acid, ammonia and galactic cosmic rays in atmospheric aerosol nucleation. Nature 476, 429–433.
Kompalli, S.K., Babu, S.S., Moorthy, K.K., Gogoi, M.M., Nair, V.S., Chaubey, J.P., 2014. The formation and growth of ultrafine particles in two contrasting environments: a case study. Annales Geophysics 32, 817–830.
Komppula, M., Lihavainen, H., Hyvärinen, A.P., Kerminen, V.M., Panwar, T.S., Sharma, V.P., Viisanen, Y., 2009. Physical properties of aerosol particles at a Himalayan background site in India. J. Geophys. Res.: Atmosphere 114, D12202.
Kontkanen, J., Järvinen, E., Manninen, H.E., Lehtipalo, K., Kangasluoma, J., Decesari, S., Gobbi, G.P., Laaksonen, A., Petäjä, T., Kulmala, M., 2016. High concentrations of sub-3nm clusters and frequent new particle formation observed in the Po Valley, Italy, during the PEGASOS 2012 campaign. Atmos. Chem. Phys. 16, 1919–1935.
Kontkanen, J., Lehtipalo, K., Ahonen, L., Kangasluoma, J., Manninen, H.E., Hakala, J., Rose, C., Sellegri, K., Xiao, S., Wang, L., Qi, X., Nie, W., Ding, A., Yu, H., Lee, S., Kerminen, V.M., Petäjä, T., Kulmala, M., 2017. Measurements of sub-3 nm particles using a particle size magnifier in different environments: from clean mountain top to polluted megacities. Atmos. Chem. Phys. 17, 2163–2187.
Kuang, C., Chen, M., Zhao, J., Smith, J., McMurry, P.H., Wang, J., 2012. Size and time-resolved growth rate measurements of 1 to 5 nm freshly formed atmospheric nuclei. Atmos. Chem. Phys. 12, 3573–3589.
Kuang, C., McMurry, P.H., McCormick, A.V., 2009. Determination of cloud condensation nuclei production from measured new particle formation events. Geophys. Res. Lett. 36, L09822.
Kuang, C., Riipinen, I., Sihto, S.L., Kulmala, M., McCormick, A.V., McMurry, P.H., 2010. An improved criterion for new particle formation in diverse atmospheric environments. Atmos. Chem. Phys. 10, 8469–8480.
Kulmala, M., Kerminen, V.-M., 2008. On the growth of atmospheric nanoparticles. Atmos. Res. 90, 132–150.
Kulmala, M., Kerminen, V.-M., Anttila, T., Laaksonen, A., O'Dowd, C.D., 2004a. Organic aerosol formation via sulphate cluster activation. J. Geophys. Res. : Atmosphere 109, D04205.
Kulmala, M., Kontkanen, J., Junninen, H., Lehtipalo, K., Manninen, H.E., Nieminen, T., Petäjä, T., Sipilä, M., Schobesberger, S., Rantala, P., Franchin, A., Jokinen, T., Järvinen, E., Äijälä, M., Kangasluoma, J., Hakala, J., Aalto, P.P., Paasonen, P., Mikkilä, J., Vanhanen, J., Aalto, J., Hakola, H., Makkonen, U., Ruuskanen, T., Mauldin, R.L., Duplissy, J., Vehkamäki, H., Bäck, J., Kortelainen, A., Riipinen, I., Kurtén, T., Johnston, M.V., Smith, J.N., Ehn, M., Mentel, T.F., Lehtinen, K.E.J., Laaksonen, A., Kerminen, V.-M., Worsnop, D.R., 2013. Direct observations of atmospheric aerosol nucleation. Science 339, 943–946.
Kulmala, M., Mordas, G., Petäjä, T., Grönholm, T., Aalto, P.P., Vehkamäki, H., Hienola, A.I., Herrmann, E., Sipilä, M., Riipinen, I., Manninen, H.E., Hämeri, K., Stratmann, F., Bilde, M., Winkler, P.M., Birmili, W., Wagner, P.E., 2007a. The condensation particle counter battery (CPCB): a new tool to investigate the activation properties of nanoparticles. J. Aerosol Sci. 38, 289–304.
Kulmala, M., Petäjä, T., Nieminen, T., Sipilä, M., Manninen, H.E., Lehtipalo, K., Dal Maso, M., Aalto, P.P., Junninen, H., Paasonen, P., Riipinen, I., Lehtinen, K.E.J., Laaksonen, A., Kerminen, V.-M., 2012. Measurement of the nucleation of atmospheric aerosol particles. Nat. Protoc. 7, 1651–1667.
Kulmala, M., Riipinen, I., Sipilä, M., Manninen, H.E., Petäjä, T., Junninen, H., Maso, M. D., Mordas, G., Mirme, A., Vana, M., Hirsikko, A., Laakso, L., Harrison, R.M., Hanson, I., Leung, C., Lehtinen, K.E.J., Kerminen, V.-M., 2007b. Toward direct measurement of atmospheric nucleation. Science 318, 89–92.

Kulmala, M., Vehkamäki, H., Petäjä, T., Dal Maso, M., Lauri, A., Kerminen, V.M., Birmili, W., McMurry, P.H., 2004b. Formation and growth rates of ultrafine atmospheric particles: a review of observations. J. Aerosol Sci. 35, 143–176.

Lampilahti, J., Leino, K., Manninen, A., Poutanen, P., Franck, A., Peltola, M., Hietala, P., Beck, L., Dada, L., Quéléver, L., Öhrnberg, R., Zhou, Y., Ekblom, M., Vakkari, V., Zilitinkevich, S., Kerminen, V.-M., Petäjä, T., Kulmala, M., 2020. Aerosol particle formation in the upper residual layer. Atmos. Chem. Phys. Discuss. https://doi.org/10.5194/acp-2020-923. https://acp.copernicus.org/preprints/acp-2020-923/.

Leena, P.P., Anil Kumar, V., Dani, K.K., Sombawne, S.M., Murugavel, P., Pandithurai, G., 2017. Evidence of new particle formation during post monsoon season over a high-altitude site of the Western Ghats, India. Toxicol. Environ. Chem. 99, 652–664.

Lehtinen, K.E.J., Kulmala, M., 2003. A model for particle formation and growth in the atmosphere with molecular resolution in size. Atmos. Chem. Phys. 3, 251–257.

Lehtipalo, K., Kontkanen, J., Kangasluoma, J., Franchin, A., Wimmer, D., Schobesberger, S., Junninen, H., Petäjä, T., Sipilä, M., Worsnop, D., Kulmala, M., Mikkilä, J., Vanhanen, J., Leppä, J., 2014. Methods for determining particle size distribution and growth rates between 1 and 3 nm using the Particle Size Magnifier. Boreal Environ. Res. 19, 215–236.

Lehtipalo, K., Rondo, L., Kontkanen, J., Schobesberger, S., Jokinen, T., Sarnela, N., Kurten, A., Ehrhart, S., Franchin, A., Nieminen, T., Riccobono, F., Sipila, M., Yli-Juuti, T., Duplissy, J., Adamov, A., Ahlm, L., Almeida, J., Amorim, A., Bianchi, F., Breitenlechner, M., Dommen, J., Downard, A.J., Dunne, E.M., Flagan, R.C., Guida, R., Hakala, J., Hansel, A., Jud, W., Kangasluoma, J., Kerminen, V.-M., Keskinen, H., Kim, J., Kirkby, J., Kupc, A., Kupiainen-Maatta, O., Laaksonen, A., Lawler, M.J., Leiminger, M., Mathot, S., Olenius, T., Ortega, I.K., Onnela, A., Petaja, T., Praplan, A.P., Rissanen, M.P., Ruuskanen, T., Santos, F.D., Schallhart, S., Schnitzhofer, R., Simon, M., Smith, J.N., Trostl, J., Tsagkogeorgas, G., Tome, A., Vaattovaara, P., Vehkamaki, H., Vrtala, A.E., Wagner, P.E., Williamson, C., Wimmer, D., Winkler, P.M., Virtanen, A., Donahue, N.M., Carslaw, K.S., Baltensperger, U., Riipinen, I., Curtius, J., Worsnop, D.R., Kulmala, M., 2016. The effect of acid-base clustering and ions on the growth of atmospheric nano-particles. Nat. Commun. 7, 11594.

Lehtipalo, K., Sipilä, M., Junninen, H., Ehn, M., Berndt, T., Kajos, M.K., Worsnop, D.R., Petäjä, T., Kulmala, M., 2011. Observations of nano-CN in the nocturnal boreal forest. Aerosol. Sci. Technol. 45, 499–509.

Lehtipalo, K., Yan, C., Dada, L., Bianchi, F., Xiao, M., Wagner, R., Stolzenburg, D., Ahonen, L.R., Amorim, A., Baccarini, A., Bauer, P.S., Baumgartner, B., Bergen, A., Bernhammer, A.-K., Breitenlechner, M., Brilke, S., Buchholz, A., Mazon, S.B., Chen, D., Chen, X., Dias, A., Dommen, J., Draper, D.C., Duplissy, J., Ehn, M., Finkenzeller, H., Fischer, L., Frege, C., Fuchs, C., Garmash, O., Gordon, H., Hakala, J., He, X., Heikkinen, L., Heinritzi, M., Helm, J.C., Hofbauer, V., Hoyle, C.R., Jokinen, T., Kangasluoma, J., Kerminen, V.-M., Kim, C., Kirkby, J., Kontkanen, J., Kürten, A., Lawler, M.J., Mai, H., Mathot, S., Mauldin, R.L., Molteni, U., Nichman, L., Nie, W., Nieminen, T., Ojdanic, A., Onnela, A., Passananti, M., Petäjä, T., Piel, F., Pospisilova, V., Quéléver, L.L.J., Rissanen, M.P., Rose, C., Sarnela, N., Schallhart, S., Schuchmann, S., Sengupta, K., Simon, M., Sipilä, M., Tauber, C., Tomé, A., Tröstl, J., Väisänen, O., Vogel, A.L., Volkamer, R., Wagner, A.C., Wang, M., Weitz, L., Wimmer, D., Ye, P., Ylisirniö, A., Zha, Q., Carslaw, K.S., Curtius, J., Donahue, N.M., Flagan, R.C., Hansel, A., Riipinen, I., Virtanen, A., Winkler, P.M., Baltensperger, U., Kulmala, M., Worsnop, D.R., 2018. Multicomponent new particle formation from sulfuric acid, ammonia, and biogenic vapors. Science Advances 4 eaau5363.

Lelieveld, J., Evans, J.S., Fnais, M., Giannadaki, D., Pozzer, A., 2015. The contribution of outdoor air pollution sources to premature mortality on a global scale. Nature 525, 367–371.

Lu, Y., Yan, C., Fu, Y., Chen, Y., Liu, Y., Yang, G., Wang, Y., Bianchi, F., Chu, B., Zhou, Y., Yin, R., Baalbaki, R., Garmash, O., Deng, C., Wang, W., Petäjä, T., Kerminen, V.M., Jiang, J., Kulmala, M., Wang, L., 2019. A proxy for atmospheric daytime gaseous sulfuric acid concentration in urban Beijing. Atmos. Chem. Phys. 19, 1971–1983.

Maher, E.F., Laird, N.M., 1985. EM algorithm reconstruction of particle size distributions from diffusion battery data. J. Aerosol Sci. 16, 557–570.

McMurry, P.H., Kulmala, M., Worsnop, D.R., 2011. Special issue on aerosol measurements in the 1 nm range. Aerosol. Sci. Technol. 45 (4), i.

Mikkonen, S., Romakkaniemi, S., Smith, J.N., Korhonen, H., Petäjä, T., Plass-Duelmer, C., Boy, M., McMurry, P.H., Lehtinen, K.E.J., Joutsensaari, J., Hamed, A., Mauldin Iii, R.L., Birmili, W., Spindler, G., Arnold, F., Kulmala, M., Laaksonen, A., 2011. A statistical proxy for sulphuric acid concentration. Atmos. Chem. Phys. 11, 11319–11334.

Mirme, S., Mirme, A., 2013. The mathematical principles and design of the NAIS – a spectrometer for the measurement of cluster ion and nanometer aerosol size distributions. Atmospheric Measurement and Techniques 6, 1061–1071.

Mirme, S., Mirme, A., Minikin, A., Petzold, A., Hõrrak, U., Kerminen, V.M., Kulmala, M., 2010. Atmospheric sub-3 nm particles at high altitudes. Atmos. Chem. Phys. 10, 437–451.

Mönkkönen, P., Koponen, I.K., Lehtinen, K.E.J., Hämeri, K., Uma, R., Kulmala, M., 2005. Measurements in a highly polluted Asian mega city: observations of aerosol number size distribution, modal parameters and nucleation events. Atmos. Chem. Phys. 5, 57–66.

Moorthy, K.K., Sreekanth, V., Prakash Chaubey, J., Gogoi, M.M., Suresh Babu, S., Kumar Kompalli, S., Bagare, S.P., Bhatt, B.C., Gaur, V.K., Prabhu, T.P., Singh, N.S., 2011. Fine and ultrafine particles at a near–free tropospheric environment over the high-altitude station Hanle in the Trans-Himalaya: new particle formation and size distribution. J. Geophys. Res.: Atmosphere 116, D20212.

Murugavel, P., Chate, D.M., 2009. Generation and growth of aerosols over Pune, India. Atmos. Environ. 43, 820–828.

Neitola, K., Asmi, E., Komppula, M., Hyvärinen, A.P., Raatikainen, T., Panwar, T.S., Sharma, V.P., Lihavainen, H., 2011. New particle formation infrequently observed in Himalayan foothills – why? Atmospheirc Chemistry and Physics 11, 8447–8458.

Nicholas, M., Jaimes-Correa, J., Petters, M., Royalty, T., Phillips, B., Zimmerman, A., Reed, R., 2019. Possible wintertime sources of fine particles in an urban environment. J. Geophys. Res.: Atmosphere 124.

Paasonen, P., Kupiainen, K., Klimont, Z., Visschedijk, A., Denier van der Gon, H.A.C., Amann, M., 2016. Continental anthropogenic primary particle number emissions. Atmospheirc Chemistry and Physics 16, 6823–6840.

Paasonen, P., Nieminen, T., Asmi, E., Manninen, H.E., Petäjä, T., Plass-Dülmer, C., Flentje, H., Birmili, W., Wiedensohler, A., Hõrrak, U., Metzger, A., Hamed, A., Laaksonen, A., Facchini, M.C., Kerminen, V.M., Kulmala, M., 2010. On the roles of sulphuric acid and low-volatility organic vapours in the initial steps of atmospheric new particle formation. Atmospheirc Chemistry and Physics 10, 11223–11242.

Patoulias, D., Fountoukis, C., Riipinen, I., Pandis, S., 2014. The role of organic condensation on ultrafine particle growth during nucleation events. Atmos. Chem. Phys. 15, 6337–6635.

Petäjä, T., Mauldin III, R.L., Kosciuch, E., McGrath, J., Nieminen, T., Paasonen, P., Boy, M., Adamov, A., Kotiaho, T., Kulmala, M., 2009. Sulfuric acid and OH concentrations in a boreal forest site. Atmos. Chem. Phys. 9, 7435–7448. https://doi.org/10.5194/acp-9-7435-2009.

Pierce, J.R., Adams, P.J., 2007. Efficiency of cloud condensation nuclei formation from ultrafine particles. Atmos. Chem. Phys. 7, 1367–1379.

Riccobono, F., Rondo, L., Sipilä, M., Barmet, P., Curtius, J., Dommen, J., Ehn, M., Ehrhart, S., Kulmala, M., Kürten, A., Mikkilä, J., Petäjä, T., Weingartner, E., Baltensperger, U., 2012. Contribution of sulfuric acid and oxidized organic compounds to particle formation and growth. Atmos. Chem. Phys. 12, 9427–9439.

Riipinen, I., Sihto, S.-L., Kulmala, M., Arnold, F., Dal Maso, M., Birmili, W., Saarnio, K., Teinilä, K., Kerminen, V.-M., Laaksonen, A., Lehtinen, K., 2007. Connections between atmospheric sulphuric acid and new particle formation during QUEST III-IV campaigns in Heidelberg and Hyytiälä. Atmos. Chem. Phys. 7, 1899–1914.

Riipinen, I., Yli-Juuti, T., Pierce, J.R., Petäjä, T., Worsnop, D.R., Kulmala, M., Donahue, N.M., 2012. The contribution of organics to atmospheric nanoparticle growth. Nat. Geosci. 5, 453–458.

Rose, C., Sellegri, K., Asmi, E., Hervo, M., Freney, E., Colomb, A., Junninen, H., Duplissy, J., Sipilä, M., Kontkanen, J., Lehtipalo, K., Kulmala, M., 2015. Major contribution of neutral clusters to new particle formation at the interface between the boundary layer and the free troposphere. Atmos. Chem. Phys. 15, 3413–3428.

Schobesberger, S., Junninen, H., Bianchi, F., Lönn, G., Ehn, M., Lehtipalo, K., Dommen, J., Ehrhart, S., Ortega, I.K., Franchin, A., Nieminen, T., Riccobono, F., Hutterli, M., Duplissy, J., Almeida, J., Amorim, A., Breitenlechner, M., Downard, A. J., Dunne, E.M., Flagan, R.C., Kajos, M., Keskinen, H., Kirkby, J., Kupc, A., Kürten, A., Kurtén, T., Laaksonen, A., Mathot, S., Onnela, A., Praplan, A.P., Rondo, L., Santos, F.D., Schallhart, S., Schnitzhofer, R., Sipilä, M., Tomé, A., Tsagkogeorgas, G., Vehkamäki, H., Wimmer, D., Baltensperger, U., Carslaw, K.S., Curtius, J., Hansel, A., Petäjä, T., Kulmala, M., Donahue, N.M., Worsnop, D.R., 2013. Molecular understanding of atmospheric particle formation from sulfuric acid and large oxidized organic molecules. Proc. Natl. Acad. Sci. Unit. States Am. 110, 17223–17228.

Sebastian, M., Kanawade, V.P., Soni, V.K., Asmi, E., Westervelt, D.M., Vakkari, V., Hyvärinen, A.P., Pierce, J.R, Hooda, R.K., 2021. New particle formation and growth to climate-relevant aerosols at a background remote site in the Western Himalaya. J. Geophys. Res.: Atmos. 126 (7) e2020JD033267.

Seinfeld, J.H., Pandis, S.N., 1998. Atmospheric Chemistry and Physics, from Air Pollution to Climate Change. John Wiley & Sons, Inc., New York.

Siingh, D., Gautam, A.S., Kamra, A.K., Komsaare, K., 2013. Nucleation events for the formation of charged aerosol particles at a tropical station - preliminary results. Atmos. Res. 132–133, 239–252.

Sipilä, M., Berndt, T., Petäjä, T., Brus, D., Vanhanen, J., Stratmann, F., Patokoski, J., Mauldin, R., Hyvärinen, A.P., Lihavainen, H., Kulmala, M., 2010. The role of sulfuric acid in atmospheric nucleation. Science 327, 1243–1246.

Sipilä, M., Lehtipalo, K., Attoui, M., Neitola, K., Petäjä, T., Aalto, P.P., O'Dowd, C.D., Kulmala, M., 2009. Laboratory verification of PH-CPC's ability to monitor atmospheric sub-3 nm clusters. Aerosol. Sci. Technol. 43, 126–135.

Smith, J.N., Barsanti, K.C., Friedli, H.R., Ehn, M., Kulmala, M., Collins, D.R., Scheckman, J.H., Williams, B.J., McMurry, P.H., 2010. Observations of aminium salts in atmospheric nanoparticles and possible climatic implications. Proc. Natl. Acad. Sci. Unit. States Am. 107, 6634–6639.

Smith, J.N., Dunn, M.J., VanReken, T.M., Iida, K., Stolzenburg, M.R., McMurry, P.H., Huey, L.G., 2008. Chemical composition of atmospheric nanoparticles formed from nucleation in Tecamac, Mexico: evidence for an important role for organic species in nanoparticle growth. Geophys. Res. Lett. 35, L04808.

Sreekanth, V., Mahesh, B., Niranjan, K., 2018. Gradients in PM2.5 over India: five city study. Urban Climate 25, 99–108.

Sulo, J., Sarnela, N., Kontkanen, J., Ahonen, L., Paasonen, P., Laurila, T., Jokinen, T., Kangasluoma, J., Junninen, H., Sipilä, M., Petäjä, T., Kulmala, M., Lehtipalo, K., 2021. Long-term measurement of sub-3 nm particles and their precursor gases in the boreal forest. Atmos. Chem. Phys. 21, 695–715.

Tröstl, J., Chuang, W.K., Gordon, H., Heinritzi, M., Yan, C., Molteni, U., Ahlm, L., Frege, C., Bianchi, F., Wagner, R., Simon, M., Lehtipalo, K., Williamson, C., Craven, J.S., Duplissy, J., Adamov, A., Almeida, J., Bernhammer, A.-K., Breitenlechner, M., Brilke, S., Dias, A., Ehrhart, S., Flagan, R.C., Franchin, A., Fuchs, C., Guida, R., Gysel, M., Hansel, A., Hoyle, C.R., Jokinen, T., Junninen, H., Kangasluoma, J., Keskinen, H., Kim, J., Krapf, M., Kürten, A., Laaksonen, A., Lawler, M., Leiminger, M., Mathot, S., Möhler, O., Nieminen, T., Onnela, A., Petäjä, T., Piel, F.M., Miettinen, P., Rissanen, M.P., Rondo, L., Sarnela, N.,

Schobesberger, S., Sengupta, K., Sipilä, M., Smith, J.N., Steiner, G., Tomè, A., Virtanen, A., Wagner, A.C., Weingartner, E., Wimmer, D., Winkler, P.M., Ye, P., Carslaw, K.S., Curtius, J., Dommen, J., Kirkby, J., Kulmala, M., Riipinen, I., Worsnop, D.R., Donahue, N.M., Baltensperger, U., 2016. The role of low-volatility organic compounds in initial particle growth in the atmosphere. Nature 533, 527–531.

Turco, R.P., Zhao, J.-X., Yu, F., 1998. A new source of tropospheric aerosols: ion-ion recombination. Geophys. Res. Lett. 25, 635–638.

Vakkari, V., Tiitta, P., Jaars, K., Croteau, P., Beukes, J.P., Josipovic, M., Kerminen, V.-M., Kulmala, M., Venter, A.D., van Zyl, P.G., Worsnop, D.R., Laakso, L., 2015. Reevaluating the contribution of sulfuric acid and the origin of organic compounds in atmospheric nanoparticle growth. Geophys. Res. Lett. 42, 10,486– 10,493.

Vanhanen, J., Mikkilä, J., Lehtipalo, K., Sipilä, M., Manninen, H.E., Siivola, E., Petäjä, T., Kulmala, M., 2011. Particle size magnifier for nano-CN detection. Aerosol. Sci. Technol. 45, 533–542.

Wang, L., Khalizov, A.F., Zheng, J., Xu, W., Ma, Y., Lal, V., Zhang, R., 2010. Atmospheric nanoparticles formed from heterogeneous reactions of organics. Nat. Geosci. 3, 238–242.

Weber, R.J., Marti, J.J., McMurry, P.H., Eisele, F.L., Tanner, D.J., Jefferson, A., 1996. Measured atmospheric new particle formation rates: implications for nucleation mechanisms. Chem. Eng. Commun. 151, 53–64.

Wehner, B., Petäjä, T., Boy, M., Engler, C., Birmili, W., Tuch, T., Wiedensohler, A., Kulmala, M., 2005. The contribution of sulfuric acid and non-volatile compounds on the growth of freshly formed atmospheric aerosols. Geophys. Res. Lett. 32, L17810.

Westervelt, D.M., Pierce, J.R., Adams, P.J., 2014. Analysis of feedbacks between nucleation rate, survival probability and cloud condensation nuclei formation. Atmos. Chem. Phys. 14, 5577–5597.

Xiao, S., Wang, M.Y., Yao, L., Kulmala, M., Zhou, B., Yang, X., Chen, J.M., Wang, D.F., Fu, Q.Y., Worsnop, D.R., Wang, L., 2015. Strong atmospheric new particle formation in winter in urban Shanghai, China. Atmos. Chem. Phys. 15, 1769–1781.

Yli-Juuti, T., Tikkanen, O., Manninen, H., Nieminen, T., Kulmala, M., 2016. Analysis of sub-3 nm particle growth in connection with sulfuric acid in a boreal forest. Boreal Environ. Res. 21, 287–298.

Yu, Ganne, H.A., You, Y., Sedlacek, A., Springston, S., Kanawade, V.P., Lee, Y.-N., Wang, J., Kuang, C., McGraw, R.L., McCubbin, I., Mikkila, J., Lee, S.-H., 2014. Sub-3 nm particles observed at the coastal and continental sites in the United States. J. Geophys. Res.: Atmosphere 119, 860–879.

Yu, Zhou, L., Liang, D., Shen, W., Dai, W., Zheng, J., Ma, Y., Chen, M., 2016. Nucleation and growth of sub-3 nm particles in the polluted urban atmosphere of a megacity in China. Atmos. Chem. Phys. 16, 2641–2657.

Yu, F., 2011. A secondary organic aerosol formation model considering successive oxidation aging and kinetic condensation of organic compounds: global scale implications. Atmos. Chem. Phys. 11, 1083–1099.

Yu, H., McGraw, R., Lee, S.-H., 2012. Effects of amines on formation of sub-3 nm particles and their subsequent growth. Geophys. Res. Lett. 39, L02807.

Yu, H., Ren, L., Kanawade, V.P., 2017. New particle formation and growth mechanisms in highly polluted environments. Current Pollution Reports 3, 245–253.

Yue, D.L., Hu, M., Zhang, R.Y., Wang, Z.B., Zheng, J., Wu, Z.J., Wiedensohler, A., He, L. Y., Huang, X.F., Zhu, T., 2010. The roles of sulfuric acid in new particle formation and growth in the mega-city of Beijing. Atmos. Chem. Phys. 10, 4953–4960.

Zhao, J., Eisele, F.L., Titcombe, M., Kuang, C., McMurry, P.H., 2010. Chemical ionization mass spectrometric measurements of atmospheric neutral clusters using the cluster-CIMS. J. Geophys. Res.: Atmosphere 115, D08205.

Check for updates

JGR Atmospheres

RESEARCH ARTICLE
10.1029/2020JD033267

Key Points:

- We present new measurement-based evidence of the contribution of new particle formation (NPF) to climate-relevant aerosols in the Western Himalaya
- NPF occurred frequently in the pre-monsoon (March–May) season
- NPF rates were higher for cleaner events than polluted events

Supporting Information:

Supporting Information may be found in the online version of this article.

Correspondence to:

V. P. Kanawade,
vijaykanawade03@yahoo.co.in

Citation:

Sebastian, M., Kanawade, V. P., Soni, V. K., Asmi, E., Westervelt, D. M., Vakkari, V., et al. (2021). New particle formation and growth to climate-relevant aerosols at a background remote site in the Western Himalaya. *Journal of Geophysical Research: Atmospheres*, *126*, e2020JD033267. https://doi.org/10.1029/2020JD033267

Received 12 JUN 2020
Accepted 5 FEB 2021

Author Contributions:

Conceptualization: Vijay P. Kanawade
Data curation: Mathew Sebastian, Vijay P. Kanawade, Rakesh K. Hooda
Formal analysis: Mathew Sebastian, Vijay P. Kanawade, Rakesh K. Hooda
Funding acquisition: Vijay K. Soni
Investigation: Mathew Sebastian, Vijay P. Kanawade, Vijay K. Soni, Eija Asmi, Daniel. M. Westervelt, Ville Vakkari, Antti-Pekka Hyvärinen, Jeffrey R. Pierce
Methodology: Mathew Sebastian, Vijay P. Kanawade, Daniel. M. Westervelt, Jeffrey R. Pierce, Rakesh K. Hooda
Project Administration: Vijay K. Soni
Resources: Vijay K. Soni, Eija Asmi, Daniel. M. Westervelt, Ville Vakkari, Antti-Pekka Hyvärinen, Jeffrey R. Pierce

© 2021. American Geophysical Union. All Rights Reserved.

New Particle Formation and Growth to Climate-Relevant Aerosols at a Background Remote Site in the Western Himalaya

Mathew Sebastian[1], Vijay P. Kanawade[1], Vijay K. Soni[2], Eija Asmi[3,4], Daniel. M. Westervelt[5,6], Ville Vakkari[3,7], Antti-Pekka Hyvärinen[3], Jeffrey R. Pierce[8], and Rakesh K. Hooda[3]

[1]Centre for Earth, Ocean and Atmospheric Sciences, University of Hyderabad, Hyderabad, India, [2]India Meteorological Department, Ministry of Earth Sciences, New Delhi, India, [3]Finnish Meteorological Institute, Erik Palmenin Aukio 1, Helsinki, Finland, [4]Servicio Meteorológico Nacional, Buenos Aires, Argentina, [5]Columbia University, Lamont-Doherty Earth Observatory, NY, USA, [6]NASA Goddard Institute for Space Studies, New York, NY, USA, [7]Atmospheric Chemistry Research Group, North-West University, Potchefstroom, South Africa, [8]Department of Atmospheric Science, Colorado State University, Fort Collins, CO, USA

Abstract New particle formation (NPF) can influence the Earth's radiative budget when the newly formed particles grow to climate-relevant sizes. Here, we present analysis of 21 months of continuous aerosol size distribution measurements at a background remote site in the western Himalaya and provide observational evidence that newly formed particles grow to cloud condensation nuclei (CCN)-active sizes (i.e., >20–100 nm in diameter). Out of total 55 NPF events, 38 (66%) events occurred in the pre-monsoon season (March–May). NPF events were classified into those with and without pollution influence as polluted and cleaner, respectively, using black carbon data. The analysis of air mass age, based on the ratio of number concentration of Aitken to accumulation mode aerosols, indicated that NPF occurred in the relatively cleaner air masses reaching to the site. The median formation rate of 10 nm particles and particle growth rates for cleaner events were three-fold and two-fold, respectively, higher than polluted events. We present the first estimates of the survival probability of newly formed particles to 50 and 100 nm size, which was not attempted in an Indian environment previously. The survival probability to 50 nm particles ranged from 44% to 98%, with a mean and standard deviation of 82 ± 18%. On average, ~60% of the particles surviving to 50 nm survived to 100 nm, making the overall survival probability of 100 nm to 53 ± 31%. This indicates that the probability of nucleated particles growing to CCN-active sizes under a large source of condensing vapor (transported from nearby lower-altitude regions) and low pre-existing particle concentrations (background mountain site) is high compared to the previous studies. These findings highlight the importance of the efficiency of nucleation events for producing CCN, which is a critical basis of aerosol indirect effects.

1. Introduction

Solid or liquid particles suspended in air are defined as atmospheric aerosols. Atmospheric aerosols affect weather, climate, human health, and air quality, thus it is of significant societal and economical importance (Chowdhury et al., 2018; IPCC, 2013; Landrigan et al., 2018). Aerosols also counteract some fraction of greenhouse gas-driven global warming (Paasonen et al., 2013), by directly scattering and absorbing solar radiation and indirectly by altering cloud properties (Rosenfeld et al., 2014; Sarangi et al., 2018). Amongst current uncertainties in the radiative forcing, aerosol-induced changes in cloud properties is the largest source of uncertainty in future climate projections at the regional and global scales (IPCC, 2013).

Aerosol nucleation is the process of formation of new particles from vapors (hereafter referred to as new particle formation, [NPF]) and it is the largest source of aerosol numbers in the atmosphere (Kulmala et al., 2013; Zhang et al., 2012). However, these newly formed aerosols of 1–2 nm in diameter need to grow further to climate-relevant cloud condensation nuclei (CCN) sizes (i.e., >20–100 nm in diameter) until they are able to influence clouds and thereby climate (Kerminen et al., 2012; Wang & Penner, 2009), even though smaller aerosols affect human health, air quality, and atmospheric chemistry (Landrigan et al., 2018; von Schneidemesser et al., 2015). NPF has been observed to take place throughout most of the

Software: Daniel. M. Westervelt, Rakesh K. Hooda
Supervision: Vijay P. Kanawade
Validation: Mathew Sebastian, Daniel. M. Westervelt
Writing – original draft: Mathew Sebastian, Vijay P. Kanawade
Writing – review & editing: Mathew Sebastian, Vijay P. Kanawade, Vijay K. Soni, Eija Asmi, Daniel. M. Westervelt, Ville Vakkari, Antti-Pekka Hyvärinen, Jeffrey R. Pierce, Rakesh K. Hooda

terrestrial troposphere, including high altitude sites (Kerminen et al., 2018; Sellegri et al., 2019). Numerical experiments over the Midwestern USA, where NPF occurred frequently on regional scale, showed that NPF inhibits growth of pre-existing aerosols to CCN sizes by reducing ambient sulfuric acid concentrations over the region, and thereby the ambient CCN concentrations and cloud albedo, leading to an overall warming effect relative to when NPF was excluded (Sullivan et al., 2018). Westervelt et al. (2014) relates CCN formation to various nucleation schemes using simulation in GEOS-Chem-TOMAS global aerosol model and highlighted that nucleation contributed to about half of the CCN concentrations. A recent study also indicated that NPF produces about 54% of CCN in the present day with an estimated uncertainty range of 45%–85% (Gordon et al., 2017). Thus, the contribution of NPF to the global CCN budget spans a relatively large range of uncertainty (Kerminen et al., 2012; Westervelt et al., 2014), which, together with our limited understanding of association between NPF and CCN, results in large uncertainties in the indirect radiative forcing by aerosols (IPCC, 2013). Thus, the evident ubiquity and heterogeneity in linkages between NPF and CCN requires long-term continuous ambient observations, aided with state-of-the-art aerosol instrumentation techniques and regional to planetary scale model simulations to bring out new insights into field measurements.

The majority of comprehensive long-term ambient observations of NPF have been made in urban, rural, and remote areas in North America and Europe in locations that are more easily accessible (Hallar et al., 2016; Kanawade et al., 2012; Manninen et al., 2010; Nieminen et al., 2018). NPF has also been studied at some high altitude sites, such as the measurements by Venzac et al. (2008) at Himalayan Nepal Climate Observatory, Pyramid (NCO-P; 5,079 m above mean sea level [amsl]) in the Khumbu Valley, Kivekäs et al. (2009) at Mount Waliguan (3,816 m amsl), a remote mountain-top station in inland China, Foucart et al. (2018) at the Maïdo observatory (2,150 m amsl), Réunion, a Southern Hemisphere site surrounded by Indian Ocean, Venzac et al. (2009) at the Puy de Dôme site (1,465 m amsl) in France, Boulon et al. (2010) and Tröstl et al. (2016) at Jungfraujoch (3,580 m amsl) in the Swiss Alps, and Hallar et al. (2011) at Storm Peak Laboratory (3,201 m amsl) in the USA. Recently, Sellegri et al. (2019) presented aerosol observations from six high altitude stations (Puy de Dôme in France, Mount Chacaltaya in Bolivian Andes, NCO-P, Maïdo observatory on La Reunion Island in the Indian Ocean, Jungfraujoch in the Swiss Alps, and the Monte Cimone site on the Northern Apennines) for which a year-long measurements were available to derive statistically relevant NPF features (frequency, formation rates, growth rates, and CCN contribution to total aerosols) and seasonal variability. Previous long-term studies from the Indian Himalaya have also characterized aerosol properties and NPF events such as the measurements by Hooda et al. (2018), Neitola et al. (2011), and Komppula et al. (2009) at Mukteshwar, a high-altitude site (2,180 m amsl) in North-western Indian Himalaya and Moorthy et al. (2011) at a high-altitude site, Hanle (4,520 m amsl), in the Trans-Himalaya. NPF frequency at Mukteshwar and Hanle sites in the Himalaya showed a clear seasonal cycle that was connected to the evolution of atmospheric boundary layer (ABL) and solar insolation, respectively. During the pre-monsoon season (March–May), the increasing boundary layer height lifted aerosols and their precursors from nearby lower-altitude regions up to the station, and the precursors combined with high solar insolation at the mountain top increased the NPF probability significantly (Moorthy et al., 2011; Neitola et al., 2011). In addition, the ground-based NPF observations in India are limited to only a few locations, including Mahabaleshwar in the Western Ghats (Leena et al., 2017), New Delhi (Mönkkönen et al., 2005), Kanpur and Pune (Kamra et al., 2015; Kanawade et al., 2020; Kanawade et al., 2014), Gadanki (Kanawade et al., 2014), and Trivandrum (Babu et al., 2016). However, none of the above previous studies in India, to our knowledge, has explored the linkage between atmospheric NPF and CCN formation.

In this study, we use 21 months (December 2016–September 2018) of continuous aerosol size distribution measurements to establish statistics on NPF rates, growth rates, seasonal variability, survival probability, and CCN formation rates of newly formed aerosols at Ranichauri measurement site. In order to explain the seasonal variability in NPF features, different months are grouped in four seasons: winter (December–February), pre-monsoon (March–May), monsoon (June–September), and post-monsoon (October and November).

21698996, 2021, 7, Downloaded from https://agupubs.onlinelibrary.wiley.com/doi/10.1029/2020JD033267, Wiley Online Library on [13/12/2023]. See the Terms and Conditions (https://onlinelibrary.wiley.com/terms-and-conditions) on Wiley Online Library for rules of use; OA articles are governed by the applicable Creative Commons License

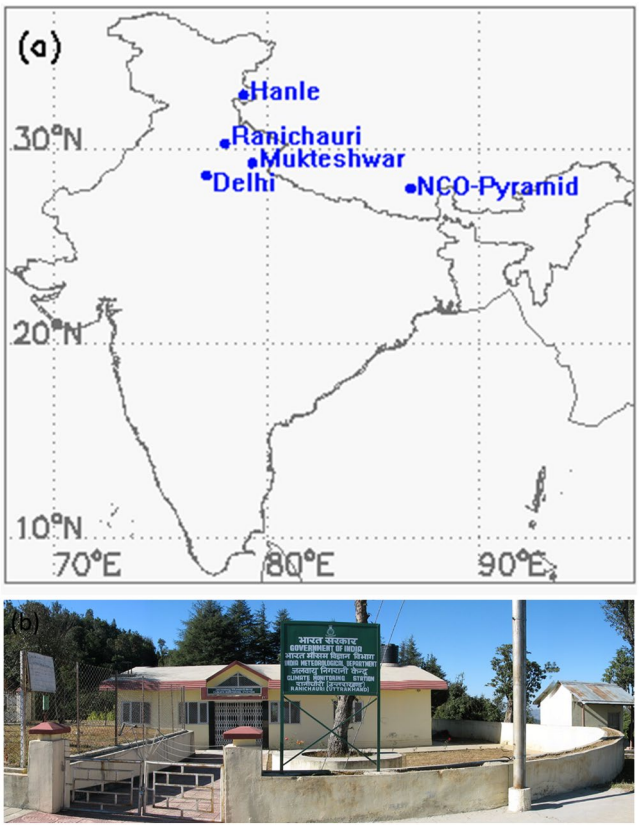

Figure 1. (a) Location of Ranichauri and surroundings locations, including high altitude sites in the Himalaya. (b) Photograph of Ranichauri Climate Observing Station.

2. Materials and Methods

2.1. Location

The village named Ranichauri is located in Tehri Garhwal district of Uttarakhand state in the southern slope of the Western Himalaya. Figure 1a shows the location of Ranichauri and surrounding locations, including three high-altitude sites in the Himalaya (Hanle, Mukteshwar, and NCO-P) from where observations of aerosol size distributions were reported in the past. The observation site (30.2°N, 78.25°E; ~1,930 m amsl) is situated on an isolated hill-top, within the campus of College of Forestry in Ranichauri (Figure 1b). The observation site is a Climate Monitoring station (hereafter referred to as Ranichauri) managed by India Meteorological Department (IMD) under the Global Atmospheric Watch (GAW) program of the World Meteorological Organization. The station is away from major sources of anthropogenic pollution and can be considered as a background observatory. But the black carbon (BC) concentrations measured at Ranichauri are considerably high for a background location (annual mean and standard deviation of 1.4 ± 1.1 μg/m^3). This is higher compared to a nearby high altitude remote site, Mukteshwar (0.9 ± 0.6 μg/m^3) (Kumar et al., 2020), particularly in the pre-monsoon season with the proximity of forest fires. The 10th, 25th, 50th, 75th, and 90th percentiles of BC at Ranichauri are 0.3, 0.6, 1.3, 2.1, and 3.2 μg/m^3, respectively. The city of Rishikesh is located about 70 km to the south, Srinagar city about 100 km to the south east and Dehradun city about 100 km to the west of Ranichauri. The topography of the region covers uneven distribution of forests, agriculture land, orchards, and small human settlements. Based on long-term observations (1985–2013), the daily maximum temperature varies from 9.4°C to 27.2°C, with mean annual total rainfall of about 1,274 mm at this site (Upadhyay et al., 2015).

Air mass history was identified using NOAA ARL PC-version HYSPLIT model (Draxler & Rolph, 2010) by calculating hourly 2-day air mass backward trajectories starting at 500 m above the ground level using gridded wind fields from the Global Data Assimilation System, which has a spatial resolution of 1° × 1° longitude by latitude and a time resolution of 1 h (Kanamitsu, 1989). BC data was used to identify if the air mass reaching the site was polluted. Figure 2 shows the 2-day backward trajectories of air masses arriving at 500 m above the ground at Ranichauri for winter, pre-monsoon, monsoon, and post-monsoon seasons. Ranichauri generally experiences a mixture of relatively cleaner free tropospheric air and polluted air from highly polluted Indo-Gangetic Plain. During winter and post-monsoon seasons, the free tropospheric flow from north-western region predominantly reaches the site. Air masses from the polluted Indo-Gangetic Plain in the south-east were dominant during the pre-monsoon season whereas air masses from the south-east and west were prevalent during the monsoon season.

The ABL influence was analyzed using the methodology explained in Hooda et al. (2018). It used specific humidity (q) as a passive tracer for ABL dynamics (Kowol-Santen et al., 2001; Serafin et al., 2018; Weigel et al., 2007). The lifting of air in the ABL was first assessed by examining the variability "∂q" in specific humidity at two sites (Delhi and Ranichauri). Furthermore, to investigate the ABL air lifting from the plains below, the hourly specific humidity difference between the two sites and corresponding undisturbed difference of q between Ranichauri and the plains (Delhi) "denoted as ΔRPq" was estimated. It was assumed, based upon "∂q" diurnal-monthly values that there was no mixing of air happening at 5:00 a.m. between the two sites (mountainous and plains). From these parameters, the fraction of air (Φq) arriving Ranichauri from the plains can be calculated as;

$$\Phi q = 1 - \frac{q_{\mathrm{DEL}} - q_{\mathrm{RANI}}}{\Delta \mathrm{RPq}}. \quad (1)$$

21698996, 2021, 7, Downloaded from https://agupubs.onlinelibrary.wiley.com/doi/10.1029/2020JD033267, Wiley Online Library on [13/12/2023]. See the Terms and Conditions (https://onlinelibrary.wiley.com/terms-and-conditions) on Wiley Online Library for rules of use; OA articles are governed by the applicable Creative Commons License

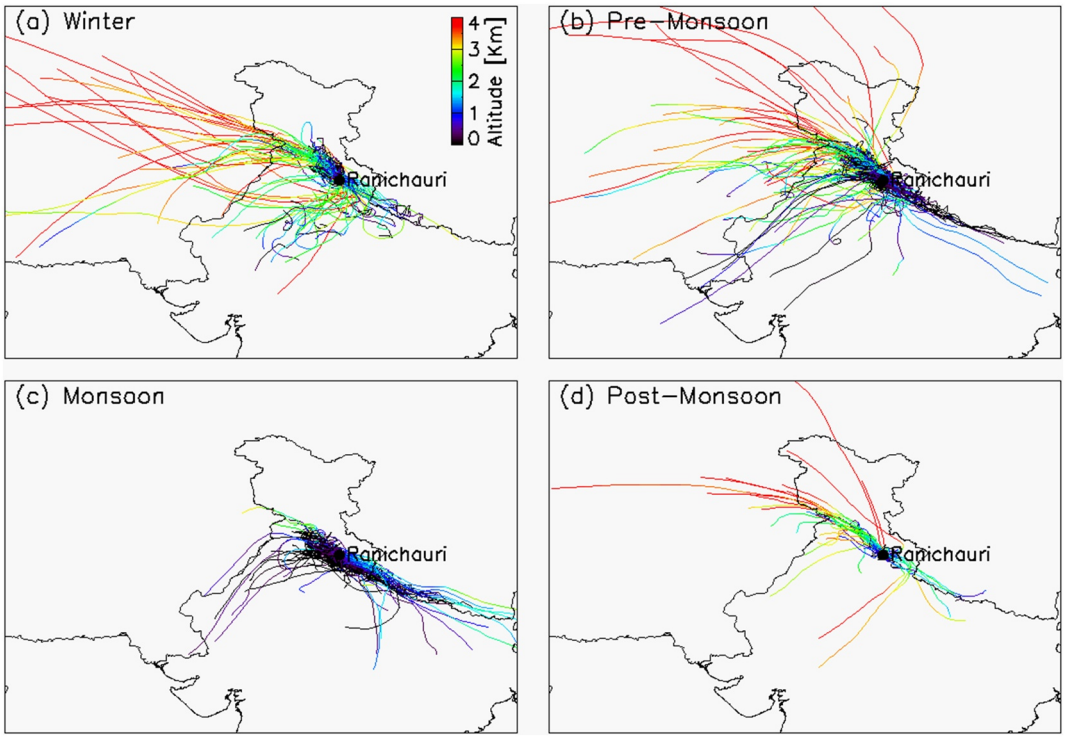

Figure 2. Two-day backward air mass trajectories starting at 500 m above the ground level for (a) winter (December–February), (b) pre-monsoon (March–May), (c) monsoon (June–September), and (d) post-monsoon (October and November) seasons. The color indicates the altitude along the air mass backward trajectory.

The influence of the Indo-Gangetic Plains boundary layer was evaluated with different threshold values of Φq (0.25, 0.5, and 0.75) and compared to the maximum mixing depth of Delhi (ERA-5 based) in terms of the fraction of the days (Figure S1). More details are provided in supporting information.

2.2. Instrumentation and Data Sets

A custom-built differential mobility particle sizer (DMPS) was used to obtain the ambient aerosol size distribution in the size range of 10–800 nm (30 size bins). The DMPS consisted of a Vienna-type differential mobility analyzer (DMA) that classifies the charged particles according to their electrical mobility, and a TSI 3772 condensation particle counter that counts particles of the selected mobility. Thus, the aerosol size information throughout the text is in electrical mobility diameter. A full aerosol number-size distribution with 30 bins was obtained every 10 min. The DMPS inlet flow rate was 1 liter per minute (LPM), and the sheath air flow rate was 5 LPM. The sample air was drawn inside through a stainless steel inlet tube of about 2 m in length and dried to less than 40% relative humidity with a Nafion dryer. Diffusion losses in the inlet and inside the DMPS were considered in the data inversion. The inversion method was identical to that presented by Wiedensohler et al. (2012), for the Finnish Meteorological Institute DMPS.

Black carbon measurements were made using Aethalometer (model AE-33) (Magee Scientific, 2016), which is deployed under IMD national network for measurements of BC at important geographical locations in India (Kumar et al., 2020). Aethalometer measures light attenuation at seven wavelengths. The BC concentrations here are derived at a wavelength of 880 nm using mass absorption cross-section value of 7.77 m^2/g (Petzold et al., 2013). This wavelength was chosen to calculate BC concentration as absorption due to other aerosols is negligible at this wavelength (Drinovec et al., 2015). Aethalometer uses a Teflon-coated glass fiber tape and the aerosols are collected on a two parallel spot measurement of optical absorption, which provides near real-time compensation for the spot loading effect. Aethalometer inlet was equipped with an impactor for removing the aerosols with aerodynamic diameters larger than 2.5 μm. More details of BC measurement and calculation can be found in Drinovec et al. (2015).

21698996, 2021, 7, Downloaded from https://agupubs.onlinelibrary.wiley.com/doi/10.1029/2020JD033267, Wiley Online Library on [13/12/2023]. See the Terms and Conditions (https://onlinelibrary.wiley.com/terms-and-conditions) on Wiley Online Library for rules of use; OA articles are governed by the applicable Creative Commons License

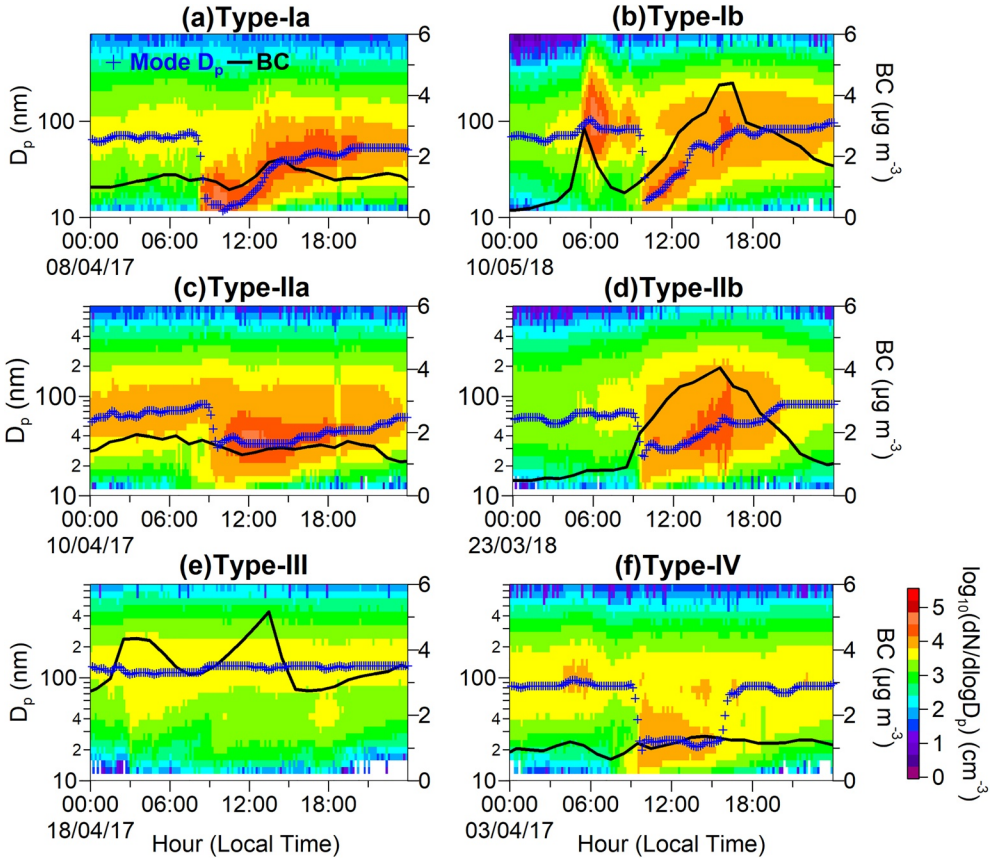

Figure 3. Temporal evolution of aerosol size distributions (filled contour), particle mode diameter (blue plus symbol), and BC mass concentrations (thick black line) for a typical Type-I NPF (a and b), Type-II NPF (c and d),Type-III nonevent (e), and Type-IV unidentified (f) days at Ranichauri. BC, black carbon; NPF, new particle formation.

2.3. Estimation of Relevant NPF Features

We classified NPF events into different types upon visual inspection of the contour plot of the aerosol size distributions (Dal Maso et al., 2005). Particle mode diameter and BC concentrations were used to classify events into subtypes. To obtain the particle mode diameter (i.e., local maximum of the aerosol size distribution), multimodal log-normal distribution upto three modes was fitted to the measured aerosol size distribution. Type-I NPF events were identified by the presence of distinctly new mode of particles with diameters smaller than 25 nm and with a steady growth in diameter of this new mode for at least 6 h such that aerosol size distributions display a "banana"-shaped aerosol growth. Type-I NPF events were further classified into two subtypes: Ia and Ib, based on BC concentrations. Type-Ia NPF event showed no or insignificant simultaneous increase in BC concentrations with new mode of particle diameter, implying a cleaner event (e.g., Figure 3a) whereas Type-Ib NPF event showed significant simultaneous increase in BC with the new mode of particle diameter, implying polluted event (e.g., Figure 3b). For these events, the particle growth rate (GR) was calculated by fitting a first-order polynomial line through growing particle mode diameter between 10 and 25 nm as a function of time and calculating its slope, following Dal Maso et al. (2005) methodology, modified and updated by Westervelt et al. (2013). The formation rate of 10 nm particles (J_{10}) was found using the simplified approximation of the general dynamic equation, describing evolution of the aerosol size distribution. The formation rate of 10 nm particles was calculated from aerosol size distributions obtained from the DMPS (10–800 nm) using the following equation:

$$J_{10} = \frac{dN_{10-25}}{dt} + F_{\mathrm{CoagS}} + F_{\mathrm{growth}} \quad (2)$$

21698996, 2021, 7, Downloaded from https://agupubs.onlinelibrary.wiley.com/doi/10.1029/2020JD033267, Wiley Online Library on [13/12/2023]. See the Terms and Conditions (https://onlinelibrary.wiley.com/terms-and-conditions) on Wiley Online Library for rules of use; OA articles are governed by the applicable Creative Commons License

Table 1
Summary of New Particle Formation Event Classification

Event type	Subtype	Features
Type-I NPF	Ia (cleaner)	A new mode of particles smaller than 25 nm size is visible with a steady growth in the particle size for at least 6 h. GR and J_{10} can be calculated. No or insignificant simultaneous increase in BC concentrations with the particle mode diameter.
	Ib (polluted)	Same as Type-Ia, but with significant simultaneous increase in BC concentrations.
Type-II NPF	IIa (cleaner)	A new mode of particles smaller than 25 nm is absent referred to as Aitken-mode growth event. GR and J_{10} can not be calculated. No or insignificant simultaneous increase in BC concentrations with the particle mode diameter.
	IIb (polluted)	Same as Type-IIa, but with significant simultaneous increase in BC concentrations.
Type-III nonevent		No distinct change in particle mode diameter during the course of the day
Type-IV unidentified		Difficult to identify whether it is one of the above event types.

Abbreviations: BC, black carbon; GR, growth rate; NPF, new particle formation.

where the first term in Equation 2 is the rate of the change of nucleation mode particle number concentrations, the second term is the coagulation loss, and the third term is the flux out of the size range 10–25 nm, that is, condensational growth.

Type-II NPF events were similar to Type-I NPF events except that the initial mode diameter was larger than 25 nm. Thus, GR and J_{10} can not be calculated for Type-II NPF events. Such events are observed when the air mass with NPF reaches the measurement site after the particles have already grown larger than 25 nm, referred to as Aitken-mode growth events. Type-II NPF events were further classified into two subtypes: IIa (cleaner) and IIb (polluted), similar to Type-I NPF events. This indicates that Type-II events can occur in both cleaner and polluted air masses. Type-IIa NPF events showed no or insignificant simultaneous increase in BC concentrations, implying a cleaner event (e.g., Figure 3c). Type-IIb NPF events showed simultaneous increase in BC concentrations, implying a polluted event (e.g., Figure 3d). The days with no evidence of distinct change in particle mode diameter were identified as Type-III nonevent (e.g., Figure 3e). Those days, which were difficult to be classified as any one of the above categories, were identified as Type-IV unidentified event days (e.g., Figure 3f). The criteria used for classifying these events are summarized in Table 1.

We also calculated size-segregated aerosol number concentrations by integrating the number concentration of aerosols from 10 to 25 nm (nucleation mode, N_{NUC}), 25 to 100 nm (Aitken mode, N_{AIT}), 100 to 800 nm (accumulation mode, N_{ACCU}), and 10 to 800 nm (total aerosols, N_{TOT}). Similarly, total aerosol surface area (SA_{TOT}), total volume (Vol_{TOT}), total mass concentration (M_{TOT}), total condensation sink (CS_{TOT}), and total coagulation sink ($CoagS_{TOT}$) in the size range of 10–800 nm were calculated following Dal Maso et al. (2005), to examine seasonal variability and diurnal patterns of NPF features. It is worth noting that there were no measurements of aerosols less than 10 nm diameter size during the study period. Therefore, it was not possible to precisely estimate the fraction of N_{NUC} originated from NPF processes, which usually starts at 1–2 nm diameter size (Kulmala et al., 2007).

2.4. Particle Survival Probability, CCN-Active Particle Formation Rates, and CCN Derived from SMPS

While particles as small as 20 nm may activate in summertime arctic clouds (Korhonen et al., 2008; Leaitch et al., 2016), in typical ambient in-cloud supersaturations, 50 and 100 nm can be considered as a good proxy for CCN concentration (Kerminen et al., 2012) at ~1.0% and 0.2% supersaturation for stratiform clouds, respectively. Here, we have calculated the particle survival probabilities to 50 nm (SP50) and 100 nm (SP100) size following the methodology explained by Pierce and Adams (2007) and first applied to ambient observations in Westervelt et al. (2013). Briefly, SP is the ratio of particle fluxes at the initial size and the CCN-active sizes (typically to 50 and 100 nm particles). The survival probability from initial size m to n (in this case, 10–50 and 10–100 nm) is calculated by the following equation:

21698996, 2021, 7, Downloaded from https://agupubs.onlinelibrary.wiley.com/doi/10.1029/2020JD033267, Wiley Online Library on [13/12/2023]. See the Terms and Conditions (https://onlinelibrary.wiley.com/terms-and-conditions) on Wiley Online Library for rules of use; OA articles are governed by the applicable Creative Commons License

$$SP_{m,n} = \prod_{k=m}^{n-1} \exp\left(-\frac{\tau_{k,k+1}^{cond}}{\tau_k^{coag}}\right) \quad (3)$$

where τ^{cond} is the condensational growth time scale required for a particle to grow to a size of interest. τ^{coag} is the inverse of the CoagS for a given size range. The formation rates of CCN-active particles (i.e., 50 and 100 nm) are calculated as, $J_{50} = J_{10} \times SP50$ and $J_{100} = J_{10} \times SP100$. J_{50} and J_{100} are the formation rate of particles of size 50 and 100 nm, respectively. While this methodology does not consider aerosol composition and mixing state, the particles larger than 50 nm will serve as CCN under typical supersaturations. Since, the aerosol size plays the major role in the aerosols ability to act as CCN rather than its composition (Dusek et al., 2006). The survival probabilities and formation rates of 50 and 100 nm particles were calculated for Type-I NPF event alone as it was not possible to derive J_{10} for Type-II NPF events.

We have also estimated the contribution of freshly formed particles to the CCN concentrations followed by Kerminen et al. (2012) methodology, which calculates $N_{CCNprior}$ and N_{CCNmax}. We used similar CCN thresholds, that is, 50 and 100 nm to calculate $N_{CCNprior}$ and N_{CCNmax}. $N_{CCNprior}$ is calculated as a 1-h average concentration immediately prior to the appearance of the newly formed nucleation mode particles, whereas N_{CCNmax} is calculated as a maximum one hour average concentration during an NPF event. The contribution of the nucleation to CCN concentrations during the observed Type-I NPF event days was then examined in both relative and absolute concentrations terms.

3. Results and Discussion

3.1. Typical NPF Events and Their Frequency

Previous study at NCO-P in the Khumbu Valley, a high altitude site in the Eastern Himalaya, using 16 months of aerosol size distributions showed that NPF events occurred very frequently when the more polluted air rising from valleys reach the site (Venzac et al., 2008). Whereas, the long-term (2005–2010) measurements of aerosol size distributions from Mukteshwar, Uttarakhand, a high-altitude site in Western Himalaya, showed that the NPF events occurred rather sporadically, except during the pre-monsoon season (Neitola et al., 2011). NPF events during the pre-monsoon season were connected to the evolution of the boundary layer up to the site elevation.

Figure 3 shows typical NPF events observed at Ranichauri site. Type-Ia and Type-Ib are identical type of events except that BC concentrations did not vary during the course of Type-Ia NPF event while BC concentrations increased sharply with particle mode diameter in case of Type-Ib NPF event. Many studies have suggested that NPF occur preferably at low aerosol loading, because high pre-existing aerosol concentrations tend to scavenge both nucleation precursors (e.g., sulfuric acid, ammonia, amines, and volatile organic compounds) and small molecular clusters (Kulmala et al., 2004; Zhang et al., 2012). However, observations in polluted environments and plumes have also revealed significant rates of NPF despite the high ambient aerosol concentrations (Nie et al., 2014; Nieminen et al., 2018; Westervelt et al., 2013; Yao et al., 2018; Yu et al., 2017; Zhang et al., 2015). Previous studies put forward the hypothesis that either reduced scavenging of nanometer-sized clusters to pre-existing aerosols or rapid cluster growth likely accounts for the nucleation and growth of nano particles in a polluted atmosphere (Dai et al., 2017; Kulmala et al., 2017). These previous studies substantiate the Type-Ib events, which have NPF within a polluted air mass. The CS_{TOT} for Type-I NPF events were in the range 1.2–52.8 $\times 10^{-3}$ s^{-1}, with a mean and standard deviation of 8.6 $\pm$ 5.8 $\times 10^{-3}$ s^{-1}. This value is higher by a factor of about 3 as compared to a high altitude site, Puy de Dôme in France (2.77 $\times 10^{-3}$ s^{-1}) and more than an order of magnitude higher than another high altitude site, Jungfraujoch in the Swiss Alps (0.15 $\times 10^{-3}$ s^{-1}) (Sellegri et al., 2019). At the NCO-P site in the Khumbu Valley, Venzac et al. (2008) found that high pre-existing aerosol concentrations prevented NPF occurrence, with NPF frequencies less than 10% for CS higher than 2.1 $\times 10^{-3}$ s^{-1}, with a NPF frequency of about 50% for CS lower than this value. This indicates that the typical CS at Ranichauri site was sufficiently high that the natural source strength of vapors cannot overcome it and thereby inhibited cleaner NPF events. For the typical Type-Ia event shown in Figure 3, the calculated growth rate in the size range 10–25 nm diameter (8.45 nm/h) was almost twofold than that of the Type-Ib event (4.69 nm/h). Overall, the growth rates for Type-Ia cleaner event days were higher than Type-Ib event days. In contrast, Neitola et al. (2011)

21698996, 2021, 7, Downloaded from https://agupubs.onlinelibrary.wiley.com/doi/10.1029/2020JD033267, Wiley Online Library on [13/12/2023]. See the Terms and Conditions (https://onlinelibrary.wiley.com/terms-and-conditions) on Wiley Online Library for rules of use; OA articles are governed by the applicable Creative Commons License

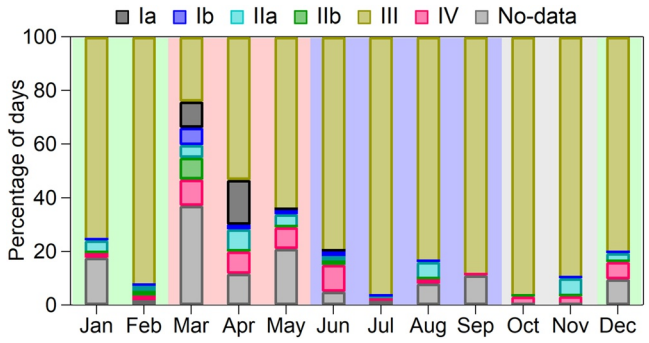

Figure 4. Monthly percentage of days for occurrence of NPF events (Ia, Ib, IIa, and IIb), nonevent (III), unidentified (IV), and no-data days at Ranichauri. The background colors (light green, light red, light blue, and light gray) indicate different seasons (winter, pre-monsoon, monsoon, and post-monsoon, respectively). NPF, new particle formation.

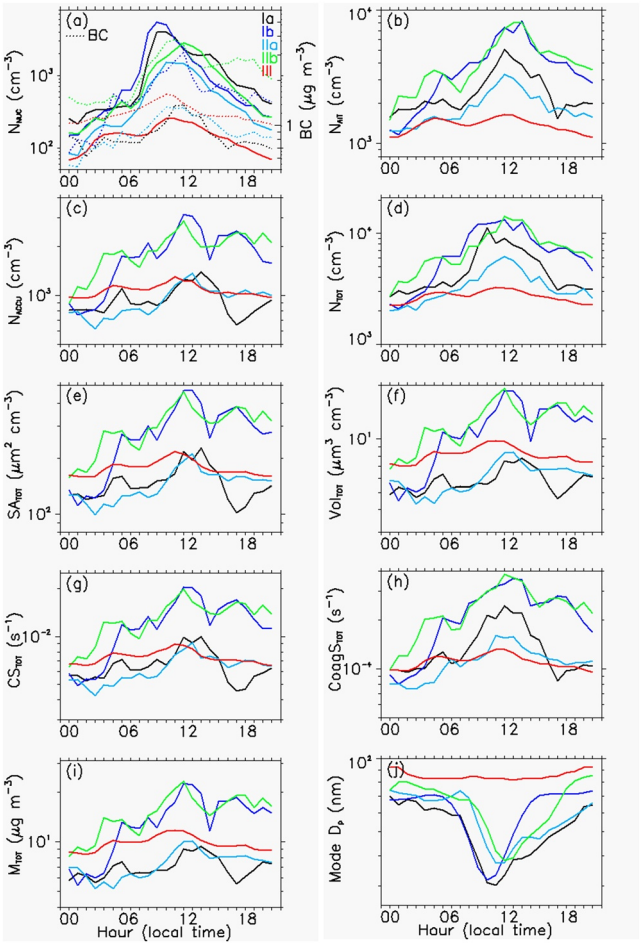

Figure 5. Averaged diurnal variation of (a) nucleation mode aerosols (solid lines) and black carbon mass concentrations (dotted line), (b) Aitken mode aerosols, (c) accumulation mode aerosols, (d) total aerosols, (e) total surface area, (f) total volume, (g) total condensation sink, (h) total coagulation sink, (i) total mass, and (j) particle mode diameter for NPF (Type-I and Type-II) event and nonevent (Type-III) days. Line color indicates the type of event. NPF, new particle formation.

reported higher growth rates at Mukteshwar site for boundary layer polluted events as compared to cleaner free tropospheric events.

Figure 4 shows the percentage of days for different types of events observed at Ranichauri during the period of the study. Out of a total of 643 days of observations, there were 24 (3.6%) Type-I and 31 (4.8%) Type-II event days. A total of 493 (76.4%) days did not show any evidence of NPF and 33 (5.1%) days were categorized as unidentified days. There were no measurements on 62 (9.7%) days. The monthly percentage of occurrence of NPF days was comparable to an earlier study at a high altitude site, Mukteshwar, in the Western Himalaya (Neitola et al., 2011), which is about 300 km to the Southeast of Ranichauri (Figure 1). Type-I NPF events occurred frequently in the pre-monsoon season (23 out of a total 24 event days). The days with no evidence for NPF were more common in the monsoon season owing to wet/cloud scavenging of condensable vapors as well as small clusters, and low solar insolation on persistently cloudy conditions during the monsoon season. A study at a rural site, Gadanki, in India also observed infrequent occurrence of NPF connected to lower aerosol precursor concentrations and weak gas-phase oxidation due to diminished solar radiation on persistently cloudy days during monsoon season (Kanawade et al., 2014).

3.2. Diurnal Variation of Aerosol Parameters

Figure 5 shows averaged diurnal variability in size-segregated aerosol number concentrations (Figures 5a–5d), BC mass concentration (dotted line, Figure 5a), total surface area (Figure 5e), Vol_{TOT} (Figure 5f), CS_{TOT} (Figure 5g), $CoagS_{TOT}$ (Figure 5h), total mass (Figure 5i), and particle mode diameter (Figure 5j). Overall, we found two main types of diurnal variation patterns in aerosol concentrations and properties. The first type was clearly connected to NPF events, showing rapid diurnal changes in aerosol number concentrations and properties during midday. The second type was characterized as the background aerosol size distribution and aerosol properties showing little or no diurnal change. These types of diurnal variation patters are similar to previous studies reporting temporal evolution of aerosol number concentrations and properties from long-term ground-based measurements (Hooda et al., 2018; Shen et al., 2011; Venzac et al., 2008). We further describe these types below.

N_{NUC} has more than an order-of-magnitude diurnal variability on days with NPF events, but a factor of 2–3 on nonevent days (Figure 5a). The morning increase in N_{NUC} does not coincide with the increase in concentrations of anthropogenic aerosol tracer, indicated by BC for Type-Ia and Type-IIa cleaner events. However, the morning peak in N_{NUC} clearly coincides with the elevated BC concentrations for Type-Ib and Type-IIb polluted events (Figure 5a). This is similar to observations at a high altitude site in the Western Himalaya reported by Venzac et al. (2008). This finding is further corroborated by the presence of higher Aitken mode and accumulation mode concentrations for polluted events (Ib and IIb) than cleaner events (Ia and IIa) (Figure 5g). The higher aerosol number concentrations on polluted days are also reflected in the diurnal variability in total surface area, Vol_{TOT}, CS_{TOT}, $CoagS_{TOT}$, and toal mass (Figures 5d–5i). In contrast, the particle mode diameter was smaller for cleaner event days than polluted event and nonevent days (Figure 5j). Similar diurnal variation of BC concentrations during Type-Ia, Type-IIa, and nonevent days

21698996, 2021, 7, Downloaded from https://agupubs.onlinelibrary.wiley.com/doi/10.1029/2020JD033267, Wiley Online Library on [13/12/2023]. See the Terms and Conditions (https://onlinelibrary.wiley.com/terms-and-conditions) on Wiley Online Library for rules of use; OA articles are governed by the applicable Creative Commons License

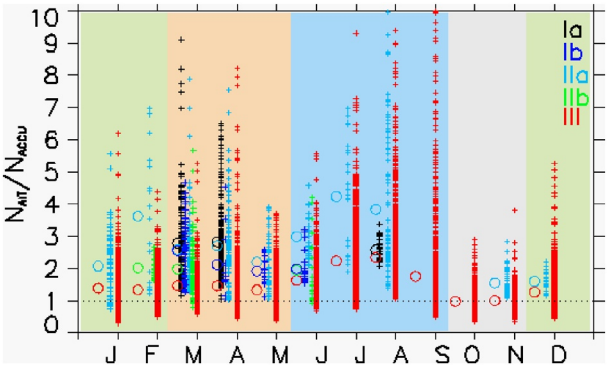

Figure 6. Hourly (plus sign) and monthly (open circle) averaged ratio of Aitken mode to accumulation mode aerosols for NPF event (Ia, Ib, IIa, and IIb) and nonevent (III) days. The background colors (light green, light red, light blue, and light gray) indicate different seasons (winter, pre-monsoon, monsoon, and post-monsoon, respectively). NPF, new particle formation.

(Figure 5a) perhaps illustrates that NPF was not prevented by the pre-existing aerosol concentrations in both cleaner and polluted air masses. In addition to pre-exisiting aerosol concentrations, there are two other factors that may strongly modulate NPF occurrence: availability of aerosol precursor concentration and solar insolation. At the high-altitude Hanle site in the Trans-Himalaya (Moorthy et al., 2011), it was observed that NPF rates were higher during pre-monsoon as the solar insolation was abundant. In their study, NPF slowed as the seasons progressed toward winter. Neitola et al. (2011) reported frequent NPF at the Mukteshwar site in the North-Western Himalaya during the pre-monsoon season. They found that the high frequency of pre-monsoon events was linked to elevated boundary layer height, indicating availability of aerosol precursors transported from valley regions. A recent review study of ground-based high altitude sites indicated that the impact of CS on the occurrence of NPF appeared to be different from one high altitude site to another (Sellegri et al., 2019). For instance, Venzac et al. (2008) found that high CS ($>2.1 \times 10^{-3}$ s^{-1}) inhibited the occurrence of NPF at the high-altitude Himalayan Nepal site, Pyramid, while the CS was higher during NPF events days (3.1×10^{-3} s^{-1}) than nonevent days (2.1×10^{-3} s^{-1}) at the Mount Chacaltaya site in Bolivian Andes (Rose et al., 2015) (implying the opposite effect of CS at Pyramid). Sellegri et al. (2019) suggested that the occurrence of NPF at high altitude sites might be determined by the abundance of condensable vapors, which are transported together with pre-existing aerosols from lower altitudes. At Ranichauri, the NPF occurred at both low (6.4×10^{-3} s^{-1}) and high (12.5×10^{-3} s^{-1}) CS conditions (Figure 5g), with the ratio between polluted and cleaner event days of about 2.

Further, we have calculated averaged diurnal variation of meteorological parameters for observed Type-I, Type-II, and Type-III event days (Figure S2). Temperature and relative humidity were slightly lower on nonevent days as compared to event days. The wind direction rapidly changed on event days as compared to nonevent days. Altogether, the meteorological parameters did not show much variation between the event and nonevent days.

The occurrence of NPF events in different air mass types is another open question. Air masses of different origin pose not only different meteorological conditions, but also varying chemical features. Therefore, the probability of occurrence of NPF at a given location not only depends on local emissions, but also the type of air mass arriving at that location (Sogacheva et al., 2005). For instance, NPF events were more common in continental polluted air masses than that of cleaner marine air masses from the Atlantic Ocean (Hussein et al., 2009; Sogacheva et al., 2007). Pierce et al. (2014) also showed that NPF rates were faster under the polluted conditions as compared to cleaner-air flow at Egbert, a mixture of forests and farmland site in Ontario, Canada. NPF has been seen to occur commonly at semi-rural and remote sites under the influence of long-range transported polluted plumes with elevated sulfuric acid concentrations via oxidation of sulfur dioxide (Creamean et al., 2011; Kanawade et al., 2012). Neitola et al. (2011) showed that NPF occurs frequently in the pre-monsoon season at a high-altitude site, Mukteshwar in the Himalayan foot hills when the boundary layer height was lifted up to the station altitude which allowed transport of aerosol precursors from valley to the station. These and numerous other studies found that NPF processes are strongly linked to the history of air masses (e.g., Asmi et al., 2011; Nieminen et al., 2014; Nilsson et al., 2001). This is not surprising since air masses arriving from different locations are likely to be affected by varying concentrations of aerosol precursors and meteorological conditions prior to their arrival at the measurement site, which determines the age of the air mass.

Hyvärinen et al. (2010) used ratio of Aitken mode to accumulation mode aerosols to determine the age of the air mass, where low values indicate an aged air mass while high values indicate the cleaner air mass often connected with NPF events. Figure 6 shows the hourly and monthly averaged ratio of Aitken mode to accumulation mode aerosols (N_{AIT}/N_{ACCU}) for NPF and nonevent days. The site is dominated by Aitken mode aerosols almost throughout the year, with the highest ratios of N_{AIT} to N_{ACCU} during monsoon and pre-monsoon seasons. N_{AIT}/N_{ACCU} values are higher for nonevent days than event days in the monsoon

21698996, 2021, 7, Downloaded from https://agupubs.onlinelibrary.wiley.com/doi/10.1029/2020JD033267, Wiley Online Library on [13/12/2023]. See the Terms and Conditions (https://onlinelibrary.wiley.com/terms-and-conditions) on Wiley Online Library for rules of use; OA articles are governed by the applicable Creative Commons License

Table 2
Summary of Particle Growth and Formation Rates for Type-I Event Days

Event type	GR_{10-25} (nm/h) Mean ± σ	GR_{10-25} (nm/h) Median (p25–p75)	J_{10} (cm^{-3} s^{-1}) Mean ± σ	J_{10} (cm^{-3} s^{-1}) Median (p25–p75)
Ia	8.51 ± 4.46	7.53 (6.15–11.18)	0.26 ± 0.27	0.21 (0.05–0.49)
Ib	4.86 ± 3.13	4.17 (3.29–10.71)	0.09 ± 0.08	0.07 (0.02–0.19)

Note. σ indicates standard deviation; p25 and p75 indicate 25th and 75th percentile values, respectively.

indicating the efficient wet scavenging of accumulation mode particles. N_{AIT}/N_{ACCU} values are higher for NPF event days than nonevent days in the pre-monsoon season, indicating the large source of Aitken mode aerosols via NPF processes. The monthly mean ratio ranged from 1.5 to 4.2, with about 75% cleaner events (Ia and IIa) of total NPF events (Figure 6).

3.3. Growth Rate, Formation Rate, and Survival Probabilities of Climate-Relevant Aerosols

Growth rates, formation rates, and survival probabilities were calculated only for Type-Ia and Type-Ib event days. Table 2 summarizes mean, median, and percentile (25th and 75th) values for $GR_{10-25\ nm}$ and J_{10} for these event days. For Type-Ia events, the median $GR_{10-25\ nm}$ was 7.5 nm/h, with 6.2 and 11.2 nm/h as 25th and 75th percentiles. For Type-Ib events, the median $GR_{10-25\ nm}$ was 4.2 nm/h, with 3.3 and 10.7 nm/h as 25th and 75th percentiles. The mean $GR_{10-25\ nm}$ was 8.51 and 4.86 nm/h for Type-Ia and Type-Ib, respectively. Figure 7a illustrates the cumulative probability distribution functions for $GR_{10-25\ nm}$ for these event days. The particle growth rates were about twofold higher for cleaner events than polluted events. This suggests that faster growth rates were favored at a lower CS. Overall, $GR_{10-25\ nm}$ values are within the large range observed at other high altitude sites (0.4–19.9 nm/h) (Sellegri et al., 2019).

The mean J_{10} was 0.26 and 0.09 cm^{-3} s^{-1} for Type-Ia and Type-Ib events, respectively. For Type-Ia event days, the median J_{10} was 0.21 cm^{-3} s^{-1}, with 0.05 and 0.49 cm^{-3} s^{-1} as 25th and 75th percentile values whereas for Type-Ib events, median J_{10} was 0.07 cm^{-3} s^{-1}, with 0.02 and 0.19 cm^{-3} s^{-1} as 25th and 75th quartile values. Figure 7b illustrates the cumulative probability distribution functions for J_{10} for these event days. García et al. (2014) reported J_{10}, at a high-altitude Izaña station in the Atlantic Ocean, in the range from 0.5 to 0.6 cm^{-3} s^{-1} whereas Venzac et al. (2008) reported, at a high altitude NCO-P site, in the range from 0.1 to 0.2 cm^{-3} s^{-1}. J_{10} at Ranichauri is comparable to these values, and to one reported for the Mukteshwar site in the Himalayan foothills (0.4 cm^{-3} s^{-1}) (Neitola et al., 2011). Nevertheless, J_{10} values at Ranichauri falls within the wide range reported for high-altitude and continental boundary layer sites across the globe (0.01–10 cm^{-3} s^{-1}) (Kulmala et al., 2004; Sellegri et al., 2019).

The contribution of atmospheric NPF to total aerosols or CCN concentrations can be estimated from the aerosol size distribution data. Kulmala et al. (2016) estimated that NPF contributes about 80% to the total aerosol number concentrations in a rural forest site, SMEAR II station at Hyytiälä, Finland. But, Tröstl et al. (2016) highlighted, based on 12-month aerosol size distribution data from the high-altitude site, Jungfraujoch, that NPF adds about 10% new particles to the aerosol concentration below 50 nm. They further emphasized that newly formed particles do not grow to CCN-active size (for an activation diameter of ~90 nm [Jurányi et al., 2011]) within observed NPF time-scales at this site (48 h), yielding low contribution of NPF to the CCN concentrations. The measurements at Mt. Tai in Shandong Province in China also showed that only about 12% of the total NPF events showed enhancement in CCN concentrations (Shen

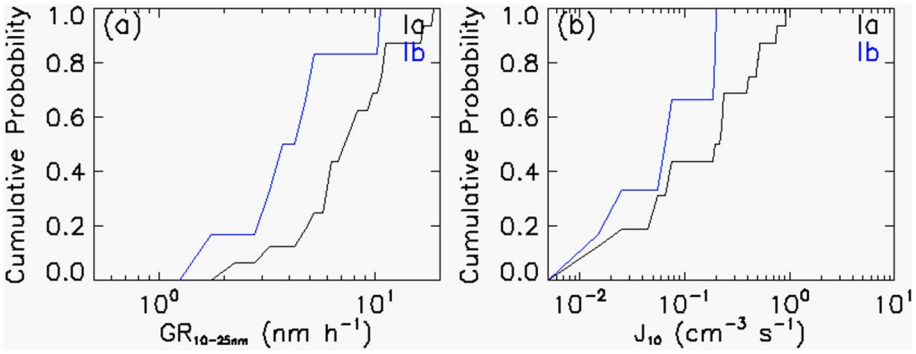

Figure 7. Cumulative probability distributions of (a) $GR_{10-25\ nm}$ and (b) J_{10} for Type-Ia and Type-Ib NPF event days. GR, growth rate; NPF, new particle formation.

21698996, 2021, 7, Downloaded from https://agupubs.onlinelibrary.wiley.com/doi/10.1029/2020JD033267, Wiley Online Library on [13/12/2023]. See the Terms and Conditions (https://onlinelibrary.wiley.com/terms-and-conditions) on Wiley Online Library for rules of use; OA articles are governed by the applicable Creative Commons License

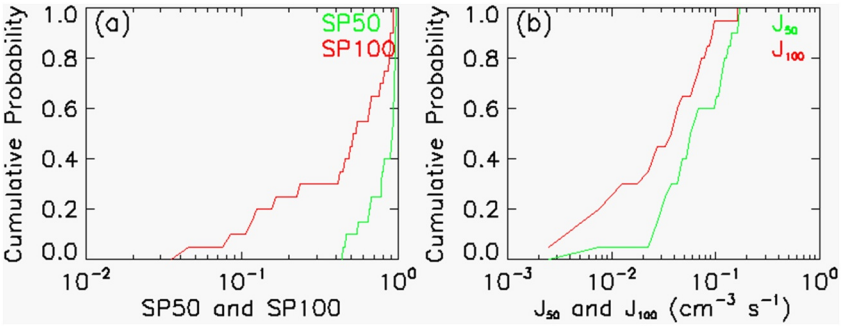

Figure 8. Cumulative probability distributions of (a) survival probability to 50 and 100 nm and (b) formation rates of 50 and 100 nm particles for the Type-I events.

et al., 2016). There is also no direct evidence of NPF contribution to CCN size at other high altitude sites, for example, NCO-P, Chacaltaya, or Storm Peak Laboratory (Hallar et al., 2016; Rose et al., 2015; Venzac et al., 2008). In addition, observations at Whistler Mountain (~1,300 m amsl) showed that freshly nucleated particles had a 10%–25% probability of growing to CCN sizes (100 nm) before being scavenged by coagulation (Pierce et al., 2012) whereas aerosol size distribution data at Chacaltaya mountain found that the potential to form CCN was about 53% in the free troposphere (Rose et al., 2017). Further, sulfuric acid is the dominant contributor to initial growth of nanoparticles from NPF, while organic compounds become more important as particles grow larger (Kulmala, Petäjä et al., 2016). Thus, the growth of nucleated particles to CCN sizes is dependent on the source and chemical makeups of the precursor compounds (Wang et al., 2017) as well as sinks (such as coagulations to pre-existing particles) (Kulmala et al., 2005). Since the growth of nucleated particles to CCN sizes takes from a few hours up to about 3 days in the lower troposphere, it is observationally very challenging to distinguish CCN formed through atmospheric NPF from those formed from growth of pre-existing aerosols (Kerminen et al., 2012).

Figure 8 shows cumulative probability distribution functions for the survival probability to 50 and 100 nm particles (SP50 and SP100) and the formation rates of 50 and 100 nm particles (J_{50} and J_{100}) for Type-I events. Table 3 summaries survival probabilities (SP) and formation rates (J) of 50 and 100 nm particles from various sites across the globe. SP50 ranged from 44% to 98%, with a mean and standard deviation of 82 ± 18% and SP100 ranged from 5% to 94%, with a mean and standard deviation of 53 ± 32%. These results show that, on average, 64% of new particle surviving to 50 nm goes on to survive to 100 nm. With the observed mean particle growth rates of 8.51 nm/h, the newly formed particles survived approximately 4–6 h to reach 50 nm. The mean value of SP50 at Ranichauri is almost double of the value reported for low-altitude forest site (33%) (Pierce et al., 2014) and comparable to the observed range at all four urban sites (31%–80%) reported by Westervelt et al. (2013). There are uncertainties in calculation of survival probabilities to 50 and 100 nm particles as previously reported by Westervelt et al. (2013). First, the primary particles may contribute to particle number concentrations of 10–25 nm, and therefore contributing to the apparent nucleation

Table 3
Summary of Survival Probability and Formation Rate of 50 and 100 nm Particles at Diverse Locations

Location	SP50 (%)	SP100 (%)	J_{50} (cm^{-3} s^{-1})	J_{100} (cm^{-3} s^{-1})	Reference
Ranichauri, India	82 ± 18	53 ± 32	0.08 ± 0.05	0.05 ± 0.04	This study
Egbert, Ontario, Canada	33	19	0.039	0.022	Pierce et al. (2014)
Pittsburgh, USA	37	2.4	0.11	0.006	Westervelt et al. (2013)
Atlanta, USA	67	3.7	0.177	0.006	Westervelt et al. (2013)
St. Louis, USA	46	1.8	1.6	0.046	Westervelt et al. (2013)
Hyytiälä, Finland	55	2.6	0.23	0.004	Westervelt et al. (2013)
Po Valley, Italy	34	4.4	0.39	0.34	Westervelt et al. (2013)
Mt. Tai, China	10–140	5–40	–	–	Zhu et al. (2020)

21698996, 2021, 7, Downloaded from https://agupubs.onlinelibrary.wiley.com/doi/10.1029/2020JD033267, Wiley Online Library on [13/12/2023]. See the Terms and Conditions (https://onlinelibrary.wiley.com/terms-and-conditions) on Wiley Online Library for rules of use; OA articles are governed by the applicable Creative Commons License

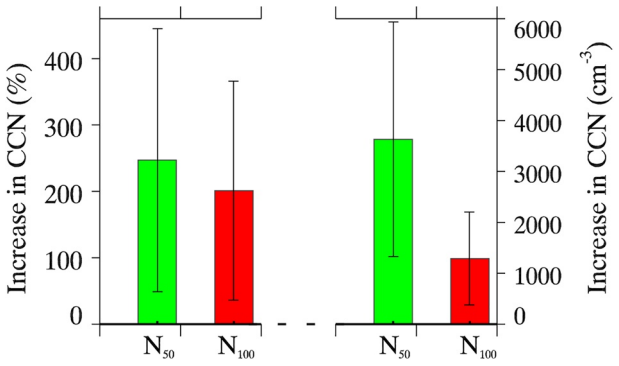

Figure 9. The relative (%) and absolute (in cm^{-3}) increase in CCN concentrations during Type-I NPF event days. CCN, cloud condensation nuclei; NPF, new particle formation.

rate. The use of two growth rates for only two size ranges (10–25 and 25–100 nm) may bias survival probabilities higher than expected. But, Westervelt et al. (2013) quantitatively addressed the survival probability uncertainty by using two methods: one method identified in the paper, and the other described by Kuang et al. (2009), wherein the ratio of N_{100} to N_3 for a given growth trajectory is defined as the survival probability. Westervelt et al. (2013) found that the two methods largely yield similar survival probabilities. J_{50} and J_{100} are the products of J_{10} and the corresponding survival probabilities. J_{50} ranged from 0.009 to 0.17 cm^{-3} s^{-1}, with a mean and standard deviation of 0.08 ± 0.05 cm^{-3} s^{-1}, which is about two times higher than a low altitude site in Egbert, Ontario, Canada (Pierce et al., 2014) where J_{50} was 0.039 cm^{-3} s^{-1} and lower by almost one-fifth to that of a highly polluted site, Po Valley (0.39 cm^{-3} s^{-1}) (Westervelt et al., 2013). J_{100} ranged from 0.004 to 0.16 cm^{-3} s^{-1}, with a mean and standard deviation of 0.05 ± 0.04 cm^{-3} s^{-1}, which is about two to three times higher than low altitude site, Egbert, Ontario, Canada (0.02 cm^{-3} s^{-1}) (Pierce et al., 2014). While J_{100} at Ranichauri was lower by an order of magnitude than that at the Po Valley (0.34 cm^{-3} s^{-1}) (Westervelt et al., 2013). The ratio of J_{100} to J_{50} ranged from 0.10 to 0.99, with a mean value of about 0.60 ± 0.31.

While the size of aerosol particle determines its ability to act as CCN, the hygroscopicity of particle also affects CCN activation (McFiggans et al., 2006). Figure 9 shows relative (in %) and absolute (in cm^{-3}) increase in CCN concentrations for Type-I nucleation event days at Ranichauri. Analogous to SP50 and SP100 calculations, nucleation events had an obvious effect on CCN concentrations. The relative increase in N_{50} ranged from 21.6% to 577.1%, with a mean and standard deviation of 247 ± 198% whereas the absolute increase in N_{50} ranged from 541 to 7,964 cm^{-3}, with a mean and standard deviation of 3,631 ± 2,603 cm^{-3}. The absolute increase in N_{50} at Ranichauri is comparable to continental background site, Botsalano, South Africa (Kerminen et al., 2012), indicative of intense nucleation events with higher growth rates. The relative increase in N_{100} ranged from 17.8% to 579.4%, with a mean and standard deviation of 201 ± 165% whereas the absolute increase in N_{100} ranged from 211 to 2,451 cm^{-3}, with a mean and standard deviation of 1,290 ± 913 cm^{-3}.

4. Conclusions

Here, we presented aerosol size distribution measurements at a background remote site in the Western Himalaya, Ranichauri, based on a 21 months (December 1, 2016 to September 14, 2018). We reported the frequency of NPF occurrence, growth rate, formation rate, seasonal variability and diurnal patterns in NPF features and illustrated survival probability of newly formed aerosols to 50 and 100 nm particles. Out of 643 observation days, Type-I (clear NPF) and Type-II NPF (Aitken-mode growth) events were observed on 3.6% and 4.8% days, respectively, with highest NPF frequency in the pre-monsoon (March–May) season. Type-I and Type-II NPF events were further classified into two subtypes: a (cleaner) and b (polluted), based on BC mass concentrations. For Type-Ia NPF event days, the $GR_{10–25\ nm}$ varied from 2.1 to 18.5 nm/h, with a mean and standard deviation of 8.51 ± 4.46 nm/h and for Type-Ib events, it varied from 1.6 to 10.7 nm/h with mean and standard deviation of 4.86 ± 3.13 nm/h. For Type-Ia events, J_{10} varied from 0.01 to 0.91 cm^{-3} s^{-1} with a mean and standard deviation of 0.26 ± 0.27 cm^{-3} s^{-1}, whereas it varied from 0.01 to 0.24 cm^{-3} s^{-1} with mean and standard deviation of 0.09 ± 0.08 cm^{-3} s^{-1} for Ib event days. The newly formed particles survival probability to 50 nm size ranged from 44% to 98%, with a mean and standard deviation of 82 ± 18%, and the survival probability to 100 nm was 53 ± 32%. Our estimates of survival probability indicate that a significant fraction of nucleated particles grow larger than 50 and 100 nm, and thus constitute an important source of CCN for cloud formations. The uplifting of the planetary boundary layer to the elevation of the measurement site appeared to carry aerosol precursor vapors for particle growth at a relatively lower background pre-existing particle concentrations. The mean formation rates of 50 and 100 nm particles were 0.08 and 0.05 cm^{-3} s^{-1}, respectively. The newly formed particles have an obvious effect on CCN number concentrations during the observed NPF event days. Overall, NPF occurred more frequently in air masses with low BC concentrations (cleaner) than polluted air masses, with faster growth rates and formation rates during

21698996, 2021, 7, Downloaded from https://agupubs.onlinelibrary.wiley.com/doi/10.1029/2020JD033267, Wiley Online Library on [13/12/2023]. See the Terms and Conditions (https://onlinelibrary.wiley.com/terms-and-conditions) on Wiley Online Library for rules of use; OA articles are governed by the applicable Creative Commons License

cleaner event days (Type-Ia). While the high CS in polluted air masses could reduce the concentrations of condensable vapors and in turn lowering NPF and growth rates, the chemistry producing condensable vapors may also significantly alter NPF and growth rates. Our results highlight that although the occurrence of NPF was lower at this site as compared to other remote high altitude sites, the high survival probability indicates that the sporadic NPF events could be a large source of climate-relevant aerosols.

In this study, we have linked, for the first time to our knowledge, NPF to climate-relevant aerosols in India. First, more emphasis should be put on combining long-term field measurements from multiple sites in India to derive statistically relevant NPF features including frequency, growth rates, formation rates, survival probability of newly formed aerosols, and CCN concentrations or some proxy for it. Second, adding chemical information and CCN concentration measurements to the existing aerosol size distribution measurements would provide new information on NPF-CCN linkages in cleaner versus polluted environments. Lastly, such analyses of field measurements should be aided with regional or parcel model simulations to aid in interpreting field measurements.

Data Availability Statement

DMPS aerosol size distribution and AE-33 Aethalometer black carbon data are archived at https://data.mendeley.com/datasets/pstmtr8gzr/2. Air mass back trajectory calculation is performed using PC windows-based HYSPLIT model, which is available publicly at https://www.ready.noaa.gov/HYSPLIT.php.

Acknowledgments
V. P. Kanawade would like to thank Department of Science & Technology (DST)-SERB Grant (ECR/2016/001333). CLIMOB (CLImate Modeling and Observations in India)—project funded by the Ministry for Foreign Affairs of Finland is acknowledged for supporting the measurements in Ranichauri. J. R. Pierce was supported by the US Department of Energy's Atmospheric System Research, an Office of Science, Office of Biological and Environmental Research program, under grant DE-SC0019000. Authors acknowledge the free use of PC-based HYSPLIT model. Authors also thank the anonymous reviewers for their many insightful comments and suggestions which helped to improve the quality of the manuscript.

References

Asmi, E., Kivekäs, N., Kerminen, V.-M., Komppula, M., Hyvärinen, A.-P., Hatakka, J., et al. (2011). Secondary new particle formation in Northern Finland Pallas site between the years 2000 and 2010. *Atmospheric Chemistry and Physics*, *11*(24), 12959–12972. https://doi.org/10.5194/acp-11-12959-2011

Babu, S. S., Kompalli, S. K., & Moorthy, K. K. (2016). Aerosol number size distributions over a coastal semi urban location: Seasonal changes and ultrafine particle bursts. *The Science of the Total Environment*, *563–564*, 351–365. https://doi.org/10.1016/j.scitotenv.2016.03.246

Boulon, J., Sellegri, K., Venzac, H., Picard, D., Weingartner, E., Wehrle, G., et al. (2010). New particle formation and ultrafine charged aerosol climatology at a high altitude site in the Alps (Jungfraujoch, 3580 m a.s.l., Switzerland). *Atmospheric Chemistry and Physics*, *10*(19), 9333–9349. https://doi.org/10.5194/acp-10-9333-2010

Chowdhury, S., Dey, S., & Smith, K. R. (2018). Ambient $PM_{2.5}$ exposure and expected premature mortality to 2100 in India under climate change scenarios. *Nature Communications*, *9*(1), 318. https://doi.org/10.1038/s41467-017-02755-y

Collaud Coen, M., Andrews, E., Asmi, A., Baltensperger, U., Bukowiecki, N., Day, D., et al. (2013). Aerosol decadal trends—Part 1: In-situ optical measurements at GAW and IMPROVE stations. *Atmospheric Chemistry and Physics*, *13*(2), 869–894. https://doi.org/10.5194/acp-13-869-2013

Creamean, J. M., Ault, A. P., Ten Hoeve, J. E., Jacobson, M. Z., Roberts, G. C., & Prather, K. A. (2011). Measurements of aerosol chemistry during new particle formation events at a remote rural mountain site. *Environmental Science and Technology*, *45*(19), 8208–8216. https://doi.org/10.1021/es103692f

Dai, L., Wang, H., Zhou, L., An, J., Tang, L., Lu, C., et al. (2017). Regional and local new particle formation events observed in the Yangtze River Delta region, China. *Journal of Geophysical Research: Atmospheres*, *122*(4), 2389–2402. https://doi.org/10.1002/2016JD026030

Dal Maso, M. D., Kulmala, M., Riipinen, I., Wagner, R., Hussein, T., Aalto, P. P., & Lehtinen, K. E. J. (2005). Formation and growth of fresh atmospheric aerosols: eight years of aerosol size distribution data from SMEAR II, Hyytiälä, Finland. *Boreal Environment Research*, *10*(5), 323–336.

De Wekker, S. F. J., & Kossmann, M. (2015). Convective boundary layer heights over mountainous terrain—A review of concepts. *Frontiers of Earth Science*, *3*, 77. https://doi.org/10.3389/feart.2015.00077

Draxler, R. R., & Rolph, G. D. (2010). *HYSPLIT—HYbrid single-particle Lagrangian integrated trajectory model*. http://ready.arl.noaa.gov/HYSPLIT.php

Drinovec, L., Močnik, G., Zotter, P., Prévôt, A. S. H., Ruckstuhl, C., Coz, E., et al. (2015). The "dual-spot" Aethalometer: an improved measurement of aerosol black carbon with real-time loading compensation. *Atmospheric Measurement Techniques*, *8*(5), 1965–1979. https://doi.org/10.5194/amt-8-1965-2015

Dusek, U., Frank, G. P., Hildebrandt, L., Curtius, J., Schneider, J., Walter, S., et al. (2006). Size matters more than chemistry for cloud-nucleating ability of aerosol particles. *Science*, *312*(5778), 1375–1378. https://doi.org/10.1126/science.1125261

Foucart, B., Sellegri, K., Tulet, P., Rose, C., Metzger, J.-M., & Picard, D. (2018). High occurrence of new particle formation events at the Maïdo high-altitude observatory (2150 m), Réunion (Indian Ocean). *Atmospheric Chemistry and Physics*, *18*(13), 9243–9261. https://doi.org/10.5194/acp-18-9243-2018

García, M. I., Rodríguez, S., González, Y., & García, R. D. (2014). Climatology of new particle formation at Izaña mountain GAW observatory in the subtropical North Atlantic. *Atmospheric Chemistry and Physics*, *14*(8), 3865–3881. https://doi.org/10.5194/acp-14-3865-2014

Gordon, H., Kirkby, J., Baltensperger, U., Bianchi, F., Breitenlechner, M., Curtius, J., et al. (2017). Causes and importance of new particle formation in the present-day and preindustrial atmospheres. *Journal of Geophysical Research: Atmospheres*, *122*(16), 8739–8760. https://doi.org/10.1002/2017JD026844

Hallar, A. G., Lowenthal, D. H., Chirokova, G., Borys, R. D., & Wiedinmyer, C. (2011). Persistent daily new particle formation at a mountain-top location. *Atmospheric Environment*, *45*(24), 4111–4115. https://doi.org/10.1016/j.atmosenv.2011.04.044

21698996, 2021, 7, Downloaded from https://agupubs.onlinelibrary.wiley.com/doi/10.1029/2020JD033267, Wiley Online Library on [13/12/2023]. See the Terms and Conditions (https://onlinelibrary.wiley.com/terms-and-conditions) on Wiley Online Library for rules of use; OA articles are governed by the applicable Creative Commons License

Hallar, A. G., Petersen, R., McCubbin, I. B., Lowenthal, D., Lee, S., Andrews, E., & Yu, F. (2016). Climatology of new particle formation and corresponding precursors at storm peak laboratory. *Aerosol and Air Quality Research*, *16*(3), 816–826. https://doi.org/10.4209/aaqr.2015.05.0341

Hooda, R. K., Kivekäs,N., O'Connor, E. J., Collaud Coen, M., Pietikäinen, J. P., Vakkari, V., et al., (2018). Driving factors of aerosol properties over the foothills of central himalayas based on 8.5 years continuous measurements. *Journal of Geophysical Research: Atmospheres*, *123*(23), 13421–13442. https://doi.org/10.1029/2018JD029744

Hussein, T., Junninen, H., Tunved, P., Kristensson, A., Dal Maso, M., Riipinen, I., et al. (2009). Time span and spatial scale of regional new particle formation events over Finland and Southern Sweden. *Atmospheric Chemistry and Physics*, *9*(14), 4699–4716. https://doi.org/10.5194/acp-9-4699-2009

Hyvärinen, A.-P., Lihavainen, H., Komppula, M., Panwar, T. S., Sharma, V. P., Hooda, R. K., & Viisanen, Y. (2010). Aerosol measurements at the Gual Pahari EUCAARI station: preliminary results from in-situ measurements. *Atmospheric Chemistry and Physics*, *10*(15), 7241–7252. https://doi.org/10.5194/acp-10-7241-2010

Hyvärinen, A.-P., Raatikainen, T., Komppula, M., Mielonen, T., Sundström, A.-M., Brus, D., et al. (2011). Effect of the summer monsoon on aerosols at two measurement stations in Northern India—Part 2: Physical and optical properties. *Atmospheric Chemistry and Physics*, *11*(16), 8283–8294. https://doi.org/10.5194/acp-11-8283-2011

IPCC *Climate change 2013: The physical science basis. Contribution of Working Group I to the Fifth Assessment Report of the Intergovernmental Panel on Climate Change*. Cambridge, UK and New York, NY, USA. https://www.ipcc.ch/report/ar5/wg1/

Jurányi, Z., Gysel, M., Weingartner, E., Bukowiecki, N., Kammermann, L., & Baltensperger, U. (2011). A 17-month climatology of the cloud condensation nuclei number concentration at the high alpine site Jungfraujoch. *Journal of Geophysical Research*, *116*(D10). https://doi.org/10.1029/2010JD015199

Kamra, A. K., Siingh, D., Gautam, A. S., Kanawade, V. P., Tripathi, S. N., & Srivastava, A. K. (2015). Atmospheric ions and new particle formation events at a tropical location, Pune, India. *Quarterly Journal of the Royal Meteorological Society*, *141*(693), 3140–3156. https://doi.org/10.1002/qj.2598

Kanamitsu, M. (1989). Description of the NMC Global Data Assimilation and Forecast System. *Weather and Forecasting*, *4*(3), 335–342. https://doi.org/10.1175/1520-0434(1989)004<0335:dotngd>2.0.co;2

Kanawade, V. P., Benson, D. R., & Lee, S.-H. (2012). Statistical analysis of 4-year observations of aerosol sizes in a semi-rural continental environment. *Atmospheric Environment*, *59*, 30–38. http://dx.doi.org/10.1016/j.atmosenv.2012.05.047

Kanawade, V. P., Shika, S., Pöhlker, C., Rose, D., Suman, M. N. S., Gadhavi, H., et al. (2014). Infrequent occurrence of new particle formation at a semi-rural location, Gadanki, in tropical Southern India. *Atmospheric Environment*, *94*, 264–273. http://dx.doi.org/10.1016/j.atmosenv.2014.05.046

Kanawade, V. P., Tripathi, S. N., Chakraborty, A., & Yu, H. (2020). Chemical characterization of sub-micron aerosols during new particle formation in an urban atmosphere. *Aerosol and Air Quality Research*, *20*, 1294–1305. https://doi.org/10.4209/aaqr.2019.04.0196

Kanawade, V. P., Tripathi, S. N., Siingh, D., Gautam, A. S., Srivastava, A. K., Kamra, A. K., et al. (2014). Observations of new particle formation at two distinct Indian subcontinental urban locations. *Atmospheric Environment*, *96*, 370–379. http://dx.doi.org/10.1016/j.atmosenv.2014.08.001

Kerminen, V.-M., Chen, X., Vakkari, V., Petäjä, T., Kulmala, M., & Bianchi, F. (2018). Atmospheric new particle formation and growth: review of field observations. *Environmental Research Letters*, *13*(10), 103003. https://doi.org/10.1088/1748-9326/aadf3c

Kerminen, V.-M., Paramonov, M., Anttila, T., Riipinen, I., Fountoukis, C., Korhonen, H., et al. (2012). Cloud condensation nuclei production associated with atmospheric nucleation: a synthesis based on existing literature and new results. *Atmospheric Chemistry and Physics*, *12*(24), 12037–12059. https://doi.org/10.5194/acp-12-12037-2012

Kivekäs, N., Sun, J., Zhan, M., Kerminen, V.-M., Hyvärinen, A., Komppula, M., et al. (2009). Long term particle size distribution measurements at Mount Waliguan, a high-altitude site in inland China. *Atmospheric Chemistry and Physics*, *9*(15), 5461–5474. https://doi.org/10.5194/acp-9-5461-2009

Komppula, M., Lihavainen, H., Hyvärinen, A. P., Kerminen, V.-M., Panwar, T. S., Sharma, V. P., & Viisanen, Y. (2009). Physical properties of aerosol particles at a Himalayan background site in India. *Journal of Geophysical Research*, *114*(D12). https://doi.org/10.1029/2008JD011007

Korhonen, H., Carslaw, K. S., Spracklen, D. V., Ridley, D. A., & Ström, J. (2008). A global model study of processes controlling aerosol size distributions in the Arctic spring and summer. *Journal of Geophysical Research*, *113*(D8). https://doi.org/10.1029/2007jd009114

Kowol-Santen, J., Beekmann, M., Schmitgen, S., & Dewey, K. (2001). Tracer analysis of transport from the boundary layer to the free troposphere. *Geophysical Research Letters*, *28*(15), 2907–2910. https://doi.org/10.1029/2001gl012908

Kuang, C., McMurry, P. H., & McCormick, A. V. (2009). Determination of cloud condensation nuclei production from measured new particle formation events. *Geophysical Research Letters*, *36*(9). https://doi.org/10.1029/2009GL037584

Kulmala, M., Kerminen, V.-M., Petäjä, T., Ding, A. J., & Wang, L. (2017). Atmospheric gas-to-particle conversion: why NPF events are observed in megacities? *Faraday Discussions*, *200*(0), 271–288. https://doi.org/10.1039/c6fd00257a

Kulmala, M., Kontkanen, J., Junninen, H., Lehtipalo, K., Manninen, H. E., Nieminen, T., et al. (2013). Direct observations of atmospheric aerosol nucleation. *Science*, *339*(6122), 943–946. https://doi.org/10.1126/science.1227385

Kulmala, M., Luoma, K., Virkkula, A., Petäjä, T., Paasonen, P., Kerminen, V.-M., et al. (2016). On the mode-segregated aerosol particle number concentration load: Contributions of primary and secondary particles in Hyytiälä and Nanjing. *Boreal Environment Research*, *21*(3–4), 319–331.

Kulmala, M., Petäjä, T., Kerminen, V.-M., Kujansuu, J., Ruuskanen, T., Ding, A., et al. (2016). On secondary new particle formation in China. *Frontiers of Environmental Science & Engineering*, *10*(5), 8. https://doi.org/10.1007/s11783-016-0857-7

Kulmala, M., Petäjä, T., Mönkkönen, P., Koponen, I. K., Dal Maso, M., Aalto, P. P., et al. (2005). On the growth of nucleation mode particles: source rates of condensable vapor in polluted and clean environments. *Atmospheric Chemistry and Physics*, *5*(2), 409–416. https://doi.org/10.5194/acp-5-409-2005

Kulmala, M., Vehkamäki, H., Petäjä, T., Dal Maso, M., Lauri, A., Kerminen, V.-M., et al. (2004). Formation and growth rates of ultrafine atmospheric particles: a review of observations. *Journal of Aerosol Science*, *35*(2), 143–176. https://doi.org/10.1016/j.jaerosci.2003.10.003

Kumar, R. R., Soni, V. K., & Jain, M. K. (2020). Evaluation of spatial and temporal heterogeneity of black carbon aerosol mass concentration over India using three year measurements from IMD BC observation network. *The Science of the Total Environment*, *723*, 138060. https://doi.org/10.1016/j.scitotenv.2020.138060

Landrigan, P. J., Fuller, R., Acosta, N. J. R., Adeyi, O., Arnold, R., Basu, N., et al. (2018). The Lancet Commission on pollution and health. *The Lancet*, *391*(10119), 462–512. https://doi.org/10.1016/s0140-6736(17)32345-0

21698996, 2021, 7, Downloaded from https://agupubs.onlinelibrary.wiley.com/doi/10.1029/2020JD033267, Wiley Online Library on [13/12/2023]. See the Terms and Conditions (https://onlinelibrary.wiley.com/terms-and-conditions) on Wiley Online Library for rules of use; OA articles are governed by the applicable Creative Commons License

Leaitch, W. R., Korolev, A., Aliabadi, A. A., Burkart, J., Willis, M. D., Abbatt, J. P. D., et al. (2016). Effects of 20-100 nm particles on liquid clouds in the clean summertime Arctic. *Atmospheric Chemistry and Physics*, *16*(17), 11107–11124. https://doi.org/10.5194/acp-16-11107-2016

Leena, P. P., Anil Kumar, V., Dani, K. K., Sombawne, S. M., Murugavel, P., & Pandithurai, G. (2017). Evidence of new particle formation during post monsoon season over a high-altitude site of the Western Ghats, India. *Toxicological and Environmental Chemistry*, *99*(4), 652–664. https://doi.org/10.1080/02772248.2016.1274031

Magee Scientific. (2016). *Aethalometer® model AE33 user manual - version 1.54*. Ljubljana, Slovenia: Aerosol d.o.o. pp. 159–195.

Manninen, H. E, Nieminen, T., Asmi, E., Gagné, S., Häkkinen, S., Lehtipalo, K., et al. (2010). EUCAARI ion spectrometer measurements at 12 European sites—Analysis of new particle formation events. *Atmospheric Chemistry and Physics*, *10*(16), 7907–7927. https://doi.org/10.5194/acp-10-7907-2010

McFiggans, G., Artaxo, P., Baltensperger, U., Coe, H., Facchini, M. C., Feingold, G., et al. (2006). The effect of physical and chemical aerosol properties on warm cloud droplet activation. *Atmospheric Chemistry and Physics*, *6*, 2593–2649. https://doi.org/10.5194/acp-6-2593-2006

Mönkkönen, P., Koponen, I. K., Lehtinen, K. E. J., Hämeri, K., Uma, R., & Kulmala, M. (2005). Measurements in a highly polluted Asian mega city: observations of aerosol number size distribution, modal parameters and nucleation events. *Atmospheric Chemistry and Physics*, *5*(1), 57–66. https://doi.org/10.5194/acp-5-57-2005

Moorthy, K. K., Sreekanth, V., Chaubey, J. P., Gogoi, M. M., Babu, S. S., Kompalli, S. K., et al. (2011). Fine and ultrafine particles at a near–free tropospheric environment over the high-altitude station Hanle in the Trans-Himalaya: New particle formation and size distribution. *Journal of Geophysical Research*, *116*(D20). https://doi.org/10.1029/2011JD016343

Neitola, K., Asmi, E., Komppula, M., Hyvärinen, A.-P., Raatikainen, T., Panwar, T. S., et al. (2011). New particle formation infrequently observed in Himalayan foothills—why?. *Atmospheric Chemistry and Physics*, *11*(16), 8447–8458. https://doi.org/10.5194/acp-11-8447-2011

Nie, W., Ding, A., Wang, T., Kerminen, V.-M., George, C., Xue, K., et al. (2014). Polluted dust promotes new particle formation and growth. *Scientific Reports*, *4*(1), 6634. https://doi.org/10.1038/srep06634

Nieminen, T., Asmi, A., Maso, M. D., Aalto, P. P., Keronen, P., Petaja, T., et al. (2014). Trends in atmospheric new-particle formation: 16 years of observations in a boreal-forest environment. *Boreal Environment Research*, *19*(B), 191–204. http://hdl.handle.net/10138/165199

Nieminen, T., Kerminen, V.-M., Petäjä, T., Aalto, P. P., Arshinov, M., Asmi, E., et al. (2018). Global analysis of continental boundary layer new particle formation based on long-term measurements. *Atmospheric Chemistry and Physics*, *18*(19), 14737–14756. https://doi.org/10.5194/acp-18-14737-2018

Nilsson, E. D., Paatero, J., & Boy, M. (2001). Effects of air masses and synoptic weather on aerosol formation in the continental boundary layer. *Tellus B*, *53*(4), 462–478. https://doi.org/10.3402/tellusb.v53i4.16619

Paasonen, P., Asmi, A., Petäjä, T., Kajos, M. K., Äijälä, M., Junninen, H., et al. (2013). Warming-induced increase in aerosol number concentration likely to moderate climate change. *Nature Geoscience*, *6*(6), 438–442. https://doi.org/10.1038/ngeo1800

Petzold, A., Ogren, J. A., Fiebig, M., Laj, P., Li, S.-M., Baltensperger, U., et al. (2013). Recommendations for reporting "black carbon" measurements. *Atmospheric Chemistry and Physics*, *13*(16), 8365–8379. https://doi.org/10.5194/acp-13-8365-2013

Pierce, J. R., & Adams, P. J. (2007). Efficiency of cloud condensation nuclei formation from ultrafine particles. *Atmospheric Chemistry and Physics*, *7*(5), 1367–1379. https://doi.org/10.5194/acp-13-8365-2013

Pierce, J. R., Leaitch, W. R., Liggio, J., Westervelt, D. M., Wainwright, C. D., Abbatt, J. P. D., et al. (2012). Nucleation and condensational growth to CCN sizes during a sustained pristine biogenic SOA event in a forested mountain valley. *Atmospheric Chemistry and Physics*, *12*(7), 3147–3163. https://doi.org/10.5194/acp-12-3147-2012

Pierce, J. R., Westervelt, D. M., Atwood, S. A., Barnes, E. A., & Leaitch, W. R. (2014). New-particle formation, growth and climate-relevant particle production in Egbert, Canada: analysis from 1 year of size-distribution observations. *Atmospheric Chemistry and Physics*, *14*(16), 8647–8663. https://doi.org/10.5194/acp-14-8647-2014

Rose, C., Sellegri, K., Moreno, I., Velarde, F., Ramonet, M., Weinhold, K., et al. (2017). CCN production by new particle formation in the free troposphere. *Atmospheric Chemistry and Physics*, *17*(2), 1529–1541. https://doi.org/10.5194/acp-17-1529-2017

Rose, C., Sellegri, K., Velarde, F., Moreno, I., Ramonet, M., Weinhold, K., et al. (2015). Frequent nucleation events at the high altitude station of Chacaltaya (5240 m a.s.l.), Bolivia. *Atmospheric Environment*, *102*, 18–29. https://doi.org/10.1016/j.atmosenv.2014.11.015

Rosenfeld, D., Sherwood, S., Wood, R., & Donner, L. (2014). Climate effects of aerosol-cloud interactions. *Science*, *343*(6169), 379–380. https://doi.org/10.1126/science.1247490

Sarangi, C., Kanawade, V. P., Tripathi, S. N., Thomas, A., & Ganguly, D. (2018). Aerosol-induced intensification of cooling effect of clouds during Indian summer monsoon. *Nature Communications*, *9*(1), 3754. https://doi.org/10.1038/s41467-018-06015-5

Sellegri, K., Rose, C., Marinoni, A., Lupi, A., Wiedensohler, A., Andrade, M., et al. (2019). New particle formation: A review of ground-based observations at mountain research stations. *Atmosphere*, *10*(9), 493. https://doi.org/10.3390/atmos10090493

Serafin, S., Adler, B., Cuxart, J., De Wekker, S. F. J., Gohm, A., Grisogono, B., et al. (2018). Exchange processes in the atmospheric boundary layer over mountainous terrain. *Atmosphere*, *9*, 102. https://doi.org/10.3390/atmos9030102

Shen, X. J., Sun, J. Y., Zhang, Y. M., Wehner, B., Nowak, A., Tuch, T., et al. (2011). First long-term study of particle number size distributions and new particle formation events of regional aerosol in the North China Plain. *Atmospheric Chemistry and Physics*, *11*(4), 1565–1580. https://doi.org/10.5194/acp-11-1565-2011

Shen, X. J., Sun, J., Zhang, X., Zhang, Y., Zhang, L., & Fan, R. (2016). Key features of new particle formation events at background sites in China and their influence on cloud condensation nuclei. *Frontiers of Environmental Science & Engineering*, *10*(5), 5. https://doi.org/10.1007/s11783-016-0833-2

Singh, N., Solanki, R., Ojha, N., Janssen, R. H. H., Pozzer, A., & Dhaka, S. K. (2016). Boundary layer evolution over the central Himalayas from radio wind profiler and model simulations. *Atmospheric Chemistry and Physics*, *16*(16), 10559–10572. https://doi.org/10.5194/acp-16-10559-2016

Sogacheva, L., Hamed, A., Facchini, M. C., Kulmala, M., & Laaksonen, A. (2007). Relation of air mass history to nucleation events in Po Valley, Italy, using back trajectories analysis. *Atmospheric Chemistry and Physics*, *7*(3), 839–853. https://doi.org/10.5194/acp-7-839-2007

Sogacheva, L., Maso, M. D., Kerminen, V.-M., & Kulmala, M. (2005). Probability of nucleation events and aerosol particle concentration in different air mass types arriving at Hyytiala, southern Finland, based on back trajectory analysis. *Boreal Environment Research*, *10*, 479–491.

Sullivan, R. C., Crippa, P., Matsui, H., Leung, L. R., Zhao, C., Thota, A., & Pryor, S. C. (2018). New particle formation leads to cloud dimming. *npj Climate and Atmospheric Science*, *1*(1), 9. https://doi.org/10.1038/s41612-018-0019-7

Tröstl, J., Herrmann,E., Frege,C., Bianchi,F., Molteni,U., Bukowiecki,N., et al. (2016). Contribution of new particle formation to the total aerosol concentration at the high-altitude site Jungfraujoch (3580 m asl, Switzerland). *Journal of Geophysical Research: Atmospheres*, *121*(19), 11692–11711. https://doi.org/10.1002/2015JD024637

21698996, 2021, 7, Downloaded from https://agupubs.onlinelibrary.wiley.com/doi/10.1029/2020JD033267, Wiley Online Library on [13/12/2023]. See the Terms and Conditions (https://onlinelibrary.wiley.com/terms-and-conditions) on Wiley Online Library for rules of use; OA articles are governed by the applicable Creative Commons License

Upadhyay, R., Ranjan, R., & Negi, P. S. (2015). Climate variability and trend at Ranichauri (Uttarakhand). *Journal of Agrometeorology*, *17*(2), 241–243

Venzac, H., Sellegri, K., Laj, P., Villani, P., Bonasoni, P., Marinoni, A., et al. (2008). High frequency new particle formation in the Himalayas. *Proceedings of the National Academy of Sciences of the United States of America*, *105*(41), 15666–15671. https://doi.org/10.1073/pnas.0801355105

Venzac, H., Sellegri, K., Villani, P., Picard, D., & Laj, P. (2009). Seasonal variation of aerosol size distributions in the free troposphere and residual layer at the puy de Dôme station, France. *Atmospheric Chemistry and Physics*, *9*(4), 1465–1478. https://doi.org/10.5194/acp-9-1465-2009

von Schneidemesser, E., Monks, P. S., Allan, J. D., Bruhwiler, L., Forster, P., Fowler, D., et al. (2015). Chemistry and the linkages between air quality and climate change. *Chemistry Review*, *115*(10), 3856–3897. https://doi.org/10.1021/acs.chemrev.5b00089

Wang, M., & Penner, J. E. (2009). Aerosol indirect forcing in a global model with particle nucleation. *Atmospheric Chemistry and Physics*, *9*(1), 239–260. https://doi.org/10.5194/acp-9-239-2009

Wang, Z., Birmili, W., Hamed, A., Wehner, B., Spindler, G., Pei, X., et al. (2017). Contributions of volatile and nonvolatile compounds (at 300°C) to condensational growth of atmospheric nanoparticles: An assessment based on 8.5 years of observations at the Central Europe background site Melpitz. *Journal of Geophysical Research: Atmospheres*, *122*(1), 485–497. https://doi.org/10.1002/2016JD025581

Weigel, A. P., Chow, F. K., & Rotach, M. W. (2007). The effect of mountainous topography on moisture exchange between the "surface" and the free atmosphere. *Boundary-Layer Meteorology*, *125*(2), 227–244. https://doi.org/10.1007/s10546-006-9120-2

Westervelt, D. M., Pierce, J. R., & Adams, P. J. (2014). Analysis of feedbacks between nucleation rate, survival probability and cloud condensation nuclei formation. *Atmospheric Chemistry and Physics*, *14*(11), 5577–5597. https://doi.org/10.5194/acp-14-5577-2014

Westervelt, D. M., Pierce, J. R., Riipinen, I., Trivitayanurak, W., Hamed, A., Kulmala, M., et al. (2013). Formation and growth of nucleated particles into cloud condensation nuclei: model-measurement comparison. *Atmospheric Chemistry and Physics*, *13*(15), 7645–7663. https://doi.org/10.5194/acp-13-7645-2013

Wiedensohler, A., Birmili, W., Nowak, A., Sonntag, A., Weinhold, K., Merkel, M., et al. (2012). Mobility particle size spectrometers: harmonization of technical standards and data structure to facilitate high quality long-term observations of atmospheric particle number size distributions. *Atmospheric Measurement Techniques*, *5*(3), 657–685. https://doi.org/10.5194/amt-5-657-2012

Yao, L., Garmash, O., Bianchi, F., Zheng, J., Yan, C., Kontkanen, J., et al. (2018). Atmospheric new particle formation from sulfuric acid and amines in a Chinese megacity. *Science*, *361*(6399), 278–281. https://doi.org/10.1126/science.aao4839

Yu, H., Ren, L., & Kanawade, V. P. (2017). New particle formation and growth mechanisms in highly polluted environments. *Current Pollution Reports*, *3*(4), 245–253. https://doi.org/10.1007/s40726-017-0067-3

Zhang, R., Khalizov, A., Wang, L., Hu, M., & Xu, W. (2012). Nucleation and growth of nanoparticles in the atmosphere. *Chemistry Review*, *112*(3), 1957–2011. https://doi.org/10.1021/cr2001756

Zhang, R., Wang, G., Guo, S., Zamora, M. L., Ying, Q., Lin, Y., et al. (2015). Formation of urban fine particulate matter. *Chemistry Review*, *115*(10), 3803–3855. https://doi.org/10.1021/acs.chemrev.5b00067

Zhu, Y., Xue, L., Gao, J., Chen, J., Li, H., Zhao, Y., et al. (2021). Increased new particle yields with largely decreased probability of survival to CCN size at the summit of Mt. Tai under reduced SO_2 emissions. *Atmospheric Chemistry and Physics Discussions*, *21*, 1305–1323. https://doi.org/10.5194/acp-2020-364

21698996, 2021, 7, Downloaded from https://agupubs.onlinelibrary.wiley.com/doi/10.1029/2020JD033267, Wiley Online Library on [13/12/2023]. See the Terms and Conditions (https://onlinelibrary.wiley.com/terms-and-conditions) on Wiley Online Library for rules of use; OA articles are governed by the applicable Creative Commons License

UNIVERSITY OF HYDERABAD

Centre for Earth, Ocean and Atmospheric Sciences
School of Physics

Plagiarism Free Certificate

This is to certify that the similarity index of this thesis has been checked by the IGM Library of the University of Hyderabad is 40%. Out of which 30% similarity is identified from the candidate's own publication which forms the major part of the thesis. The details of the student publications are as follows.

- **Sebastian, M.,** Kanawade, V.P., et al., *Observations of particle number size distributions and new particle formation in six Indian locations,* Atmospheric Chemistry and Physics, 22, 2022. (Chapters 3 & 5)
- Kanawade, V.P., **Sebastian, M.** and Dasari. P., *New particle formation and growth suppressed during COVID-19 lockdown in urban Hyderabad,* Journal of Geophysical Research-Atmospheres, 127, 2022. (Chapter 3)
- Kanawade, V.P., **Sebastian, M.**, et al., *Atmospheric new particle formation in India: Current understanding and knowledge gaps*, Atmospheric Environment, 270, 2022. (Chapter 1)
- **Sebastian, M.,** Kanawade, V. P., and Pierce, J. R., *Observation of sub-3nm particles and new particle formation at an urban location in India.* Atmospheric Environment, 256, 2021. (Chapter 3)
- **Sebastian, M.,** V.P. Kanawade et al., *New particle formation and growth to climate-relevant aerosols at a background remote site in the Western Himalaya*, Journal of Geophysical Research-Atmospheres, 126, 2021. (Chapter 5)

The remaining 10% similarity was identified from the external sources in the present thesis which is according to prescribed regulations of the University. All the publications related to the thesis have been appended at the end of the thesis. Hence, the present thesis is considered to be plagiarism-free.

V Kanawade
21/12/2023

Dr. Vijay P. Kanawade
UGC-Assistant Professor
Centre for Earth, Ocean & Atmospheric Sciences
University of Hyderabad
Hyderabad-500 046, Telangana, INDIA.

Atmospheric New Particle Formation and Growth in Diverse Environments in India

by Mathew Sebastian

Librarian
Indira Gandhi Memorial Library
UNIVERSITY OF HYDERABAD
Central University P.O.
HYDERABAD-500 046.

Submission date: 21-Dec-2023 12:45PM (UTC+0530)
Submission ID: 2263547333
File name: hewSebastian_PhDThesis_Final_21Dec2023_Without_bibliography.docx (13.7M)
Word count: 30603
Character count: 170612

21/12/2023

Dr. Vijay P. Kanawade
UGC-Assistant Professor
Centre for Earth, Ocean & Atmospheric Sciences
University of Hyderabad
Hyderabad-500 046, Telangana, INDIA.

Atmospheric New Particle Formation and Growth in Diverse Environments in India

ORIGINALITY REPORT

40%	23%	38%	2%
SIMILARITY INDEX	INTERNET SOURCES	PUBLICATIONS	STUDENT PAPERS

PRIMARY SOURCES

1	acp.copernicus.org Internet Source	11%
2	Mathew Sebastian, Vijay P. Kanawade, Jeffrey R. Pierce. "Observation of sub-3nm particles and new particle formation at an urban location in India", Atmospheric Environment, 2021 Publication	6%
3	V. P. Kanawade, M. Sebastian, P. Dasari. "Reduction in anthropogenic emissions suppressed new particle formation and growth: Insights from the COVID-19 lockdown", Journal of Geophysical Research: Atmospheres, 2022 Publication	5%
4	Vijay P. Kanawade, Mathew Sebastian, Rakesh K. Hooda, Antti-Pekka Hyvärinen. "Atmospheric new particle formation in India: Current understanding and knowledge gaps", Atmospheric Environment, 2022 Publication	3%

21/12/2023
Dr. Vijay P. Kanawade
UGC-Assistant Professor
Centre for Earth, Ocean & Atmospheric Sciences
University of Hyderabad
Hyderabad-500 046, Telangana, INDIA.

5	M. Sebastian, V. P. Kanawade, V. K. Soni, E. Asmi et al. "New Particle Formation and Growth to Climate-relevant Aerosols at a background remote Site in the Western Himalaya", Journal of Geophysical Research: Atmospheres, 2021 Publication	3%
6	V. P. Kanawade, M. Sebastian, P. Dasari. "Reduction in Anthropogenic Emissions Suppressed New Particle Formation and Growth: Insights From the COVID-19 Lockdown", Journal of Geophysical Research: Atmospheres, 2022 Publication	1%
7	www.researchgate.net Internet Source	1%
8	Mathew Sebastian, Vijay P. Kanawade, Vijay K. Soni, Eija Asmi et al. "New Particle Formation and Growth to Climate-Relevant Aerosols at a Background Remote Site in the Western Himalaya", Journal of Geophysical Research: Atmospheres, 2021 Publication	1%
9	Mathew Sebastian, Sobhan Kumar Kompalli, Vasudevan Anil Kumar, Sandhya Jose et al. "Observations of particle number size distributions and new particle formation in six	<1%

Dr. Vijay P. Kanawade
UGC-Assistant Professor
Centre for Earth, Ocean & Atmospheric Sciences
University of Hyderabad
Hyderabad-500 046, Telangana, INDIA.

	Indian locations", Atmospheric Chemistry and Physics, 2022 Publication	
10	hdl.handle.net Internet Source	<1%
11	Nucleation and Atmospheric Aerosols, 2007. Publication	<1%
12	iopscience.iop.org Internet Source	<1%
13	home.iitk.ac.in Internet Source	<1%
14	amt.copernicus.org Internet Source	<1%
15	agupubs.onlinelibrary.wiley.com Internet Source	<1%
16	www.ndtv.com Internet Source	<1%
17	coek.info Internet Source	<1%
18	Submitted to University of Hyderabad, Hyderabad Student Paper	<1%
19	T. Hussein, H. Junninen, P. Tunved, A. Kristensson et al. "Time-span and spatial-scale of regional new particle formation events	<1%

over Finland and Southern Sweden", Copernicus GmbH, 2009
Publication

20	meetingorganizer.copernicus.org Internet Source	<1%
21	"Aerosol Measurement", Wiley, 2011 Publication	<1%
22	www.science.gov Internet Source	<1%
23	helda.helsinki.fi Internet Source	<1%
24	www.mdpi.com Internet Source	<1%
25	Jinping Ou, Qihou Hu, Haoran Liu, Shiqi Xu, Zhuang Wang, Xiangguang Ji, Xinqi Wang, Zhouqing Xie, Hui Kang. "Exploring the impact of new particle formation events on PM2.5 pollution during winter in the Yangtze River Delta, China", Journal of Environmental Sciences, 2022 Publication	<1%
26	Vijay P. Kanawade, Mathew Sebastian, Rakesh K. Hooda, Antti Hyvärinen. "Atmospheric new particle formation in India: Current understanding and knowledge gaps", Atmospheric Environment, 2021 Publication	<1%

27	Renyi Zhang, Alexei Khalizov, Lin Wang, Min Hu, Wen Xu. "Nucleation and Growth of Nanoparticles in the Atmosphere", Chemical Reviews, 2011 Publication	<1 %
28	Sobhan Kumar Kompalli, Vijayakumar S. Nair, V. Jayachandran, Mukunda M. Gogoi, S. Suresh Babu. "Particle number size distributions and new particle formation events over the northern Indian Ocean during continental outflow", Atmospheric Environment, 2020 Publication	<1 %
29	V. Singla, S. Mukherjee, P.D. Safai, G.S. Meena, K.K. Dani, G. Pandithurai. "Role of organic aerosols in CCN activation and closure over a rural background site in Western Ghats, India", Atmospheric Environment, 2017 Publication	<1 %
30	theses.lib.polyu.edu.hk Internet Source	<1 %
31	A. Dinoi, K. Weinhold, A. Wiedensohler, D. Contini. "Study of new particle formation events in southern Italy", Atmospheric Environment, 2021 Publication	<1 %

32	kanazawa-u.repo.nii.ac.jp Internet Source	<1 %
33	mafiadoc.com Internet Source	<1 %
34	V.P. Kanawade, A.K. Srivastava, K. Ram, E. Asmi, V. Vakkari, V.K. Soni, V. Varaprasad, C. Sarangi. "What caused severe air pollution episode of November 2016 in New Delhi?", Atmospheric Environment, 2020 Publication	<1 %
35	Kupiainen-Määttä, Oona, Tinja Olenius, Hannele Korhonen, Jussi Malila, Miikka Dal Maso, Kari Lehtinen, and Hanna Vehkamäki. "Critical cluster size cannot in practice be determined by slope analysis in atmospherically relevant applications", Journal of Aerosol Science, 2014. Publication	<1 %
36	S. Suresh Babu, Sobhan Kumar Kompalli, K. Krishna Moorthy. "Aerosol number size distributions over a coastal semi urban location: Seasonal changes and ultrafine particle bursts", Science of The Total Environment, 2016 Publication	<1 %
37	www.osti.gov Internet Source	<1 %

38	Ignacio Pisso, Espen Sollum, Henrik Grythe, Nina I. Kristiansen et al. "The Lagrangian particle dispersion model FLEXPART version 10.4", Geoscientific Model Development, 2019 Publication	<1 %
39	Vijay P. Kanawade, Sachchida N. Tripathi, Abhishek Chakraborty, Huan Yu. "Chemical Characterization of Sub-micron Aerosols during New Particle Formation in an Urban Atmosphere", Aerosol and Air Quality Research, 2020 Publication	<1 %
40	gupea.ub.gu.se Internet Source	<1 %
41	dokumen.pub Internet Source	<1 %
42	"Aerosol Science", Wiley, 2013 Publication	<1 %
43	Anil Patel, Neeraj Rastogi. "Oxidative Potential of Atmospheric Aerosols over Different Regions of India and Surrounding Oceans", ACS Earth and Space Chemistry, 2023 Publication	<1 %
44	Katri Leino, Janne Lampilahti, Pyry Poutanen, Riikka Väänänen et al. "Vertical profiles of sub-3 nm particles over the boreal forest", Copernicus GmbH, 2018	<1 %

Publication

45	eprints.qut.edu.au Internet Source	<1%
46	Kenjiro Iida, Mark Stolzenburg, Peter McMurry, Matthew J. Dunn, James N. Smith, Fred Eisele, Pat Keady. "Contribution of ion-induced nucleation to new particle formation: Methodology and its application to atmospheric observations in Boulder, Colorado", Journal of Geophysical Research: Atmospheres, 2006 Publication	<1%
47	Buddhi Pushpawela, Rohan Jayaratne, Lidia Morawska. "Differentiating between particle formation and growth events in an urban environment", Atmospheric Chemistry and Physics, 2018 Publication	<1%
48	Jing Wang, Mengren Li, Lingjun Li, Ronghua Zheng, Xiaolong Fan, Youwei Hong, Lingling Xu, Jinsheng Chen, Baoye Hu. "Particle number size distribution and new particle formation in Xiamen, the coastal city of Southeast China in wintertime", Science of The Total Environment, 2022 Publication	<1%
49	ir.lib.uwo.ca Internet Source	<1%

50	iris.unige.it Internet Source	<1%
51	L Keck. "Comprehensive Measurement of Atmospheric Aerosols with a Wide Range Aerosol Spectrometer", Journal of Physics Conference Series, 07/06/2011 Publication	<1%
52	Magdalena Okuljar, Heino Kuuluvainen, Jenni Kontkanen, Olga Garmash et al. "Measurement report: The influence of traffic and new particle formation on the size distribution of 1–800 nm particles in Helsinki – a street canyon and an urban background station comparison", Atmospheric Chemistry and Physics, 2021 Publication	<1%
53	Pierce, J. R., D. M. Westervelt, S. A. Atwood, E. A. Barnes, and W. R. Leaitch. "New-particle formation, growth and climate-relevant particle production in Egbert, Canada: analysis from 1 year of size-distribution observations", Atmospheric Chemistry and Physics, 2014. Publication	<1%
54	V.P. Kanawade, S. Shika, C. Pöhlker, D. Rose et al. "Infrequent occurrence of new particle formation at a semi-rural location, Gadanki, in	<1%

tropical Southern India", Atmospheric Environment, 2014
Publication

---

55 Peng Du, Huaqiao Gui, Jiaoshi Zhang, Jianguo Liu, Tongzhu Yu, Jie Wang, Yin Cheng, Zongbo Shi. "Number size distribution of atmospheric particles in a suburban Beijing in the summer and winter of 2015", Atmospheric Environment, 2018 <1 %
Publication

---

56 Yunyan Zhang, Bjorn Stevens, Brian Medeiros, Michael Ghil. "Low-Cloud Fraction, Lower-Tropospheric Stability, and Large-Scale Divergence", Journal of Climate, 2009 <1 %
Publication

---

57 www.atmos-chem-phys.net <1 %
Internet Source

---

58 Shiyi Lai, Xin Huang, Ximeng Qi, Liangduo Chen et al. "Vigorous new particle formation above polluted boundary layer in the North China Plain", Geophysical Research Letters, 2022 <1 %
Publication

---

59 Vijay P. Kanawade, Sachchida N. Tripathi, Abhishek Chakraborty, Huan Yu. "Chemical Characterisation of Sub-micron Aerosols During New Particle Formation in an Urban <1 %

Atmosphere", Aerosol and Air Quality Research, 2020
Publication

60	Huan Yu, John Ortega, James N. Smith, Alex B. Guenther et al. "New Particle Formation and Growth in an Isoprene-Dominated Ozark Forest: From Sub-5nm to CCN-Active Sizes", Aerosol Science and Technology, 2014 Publication	<1 %
61	asian-transactions.org Internet Source	<1 %
62	tsi.com Internet Source	<1 %
63	www.collectionscanada.ca Internet Source	<1 %
64	A. Asmi. "Number size distributions and seasonality of submicron particles in Europe 2008–2009", Atmospheric Chemistry and Physics, 06/15/2011 Publication	<1 %
65	Berhane Temelso, Thomas E. Morrell, Robert M. Shields, Marco A. Allodi et al. "Quantum Mechanical Study of Sulfuric Acid Hydration: Atmospheric Implications", The Journal of Physical Chemistry A, 2012 Publication	<1 %

66	Cusack, M., A. Alastuey, and X. Querol. "Case studies of new particle formation and evaporation processes in the western Mediterranean regional background", Atmospheric Environment, 2013. Publication	<1 %
67	es.scribd.com Internet Source	<1 %
68	J. M. Desantes, V. Bermúdez, J. V. Pastor, E. Fuentes. "Investigation of the Influence of Post-Injection on Diesel Exhaust Aerosol Particle Size Distributions", Aerosol Science and Technology, 2006 Publication	<1 %
69	JOST HEINTZENBERG. "?How to find bananas in the atmospheric aerosol?: new approach for analyzing atmospheric nucleation and growth events", Tellus B, 4/2007 Publication	<1 %
70	Submitted to Uttar Pradesh Technical University Student Paper	<1 %
71	moam.info Internet Source	<1 %
72	C.-H. Jeong. "Particle formation and growth at five rural and urban sites", Atmospheric Chemistry and Physics, 08/27/2010	<1 %

Publication

73	HENRIK WIINIKKA, RIKARD GEBART. "THE INFLUENCE OF FUEL TYPE ON PARTICLE EMISSIONS IN COMBUSTION OF BIOMASS PELLETS", Combustion Science and Technology, 2006 Publication	<1 %
74	TAREQ HUSSEIN. "Observation of regional new particle formation in the urban atmosphere", Tellus B, 09/2008 Publication	<1 %
75	homepages.see.leeds.ac.uk Internet Source	<1 %
76	Hajime Akimoto, Jun Hirokawa. "Atmospheric Multiphase Chemistry", Wiley, 2020 Publication	<1 %
77	Liya Ma, Yujiao Zhu, Mei Zheng, Yele Sun, Lei Huang, Xiaohuan Liu, Yang Gao, Yanjie Shen, Huiwang Gao, Xiaohong Yao. "Investigating three patterns of new particles growing to the size of cloud condensation nuclei in Beijing's urban atmosphere", Atmospheric Chemistry and Physics, 2021 Publication	<1 %
78	Markku Kulmala, Heikki Junninen, Lubna Dada, Imre Salma et al. "Quiet New Particle	<1 %

Formation in the Atmosphere", Frontiers in Environmental Science, 2022
Publication

79	V. Fiedler. "The contribution of sulphuric acid to atmospheric particle formation and growth: a comparison between boundary layers in Northern and Central Europe", Atmospheric Chemistry and Physics, 07/20/2005 Publication	<1 %
80	pdffox.com Internet Source	<1 %
81	www.inq7.net Internet Source	<1 %
82	www.tucson.ars.ag.gov Internet Source	<1 %
83	Derek V. Mallia, Logan E. Mitchell, Andres Eduardo Gonzalez Vidal, Dien Wu, Lewis Kunik, John C. Lin. " Can We Detect Urban-Scale CO Emission Changes Within Medium-Sized Cities? ", Journal of Geophysical Research: Atmospheres, 2023 Publication	<1 %
84	G. Mordas, K. Plauškaitė, N. Prokopčiuk, V. Dudoitis, C. Bozzetti, V. Ulevicius. "Observation of new particle formation on Curonian Spit located between continental	<1 %

Europe and Scandinavia", Journal of Aerosol Science, 2016
Publication

85 Hari. "From Processes and Transport to Trees, Ecosystems and Atmosphere", Boreal Forest and Climate Change, 2008 <1%
Publication

86 Lubna Dada, Hélène Angot, Ivo Beck, Andrea Baccarini et al. "A central arctic extreme aerosol event triggered by a warm air-mass intrusion", Nature Communications, 2022 <1%
Publication

87 S D PAWAR, P MURUGAVEL, V GOPALAKRISHNAN. "New particle formation by ion-induced nucleation during dissipation stage of thunderstorm", Journal of Earth System Science, 2011 <1%
Publication

88 Ulrich Pöschl, Manabu Shiraiwa. "Multiphase Chemistry at the Atmosphere–Biosphere Interface Influencing Climate and Public Health in the Anthropocene", Chemical Reviews, 2015 <1%
Publication

89 Ying Zhou, Lubna Dada, Yiliang Liu, Yueyun Fu et al. "Variation of size-segregated particle number concentrations in winter Beijing", Copernicus GmbH, 2019 <1%

Publication

90	karws.gso.uri.edu Internet Source	<1%
91	Chenjuan Deng, Yueyun Fu, Lubna Dada, Chao Yan et al. "Seasonal Characteristics of New Particle Formation and Growth in Urban Beijing", Environmental Science & Technology, 2020 Publication	<1%
92	Giechaskiel, B.. "Evaluation of the particle measurement programme (PMP) protocol to remove the vehicles' exhaust aerosol volatile phase", Science of the Total Environment, 20101001 Publication	<1%
93	Kevin Berland, Clémence Rose, Jorge Pey, Anais Culot et al. "Spatial extent of new particle formation events over the Mediterranean Basin from multiple ground-based and airborne measurements", Atmospheric Chemistry and Physics, 2017 Publication	<1%
94	Submitted to UC, Irvine Student Paper	<1%
95	Submitted to University of Leeds Student Paper	<1%

96	Vyoma Singla, Subrata Mukherjee, Adam Kristensson, Govindan Pandithurai, Kundan K. Dani, Vasudevan Anil Kumar. "New Particle Formation at a High Altitude Site in India: Impact of Fresh Emissions and Long Range Transport", Copernicus GmbH, 2018 Publication	<1%
97	Xinghua Zhang, Yangmei Zhang, Junying Sun, Xuejin Zheng, Gang Li, Zuqing Deng. "Characterization of particle number size distribution and new particle formation in an urban environment in Lanzhou, China", Journal of Aerosol Science, 2017 Publication	<1%
98	Zhou Zhang, Xinming Wang, Yanli Zhang, Sujun Lü, Zhonghui Huang, Xinyu Huang, Yuesi Wang. "Ambient air benzene at background sites in China's most developed coastal regions: Exposure levels, source implications and health risks", Science of The Total Environment, 2015 Publication	<1%
99	etheses.bham.ac.uk Internet Source	<1%
100	scholars.unh.edu Internet Source	<1%

Exclude quotes	On	Exclude matches	< 14 words
Exclude bibliography	On		